LATE QUATERNARY LANDSCAPE EVOLUTION IN THE GREAT KAROO, SOUTH AFRICA: PROCESSES AND DRIVERS

Thesis submitted in accordance with the requirements of the University of Liverpool for the degree of Doctor in Philosophy by

Christopher James Oldknow

21st July, 2016.

Table of Contents

Abstract

The Great Karoo spans the north-central part of South Africa at a major climatic boundary. The characteristics, spatial patterns and drivers of river channel response to Late Quaternary climate changes in the Sneeuberg, South Africa remain unclear due to the discontinuous alluvial stratigraphic record and the lack of dated palaeoclimatic archives. Dendritic channel networks in the upper Sundays River are deeply incised exposing terrace fills of varying thickness (2-6 m), extent (1 - > 10km) and pedogenic overprinting. Channels exhibit 'stepped' long profiles where resistant rock strata (dolerite, sandstone) cross valley floors, but are now partially or completely breached. DGPS surveys, sediment logging, mineral magnetic measurements and radiometric dating (OSL and ^{14}C) were used to determine the source, age structure and depositional process of valley fills and ascribe intensity of pedogenic overprinting. A conceptual model of terrace development in relation to changing conditions of connectivity was tested.

First order streams were desensitised to late Quaternary base level changes downstream due to the blocking effect of two barriers, with localised autogenic "cut and fill." Contrastingly, the continuity of 4 fill terraces over incised barriers in 2^{nd} – 4^{th} order tributaries indicate relatively high sensitivity to post-LGM climatic change. However, deposition of alluvium (T2) inset within periglacial deposits (T1) was partly a complex response to re-connection of the channel network with deep upland colluvial stores resulting in the valleys becoming choked with sediment. This caused a rise in groundwater and formation of extensive (> 10 km^2) rootmats on valley floors, restricting depth of subsequent channel entrenchment (T3/T4).

This study presents one of the first attempts in South Africa to test and explain terrace genesis and correlation using existing conceptual models for sediment connectivity. The relative roles of periglaciation and fluvial activity are shown to be key influences on dynamics of Quaternary sedimentation, pedogenesis and erosion and help to explain how sediments can be preserved over long periods (10^4 years) in catchments subject to base level fall.

Acknowledgements

I thank the University of Liverpool and specifically, the Department of Geography and Planning for the support and facilities provided for this study. This PhD project was conducted on a NERC-algorithm studentship (1093015).

Many thanks are due to my supervisors: Professor Janet Hooke, Professor Andreas Lang and Dr Barbara Mauz for their guidance and support during period of candidature.

Additionally, I would like to thank: Professor Frank Oldfield (University of Liverpool) and Dr Ian Candy (Royal Holloway, University of London) for their specialist guidance in the respective fields of mineral magnetism and soil micromorphological analysis; Kate Rowntree (Rhodes University) for providing us with field equipment and digitised aerial photographs of the study region and Hester and JP of Ganora farm, South Africa for granting us permission to work on their farmland.

Thank you to my many friends and family who have supported and encouraged me during the last four years.

Chapter 1: Introduction and aims

1.1 Introduction

Terraces are formed by phases of cyclic cutting and filling of vertical accumulations of alluvial sediments. Several periods of cutting and filling can produce complex stratigraphic and topographic relationships (Leopold and Miller, 1954). The causes of floodplain abandonment are varied and can broadly be classified into two groups: 1) allogenic and 2) autogenic. Climatic, tectonic, eustatic fluctuations and land use changes constitute allogenic drivers of terrace development (Leopold et al., 1964; Born and Ritter, 1970; Merrits et al., 1994; Bridgland and Westaway, 2008). However, exceedance of geomorphic thresholds and complex response can result in terrace incision, aggradation and stabilisation in response to direct climate forcing but also independently from climate (Schumm, 1973; 1977; Patton and Schumm, 1981; Young and Nanson, 1982; Tooth et al., 2004; Erkens et al., 2009). Removal of channel obstructions and progressive fluvial downcutting can also act as intrinsic controls on terrace development (Hadley, 1960; Warner, 1972; Tooth et al., 2004; 2007; Cheetham et al., 2010).

Individual terraces represent changes in river behaviour and sediment supply (Schumm, 1977). Analysis of terrace morphology can yield insights into fluvial system evolution over a range of spatial scales. Establishing the lateral (cross-section) and longitudinal (long-section) limits of terraces can provide an initial morphostratigraphic framework to facilitate correlation between terraces (Leopold and Miller, 1954; Leopold et al., 1964). This is particularly useful where traditional ‘terrace staircases’ are not preserved but rather terrace remnants occur as small discontinuous pockets (Brierley and Fryirs, 1998; Cheetham et al., 2010a). Presence of pocket fills may reflect terminal channel processes inducing reach scale phases of cutting and filling (Bull, 1997; Billi, 2007), catchment or tributary disconnectivity (Brierley and Fryirs, 1997; 1998; Fryirs et al., 2007) and also diminishing geomorphic system memory as formerly continuous terraces are reworked (Keen-Zebert et al., 2013).

Correlation of terrace remnants requires a multi-faceted approach. The sedimentology (sorting, grain-size and sedimentary structures) of terraces indicates

conditions of deposition. Stratigraphy of terrace fills indicates changes in fluvial regime, the conditions and rates of accretion (Born and Ritter, 1970; Warner, 1972; Young and Nanson, 1982; Merritts et al., 1994). Palaeosols represent phases of geomorphic stability. Macro-pedological features (soil structure, texture, organic content, colour) characterise distinct soil horizons and general conditions of formation, whilst micromorphological features (secondary carbonate accumulations, iron mottling, illuviated clays) can be used to semi-quantitatively characterise soil maturity, conditions of formation, changes in sediment source and degree of soil polygenesis (Wehmueller, 1993). Palaeosols may contain useful information about the nature of climate during phases of geomorphic inactivity (Candy et al., 2002). They may also constitute important pedo-stratigraphic discontinuities, evidencing abrupt changes in geomorphic state (Botha and Fedoroff, 1995; Clarke et al., 2003). Mineral magnetic measurements can establish which sedimentological and pedological units within terraces display similar concentrations of ferrimagnetic (magnetite/maghemite) and anti-ferromagnetic minerals (haematite/goethite) to: 1) semi-quantitatively ascribe pedogenic intensity; and 2) infer changes in catchment source area (Oldfield et al., 2009). Chronometric data is crucial to test for the contemporaneity of terrace fills, calculate sedimentation rate (Cheetham et al., 2010a), establish duration of alluvial preservation (Lewin and Macklin, 2003; Keen-Zebert et al., 2013) and evaluate the leads and lags of river channel response to extrinsic drivers of climate change (Lyons et al., 2014).

Cyclic incision and aggradation is a feature of the Great Escarpment in South Africa. Botha et al. (1994) recognised four colluvial geomorphic cycles spanning the last 135,000 years in the KwaZulu-Natal but fills were diachronous between sites implying the agency of local geomorphic thresholds (Schumm, 1977). This contrasts with the Klein Seekoi valley (20 km north of the Sundays River) draining the landward side of the Sneeuberg (Fig. 1.1) where a combination of geologic and climatic factors mean that localised autogenic cut and fill processes dominate with no explicit terrace stratigraphy pre-dating the mid-Holocene (Bousman et al., 1988; Holmes et al., 2003; Grenfell et al., 2014). The Klein Seekoi is not incised to the same extent as the Sundays. Other researchers have attempted to make explicit links between quantitative palaeoclimatic archives and geoproxy records with mixed success (Clarke et al., 2003; Temme et al., 2008; Lyons et al., 2014). The major

problems with this approach include, i) extrapolation of climate records over large geographic distances, ii) the varied response of different proxy records to the same environmental forcing (Stone, 2014), iii) inadequate dating coverage and temporal precision where dating is available (Lyons et al., 2013), iv) failure to adequately characterise local thresholds that can produce leads and lags to allogenic forcing (Patton and Schumm, 1981).

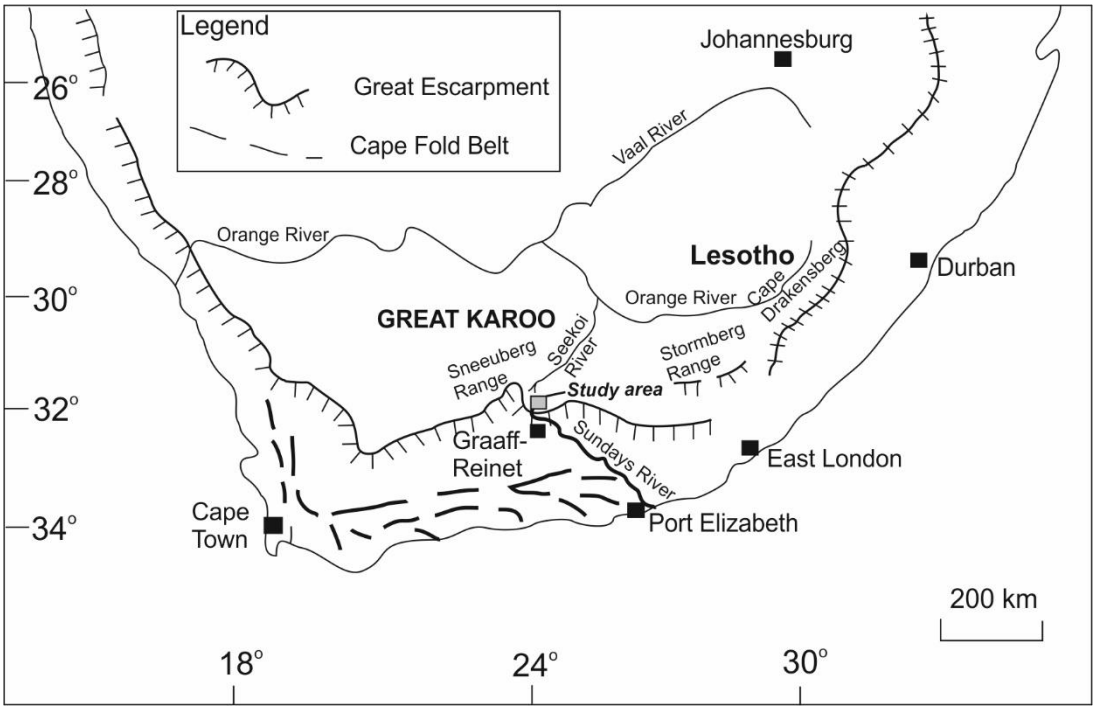

Figure 1.1 – study area location in relation to Great Escarpment and other major mountain ranges and rivers of South Africa. Modified from Holmes et al. (2003).

The south-flowing Sundays River originates in the Sneeuberg just north of the Great Escarpment and terminates in the Southern Ocean near Port Elizabeth (Fig. 1.1). Terrace sedimentology and stratigraphy of the lower Sundays River, South Africa has been investigated by Hattingh and Rust (1999) where 13 Miocene to Holocene-aged terraces were originally linked to allocyclic drivers of eustasy and epeirogenic uplift (Erlanger et al., 2012). The headwaters of the Sundays River, which are the focus of this study, originate in the Sneeuberg in the Great Karoo at a major climatic boundary between summer and winter dominated rainfall zones (Fig. 1.1; Chase and Meadows, 2007; Chase et al., 2015). This region has been tectonically stable since the Late Pliocene and buffered from effects of Late Quaternary eustatic sea level changes. Valleys are deeply incised in response to the landward retreat of the Great

Escarpment. Dendritic first order gullies and second to fourth order tributaries have exposed up to 6 m of colluvium and alluvium exhibiting complex stratigraphy in relation to major geological and geomorphic barriers of different configuration and longevity. Work to date in these upland catchments has centred on reconstructing erosion histories since the late 19th century (Foster et al., 2007; Boardman et al., 2010; Rowntree et al., 2012). The Upper Sundays therefore provides a unique opportunity to compare and contrast the characteristics, drivers and mechanisms of cutting and filling with those reported from fills to the north of the Sneeuberg (Holmes et al., 2003; Grenfell et al., 2014). The complexity of the terrace deposits and distribution of different kinds of barriers to sediment movement (Fryirs et al., 2007) make these valleys ideal for refining and applying ideas of connectivity to understand the mechanisms and trajectories of palaeo-sediment fluxes both at the channel (Hooke, 2003) and catchment scale (Tooth et al., 2004; Fryirs et al., 2012).

1.2 Research aim and objectives

The overarching aim of this research is to develop an understanding of the characteristics, mechanisms and drivers of terrace formation in the headwaters of the upper Sundays River, South Africa. Specifically, two low-order tributaries (Africanders and Wilgerbosch Kloof) and several reaches of the higher-order Wilgerbosch tributary were selected. This research aim is achieved through longitudinal and cross-sectional correlation of terrace fills by geomorphologic, stratigraphic, pedologic and chronometric analyses.

The objectives of this study are to identify and characterise the different valley fills present and establish their continuity, to reconstruct the physical linkages (connectivity) between different landscape components from the sedimentology, stratigaphy and pedology of deposits and to establish a chronology of terrace formation and incision and compare with other regional and continental dryland fluvial records. This study provides the first comprehensive, multi-proxy reconstruction of Late Quaternary terrace evolution in the Sundays River headwaters.

Chapter 2: Study area and literature review.

2.1 Introduction

The objectives of this literature review are to provide: i) an introduction to the study area; ii) brief summaries of both the geological and climatological context for the study region; and iii) a review of the characteristics, mechanisms and drivers of alluviation and colluviation illustrated by case studies from valleys in the USA, Australia, South Africa and across the Mediterranean.

2.2 Study area

The Great Karoo is a vast (30% total land surface of South Africa), dissected landscape of plains and flat-topped mountains, characterised by east-west orientated mountain ranges, an example being the Sneeuberg in which the Sundays River originates (Fig. 1.1). Compassberg is the second highest peak (2502 m) in the Eastern Cape Escarpment (Boardman et al., 2003). Vegetation consists of Karroid scrub on plains and sourveld in mountain reaches (Sugden, 1989).

The headwaters of the Sundays River and its tributaries drain deeply incised slopes and valleys south of Compassberg. The river flows through the Great Karoo before reaching the quartzite/sandstone rich Klein Winterhoek Mountains to the south. Upstream of the mountains, a few terrace deposits are preserved as isolated features. Upon exiting the mountains, the Sundays drains soft mudstones and shales associated with the Cretaceous Algoa basin (Hattingh, 1996), where a well-developed flight of terraces has formed along its entire length. Hattingh (1996) identified thirteen terraces providing an almost continuous depositional record from the Late Miocene to Holocene. However, Hattingh's (1996) proposition that fluvial incision of the Sundays terraces resulted from eustatic sea-level fall (up to 450 m since the Miocene) has recently been criticised as irreconcilable with the subsequent net increases in global ice volume. Bridgland and Westaway (2008) deduced two key phases of epeirogenic uplift in the late Pliocene and Mid-Pleistocene – the latter coinciding with a switch from aggradation of the Sundays to incision of a narrow gorge (see T4 – Hattingh and Rust, 1999). Westaway (2002a) proposed the most likely forcing agent, in the absence of any Pleistocene glaciation in South Africa, was erosion and cyclic loading of the continental crust beneath the offshore continental

shelf which occurred in response to global sea-level fluctuations. The relatively high Late Pliocene uplift rates have been attributed to enhanced erosion arising from a much wetter climate regime that prevailed at that time (Tankard et al., 1982; Tyson, 1986; Bridgland and Westaway, 2008a).

The Sundays Headwaters are deeply incised but the timing and causes of the present 'cut' phase have been the subject of considerable debate (Rowntree et al., 2004). From a combined analysis of aerial photographs and historical records, Boardman (2014) proposed that the present 'cut' phase initiated in the mid to late 19th century in response to poorly managed grazing systems implemented by European settlers, but as yet, chronometric data has not been obtained and thus constraining the exact timing of this incision has not been possible.

In the last nine years, a broad study investigating the use of environmental magnetism and gamma spectrometry as methods for reconstructing the erosional history of small Sneeuberg catchments has been ongoing (Foster et al., 2007; Boardman et al., 2010; Rowntree et al., 2012; Pulley and Rowntree, 2016).

Dendritic gully networks and mixed alluvial-bedrock channels up to 6 m deep are common in the Upper Sundays. Gullying has exposed a complex alluvial and colluvial terrace-stratigraphy with marked sedimentological and pedological differences that may be testament to a legacy of prior 'cut and fill' episodes, but the spatial and temporal scales and drivers of these phases have yet to be investigated. Despite the extent of incision, pockets of relatively intact fill occur in narrow valley settings, juxtaposed with fills that are extremely denuded where badlands have developed (Keay-Bright and Boardman, 2009). Soil erosion associated with this incision continues to reduce land productivity for grazing and cultivation (Rowntree et al., 2004) as well as exacerbating problems of reservoir and check dam siltation (Foster et al., 2007; Rowntree et al., 2012).

Thus, until our study conducted from 2012-2015, work in the upper Sundays has focused on clarifying the drivers of the current incision phase and reconstructing historical catchment erosion histories but with no attention paid to the Late Quaternary fluvio-geomorphic evolution of these valleys. Extensive colluvial deposits are a feature of the Great Escarpment but studies have mainly focused on rivers and slopes draining its landward side (Scott, 1989; Botha et al., 1994; Clarke et al., 2003;

Holmes, 2003; Boardman et al., 2005) and, as a result, the age, sedimentology and stratigraphy of deposits contained within the Sundays headwaters have yet to be investigated.

2.3 Geology

The Sundays headwater valleys are dominated by Permian/Triassic Karoo Supergroup rocks which exhibit negligible dip (Boardman et al., 2003; Pulley and Rowntree, 2016). Rocks of the upper Beaufort Group comprise the sedimentary strata outcropping in these valleys. Two geological formations are represented (Fig. 2.1).

Firstly, the Middleton Formation consists of a thick mudrock-dominated succession which reflects shallow lacustrine facies at the base, overlain by vertically stacked fining-upward sequences ranging from 200-600 m thick (Johnson, 1976). Secondly, the Balfour Formation comprises a mixture of fining-upward sandstone-dominated sequences laid down by a network of low sinuosity streams (Oudeberg member – Turner, 1978). The top of this formation consists of lacustrine mudstones, shales, rhythmites and sandstones with wave ripples (see Fig. 2.2) which becomes sandier and redder towards the top (Catuneanu et al., 2005).

Drakensberg Group dolerite sills and dykes constitute the major igneous rock component, emplaced approximately 183 Ma, forming the highlands of the Eastern Cape region and Lesotho (Duncan et al., 1997). The majority of these sills are strata bound by the Beaufort Group rocks with widespread contact metamorphism (Neuumann et al., 2011).

Following the emplacement of the doleritic province across the Karoo basin, the Gondwanan supercontinent started to break up due to marginal rift faulting involving tilted blocks and horst and graben structures (Maud, 1996; Catuneanu et al., 2005). Breakup occurred first along the east coast (160 Ma), but at approximately 130 Ma along the western flank.

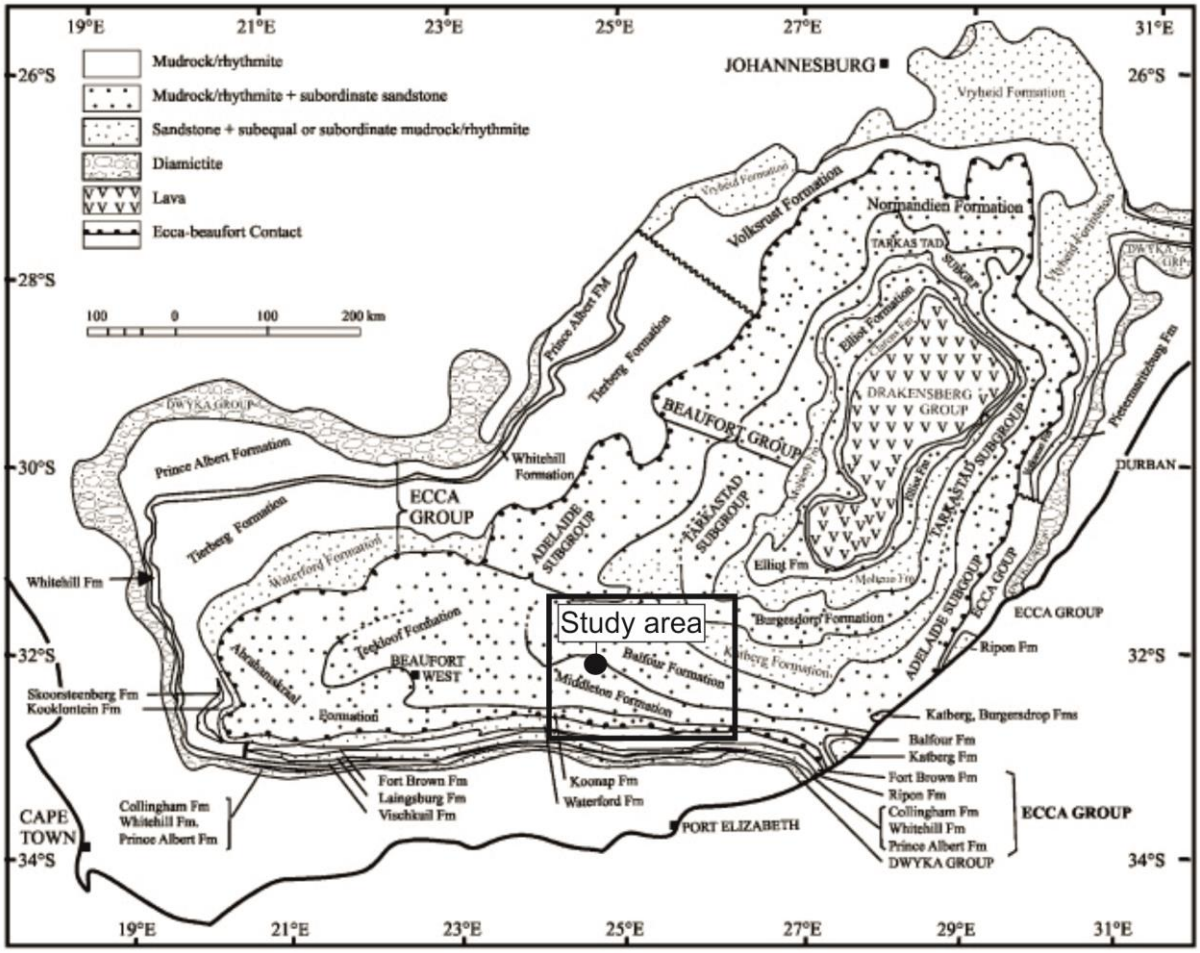

Figure 2.1 – geological map showing distribution of the different subgroups and associated formations of the Beaufort Group. The area enclosed within the square straddles the Great Escarpment and Sneeuberg, where siltstones, shales and subordinate sandstones associated with the Middleton and Balfour formations occur. Modified from Catuneanu et al., (2005).

Prior to continental break-up, South Africa was central within Gondwana and its altitude high relative to the other proto-continents (1,800–2,400 m.a.s.l). Following break-up, erosion commenced on the newly formed high and steep margins of the South African subcontinent, forming the 'Great Escarpment'. This geomorphic feature still separates the steep and deeply dissected marginal portions of the subcontinent from the high plains that characterise the interior. At 120 Ma ago, the formation of the major fluvial systems draining the Escarpment occurred (Hattingh, 1996; Maud, 1996).

Additionally, two major erosion surfaces are superimposed on the Karoo landscape. According to Partridge and Maud (1987), 100-200 m of epeirogenic uplift occurred roughly 18 Ma ago in the Eastern Cape region, with the initiation of a new erosion cycle as rejuvenated rivers cut down to new base levels and also coastal areas being tilted seaward. However, this work has been challenged more recently. Burke

and Gunnell (2008) have argued that tilting occurred due to crustal swelling associated with eruption of the “Afar plume” after 31 Ma. Large escarpments then formed on swell flanks as they began to rise in the last 30 Ma.

Nevertheless this tilting of the proto-Eastern Cape led to a marine transgression, expressed in the form of a marine bench, which now forms a gently seaward-sloping plain (150-250 m elevation) seaward of the mountain ranges extending westwards from Port Elizabeth. Sea level curves for the Algoa Bay also indicate a fluctuation between 280 m above and below present sea level, but with an overall lowering from the Late Miocene to the Holocene (Le Roux, 1989; Hattingh, 1996; Maud, 1996).

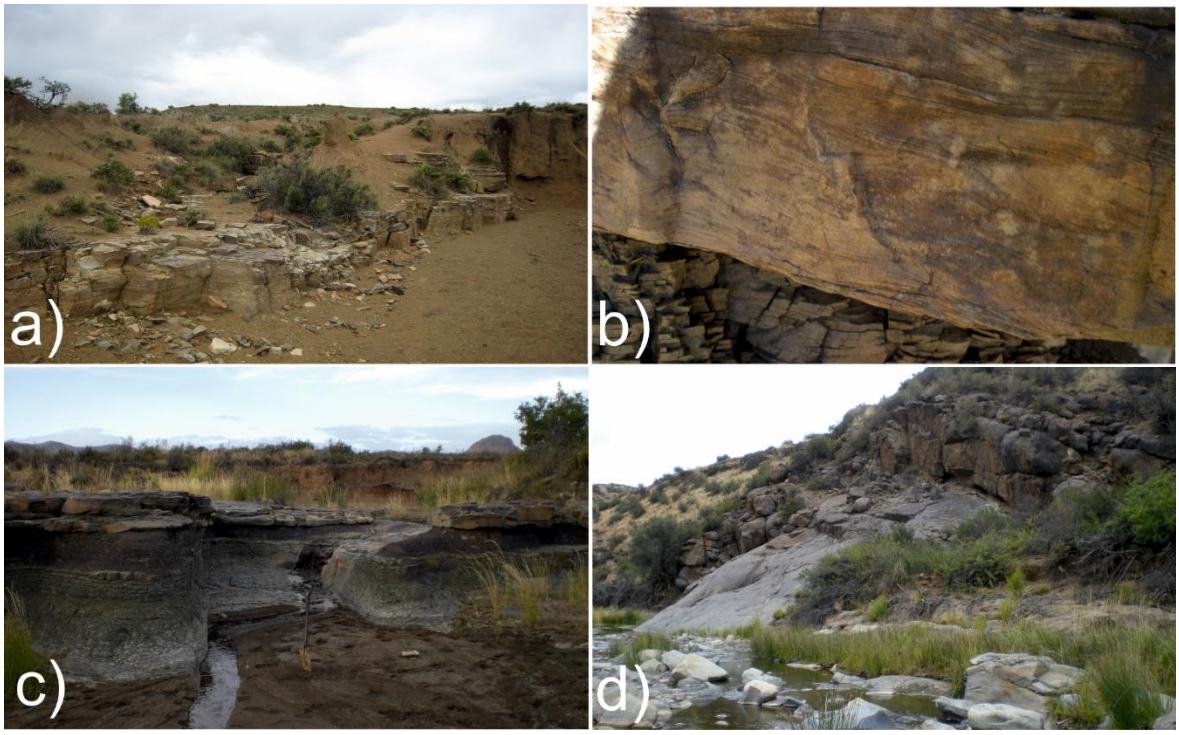

Figure 2.2 – photographs of Karoo Supergroup rocks. 2.2a – sandstone rock of the Balfour Fm 2.2b – sandstone with wave ripples, 2.2c – channel headcut through Balfour Fm. shales and siltstones, the latter indicated by dark reddish/brown colour, 2.2d – example of intrusive dolerite dyke.

However, this post-African I erosion cycle was terminated by further major uplift and seaward tilting of the coastal hinterland in the Early-Mid Pliocene (4 Ma ago). This second major epeirogenic uplift phase initiated river incision and differential dissection of the topography according to the erodibility of the substrate. This is recorded in the Sneeuberg study area as flat-topped hills, capped by resistant dolerites or sandstones, which, due to being relatively resistant to erosion, rise above areas controlled by structurally weaker mudstones and shales (Maud, 1996).

The subcontinent is now a stable craton, but there have been phases of epeirogenic uplift in the late Pliocene and Pleistocene (see Section 2.2).

2.4 Climate

The Sneeuberg lies within the eastern region of the Warm Temperate Zone (Sugden, 1989). The area lies at a major climatic boundary with influences from both summer and winter dominated rains, making it a climatically sensitive region (Chase and Meadows, 2007). Annual rainfall is typically 350 mm a^{-1}, concentrated in the late summer/early autumn (Schultz, 1980; Sugden, 1989; Rowntree et al., 2012). Nearby instrumental rainfall records show high coefficient of variance in precipitation since 1908 (Fig. 2.3), with three distinct drought phases from 1908-1930, 1964-1972 and 1992-2001 (Grenfell et al., 2014). Diurnal and seasonal temperatures show large fluctuations: summer maxima of ca. 30^{o}C and winter minima of below -10^{o}C (Schulze, 1980). Rainfall in the 19th and 20th centuries has shown no net increase or decrease, but the record exhibits pronounced multidecadal variability (16-20 years), which is a well-established feature of southern African rainfall (Tyson, 1986; Folland et al., 1998; Boardman et al., 2003).

Until recently, there has been considerable disagreement between palaeoclimatic models with respect to temperature and wetness since the Last Glacial Maximum. For instance, there has been much discussion over the degree to which expansion of Antarctic sea ice during glacial times, displaces the westerlies equatorward leading to enhanced humidity and concurrent winter rainfall in south-west Africa (van Zinderen Bakker, 1976; Stuut et al., 2004). van Zinderen Bakker (1967) first applied the idea of a latitudinal shift of circulation systems over glacial-interglacial timescales to assess the nature of climate change over the South African subcontinent. The ensuing model called for expansion of winter rains across all of South Africa (WRZ) south of 25^{o}S during glacial periods. A later model by Butzer et al. (1978) emphasised a stronger rather than displaced circulation system. Their model suggests a minimal shift in the westerlies during glacial times (based on Tufa deposts of the Gaap Escarpment: 37.5-19.7 ka) with drier conditions resulting in all except the southwestern most zones of the winter rainfall zone (WRZ). Crucially, this model argued for an increase in precipitation in the summer rainfall zone (SRZ) as a function of interhemispheric pressure variations leading to a southward displacement

of the ITCZ. Based on stromatolite ages (19.4-18.6 ka) from the Urwi Pan in the central Kalahari, precipitation was estimated to increase by 150-200% at the LGM, which may evidence this southward shift in the ITCZ (Lancaster, 1979). While some agreement existed between model results and palaeoenvironmental records, the degree to which this association was merely circumstantial remains unclear.

Cockcroft et al. (1987) developed arguably more reliable climate models of South Africa, on the basis that they incorporated more numerical information on contemporary weather patterns, as well as their *longitudinal* variability (the previous examples cited employed models that only considered *latitudinal* variability). Their model rekindled the notion of an expanded Antarctic glacial ice induced equatorward shift in the westerlies leading to a much larger WRZ in South Africa. A reduction in the meridional Walker circulation during glacial times resulting in weaker tropical easterlies, leading to significantly reduced SRZ totals in more eastern parts of South Africa. Conversely, during interglacial times, this circulation is strengthened with the resulting higher intensity tropical easterlies supplying more moisture to the continent resulting in an expanded SRZ at the expense of the WRZ, the latter curtailed as the westerlies are shifted southward only grazing the southwestern most fringes of the subcontinent. Despite being useful on a broad scale, the proposed WRZ dynamics still did not accord with some palaeoenvironmental records. A pollen record from Namibia as well as a stable carbon isotope record from the South African interior (Scott et al., 2004; Lee-Thorp and Beaumont, 1995) implied a far more muted response in the WRZ to forcing by distal glacial expansion. The model also does not account for smaller spatial and temporal scale climate variability.

Nevertheless, a suite of advances including more refined dating techniques (OSL - Rodnight et al., 2006) and the discovery of new proxy data sources (e.g. marine cores off the Namibian coast: Shi et al., 2001; Stuut et al., 2002; Dupont and Wyputta, 2003; Hyrax middens – Chase et al., 2012, 2013, 2015 a and b) have allowed for the first palaeoenvironmental transects to be constructed and analysed (Chase and Meadows, 2007; Gasse et al., 2008; Lewis et al., 2011; Stone, 2014). However, the spatial patterning of wetter and drier conditions than present and the position of mid-latitude westerlies during the LGM are still greatly debated. Furthermore, the fact that differet proxies may respond to different forcings introduces ambiguities in interpretations of palaeoclimate (Stone, 2014). Recently it

has been proposed that via inter-hemispheric teleconnections, patterns of warming and cooling post-MIS2 occurred in phase between northern and southern hemispheres (He et al., 2013). New data from hyrax middens across South Africa, Chase et al. (2015) proposed that following the LGM, westerly storm tracks shifted southward with increased flow of warm Agulhas Current waters into the SE Atlantic. As a result, reduced northward heat transport in the Atlantic Meridional Overturning Circulation (AMOC) favoured warming sea-surface temperatures and increasing advection of tropical easterlies to the southwestern Cape (Reason et al., 2006). Crucially, this model purports that the SRZ expanded across much of southern Africa from 18-14.6 ka and that subsequent climate changes were in phase with the North Atlantic (He et al., 2013; Chase et al., 2015), but this does not accord with other reconstructions of palaeoprecipitation from Blood River donga sediments which imply climatically dry conditions until 15 ka (Lyons et al., 2014).

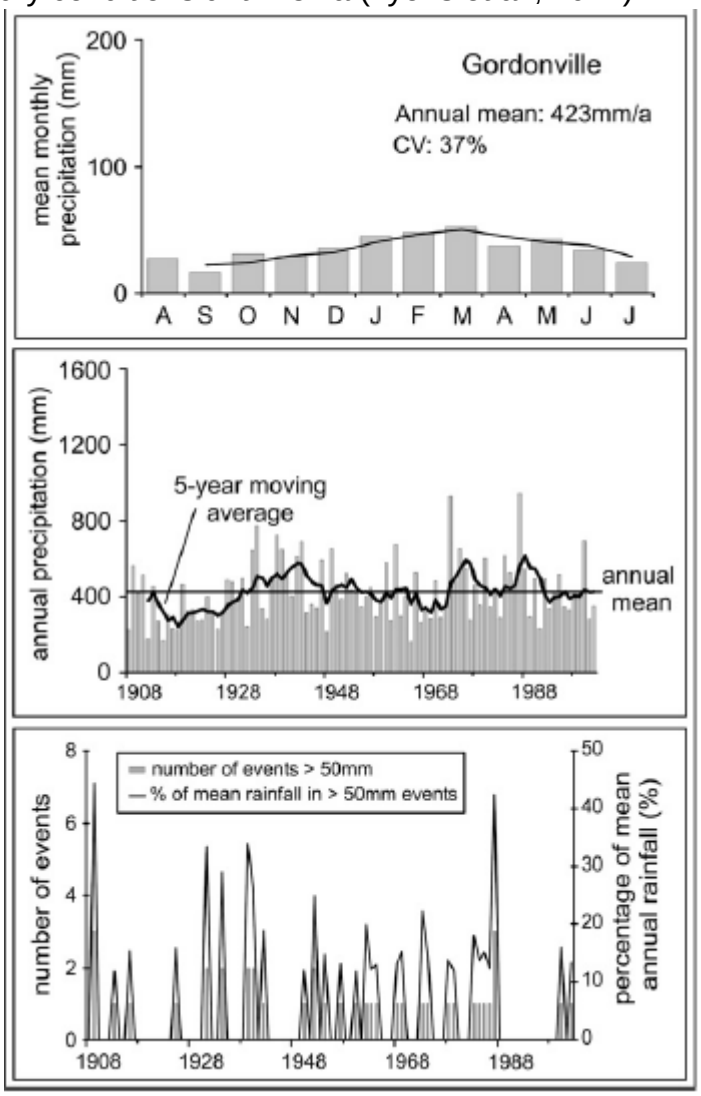

Figure 2.3 – Climate data for Gordonville in the Karoo, indicating seasonality, inter-annual variability and flashiness (After Grenfell et al., 2014).

2.5 Characteristics and drivers of valley alluviation

2.5.1 Introduction

Alluvial terraces represent packages of vertically accreted floodplain and channel sediment during phases of net valley aggradation. Floodplains become terraces when channels are entrenched to sufficient depth to prevent sedimentation on the former floodplain (terrace) surface.

Conventionally, terrace staircases have been used to analyse and reconstruct fluvial system evolution (Schumm, 1977). In dryland ephemeral channels, the highly episodic, 'flashy' nature of hydrological responses to storms predominantly results in 'disequilibrium' channel forms such as terminal gullies or arroyos (Bull, 1997), as opposed to 'equilibrium forms' more commonly associated with humid drainage settings where channel form more commonly is adjusted to a mean 'channel-forming discharge' (Knighton, 1997).

'Arroyos' are trenches with an approximately rectangular cross-section excavated in valley-floor alluvium with a major stream channel at the base. The term was first used in a scientific context by Dodge (1902), but used in Spanish literature since at least 775 AD (Graf, 1983). The arroyo cycle is a well-established concept: phases of channel entrenchment may be rapid, occurring in less than 100 years, but conversely, filling of channels can take over 500 years (Bull, 1997; Gellis et al., 2012). Exposures of palaeo-arroyos in the SW USA attest to phases of Late Quaternary cut and fill (Bailey, 1935; Hack, 1942; Haynes, 1968; Waters et al., 2001; Harden et al., 2010).

'Gullies' are smaller than arroyos, comprising V or U-shaped trenches in unconsolidated materials with a small channel at the base. They are typically not collocated with major stream channels and thus often discontinuous in nature (Graf, 1983; Harvey, 2001; Chiverrell et al., 2007). Interest in the arroyo and gullying phenomenon stems from geomorphic, archeologic and land management problems directly related to their incision and evolution (Patton and Schumm, 1981).

Alluvial archives have been used for palaeoenvironmental reconstructions in semi-arid landscapes worldwide (e.g. Erkens et al., 2009; Harvey et al, 2011; Macklin et

al., 2012; Lyons et al., 2014). Two main disciplinary approaches to their investigation are recognised.

Firstly, the stratigraphy of alluvial deposits is analysed, mapped and interpreted (Born and Ritter, 1970; Warner, 1972; Cooke and Reeves, 1976; Young and Nanson, 1982; Merritts et al., 1994; Erkens et al., 2009). In most dryland settings, major exposures reflect historic arroyo (Schumm and Hadley, 1957) or gully incision in the late 19th century (Brierley and Fryirs, 1999; Boardman et al., 2014), but cycles of cutting and filling have occurred throughout the Holocene (Bailey, 1935; Hack, 1942; Haynes, 1968; Lyons et al., 2013) and Late Pleistocene at some locations in South Africa, Greece, Crete and Spain (Botha et al., 1994; Botha and Fedoroff, 1995; Woodward et al., 2008; Macklin et al., 2010; Soria-Jáuregui et al., 2016).

Various techniques have been developed to establish the (dis)continuity of terrace units including detailed lateral and longitudinal surveys (Leopold and Miller, 1954; Leopold et al., 1964; Cheetham et al., 2010). Refined dating approaches (OSL, ^{14}C) have permitted more precise alluvial chronologies to be constructed to evaluate the degree of synchronism between different alluvial deposits both locally and regionally, as well as assess leads and lags to records of Late Quaternary climate change (Rodnight et al., 2006; Temme et al., 2008; Erkens et al., 2009; Harden et al., 2010; Keen-Zebert et al., 2013; Lyons et al., 2013).

Secondly, slackwater flood deposits in canyons have been used to reconstruct pre-instrumental flood histories with mixed success (Baker et al, 1979; Patton et al, 1979; Kochel and Baker, 1988). For the USA, a large inventory of Holocene palaeoflood records was compiled based on slackwater deposits (Baker et al., 1983; Webb, 1985; Ely and Baker, 1985; Ely, 1992; O' Connor et al, 1994; House, 1996). However, relations between arroyo cutting and filling and slackwater deposits in canyons have not been considered. In a recent study, Harvey et al. (2011) have demonstrated that slackwater records are controlled by upstream geomorphic changes as much as temporal variability in storm frequency. Additionally, use of slackwater deposits in 1D hydraulic modelling studies is necessarily limited to bedrock gorges that are incapable of adjusting their cross sectional geometry (Thorndycraft et al., 2005).

2.5.2 Controls on terrace development

The causes of cyclical incision and aggradation are varied and the relative roles of different drivers still contested (Cooke and Reeves, 1976; Leopold, 1976; Schumm, 1977; Graf, 1983; Karlstrom and Karlstrom, 1987; Erkens et al., 2009). Refinements to our understanding of the causes of episodic "cutting and filling" are needed for land management, for reconstructing the impact of Late Quaternary climate change on river terrace development and for the prediction of future landscape response to climate variations (Hereford, 2002).

The most well-established **allogenic** drivers of terrace formation include climatic, tectonic and eustatic fluctuations (Leopold et al., 1964; Born and Ritter, 1970; Balling and Wells, 1990; Merritts et al., 1994; Rinaldo et al., 1995; Hattingh, 1996; Bridgland and Westaway, 2008; Harden et al., 2010). Recently, it was demonstrated that climate overrode local variations in tectonism across the Mediterranean in the production of terrace fills in Greece, Libya and Spain (Macklin et al., 2002). High rates of crustal uplift were shown to be important in creating accommodation space for a suite of terraces, but sensitivity of fluvial response to climate changes since 200 ka was attributed to the degree of hillslope-channel coupling (Macklin et al., 2002). Vegetation cover, partly driven by climate, is often a key control determining whether channels have incised, particularly if vegetation and rainfall are out of phase (Knox, 1972). However, vegetated slopes and floodplains can change the relationship between channel discharge and sediment load and trigger incision (Soria-Jáuregui et al., 2016). Overgrazing and land mismanagement are well-established drivers of arroyo (Bailey, 1935; Thornthwaite et al., 1942; Antevs, 1952) and gully incision (Brierley and Fryirs, 1999; Boardman et al., 2003; Rowntree et al., 2004).

Traditionally, individual terrace units were assumed to reflect direct climate change (Bryan, 1940; Euler et al., 1979), but terraces can also result from exceedance of geomorphic thresholds and complex response (Schumm, 1973; Erkens et al., 2009).

Schumm and Hadley (1957) recognised the importance of non-climatic drivers of channel entrenchment. For example, at Twentymile Creek, Wyoming, 1/3 of tributaries were graded to a terrace surface above the main channel (Hadley and Schumm, 1961). This disconnect was attributed to loss of competence due to infiltration of water through the channel bed causing an increase in sediment

concentration downstream, thereby blocking and inducing backfilling of the tributaries. Concepts of ‘geomorphic thresholds’ and ‘complex response’ that could explain the persistence of evidence of cyclic behaviour in geomorphic systems, provide an alternative to traditional equilibrium approaches in geomorphology (Schumm, 1973; 1977; Graf, 1983). Such concepts revolutionised interpretation of Quaternary terrace sequences and how cut and fill may be decoupled from direct climate forcing (Patton and Schumm, 1981).

In the Wolumla catchment, Australia, Brierley and Fryirs (1999) demonstrated that the position of the trunk stream channel within the valley floor is a key determinant of whether tributaries have incised and thus shifts in the positioning and functioning of geomorphic process zones can override controls of slope and catchment area (Brierley and Murn, 1997). Additionally, bedrock steps may protect tributaries from base level change on the trunk river (Jones et al., 2010). Larger bedrock barriers may retard incision on rivers, restricting terrace development. For example, Tooth et al. (2004) demonstrated the effects of Drakensberg group dolerite sills on the fluvial evolution of the Klip River, South Africa. Low energy meandering channels planed lithologically weaker sandstone upstream of doleritic intrusions creating frequent channel avulsions, meander cut-offs and wetlands. Incision of the sill resulted in abandonment of wetlands and floodplains.

With the advent of multi-faceted dating approaches (^{14}C, OSL), lack of accordance in timing of incision across “cut and fill” landscapes has often been used to evaluate the effects of complex response and resultant leads and lags to climate change (Patton and Schumm, 1981; Patton and Boisson, 1986; Prosser, 1991; Prosser and Winchester, 1996; Macklin et al., 2002; Erkens et al., 2009; Lyons et al., 2013). However, diachronous alluvial deposits can also reflect variable alluvial preservation potential (Lewin and Macklin, 2003; Macklin et al., 2012; Keen-Zebert et al., 2013). Efforts to link terrace development in South Africa to phases of climate change are often hampered by restricted dating precision and the large geographic distances between fluvial archives of interest and available palaeoclimatic archives (Botha et al., 1992; Partridge et al., 1997). The close relations between cycles of cut and fill across the Mediterranean and late Quaternary palaeoclimatic records for the North Atlantic highlight the usefulness of this approach, however (Macklin et al., 2002;

Benito et al., 2008; Woodward et al., 2008; Vis et al., 2010; Soria-Jáuregui et al., 2016).

With respect to the dynamics and controls on aggradation, Love (1977) proposed that the arroyo filling in Chaco Canyon, New Mexico was due to two feedbacks: 1) periods of decreased rainfall resulted in accretion of alluvial banks which stabilised and; 2) aggradation of active channel during such periods causes adjustment of flood geometry resulting in more frequent overbank flooding of the canyon floor and enhanced infilling due to loss of flow competence. This example demonstrates how an initial switch to drier conditions results in a series of positive feedbacks leading to the infilling of the arroyo. Aggradation may also be induced by terminal channel fans which act to block valley floors triggering backfilling which propagates upstream (Schumm and Hadley, 1957). Sediment 'slugs' may also plug valleys triggering backfilling (Nicholas et al., 1995). The key implication of these examples is that an initial climatic perturbation of sufficient magnitude to override local autogenic controls (Erkens et al., 2009) may trigger a fundamental mode shift in the geomorphic system, which then determines behaviour of the fluvial system for multiple millennia (Nicholas et al., 1995). This exemplifies the need to understand the antecedent conditions of landscape development to contextualise subsequent responses.

Working in the Paria basin, Southern Utah, Hereford (1986) found that up to 3 m of alluviation occurred after 1940. This was attributed to decreased warm-season rainfall frequency associated with a muted ENSO (Hereford and Webb, 1992). Balling and Wells (1990) also attributed infilling of arroyos in the Zuni River basin, New Mexico to be related to fewer intense summer storms and lower annual rainfall after 1940, corroborating the findings of Love (1977) and Hereford and Webb (1992). These case studies also illustrate that phases of aggradation can occur more rapidly than elsewhere (Bull, 1997) and thus enhance the prospects of reversing the erosion cycle within human lifespans.

Aggradation during glacial (cold, dry) periods is a feature of the upper River Ebro on the Iberian Peninsula. Reduced vegetation cover on slopes resulted in incision of slopes and deposition of coarse material on valley floors causing aggradation during MIS6, 5d, 4 and 2 (Soria-Jáuregui et al., 2016). Periglacial features such as stratified slope deposits are present elsewhere in the Catabrian Mountains evidencing mass-

wasting processes under cold, dry conditions that lead to aggradation (González-Amuchastegui and Serrano, 2013). Major phases of aggradation occurred during mid-late Pleistocene glacial periods across the Mediterranean even in non-glaciated catchments, attributed to more intense physical weathering and more extreme floods which flushed regolith to valley floors (Vita Finzi, 1969; Woodward et al., 2008; Macklin et al., 2012).

Bedrock type has also been found to be an important determinant of whether arroyos have incised or filled. Two examples are given. Firstly, McFadden and McAuliffe (1997) found that discontinuous arroyos prevailed on erodible Bidahochi formation mudrock, whereas continuous arroyos occurred on Cretaceous sandstones on the Colorado Plateau. The soft mudrock generated high sediment yields which overwhelmed stream power triggering aggradation and backfilling up to 20 km upstream over several thousand years (Bull, 1991; McFadden and McAuliffe, 1997). Secondly, Jones et al. (2010) working at Gibbler Gulch, W Colorado, identified slow headwater aggradation over a 6-7,000 year period followed by a single subsequent aggradation and incisional phase, contrasting with four major terraces exhibiting major cut and fill architecture downstream of a bedrock canyon. They proposed that free-draining slopes of sandstone in the headwaters diminished stream power and initiated aggradation.

In conclusion, the drivers of terrace ‘cut and fill’ are varied and complex. Alluvial records cannot always be conveniently linked to established chronologies of Late Quaternary climate change, but useful information regarding changes in intrinsic thresholds and complex response within the fluvial system may be obtained instead. Although radiometric dating approaches can assist in quantifying the leads and lags of river response to climate change where palaeoclimatic data is available (Schumm, 1973; Schumm and Parker, 1973; Patton and Schumm, 1981; Temme et al., 2008; Erkens et al., 2009; Lyons et al, 2013), the possible effects of autogenesis on terrace development need to be evaluated and, if possible quantified (Rinaldo et al., 1995) on a site by site basis to understand the mechanisms of fluvial system evolution.

2.5.3 Conceptual models of sediment fluxes

For over 30 years, geomorphologists have been examining the fate of eroded sediment and the pathways and timeframes of transport and storage within

catchments. Ferguson (1981) described river channels as “jerky conveyor belts” of sediment. The “sediment delivery problem” describes how only a small % of catchment-eroded sediment will reach the basin outlet (Walling, 1983) with sediments being stored over varying spatial and temporal scales (Meade, 1982; Trimble, 1983; Otto et al., 2009). Sediment **stores** are transient in nature, including channel features such as bars and benches, whereas **sinks** constitute more permanent storage zones such as slopes, floodplains and terraces (Fryirs and Brierley, 2001).

The spatial and temporal extent of coupling between different landscape and channel compartments has been a major focus of research. Nicholas et al, (1995) recognised large pulses of sediment known as waves or ‘slugs’ and the implications for valley-floor restructuring. Brierley and Fryirs (1998, 1999) and Fryirs and Brierley (2001) have considered the long-term dynamics of coupling in a disturbed catchment in New South Wales. Reid et al. (2007a) have argued that geomorphologists are still lacking understanding of how processes of sediment delivery and mechanisms of storage are coupled or decoupled in different types of catchment cascades.

In the past two decades the concept of ‘connectivity’ in geomorphic systems has been introduced at the scale of alluvial channels (Hooke, 2003) and the wider landscape (Brierley and Fryirs, 1999). ‘Connectivity’ can be defined as the water mediated transfer of sediment between different compartments of the catchment sediment cascade. This concept allows geomorphologists to explain how the “jerky conveyor belt” operates in any given system (Fryirs, 2013).

Fryirs et al. (2007) introduced a conceptual framework to differentiate the kinds of linkages and blockages in the sediment transport system. For example, **buffers** refer to landforms preventing sediment entering channels (i.e. floodplains/terraces – Schumm and Hadley, 1957; Brierley and Fryirs, 1999). **Barriers** disrupt longitudinal linkages of sediment through their effect on base level or bed profile of a channel. Barriers may be geological in nature (i.e. resistant rock strata impeding channel downcutting – Tooth et al., 2004), but also can include overwidened channels triggering loss of competence (Bull, 1997), aggrading channels restructuring flood geometry (Love, 1977) or emplacement of sediment ‘slugs’ which may plug channels and cause backfilling (Nicholas et al., 1995). The disruptive effects of in-channel

vegetation on connectivity have also been demonstrated (Sandercock et al., 2007; Sandercock and Hooke, 2011). **Blankets** act to disrupt vertical linkages by smothering sediment stores. An example could be a mature pedogenic calcrete mantling slopes or valley floors preventing incision, immobilising underlying sediment. The position and characteristics of such impediments determine "the effective catchment area": the proportion of a catchment that can contribute sediment to or transport along the channel system (Fryirs et al., 2007). By determining where such disruptions occur and timescales of reworking, this permits a more detailed understanding of the internal dynamics of sediment fluxes in catchments compared to traditional sediment budget approaches (Fryirs, 2013). In this respect, a model of (dis)connectivity can be developed, conceptualising sediment transfer systems in terms of a series of switches that turn on or off under varying magnitude-frequency conditions (Fryirs, 2013).

These frameworks signify a shift from conceptualising sediment transfer between different, discrete stores (Schumm, 1977) to a continuum-based approach (Fryirs et al., 2007; Fryirs, 2013), but have been criticised as incomplete, as they focus on disconnectivity and the movement of sediment by water. Bracken et al. (2015) argue for the incorporation of the effects of frequency-magnitude distributions on sediment detachment as well as the spatial and temporal feedbacks between that and transport dynamics. However, conceptualising geomorphic systems in terms of a series of switches is still presently useful for reconstructing, in concert with techniques that reveal the extent and characteristics of cut and fill, the long-term operation of different parts of catchments over centennial to millennial timescales and thus should feature in any analysis of Late Quaternary palaeo-fluvial evolution. Understanding and establishing the extent of connectivity within catchments helps to account for why morphologic adjustments take time to propagate and lag changes in allogenic controls (Erkens et al., 2009), but the explicit application of frameworks of connectivity in the context of river terrace development has yet to be investigated.

2.5.4 South Africa: Case studies of 'cut and fill'

The most recent and one of only a few Quaternary-based studies in the Sneeuberg was carried out in the headwaters of the Klein Seekoi River – relatively close (20 km north) to the study area in this thesis, but flowing north (Holmes et al., 2003). They

proposed that fills are of greater antiquity than previously stated in earlier studies (Bousman et al., 1988; Marker, 1995), later reinforced by a preliminary OSL age obtained from a colluvial fan (48.9 ± 5.4 ka – Boardman et al., 2005). However, the stratigraphic record lacked the scale and complexity of 'cut and fill' features recognised by Botha et al., (1994) in colluvial deposits in the more humid (SRZ dominated) KwaZulu-Natal (KZN herein) to the east.

In the Klein Seekoi headwaters, a single dominant phase of late Holocene incision post-dating the 19th century European occupation is evident in all valley fills documented by Neville (1996), Holmes et al. (2003) and Boardman (2014). Prior to this incision, chains of ponds formerly occupied valley floors, similar to those reported in Australia (Fryirs and Brierley, 1999). Processes of valley cut and fill differ from those reported in the KZN, with discontinuous channels and floodouts represented in the stratigraphic legacy attributed to local valley morphodynamics (Grenfell et al., 2009; 2012). In light of these more recent findings, the palaeoclimatological significance of the mid-Holocene 'organic phase' documented by Holmes et al. (2003) is questionable, as palaeosols and wetland formation have clearly been dominated by autogenic behaviour controlled by local valley morphology and feedbacks of sedimentation and channel avulsion. Grenfell et al, (2014) have subsequently proposed that these discontinuous gullies and floodouts reflect the highly episodic flows that occur in response to intense late summer storms. The 'step-like' valley long profile here implies that the Klein Seekoi valley is not incised to the same degree as the upper Sundays River. Ongoing cycles of local sedimentation and incision appear to be as much related to the disruptive effects of geological barriers crossing the valleys (Tooth et al., 2004; Fryirs et al., 2007), as local aridity means that perennial flow discharge cannot be sustained.

Botha et al. (1994), in contrast to Holmes et al. (2003), recognised at least four geomorphic cycles comprising gully cut and fill features and intervening palaeosols in the KwaZulu-Natal spanning the last 135,000 years, but fills between sites were found to be diachronous. This was attributed to differential local hillslope geomorphic threshold conditions. Intrinsic controls may include exceedance of a critical slope angle (Schumm, 1977), changing vegetation dynamics (Knox, 1972) and also intrinsic differences in the erodibility of soil as a function of local variations in lithology (Rienks et al., 2000).

Other work in KZN has more explicitly attempted to examine and link colluvial and pedogenic episodes to records of palaeoclimate, but these records lack the extent of cut and fill reported by Botha et al. (1994). Clarke et al. (2003) investigating colluvial sediments at the Voordrag site in the KZN noted a distinct absence of cut and fill features, but fills were found to be of similar age (90-100 ka) to other published dates (Botha et al., 1994; Wintle et al., 1995a). They proposed that accumulations of sandy colluvium required an initial humid period during which chemical weathering could produce large volumes of regolith and, subsequently, an arid phase where vegetation cover is minimal, where slopewash could transfer this colluvium to the valley floor. Crucially, their record indicates variable climate conditions during the LGM - predominantly arid, but relatively wet periods indicated by four interspersed palaeosols. This contrasts with Temme et al's (2008) landscape reconstruction on Masotcheni formation sediments, where they infer from IRSL ages that no deposition whatsoever during the LGM was attributed to continental aridity (Partridge et al., 1997), a proposition that is hard to reconcile with other palaeogeomorphic evidence of sedimentation during the LGM. On the Blood River, KZN, Lyons et al., (2013) reported a slow, continuous phase of colluvial sedimentation from prior to 22 up to 0.89 ka with no major cut and fill features. Unlike the Sneeuberg, gully incision here appears to have been the result of abrupt climate changes in the Late Holocene (Tyson et al., 2001; Lyons et al., 2013; Nicholson et al., 2013).

River terrace palaeosols have been investigated as a source of palaeoenvironmental data in South Africa. From the applied combination of OSL dating, diffuse reflectance spectroscopy and soil magnetic measurements, Lyons et al. (2014) demonstrated that climate was the primary soil-forming factor controlling pedogenesis in overbank sediments of the Modder River. Provided there are opportunities for radiometric dating to link geoproxy archives with palaeoclimatic records, this approach may be applied to other terrace palaeosols. However, confident ascription of palaeoclimate as the dominant control on the magnetic properties of soil may not always be straightforward because of other factors such as parent material, relief and time controlling pedogenesis (Jenny, 1941). Furthermore, terrace soils may be polygenetic, reflecting multiple phases of iron oxide transformation (Chadwick, 1995; Maher, 2011). In these cases, the conventionally used set of magnetic measurements (Dearing et al., 1996) are likely to represent the integrated effects of

iron oxidation/reduction associated with several, varied environmental conditions, as well as illuviated clay/silt infillings produced by bioturbation. Micromorphological investigation of palaeosols can provide an independent means of semi-quantitatively establishing extent of soil polygenesis and the conditions under which different pedogenic phases occurred (Wehmueller, 1993). This, coupled with mineral magnetic measurements, offers a unique way of evaluating the extent to which soil characteristics can be robustly tied to a definitive external forcing.

Magnetic signatures are also strongly affected by sediment particle size (Maher, 1988; Blake et al., 2006). A range of studies have shown a remarkably consistent relationship between particle size and magnetic grain size (Zheng et al., 1991; Oldfield and Yu, 1994; van der Post et al., 1997; Chiverrell et al., 2008; Oldfield et al., 2009). Combined particle size separation and magnetic measurements have made it possible to distinguish between components of bulk sediments that reflect different processes and sources. For instance, Hao et al. (2008b) note the concentration of ultrafine superparamagnetic (SP) grains and single domain (SD) grains in the clay (0-2 μm) grade within Chinese Loess. Working on Saharan and Sahelian dusts, Lyons et al. (2010) successfully discriminated between sediments inherited from different parent rocks, manifesting as coarse multi-domain magnetite in the coarse silt fraction (32-63 μm). In this respect, even before problems of soil polygenesis are considered, bulk samples measured for their magnetic susceptibility and remanence are likely to exhibit characteristics that are the sum of pedogenic, diagenetic and lithogenic controls (Foster et al., 1998; Pulley et al., 2016). The application of soil magnetic measurements in the upper Sundays River have been, until now, restricted to fingerprinting historical catchment sediment fluxes. Its role in reconstructing changing ancient sediment fluxes and modes of soil development in these valleys has yet to be explored.

2.6 Research gap and study aims and objectives

The studies cited in Section 2.5 highlight a need for better understanding of the controls, mechanisms and processes responsible for terrace genesis. Specifically, identification of thresholds of allogenic forcing needed to override autogenic controls within past environmental phases is important if geomorphologists are to draw on sedimentary archives for narratives of past-climate change. Even where allogenic

drivers can be confidently demonstrated, landscape response is equally dependent on current and antecedent dynamics of sediment supply generation, storage and extent of connectivity between landscape components. So far, current interpretive frameworks of connectivity have yet to be applied explicitly for the purpose of understanding dynamics terrace of development and nuancing ideas of complex response in catchments with barriers of different configuration and longevity. This coupled with a lack of geoproxies across South Africa continues to obstruct efforts to derive coherent palaeoenvironmental syntheses of late Quaternary landscape response. Despite the abundance of slope and alluvial deposits in tributaries of the upper Sundays River, South Africa, there remains a deficit in understanding whether these deposits reflect allogenically or autogenically driven geomorphic features, since studies in this area have exclusively focused upon contemporary land degradation.

Therefore, the overarching aim of this research is to develop an understanding of the characteristics, mechanisms and drivers of terrace formation in three low order tributaries of the upper Sundays River, South Africa. To address this aim, several objectives have been defined:

1) To identify and characterise the different valley fills present and establish their continuity

To achieve objective 1, extensive field reconnaissance of valleys, channels and their deposits were conducted. The major types of fill were defined in the field, initially distinguished on the basis of colour (i.e. rubified, brown, grey fill). Major types of barriers, buffers and blankets were similarly defined and their relations to different types of fill noted. We used differential GPS (dGPS herein) to perform high precision (± 2 cm) surveys of channel long and cross sections as well as terrace elevation. The limits of each major class of fill were physically traced in the field and georeferenced using the d-GPS approach, but supplemented by measurements using the GMS-2 GPS system, which affords ± 30 cm precision. The location of barriers, buffers and blankets was also georeferenced (see ch.3 for details).

From this data, in combination with digitised aerial photographs, georeferenced, high precision maps were derived showing the longitudinal and lateral limits of deposits in the headwater and trunk valleys. This information is then used to address the

following key questions: 1) Are unconfined valleys more prone to terminal channel and floodout processes? 2) Are the same stratigraphic sequences preserved in contrasting valley types? 3) Are a greater number of terrace preserved in the unconfined valleys due to enhanced preservation potential?

2) To reconstruct the physical linkages (connectivity) between different landscape components from the sedimentology, stratigraphy and pedology of deposits

To achieve objective 2, sedimentary sections were logged at over 35 outcrop locations. Choice of location was guided by initial mapping of extents of deposits and major lateral, vertical and longitudinal boundaries. Hand-collected samples were obtained from principal stratigraphic units and used to conduct grain-size analysis on the < 2 mm fraction as well as to measure geochemical and mineral magnetic properties to reconstruct changes in sediment provenance and semi-quantitatively ascribe intensity of pedogenesis. Block samples were collected for thin section development to reconstruct degree of soil polygenesis and compare against soil magnetic data.

3) To establish a chronology of terrace formation and incision and compare with other regional and continental dryland fluvial records.

To achieve objective 3, several outcrops (of those logged) were evaluated in terms of possible suitability for 1) Optical Dating of sedimentary quartz (OSL) and 2) AMS radiocarbon dating on plant macrofossils. Sampling was targeted in such a way that could allow the vertical and lateral and longitudinal age structure of fills to be evaluated. See chapter 3 for a full list of sampling and analytical procedures.

Chapter 3: Methodology

This chapter provides an overview of the field sites, field methods, sample collection and treatment procedures and techniques that have been used to realise project aims/objectives as outlined in section 2.6.

3.1 Field area

3.1.1 The Sundays River

Tributaries of the upper Sundays River consists of a dendritic drainage network comprising both continuous and discontinuous first order gullies as well as second to fourth order mixed bedrock/alluvial channels that have incised following the European incursion (Boardman, 2014). These are deeply incised into Drakensberg dolerite sills and dykes and also sandstone/siltstones of the Balfour Formation (see section 2.3). The relative expressions of each lithologic component vary between sub-catchments (see Fig. 2.2). Mesas separating sub-catchments are typically 'flat-topped' where they are capped by Karoo dolerite sills. Sills where they are exposed subaerially, form prominent ridges and deeply weathered upstanding tors on footslopes, but deep knickpoints have formed through many former ridges on footslopes and valley floors.

Check dams, weirs and reservoirs have been constructed in the last century across the catchment for irrigation and domestic uses, but have rapidly filled with sediment (Foster et al., 2009; Boardman et al., 2010). The erosion history of the Ganora catchment has been studied by Foster et al, (2007); Boardman et al, (2010) and Rowntree et al, (2012), but this was limited to the post-European settlement period.

3.1.2 Site selection and justification

Channel properties and terraces from two headwater tributaries and a 10 km segment of the trunk river were investigated for this study (Fig. 3.1). Satellite and areal imagery available through Google Earth and photographs of channels and terraces (Hooke, pers comm.) were used to perform initial aerial reconnaissance of tributaries, determine extent of fills and assess potential sampling locations. The approach was then to do fieldwork, collect and return samples to University of Liverpool for subsequent analyses.

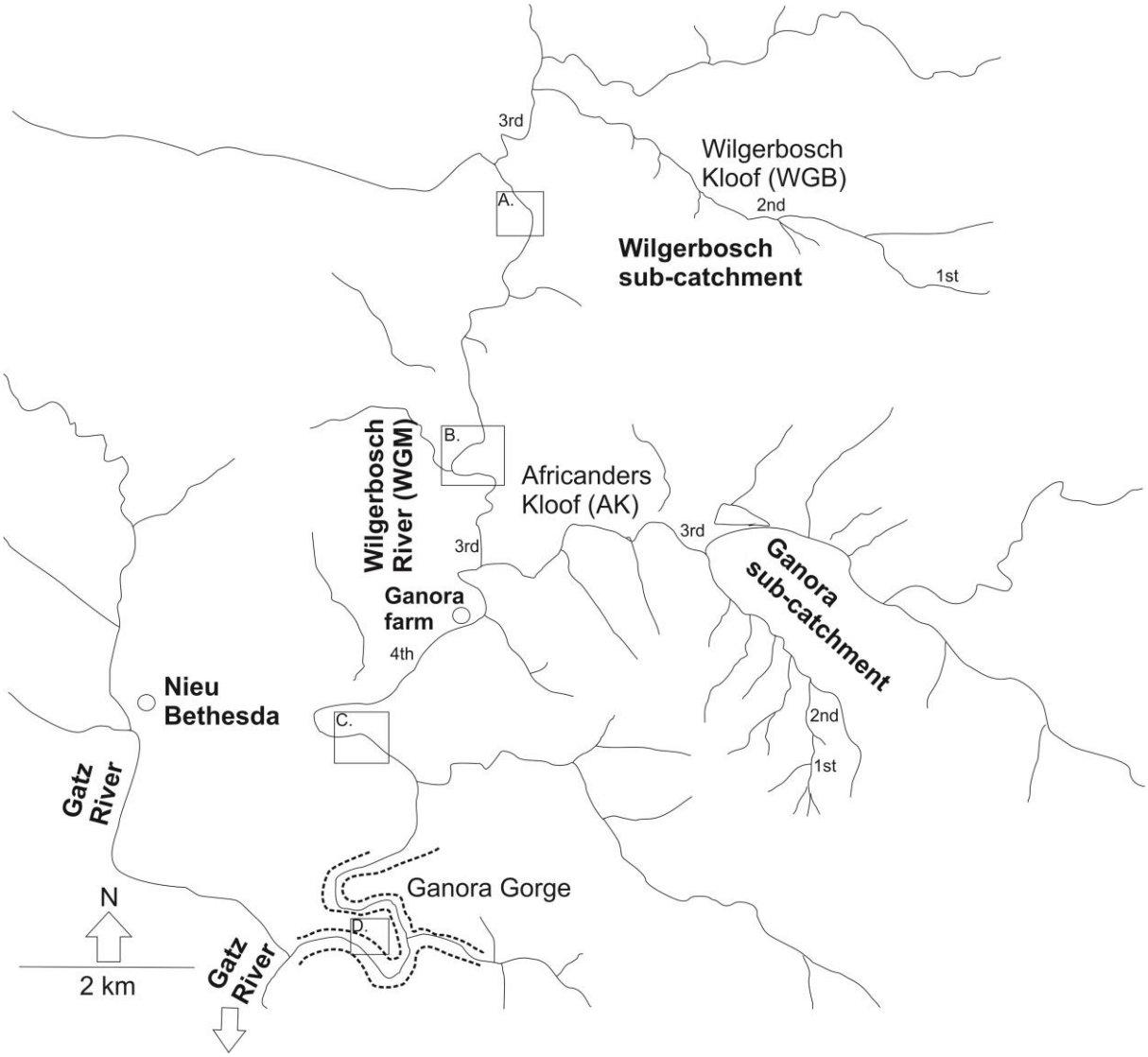

Figure 3.1 – map of study area showing headwater tributaries of the Gatz River (a tributary of the Sundays). Labelled boxes (A-D) represent study reaches of terrace analysis conducted on the trunk river, chosen on the basis of completeness of preservation.

3.2 Fieldwork

Two seasons of fieldwork were conducted in March–April 2012 and 2013 at indicated sites (Fig. 3.1). Several days of field reconnaissance were carried out to identify the nature and completeness of deposits in valleys of varying morphology. Valley morphology is strongly controlled by the occurrence, distribution and degree of incision of dolerite sills and dykes in this area (Holmes et al., 2003; Grenfell et al., 2014). Tributaries incised into dolerite are thus narrow and steep, whereas those incised into the softer Beaufort group rocks are typically wider and less steep. In season one, following reconnaissance activities, Africanders Kloof was therefore chosen on the basis of three key elements: 1) a narrow and steep tributary with

slopes of sandstone, but also intrusive dolerite sills and dykes at various stages of incision outcropping on slopes and in valleys, 2) the valley contained the most complex and well preserved series of distinct fills compared to other sites explored, some of which appeared more continuous than others; and 3) the feasibility of establishing the longitudinal and lateral variability in the kinds of fills due to the depth and extent of gullying.

Compared to Africanders, Wilgerbosch Kloof is subject to abrupt changes in degree of valley confinement. This tributary was selected for investigation in season 2, as an example of a relatively wide, low-gradient valley due to the dominance of mudstone over dolerite.

In addition, four sites along the Wilgerbosch River (Fig. 3.1) were selected for analysis on the basis of completeness of the deposits. This was carried out to test whether the same sequences in the headwater tributaries were present in the trunk river and reconstruct the extent of connectivity between them. Restricted access to the channel following a flood in between these outcrop locations prevented detailed logging and interrogation of sediments in the middle of the canyon, and as a result, the approximate extents of alluvium are noted from field observation and aerial photographic analysis.

3.2.1 Surveys: Strategy and rationale.

Surveys of channel long sections, terrace bank height and channel cross sections were carried out using a TOPCON HiPer II D-GPS system. This technique has the advantage of providing very high precision (± 2 cm) survey data. The major types of fill present in all valleys were identified and classified on the basis of approximate grain size, colour and nature of bedding. The longitudinal and lateral limits of these fills were physically traced where possible and digitally mapped using a TOPCON GMS-2 handheld GPS unit, which provided precision of ± 30 cm. Major stratigraphic junctions were mapped. The locations of **barriers** (geological: dolerite sills and dykes; geomorphic: laterally impinging fans), **blankets** (carbonate cements) and **buffers** (hillslope-channel distance) were also mapped. These features were mapped in order to establish whether or not 1) certain alluvial fills graded to (i.e. terminated at) bedrock steps or 2) whether lithostratigraphic units were mappable over discontinuities in valley base level. 15 cross sections at both Africanders and

Wilgerbosch Kloof were obtained at 1) major stratigraphic junctions and 2) up and downstream of major rock barriers as determined from initial field reconnaissance. Wetlands in the lower Africanders Kloof and along stretches of the Wilgerbosch River and gorge restricted access to the channels in some reaches and in addition, there were problems of signal acquisition, resulting in gaps in long profile survey data, reported in Chapter 4. Where possible, the GMS-2 unit was used to obtain terrace elevation (± 30 cm precision) in the Wilgerbosch River (Fig. 3.1).

3.2.2 Sediment logging

20 outcrops were selected at Africanders Kloof, 12 at Wilgerbosch Kloof and 7 along the Wilgerbosch trunk river (Fig. 3.2) to i) ensure representation of major differences in terrace stratigraphy as established through surveys of the lateral and longitudinal extents of deposits and ii) establish the (dis)continuity of lithostratigaphic units over mapped barriers. The comparatively large distance between outcrop locations in the WGM channel and gorge is due to the relatively discontinuous alluvial fills here and problems of access to channels. Logs were initially sketched in the field and the location of major stratigraphic discontinuities noted.

A schematic of a sedimentary log is provided in Figure 3.3. All outcrops were cleaned to facilitate clear identification and description of the facies. As far as possible, exposures were selected where it was possible to log every unit in detail. However, the deep nature of some of the gullies and channels (up to 6 m) meant that detailed logging of only 3-4 m in some cases above the modern channel bed could be achieved. In these cases, the sedimentologic and bedding characteristics were noted from visual observation only. The position of samples is indicated on the logs and referred to by height above the channel.

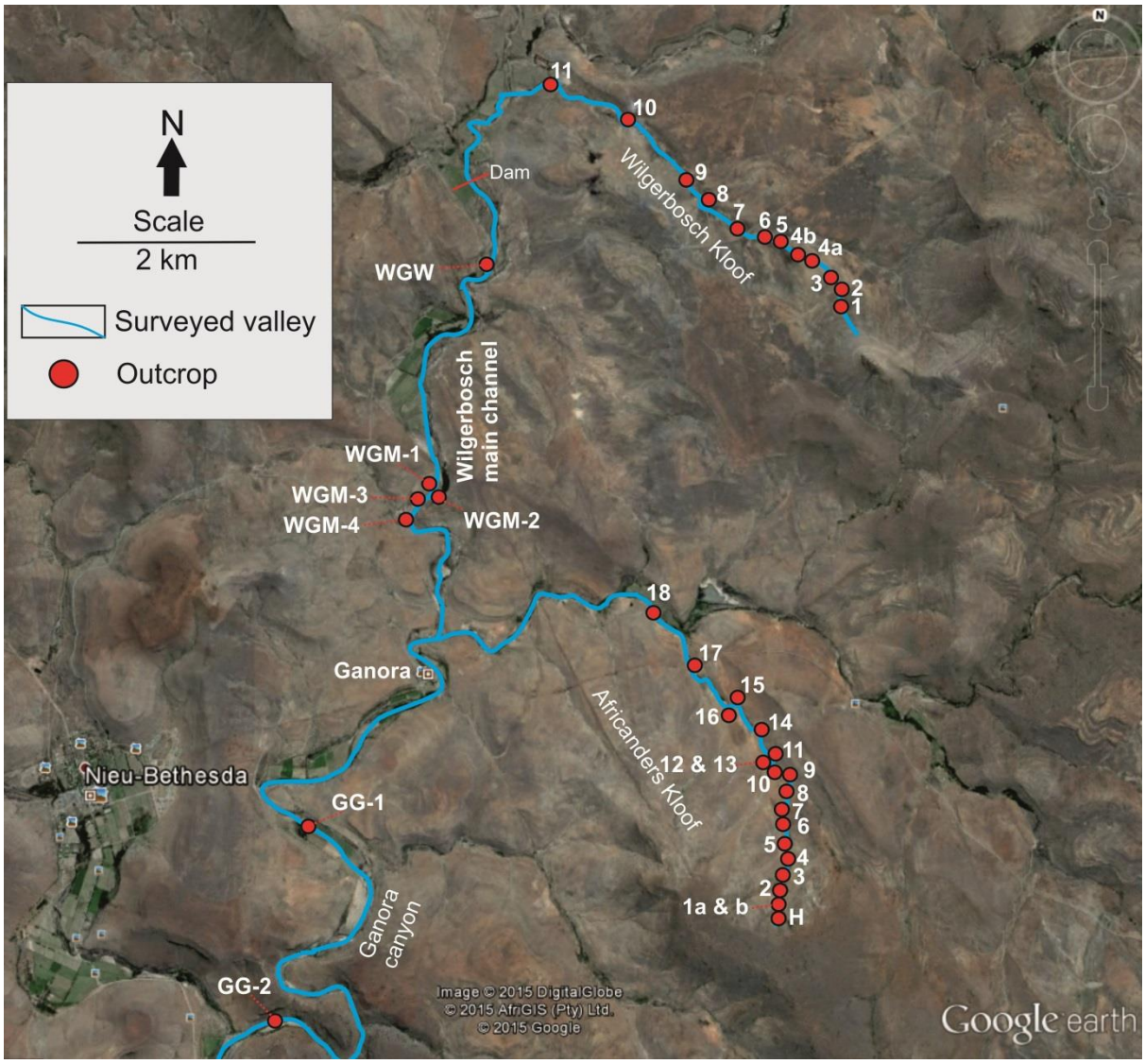

Figure 3.2 – locations of logged outcrops across the study area. Note log sites are reported in the text with following abbreviations: Africanders Kloof (AK), Wilgerbosch Kloof (WGB), Wilgerbosch Main Channel (WGM) and Ganora Gorge (GG).

Graphic sediment logs were constructed. A series of facies codes were developed to represent the range of facies characteristics recorded in the valley fills. The classification by Tucker (2011) for sedimentary structures and bedding characteristics was used (Fig. 3.4).

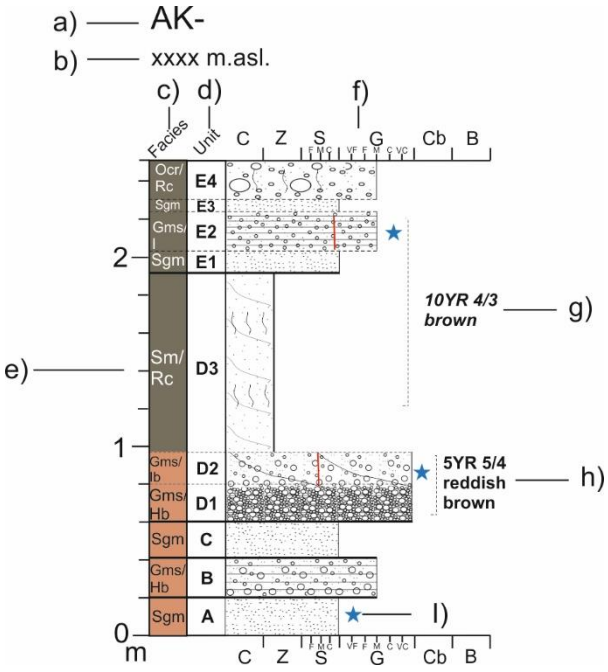

Figure 3.3 – template of graphic sedimentary log: a) Site code/exposure number, b) Elevation in metres above sea level (obtained using GMS-2), c) facies codes and Munsell colour, d) unit and subunit, e) height above channel in metres, f) grain size scale following Wentworth (1922), g) italicised Munsell colour measurement indicating reading obtained in field (note non-italicised convention representative of munsell colour obtained from air dried samples) h) sedimentary unit scaled according to dominant clast size, in this case gravel (Gms) with red line to indicate D_{50} of matrix (0-2 mm) determined from coulter granulometric analysis, i) sedimentary unit devoid of clasts > 2 mm and thus scaled according to sediment D_{50} as determined from coulter granulometric analysis (very coarse sand - Sgm).

Coulter laser granulometry was used to characterise the different mixtures of fine grained (clay–very coarse sand) sediments (see Table 3.1 and 3.2 for terminology). For sampled clast-poor units (i.e. dominated by very coarse sand or finer), sedimentary logs were scaled according to the D_{50} geometric grain size as determined from Coulter granulometric analysis (Blott and Pye, 2001). Where Coulter data is unavailable, logs are scaled based on in-field evaluation of texture. For units dominated by gravels or coarser material, logs are scaled according to dominant clast size following the Udden-Wentworth classification system - see Table 3.3. Where possible, this was determined by measuring the b-axis of 50 clasts on collected samples or in the field and where not possible, mean clast size was estimated from visual observation. For sampled clast-rich units, the D_{50} of the matrix is indicated on the logs as a red line corresponding to the Wentworth grain size scale on the X axis (Fig 3.3f). Munsell colours were recorded in the field, but later remeasured on air-dried samples in the lab.

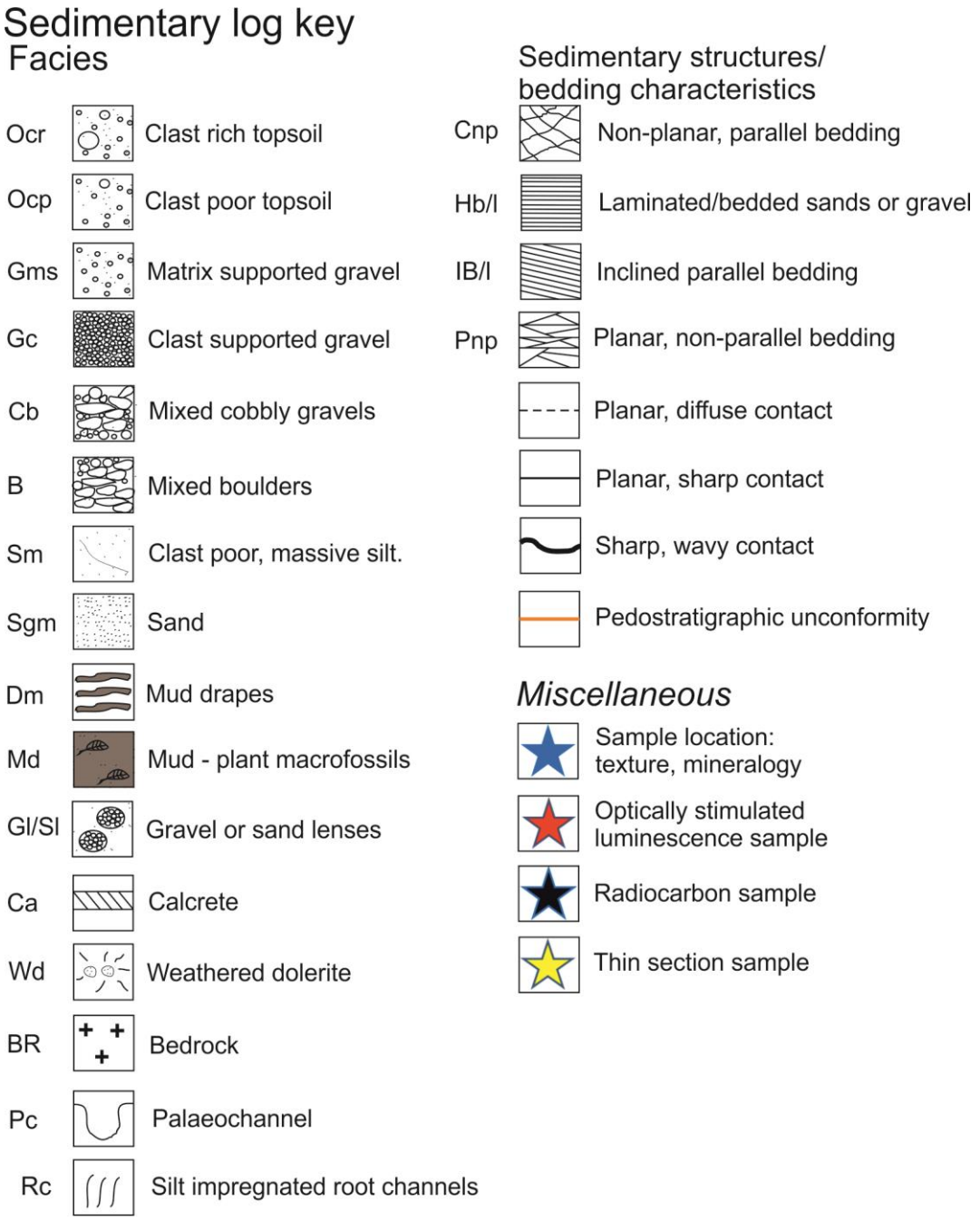

Figure 3.4 – sedimentary log key with symbols that characterise facies, bioturbation, occurrence of sedimentary structures and bedding characteristics. Facies codes were developed to accommodate the range of facies discovered at the field sites. Sedimentary structures/bedding characteristics were adapted from Tucker (2011). Under 'miscellaneous', samples collected for different tests are represented: Blue star – sediment collected to determine magnetic mineralogy, total elemental geochemistry, loss on ignition and coulter granulometry; Red star – samples collected for luminescence (OSL) dating; Black star – samples collected for radiocarbon (C14) dating; Yellow star – location of samples collected for thin section preparation and analysis.

Table 3.1 – grain size scale in microns and phi units used in the Gradistat program and in this study to describe fine sediments (0-2 mm). Adapted from Blott and Pye, (2001).

Microns (μm)	Phi (Φ)	Descriptive terminology: GRADISTAT program
1000-2000	-1	Very coarse sand.
500-1000	0	Coarse sand.
250-500	1	Medium sand.
125-250	2	Fine sand.
63-125	3	Very fine sand.
32-63	4	Very coarse silt.
16-32	5	Coarse silt.
8-16	6	Medium silt.
4-8	7	Fine silt.
2-4	8	Very fine silt.
0-2	9	Clay.

Table 3.2 – Particle size mixture terminology used throughout thesis to describe sediment mixtures for sediments under 2 mm. *Note silty clay refers to situations where measured clay is >25% and clayey silt for where clay <25%.

% sand	Descriptive mixture terminology
> 90	Sand
50 - 90	Sandy silt
10-50	Silty sand
< 10	*Silty clay / clayey silt

An alternative approach to the characterisation of sand and gravel components would have been to separate them and record their respective % weight. However, the development of soil aggregates at most locations meant that it would have been necessary to disperse and wet sieve all samples to accurately quantify these components. This was not executed due to time constraints.

Table 3.3 – grain size scale in millimetres and associated terminology to classify coarse sediments (larger than 2 mm). Modified from Wentworth (1922).

Millimetres (mm)	Descriptive terminology: Wentworth size class
> 256	Boulders
64-256	Cobble
32-64	Very coarse gravel.
16-32	Coarse gravel.
8-16	Medium gravel.
4-8	Fine gravel.
2-4	Very fine gravel.

Table 3.4 – Terminology of bed thickness. After Tucker (2011)

Scale	Bed thickness
> 1 m	Very thickly bedded.
0.3 – 1 m	Thickly bedded.
0.1 – 0.3 m	Medium bedded.
0.03 – 0.1 m	Thinly bedded.
10 mm – 0.03 m	Very thinly bedded.
3 – 10 mm	Thickly laminated
Less than 3 mm	Thinly laminated.

3.2.3 Sampling of valley fills

A total of 191 samples were collected from exposures at the side of the present channel using a trowel. Sampling was conducted in order to characterise major stratigraphic units and palaeosols with respect to their grain size, magnetic, geochemical and organic composition as well as final burial age (OSL). Three illustrative examples from contrasting outcrops are given in Fig. 3.5. Sampling density was dependent on 1) stratigraphic resolution, 2) major changes in soil colour and 3) accessibility of units. AK-3 is an example of an outcrop with low stratigraphic resolution, but changes in colour between units B1 and 2.

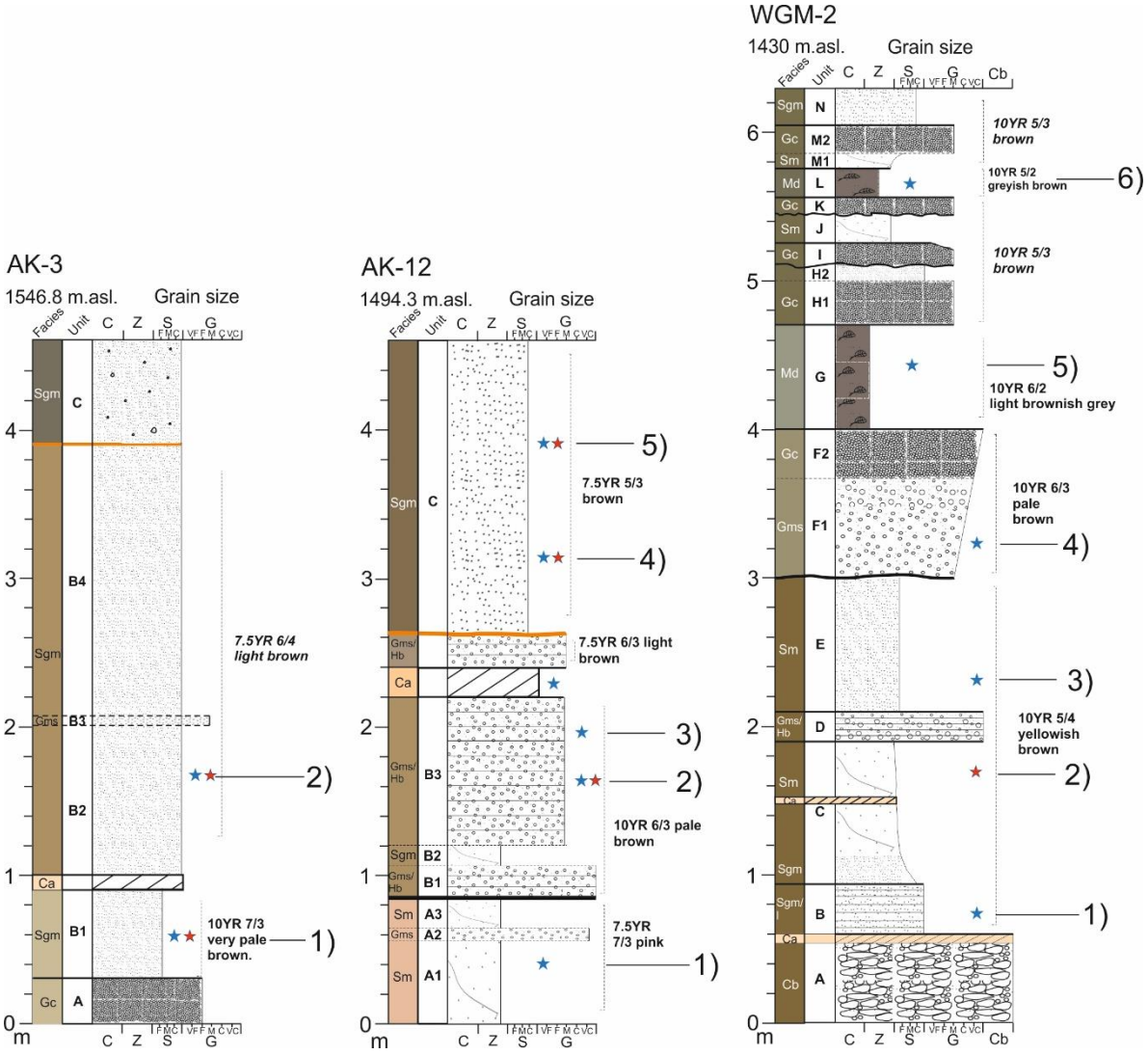

Figure 3.5 – approach to sampling the valley fills illustrated by three contrasting sedimentary logs. AK-3: Note sampling either side of a carbonate horizon. AK-12: Note sampling across major litho and pedostratigraphic (see orange line) boundaries. WGM-2: Note samples 1-3 were taken below a major stratigraphic unconformity; 4-6 from above this unconformity.

Therefore, two samples were collected from either side of the major carbonate horizon. In contrast, at AK-12, five samples were collected from horizons exhibiting different colour and texture, bracketing two possible unconformities (Fig. 3.5). At WGM-2, the same approach is repeated but two small intervening possible palaeosols (units G and L) were sampled to determine the conditions under which they formed (Fig. 3.5).

The overarching aim of employing OSL dating was to determine the age structure of valley fills across the region, supplemented by C14 dating where appropriate. Three key objectives were defined:

1) To establish vertical rates of aggradation for each terrace;

2) To establish a chronology of terrace 'cut and fill' in each tributary and evaluate spatial differences in burial age;

3) To reconstruct palaeo-connectivity between landscape compartments and the direction of valley filling.

A total of 15 outcrops were selected for OSL dating, representing the optimum trade-off between ensuring as complete a coverage of deposits as possible but avoiding sections potentially unsuited to sampling on the basis of 1) bioturbation in the form of root channels and/or animal burrows and 2) lack of homogeneous sandy units – hence the relatively few outcrops sampled from Wilgerbosch (Fig. 3.2 and Table 3.5). 32 samples were obtained from horizons where there was at least a 20 cm gap between bracketing units or bedrock (Table 3.5). Sampling was conducted at night time under red torch light as terrace fills were too heavily cemented to sample using conventional plastic tubes. Sections were cleaned thoroughly to ensure daylight-exposed surfaces were completely removed. Sediment was then shovelled into opaque plastic bags, sealed and double-bagged. Repeat samples were collected from the same horizon to determine dose rate and moisture content. All samples were stored at 4^{o}C prior to shipping to preserve moisture content.

A further 9 samples from palaeo-wetlands preserved in terrace fills were collected for C14 dating to augment the OSL samples (Table 3.6). Horizons were chosen that possessed high concentrations of fossilised plant stems and leaves.

5 samples were also collected at three locations for thin section development and subsequent micromorphological analysis. **1.** A distinct, continuous carbonate horizon was found at Africanders Kloof (AK-12 – Fig. 3.5 and 3.6A). Two blocks were carved out of the section and enclosed in bubble-wrap to avoid generating cracks and/or fissures. The purpose of collecting these samples was to determine: a) whether the carbonate deposit is dolomite or calcite; b) if it is caliche, was the mode of genesis related to biological processes controlled by the position of a former water-table (Wright et al., 1995; Candy, 2002) or rather, by abiotic processes relating to successive infiltration and evaporation (Machette, 1985); c) assess its possible suitability for U/Th dating via the isochron method (Candy et al., 2005); and d) to evaluate the extent to which the soils which are overprinted by the carbonate are

polygenetic (i.e. how many phases of pedogenesis have they undergone) and assess the usefulness of the magnetic properties for indicating discrete environmental phases.

Table 3.5 – samples collected for OSL dating, log number and height, sample texture and depositional setting.

Sample code	Outcrop/Height (cm)	Texture	Depositional setting
LV616	AK-1B 20 – 30	Gravelly sand	Alluvial fan channel.
LV617	AK-1B 95 – 100	Sandy silt	Alluvial fan channel.
LV509	AK-2 75 – 85	Gravelly sand	Alluvial fan channel.
LV510	AK-3 55 – 65	Sandy silt	Slopewash deposit.
LV621	AK-3 165 – 175	Sandy silt	Slopewash deposit.
LV511	AK-4 60 – 70	Gravelly sand	Slopewash deposit.
LV512	AK-5 155 – 165	Sandy silt	Palaeochannel.
LV513	AK-8 55 – 60	Gravelly sand	Slopewash deposit.
LV514	AK-8 180 – 185	Sandy silt	Alluvial fan.
LV515	AK-10 195 – 205	Sandy silt	Floodplain.
LV625	AK-10 290 – 295	Silty sand	Floodplain.
LV626	AK-10 415 – 425	Sandy silt	Floodplain.
LV516	AK-12 160 – 170	Gravelly sand	Palaeochannel.
LV517/628	AK-12 315 – 325	Sandy silt	Floodplain.
LV627	AK-12 395 – 405	Sandy silt	Floodplain.
LV629	AK-16 190 – 200	Sandy silt	Floodplain.
LV630	AK-16 315 – 325	Sandy silt	Floodplain.
LV631	AK-16 470 – 480	Sandy silt	Floodplain.
LV518	AK-17 190 – 200	Sandy silt	Floodplain.
LV607	WGB-4B 20 – 30	Gravelly sand	Channel bar.
LV608	WGB-4B 160 - 170	Sandy silt	Floodplain.
LV632	WGB-6 75 – 85	Silty sand	Floodplain.
LV633	WGB-6 130 – 140	Gravelly sand	Channel dunes.
LV609	WGM-1 30 – 40	Sandy silt	Wetland channel deposit.
LV610	WGM-1 165 – 175	Sandy silt	Floodplain.
LV611	WGM-1 295 – 305	Sandy silt	Floodplain.
LV612	WGM-2 175 – 180	Silty sand	Floodplain.
LV604	GG-1 110 – 115	Silty sand	Floodplain.
LV605	GG-1 285 – 295	Gravelly sand	Channel bar.
LV606	GG-1 375 – 385	Gravelly sand	Channel bar.

Table 3.6 – samples collected for C14 dating, log number and height, sample texture and depositional setting.

Sample code	Outcrop/height (cm)	Texture	Depositional setting
AK-4-1	AK-4: Inset grey fill 20 cm below modern channel	Silty sand.	Wetland at channel terminus upstream of rock step.
AK-4-2	AK-4: Inset grey fill 20 cm above modern channel	Sandy silt	Wetland at channel terminus upstream of rock step.
AK-18-1	AK-18 140-150	Silty sand.	Wetland.
AK-18-2	AK-18 150-160	Silty sand.	
AK-18-3	AK-18 185-195	Sandy silt	
WGW-1	WGW 110-120	Sandy silt	
WGM-1-1	WGM-1 265-275	Sandy silt	
WGM-1-2	WGM-1 315-325	Sandy silt	
WGM-2-1	WGM-2 455-465	Silty clay	
WGM-2-2	WGM-2 560-570	Silty sand	

2. Slopewash deposits at site WGB-8 (Fig. 3.2 and 3.6B). One block was obtained for thin section development in order to determine soil maturity. **3.** Palaeochannel sediments at site WGB-9. The relatively friable nature of the sediments permitted sampling using conventional Kubiena tins (9 x 6 cm): two samples were obtained (Fig. 3.2 and 3.6C) either side of a gradational bed contact. This was done for two reasons: 1) To compare extent of pedogenic overprinting between units and 2) compare with WGB-8 and merge with survey data of extents of deposits to infer relative age. This between-site comparison was particularly crucial, as bioturbation (root channels) rendered these sections unsuitable for OSL dating.

3.3 Data processing and outputs

The mapped spatial limits of main terrace deposits, channel long section, the type and extent of barriers, and both outcrop and cross section locations were plotted onto digitised aerial photographs (20 m resolution) using ArcMap 10.1. From this, scaled maps were derived and graphed using CorelDraw. Channel long sections, terrace bank level and cross sections were plotted in Microsoft Excel. Sedimentary logs were developed in CorelDraw. Channel long sections were subdivided into 1-1.1 km segments and presented as 3-4 separate figures.

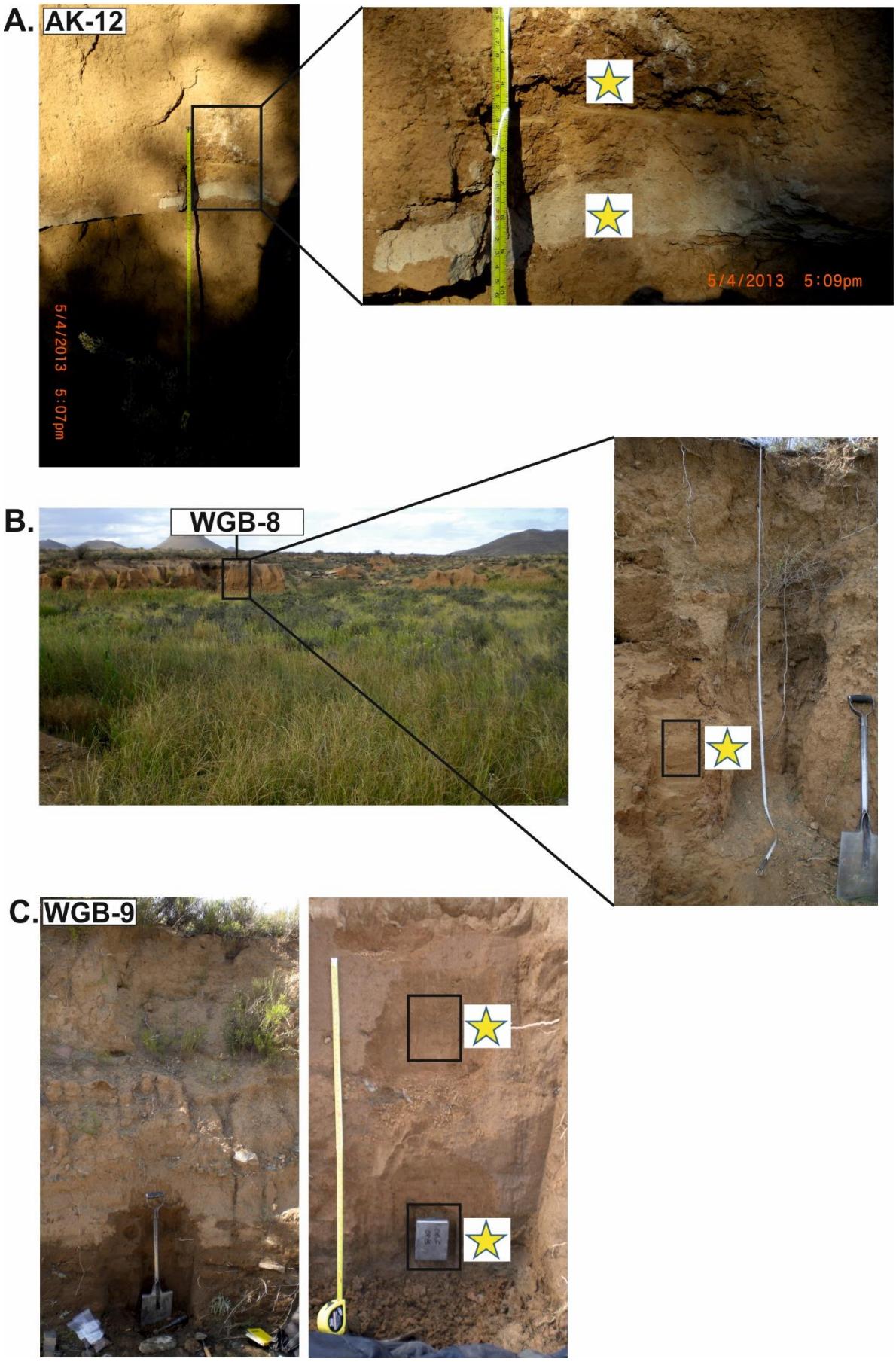

Figure 3.6 – photographs of locations sampled for micromorphological analysis: **A.** AK-12, **B.** WGB-8, **C.** WGB-9.

This was done in order to clearly graph the vertical and longitudinal limits of terrace units as portrayed in detail, in the respective sedimentary logs. Cross sections were edited to display the major lateral junctions between terrace fills.

3.4 Laboratory methods and analyses

3.4.1 Soil magnetism: preparative techniques

A standard set of soil magnetic measurements were conducted on all samples from terrace fills (Dearing, 1994). These were applied to 1) 'bulk' samples (0-63 μm) and 2) clay/very fine silt (0-4 μm) and very coarse silt (32-63 μm) extracts. The 'bulk' samples were measured in order to: 1) provide preliminary characterisations of the total ferrimagnetic concentration, grain size and mineralogy of all terrace fills; 2) determine, in concert with soil micromorphological and macro-pedological evidence, the primary conditions of soil formation in different valley contexts; 3) evaluate the usefulness of magnetic susceptibility and remanence parameters as a basis for reconstructing terrace continuity.

Of the 149 samples measured for their magnetic properties, 20 were selected for particle size separation. These were selected from sites proximal to different geological sources: dolerite, sandstone and mixed sources (Table 3.7). The objectives of this work included: 1) the identification of a particle size cut-off for pedogenic magnetic signatures in the different geological settings; 2) the identification of the grade in which any lithogenic signatures persist and whether discrimination between rock source is possible; 3) to determine the extent to which magnetic susceptibility and remanence in the 'bulk' samples is dominated by the respective pedogenic or lithogenic components, and thus whether the bulk measurements are better indicators of changing source and or intensity of pedogenesis; and 4) to compare pedogenic fine-grained signatures from both poorly and well drained settings to investigate extent of ferrimagnetic dissolution and diagenesis. The bulk samples were gently disaggregated using a pestle and mortar. A dry sieve shaker was used to isolate the <63 μm fraction for soil magnetic susceptibility and remanence measurements. Samples were packed into 10 cc plastic pots using cling film and weighed to two decimal places.

Table 3.7 – samples to which Atterberg particle separation technique was applied. *Coulter measurements obtained on 4-8 and 32-63 μm to test effectiveness of Atterberg separation.

Outcrop/height (cm)	Local geological source	Depositional setting
*AKH 60	Dolerite	Fan channel deposits.
*AK-1A 5-10	Dolerite	
*AK-1A 75-85	Dolerite	
*AK-1A 175-185	Dolerite	
*AK-2 25-35	Dolerite	
*AK-2 140-150	Dolerite	
*AK-2 215-225	Dolerite	
*AK-7 65-75	Dolerite	Debris-flow.
*AK-9 30-40	Dolerite	In situ soil.
*AK-9 390-400	Sandstone	Wetland / gleyed soil.
*AK-12 40-50	Dolerite	Slopewash deposits
*AK-12 160-170	Dolerite	Palaeochannel.
WGBLP91	Sandstone	Overland flow deposit.
WGBLP92	Sandstone	Alluvian fan.
WGBLP96	Sandstone	Alluvian fan.
WGB-1 80-85	Sandstone	Alluvian fan.
WGB-8 90-100	Mixed	Slopewash deposits
WGM-4 270-280	Mixed	Channel deposits.
GG slope	Mixed	Colluvial deposit.

Clay and silt fractions from 20 samples were obtained by the Atterberg method. 20 g of sample was added to two beakers and soaked in a mixture of calgon (25 ml) and double-distilled water (175 ml). For very coarse samples, 3 beakers were used (60 g) to maximise the chance for large enough extracts from each particle size window. Beakers were shaken continuously for 24 hours to disperse the silts and clays. Dispersed material was then washed through a 63 μm brass sieve and poured into Atterberg cylinders (up to 3 per sample).

Cylinders were placed in a heated, concrete water tank. For the first batch of samples, temperature was set to 20^{o}C (just above room temperature). Tubes were left for ½ hour to ensure equilibration between a) temperature of water in tank and b) temperature of water in tubes (as this affects water density). Settling times for the size fractions 0-2, 2-4, 4-8, 8-16 and 16-32 μm were determined from tables, the values of which accord to temperature and consequent water density (Table 3.8). The second batch of samples was immersed at 21^{o}C, with adjusted settling times as shown (Table 3.9).

Table 3.8 - Settling times obtained for fluid with a specific gravity of 2.55 at 20°C. Three siphons, the first two at 19 cm and the third at 20 cm tube depth were obtained.

Grain size (μm)	Settling time (hr: min: sec)
0-2	17: 20: 00
2-4	4: 20: 00
4-8	1: 05: 00
8-16	0: 16: 14
16-32	0: 04: 02

Table 3.9 - Settling times obtained for fluid with a specific gravity of 2.55 at 21°C. Three siphons, the first two at 19 cm and the third at 20 cm tube depth were obtained.

Grain size (μm)	Settling time (hr: min: sec)
0-4	4: 13: 46
4-8	1: 03: 26
8-16	0: 15: 50
16-32	0: 03: 56

Siphoned extracts were collected in clearly labelled beakers, centrifuged, rinsed and freeze-dried as oven-heating above 40°C has been shown to change the magnetic properties of sediment (Thompson and Oldfield, 1986). Samples were packed into 10 cc plastic pots and weighed.

The effectiveness of the siphoning procedure on resultant grain-size extracts was evaluated for the Africanders Kloof samples (Table 3.7) using the Coulter LS 200. Coulter grain-size data were obtained on the 4-8 and 32-63 μm fractions from the AK subset. The 0-4 μm fraction is not reported, as the Coulter underestimates clay.

3.4.2 Magnetic measurements

Both sample batches were subject to a series of routine magnetic measurements at the University of Liverpool Magnetics lab (Walden et al., 1999) including: 1) initial low frequency (0.47 kHz) volume susceptibility (k) measurements; 2) low frequency (0.47 kHz) magnetic susceptibility (X_{LF}); 3) high frequency (4.7 kHz) magnetic susceptibility; 4) susceptibility of anhysteretic remanent magnetisation (X_{ARM}); 5) isothermal remanent magnetisation (IRM_{1T}); and 6) isothermal remanence magnetisation at incremented reverse fields of -20, -40, -100 and -300mT.

Samples were initially measured for magnetic susceptibility (k) using the KLY-3 Kappabridge system. This has the advantage of allowing i) precise calibration using

a known reference standard and ii) diamagnetic effects from plastic pots and cling film are removed from the resulting volume susceptibility values.

To assess bulk magnetic mineral concentration and calculate frequency-dependent susceptibility X_{FD} (Dearing et al., 1996), the Bartington MS2B sensor was used to determine both low (0.46 KHz) and high (4.6 KHz) frequency susceptibility. The loss of susceptibility between these two frequencies reflects changing concentrations of grains at the border (0.025 μm diameter grains) between single domain (SD) and superparamagnetic (SP) grains commonly associated with weathering (Maher, 1988).

Susceptibility readings were compared with those obtained from the Kappabridge system to check for repeatability. The sensor was calibrated using a reference standard that produces κ values of 3152 10^{-10} m^3. Drift was corrected for using: κ (corrected) = sample κ - {(first air κ + second air κ)/2}.

Strongly magnetic samples (κ > 50) were measured on the low sensitivity '1.0' scale and repeated three times unless readings varied by > 1 S.I. unit, in which case a further three measurements were obtained. Weakly magnetic samples (κ < 50) were measured on the high sensitivity 0.1 scale. Strong and weak samples were measured in two groups and the sensor re-calibrated in between. Samples exhibiting κ 0-30 were measured 10 times to obtain a better average than would be obtained if the standard three repeats were conducted (Dearing, 1999). **Volume susceptibility** (κ) readings were divided by sample density (ρ) to give **mass specific susceptibility** (χ). Mass specific readings were then divided by 100 to normalise the power to 10^{-8} m^3 kg^{-1}. For example, for a hypothetical κ_{LF} reading of 25 (10^{-10} m^3) and sample mass of 3.5 g: 25 / (3.5/1000) / 100 = 71.42 10^{-8} m^3 kg^{-1}. For the raw IRM_{1T} readings, units are 10^{-8} Am^2. Thus, the only exception to the previous formula when applied to the IRM_{1T} is that mass specific values are divided by 1000 instead of 100 to yield 10^{-5} Am^2 kg^{-1}.

Anhysteretic remanence magnetisation (ARM) was employed using a DTECH alternating field demagnetiser, with a peak alternating field of 100 mT in conjunction with a steady field of 0.1 mT superimposed. Measurements were then obtained using a Molspin fluxgate spinner magnetometer. This measurement is sensitive to changing concentrations of SD grains (Thompson and Oldfield, 1986, Table 3.10a).

The IRM_{1T} and associated backfields were imparted using a pulse magnetiser, with readings then obtained from the Molspin fluxgate magnetometer. Samples were measured in batches of 10-13, as samples exhibiting low viscosity-magnetism are susceptible to remanence losses over extended time intervals. The spinner magnetometer was calibrated using a reference standard at the beginning and end of each batch of measurements. The IRM_{1T} provides an indication of the total concentration of remanence carrying ferrimagnetcs (Evans and Heller, 2003, Table 3.10a). A maximum field of 1 T was selected because magnetite saturates at or below -500 mT and any further growth in IRM above can relate to the presence of haematite, which is a common iron oxide found in semi-arid soils (Oldfield, 1991) and also goethite under moister conditions (Balsam et al., 2004).

Two low back-fields (-20, -40 mT) were selected as these have been found to exclude contributions from magnetically 'hard' fine grained haematite and thus approximate remanence carried in ferrigmagnetic minerals (i.e. magnetite concentration) independently from magnetic grain size (Oldfield, 1991; Wang et al., 2009). The two high reverse field measurements (-100 mT and -300 mT) were carried out to calculate 'S' values (S_{-100}% and S_{-300}%), which evaluate changing proportions of soft (S_{-100}%) and hard magnetic minerals (S_{-300}%, Table 3.9b).

To estimate changing total concentrations of all *hard*, antiferromagnetic minerals (haematite/goethite), the hard isothermal remanence (HIRM) parameter ((IRM_{1T} + -IRM_{300mT}) / mass)) was calculated (Table 3.10a). To estimate changing concentrations of all *soft* magnetic minerals (magnetite, maghemite), the 'Soft_IRM' parameter was calculated (Lyons et al., 2010, Table 3.10a). Several further parameters were calculated from magnetic measurements to characterise ferrigmagnetic granulometry (Table 3.10c). X_{FD} is given as a % as this provides a more conservative estimate of the concentration of SP/SSD grains where total susceptibility is high (Table 3.10c).

The X_{ARM}/X_{LF} and X_{ARM}/X_{FD} ratios are used to investigate relative contributions of SP and SD grains to the bulk signal (Evans and Heller, 2003, Table 3.10c). These ratios can be useful for discriminating between lithogenic and pedogenic magnetic signatures provided assemblages are exclusively dominated by grains ranging from SP–SD size (0.025 – 0.069 μm, Oldfield and Crowther, 2007).

However, where multi-domain grains (> 0.07 μm) predominate, the X_{ARM}/X_{LF} ratio becomes unsuitable due to the grain size dependency of X_{LF} which reduces above the SD/PSD limit (Evans and Heller, 2003). As the X_{ARM} is the numerator, smaller values of X_{LF} can produce large quotient values, misleadingly indicating an SD pedogenic signature, where MD grains in fact predominate. Following the recommendation of Oldfield (1994), the X_{ARM}/IRM_{1T} ratio was calculated (Table 3.10c). Only where values > 0.6 x (10^{-3} mA^{-1}) and $X_{FD}\%$ > 1 are assemblages dominated by 0.025–0.069 μm grains and thus suitable for analysis via the bilogarithmic plot of X_{ARM}/X_{LF} and X_{ARM}/X_{FD} (Maher, 1988; Oldfield, 1994; Oldfield and Crowther, 2007).

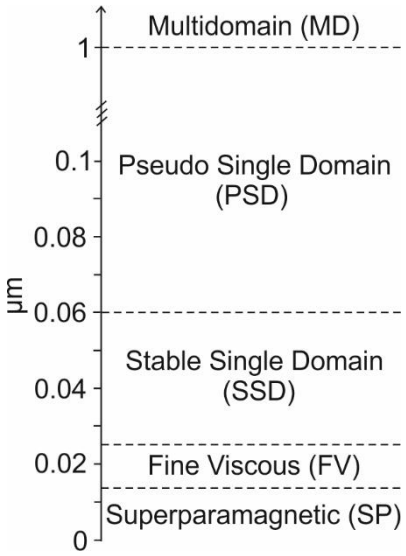

Figure 3.7 – magnetic grain size and associated magnetic domains (according to Maher, 1986; Oldfield, 1994).

3.4.3 X-ray fluorescence measurements

XRF measurements using the Bruker S2 Ranger system were carried out on all samples for four major purposes: 1) to calculate chemical weathering indices to better constrain the relative age of the terrace fills; 2) to compare these indices with OSL chronometric data; 3) to quantify secondary carbonate and salt accretions; and 4) to measure bromine (ppm) content.

Table 3.10a – concentration dependent magnetic parameters referred to in the text, their units, definition and associated interpretation.

Magnetic parameters: *Concentration*	Units (SI)	Definition	Interpretation
X_{LF} / X_{HF}	$10^{-8}\ m^3\ kg^{-1}$	Mass specific susceptibility at low (0.46 kHz) and high (4.6 kHz) frequency. X = *M* / *ρ H* (*ρ* = density; *M* = magnetic moment; *H* = applied field).	Initial low and high field magnetic susceptibility. Its value reflects the composite effects of ferrimagnetic, anti-ferromagnetic, diamagnetic and paramagnetic minerals within the sample.
X_{fd}	$10^{-8}\ m^3\ kg^{-1}$	Frequency dependent susceptibility.	Sensitive to changing concentrations of grains close to the border between Single Domain (SD, 25- 100 nm) and superparamagnetic (< 25 nm) grains (Maher, 1988).
X_{arm}	$10^{-8}\ m^3\ kg^{-1}$	Mass specific anhysteretic remanence magnetisation.	ARM is roughly proportional to the concentration of ferrimagnetic grains (magnetite, maghemite) in the stable single domain grain size range (0.02-0.4 μm).
SIRM or IRM_{1T}	$10^{-5}\ m^3\ kg^{-1}$	Mass specific saturation isothermal remanence magnetisation.	SIRM is the highest amount of magnetic remanence that can be produced in a sample by applying a large magnetic field. It is related to concentrations of all remanence-carrying minerals in a sample but also dependent on grain size. Some anti-ferromagnetic minerals (e.g. goethite) may not be saturated at this field hence the specific use of IRM_{1T} to denote that full saturation may not have occurred.
Soft_IRM_{-100mT}	$10^{-5}\ Am^2\ kg^{-1}$	The magnetic remanence (unreversed) that remains after demagnetization in a reverse field of -100 mT, calculated as (IRM_{1T} + -300mT / 2) / mass (g).	Rough proxy for changing concentration of the ferrimagnetic minerals: magnetite and maghemite.
$HIRM_{-300mT}$	$10^{-5}\ Am^2\ kg^{-1}$	The magnetic remanence (unreversed) that remains after demagnetization in a high reverse field of -300mT, calculated as (IRM_{1T} + -300mT / 2) / mass (g).	Rough proxy for changing concentration of antiferromagnetic minerals, predominantly, though not exclusively haematite.

Table 3.10b – magnetic parameters which characterize magnetic mineralogy referred to in the text, their units, definition and associated interpretation.

Magnetic parameters: *Mineralogy*	Units (SI)	Definition	Interpretation
S_{100}%	%	% remanence unreversed after exposure to weak -100mT backfield. Obtained by (-100mT / SIRM) / mass. Then: 100 – (-100mT%).	Indicators of relative proportions of ferrimagnetic (magnetite/maghemite) and anti-ferromagnetic minerals (haematite/goethite).
S_{300}%	%	% remanence unreversed after exposure to weak -100mT backfield. Obtained by (-300mT / SIRM) / mass. Then: 100 – (-300mT%).	

Table 3.10c – magnetic parameters which characterize magnetic grain size referred to in the text, their units, definition and associated interpretation.

Magnetic parameters: *Granulometry*	Units (SI)	Definition	Interpretation
X_{fd}	%	Percentage frequency dependent susceptibility: (X_{LF} - X_{HF} / X_{LF}) x 100.	Reflects concentration of grains at the stable single domain (SSD) and superparamagnetic (SP) boundary. % values provide more conservative estimate of fine-viscous SP grains than mass specific, especially where X_{LF} is very high.
X_{arm}/Xlf	-	Quotient.	Grain size indicator reflecting relative contributions of SP and SD grains to bulk magnetic signal, but interpretation depends on magnetic grain size distribution (see text for full explanation).
X_{arm}/X_{fd}	-	Quotient.	Grain size indicator. This quotient is positive correlated with increasing grain size up to the SSD limit.
X_{arm}/IRM_{1T}	10^{-3} mA^{-1}	Quotient.	Reflects increasing contributions of remanence carrying SD grains.

Various element ratios have been proposed in the literature to quantify degree of chemical weathering (Table 3.11). The concept of weathering indices is predicated on the selective removal of soluble and mobile elements compared to the relative enrichment of immobile and non-soluble elements (Buggle et al., 2011). The XRF provides a rapid, non-destructive means of obtaining geochemical data from which to derive elemental ratios such as Al, Na, Ca and K. Weathering indices which employ Ca are likely to be inappropriate for the terrace fills of this study, because although Karoo dolerite contains abundant calcium plagioclase (Neumann et al., 2011), Ca leached from the host rock is likely to accumulate in soils as secondary carbonate (Botha et al., 1994).

For this reason, the 'chemical proxy of alteration' (CPA herein) by Buggle et al., (2011) is employed in our study as Na is used as the soluble element. A disadvantage of using the XRF in this case is that Na measurement is 'noisy' (Boyle, pers. comm.).

Table 3.11 – weathering indices quoted as molecular proportions. [a] Chemical proxy of alteration (Buggle et al., 2011); [b] Chemical index of alteration (Nesbitt and Young, 1982); [c] Index B (Kronberg and Nesbitt, 1981); [d] Chemical index of weathering (Harnois, 1988); [e] Plagioclase index of alteration (Fedo et al., 1995). Note CaO* refers to silicatic Ca. After Buggle et al., (2011).

$CPA^{a} = [Al_2O_3 / (Al_2O_3 + Na_2O)] \times 100$
$CIA^{b} = [Al_2O_3 / (Al_2O_3 + Na_2O + CaO^* + K_2O)] \times 100$
$Index\ B^{C} = (CaO^*\ \ Na_2O + K_2O) / Al_2O_3 + CaO^* + Na_2O + K_2O)$
$CIW^{d} = [Al_2O_3 / (Al_2O_3 + Na_2O + CaO^*)] \times 100$
$PIA^{e} = [Al_2O_3 - K_2O) / (Al_2O_3 + CaO^* + Na_2O - K_2O)] \times 100$

The halogen 'bromine' is measured by the XRF and has been investigated as another possible proxy for organic content. Bromine mainly exists in the inorganic form of 'bromide' and is found in rainfall, cloud water, stream and groundwater (Neal et al., 2007). Previous research has shown that bromide is correlated strongly with organic matter in soils and especially enriched in peat (Hughes et al., 1998; Biester et al., 2004). Bromine in rainwater can sorb onto humus contained within soil profiles and be involved in biogeochemical cycling (Korom, 2000). High soil moisture content associated with flooding has been shown to be the most important factor governing bromine dissolution and its release from soil systems may be highly seasonal (Hughes et al., 1998). Recently, Abderrahim et al., (2011) demonstrated the

effectiveness of bromine quantification (ppm) via X-ray fluorescence analysis on a series of vadose-zone soil samples collected in Morocco. Bromine in content is reported alongside LOI% data in Chapters 5 - 7.

3.4.4 Laser Granulometry

To establish the 0–2 mm sedigraph composition, samples collected from major stratigraphic horizons were measured using an LS200 Beckman Coulter Granulometer. The following preparative steps were taken:

1) All samples were treated with H_2O_2 to remove plant/organic material. Larger detritus (i.e. ostracod shells) were removed manually. 2) Samples were then dispersed using Calgon prior to measurement. 3) For clay/silt rich samples, the in-built 'sonicate' function on the LS 200 was used to further aid dispersion, though laser diffraction is known to underestimate clay content (Fedotov et al., 2007). Results were analysed and presented using the GRADISTAT program (Version 8 – Blott, 2010).

3.4.5 Loss on Ignition (LOI)

To characterise the organic content of the valley fills, LOI measurements were conducted. Excess moisture was removed by heating samples to 105^{o}C for 12 hours. As most of the sediments contained carbonates, samples were heated at 450^{o}C for 4 hours and weighed before and after. LOI values are reported in Chapters 5-7 as a %.

3.4.6 Thin section development

Samples collected for thin section development were air dried and prepared for thin section development by the University of Stirling. Thin sections were analysed using a cross-polarised microscope to provide qualitative descriptions of the 'skeleton' (features such as grain size, sorting, grain-angularity and bed contacts) and groundmass (calcite hyper and hypocoatings, iron cements, rhizocretions, voids and channels, inset laminated clay coatings and geopetal fills).

For the AK-12 carbonate horizon, several additional tests to assess its possible suitability for U/Th dating were conducted. These included: 1) XRF geochemical analysis to establish whether the carbonate was dolomite or calcite; 2)

cathodoluminescence microscopy to evaluate degree and extent of diagenesis (neo-sparite formation); 3) ICP-MS measurements of carbonate dissolved in 2.5% nitric acid to establish presence and concentration of uranium (Rasbury et al., 2000; Kelly et al., 2003); and 4) determination of total carbonate content via the acid-soluble weight loss method (Chaney et al., 1982).

3.4.7 OSL measurements

The samples were prepared for D_b (burial dose) determination following the procedure outlined in Fig. 3.8. Because many samples possessed a high proportion of silt and clay particles, fines were removed by 1) manual disaggregation of aggregates; 2) dispersion using ammonium hydroxide and; 3) wet sieving. Carbonates were removed using 10% HCl and again using 33%. Organics were removed using 10 and 30% H_2O_2. A steady reaction with H_2O_2 was produced for most samples and may reflect the breakdown of iron oxides. Samples were wet sieved again to remove any fine particles to ensure the heavy liquid was not contaminated. Samples were then separated on the basis of density ($2.62 < \rho < 2.76$ s.g.) to concentrate quartz. All samples possessed high 'feldspar' (sensu lato) content reflected in large amount of grains retained during density separation.

Samples strongly reacted to the HF etch, yielding very low quartz amounts. This necessitated utilising abnormally large grain size windows – typically 90-200 μm, but occasionally 90-300 μm (Appendix A). This is not ideal, since the broader the window, the more inclusion there is of grains that have received differential environmental radiation dose rates and transport histories. Fine grains have also been found to be more prone to effects of poor bleaching in fluvial systems (Truelsen and Wallinga, 2003) and are also susceptible to illuviation. 1 mm aliquots were thus measured in order to keep the number of grains per disc to the minimum.

Even with these large grain size windows, quartz amounts were typically negligible (several grams) and the main reason for abandoning samples. All measurements were carried out using Risø DA-15 B/C reader equipped with 21 blue LEDs (470Δ30 nm) for stimulation providing ~30mW cm^{-2}. OSL was detected through a Hoya U340 filter (transmitting 320-390 nm). Initial measurements of equivalent dose on 3-5 aliquots per sample were carried out to check the behaviour of the quartz, assess

typical ranges of D_e values and assess suitability of the SAR protocol (Murray and Wintle, 2000) with a view to possible re-sampling during next season of fieldwork. Samples typically failed to recycle the low regenerative dose point evidencing recuperation (LV506, 507, 511-3; Appendix A). Other samples exhibited saturated quartz as the regenerative dose points used failed to attain the magnitude of the natural OSL signal (LV508, 510, 511-3; Appendix A).

Table 3.12 – aliquot acceptance criteria, explanation and associated publication. *Applies to SAR dose recovery test only.

Aliquot acceptance criteria	**Explanation**	**Reference**
i. Recycling of low dose ± 10%	Used as a means of checking whether the test dose response has adequately corrected for sensitivity changes to quartz electron trapping centres. Values should approximate unity.	Murray and Wintle (2000)
ii. Infrared depletion ratio ± 10%	Electrons stored within feldspar minerals have been found to be sensitive to stimulation by infrared light. IR depletion ratio is therefore a test of purity.	Duller (2003)
iii. $D_e < 2b$	Parameter *b* describes the slope of the regenerative dose curve. If equivalent dose value (D_e) is greater than 2x*b*, this indicates the sample is close to saturation (i.e. the luminescence traps are full).	Galbraith and Roberts (2012)
*iv. Dose recovery ± 10%	Recovered D_e values must be within 10% of applied dose	-

Samples LV509 and 515 were successfully dated. Since the methodological aspect was iterated in response to results from a variety of screening tests, the details of the justification for and choice of specific measurement protocols and their results are reported in Appendix B.

3.5 Summary

Work carried out over two field seasons involved the mapping of 20 km of channel from low order tributaries (Africanders and Wilgerbosch Kloof) to the higher order Wilgerbosch River and collection of samples for subsequent laboratory analysis (Tables 3.13 and 3.14).

The integration of high precision dGPS survey data of channel sections (long and cross), terrace height, the spatial extent of major terrace fills, the location of barriers and sediment logging with analyses of soil magnetism, geochemical composition (XRF), particle size and micromorphological features from major stratigraphic units

has facilitated the first comprehensive investigation into the characteristics, mechanisms and drivers of Late Quaternary terrace development in the Upper Sundays River.

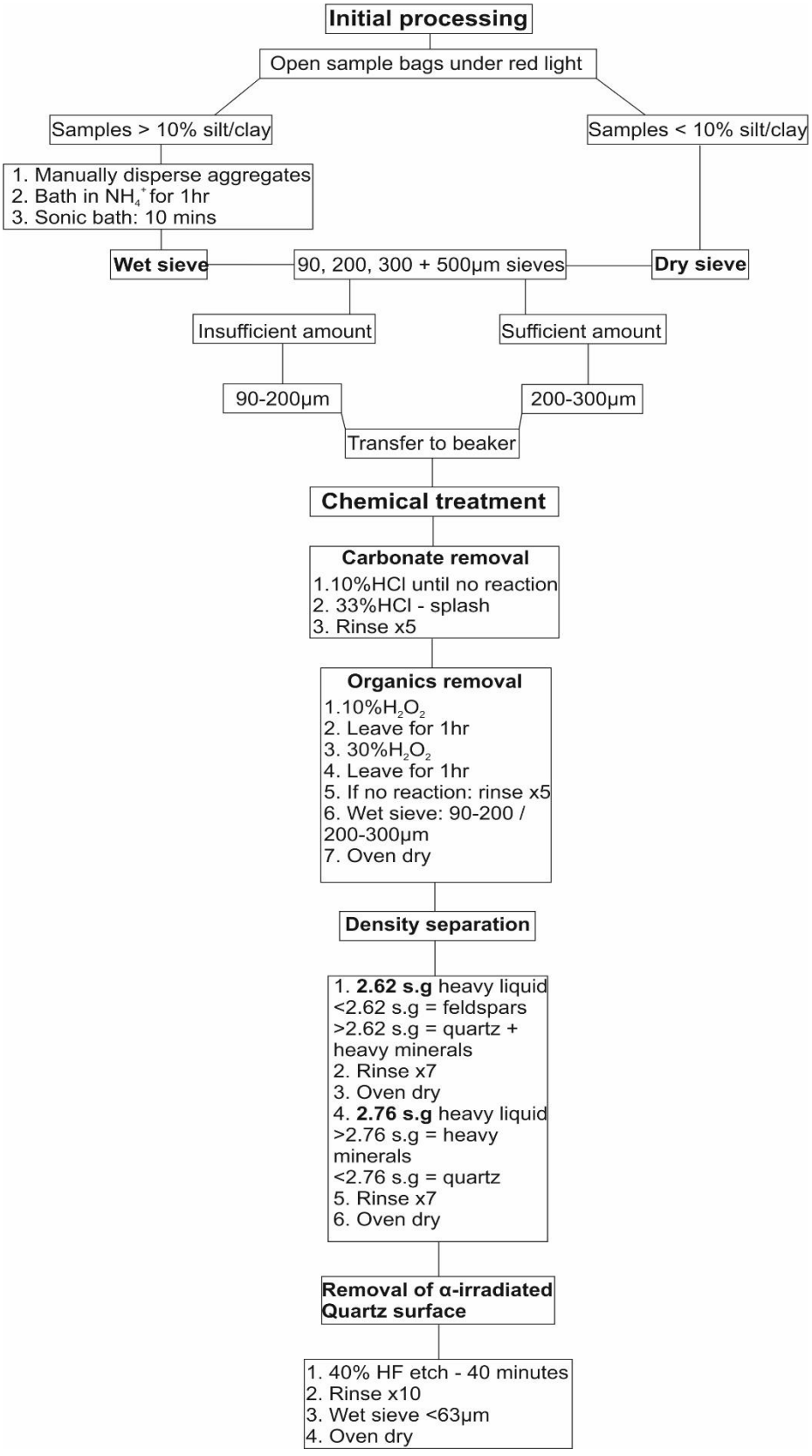

Fig. 3.8 – Summary of laboratory methods for OSL samples

Table 3.13 – number of cross sections, outcrops and samples obtained during fieldwork. *Samples collected for magnetic, geochemical, micromorphological and particle size analysis. **Samples collected for radiometric dating.

Fieldwork	**Number obtained**
Cross sections	30
Outcrops	39
*Samples i	149
**Samples ii	42

Table 3.14 – number of samples subject to each of laboratory techniques.

Technique	**Samples measured**
Soil magnetism (0-63µm)	143
Soil magnetism (particle size extracts – Atterberg technique).	20
Coulter measurements.	144
XRF geochemistry	144
Loss on Ignition	135
Thin section development.	5
OSL	26
Radiocarbon	10

Chapter 4: Results i - Contemporary valley and channel morphology

4.1: Introduction

The aim of this chapter is to characterise the morphology of the different valleys and channel systems of this study and provide the framework of the valley fills for detailed analysis of logged sections in Chapters 5-7 (Fig. 4.1). The headwater tributaries of Africanders and Wilgerbosch Kloof are treated first, then the Wilgerbosch River. From this combination of evidence, a series of possible analogues are developed to assist in the classification of palaeochannel processes and their forms as reflected in the terrace legacy.

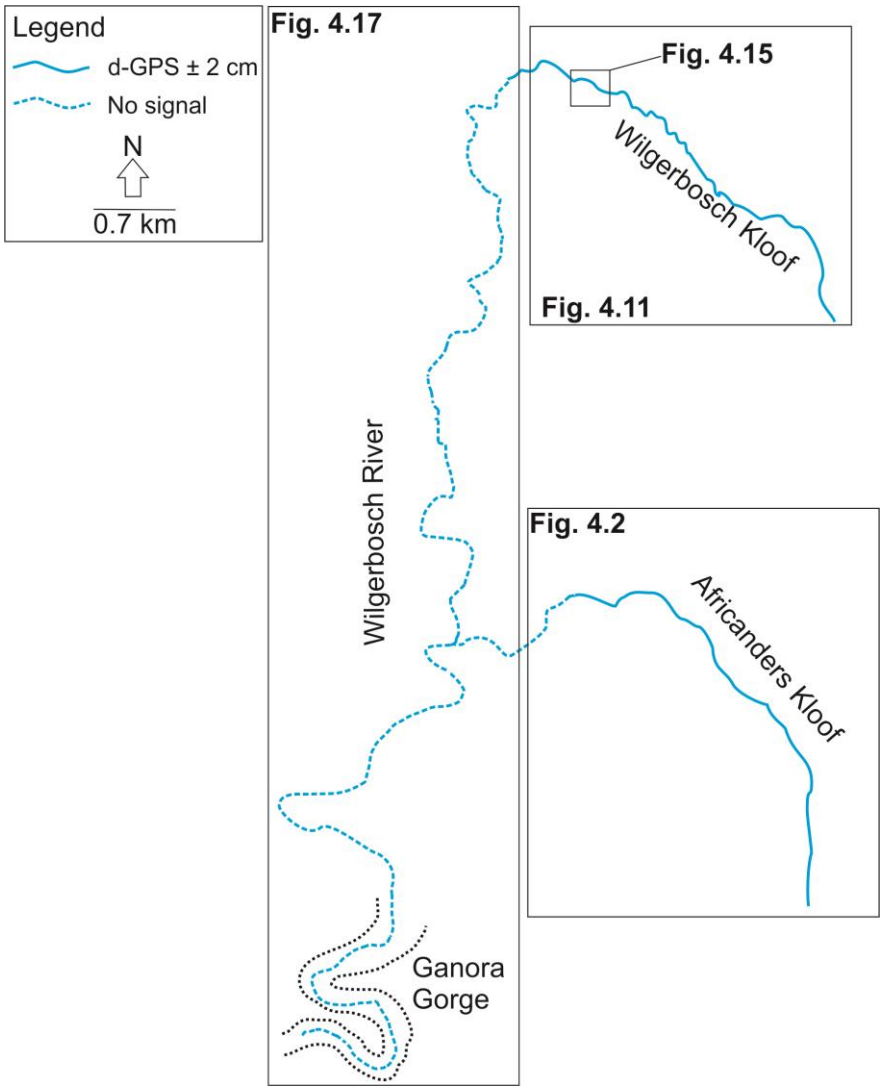

Figure 4.1 – extent and quality of d-GPS channel long-section data. Note: blue dashed line indicates where there were problems of signal acquisition and/or access to the channels.

4.2: Africanders Kloof

The following analysis of channel and valley systems is subdivided into three major valley components (Fig. 4.2). Barriers to sediment movement have been divided into three types, based on their morphology (Fig. 4.3). The upper valley is characterised by a steep (0.056 m/m – Table 4.2), continuous first order, U-shaped ephemeral gully, which extends upwards to the footslopes (Fig. 4.4 and 4.5). The gully contains a mixed load of sand and gravel, dissecting up to 2.5 m of sediments that comprise a fan-like landform originating from the upper slope (Fig. 4.6a). Other morphological evidence in the form of terrace surfaces which dip away from the gully (see CS-1 and 2 – Fig. 4.7) implies a lobate landform consistent with a fan.

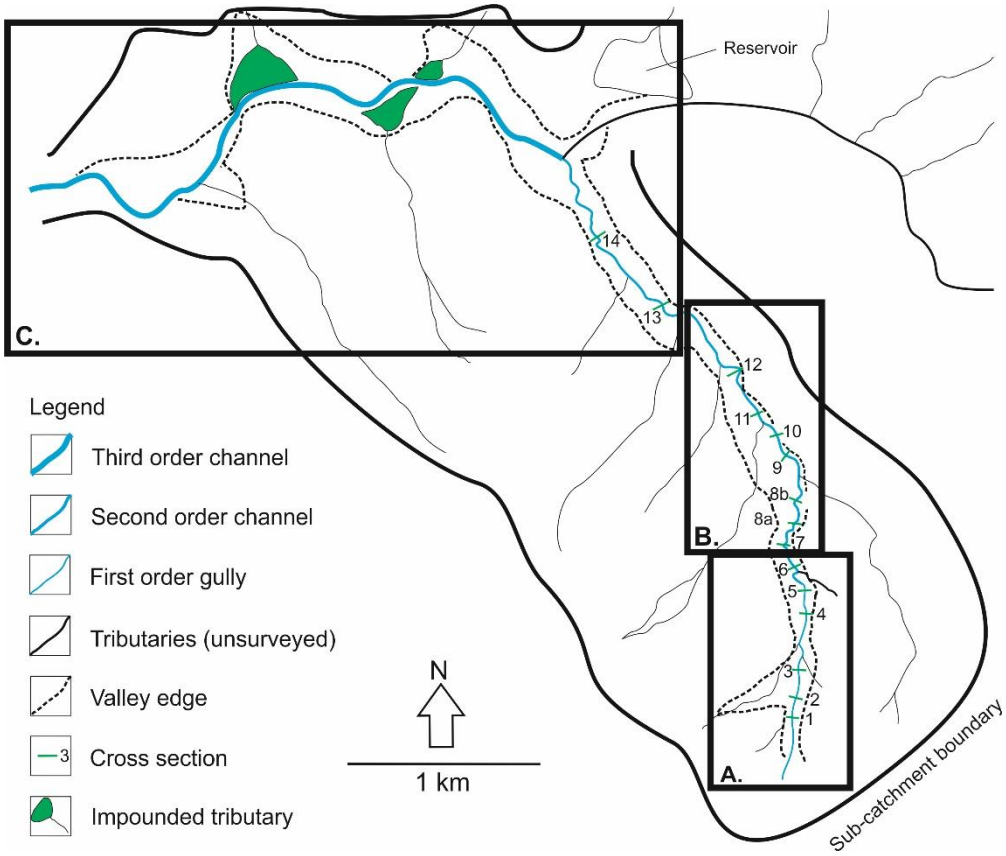

Figure 4.2 – geomorphic map showing valley edge, the location of first, second and third order channels and the locations of surveyed cross sections (Fig. 4.7). Note the map is divided into three compartments: A: Upper valley; B: Central valley and C: Lower valley. Valley and channel characteristics follow this order in text.

The junction between reaches 2 and 3 (Fig. 4.4) is marked by an 80 cm knickpoint incised into alluvium and, thereafter, the gully deepens to 4 m (Fig. 4.6b). The top of this knickpoint corresponds to an incised 'whitish,' clayey soil formed on dolerite (Fig.

4.6c) implying that this was once a barrier retarding channel downcutting (see (Fig. 4.3 - ‘1: Breached rock barrier’).

Barriers	Description	Effects
1 Breached rock barrier (long view).		
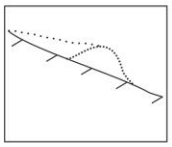	Exclusively related to **dolerite**. Incision of bedrock outcrops which formerly dammed sediment. Solid black line signifies new channel base level.	Re-connection of sediment sinks with channel network.
2 Rock steps (long view).		
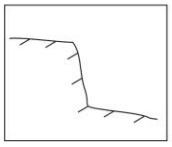	Exclusively related to **sandstone**. Up to 3 m high. Mostly limited to upper headwater valleys.	Reduction in channel gradient and confinement upstream.
3 Knickpoint retreat (long view).		
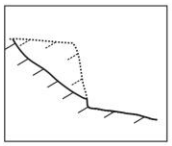	Applicable to **dolerite**, **sandstone** and **mudstone**. Fluvial incision of rock step resulting in steepening of channel bed. Common in 2nd and 3rd order tributaries.	Boost stream power and sediment exchange between reaches.
Buffers		
1. Elevated terraces (cross-view).		
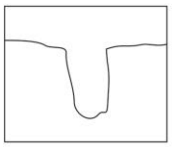	Terraces up to 5 m high.	Reduced slope-channel coupling.
2. Intact valley fill (planform).		
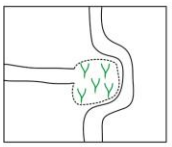	Intact valley fill up to 5 m high with tributary terminating in a localised wetland.	Disconnectivity induced between tributary and trunk stream.
Blankets		
1. Sediment texture		
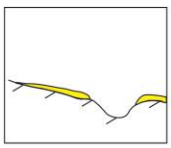	Clay/silt rich deposits directly overlying dolerite.	Facilitated preservation of T1 even in high energy reaches. Protected underlying bedrock from fluvial incision.
2. Carbonate cements		
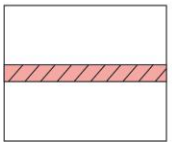	Carbonate deposits, thickest (up to 10 cm) in central and lower valleys.	Base level anchor slowing knickpoint retreat through rubified deposits in 1st and 2nd order streams.

Figure 4.3 – definition, description and effects of barriers, buffers and blankets documented across the study region. Note that ‘barriers’ are colour coded and marked on the geomorphic maps (Fig. 4.4, 4.5, 4.9, and 4.11).

From reach 2 downstream, the terrace deposits thicken (up to 5 m) and are overprinted by a thin calcrete horizon which was traced to the height of breached rock barrier 1 (Fig. 4.3 and 4.4). Morphologically, the gully is considerably deeper and narrower, and the terrace surfaces, in contrast to upstream, dip toward the gully (see Fig. 4.6d and CS-3 – Fig. 4.7). Gully depth and confinement progressively decrease in reach 4 (see Fig. 4.3 and CS-4 - Fig. 4.6) with proximity to dolerite rock step 4 (Fig. 4.3, 4.4 and 4.7). A greyish deposit is inset within the rubified deposits (Fig. 4.6e), representing the first case of 'fill within fill.' Additionally, due to reduced terrace height, up to 50 cm of modern floodplain sediments have accreted on top of and also are inset within the rubified deposits at CS-4 (Fig. 4.4 and 4.6f).

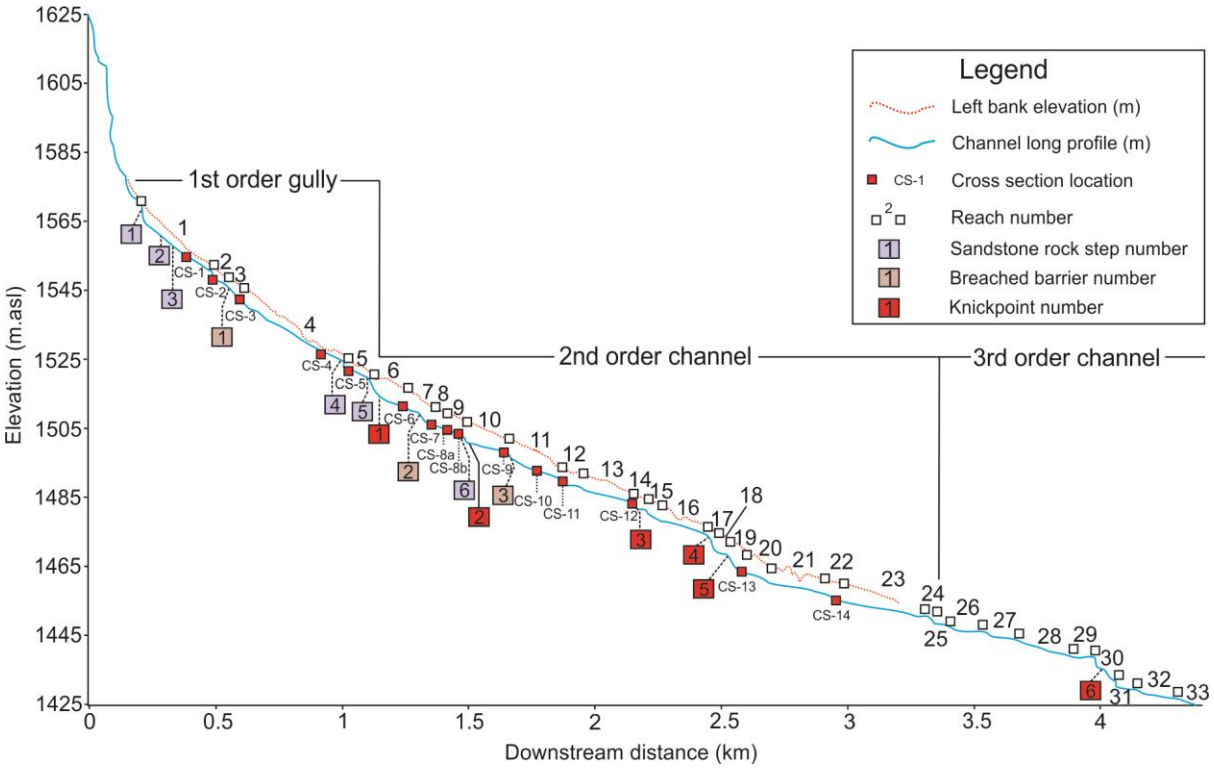

Figure 4.4 – channel long section for Africanders Kloof. Displayed are a) locations of cross sections, b) reach numbers and c) stream order.

In reach 5, the rubified deposits continue but, preserved within the terrace, are clearly defined palaeochannel structures and the 'greyish fills' are absent (Fig. 4.6g). The first order gully joins a second order bedrock channel after rock step 5 (Fig. 4.3, 4.4 and 4.6h). This second-order stream (reach 6) transitions from a narrow and steep (0.114 m/m – Table 4.1) bedrock channel to a mixed bedrock-alluvial stream. Notably, this stretch of channel is perennial: fed by groundwater flow, with abundant in-channel vegetation.

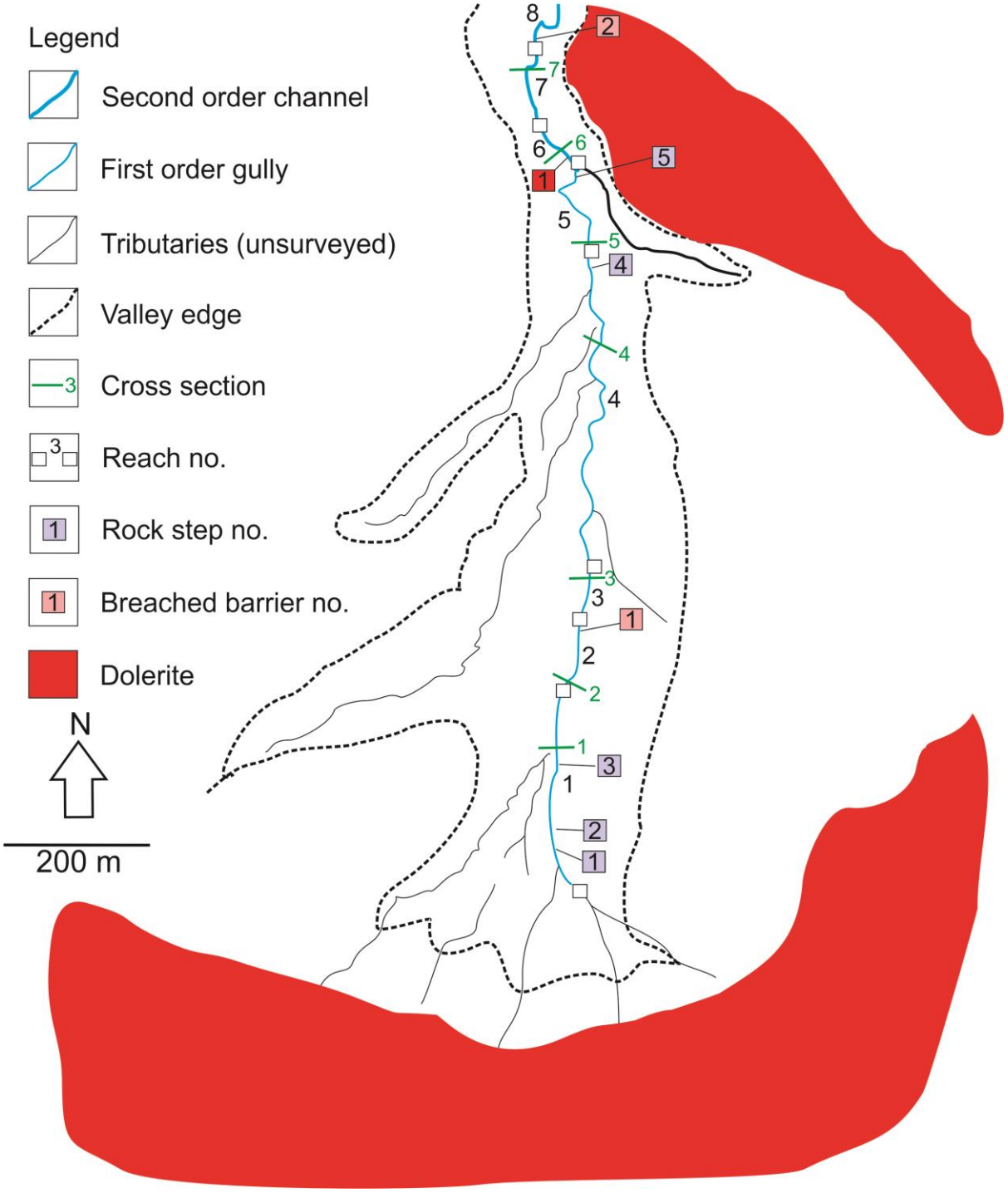

Figure 4.5 – geomorphic map of upper Africanders Kloof (see Fig. 4.2A). Note labelled channel reaches corresponding to those shown in the long-section (Fig. 4.4) and colour coded barriers (Fig. 4.3).

Up to 3 m of rubified terrace fills are present, with the re-emergence of pockets of the inset grey fills in reaches 7-9. In reach 8, the channel steepens (0.085 m/m), alternating between being terrace and bedrock (dolerite) confined. The inset grey fill terminates upstream of a major dolerite barrier with the rubified fills impounded

behind it (Fig. 4.8a). This constriction acts as a major discontinuity for coarse sediment in the modern channel system: well-rounded dolerite boulders and cobbles are present upstream of the constriction, but absent downstream. The terrace fills are characterised by well bedded, matrix-supported, deeply rubified, coarse (cobble–boulder) dolerite clasts, similar to those on the flanking slopes (Fig. 4.8b).

At CS-8a and b (Fig. 4.7 and 4.9), these deposits have been cross-cut by the inset grey fill (Fig. 4.8c). The end of reach 9 is delimited by knickpoint 2 (Fig. 4.4 and 4.9). In contrast with the knickpoint at the end of reach 5 (the confluence between first and second order streams), this knickpoint exhibits comparatively deep incision (Fig. 4.8d) and, notably, the rubified terrace deposits are continuous between reaches 9 and 10 instead of grading to the top of the bedrock (Fig. 4.4).

Reaches 10–14 exhibit relatively low slope (Table 4.1) compared to upstream, alternating between being channel and bedrock confined. Small strands of inset floodplain have formed in wider segments of reaches 11 and 13 (Fig 4.8e), and are colonised by wetland plants such as Juncus and Phragmites (Fig. 4.8f). The terrace deposits exhibit the greatest complexity in these reaches. Three main types are recognised: 1) rubified deposits overprinted by a thin, laterally continuous carbonate horizon; 2) inset grey fills; and 3) intermediate ‘brown’ fill that is relatively unconsolidated, consisting of angular mudstone fragments from the proximal slope (Fig. 4.8g). Large dolerite boulders up to 80 cm (b axis) in diameter are present in the channel (reach 13), derived from the proximal dolerite slope to the west (Fig. 4.8h). A ‘whitish’ clay similar to that reported earlier (reaches 2–3) was found mantling dolerite exposed in the channel (Fig. 4.8i). The channel is deflected by dolerite at the junction with reach 14, forming the first distinct meander, with a small point bar on the inside of the bend. The channel is relatively unconfined here (CS-12 – Fig. 4.7).

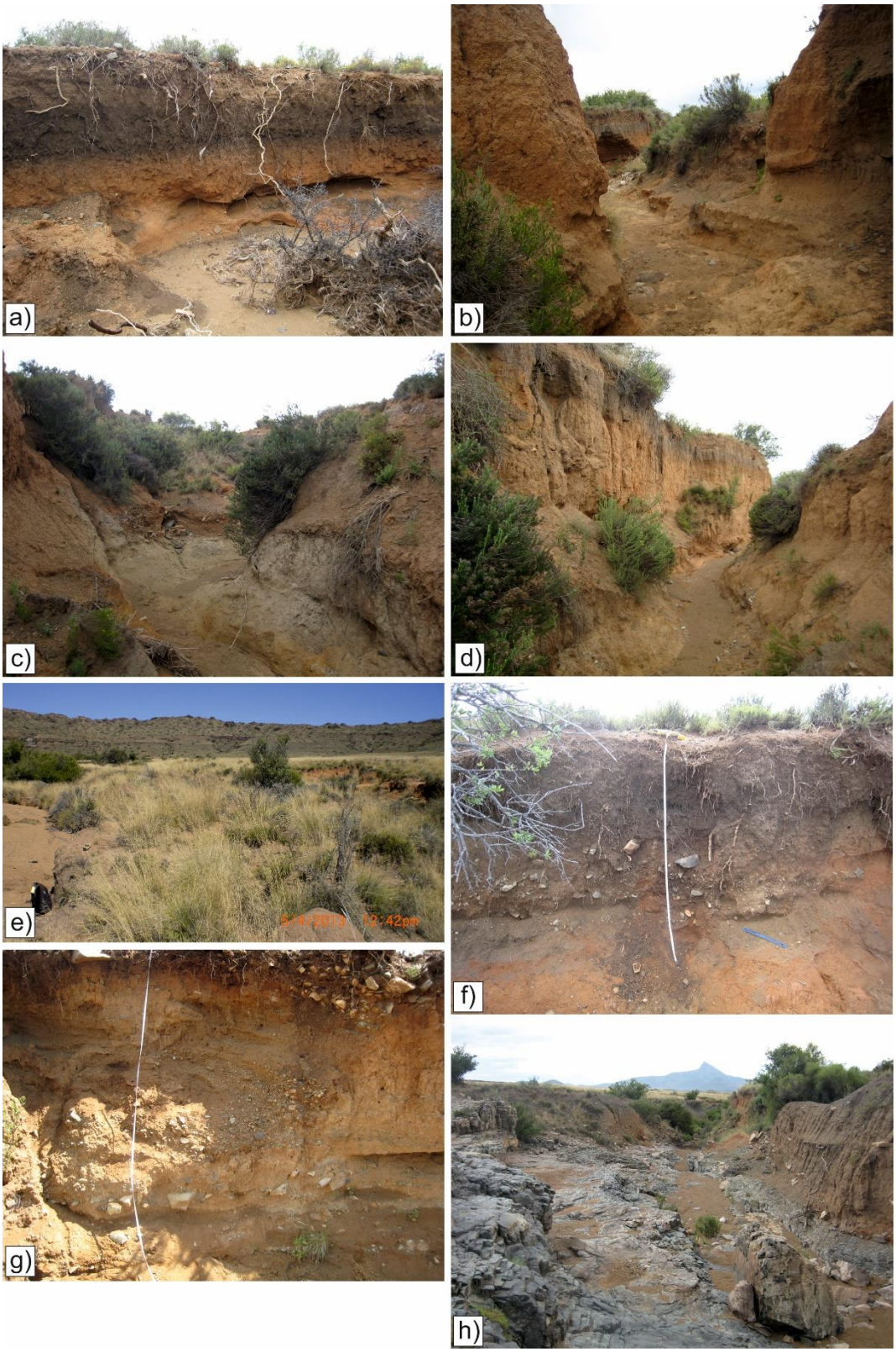

Figure 4.6 – photographs of a) palaeofan sediments incised by first order gully, b) retreating knickpoint the top of which corresponds to c) the height of a former dolerite barrier; d) narrow, deep gully downstream of breached rock barrier no.1; e) 'black palaeosol' inset within rubified deposits just upstream of rock step 4 (Fig. 4.5); f) modern floodplain deposits burying rubified fills upstream of rock step 4 (Fig. 4.5); g) first occurrence of inset grey fill architecture preserved within the left bank terrace at CS-5 (Fig. 4.7); h) confluence with second order channel in reach 6 (Fig. 4.5) – note the large rock step to left of photo acting as barrier to first order gully, but the bedrock channel to right.

Table 4.1 – Africanders Kloof gradient data derived from d-GPS of channel long section.

Stream order	Reach	Gradient (m/m)	Integrated stream order gradient (m/m)
1	1	0.06	0.056
	2	0.062	
	3	0.063	
	4	0.042	
	5	0.05	
2	6	0.114	0.057
	7	0.024	
	8	0.085	
	9	0.027	
	10	0.028	
	11	0.039	
	12	0.003	
	13	0.024	
	14	0.04	
	15	0.112	
	16	0.022	
	17	0.229	
	18	0.035	
	19	0.137	
	20	0.029	
	21	0.018	
	22	0.044	
	23	0.014	
	24	0.102	
	25	0.017	
	26	0.017	0.027
	27	0.013	
	28	0.023	
	29	0.004	
	30	0.094	
	31	0.031	
	32	0.009	
	33	0.027	

The stretch of channel between cross sections 12 and 14 (Fig. 4.4 and 4.9) consists of alternating shallow and steep reaches (Table 4.1) which switch between being bedrock and terrace confined. Steep reaches include 15, 17 and 19, where large knickpoints have formed on dolerite (Fig. 4.8j). The rubified deposits and inset black palaeosol are inter-fingered, producing unpaired terraces (CS-13 – Fig. 4.7), with most complete expression in reaches 19 – 23 where the valley becomes relatively unconfined (Fig. 4.8k and l). The wider valley has permitted the channel to meander

(reach 22). Point bars have formed in overwidened segments of meandering channel (30 – 40 m). During low flows, the channel thalweg cuts through this bar (Fig. 4.8m), and the meander apex remains disconnected from the sediment transport system.

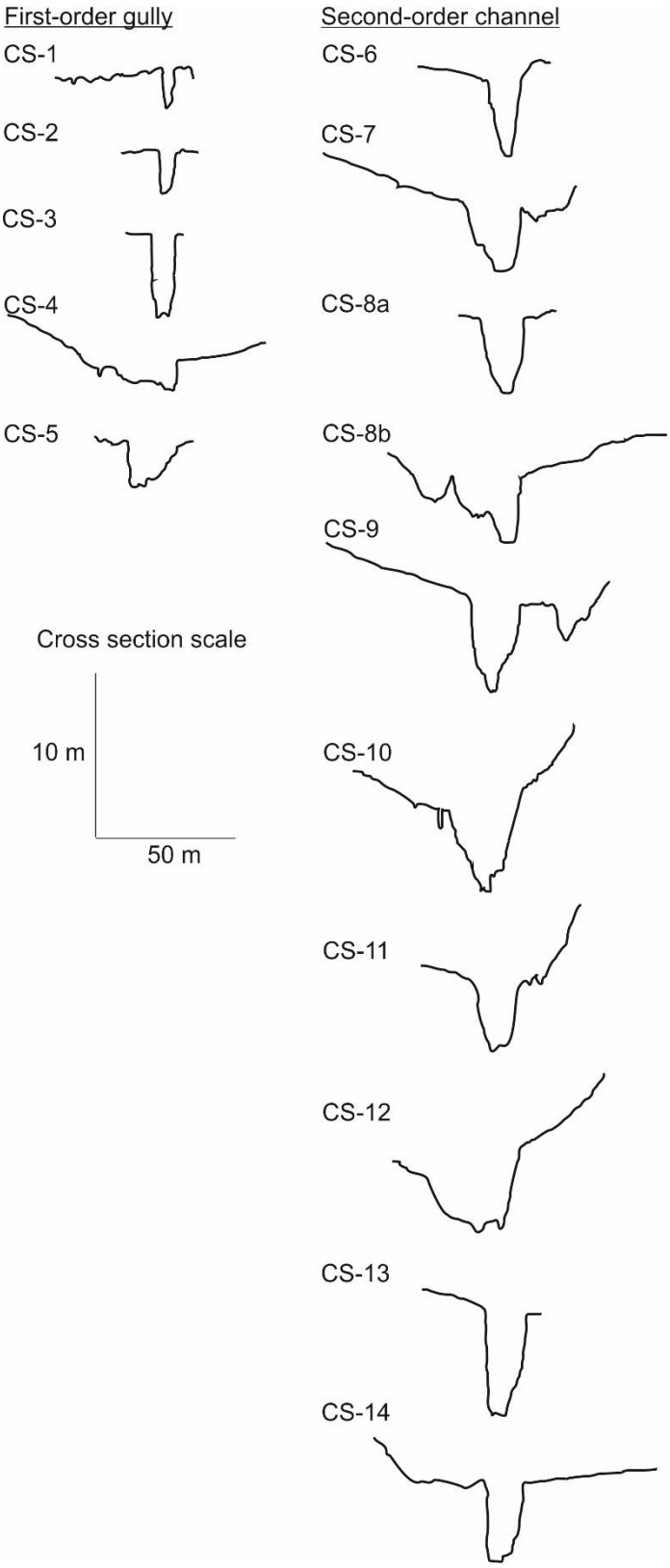

Figure 4.7 – Africanders Kloof valley cross sections, see Fig. 4.2 and 4.3 for locations.

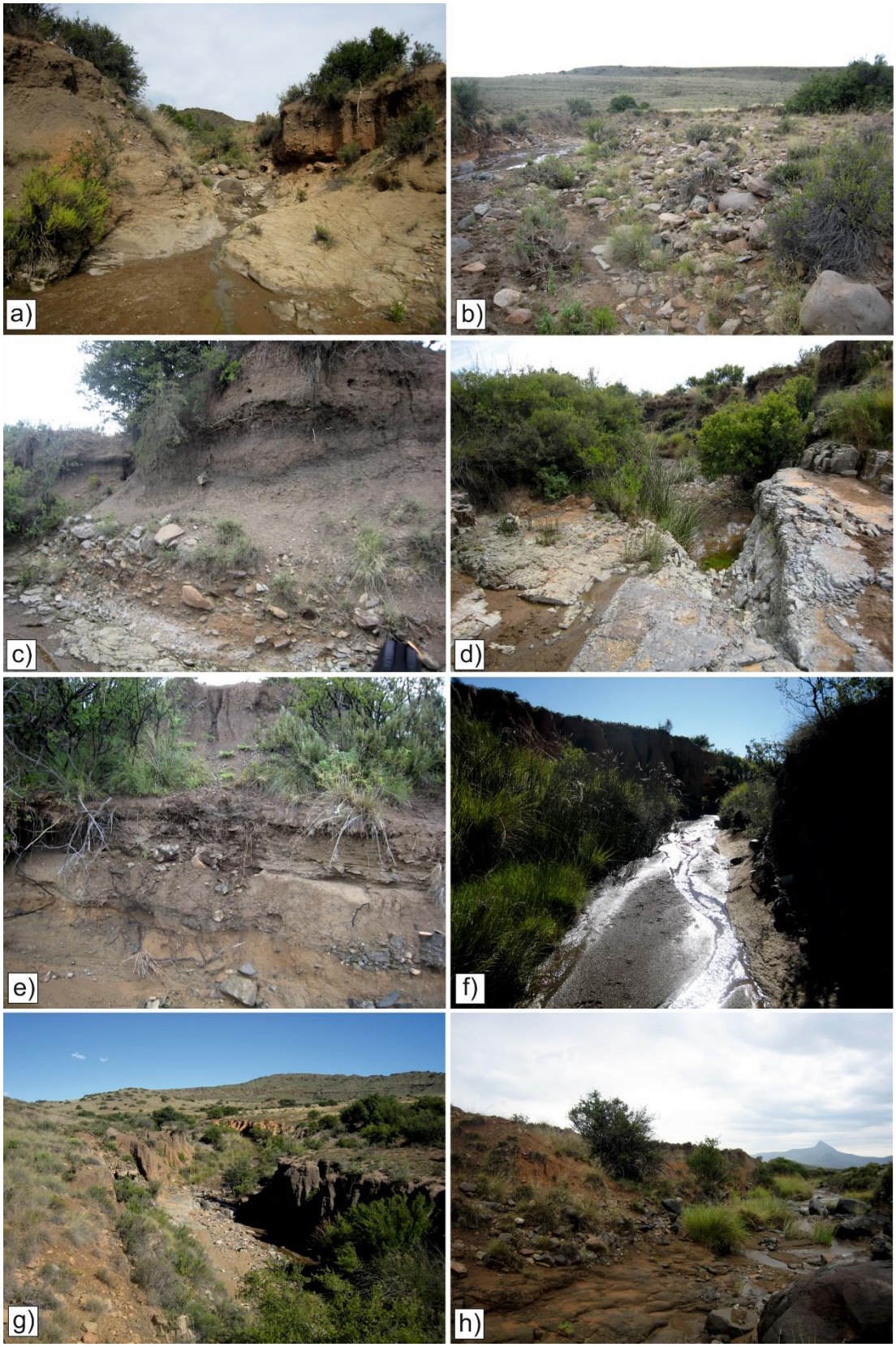
a)
b)
c)
d)
e)
f)
g)
h)

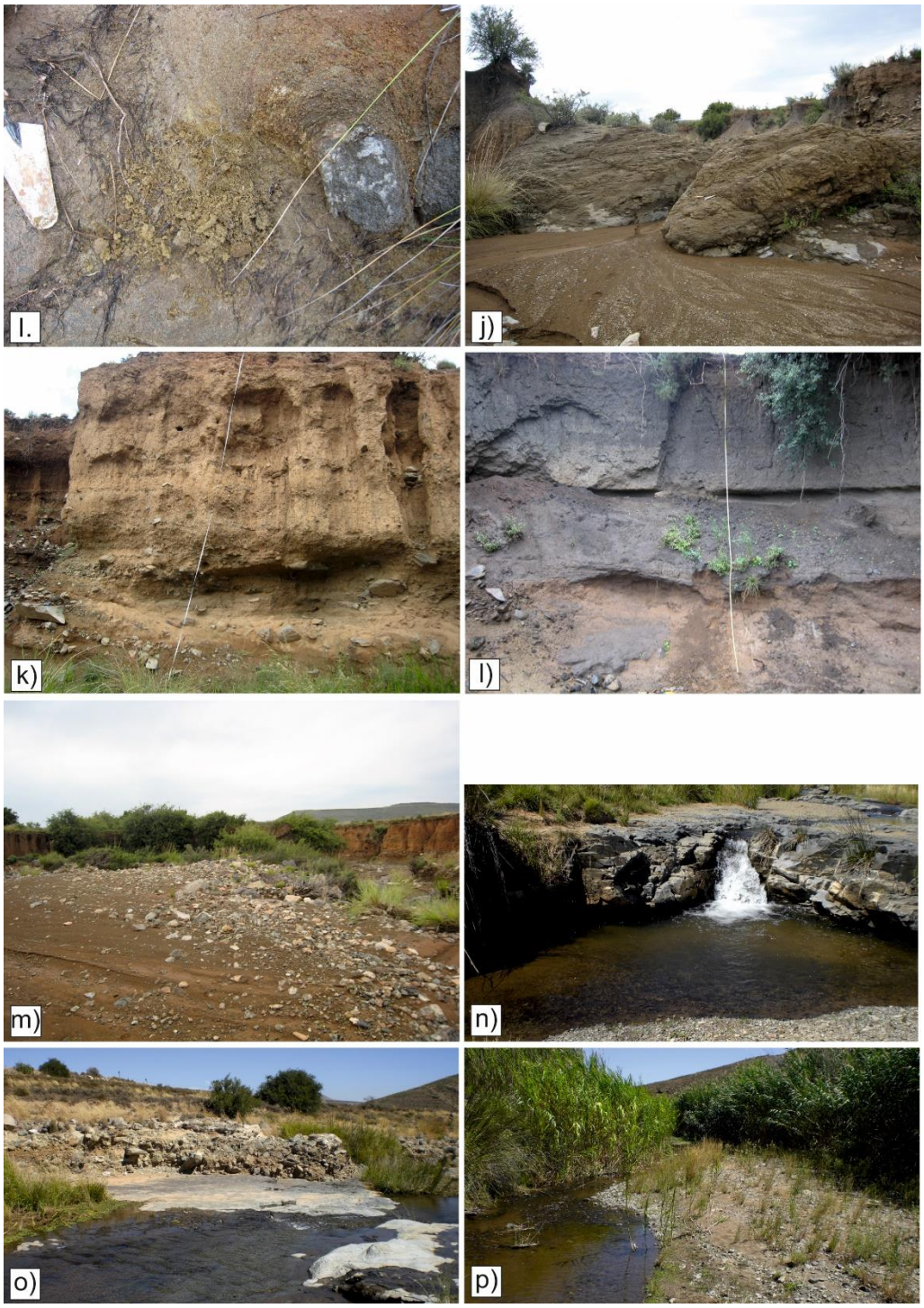

Figure 4.8 – photographs from central and lower AK valley: a) view upstream of breached rock barrier 2 (see reach 8 - Fig. 4.9) with rubified terrace fills impounded upstream – note the dolerite boulders upstream of the constriction; b) dolerite cobbles and boulders mantling slope to east of channel in reach 8; c) rubified coarse deposits cross-cut by inset grey fills and overlying brown sands in reach 8/9; d) knickpoint 2 – channel downcutting through sandstone (see Fig. 4.9) at end of reach 9; e) example of inset floodplain in wider channel sections of reaches 11 and 13; f) perennial streamflow in reach 11 – note abundant wetland vegetation at channel margins; g) juxtaposition of rubified, grey and intermediate brown fills in reach 11 (view upstream); h) dolerite boulders in channel sourced from proximal slope; i) soil mantling dolerite outcrop in channel; j) knickpoint 3 (see Fig.4.9) at end of reach 18; k) 6 m of rubified deposits with l) inset grey fill opposite at the base of knickpoint 3 (CS-13 – Fig. 4.6); m) large point bar deposit (reach 22 – Fig. 4.9); n) knickpoint 5 through sandstone (reach 30 – Fig. 4.10); o) marginal channel bar deposits; p) example of wetlands straddling the channel (reach 33).

Segments of inset floodplain are common in the lower part of the second order tributary. Notably, terrace depth progressively reduces from 6 m in reach 20 to approximately 2 m at the confluence with the third order tributary (Fig. 4.4 and 4.9).

The valley widens at this confluence (up to 350 m). Notably, the rubified deposits and carbonate are continuous at the margins of the valley. Up to 3 m of grey, relatively unconsolidated terrace fills are inset, and, unlike the inset grey fills described earlier, these directly overlie bedrock.

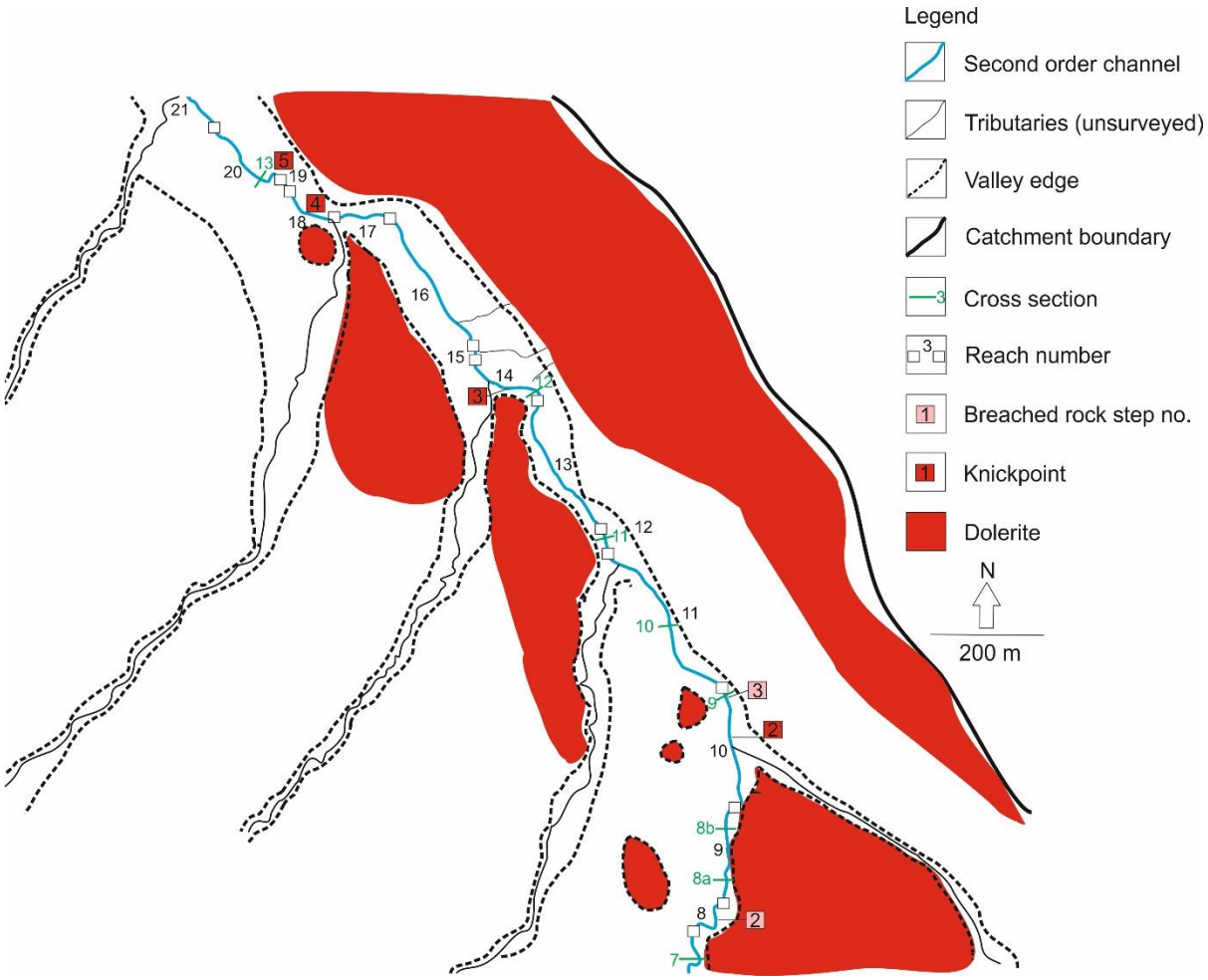

Figure 4.9 – geomorphic map of the AK central valley (see Fig. 4.2B). Note labelled channel reaches corresponding to those shown in the long-section (Fig. 4.3).

The third order channel is a perennial, mixed-load stream. Valley confinement varies between 80 – 300 m (Fig. 4.10). Channel gradients are typically low, except reach 30 (0.094 m/m – Table 4.1), where a 1 m knickpoint has formed through sandstone (Fig. 4.8n). Upstream of this knickpoint, imbricated boulders and cobbles occur at the channel margins (Fig. 4.8o). Small riffles have developed immediately upstream of

and in bedrock reaches, with pools in intermediate reaches. Narrow corridors of wetland straddle the modern channel associated with low-energy sand-dominated reaches at the base of knickpoints, though coarser gravel material is stored on bars (Fig. 4.8p and 4.10).

Several other second-order tributaries are disconnected from the main AK tributary by pockets of intact valley fill – similar to situation reported by Brierley and Fryirs (1999).

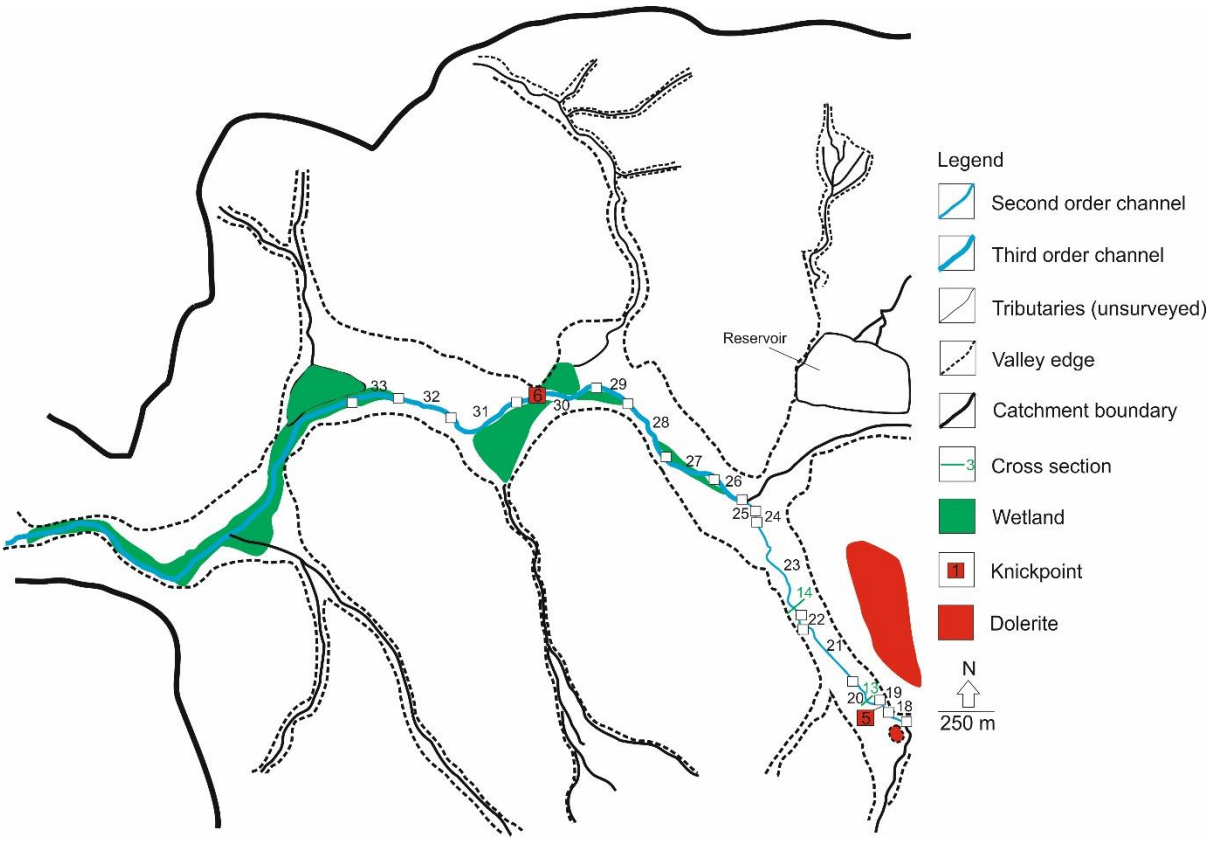

Figure 4.10 – geomorphic map of lower AK valley (see Fig. 4.2C). Note labelled channel reaches corresponding to those shown in the long-section (Fig. 4.4).

4.3: Wilgerbosch Kloof

The Wilgerbosch Kloof is incised into Beaufort Group sandstone and mudstone flanked by dolerite primarily to the north-east (Fig. 4.11). The first order channel drains steep (up to 0.18 m/m – Table 4.2) sandstone slopes – exposing up to 4 m of palaeofan sediments in reaches 1–5 (Fig. 4.11). The palaeofan is heavily degraded, exhibiting badland topography (Fig. 4.14b). The long profile exhibits a stepped morphology (Fig. 4.12), with a major break in slope in reach 2 (0.065 m/m – Table 4.2) where the channel crosses rock step 1 (Fig. 4.7, 4.11 and 4.12).

Between reaches 5 - 13, the valley becomes unconfined (Fig. 4.11). The channel is typically terrace confined and relatively wide compared to the headwaters (up to 10 m – CS-4 and 5 – Fig. 4.13), situated just above bedrock. Terrace fills typically comprise up to 2 m of rubified, well bedded deposits buried by friable, brown sands, but lack secondary carbonate (Fig. 4.14c). The channel steepens in reaches 8, 10 and 13 (Fig. 4.11; Table 4.2) where deep knickpoints (1-3 – Fig. 4.11 and 4.12) have formed through sandstone. Knickpoint 1 in reach 8 has carved into inclined beds of sandstone, which reflect local contact metamorphism with the remnants of a dolerite intrusion to the right of the channel (Fig. 4.11). Notably in reach 8, grey fills cross-cut by palaeochannel deposits appear inset within the rubified deposits formerly described (Fig. 4.14d).

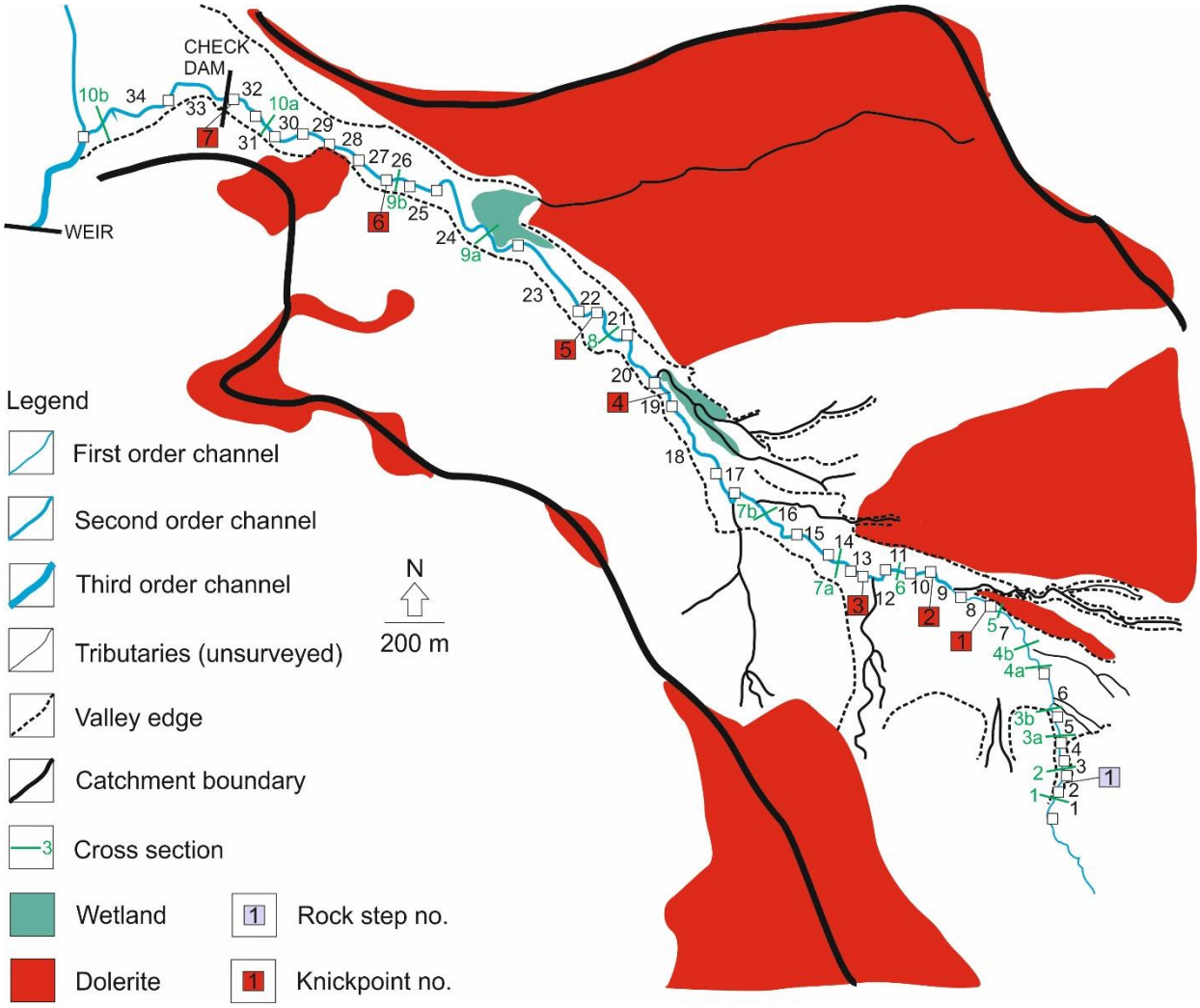

Figure 4.11 – geomorphic map of the Wilgerbosch Kloof. Note labelled channel reaches corresponding to those shown in the long-section (Fig. 4.12).

The adjoining first order tributary in reach 9 (Fig. 4.11) is a low energy channel with abundant vegetation (Fig. 4.14e). Upstream, this tributary is carved into dolerite

bedrock, and is very narrow (4-5 m), but becomes an alluvial reach near the confluence with the surveyed second order channel (Fig. 4.11) where it becomes relatively wide (10 – 15 m). Seepage from a nearby aquifer, in concert with this loss of confinement has facilitated vegetation growth and disconnectivity of fine sediment such that localised aggradation of the tributary is occurring.

After reach 13 (Fig. 4.11 and 4.12), the valley becomes confined (150 – 200 m) with slopes of dolerite to the northeast and mudstone to the southwest (Fig. 4.13). Terrace height increases to 5.5 m (CS-7b – Fig. 4.13). Crucially, in addition to the rubified fills, a grey horizon capped by brown sands similar to that reported at AK is present, extending down the valley at least as far as reach 18, where it is distinctively inset (Fig. 4.14f). Reaches 15-18 are low gradient (Table 4.2) with narrowing of the channel due to densely vegetated, inset banks of alluvium (Fig. 4.11, 4.13 (CS-7b) and 4.14g).

Channel steepening occurs in reach 19 where two knickpoints (no. 4 and 5 – Fig. 4.11 and 4.12) are carved into mudstone (Table 4.2 and Fig. 4.14h). Large mudstone boulders at the channel margin reflect in situ break up of bedrock (Fig. 4.14i) and may be analogous to coarse accumulations noted elsewhere in terrace segments immediately downstream of knickpoints, or close to weathering slopes.

Reaches 20–26 are low energy sand-dominated perennial reaches. Coarser gravel is stored on point bars in meandering stretches (Fig. 4.14j) and in-channel vegetation is pervasive. An adjoining first order tributary in reach 20 terminates as a wetland (Fig. 4.11 and 4.14j). Up to 3 m of highly denuded brown fill occur at the valley margin.

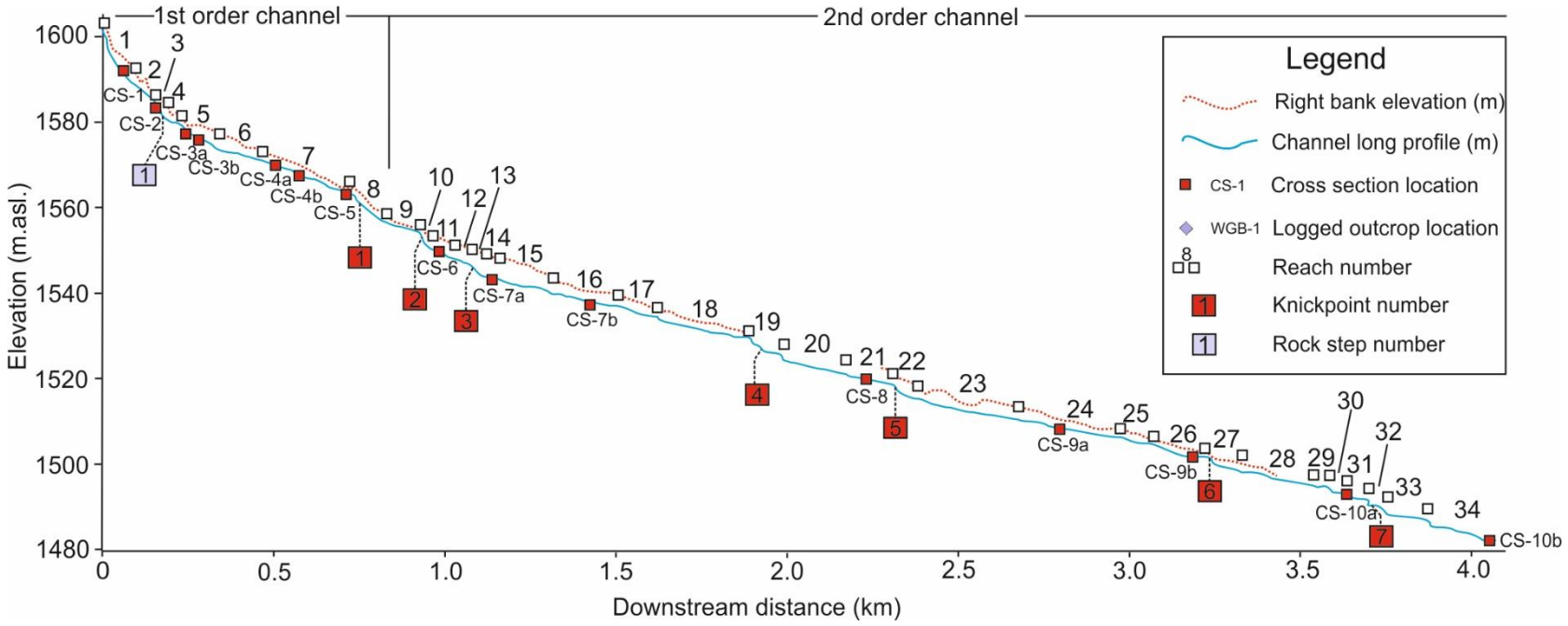

Figure 4.12 – channel long section for Wilgerbosch Kloof. Displayed are a) locations of cross sections, b) reach numbers and c) rock step and knickpoint numbers.

Table 4.2 – Wilgerbosch Kloof gradient data derived from d-GPS of channel long section.

Stream order	Reach	Gradient (m/m)	Integrated stream order gradient (m/m)
1	1	0.17	0.052
	2	0.065	
	3	0.184	
	4	0.035	
	5	0.057	
	6	0.021	
	7	0.03	
	8	0.078	
2	9	0.025	0.023
	10	0.114	
	11	0.024	
	12	0.034	
	13	0.119	
	14	0.016	
	15	0.018	
	16	0.018	
	17	0.022	
	18	0.019	
	19	0.041	
	20	0.023	
	21	0.02	
	22	0.068	
	23	0.016	
	24	0.016	
	25	0.012	
	26	0.011	
	27	0.024	
	28	0.026	
	29	0.007	
	30	0.032	
	31	0.049	
	32	0.041	
	33	0.012	
	34	0.022	

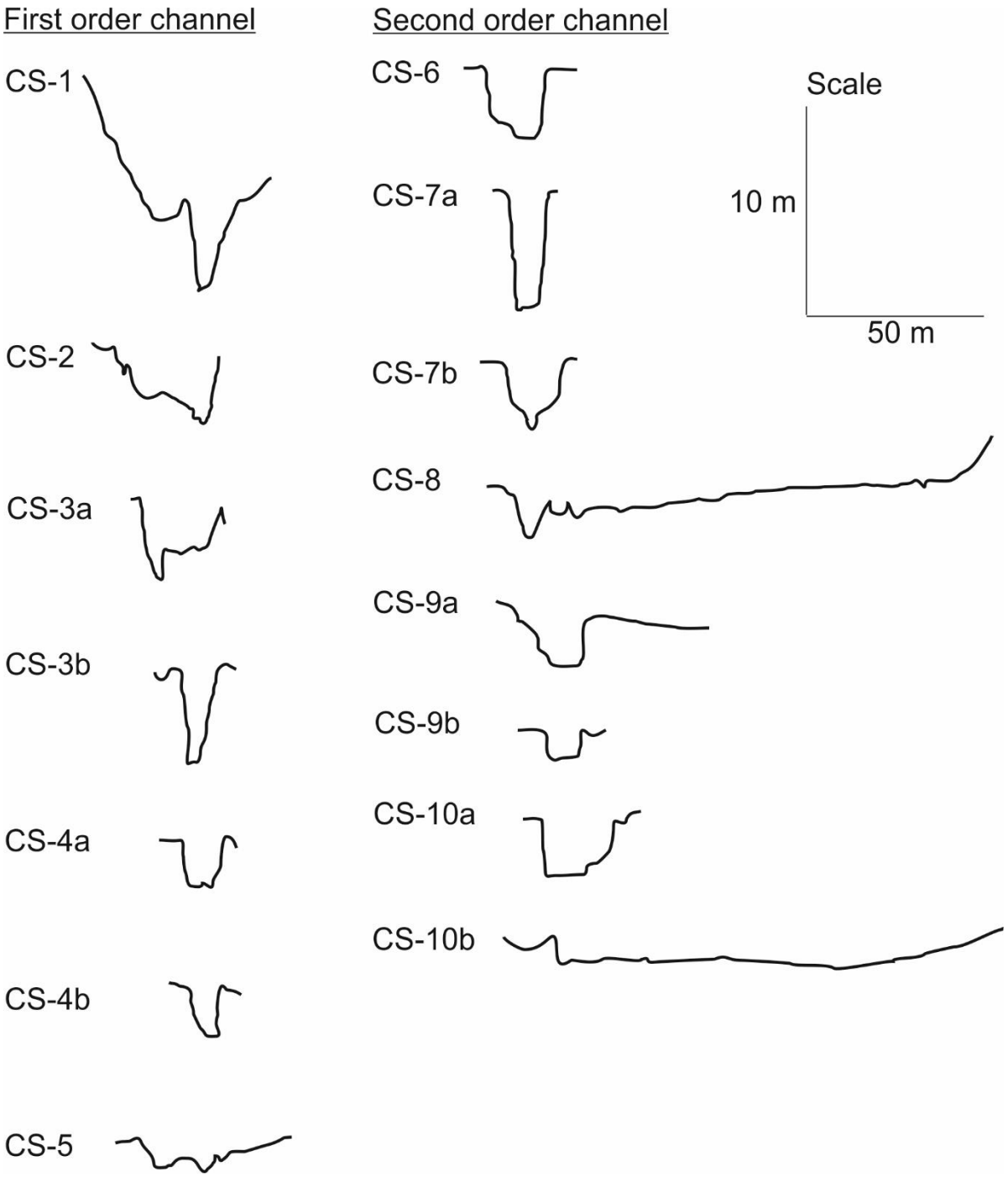

Figure 4.13 – Wilgerbosch Kloof valley cross sections, see Fig. 4.10 and 4.12 for locations.

The channel widens downstream of a major knickpoint (no. 6 – Fig. 4.11 and 4.12) through mudstone after reach 22 (Fig. 4.14m), increasing from approximately 5 m wide (CS-8) to 10-15 m wide at CS-9a and b (Fig. 4.13). Notably, the rubified deposits re-emerge in terrace fills downstream of reach 23 and are overprinted by a thin carbonate horizon similar to that reported at AK. Additionally at CS-8 (Fig. 4.13), up to 3 m of pale brown deposits are inset within the grey sediments (Fig 4.14n and o).

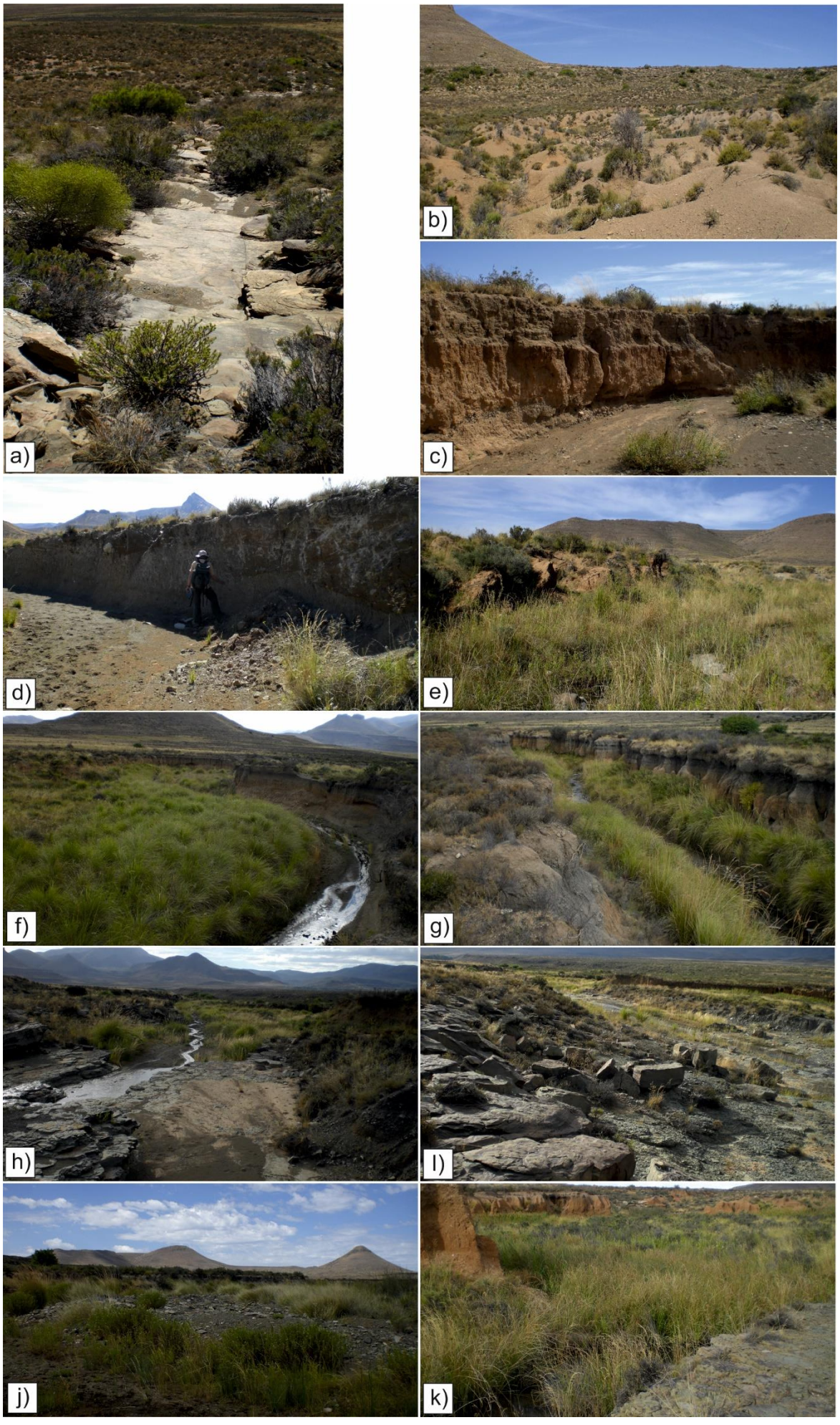
a)
b)
c)
d)
e)
f)
g)
h)
l)
j)
k)

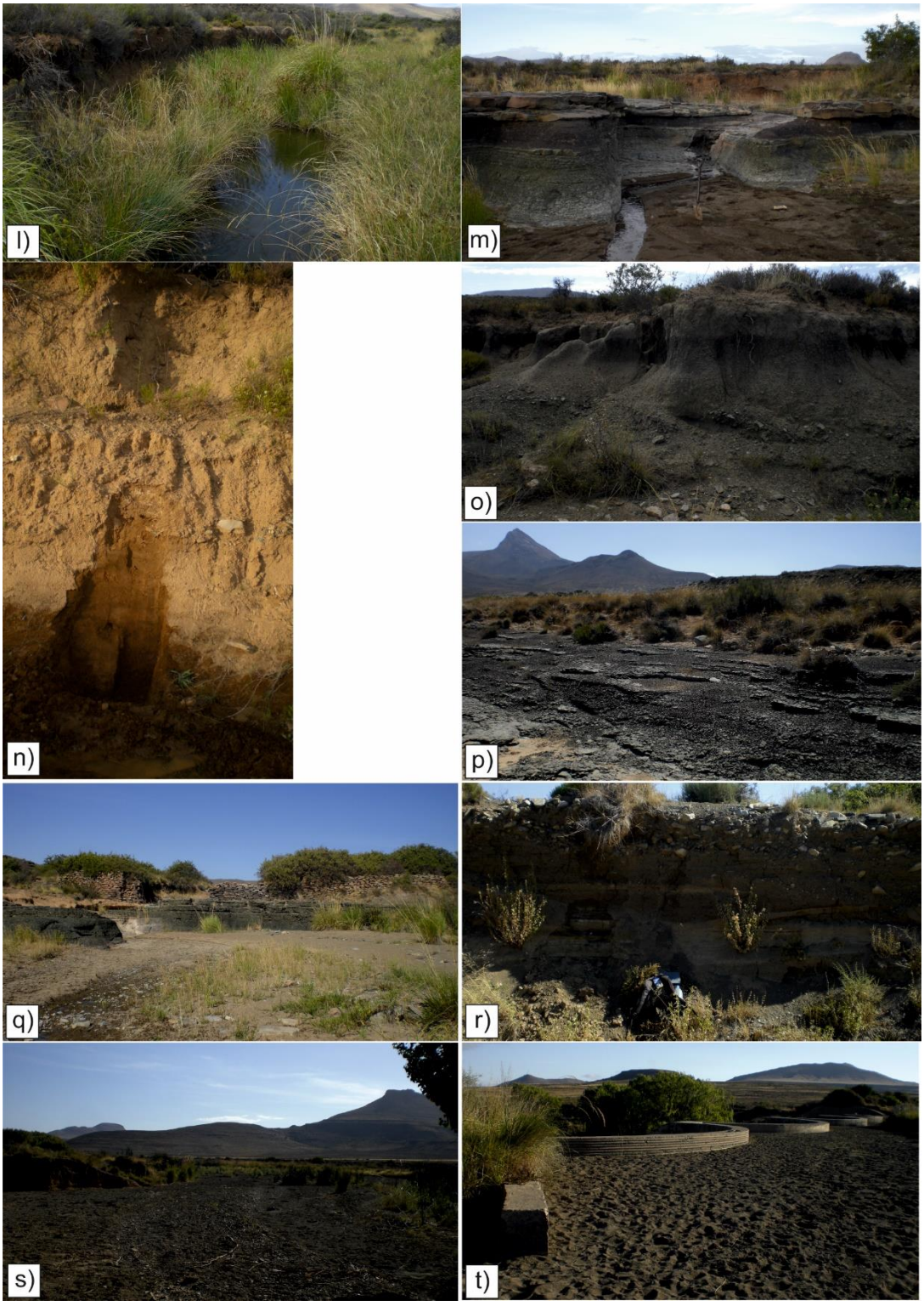

Figure 4.14 – photographs from WGB valley: a) headwater sandstone slopes; b) view upstream of degraded palaeofan mantling slopes of sandstone; c) rubified deposits overlain by brown sands (reach 7); d) pocket grey fills cross-cut by palaeochannel; e) aggraded adjoining first order tributary with wetlands (reach 9); f) rubified deposits cross-cut by grey deposits; g) thick terrace deposits (5 m) in reach 17 with inset, vegetated alluvial banks; h) 1 m knickpoint through mudstone (reach 19/20); i) in situ break up of mudstone bedrock supplying coarse material to channel; j) large point bar; k and l) aggraded first order tributaries with wetlands; m) 1 m mudstone knickpoint (reach 23); n) pale brown deposits inset within o) grey fills; p) degraded remnants of strath terraces deposited on mudstone; q) mudstone knickpoint with remnants of dam wall on top; r) sediments impounded behind

dam; s) infilled channel near confluence with 3rd order tributary in response to t) large weir 300 m downstream.

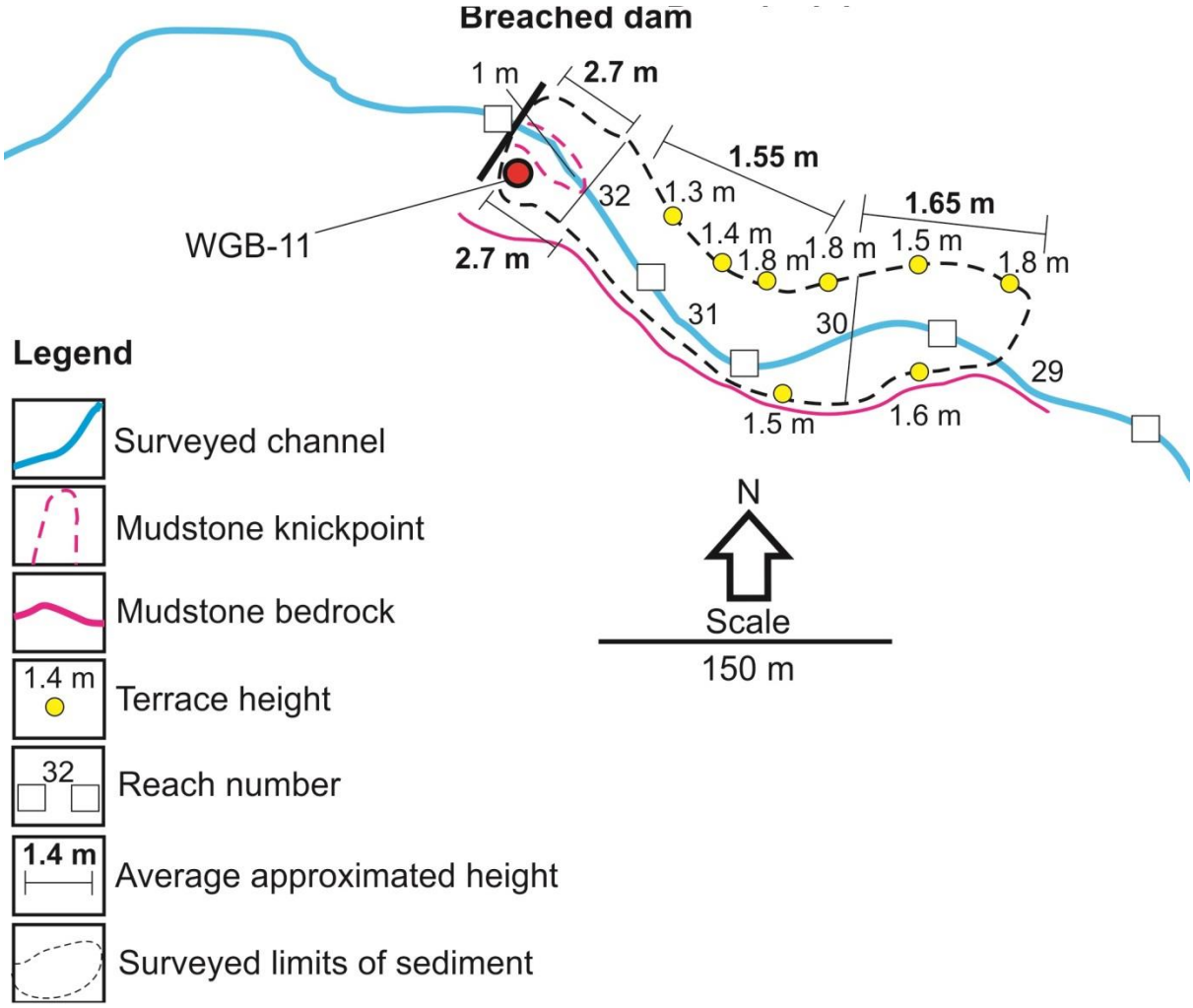

Figure 4.15 – digitally referenced map of the base of the Wilgerbosch tributary showing the spatial extent of filling behind the breached dam, with point terrace height measurements used to estimate approximate sediment thickness.

Reaches 26–32 are incised into mudstone with several deep knickpoints (no. 7-9 – Fig. 4.11 and 4.12) and strath terraces (CS-10a) preserved at the valley margins, though these have been highly degraded in places (Fig. 4.14p). In contrast with upstream, there is an abundant gravel bedload derived from in situ weathering and erosion of the underlying mudstone.

The end of reach 32 is marked by another deep 1 m mudstone knickpoint (no. 10 – Fig. 4.11). A check dam was built here in 1974 (Fig. 4.14q and r). The sediments stored behind the dam extend approximately 250 m upstream (Fig. 4.15), the characteristics of which range from cross bedded sands to varying grades of matrix

supported gravels, cobbles and boulders (Fig. 4.16). A sediment budget was calculated by dividing surveyed area into rectangles and triangles and multiplying length, width and height. Height was estimated using measured terrace elevation above bedrock (Fig. 4.15).

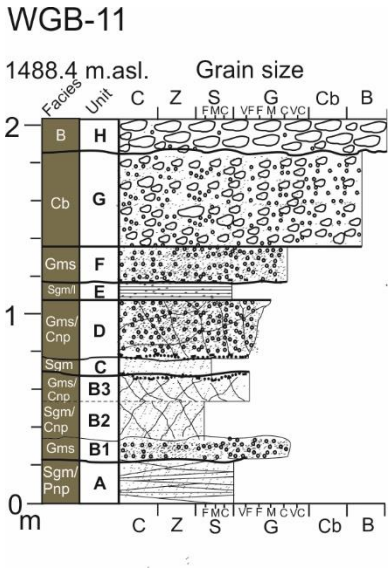

Figure 4.16 – sedimentary log obtained from outcrop WGB-11, 5 m upstream of the breached check dam.

In the segment of channel immediately upstream of the dam, sediment infill was calculated as 3.7 m depth, as there has been downcutting through mudstone rock to a depth of 1 m. The sum of individual sediment volumes was obtained as 15,404 m^3. This implies that up to 250 m of backfilling occurred within a maximum period of 38 years. The dam is now breached.

The Wilgerbosch Kloof joins a third order stream after reach 34. This 3rd order channel is impounded by a 10 m high weir (Fig. 4.11 and 4.17), which has caused backfilling such that 4 m rubified terrace fills are now buried (Fig. 4.13 - CS-10b and 4.14s and t).

4.4: Wilgerbosch River

The Wilgerbosch River is a 3rd to 4th order tributary of the Gatz River (Fig. 4.17). It is a mixed-load channel that alternates between being terrace and bedrock confined. The channel has a perennial flow of water and vegetation is abundant compared to the headwater tributaries. Straight reaches alternate with sharp, structurally controlled meander bends. The following analysis is presented in the form of 4 case

studies that represent the typical kinds of channel reaches and their deposits, as well as the older terrace fills as shown in Fig. 4.17 (boxes A-D).

A. This stretch of valley is characterised by abrupt changes in accommodation space. Reaches dominated by mudstone are wider; those dominated by dolerite are relatively constricted (Fig. 4.17). The valley downstream of the weir is approximately 400 m wide accommodating up to 5 m of predominantly grey, friable fills. The channel exhibits local braiding and flow bifurcation around vegetated pockets of matrix-supported cobble bars (Fig. 4.18a). Former channel bed deposits at the margins of the valley are capped by fresh deposits of gravels and cobbles deposited under conditions of high flow. The resulting vertical succession exhibits inverse grading.

The widest sections of channel are characterised by very coarse cobble and boulder deposits at the margins, often interstitially filled by finer deposits of sand and gravel and colonised by vegetation (Fig. 4.18b). Notably, there are frequent occurrences of dead trees both within the channel and on the floodplain, with flood marks up to 2 m above the channel bed (Fig. 4.18c).

Approximately 700 m downstream of the weir, a major valley constriction occurs where dolerite crosses the channel. No terrace fills are preserved here. Furthermore, much coarse sediment is stored on bars, with abundant wetland vegetation at the channel margins upstream of a major knickpoint through dolerite (Fig. 4.18d and e). Downstream of the knickpoint, the channel widens abruptly, with wetlands at the margins and a distinct absence of coarse sediment (Fig. 4.18f). The build-up of coarse sediment upstream of the knickpoint implies that this is acting as a major discontinuity.

A similar constriction in the valley due to intrusive dolerite occurs at the southernmost extent of segment A, though the channel has breached this barrier and is presently incising mudstone bedrock (Fig. 4.17 and 4.18g). This reach is steep relative to the previous example where the channel was actually superimposed on dolerite. Downstream of the knickpoint, the channel gradient is relatively low, with development of wetlands at the margins. This sequence of alternating high and low energy reaches continues downstream into segment B.

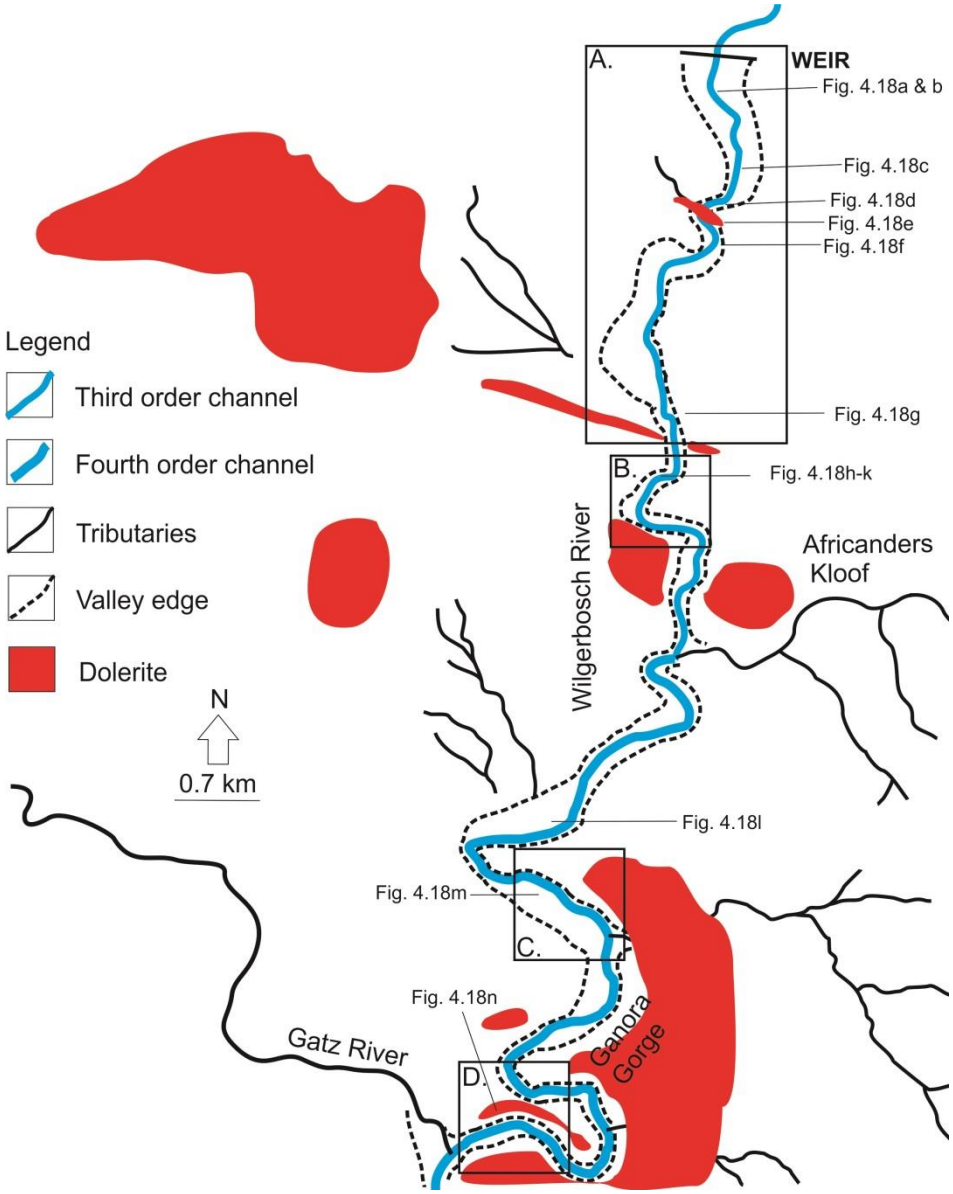

Figure 4.17 – map showing changing valley width, distribution of dolerite and major confluences along the Wilgerbosch trunk river.

B. The channel through segment B is predominantly bedrock-confined (mudstone), with unpaired, strath terraces on each side of the channel. This reach contains the most complete and accessible terrace remnants, including rubified deposits up to 4 m thick, overprinted by up to two carbonate horizons (Fig. 4.18h). Similar to the tributaries, these are cross-cut by friable, gleyed deposits (Fig 4.18i), but a separate inset terrace (Fig. 4.18j) and slope deposits (Fig. 4.18k) were also noted.

The stretch of channel between Ganora and upstream of the gorge (box C – Fig. 4.17), is predominantly bedrock confined, with structurally controlled meander bends. Terrace fills in this stretch of channel are highly degraded (Fig. 4.18l). **C.** Upstream of the Ganora gorge (Fig. 4.17), up to 5 m of rubified deposits were noted, again overprinted by carbonate deposits, but this time inset within deposits which appear to

be sourced from the nearby slope (Fig. 4.18m). Downstream, the carbonate-overprinted rubified fills inter-finger grey, friable fills. **D.** Within the gorge itself, much thicker accumulations of slope-derived deposits occur which lack carbonate (Fig. 4.18n). However, carbonate-overprinted rubified fills, appear to lie inset within these thicker slope deposits in places.

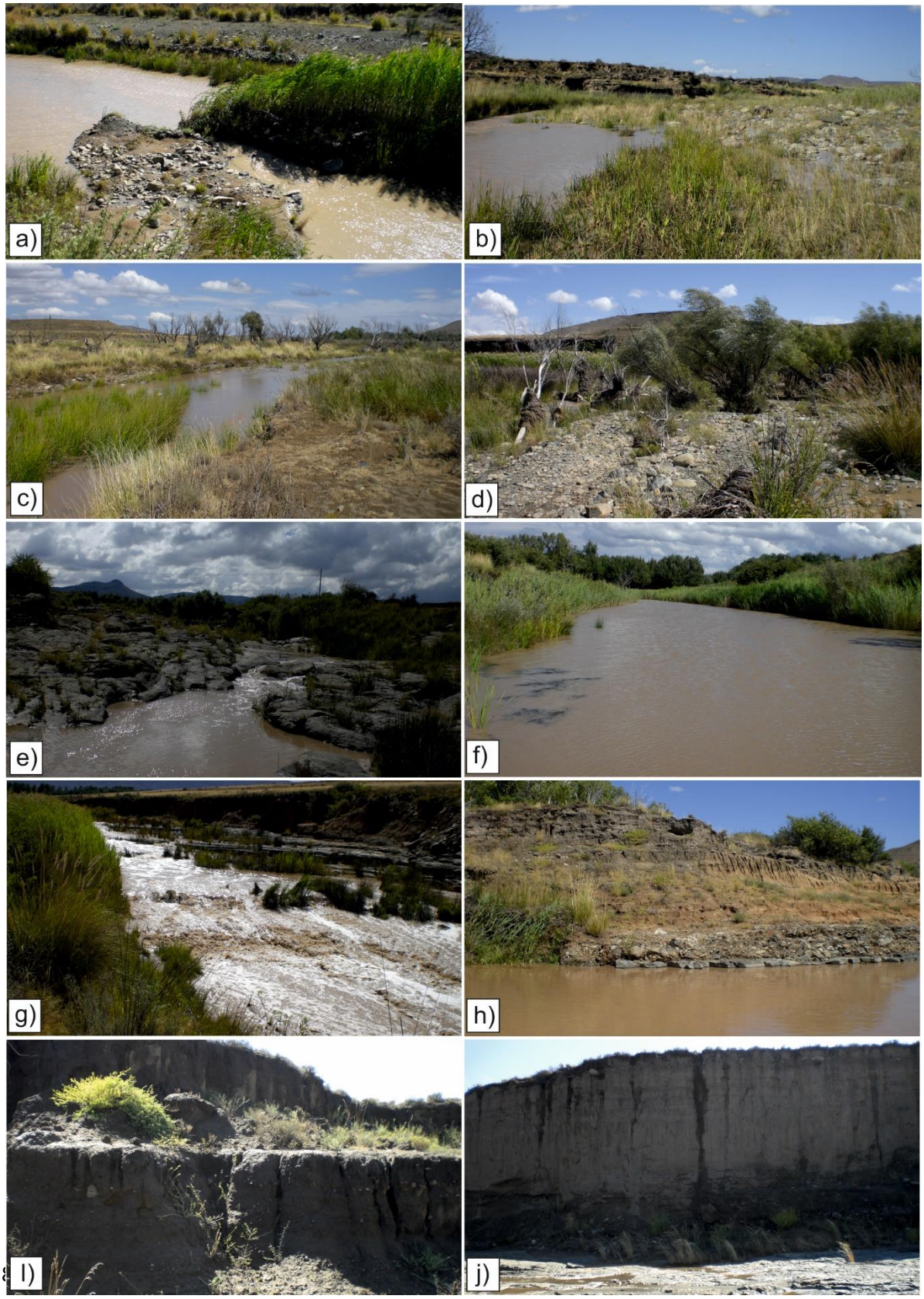

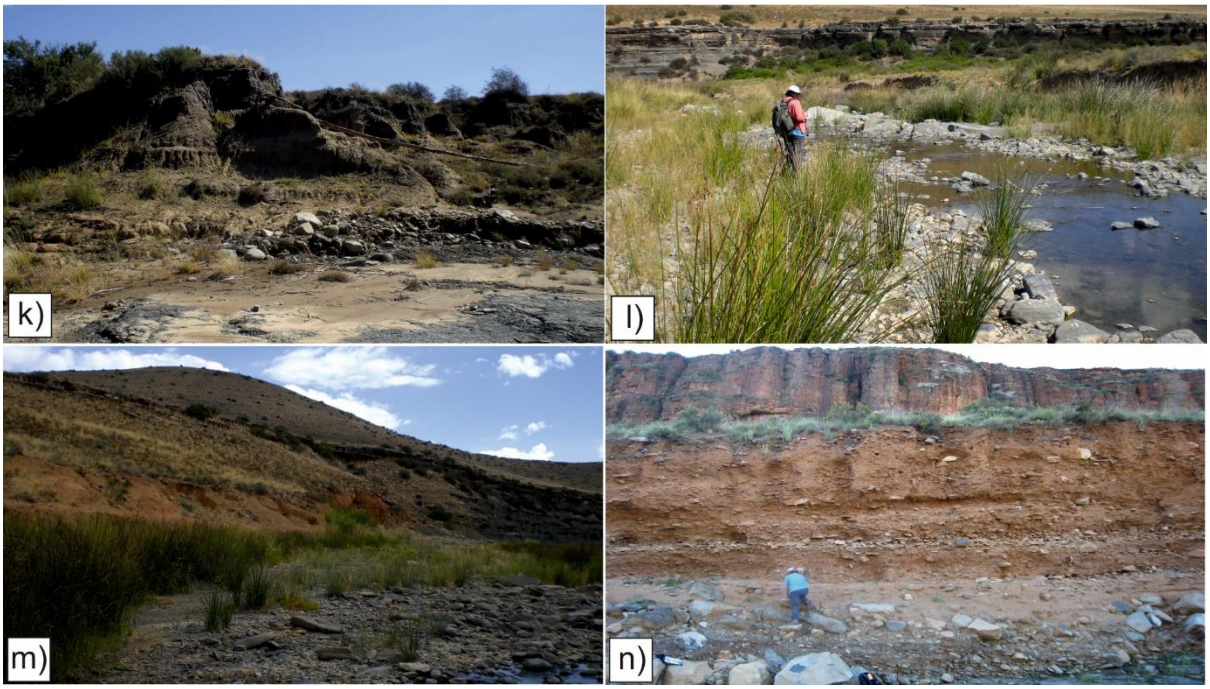

Figure 4.18 – photographs of the Wilgerbosch trunk river displayed following order reported in the text, a) channel downstream of weir, note coarse mid-channel bars; b) cobble/boulder deposits partially colonised by reeds in widest channel segments; c) dead trees with flood marks (2 m above channel); d) locally braided channel, with aggradational gravel bars upstream of dolerite intrusion; e) riffle formed on dolerite knickpoint; f) pool formed at base of dolerite sill – note the absence of coarse sediment; g) riffle formed on steepening reach upstream of deep mudstone knickpoint; h and i) rubified deposits overprinted by carbonate accumulations with inset grey deposits; j) separate inset terrace; k) slope deposits juxtaposed between deposits shown in h-j; l) example of discontinuous, denuded terrace fills in stretch of channel immediately downstream of Ganora, just upstream of bedrock-confined meander bend; m) rubified terrace fills inset within slope deposits upstream of the Ganora Gorge; n) thick slope deposits preserved within the gorge. See Fig. 4.17 for locations of photographs.

4.5: Modern analogues

From the morphologic and photographic evidence of the kinds of channel systems and their deposits, five modern analogues have been derived and linked to later chapters to guide interpretation of facies represented in terrace fills (Table 4.3).

1. Localised pockets of wetland occur at tributary confluences, where the tributary is impounded by a rock barrier, or subject to rapid loss of confinement. The pocket-like appearance of ‘grey’ fill upstream of major rock steps at Africanders Kloof and Wilgerbosch Kloof may therefore reflect palaeo-wetlands that reflect localised rather than regional geomorphic conditions.

2. Rubified terrace fills often possess a coarse basal unit immediately downstream of channel knickpoints and rock steps. These basal units may therefore reflect in situ weathering of the underlying bedrock or the products of local mass movement processes where slope-channel coupling is high.

Table 4.3 – summary of distinct contemporary deposits which may be hypothetical analogues to facies in terrace fills reported in chapters 5-7. The modern context in which these deposits occur is provided accompanied by photographic evidence from this chapter.

Analogue number	**Modern context / Figure no.**	**Depositional environment**	**Hypothetical terrace equivalent (outcrop no.)**
1	Upstream of rock steps and/or at junctions between first and second order tributary. Fig. 4.14 e, k and l.	Disconnect between tributaries and trunk due to reduced gradient and loss of confinement. Localised wetlands formed.	AK-4 inset grey fill – Ch. 5.2.6 WGB-5 – Ch. 6.6
2	Bedrock slopes at valley margin and/or downstream of knickpoints. Fig. 4.8 b and c.	In situ break-up of rock slope.	AK-7 unit B – Ch. 5.3.1. AK-16 – Ch. 5.4.2.
3	Low gradient, perennial channel reaches. Fig. 4.8f, 4.14g.	Low energy wetland reaches with deposits of sand, silt and clay.	AK-7 unit C – Ch. 5.3.1 AK-15 units D-F – Ch. 5.4.1
4	Low gradient perennial reaches upstream of sandstone or dolerite knickpoints. Fig. 4.8p, 4.18d	Aggradational wetland reaches due to base level set by rock barrier. Alternating beds of gravel, sand and mud reflecting migrating single thread channel.	AK-15 – units A-D (Ch. 5.4.1). AK-18 – Ch. 5.4.4 WGM-1 unit A-I – Ch. 7.3 WGM-2 unit F2-N – Ch. 7.4
5	Gravel-bed reaches on higher order streams. Fig. 4.8o, 4.18a.	Inversely graded coarse-fine deposits at channel margins.	AK-16 – Ch. 5.4.2 WGW – unit F – Ch. 7.2 WGM-2 unit F1 – Ch. 7.4 WGM-4 – Ch. 7.6

3. Low gradient perennial sand reaches downstream of knickpoints are commonly associated with wetland vegetation. The occurrence of vegetated inset alluvial banks reflects local aggradation. Downstream, in steeper reaches, there can be mid-channel bars. The representation of fine-grained organic rich sands and then coarse channel lag deposits within the same terrace unit may thus reflect alternating high and low energy reaches.

4. Accumulation of coarse deposits upstream of knickpoints was noted particularly in the WGM channel. The position of the channel at or just above bedrock in these reaches means that perennial flow occurs, fed from groundwater sources upstream. Due to this water supply and accretion of fine-grained deposits in zones of slackwater, a range of vegetation types (both wetland and non-wetland) have colonised bars and backwater areas. Dense areas of vegetation are frequently mantled by coarse deposits (gravels, cobbles etc) during floods. Therefore, alternating coarse deposits with gleyed, organic rich muds preserved in terrace fills may reflect localised channel braiding, with zones of slackwater being periodically inundated under conditions of stormflow.

5. Inversely graded sands, gravels and cobbles were noted at the channel margins at the base of Africanders Kloof and in the Wilgerbosch Main Channel. Gravels and cobbles were frequently accompanied by flood marks such as woody debris and/or dead trees/plants. Therefore, these sequences can reflect deposition on bars during conditions of stormflow. This facies set is distinguished from progradational features on fans that can produce inverse grading structures and are recognised in the literature (Hooke, 2004).

4.6: Conceptual model of valley filling

Rock barriers can act as major discontinuities with respect to sediment connectivity as they retard river downcutting (Tooth et al., 2004). Sections 4.2 and 4.3 documented several examples of where such discontinuities occur in the present channels, as well as evidence for possible *former* discontinuities that *may* be relevant to reconstructing the pathways and mechanisms of sediment connectivity represented in terrace fills. The following conceptual model is proposed that considers i) how sediment is generated on hillslopes, ii) the conditions under gullying may be initiated, iii) the conditions and controls by which sediment is transmitted and stored and iv) terrace development in response to changing barrier configuration across the landscape. This model is then tested using field evidence in Chapters 5-7 and discussed in Chapter 8.

The model presents a system in which aggradation and incision occur in a compartmentalised fashion (Fig. 4.19). ‘Compartmentalised filling’ means that certain reaches may aggrade and incise independently from others downstream due to

effects of disconnectivity induced by barriers of different configuration and type. Thus, geomorphic change in one part of the system may not propagate to other areas and, according to the model, may result in mappable, distinct terrace surfaces.

Fig. 4.19i and ii show two major reaches of a headwater valley delimited on the basis of two major discontinuities. i) Colluvium on the upper slope accumulates by processes of in situ weathering, slopewash and soil creep. These deposits are then incised by a gully, the drivers of which may include: 1) Slope oversteepening such that a critical threshold for incision is exceeded, 2) loss of vegetation and 3) a catastrophic flood. Headward erosion of the gully may trigger on-slope deposition in floodouts (Manjoro et al., 2012). The floodout sediments fine distally, impounded behind a rock barrier. There is no sediment connectivity between reaches 1 and 2. Aggradation of reach 2 is dependent on local supply from hillslopes, which may accumulate due to a second discontinuity downstream. ii) A second incision phase occurs as a complex response to exhaustion of colluvium on the upper slope. As before, floodout deposition occurs upstream of the discontinuity due to loss of valley confinement and slope. The 'grey' fill indicates soil development with vegetation cover which has developed as a feedback response to deposition behind the barrier. Floodout progradation buries this soil. This sequence may be analogous to the inset grey fills capped by brown sands discussed earlier. As the space behind the barrier is now filled to capacity, some limited exchange of sediment may occur between reaches 1 and 2 – permitting reach 2 to aggrade relatively rapidly in response to the next discontinuity. In these cases, well-bedded deposits would be expected upstream of the discontinuity, but absent downstream.

Fig.4.19 iii – iv demonstrates the consequences of partial breaching of the first rock barrier. Processes of gullying and floodout deposition are the same, but a reforming channel occurs downstream of the floodout. The 'green light' symbol indicates connectivity between reaches 1 and 2, but disconnectivity again (red light) at end of reach 2 due to a major rock step which induces floodout deposition (iii). As a result, backfilling occurs to produce a graded landsurface from the floodout apex all the way to the second discontinuity (iv).

The consequences of compartmentalised filling for stratigraphic evolution are that terrace fills are 1) likely to be diachronous when compared to deposits in areas

lacking discontinuities, 2) exhibit cyclical behaviour governed by changing local morphodynamics (autogenesis) rather than 3) allogenic drivers. In summary, extent of connectivity between reaches controlled otherwise by major barriers depends upon, 1) the accommodation space being filled to capacity such that the barrier may be 'overtopped', 2) circumvention or 3) incision of the barrier.

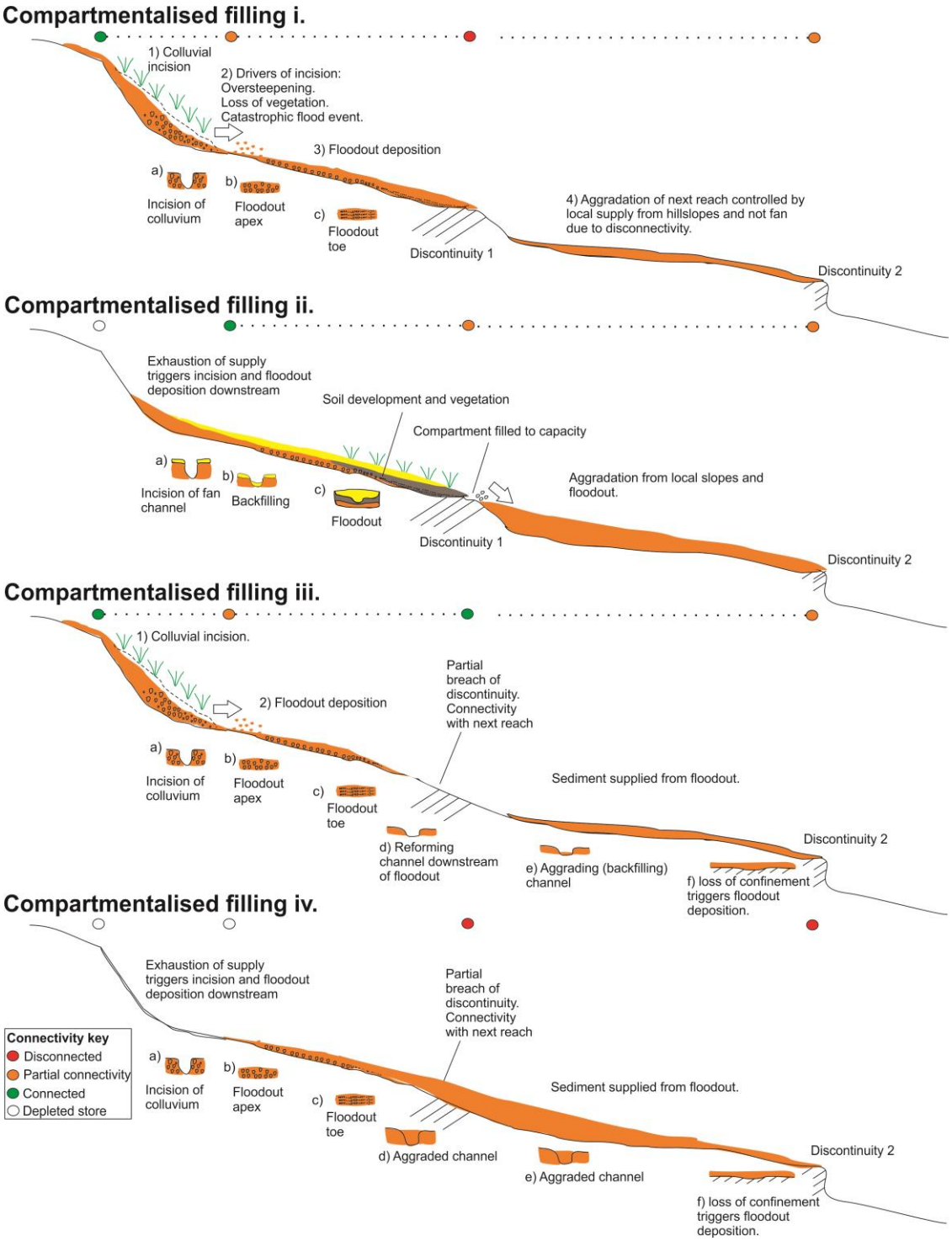

Figure 4.19 – conceptual model detailing possible mechanisms and trajectories of incision (cut) and aggradation (fill) in a tectonically stable headwater valley with geological barriers of different configuration.

Fig. 4.20 integrates the headwater system within a wider hypothetical fluvial network. Aggradation behind several discontinuities results in ‘compartmentalised’ filling (1). Soil type is primarily controlled by conditions of local drainage. The discontinuities act to block headward erosion, disconnecting these reaches from major base level changes lower down the fluvial system. The age of sediments stored behind these barriers is dependent upon: a) rates of flushing through of sediment bypassing the barrier, b) incision of the barrier.

Stage 2 depicts breaching of discontinuities 3 and 4 causing headcutting to propagate upstream. This reconnects sediment sinks with the channel network. Cross sections a-e lack the number of terraces present at f due to their disconnection from the rest of the system. Stage 3 shows a rise in base level at cross section f which triggers backfilling upstream. The subsequent incision stage (4) produces a continuous terrace. The drivers of cut and fill phases expressed at cross section f could signify a complex response to 1) the position of the trunk river on the valley floor downstream (Brierley and Fryirs, 1999; Grenfell et al., 2008), 2) loss of channel confinement downstream triggering backfilling (Schumm and Hadley, 1957; Patton and Schumm, 1983), 3) downcutting or bypassing rock barriers downstream (Tooth et al., 2004).

If the system follows a ‘backfilling’ trajectory, depending on rate of filling, the final burial age of sedimentary quartz (OSL) preserved in terrace fills would be expected to decrease upstream and be diachronous with fills impounded behind former barriers.

In summary, the conceptual model of valley filling predicts that there may be: 1) multiple phases of cut and fill recorded in some reaches but not others controlled by the connectivity of the system, 2) juxtaposition of discontinuous and continuous terraces with different modes of genesis and 3) large age differences between fills impounded behind barriers compared to those downstream subject to changing extrinsic drivers or intrinsic controls elsewhere in the system.

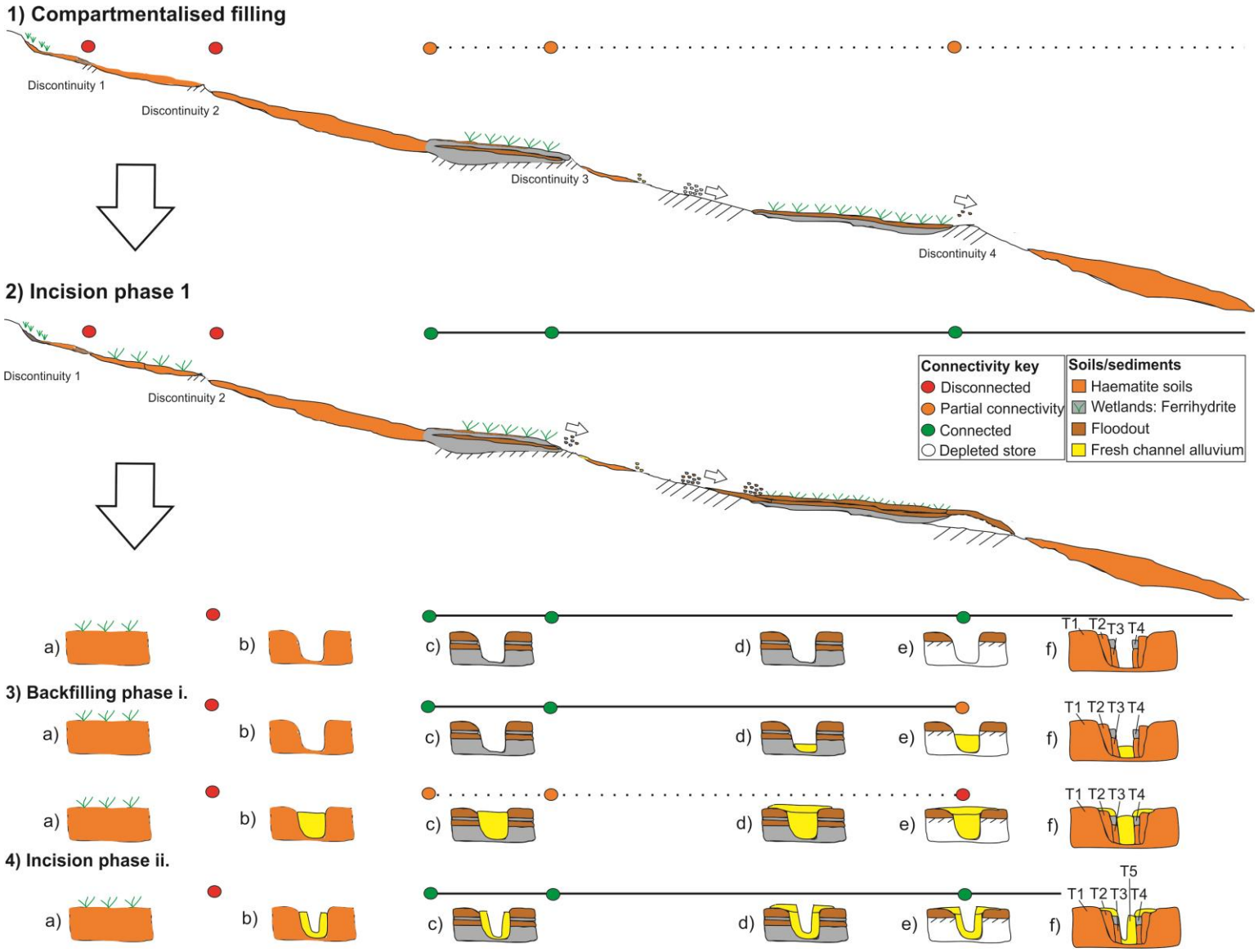

Figure 4.20 – conceptual model for wider hypothetical tectonically stable fluvial system displaying evolution from 1) system with compartmentalised filling and soil development controlled by bedrock barriers to 2) system with incision of two major barrier allowing upstream reaches to register changes in base level lower down the system.

4.7: Summary

First-order ephemeral gullies connect upland headwater sediment sources with the larger fluvial network. 2nd–4th order channels are characterised by perennial flow sourced by aquifer fed groundwater. Channel morphology is strongly determined by the occurrence and distribution of dolerite intrusions, with discontinuities in coarse sediment connectivity upstream of barriers, though many of these barriers are at least partially incised. Crucially, the juxtaposition of coarse bar deposits and zones of slackwater colonised by reeds upstream of knickpoints attests to channel thalweg migration. As a result, inter-bedded coarse-fine-coarse deposits may reflect local processes of autogenesis and not catchment wide phases of vegetation growth and soil formation. In wider valley segments, first order tributaries are commonly impounded by pockets of intact alluvium, terminating as localised wetlands flanking the channels due to transmission losses. The best preserved terrace fills occur upstream of major valley constrictions, though thick fills (up to 6 m) are preserved in the narrow, steep Africanders Kloof. Several major types of deposits have been identified across the study region. These include: 1) palaeofan sediments in headwater valley settings; 2) thick rubified fills (up to 5 m) often overprinted by up to two discrete carbonate horizons; 3) friable, grey deposits occurring as pockets, but distinctly inset within rubified terrace fills. These are in contact with bedrock in 3rd and 4th order channels; 4) brown fills inset within the rubified and grey fills present at Wilgerbosch Kloof and in segment B of the Wilgerbosch trunk river. Several analogues were derived from analysis of modern channel deposits and their position within the valleys to aid interpretation of facies preserved in terrace fills. A conceptual model detailing possible trajectories of valley aggradation was developed

The next three chapters characterise the sedimentology, pedology and stratigraphy of terrace fills, cross referencing as appropriate with the examples of the modern channel systems and their deposits presented in this chapter. This evidence is used to test the conceptual model of valley cut and fill, the synthesis of which is presented in chapter 8.

Chapter 5: Results ii: Sedimentology and pedology of valley fills – Africanders Kloof

5.1 Introduction

This chapter presents detailed analytical evidence of the sedimentological and pedological characteristics of the valley fills at Africanders Kloof. The analytical sections present the following: 20 sediment logs (see ch. 3 for log template and codes), sedigraph data from Coulter laser measurements, mineral magnetic data, valley and channel-cross section morphology, results of thin section analysis on crucial soil horizons, selected XRF-geochemical proxies, geochronological (OSL) and loss on ignition data. These are used to characterise the sediments in detail and then to interpret their depositional process and evaluate mode and intensity of soil formation. The nature of bedding contacts in concert with soil magnetics evidence is used to determine which contacts are unconformities signalling prolonged hiatuses in the sediment cascade and the sequence of events preserved within each section is interpreted. These principal lithostratigraphic units are used to reconstruct former extents of palaeo-landforms (fans, channel systems etc) which are then discussed in terms of morphostratigraphic relations in the final synthesis chapter (8).

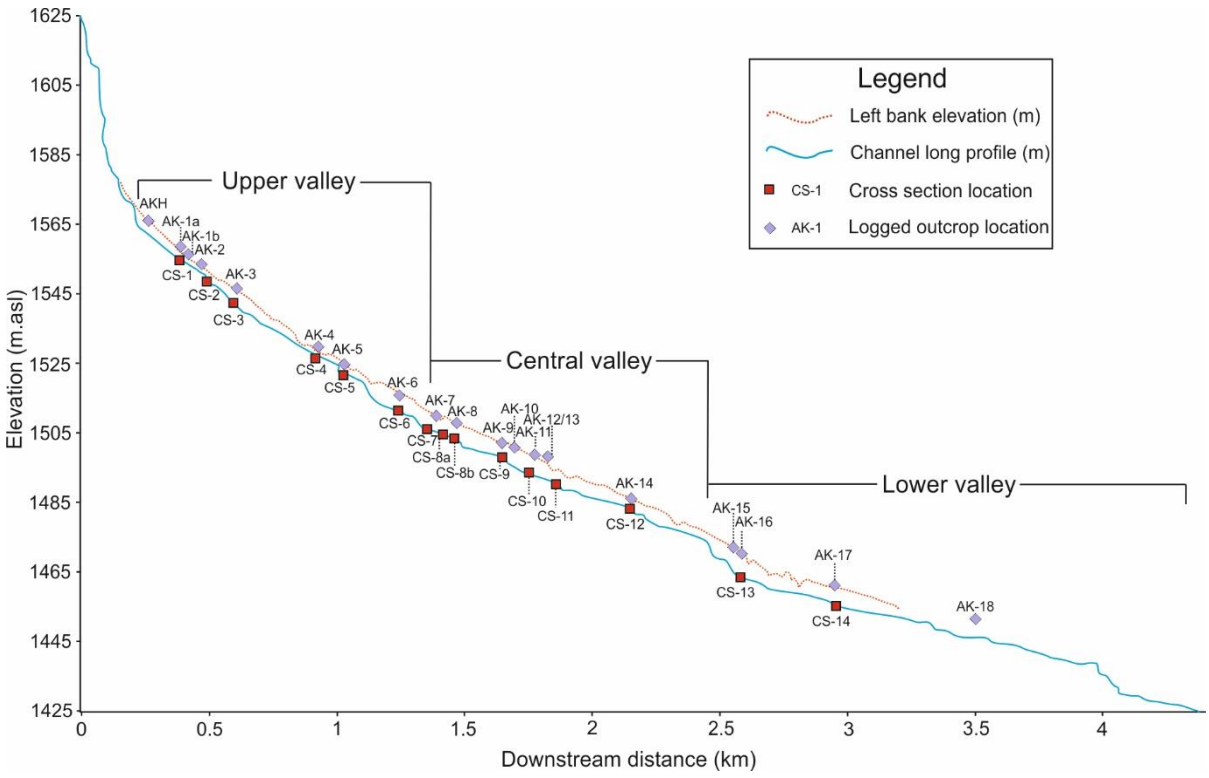

Figure 5.1 – valley long profile for Africanders Kloof tributary highlighting sediment outcrop locations and valley cross sections analysed and discussed in the text.

The following analysis of the AK valley is divided into three components: 1) Upper valley (AKH–AK-6). This stretch of valley includes the first order gully and its confluence with the second order tributary after AK-5 (see section 4.2); 2) Central valley (AK-7–AK-14). The basis for this division is the major sandstone knickpoint (no. 4 – see Fig. 4.4, section 4.2) just upstream of AK-15; and 3) Lower valley (AK-15–18).

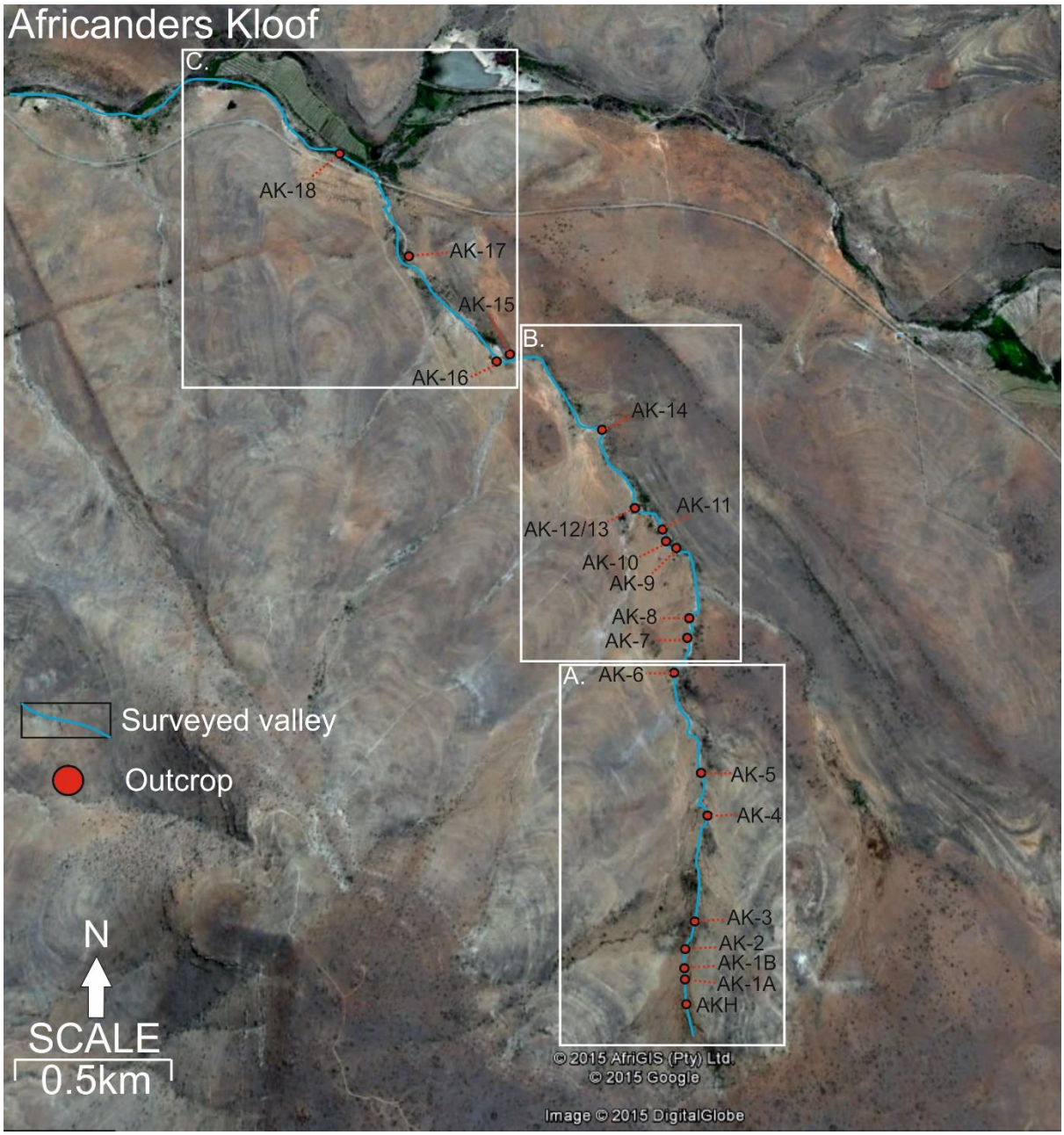

Figure 5.2 – Google Earth satellite imagery of Africanders Kloof. Note subdivision of valley as stated in text.

5.2 Upper valley: AKH – AK-6

5.2.1a AKH analysis

Log AKH was obtained from a 2.4 m gully sidewall in the upper headwaters of Africanders Kloof (Figure. 5.1, 5.2 and 5.3).

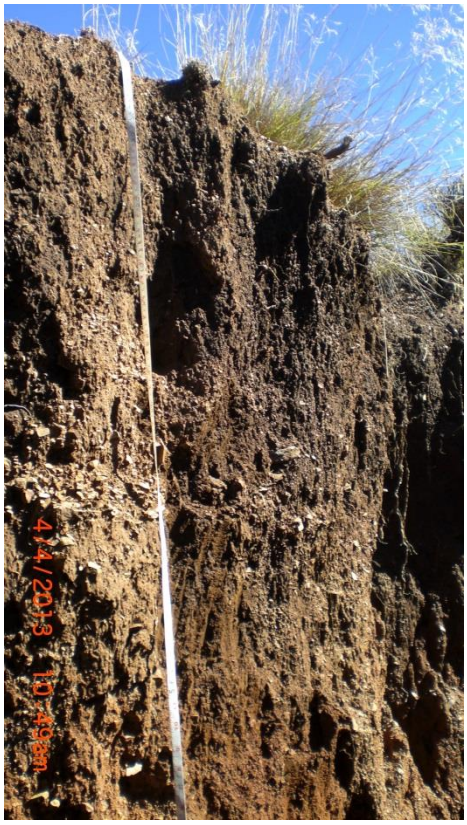

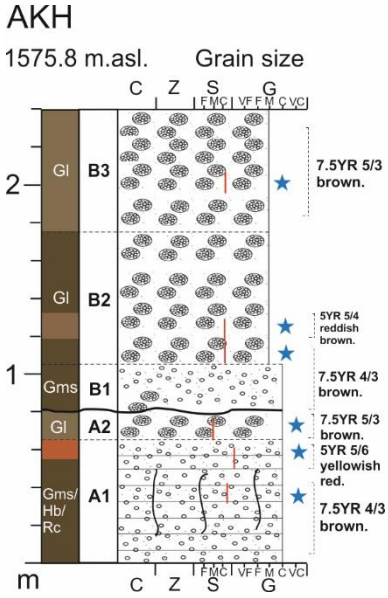

Figure 5.3 – sedimentary log and photo of outcrop AKH (see Fig. 3.4 for key).

Subunit A1 (40-50 cm) consists of thinly bedded matrix-supported angular gravels (Gms). Median grain size of the matrix is 313 µm (10.5% medium sand) with two secondary modes of fine sand and silt. Collectively 42.3% of this sample consists of coarse to very coarse sand (Fig. 5.4a). Illuviated silts occur in root channels. Loss on ignition values are slightly higher at the base (2.5%) compared to the top (55-65 cm) of the subunit (1.43% - Table 5.1), where a marked colour change from 7.5YR 4/3 brown to 5YR 5/6 yellowish red occurs. The structure of the soil is crumbly, with weakly developed blocks up to several cm in diameter. Combined coarse to very-coarse sand content is substantially higher (74.5%) at 55-65 cm compared to 40-50 cm (Fig 5.4a-b). The top of the subunit (55-65 cm) is also marked by a large reduction in most of the concentration related magnetic proxies (see unit A1-B Fig.

5.5a) - χ_{LF} drops from 162 to 69. In contrast, granulometric magnetic proxies are comparable to 40-50 cm, but the S values peak at 55-65 cm with 19% and 3.3% of the applied remanence unreversed at -100mT and -300mT, respectively (Fig. 5.5c). χ_{LF} obtained for each of the five different particle size fractions (Fig. 5.6) exhibits two distinct peaks in the fine (0-4µm) and coarsest (32-63µm) fractions. IRM_{1T} increases with particle size (Fig. 5.6a) whereas X_{FD}%, $X_{ARM/\chi LF}$ and $X_{ARM/IRM1T}$ decline with increasing particle size (Fig. 5.6b). The clay fraction possesses a small hard component (S_{-300}% - 1.6%), whilst S_{-100}% peaks for the 4-8 and 8-16µm fractions (17 and 18%, respectively – Fig. 5.6c).

Subunit A2 consists of lenticular (few cm - dms) clast-supported angular gravels with some interstitial coarse sands (Fig. 5.3). The lenses occur in an otherwise weakly stratified, very poorly sorted package of very coarse sand and minor gravels. Median grain size of the matrix is 261.4 µm (10% medium sand) with a large coarse to very-coarse sand component (40.6%- Fig. 5.4c). The magnetic properties of subunit A2 are virtually identical to the base of unit A1 (Fig. 5.5).

An undulating, erosive contact separates subunits A2 and B1 (80 cm, Fig. 5.3). Subunits B1 and B2 consist respectively, of medium and fine lenticular clast-supported gravels within a poorly sorted matrix of sand. Colour is typically 7.5YR 4/3 brown, but locally varies (5YR 5/4 reddish brown at 120-130 cm – Fig 5.3). The soil is characterised by a friable, weakly developed crumb structure.

Table 5.1 – percentage loss on ignition and bromine (ppm) data for sampled horizons at AKH.

Unit	Height (cm)	Loss on ignition (%)	Bromine (ppm)
A1	40-50	2.5	24.9
A1	55-65	1.4	1.8
A2	70-80	2.5	15.8
B2	110-120	3.0	16.3
B2	120-130	1.4	13.0
B3	195-205	1.7	22.2

The matrix of B2 is much coarser (35.8% - 37.5% very coarse sand- Fig. 5.4d and e) and slightly better sorted than unit A2. The magnetic properties of the base of subunit B2 (110-120 cm) are indistinguishable from A2, but a large reduction in

susceptibility occurs at 125-135 cm akin to 55-65 cm discussed earlier (Fig. 5.5). Subunit B3 is distinguished from B2 on the basis of more continuous areas of gravel amidst lenses comparable in character to those below (B2). The matrix of subunit B3 is slightly coarser than B2 (42.1% very coarse sand) with a slight change in colour to 7.5YR 5/3 brown (Fig. 5.3 and 5.4f). The soils of units B2 and B3 exhibit crumb structure (5-10 mm). The magnetic properties of subunit B3 are similar to the base of subunit B2, but enhanced in terms of χ_{FD}% and $X_{ARM/IRM1T}$ (Fig. 5.5c).

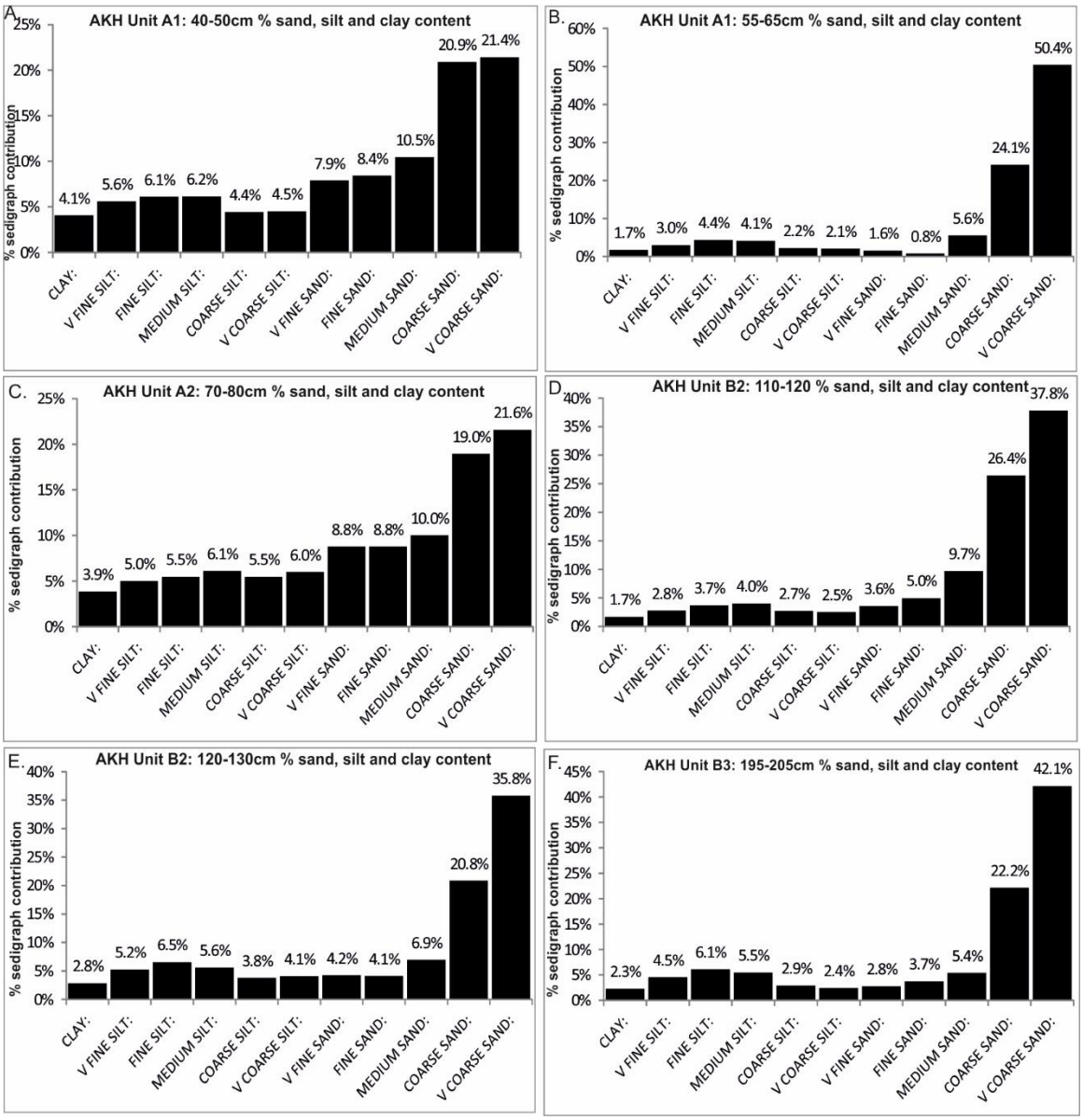

Figure 5.4 – % sand, silt and clay content derived from Coulter grain size analysis on samples collected from outcrop AKH.

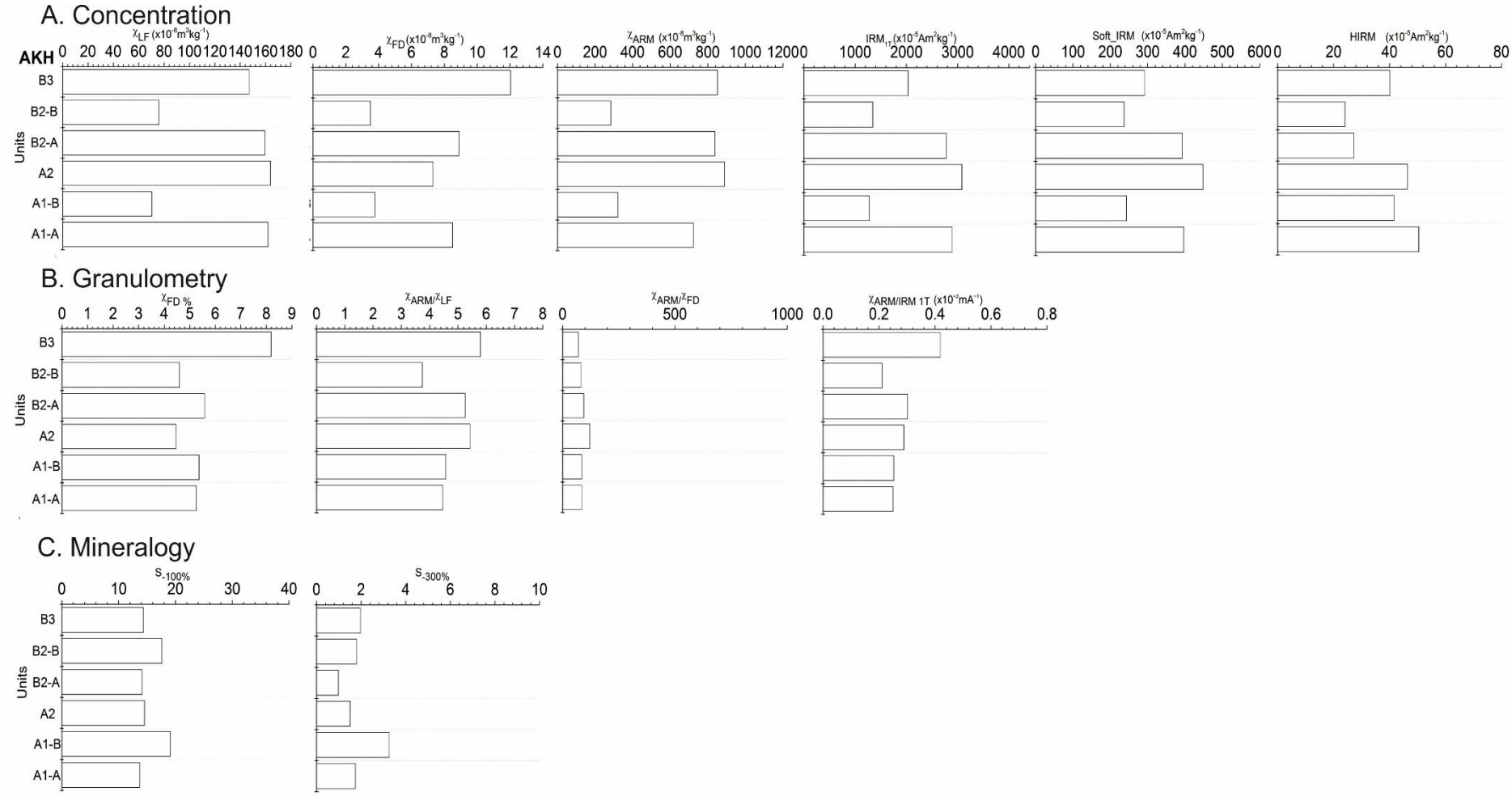

Figure 5.5 – mineral magnetic parameters from outcrop AKH.

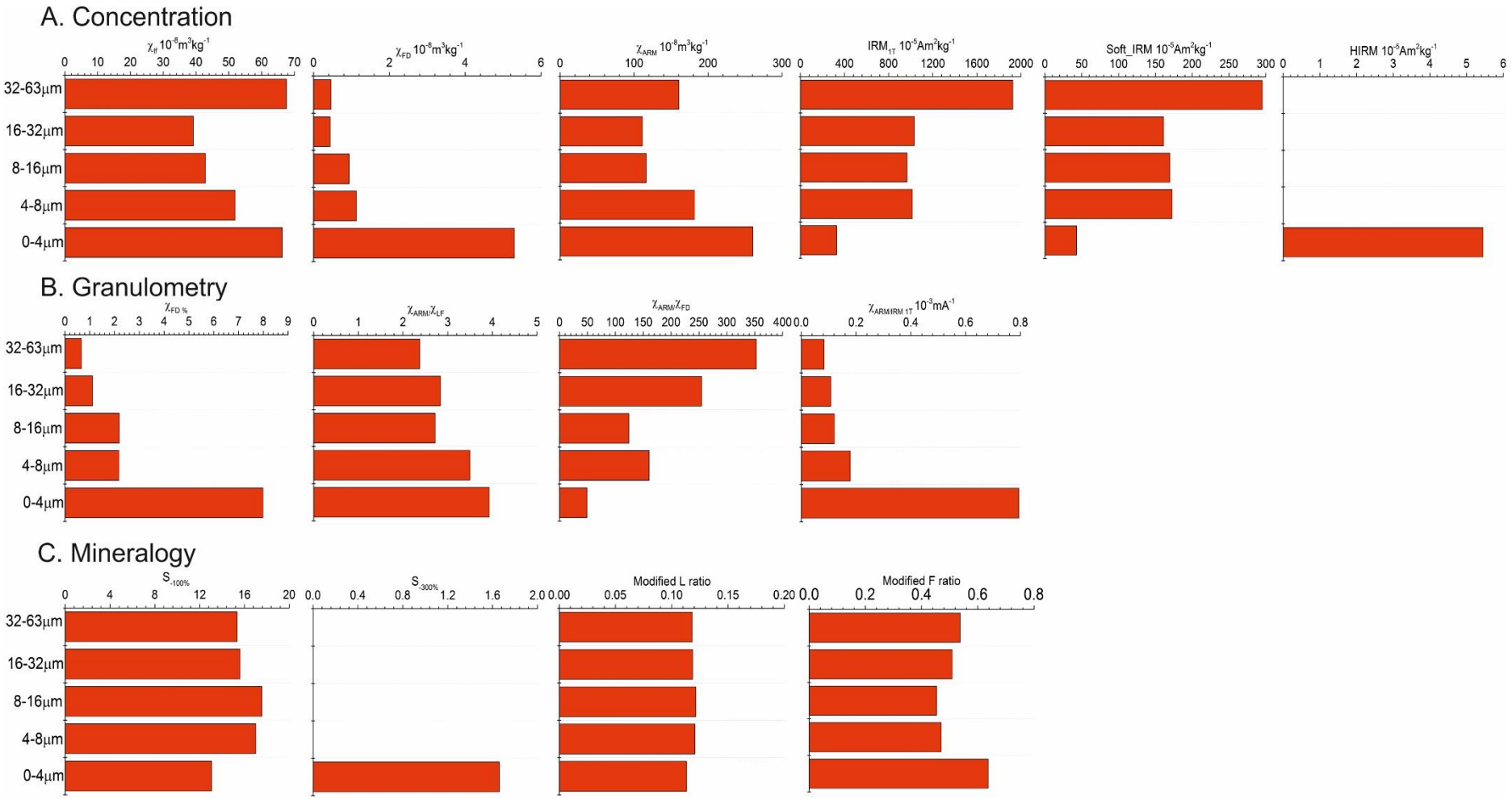

Figure 5.6 – mineral magnetic parameters from AKH unit A1 (55-65cm) obtained for five particle size fractions.

5.2.1b: AKH interpretation

The local valley morphology favours deposition in the form of a floodout. There is an abrupt reduction in slope after 200 m and a switch from a confined hillslope gully (Fig. 5.1), to a relatively unconfined valley floor. Floodouts have been found in the adjacent tributary at the base of the upper slopes where the valley locally widens. This occurs as a relatively narrow, lobate sediment body with convex surface topography.

The horizontally bedded nature of the deposits represented in unit A implies deposition by currentflow. The coarse calibre of gravel implies deposition under upper-flow regime conditions. Individual bed thickness (7-8 cm at most) is too low to infer deposition by debris or mudflow processes. In the context of sedimentation processes on alluvial fans, Sharp and Nobles (1953) noted thickness of individual debris flow units as being up to several dms thick and that clasts may be orientated vertically depending on the plasticity of the flow. Bull (1964a and b) noted that mudflow deposits on fans typically exhibited significant clay infillings (up to 31% of the sedigraph) of inter-granular voids - an order of magnitude above that observed for unit A1. Rather, the very-poorly sorted matrix of sandy silt here (Fig. 5.4a) reflects a combination of two distinct processes: 1) Interstitial filling of the gravels during the recessional phases of flow and 2) illuvial contributions of silt, clay and fine sand. Evidence for the latter is found in the form of infilled root channels, the presence of weakly developed blocky soil peds and the relative depletion of fines above (55-65 cm – Fig. 5.4b). The exceptionally high bromine content (24.9 ppm) at 40-50 cm is probably due to illuviation, hence the anomalously low concentration at 55-65 cm (1.8 ppm). The sheet-like stacking of individual beds is interpreted to indicate sheet-flood deposition due to widening of flow into a shallow braided area. This implies that the facies represent the transition from an entrenched to an unconfined or ‘terminal’ channel permitting flow spreading (Grenfell et al., 2014). Relatively slow rates of aggradation are implied by the low bed thickness (compared to above units), which can be characteristic of the distal margins of terminal distributary channels (Grenfell et al., 2012).

The dissection of the bedded gravels (subunit A1) by lenticular clast-support gravelly sands (subunit A2) implies the latter stages of sheet-flow, where it separates into small channels which incise the underlying sediment sheet (Bull, 1972).

The massive nature of the gravel unit (B1) indicates high energy conditions of flow with scour and fill structures at the base. The lenticular gravels and sands above (units B2 and B3) evidence further scour-fill structure consistent with channelized flow and reworking of previous channel deposits (Collinson, 1996). The notable drop in %silt/clay content (relative to unit A2) may indicate depletion of fines from nearby hillslopes, or that fines were preferentially transmitted downstream resulting in proximal-distal fining.

χ_{LF} values ranging from 69-166 indicate very high concentrations of ferrimagnetic minerals, further supported by the typically very high χ_{ARM} and IRM_{1T} values. Values for $\chi_{FD}\% > 4$ indicate moderate to high concentrations of fine-viscous super-paramagnetic grains for each unit. Thus, with the exception of unit B2-B (120-130 cm), all units would plot within Oldfield and Crowther's (2007) "pedogenic envelope". As outlined in Chapter 3, the suitability of this plot and associated granulometric quotients is tested following the recommendation of Oldfield (1991).

Only three samples plot above the threshold for <0.07 μm SP/SD grains, whilst the majority plot below but with highly varied $\chi_{FD}\%$ including all of the AKH samples (Fig. 5.7). Thus, only 3/69 are suitable for the bilogarithmic plot (Oldfield and Crowther, 2007), despite the fact that n=28 plot within the 'pedogenic envelope', and of the AKH samples, only unit B2-B (120-130 cm) plots outside (Fig. 5.8).

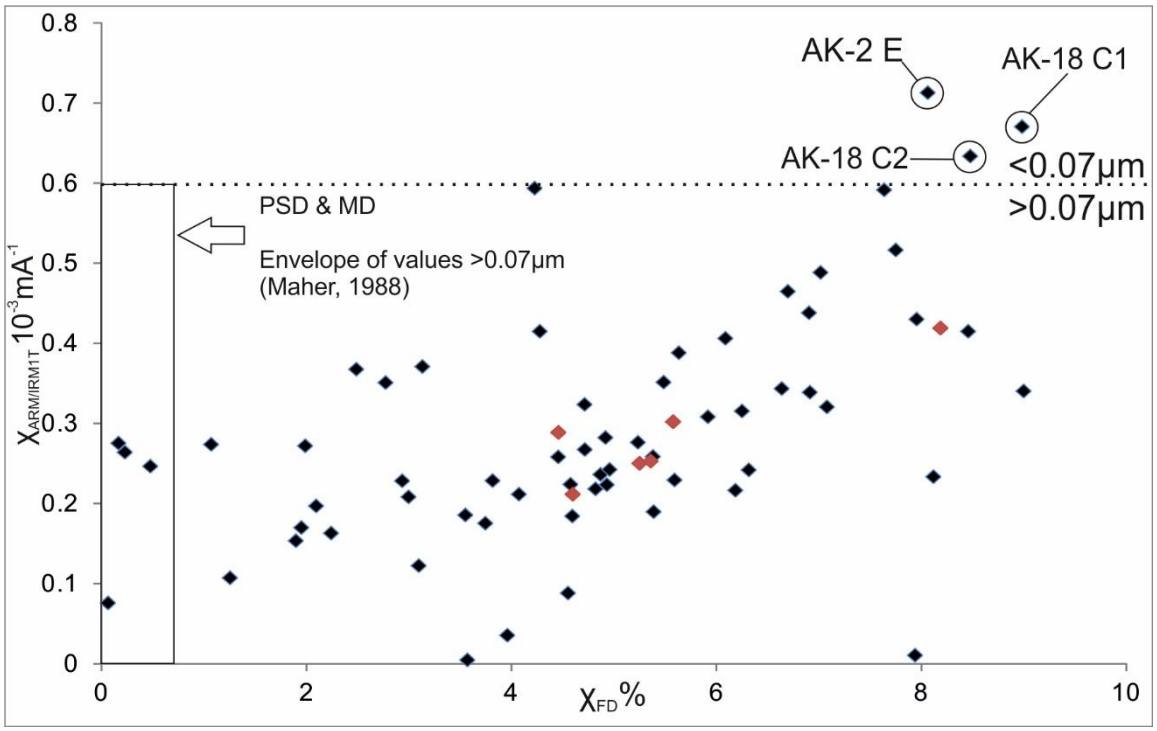

Figure 5.7 – bi-plot of χ_{FD}% versus $\chi_{ARM/IRM1T}$ for entire Africanders Kloof dataset (see appendix A). Samples from AKH are highlighted in red. Note n=3/69 samples plot above 0.6 x 10^{-3} mA^{-1} – the cut off for between coarse PSD/MD grains >0.07 µm and SP/SSD grains <0.07 µm.

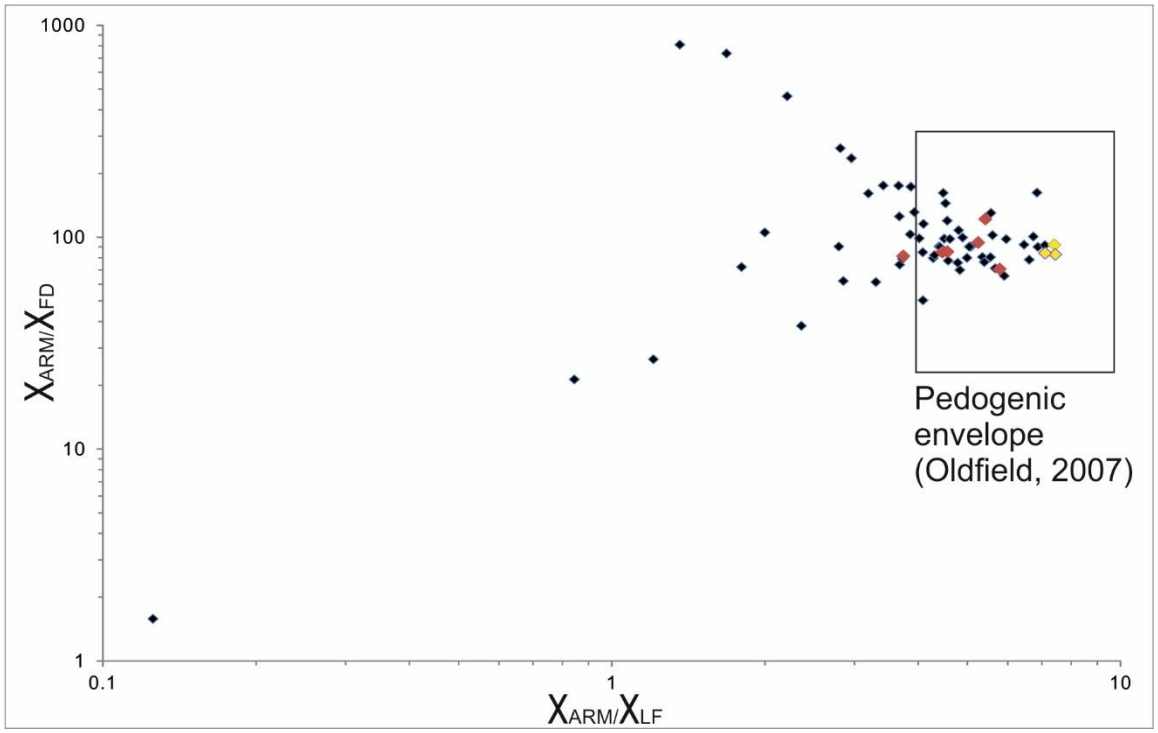

Figure 5.8 – bilogarithmic plot of the quotients χ_{ARM}/χ_{LF} and χ_{ARM}/χ_{FD} for the entire Africanders dataset, with AKH samples (red diamonds) and samples which exhibited $\chi_{ARMIRM1T}$ values >0.6x10^{-3} mA^{-1} (yellow diamonds).

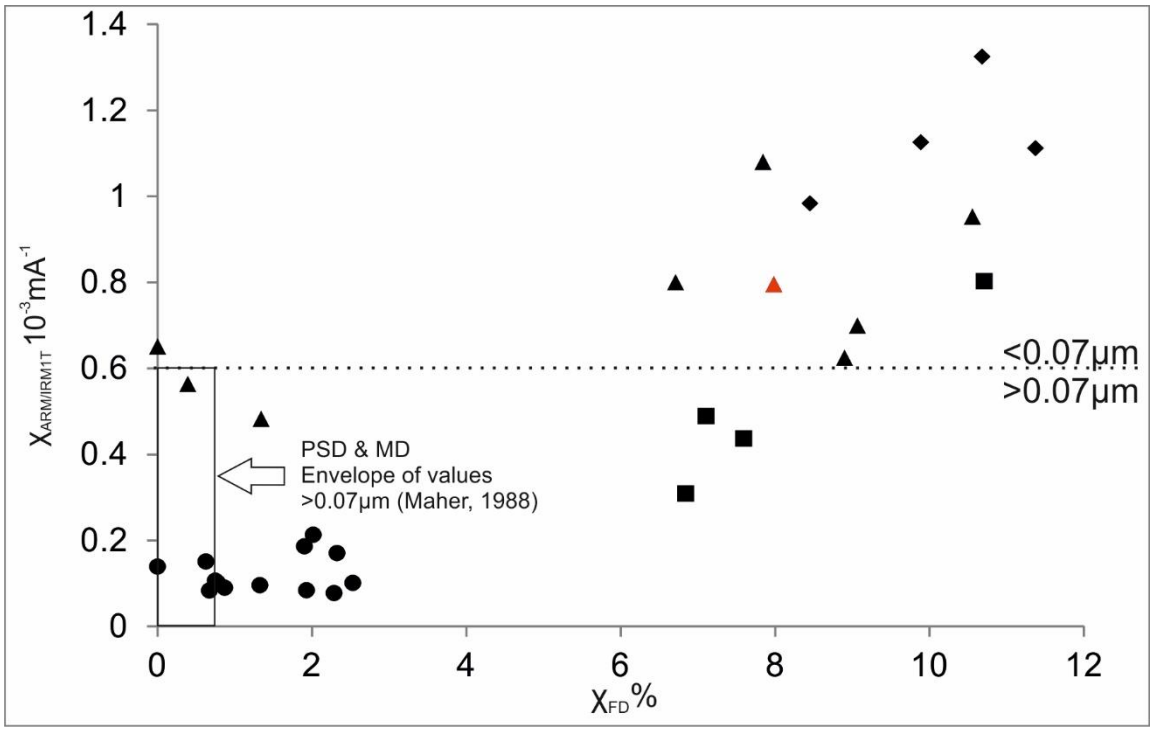

Figure 5.9 – bi-plot of χ_{FD}% versus $\chi_{ARM/IRM1T}$ for particle sized extracts (diamonds = 0-2µm; squares = 2-4µm; triangles = 0-4µm; circles = 32-63 µm) from a subsample of the Africanders dataset (n=13). AKH unit A (55-65 cm) is highlighted in red. Note the clear distinction between the coarse and finer grades.

Where particle-sized specific fractions from a sub-sample (n= 12/69) are considered, the clays, very fine silts and coarse silts show very good discrimination on the basis of magnetic grain size assemblages below and above the SD/PSD limit respectively (Fig. 5.9). Two distinct ferrimagnetic components are evident – one of pedogenic origin concentrated in the clays (high $\chi_{ARM/IRM1T}$ and χ_{FD}%) and one of lithogenic origin concentrated in the coarse silts, characterised by a form of multi-domain magnetite.

A review of Fig. 5.6 (AKH unit A: 55-65 cm) further testifies to a strong remanence carrying multi-domain ferrimagnetic signature in the 32-63 µm fraction with total ferrimagnetic concentration equalling, if not slightly exceeding that contained within the distinctive pedogenic mode (0-4 µm). When relating these patterns to the bulk magnetic susceptibility data (0-63 µm), it is clear that the strong-remanence carrying MD lithogenic magnetite component dilutes the pedogenic component expressed as low $\chi_{ARM/IRM1T}$ and relatively low χ_{FD}% (bulk = 5.4% - Fig. 5.5b) – verified by comparison the 0-4 µm clay fraction where both parameters clearly signify SP/SD dominated assemblages (Fig. 5.6). This re-affirms that for these soil samples, only the clay fraction is suitable for analysis and interpretation of SP/SD ferrimagnetic

composition via the bi-log plot (Fig. 5.9). The strength of the χ_{FD}% signature for interpretation of the bulk samples is thus the most reliable proxy for concentration of pedogenic clays, whereas the $\chi_{ARM/IRM1T}$ is most sensitive to lithogenically derived MD grains.

Thus, it follows that two forms of magnetite are under consideration: primary authigenic magnetite (Fe_3O_4) contained within the host (predominantly dolerite) rocks now exposed at the surface and secondary magnetite relating to weathering and pedogenesis. Characterising the degree of in situ pedogenesis and weathering is further complicated by the time that the regolith resided on the hillslopes before arriving at the valley floor. Dolerite weathers to rounded corestones through hydrolytic weathering reactions and exfoliation, with slope regolith commonly accompanied by ferruginous sands (Holmes et al., 2003). Thus, the pedogenic ferrimagnetic signature is partly inherited from the proximal slopes.

Taken collectively, all sedimentary units at AKH indicated by magnetic proxies indicate intense weathering, yet the evidence for in situ soil formation (soil blocks, root traces, illuviated silts/clays, iron mottling) is restricted mainly to unit A. The overall degree of pedogenic development of the units above is low. Nevertheless, the top of subunit A1 is characterised by a distinct reddening (5YR 5/6 yellowish red), reduced χ_{LF} and crucially the highest S_{-300}% values from the bulk magnetic measurements. The same is true for subunit B2 (120-130 cm – 5YR 5/4 reddish brown). This implies the reduction in susceptibility is related to higher concentrations of canted anti-ferromagnetic minerals such as pedogenic haematite at the expense of some of the original inherited magnetite. However, for subunit A2, the fact that this occurs beneath an unconformity (80 cm) indicates that haematite formation was most likely in situ and thus signifies an incised palaeogeomorphic surface. In this regard, the top of this stratigraphic unit represents a hiatus of floodout sedimentation of sufficient duration to permit soil formation. This is reinforced by the relatively high soil organic matter content reflected in the bromine values at subunit A1. Assuming that the S_{-100}% is indeed a rough proxy for degree of pedogenic haematite (following claims of Liu et al., 2015), the peak of 16% in the fine-intermediate silt grades (4-8 and 8-16 μm) could be due to the development of in-situ weathering rinds on larger grains. However, Coulter granulometry measurements on the 4-8 μm silt fraction

indicated that the true grain size of the siphoned extracts is broad, with some clay even in the coarsest grade (Table 5.2). As a result, the re-surgence of χ_{FD}% and S values in the intermediate and coarsest grades respectively has no environmental significance.

Table 5.2 – D_{10}, D_{50} and D_{90} grain size (µm) parameters obtained for [1]4-8 µm and [2]32-63 µm from the AK sub-sample set. Note that measured clay% is provided for the 32-63 µm extracts.

Outcrop	Unit	$^1D_{10}$	$^1D_{50}$	$^1D_{90}$	$^2D_{10}$	$^2D_{50}$	$^2D_{90}$	%clay
AK-1	A	2.1	5.7	13.7	29.9	52.2	78	1.9
AK-1	E1	2.1	5.8	14	26.5	47.8	74	1.5
AK-1	F1	2.9	10.5	39.1	26.1	47.8	74.5	1.5
AK-2	B	1.9	5.6	12.5	27	47.8	72.8	1.5
AK-2	E	2.9	10.8	45.9	24.5	45.8	71.9	1.6
AK-2	F2	2.9	10.7	41.3	26.8	49.2	76.8	1.4
AK-7	B	1.9	6.6	17.8	40.8	61.6	88.2	0
AK-9	A	1.9	5.3	11.8	26.3	47.8	74	1.5
AK-9	B2	1.9	5.5	13.8	26.2	47.5	73.4	1.5
AK-9	D	2.7	7.8	40.1	27.3	48.2	74.4	1.5
AK-12	A1	2.2	6.9	60.3	29.6	49.6	74	1.4
AK-12	B3	1.9	5.9	10.8	26.9	46.6	71.3	1.5

The significance of the S_{-300}% for 120-130 cm is less clear on two grounds: 1) the fact that no obvious unconformity otherwise used to infer depositional hiatus (local or otherwise) occurs above, 2) there is no distinctive change in soil structure or bioturbation to give clear soil horizonation. Compared to subunit A1 (55-65 cm), bromine is much higher (13 ppm), but there is little evidence for local eluviation of silt/clay. Its similitude with subunit A1 in terms of ferrimagnetic granulometry implies that the change in S_{-100}% is not to do with a shift in ferrimagnetic grain size but rather signifies inherited pedogenic haematite (Thompson and Oldfield, 1986).

Finally, the enhanced χ_{FD}% values obtained from subunit B3 most likely relate to enhanced wetting/drying at the soil surface permitting the development of pedogenic maghemite (Torrent et al., 2006). In the absence of clear palaeogeomorphic boundaries, 80-240 cm (Unit B) is assigned as local stratigraphic member B.

5.2.2a: AK-1A analysis

Log AK-1A was obtained from a 2.4 m gully exposure 387 m downstream from the headwaters (Figure 5.1, 5.2 and 5.10).

Unit A consists of subangular well sorted gravel lenses which populate a bimodal silt/coarse sand matrix. Total magnetic susceptibility is high (χ_{LF} = 85), but the χ_{FD}% is lowest (3.8%) accompanied by very low $\chi_{ARM}/_{IRM1T}$ (0.18 – Fig. 5.12). Highest $S_{-100\%}$ values are found for this unit with 17.5% of the applied remanence unreversed at -100mT (Fig. 5.12c). Unit B consists of matrix-supported subangular gravels, unconformably overlying unit A and differing substantially in colour (5YR 5/4 reddish brown). Unit C1 consists of clast-poor bimodal sands and silts with root channels, which transitions to clast supported, moderately sorted gravel lenses within a silty sand matrix (C2).

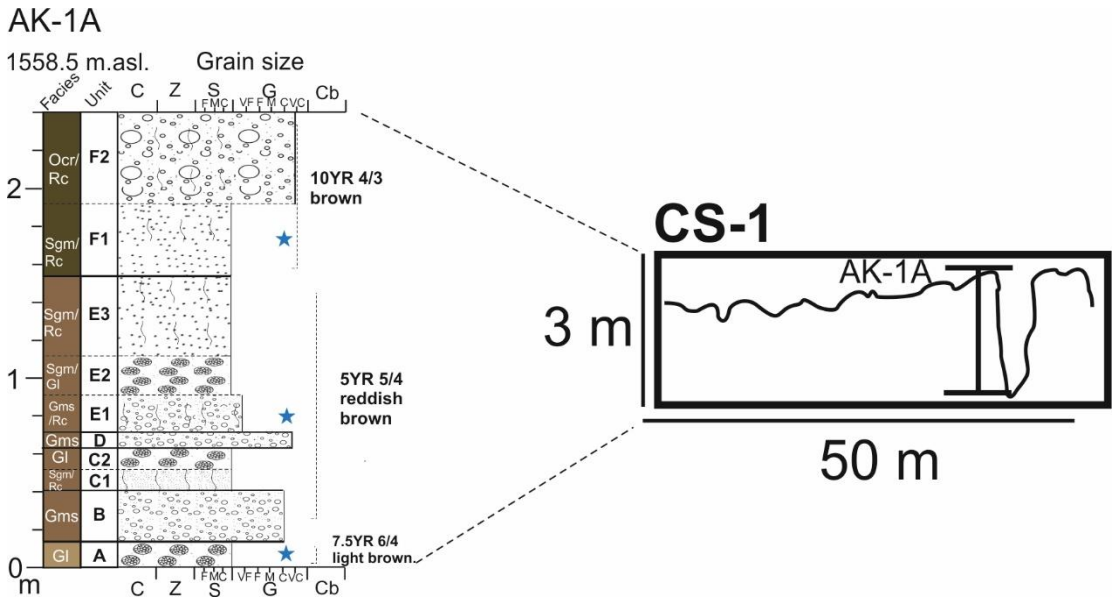

Figure 5.10 – sedimentary log AK-1A and cross section.

A sharp contact punctuates unit C2 and D. Unit D consists of predominantly clast-supported laterally discontinuous gravels, which laterally grades to gravel. Unit E1 marks an abrupt transition back to bimodal very coarse sands and silts with occasional angular gravel clasts, that coarsens slightly back to matrix-supported (coarse sand) lenticular gravels (E2). The lenses pinch out to leave a generally massive matrix of coarse sand and local minor gravels which comprises unit E3. The soil for units A-E exhibits crumb structure.

Unit F1 displays a slight coarsening in modal clast size (very coarse sand) and a distinct colour change (10YR 4/3 brown). The soil exhibits a weakly developed blocky structure that is friable. This unit exhibits strong magnetic enhancement, reflected predominantly in the χ_{LF} (149), χ_{FD} (12.6) and χ_{ARM} (995 – Fig 5.12a). The

granulometric proxies (except χ_{ARM}/χ_{FD}) also show distinct enhancement (Fig. 5.12b), but the mineralogical proxies are the same (Fig. 5.12c). Unit F2 is a massive, very poorly sorted matrix-supported gravel units. Both sub-units are extensively bioturbated through activity of roots and illuviation of silt.

Figure 5.11 – photograph of outcrop AK-1A

For units A and E1, the coarse grade (32-63μm) exhibits the highest χ_{LF} and IRM_{1T} values followed by the clay grade which also exhibits the highest values of χ_{FD}%, χ_{ARM} and $\chi_{ARM/IRM1T}$ (Table 5.3). Furthermore, S_{-300}% typically peaks in the clay grade for all samples, although values of 5.6% in concert with high S_{-100}% (20%) were obtained for the medium silt fraction (8-16μm) from unit E1. Unit F1 by contrast exhibits substantially higher χ_{LF} values for the clay grade (221.1), with over a 50% reduction in the coarsest grade (104.8).

From this data, it is clear that the $\chi_{ARM/IRM1T}$ is biased heavily by the high values of IRM_{1T} yet low χ_{ARM} in the coarse grade (32-63 μm) such that the signature of the finest grade is underestimated. Similarly, the χ_{FD}% is underestimated due to the very low values in the intermediate-coarse fractions. This is particularly the case for unit A, where 9.9% was obtained for the 0-2 μm fraction yet only 3.75% was registered for the bulk.

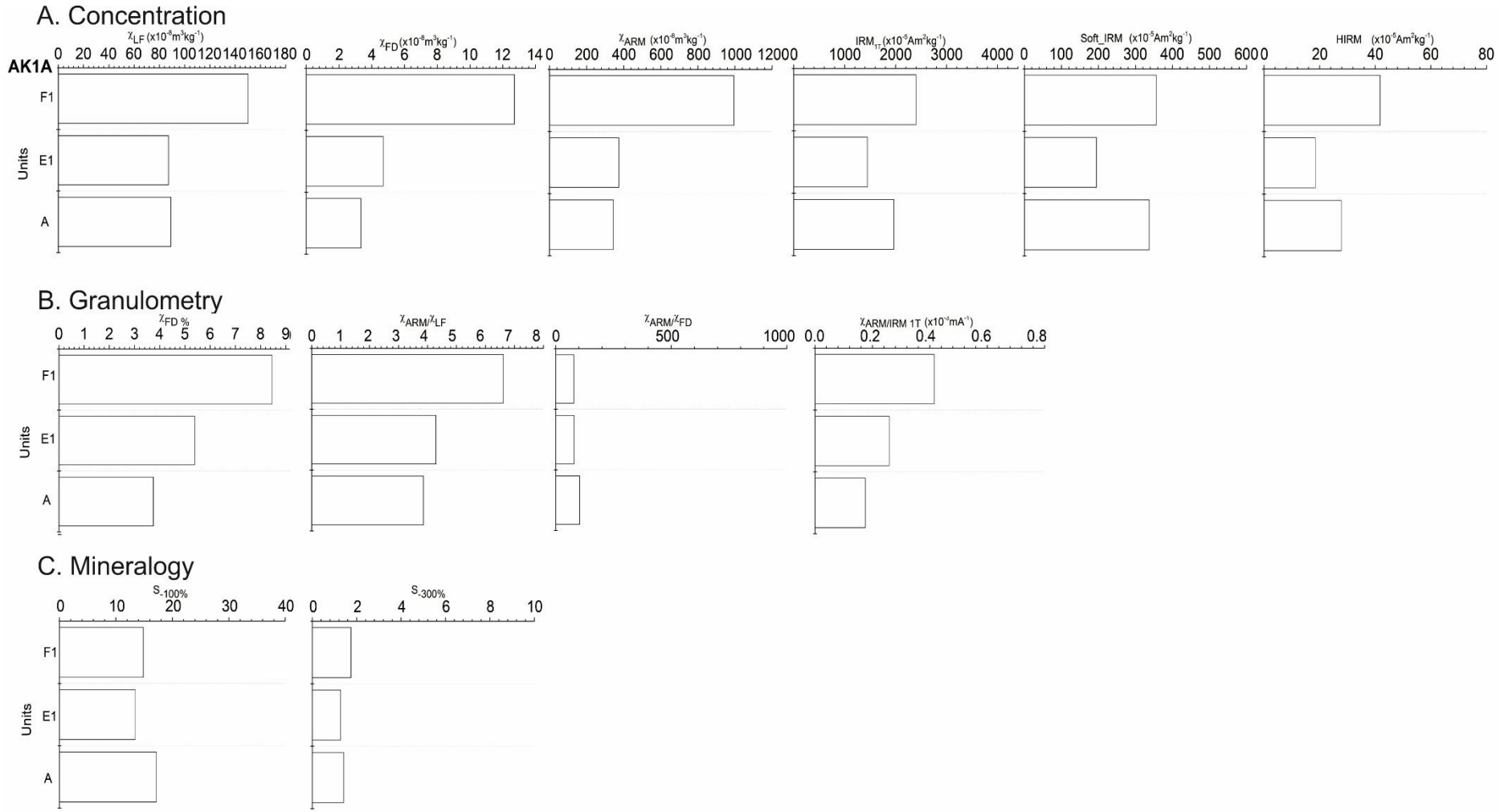

Figure 5.12 – mineral magnetic parameters from outcrop AK-1A.

Table 5.3. Magnetic parameters obtained for three particle sized fractions compared to the bulk samples from units A, E1 and F1 at outcrop AK-1A.

AK-1A: Unit A.	**X_{LF}**	**X_{FD}%**	**X_{ARM}**	**IRM_{1T}**	**Soft_IRM**	**HIRM**	**X_{ARM}/X_{LF}**	**X_{ARM}/X_{FD}**	**$X_{ARM/IRM1T}$**	**S_{-100}%**	**S_{-300}%**
0-2 μm	80.2	9.9	335.3	298.1	35.2	15.3	4.18	42.3	1.12	11.8	5.1
2-4 μm	49.4	6.8	251.6	814.5	146.9	43.2	5.10	74.5	0.31	18.0	5.3
32-63 μm	105.3	0.7	213.9	2019.9	99.8	0	2.03	271.4	0.11	4.9	0
Bulk	89.1	3.75	343.8	1963.4	194	18.5	3.86	103	0.18	17.17	1.4
AK-1A: Unit E1.	**X_{LF}**	**X_{FD}%**	**X_{ARM}**	**IRM_{1T}**	**Soft_IRM**	**HIRM**	**X_{ARM}/X_{LF}**	**X_{ARM}/X_{FD}**	**$X_{ARM/IRM1T}$**	**S_{-100}%**	**S_{-300}%**
0-2 μm	74.9	8.5	293.5	298.6	34.7	16.3	3.92	46.4	0.98	11.6	5.5
2-4 μm	66.7	7.6	232.2	531.5	73.8	17.7	3.48	45.8	0.44	13.9	3.3
32-63 μm	89.9	0.6	263.7	1754.1	165.3	27.4	2.93	466.4	0.15	9.4	1.6
Bulk	87.2	5.38	373.8	1446.3	194.7	18.5	4.28	79.6	0.26	13.5	1.3
AK-1A: Unit F1.	**X_{LF}**	**X_{FD}%**	**X_{ARM}**	**IRM_{1T}**	**Soft_IRM**	**HIRM**	**X_{ARM}/X_{LF}**	**X_{ARM}/X_{FD}**	**$X_{ARM/IRM1T}$**	**S_{-100}%**	**S_{-300}%**
0-2 μm	221.1	10.7	1279.9	966.8	70.7	37.9	5.79	54.2	1.32	7.3	3.9
2-4 μm	168.4	7.1	869.2	1776.5	201.9	40.9	5.16	72.6	0.49	11.4	2.3
32-63 μm	104.8	1.3	212.0	2223.4	161.4	0	2.02	152.4	0.1	7.3	0
Bulk	150.3	8.5	994.6	2397.9	356.1	41.7	6.62	78.2	0.41	14.9	1.7

5.2.2b: AK-1A interpretation

The local topography slopes away from the gully banks indicating alluvial deposition in the region around the modern gully rather than sedimentation directly from the hillslopes (Fig. 5.10). The sediment body in this area thus exhibits lobate morphology. A similar landform was also observed in a neighbouring tributary at Africanders Kloof (Fig. 5.13).

Figure. 5.13 – A floodout deposited on the footslopes in an adjacent tributary at Africanders Kloof.

Elsewhere in the Sneeuberg, these lobate landforms have been linked to discontinuous gully processes where gullies terminate in a 'floodout' (Grenfell et al., 2012). This term is roughly synonymous with 'terminal fans' in the context of fluvial distributary systems (Parkash et al., 1983), but there is a wide range of sedimentological and morphological variation reported in the literature (Kelly and Olsen, 1993; Sadler and Kelly, 1993; Tooth, 1999; Billi, 2007). Floodouts follow the same basic principles of deposition in alluvial fan settings: loss of flow confinement resulting in rapid energy dissipation and deposition of a lobe of sediment that may exhibit progradational features such as proximal-distal fining.

The horizontally bedded nature of the facies at AK-1A indicates stream-dominated deposition rather than emplacement by debris or mudflows surging over the surface. The fine gravel lenses 'floating' within coarse sands and silts indicate dissected sheet-flood deposits during the latter stages of flow (A) similar to that analysed for AKH subunit A2. The sharp, planar contact at 15 cm indicates an erosion surface which may be coeval with the unconformity discussed for AKH (80 cm).

The overlying coarse, matrix-supported gravels indicate deposition under upper-flow regime conditions (B), with deposition of coarse sands during waning flow (C1). The coarse-sand bed appears to have been dissected by small channels or rills with the emplacement of fine lenticular gravels (C2). Unit E similarly exhibits a weakly graded profile indicating deposition under upper-flow regime (E1), with the better sorted coarse sands then dissected by micro-channels with lenses of fine gravel deposited in them (E2). The slight upward fining characteristics of unit E are likely a feedback response due to aggradation reducing the local valley slope and may represent retreat of the aggradational system upstream (Grenfell et al., 2012).

The switch to inversely graded sands and then matrix-supported very coarse gravels above the erosional contact (155 cm) is interpreted to indicate a renewed phase of floodout progradation (Grenfell et al., 2012). The evidence for this is found in 1) the palaeoslope (Fig. 5.14) and 2) valley fills exposed in a neighbouring gully 50 m to the west (Fig. 5.15):

1) Palaeo-slope: outcrop AK-1A is located 30 m upstream of a significant reduction in slope gradient from 0.073 m/m to 0.05 m/m. Furthermore, the inversely graded sand/gravel package (unit F) only appears within 50 m upstream of AK-1A. Thus, the most probable impetus for incision into the upper floodout surface (AKH) was driven by oversteepening at its distal margin (Patton and Schumm, 1983).

2) Valley fills in adjacent gully: the unit F facies (member B – AK-1A), which dip away from the gully re-appear as a greyer, finer-grained unit in the adjacent gully as shown in Fig. 5.15 and 5.16, capped by a sand unit. Furthermore, the angle of dip of these sediments precludes the possibility of their having overtopped the local valley margin (Fig. 5.15e and Fig. 5.16). The undulating bed contact between unit F sediments and this sand unit implies an erosion surface, but the lack of well-developed channel architecture implies that local incision of the floodout surface was restricted to slopewash and/or rilling. Stratigraphically, this sequence virtually matches that recorded at AK-2 (discussed in later section) the only exception being that the sandy unit here is laterally discontinuous perpendicular to the gully (Fig. 5.15c and d) whereas at AK-2, a series of palaeochannels have back-cut into the distal margins of the floodout. The surface of the floodout is highly vegetated by Karooid vegetation

accounting for the development of blocky soil structure due to abundant root penetration. In summary, these sediments represent local stratigraphic member C.

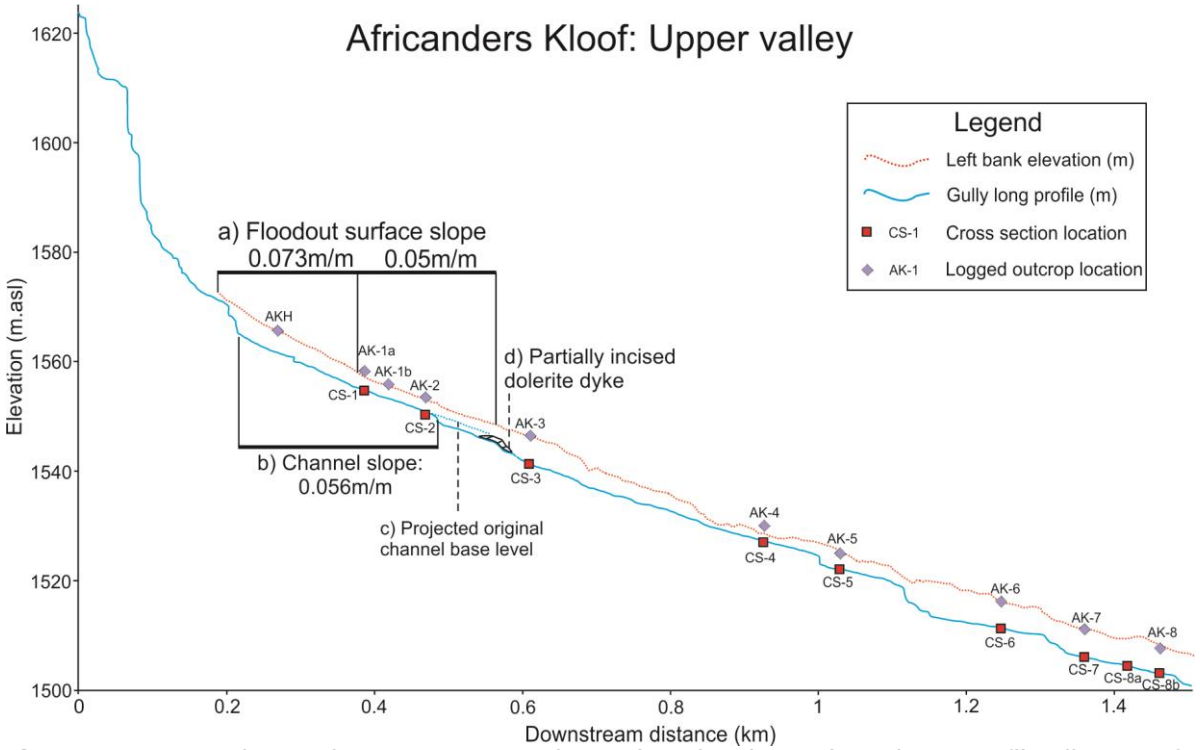

Figure. 5.14 – enhanced contemporary channel and palaeo-slope long profile diagram for the upper slopes at Africanders Kloof showing: a) floodout surface slope gradient change from 190-406 m and 406-570 m downstream (x axis), b) contemporary channel slope from 214.7-479.2 m downstream taken as representative of c) original channel base level prior to d) partial incision of dolerite dyke.

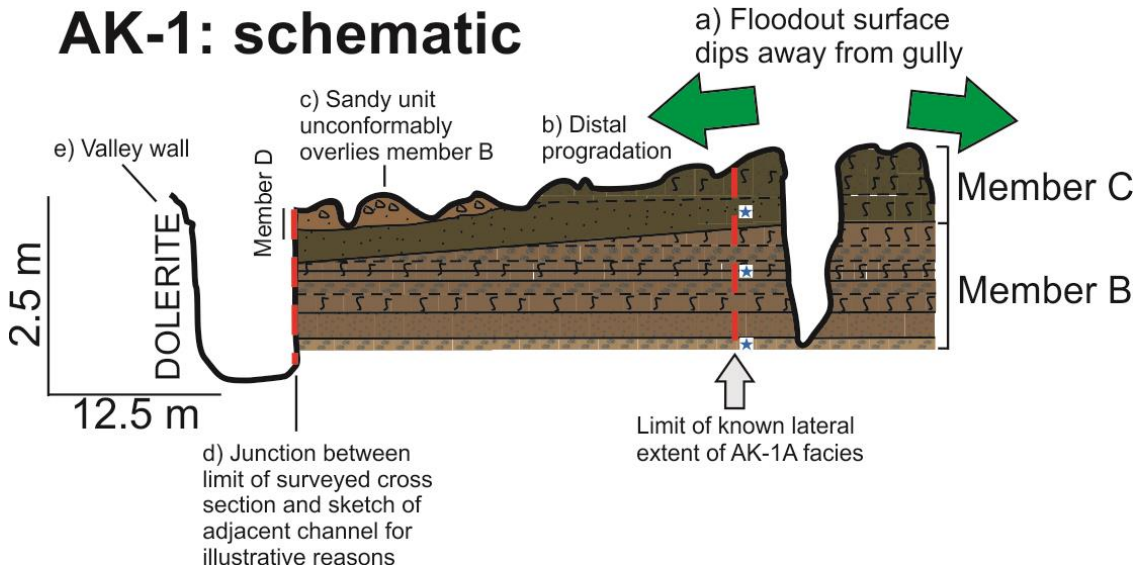

Figure. 5.15 – enhanced valley cross section capturing the floodout morphology and associated facies as recorded at outcrop AK-1A – A) Note the surface morphology promoting sedimentation away from the modern gully and B) The relative depletion of gravel expressed in member B sediments cut into by the gully to the left indicating distal progradation, C) The sandy sediment package absent at outcrop AK-1A exhibiting a sharp, undulating contact implying and erosion surface, D) Note the gully is sketched for illustrative

purposes, crucially to show relations of the dipping units associated with the floodout could not have overtopped E) The valley wall composed of dolerite.

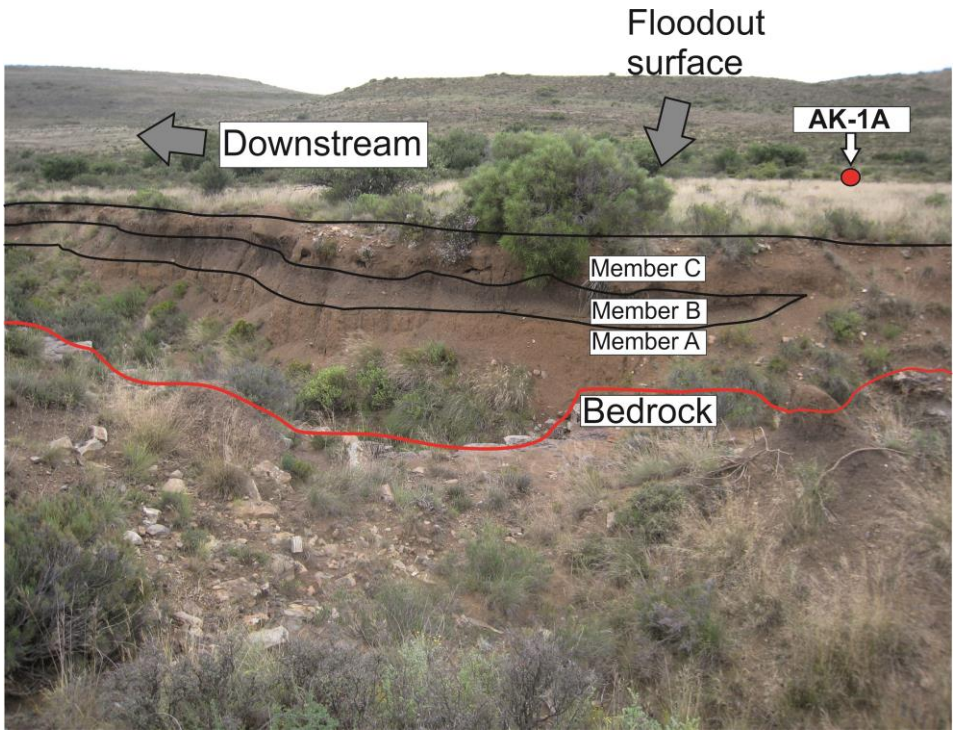

Figure. 5.16 – photograph of adjacent gully to AK-1A (see Fig. 5.15d-e). Note the dipping floodout surface toward the dolerite bedrock wall (red line). Note also the thicker, finer-grained member B sediment package – coeval with the top of unit AK-1A, which here is capped by well sorted sands and a thin veneer of laterally discontinuous, very coarse gravels.

The magnetic susceptibility data from the bulk (0-63 μm) samples for unit A indicates an assemblage dominated by predominantly multi-domain magnetite on the basis of 1) the very low $\chi_{ARM/IRM1T}$ values (0.2) and 2) high χ_{LF} and IRM_{1T}. The high S_{-100}% may be indicative of pedogenic haematite (Liu et al., 2015). The particle-size specific susceptibility data indicates two ferrimagnetic components: a pedogenic component targeted in the 0-2 μm fraction, but a stronger remanence carrying multi-domain lithogenic signature in the 32-63 μm fraction. It follows that the bulk susceptibility measurements are biased strongly by this multi-domain lithogenic magnetite component, such that SP grain (χ_{FD}% = 3.75%) concentration is clearly under-estimated. Furthermore, it appears the highest concentrations of AF minerals reside in the 0-4 μm fraction, with no resurgence in the coarsest grades. This is highlighted in Table 5.4 which compares the lithogenic fraction from AKH 55-65 cm and AK-1A. The multi-domain ferrimagnetic signature is much stronger for AK-1A than for AKH, whilst iron oxide coatings (S_{-100}%) are apparently less significant for AK-1A. This implies that, although S_{-100}% of the bulk samples are similar between these samples,

the lithogenic fraction exhibits little evidence of in situ weathering compared to AKH. Therefore, despite the fact that AK-1A unit A occurs beneath an erosion surface, degree of pedogenic overprinting is not comparable with AKH and thus the two are not advanced as being stratigraphically coeval.

Table 5.4. Magnetic parameters obtained for the 32-63 μm lithogenic fraction for comparison between AKH 55-65 cm and AK-1A 5-15 cm.

Outcrop/Unit	Br (ppm)	X_{LF}	$X_{FD\%}$	X_{ARM}	IRM_{1T}	S_{-100}%	S_{-300}%	$X_{ARM/IRM1T}$
AKH / A1-B	1.8	67.6	0.67	160.5	1,925.7	15.3	0	0.08
AK-1A / A	1.7	105.3	0.7	213.9	2,019.9	4.9	0	0.11

Unit E1 exhibits softer magnetism (lower S_{-100}%) and crucially displays a significantly higher SP grain contribution (χ_{FD}% = 5.38) as per the bulk susceptibility data. However, it is likely that this enrichment in finer weathering particles (SP grains) may be sourced from the top unit due to downward translocation of silts/clays in root channels.

Unit F1 in direct contrast exhibits identical bulk (0-63 μm) magnetic parameters to that observed for the top unit (B3) at outcrop AKH although slightly enhanced with respect to χ_{ARM} and IRM_{1T} indicating a larger proportion of remanence carrying SD grains (Fig. 5.12). This implies that the sediment here was derived from erosion of the AKH surface as indicated earlier. Compared to the units below, the χ_{ARM} of the clay fraction is 4-6 times higher, indicating relatively high concentrations of pedogenic SD grains. In particular, the 0-2 μm fraction exhibits extremely high concentrations of fine-grained ferrimagnets compared to units A and E1 that indicate a distinctive pedogenic origin. Whilst the χ_{FD}% of the bulk in this case is similar (8.5%) to that of the clay fraction (10.7% - Table 5.3), the concentration of remanence carrying SD particles reflected in the $\chi_{ARM/IRM1T}$ is still severely underestimated for the bulk measurements as was the case for the previous samples.

There have been several proposed mechanisms to explain enhanced topsoil susceptibility. Among them are processes intrinsic to natural soil formation such as alternating reducing and oxidising conditions (Maher and Taylor, 1989), although under conditions of persistent reduction, greigite (iron sulphide) may form

(Fassbinder and Stanjek, 1994). Further, the role of magnetotactic bacteria in the production of magnetite as well as firing of soil have been found to increase susceptibility (Oldfield, 1994; Oldfield and Crowther, 2007). Soil magnetism is also greatly determined by maghemite content (γ-Fe_2O_3) which can form via the oxidation of magnetite (Fe_3O_4) (Murad and Schwertmann, 1993).

The porosity of the soil here is high, with a sand-dominated matrix containing frequent root channels. There is no evidence of gleying. Thus, conditions of free drainage would favour wet/dry phases (reducing/oxidising) largely driven by seasonality. Further, the role of fire cannot be ruled out as burning associated with summer storms is common in this area, but there was no clear evidence in the logged section to indicate burning (charcoal fragments) and the granulometric quotients for the clay fraction are too marginal to ascribe to burning-induced SP grain production (Oldfield and Crowther, 2007). Therefore, in addition to effects of inheritance of weathered sediment from further upslope (AKH), the major increase of susceptibility in the fine fraction relative to the coarse fraction is most likely due to oxidation of the original authigenic magnetite to pedogenic maghemite (Barrón and Torrent, 2002).

Finally, the relatively low 'S values' in the 0-2 μm fraction implies distinctively less haematite compared to the sediments which constitute member A (AKH) and member B (AK-1A), which is probably related to member C sediments being relatively younger. Torrent et al., (2006) have argued for the paragenetic formation of maghemite and haematite. It is possible that the declining magnetic susceptibility with depth for this profile thus relates to increased oxidation to haematite at the expense of the intermediate products of pedogenic SP maghemite confirmed in the lower χ_{FD}% but higher S values.

5.2.3a: AK-1B analysis

Log AK-1B was obtained from a 2.2 m gully exposure 418.7m downstream of the headwaters on the left bank (Fig. 5.1 and Fig. 5.17).

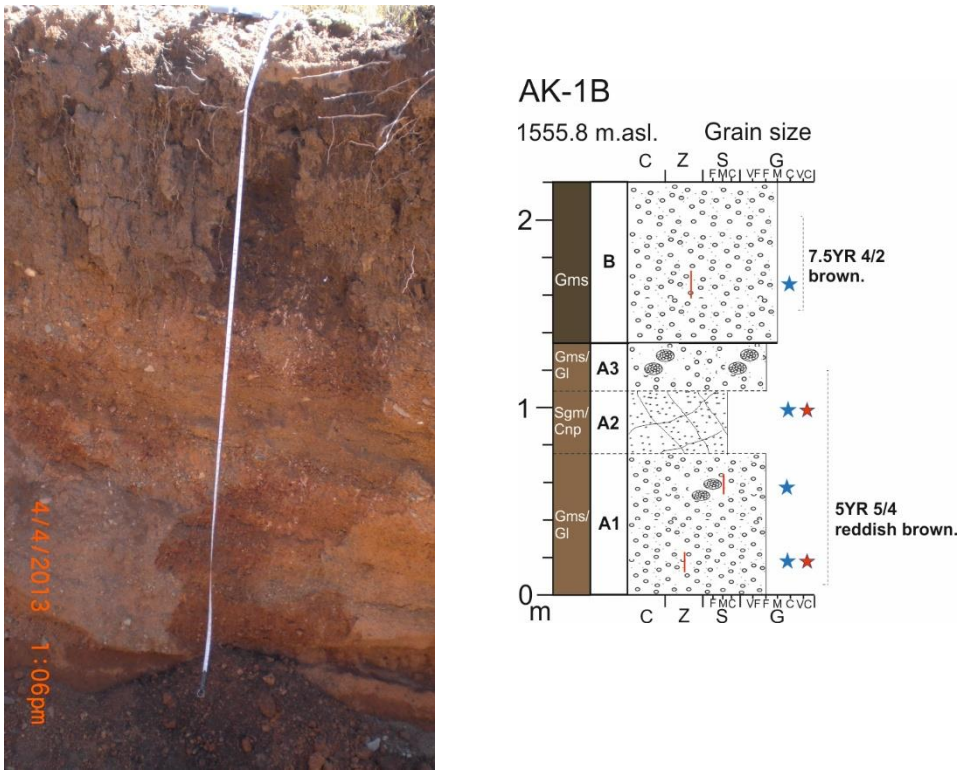

Figure 5.17 – photograph and log of outcrop AK-1B.

Subunit A1 consists of poorly sorted, abundant, matrix-supported, angular fine gravels, locally with lenses of clast-supported gravels (Fig. 5.17). The matrix at 20-30 cm is characterised by very poorly sorted silty sand (Fig. 5.18a), but at 55-65 cm is dominated by coarse to very-coarse sand (51.65 – Fig. 5.18b). Unit A2 consists of predominantly coarse to very-coarse sand (78.4% - Fig. 5.18c) and very fine gravels, exhibiting curved non-parallel bedding. Bromine content is high (11.7 ppm) relative to the bracketing units (Table 5.5). Subunit A3 consists of poorly sorted matrix-supported gravelly sand with some gravel concentrated into clast-supported lenses. The matrix is compositionally similar to A2 (Fig. 5.18d). Soil exhibits weakly developed granular structure and is friable. Unit B consists of massive matrix-supported angular medium gravels. The matrix consists of very poorly sorted silty sands Fig 5.18e). Root channels and infilled dessication cracks are common. Soil exhibits a weakly developed blocky structure and colour changes to 7.5YR 4/2 brown. Bromine and LOI% values peak for this unit (Table 5.5).

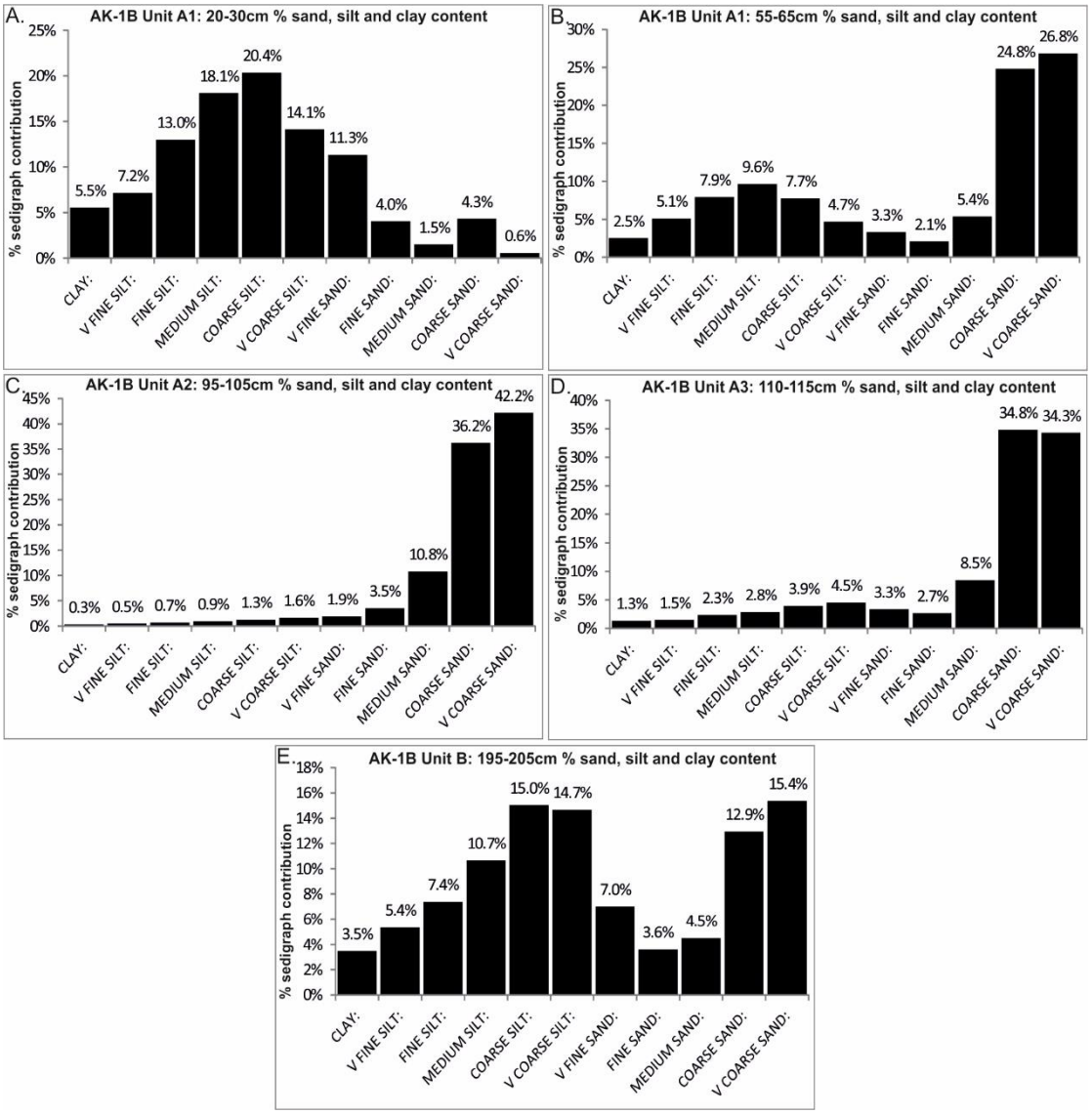

Figure 5.18 – % sand, silt and clay content derived from Coulter grain size analysis on samples collected from outcrop AK-1B.

Total magnetic susceptibility is inversely related to depth below terrace surface, with distinct surface enhancement - particularly high χ_{FD} and χ_{ARM} (unit B – Fig. 5.19a). Unit B is similarly characterised by very high χ_{FD}% (Fig. 5.19b). S_{-300}% declines with depth too, peaking at unit B (3.4% of applied remanence unreversed- Fig. 5.19c).

Table 5.5 – percentage loss on ignition and Bromine (ppm) content for sampled horizons at AK-1B.

Unit	Height (cm)	Loss on ignition (%)	Bromine (ppm)
A1	20-30	2.4	2.4
A1	55-65	1.8	3.3
A2	95-105	0.8	11.7
A3	110-115	1.7	-
B	160-170	3.3	25.0

5.2.3b: AK-1B interpretation

The thickness of the basal gravel unit indicates rapid emplacement under upper flow regime conditions. Illuviation is not deemed to be a primary process responsible for the concentration of fines, as soil organic matter content is particularly low (bromine - 2.4 ppm) and there is no evidence of root channels. The very poorly sorted matrix of silty sand is thus related to interstitial filling during flow cessation. Minimal pedogenic overprinting is indicated by the typically friable, weakly granulated structure, but deep rubification of the clasts implies in situ weathering. The appearance of lenses at 60 cm, as before, is interpreted as indicating flow recession with flow division into several smaller channels reworking the gravels. However, this is capped by further massive gravels, implying a return to high-flow conditions. Flow cessation is indicated in unit A2 with a switch to cross-bedded coarse sands. The re-appearance of lenticular gravels above implies incision and reworking of the gravel-spread as before. Collectively, these facies are consistent with channelized flow rather than sheet-floods radiating laterally due to loss of confinement similar to AKH and AK-1A (units A and F respectively).

The planar contact is interpreted as an unconformity, with unit B exhibiting greater bioturbation than A evidenced by abundant root channels, infilled dessication cracks and the largest bromine values evidencing high organic matter content). Compared to AK-1A unit F, modal clast size for this unit is smaller, but bromine content is identical (AK-1A unit E: 23.7 ppm). The slightly higher organic matter content is argued to be thus related to slope-induced catenary soil processes with increasing distance from the floodout apex (30 m upstream of AK-1A).

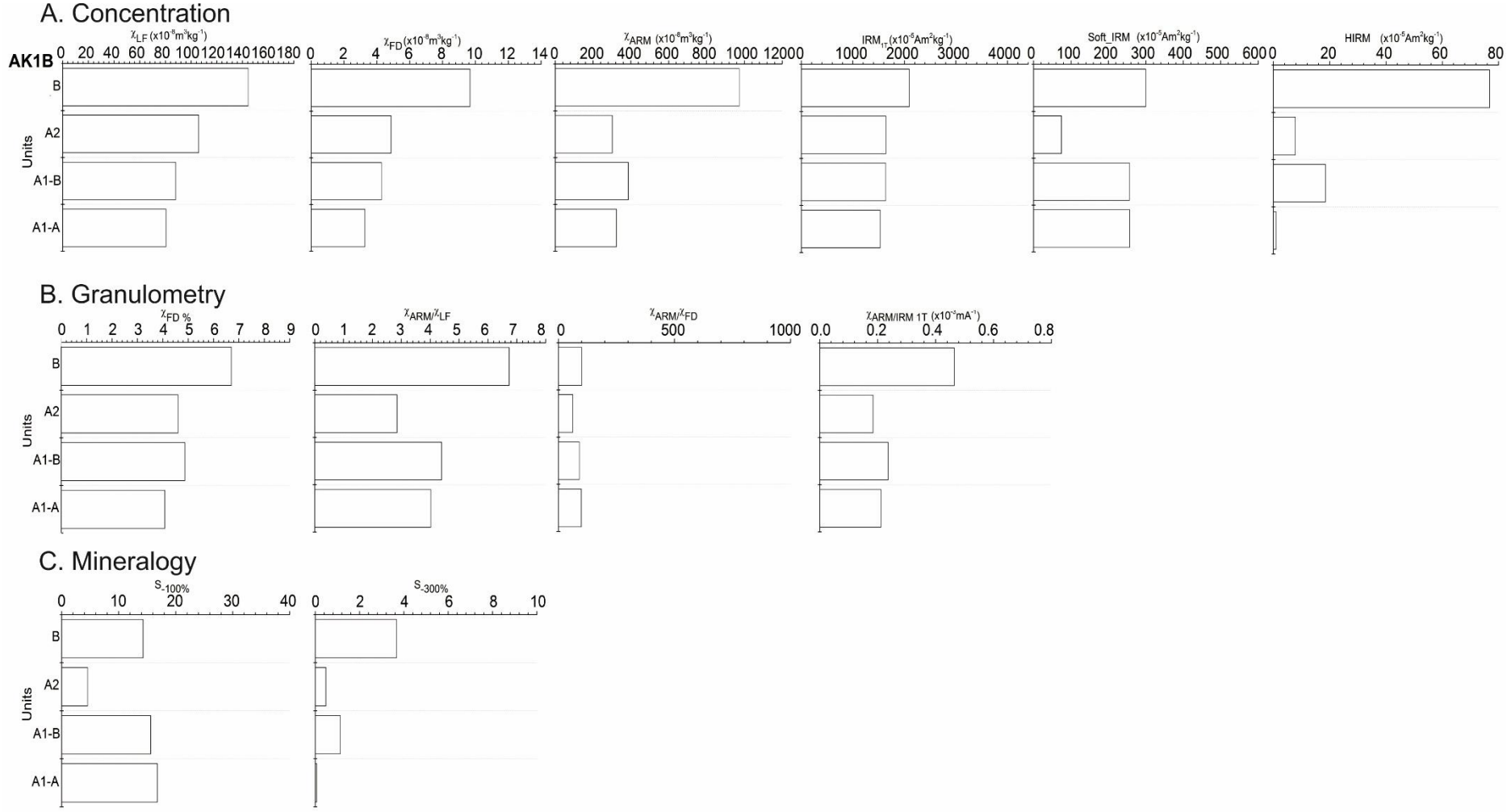

Figure 5.19 – mineral magnetic parameters from outcrop AK-1B.

The high values of concentration-related proxies attest to high concentrations of ferrimagnetic minerals throughout the profile similar to the previous two outcrops. The very low values of $\chi_{ARM/IRM1T}$ need to be interpreted in the light of the caveats informed from analysis of the different particle-size fractions before. Without that information, the combination of such low quotient values yet high χ_{FD}% could be taken as evidence for concentration of grains on the SP side of the narrow viscosity band, again underplaying the contribution of any SD magnetite/maghemite to total susceptibility. Each sampled unit shows a strong ferrimagnetic, pedogenic overprint (χ_{FD}%). The relation between diminishing ferrimagnetism with increasing depth and the relatively large increases in S_{-100}% is most probably to do with the progressive ageing of SP maghemite to pedogenic haematite which, given the 'redder' colour of unit A (5YR 5/4), is a reasonable postulation. For samples collected at AK-1A, the highest concentrations of remanence carrying ferrimagnets were found in the 32-63 μm grade, pertaining to a lithogenic MD magnetite origin. It follows that for the stratigraphically younger (i.e. above AK-1A unit E) floodout deposits expressed here (AK-1B unit B) the high IRM_{1T} values indicate similarly relatively 'young' unweathered lithogenic grains. The similar S_{-100}% signature is most likely to do with pedogenic haematite having been inherited from incision into member B sediments upstream (AKH – AK-1A). The reason for the relatively large S_{-300}% is unclear but may also be due to sorting effects concentrating clay/fine silt based pedogenic products inherited from upstream. As mentioned before, it has been found that maghemite and haematite can form paragenetically in soils from ferrihydrite (Balsam et al., 2004; Torrent et al., 2006), the difference here being that the probable maghemite source in question has been derived primarily from the oxidation of authigenic magnetite (Barrón and Torrent, 2002).

5.2.4a: AK-2 analysis

Log AK-2 was obtained from a 2.5 m gully exposure 469.3 m downstream of the headwaters on the left bank (Figure. 5.1, 5.20 and 5.21).

Unit A consists of a structureless, poorly sorted matrix of very coarse sand and silt. Unit B sharply overlies unit A, consisting of thinly bedded, laterally discontinuous, angular, matrix-supported gravels (Fig. 5.20). The matrix consists of predominantly coarse to very-coarse sand (58.8% - Fig. 5.23a). A subordinate mode exists in the

fine sand class (7%) with abundant silt and clay (23% collectively) (Fig. 5.23a). The bulk magnetic properties are similar to AK-1B unit A analysed in the previous section, whilst the particle-size specific magnetic measurements exhibit two distinct modes in χ_{LF} in the finest and coarsest grades respectively, whilst IRM_{1T} increases with increasing particle size (Table. 5.6). Whilst IRM_{1T} increases with particle size, χ_{ARM} decreases, resulting in progressively smaller values of $\chi_{ARM/IRM1T}$ in the coarser grades. These patterns mirror those obtained from the particle-size magnetic susceptibility data for AK-1A. Taken collectively, the $\chi_{ARM/IRM1T}$ from the bulk susceptibility measurements is clearly biased by the low χ_{ARM} yet very high IRM_{1T} of the coarsest grade, whilst the χ_{FD}% signal of the bulk sediment is dominated by the finest fractions.

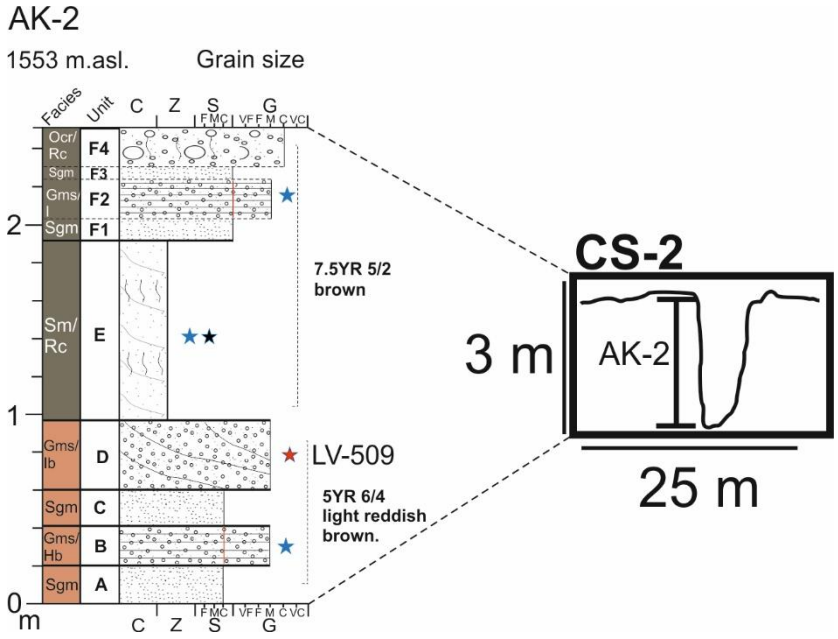

Figure 5.20 – log AK-2 and cross section.

Unit C consists of a structureless, poorly sorted matrix of very coarse sand and silt identical to unit A. A sharp, planar contact exists between units C and D. Subunit D1 consists of thin to very thinly bedded, clast rich matrix-supported medium gravels. The matrix consists of abundant coarse sands and subordinate silt. Subunit D2 is characterised by fewer clasts between 80-95 cm and reduced silt content in the matrix. Collectively, units A-D2 are 5YR 6/4 yellowish red.

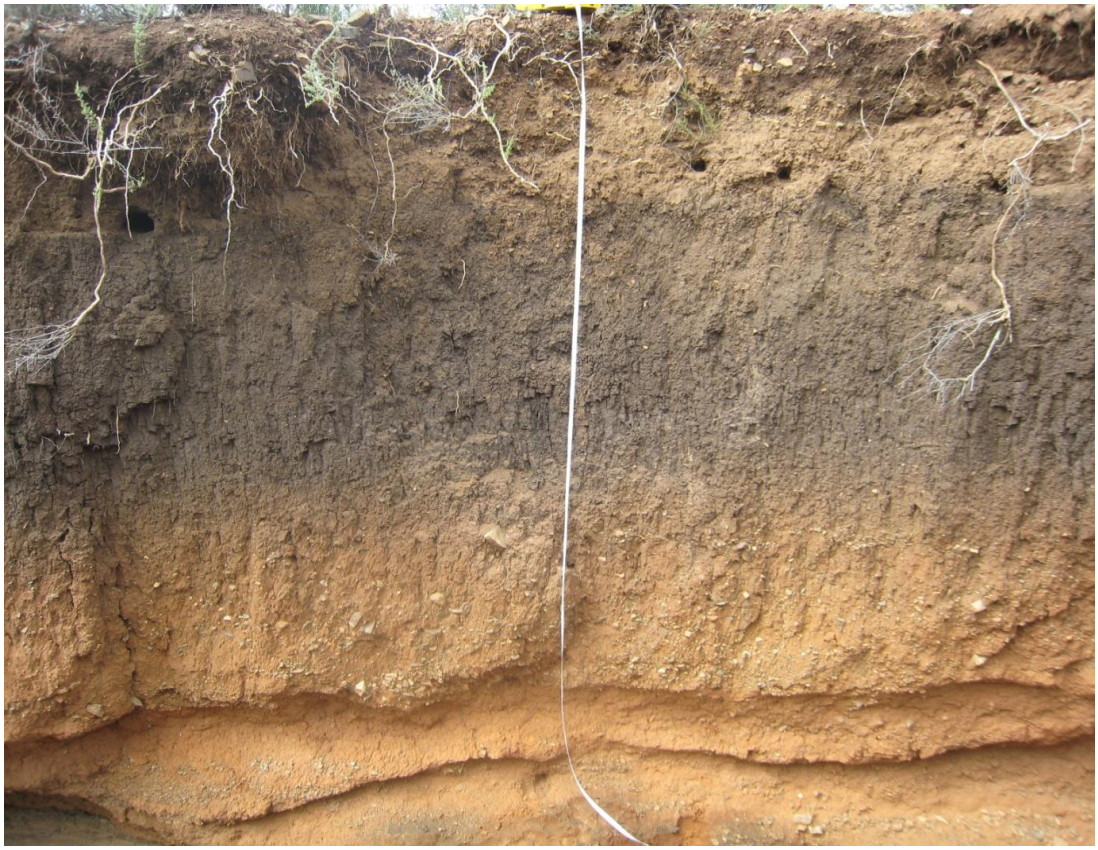

Figure 5.21 – photograph of log AK-2.

Unit E by contrast consists of very poorly sorted silty clays, which comprise 94.5% of the sedigraph (Fig. 5.23b). D_{50} is 9.6 µm. This unit reaches a maximum thickness of 0.95m but this reduces to 30cm at the point of intersect with a dolerite intrusion approximately 150m downstream where it also becomes lighter in colour (Fig. 5.22). The soil here exhibits well developed prismatic structure with abundant root channels with illuviated silts. LOI% and bromine values are relatively high compared to other sampled units (4.9% and 20.2 ppm respectively – Table 5.6). Colour is 7.5YR 5/2 brown. The nature of the contact between unit E and F1 is sharp and undulating. Unit E exhibits very strong bulk magnetic susceptibility (χ_{LF} = 142.6), but is distinctive in terms of χ_{FD} and χ_{ARM} (Fig. 5.24a). Similarly, the granulometric proxies are all distinctively high (Fig. 5.24b).

Table 5.6 – percentage loss on ignition and bromine (ppm) data for sampled horizons at AK-2.

Unit	Height (cm)	Loss on ignition (%)	Bromine (ppm)
B	25-35	2.4	2.2
E	140-150	4.9	20.2
F2	210-220	1.7	7.3

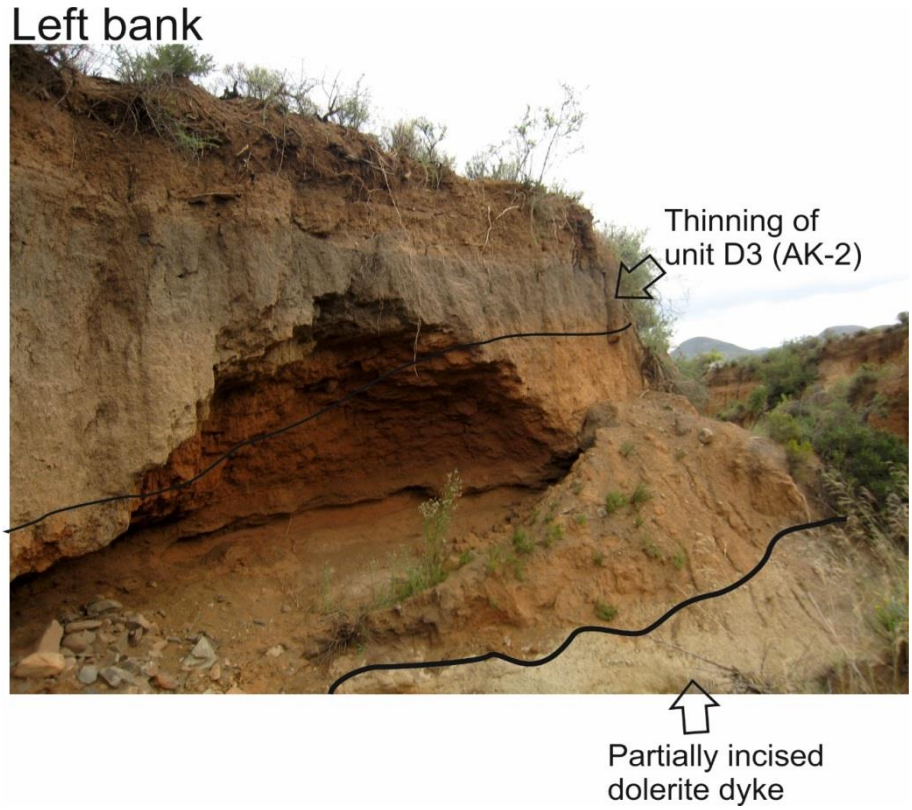

Figure 5.22 – photograph demonstrating the progressive thinning of AK-2 unit D at the intersection point with a deeply weathered and incised dolerite intrusion.

Similarly to AK-1A unit F1, unit E exhibits higher total susceptibility in the fine fractions (0-2 and 2-4 μm) compared to the coarse fraction. In contrast to the other particle size data, unit E displays highest χ_{ARM} and IRM_{1T} values in the 2-4 μm fraction and compared to unit B, exhibits relatively low S values (Table 5.7). $\chi_{ARM/IRM1T}$ values decline with increasing particle size as before. Compared to unit B, the bulk magnetic measurements do not underestimate concentration-related proxies in the fine fraction to the same degree – in particular the $\chi_{ARM/IRM1T}$ and χ_{FD}% remain relatively high (0.71 and 8.1% respectively – Fig. 5.24b).

Subunits F1 and F3 consist of massive or very thinly bedded very coarse sands. Unit F2 is characterised by massive, well sorted, coarse to very-coarse sand (89.9% - Fig. 5.23c), which is separated by thin to very thinly bedded laterally discontinuous gravels. Subunit F4 is a very poorly sorted mix of angular gravels held within a matrix of sandy silt. Root channels are abundant and the colour of Unit F is identical to unit E.

Total susceptibility as revealed by the bulk magnetic measurements (subunit F2) is slightly higher than unit E (χ_{LF} = 145), but crucially exhibits much higher IRM_{1T} (2580)

and HIRM values (72 – Fig. 5.24a). χ_{FD}% is still relatively high (5.4%), but crucially S_{-300}% peaks for this unit (2.8% remanence unreversed – Fig. 5.24c).

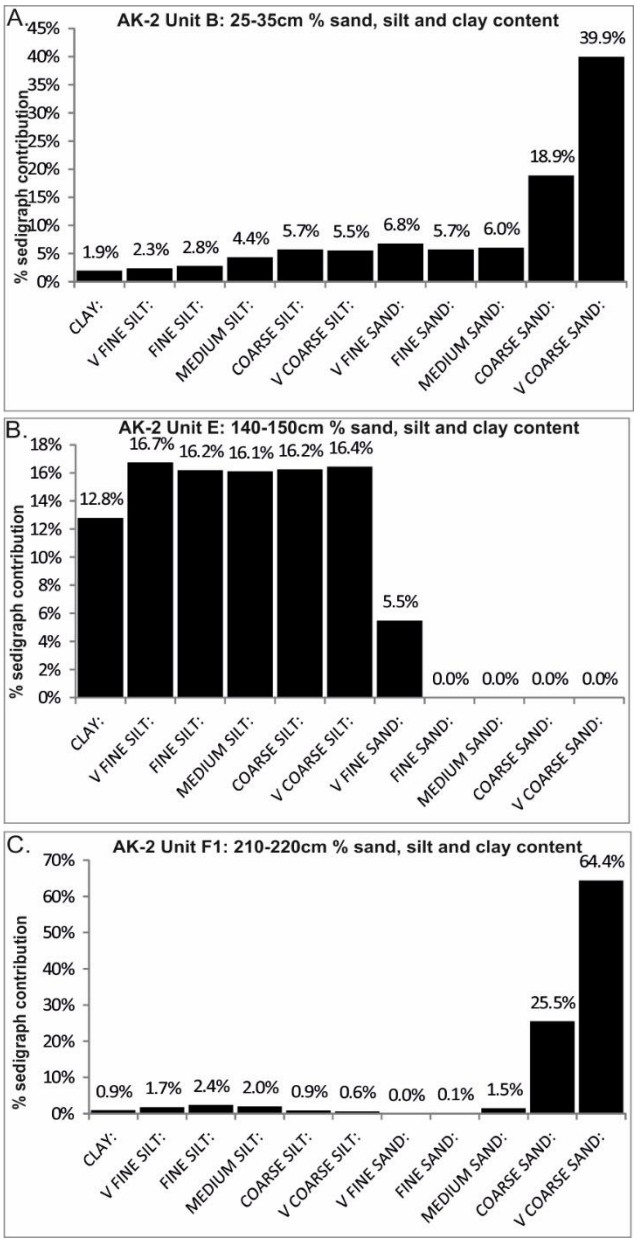

Figure 5.23 – % sand, silt and clay content derived from Coulter grain size analysis on samples collected from outcrop AK-2.

The particle-size magnetic measurements, similar to unit E, display a distinct mode in χ_{LF}, χ_{FD} and χ_{ARM} for the 0-4 μm fraction which exceeds, as was the case for AK-1B unit B, the magnetic susceptibility of the coarsest (32-63 μm) fraction. A secondary mode of IRM_{1T} values resides in the 4-8 μm fraction (1987.7), peaking in the very coarse silt grade, but $\chi_{ARM/IRM1T}$ declines with increasing particle size as noted earlier (Table 5.7).

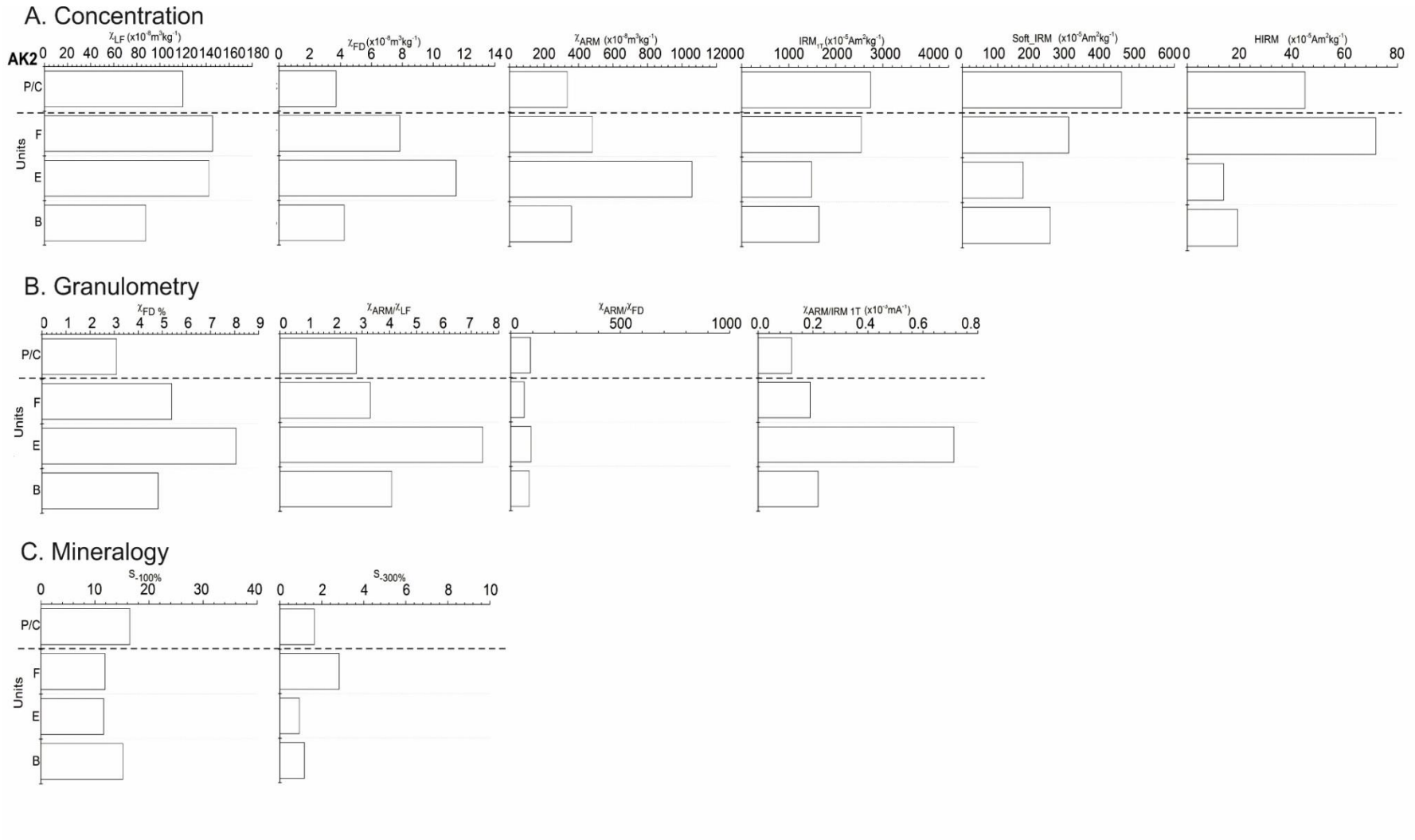

Figure 5.24 – mineral magnetic parameters from outcrop AK-2.

Table 5.7. Magnetic parameters obtained for six particle sized fractions from units B, E and F at outcrop AK-2.

AK-2: Unit B.	**X_{LF}**	**X_{FD}%**	**X_{ARM}**	**IRM_{1T}**	**Soft_IRM**	**HIRM**	**X_{ARM}/X_{LF}**	**X_{ARM}/X_{FD}**	**$X_{ARM/IRM1T}$**	**S_{-100}%**	**S_{-300}%**
0-4	89.7	9.1	359.6	514.9	68.6	13.5	4.01	44.2	0.7	13.3	2.6
32-63	106.8	0.9	228.4	2549.5	371.9	75.7	2.14	245.4	0.09	14.6	3
Bulk	87.8	4.8	358.8	1644.3	249.1	19.2	4.09	84.8	0.22	15.2	1.2
AK-2: Unit E.	**X_{LF}**	**X_{FD}%**	**X_{ARM}**	**IRM_{1T}**	**Soft_IRM**	**HIRM**	**X_{ARM}/X_{LF}**	**X_{ARM}/X_{FD}**	**$X_{ARM/IRM1T}$**	**S_{-100}%**	**S_{-300}%**
0-2	210.2	11.4	1052.2	946.8	54.4	24.4	5.01	44	1.11	5.7	2.6
2-4	293.6	10.7	1849.7	2305.1	111.2	58.4	6.3	58.8	0.80	4.8	2.5
32-63	81.9	1.9	134.2	1596.2	183.8	51.1	1.64	84.7	0.08	11.5	3.2
Bulk	142.6	8.1	1057.3	1483.5	172.2	13.8	7.42	92	0.71	11.6	0.9
AK-2: Unit F.	**X_{LF}**	**X_{FD}%**	**X_{ARM}**	**IRM_{1T}**	**Soft_IRM**	**HIRM**	**X_{ARM}/X_{LF}**	**X_{ARM}/X_{FD}**	**$X_{ARM/IRM1T}$**	**S_{-100}%**	**S_{-300}%**
0-4	189.3	8.9	969.7	1553.9	145.1	41.6	5.12	57.5	0.62	9.3	2.7
32-63	146.8	0.8	294.5	2911.4	267	0	2.01	256.8	0.1	9.2	0
Bulk	145.6	5.4	481.3	2538.6	300.7	71.8	3.31	61.3	0.19	11.8	2.8

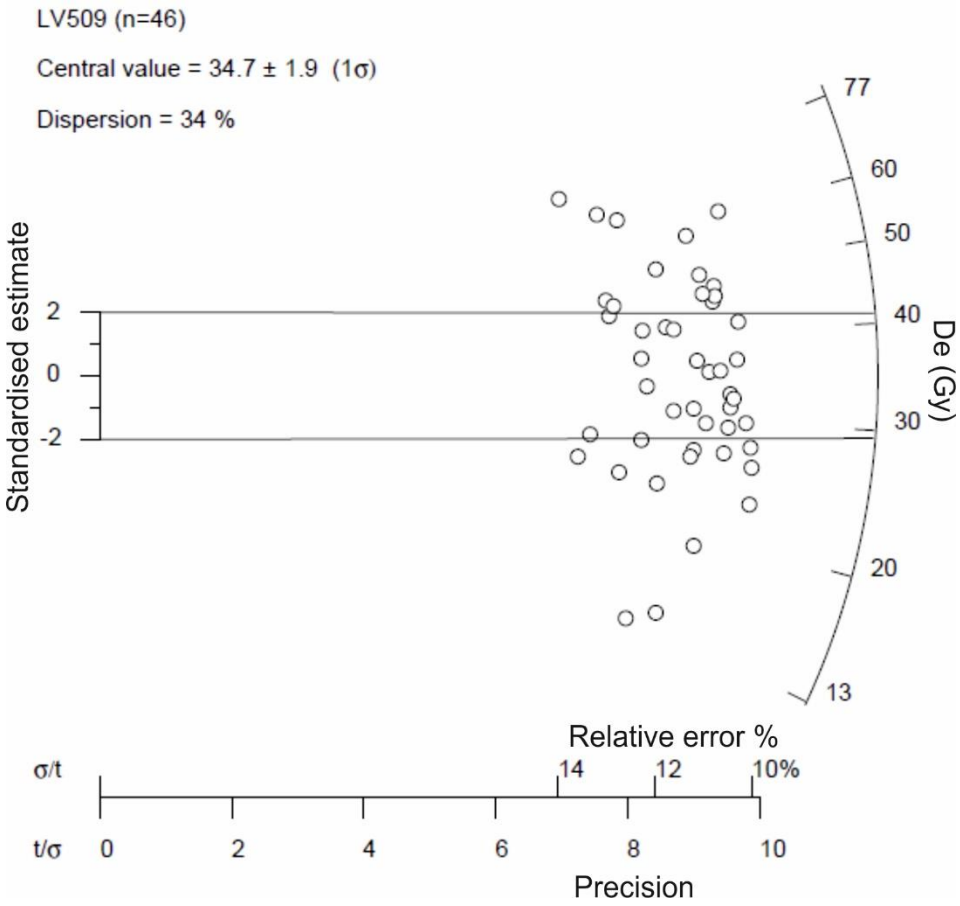

Figure 5.25 – radial plot showing 46 D_e values for LV509. The dose calculated using the central age model is shown in the horizontal bar (34.7 ± 1.9).

A final OSL age of 8.2 ± 1.5 ka (1σ) was obtained for AK-2 unit D (Table 5.18. There is a 66% chance that the true burial age lies between 11.2 – 5.2 ka. n = 14 plot with higher D_e values; n = 13 have lower values with two outliers that show 13-15 Gy (Fig. 5.25).

5.2.4b: AK-2 interpretation

The cross-sectional morphology (CS-2) shows the local topography sloping away from the gully comparable with CS-1 (AK-1A - Fig. 5.10). This indicates that the facies of the logged outcrop (AK-2) still pertain to the floodout sequence identified at outcrops AKH-AK-1B.

Compared to outcrop AK-1B, AK-2 possesses smaller units of sand and gravel. The absence of sedimentary structure in the sands (units A and C) is partly attributed to weathering and bioturbation. In the same reach, 20 m downstream on the right bank, the base of the succession consists of well sorted sands that exhibit well developed

planar-cross bedding interdigitating with some discontinuous, very thin gravel beds. The fining and better sorting of the deposits is consistent with reported facies for the distal margins of floodout sequences (Grenfell et al., 2012). The laterally discontinuous thinly bedded gravels (unit B) indicate deposition under upper flow regime conditions and evidence loss of flow confinement possibly at the terminus of a palaeogully, with the overlying sands indicating flow recession (unit C). The fact that the gravels (unit B) grade to planar cross-bedded sands 20 m downstream further evidence progressive reduction in energy conditions, associated with loss of confinement, with progradation of finer material further downstream. The switch to matrix-supported gravels (unit D) reflects floodout progradation under upper-flow regime conditions. The sharp bed contact with unit C and coarse calibre of material implies plane bed deposition. This phase of progradation occurred at 8.2 ± 1.5 ka. The imprecision associated with age LV509 likely has three main causes: 1) incomplete zeroing of the OSL signal due to high energy mode of emplacement; 2) illuviated, younger grains from above; 3) the broad grain size window encompassing grains with different environmental dose histories. This date provides a very preliminary indication of final burial age, which is better described in terms of 'Early-Mid Holocene.'

Downstream, unit D terminates as massive sand indicating distal fining probably in response to local valley impoundment by the dolerite barrier (Fig. 5.22). The sharp, planar contact between units D and E represent an unconformity. By establishing the longitudinal limits of the beds, unit E was found to be stratigraphically coeval with units F and B of sections AK-1A and 1B respectively. Unit E is interpreted as representing the distal margins of the floodout sequence which commenced just upstream of AK-1A. Upward fining in such contexts has been ascribed to the retreat of the aggradational system upstream (Grenfell et al., 2012). There are three distinct lines of evidence in support of this: 1) the fine-grained nature of the soil (94.5% silt/clay) with no gravel, 2) an order of magnitude increase in bromine content (20.2 ppm) compared to unit B (2.2 ppm), 3), an abrupt change in colour to 7.5YR 5/2 brown and a prismatic soil structure. This attests to riparian vegetation growth at the margins of the floodout. Riparian plants have been shown to spread flow and reduce velocity, facilitating deposition of silts and clays that favour further plant growth (Bull, 1997; Grenfell et al., 2012).

Table 5.8 – age modelled D_e values, D_r values and calculated age for samples **LV509**. Overdispersion, skewness and standardised kurtosis parameters are also provided. Central Age Model was used following procedure of Arnold et al., (2007). Note associated error bar on final age is quoted to 1σ . *Cosmic dose value was obtained for northern hemisphere equivalent latitude. [a] Water content measured from field sample. [b]Hypothetical water content accounting for saturation prior to terrace incision – final age is calculated using this value.

Sample	**n**	**D_e (Gy)**	**Water content (%)**	**K%**	**Th (mg/g)**	**U (mg/g)**	***Dcosmic Gy/Ka**	**Skew of lnDe *c***	**Standardised Kurtosis *k***	**Overdispersion σ (%)**	**Age model**	**Final age (ka) (1 σ)**
LV509	46	34.7 ± 1.9	2.5	2.51 ± 0.06	14.53 ± 0.26	2.64 ± 0.07	0.21 ± 0.01	-0.22	0.55	34	CAM	8.2 ± 1.5

The relations between the reduction in local slope, the abrupt fining characteristics of the floodout (unit E) and the formation of organic-rich soil due to the disruptive effects of the dolerite barrier downstream (Fig. 5.22) calls into question the extent to which this headwater floodout sequence (AKH-AK-2) was a source of sediment downstream. This segment of the valley may have filled up as a compartment and stabilised such that sediment disconnectivity between AKH - AK-2 and AK-3 – AK-4 prevailed during soil formation of the distal margins of the floodout. This is explored and tested in the forthcoming sections.

Under conditions of high vegetation cover, the probability of fire is clearly enhanced and some evidence in the form of micro-charcoal shards was found using low-powered microscopy on the remaining bulk sample from unit E. This firing of the vegetation here is advocated as being a probable trigger for local incision of the floodout represented by the well sorted coarse sands of unit F. However, it is still unclear as to how far down the valley sediment from these headwater zones propagated during incision of unit F.

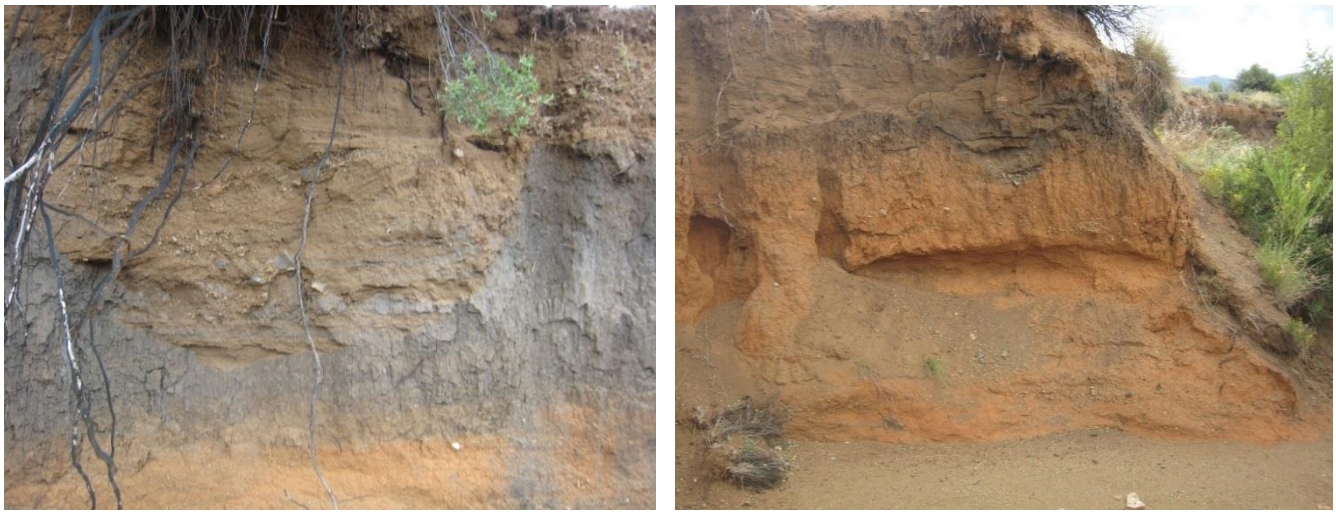

Figure. 5.26 – palaeogully architecture incised into AK-2 unit E soil a) palaeochannel incised to a maximum depth of 40 cm, b) evidence for stripping of unit E by erosion and capping by cross-bedded sands.

Originally, it was postulated that these sands represented overbank sedimentation contemporaneous with the incision of the modern gully. However, their close association with several shallow palaeochannels (see Fig. 5.26a) negates this. Rather, unit E has been incised and even completely stripped by erosion in places (Fig. 5.26b). This implies a re-working of upstream floodout sediments. The fact that

the current channel banks slope away from the channel implies that these infilled palaeo-gullies (Fig. 5.26) drained away from the modern gully and did not dissect the alluvial cover going over the dolerite dyke represented in Fig 5.22. This is also indicated by the relative thinning of the brown sand (unit F) cover at the apex of the dolerite barrier (Fig. 5.22), although not as pronounced as the thinning of the palaeosol (unit E). This implies that sedimentation continued over the barrier due to the valley upstream having been filled to capacity (see Fig. 4.19 “compartmentalised filing stage ii”). Grenfell et al., (2012) showed that sedimentation downstream of floodout termini is restricted to low energy sheet-flows with deposition of relatively fine sediment. Although the exact terminus of the palaeogully is unknown, its diversion perpendicular to the long-axis of the floodout is a logical response to the obstructive effect of the dolerite barrier prior to its partial incision and indicates that some sediment from the upper-most reaches (AKH-AK-2) may have been transmitted to lower sectors of the valley. The laminated sands (unit E) flanking and capping the palaeochannels are interpreted to be a mixture of overbank facies and floodout deposits associated with the infilling of these smaller channels (Fig. 5.26). It is also possible that the few palaeochannels exposed are part of a larger network of infilled channels draining in a similar direction dictated by the local valley morphology.

If taken in isolation, the bulk magnetic proxies for unit B would indicate a ferrimagnetic assemblage dominated by both MD and SP grains. As reported earlier on, the finest and coarsest grades (0-4 μm and 32-63 μm) exhibit magnetic signatures of a pedogenic and lithogenic origin respectively. Thus SP/SD grains are significant for the fine fraction whilst PSD/MD grains dominate the coarse fraction which biases the bulk susceptibility data. Although this unit exhibits only a very small hard (S_{-300}%) component, the ‘redder’ colour (5YR 6/4) in concert with high S_{-100}% values (16%) may indicate pedogenic haematite similar to the basal units at AK-1A and 1-B. However, the absence of an unconformity and no hard component means that this basal unit is not stratigraphically coeval with the palaeosol represented at the base of outcrop AKH (section 5.2.1).

The bulk susceptibility parameters for unit E indicate a predominantly fine-grained SP/SD dominated ferrimagnetic assemblage on the basis of the exceptionally high χ_{FD} and χ_{ARM}. $\chi_{ARM/IRM1T}$ values reported are highest for the entire bulk sample set

(0.73) attesting to the relatively very large SP/SD grain contributions. This unit pedologically and magnetically shows the highest pedogenic maturity compared to other lithostratigraphic floodout units and is 1 of just 4 samples (from entire dataset) suitable for plotting on the bilogarithmic graph (Fig. 5.7 and 5.8). The role of fire in driving the magnetic characteristics is unclear. If plotted on Oldfield and Crowther's (2007) pedogenic envelope, the χ_{ARM}/χ_{LF} and χ_{ARM}/χ_{FD} for unit E1 plot in the very top right hand corner overlapping the 'unburnt English soils'. It is possible that the lack of overlap with the 'burnt soils' is linked to 1) point of sampling (mid-point of E1) and/or 2) the differential response of sediment derived predominantly from an igneous origin under a sub-tropical weathering regime. In the case of (1), if the fire was not of particularly high intensity, heating related production of SP grains may have been limited to the top several cm or post-fire illuviation was ineffective in conveying substantial quantities of charcoal (content was minimal) to greater depths within the profile. Burnt material may have been carried away by overland flow to the south, especially as the local valley morphology slopes away from the location of the contemporary channel. In the case of (2) it is unclear what the interaction between MD magnetite sourced from dolerite and fire would be, or just that the proportions of pedogenic SD/SP grains overshadow a fire-driven SP increase such that the inter-parametric ratios have not responded.

The magnetic parameters obtained from the different particle-size fractions are radically different to the other sampled units. For instance, the 2-4 μm fraction shows the highest contributions to susceptibility from remanence carrying ferrimagnets (IRM_{1T}) whereas this is normally restricted to the coarse grade and lithogenic in origin. A high proportion of this remanence is carried by SD rather than MD grains, confirmed in the high $\chi_{ARM/IRM1T}$ values (0.8 – Table 5.7). It follows that the 2-4 μm shows the highest indications of weathering and pedogenesis based on this and also the highest χ_{LF} values. The relatively low IRM_{1T} for the 32-63 μm fraction could be due to two factors: 1) Relatively rapid development of pedogenic magnetite at the expense of the original MD lithogenic magnetite and/or 2) A sorting effect to do with the progradation of the floodout – hence concentrating finer silts and clays such that the syn-depositional lithogenic coarse component is relatively small. Since this palaeosol (unit E) grades to the top of the dolerite barrier where it thins, it implies the dolerite barrier formed a local base level anchor, reducing slope sufficiently to

promote slower aggradation at the distal floodout margins to encourage colonisation by vegetation. A review of outcrops AK-1A and 1B show the evolution of the floodout, fining from matrix-supported coarse to then medium gravels, terminating in the gravel-free fine silty clays reported in this section. The underlying member B sediments do not exhibit discernible progradational characteristics and appear to pertain to aggrading fan channels. Although the 0-2 mm sedigraph is characterised by 12% clay for unit E, Coulter granulometry tends to underestimate clay content. Either way, clay content is considerably higher compared to the floodout apex (AK-1B unit B) where 5.5% was obtained (Fig. 5.18a). This reinforces the notion of progradation-related distal fining concentrating clays and associated pedogenic products in tandem with subsequent in situ pedogenic overprinting. This also accounts for why the lithogenic magnetic component is smaller relative to the sediments beneath the unconformity.

The bulk magnetic properties of the palaeochannel (Fig. 5.24a) are intermediate between units A2 and B of AK-1B (the nearest outcrop upstream). While it is unknown at what point palaeochannel entrenchment occurred (i.e. which upstream sediment source it tapped) or its maximum depth upstream (how deeply it reworked sediments at sampled locations upstream), it is tentatively asserted that channel incision did not progress further than AK-1B upstream on the basis of the stronger concordance with units A2 of AK-1B in particular. Interpreting the magnetic properties of unit F is more ambiguous with respect to disentangling source from pedogenic modification. Compared to the palaeochannel, unit F exhibits markedly higher concentrations of SP grains (χ_{FD}% = 5.4%) with HIRM and S_{-300}% values that compare much more closely with AK-1B unit B. As the latter parameters are a measure of anti-ferromagnetic mineral concentration and with the exception of sample A1-B from the headwater fan (AKH), no other sampled units at either AK-1A or 1B exhibit this signature, it is most reasonable to postulate that unit F (AK-2) was supplied primarily from AK-1B (unit B).

5.2.5a: AK-3 analysis

Log AK-3 was obtained from a 4.5 m deep gully exposure on the right bank approximately 651.1m downstream of the headwaters in the centre of a topographic depression (Fig. 5.1, 5.27 and 5.28). This outcrop is also just downstream (20 m) of

the incised dolerite intrusion reported earlier (Fig. 5.22). This section was only logged in detail up to 3.5 m above the gully floor, as vertical gully sidewalls precluded detailed description and sampling above this height. Total log height was obtained from dGPS survey of the gully cross section and principal unit boundaries assigned on the basis of visual observation.

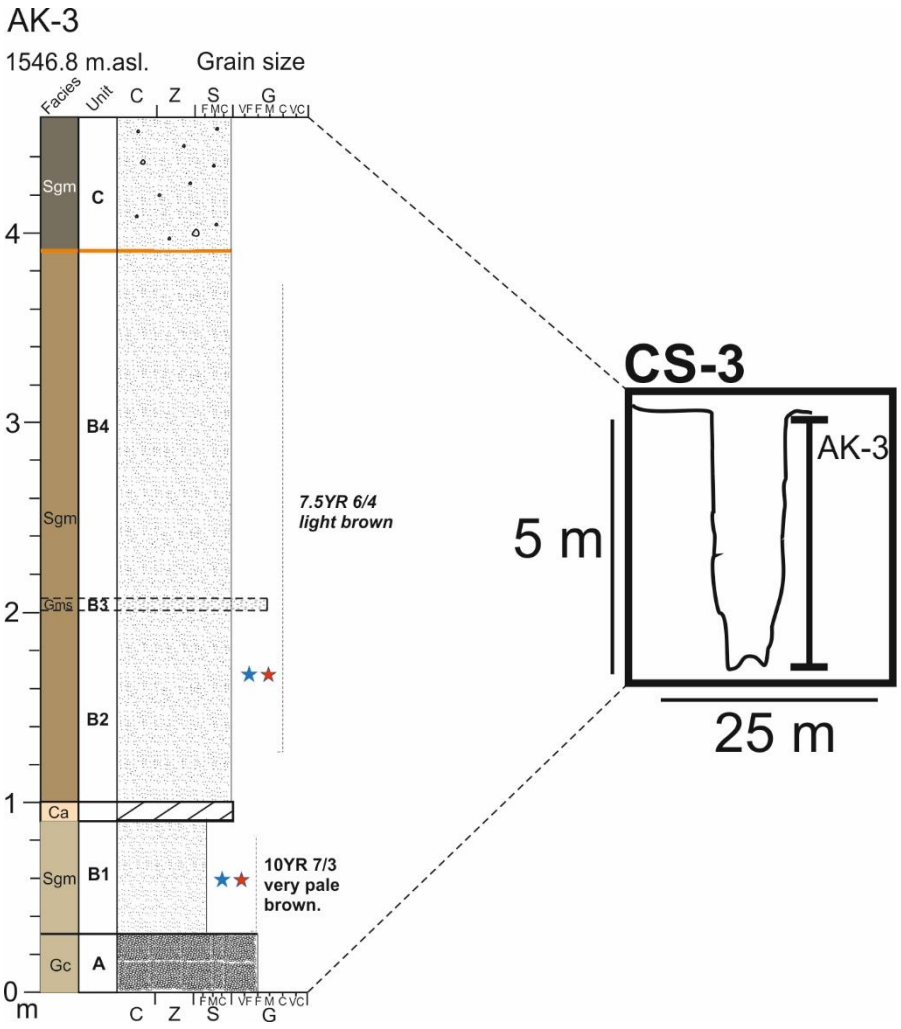

Figure 5.27 – log AK-3 and cross section.

Table 5.9 – percentage loss on ignition data and bromine content (ppm) for sampled horizons at AK-3. *This unit is treated individually in text and illustrated in figure 5.11.

Unit	Height (cm)	Loss on ignition (%)	Bromine (ppm)
*Basal soil 15m upstream	20-30	1.42	0.1
B1	55-65	1.5	0.5
B2	170-180	1.59	0.7

Unit A consists of calcretised, clast-supported gravels with local cobbles. A sharp contact between unit A and B1 exists, the latter consisting of very poorly sorted, silty

clays. Colour is 10YR 7/3 very pale brown, distinctive from other units on the upper slopes. 20 m upstream from AK-3, the deeply weathered dolerite dyke consists of very poorly sorted silty clays (77.3% combined – Fig. 5.29a) the colour of which is 2.5Y 8/2 pale brown. This unit is similar in magnetic characteristics to unit B1 (AK-3) on the basis of very weak concentration-related proxies (Fig. 5.30a), but exhibits distinctively high $\chi_{ARM}/_{IRM1T}$ values (0.38), S_{-300}% (7.9% of applied remanence unreversed - Fig. 5.30b and c).

Unit B2 consists of a poorly sorted coarse to very coarse sand (collectively 55.9%). A subordinate fine sand mode exists (96μm), with minor silt and clay (12.1% collectively – Fig. 5.37b). χ_{LF} and IRM_{1T} in particular peak for this unit (Fig. 5.38a). χ_{FD}% is moderately high (4%), but crucially the $\chi_{ARM}/_{IRM1T}$ is negligible (0.02 – Fig. 5.38b). This unit is also distinctive on the basis of S_{-100}% (74% of applied remanence reversed – Fig. 5.38c). All sampled units exhibit negligible bromine and LOI% values (Table 5.17).

Figure 5.28 – photograph of outcrop AK-3.

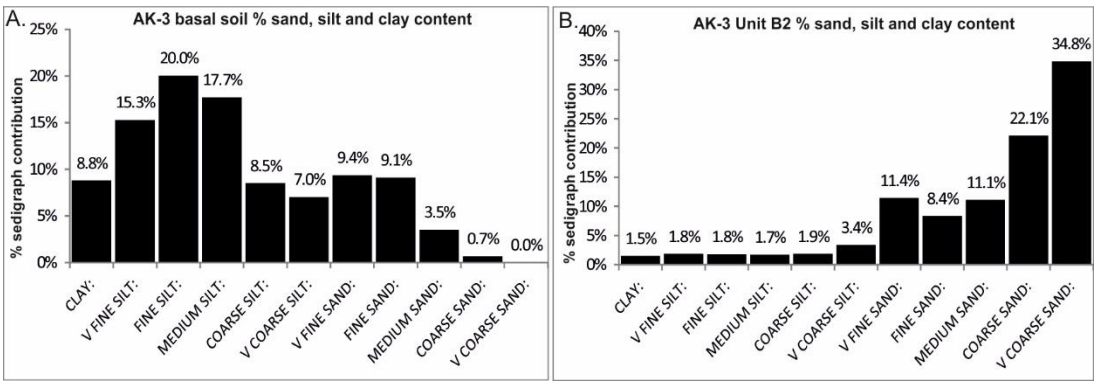

Figure 5.29 – % sand, silt and clay content derived from Coulter grain size analysis on samples collected from outcrop AK-3.

The following units were difficult to access, excavate and analyse, so only general details are provided. Unit B3 is a thin bed of matrix-supported gravel within an otherwise apparently uniform matrix as described for unit B2 and similarly for B4. Colour is 7.5YR 5/6 strong brown, but there is local reddening at the very top of the unit with a sharp, planar contact between B4 and C. Unit C appears to be a weakly bedded sandy unit similar in characteristics to that reported at AK-2 (unit F) just upstream from the dolerite barrier.

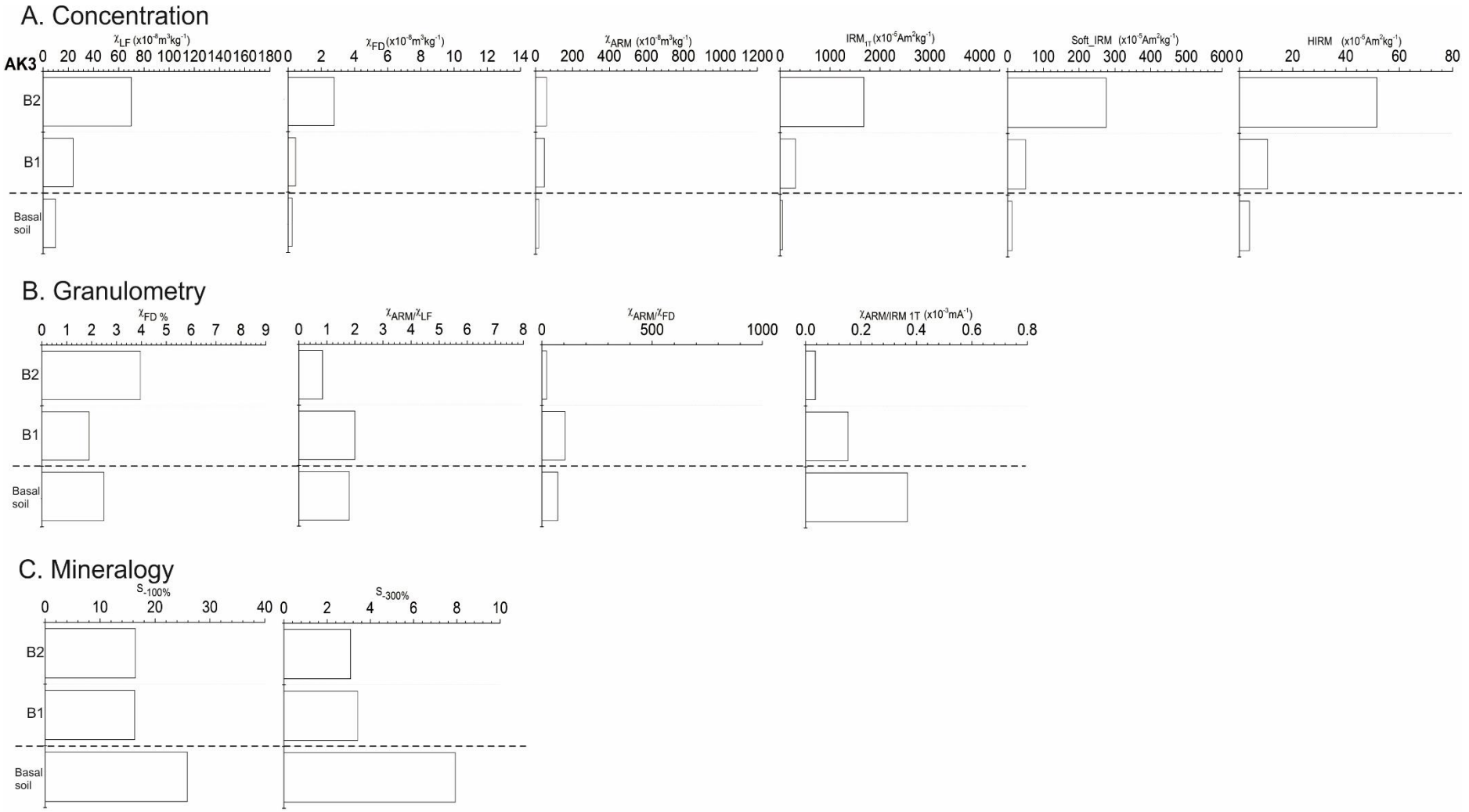

Figure 5.30 – mineral magnetic parameters from outcrop AK-3.

5.2.5b: AK-3 interpretation

In contrast to the valley-cross section morphology at AK-1 and AK-2, the local topography slopes towards the gully at CS-3. The facies here exhibit markedly different characteristics to the floodout upstream.

The fact that the basal clast-supported gravels are doleritic implies they have been locally sourced. An in situ soil is ruled out here as a clear upward fining is absent and the facies exhibit poor matrix development. Rather, the fine gravel implies sorting by current flow. As they occur at the base of the succession, overland flow over the dolerite bedrock upstream could have emplaced these clast-supported gravels, or alternatively, they could have been delivered from the hillslopes to the north east.

The colour of the massive sand unit (B1) shows evidence of gleying (10YR 7/3 very pale brown), as well as exhibiting mottled calcite leached from the calcrete horizon at 95-100 cm. This attests to the role of groundwater in producing these gleyed characteristics. Groundwater is primarily sourced from natural aquifers associated with the dolerite intrusions in this region (Meiklejohn, 2013 – pers. comm). Botha et al, (1994) also recognised that the Karoo dolerites are rich in calcium and thus Ca^{2+} ions are easily liberated in solution and carried to valley floors via runoff. Although the micromorphology of the calcrete at AK-3 is not analysed in detail here, it is interesting to note that the thin (7-9 cm) calcic horizon grades to the top of the deeply weathered dolerite barrier 20-30 m upstream implying that the dolerite was the source of Ca for carbonate fixing.

The structureless, fine-grained nature of the facies above the calcrete (unit B2) indicates low energy sedimentation. The local topography indicates this is not a fan or floodout (AKH-AK2). If the deposit was a laterally impinging fan associated with a discontinuous gully, the cross-section morphology would exhibit evidence of a distinct slope perpendicular to the contemporary gully. The most reasonable alternative is that the deposits were laid down primarily by slopewash transporting sediment from the nearby hillslopes to the east. The paler colour of these deposits (7.5YR 6/4 light brown) in concert with the extremely low bromine and LOI% values indicate the soil is leached compared to those sampled upstream. Although not excavated and analysed in detail, the local reddening at the top of unit B, may be indicative of a palaeosol (B horizon), now capped by overbank sediments (unit C)

associated with the incision of the modern gully. The relatively dark, organic rich horizon in the left bank (Fig. 5.31) may signify a polygenetic soil, with organic inputs from the contemporary vegetated surface overprinting the aforementioned rubified palaeosol surface.

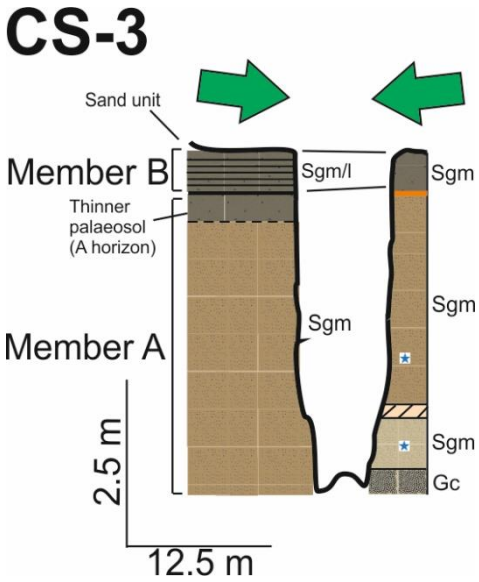

Figure. 5.31 – cross-section schematic at AK-3. Note the thicker grey soil horizon exposed in the left bank.

Downstream from AK-3, there is evidence for a number of infilled palaeogullies preserved within the left terrace. These occur as: 1) isolated pockets of minerogenic clast-supported cobbly gravels overlain by matrix-supported very poorly sorted gravels (Fig. 5.32) and 2) larger, fine-grained gleyed palaeochannel structures (Fig. 5.33). These infill deposits probably represent high energy flows from the hillslopes to the valley floor. Notably, the fine-grained silty sands into which they have cut and filled are pervasive downstream as far as AK-5, discussed in section 5.2.7.

The deeply gleyed, infilled channel shown in Fig. 5.33 is most likely indicative of a channel in a former wetland. The fact that these palaeochannels occur just above the elevation of the contemporary channel indicates that a similar base-level once existed prior to valley infilling by slopewash deposits and that sediment was once conveyed by a gully downstream at least as far as the next sandstone rock step.

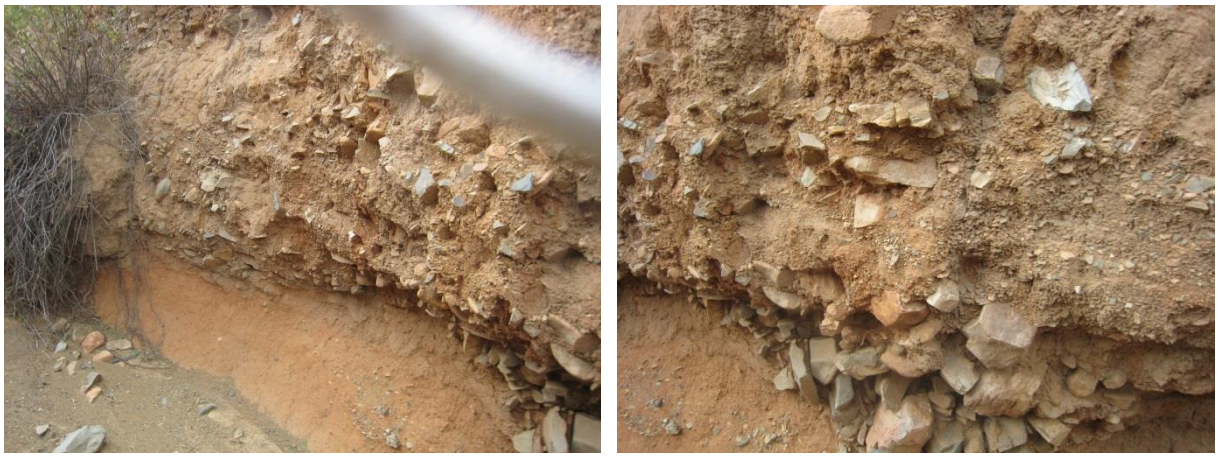

Figure. 5.32– small palaeo-gullies infilled with very coarse material locally sourced from nearby hillslopes. Note also the fine-grained light brown silty sand unit into which the palaeo-gullies are incised.

Figure. 5.33 – view upstream showing junction between the orange, slopewash material and a deeply gleyed, infilled palaeochannel approximately 60 m downstream of AK-3.

Subunit B1 is characterised by a weak magnetic assemblage with a very small ferrimagnetic component. Considering the evidence quoted for groundwater influence, it is likely that the magnetic signature is largely diluted by diamagnetic effects related to the presence of leached calcite as well as the dissolution of magnetite/maghemite. As a result, it is difficult to establish the extent to which the soil is polygenetic from the magnetic measurements alone. For instance, the silty sands deposited by slopewash are likely to have initially carried a strong ferrimagnetic signature comparable to that observed upstream of the dolerite barrier.

However, the extent of pedogenic modification reflected in a net grain size shift toward SP/SD grains has been erased due to groundwater-induced dissolution of magnetite resulting in a distinctive (albeit weak) MD ferrimagnetic signature. Furthermore, the very low concentrations of remanence carrying ferrimagnets reinforce the notion of diamagnetic inputs primarily from leached calcite and secondarily, quartz. Paramagnetic minerals like ferrihydrite are also likely to be present under waterlogged soil conditions. However, as both diamagnetic and paramagnetic minerals (quartz and calcite; ferrihydrite etc) exhibit no magnetic remanence, it follows that the relatively large S values (although < 4%), represents a canted anti-ferromagnetic (AF) assemblage, probably goethite, which preferentially forms 'wetter' soil conditions than haematite as well as high organic matter and aluminium content (Schwertmann and Taylor, 1989; Balsam et al., 2004). The pale colour (10YR 7/3) is distinct from the other soils examined thus far, but this may be due to leached calcite diluting the 'redder' hue of the original soil.

Unit B1 is also very clearly differentiated from the basal dolerite soil which displays the highest concentration of AF minerals compared to anything observed thus far. This soil formed directly on the dolerite is heavily leached (2.5Y 8/2 pale brown) pointing to conditions of persistent reduction, producing goethite as well as paramagnetic minerals.

Unit B2 in contrast displays a distinct ferrimagnetic signature (χ_{LF} = 69) comparing well with published values for Beaufort Group sandstone rather than dolerite (Rowntree et al., 2012). This clearly indicates that the palaeo floodout (AKH – AK-2) was not the primary source of sediment to AK-3. Rather, slopewash draining the sandstone slopes to the east resulted in slow aggradation out of sync with the floodout. The S values indicate a measurable AF contribution (S_{-300}% = 3), probably haematite, as this is above the threshold of water-table influence as per the elevation of the gleyed soils (unit B1).

5.2.6a: AK-4 analysis

Log AK-4 was obtained from a 1.8 m gully exposure 926.4 m downstream of the headwaters on the right bank (Fig. 5.1, 5.34 and 5.35).

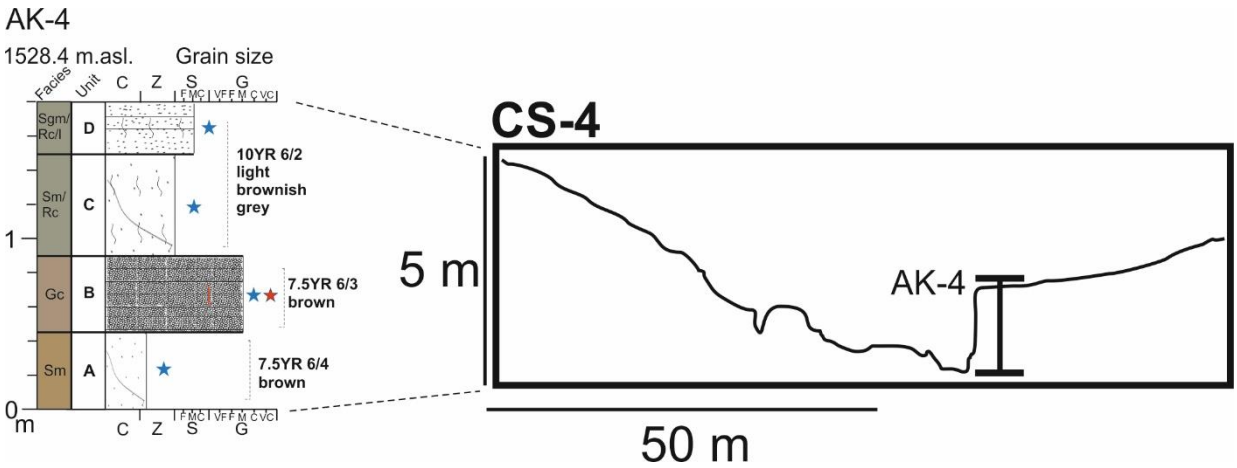

Figure 5.34 – sedimentary log AK-4 and cross section.

Unit A was traced all the way up to AK-3. It consists of a very poorly sorted, fine grained polymodal matrix (collectively 76.8% silt and clay; 23.2% sand), with subangular-angular very fine gravels (Fig. 5.36a). The unit exhibits high cohesivity owing to the high clay content (11.3%). Colour is 7.5YR 6/4 brown. Total magnetic susceptibility is high (χ_{LF} = 115), but χ_{ARM} is extremely low (Fig. 5.48a). As a result, the granulometric quotients are all nearly zero (Fig. 5.40b). A sharp, planar contact exists between units A and B (Fig. 5.34).

Unit B consists of friable, faintly horizontally bedded, matrix-supported subangular medium gravels. Some pockets of clast-supported material occur. The matrix is mainly coarse to very-coarse sand (79% - Fig. 5.36b). Colour is slightly darker than unit A: 7.5YR 6/3 brown. Magnetic properties differ from unit A primarily on the basis of the large χ_{ARM} (487) and HIRM (58 – Fig. 5.40a). Thus, the granulometric quotients are all relatively high, but also, S_{-300}% is larger than the other units, with 3.8% of the applied remanance unreversed at -300mT (Fig. 5.40b).

Figure 5.35 – photograph of outcrop AK-4.

Table 5.10 – percentage loss on ignition and bromine (ppm) data for sampled horizons at AK-4.

Unit	Height (cm)	Loss on ignition (%)	Bromine (ppm)
A	20-30	1.9	3.6
B	60-75	1.4	5.8
C	115-125	2.4	21.8
D	155-165	2.7	6.5

Unit C possesses frequent root channels and only occasional lenses of very coarse sand preserved in the parent sediment. The sedigraph for unit C is polymodal with coarse to very-coarse sand (36.6%) and very fine silt to clay (27.8% - Fig. 5.36c). Colour is 7.5YR 4/2 brown. Unit C is distinctive from A and B with very low concentration-related magnetic proxies, but relatively large granulometric quotients; $\chi_{ARM/IRM1T}$ – 0.6, for example (Fig. 5.40b). Unit D consists of a medium-sand dominated matrix with silt and relatively well sorted compared to unit C. The unit is punctuated by two distinct laminations of gravel and capped by a thin veneer of well-sorted sands. This unit exhibits a distinctively high S_{-100}% value (36.5% unreversed

at –100mT - Fig. 5.40c). Colour is 10YR 4/3 brown. Units C and D exhibit the highest LOI% and bromine values (Table 5.10).

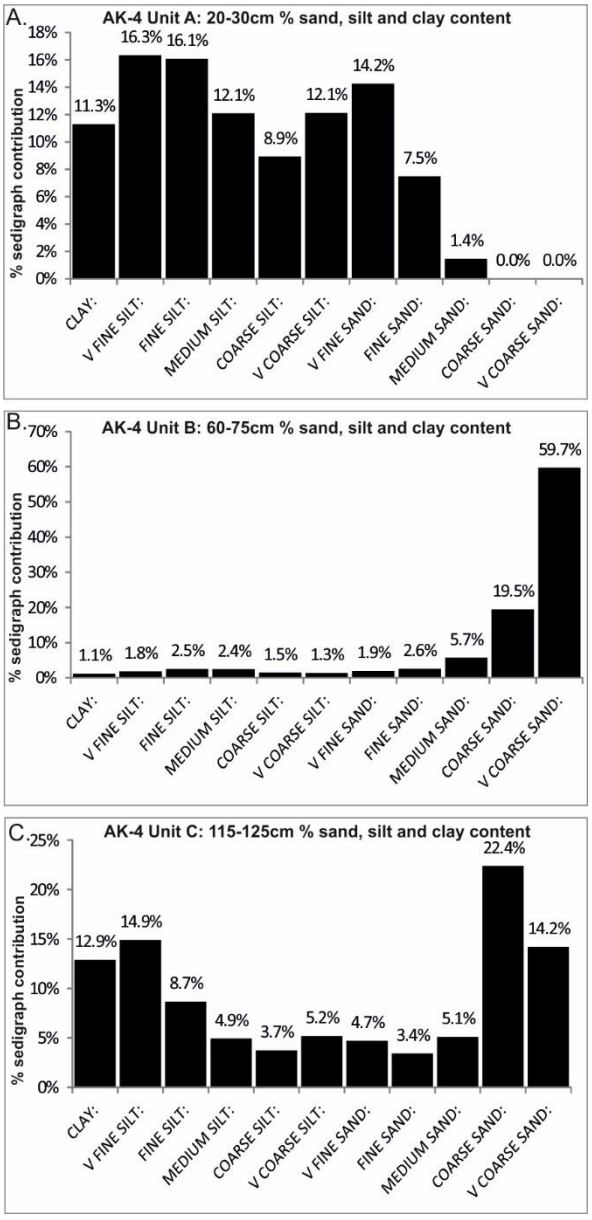

Figure 5.36 – % sand, silt and clay content derived from Coulter grain size analysis on samples collected from outcrop AK-4.

Inset within the sediments reported at AK-4, is a fine-grained, greyish brown deposit (10YR 5/1 -10YR 5/2) capped by a veneer of brown sand (Fig. 5.37). This inset deposit exhibits a sharp contact with the flanking orange-brown sediment (Fig. 5.37).

Figure 5.37 – photograph looking upstream with inset grey deposits within the orange fill at the valley margins.

Soil augering identified 65 cm of contemporary channel deposits capping these inset sediments (Fig. 5.38). The sample collected below the modern channel consists of 97.3% silt/clay combined. The unit above is relatively well sorted (67.6% coarse to very-coarse sand - Fig. 5.39).

Figure. 5.38 – auger hole through modern channel deposits of sand and gravel at AK-4.

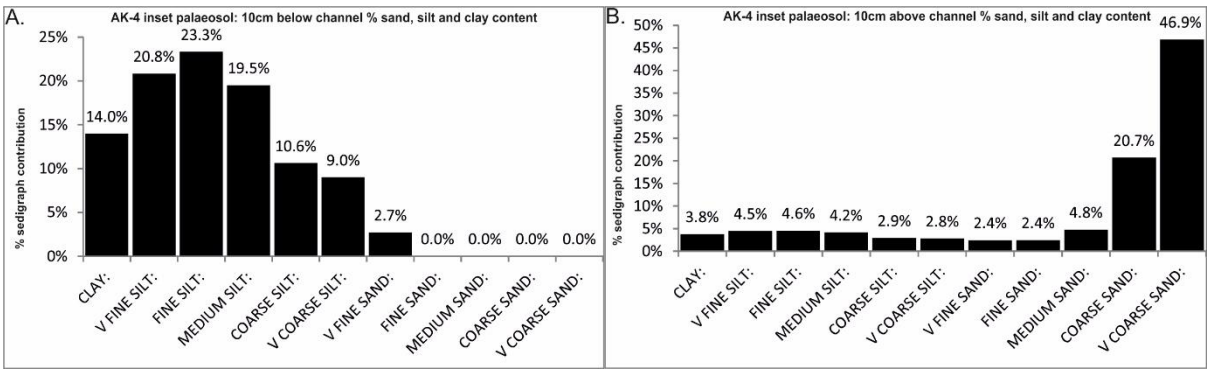

Figure 5.39 – % sand, silt and clay content obtained for the inset grey fills at 10cm below and above the contemporary channel surface respectively.

Magnetically, both samples are very similar with general low concentration related proxies (Fig. 5.40a). However, the sample below the channel exhibits relatively large $\chi_{ARM/IRM1T}$ (0.8) compared to above (0.49 - Fig. 5.40b). The latter lacks any measurable hard component reflected in the HIRM and S_{-300}% values (Fig. 5.40c).

5.2.6b: AK-4 interpretation

The grain-size composition of unit A implies deposition under low energy conditions. Given the local cross-section morphology which favours deposition toward the valley centre, as well as the traced continuity of unit A, it is more probable that these silty sands represent slopewash rather than channel deposits. Furthermore, the proximity of unit A to bedrock may have resulted in the accumulation of illuviated silt and clay from above, also evidenced by the distinctly low silt/clay of unit B (10.7%) and abundant root channels.

The contact between the matrix-supported fine gravels above (unit B) and the fine silty sands (unit A) is similar to that reported for the infilled bank gullies upstream (section 5.2.5). The laterally discontinuous, angular nature of the gravels indicates they have most likely been locally sourced and carried to the valley floor by slopewash. The sharp, planar contact between units B and C is interpreted as an unconformity. Unit C and D represent modern floodplain sediment associated with the loss of local valley confinement. They are clearly inset within the slopewash deposits of unit A. The overbank facies of unit C in particular displays evidence for high organic content, reflected in the high bromine values (21.8 ppm) and darker colour (10YR 6/2 light brownish grey). This reflects progressive organic matter inputs from vegetation on the contemporary floodplain surface (unit D).

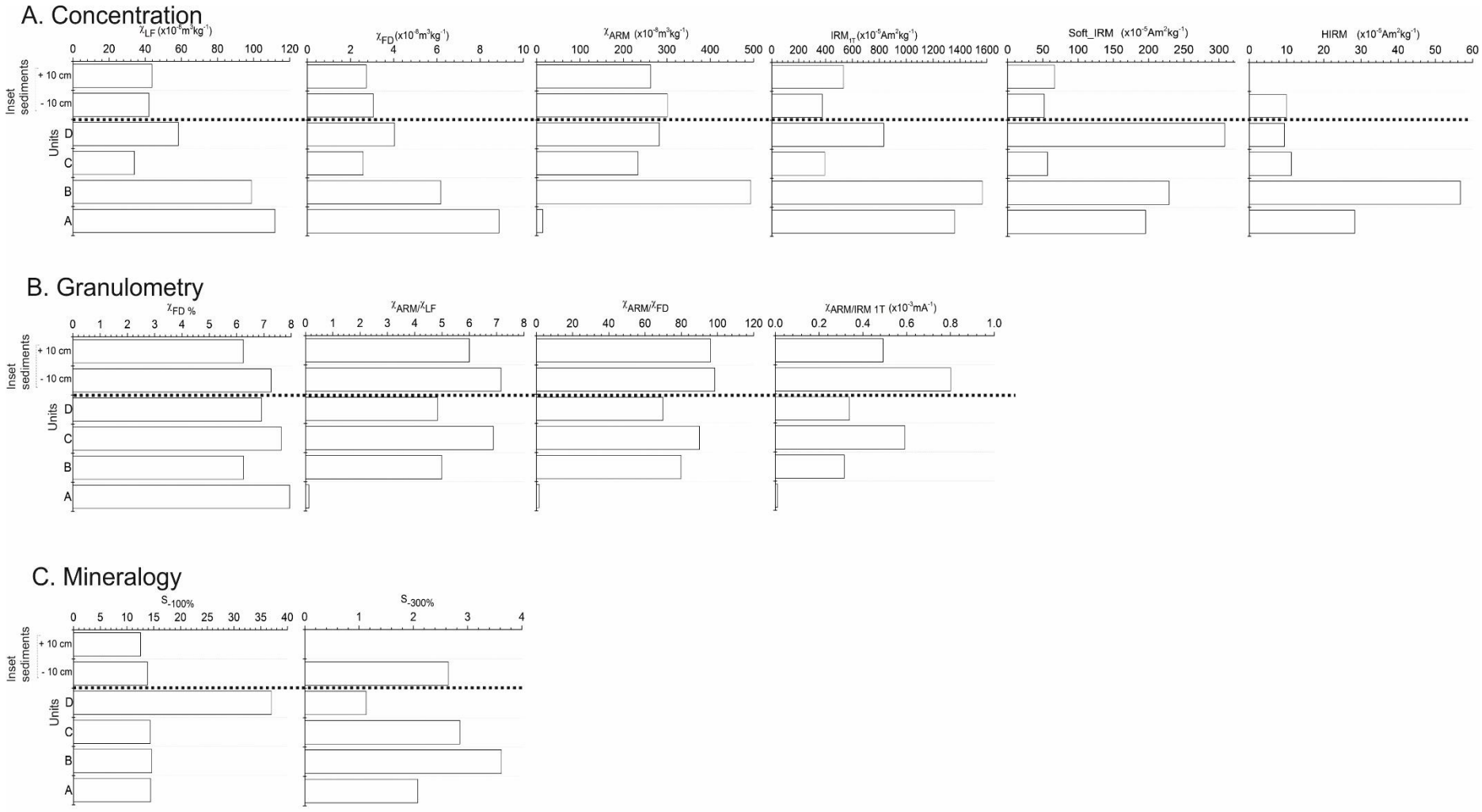

Figure 5.40 – mineral magnetic parameters from outcrop AK-4 and the inset grey fills sampled at +10 and -10 cm above and below the channel respectively.

The sharp lateral boundary between the slopewash deposits identified (AK-3 – AK-4) and the inset grey sediment package indicates that they are unconformable (Fig. 5.37). These grey fills are clearly inset within the orange fill (AK-4), signifying a major stratigraphic junction exists between the two. The friable nature of these sediments compared to the deeply weathered slopewash deposits (AK-4 unit A and B) implies they are much younger. The fine-grained nature of the deposits, in concert with their 'grey' colouration implies a low energy depositional environment such as a wetland. The association with this palaeowetland (grey fills) and loss of confinement upstream of a major rock step is analogous to modern wetlands formed in areas of impoundment behind rock barriers reported in Chapter 4 (Table 4.3: analogue 1).

Both units A and B are dominated by a strong ferrimagnetic assemblage (χ_{LF} – 98-112), but there are distinct differences in associated ferrimagnetic grain size. For instance, the negligible $\chi_{ARM}/_{IRM1T}$ (0.01) implies contribution of SD grains to total remanence to be miniscule. Further, the very high IRM_{1T} values probably reflect a distinct lithogenic origin as reported earlier for both bulk and particle-size magnetic susceptibility data (AK-1–AK-2). It is interesting to note that AK-3 unit B2, is the only other sample found to exhibit such low values of $\chi_{ARM}/_{IRM1T}$ and both that and AK-4 unit A are slopewash deposits sourced from the hillslopes to the east. In this respect, these sediments are clearly distinguished from those mantling the upper slopes (AKH-AK-2). Nevertheless, there is evidence for a distinct SP grain size signature which probably resides in the clay fraction (see section 5.2.3), but this is likely to have been concentrated by the illuviation of clays into unit A from B.

Unit B by contrast exhibits higher concentrations of SD as well as SP grains on the basis of the χ_{ARM} and χ_{FD}%. The higher S_{-300}% values for this unit indicate a larger AF mineral contribution, probably haematite compared to unit A, although an AF presence is still indicated for the latter. The fact that this occurs beneath an unconformity indicates that this is a palaeogeomorphic surface that is stratigraphically coeval with the top of unit B2 at AK-3 and is thus classified as member B sediment.

Unit C exhibits a weak ferrimagnetic signature but shows proportionally more SP/SD grains relative to MD on the basis of the greater $\chi_{ARM/IRM1T}$ (0.6). The total magnetic properties (χ_{LF} and IRM_{1T}) are very similar to the basal unit at AK-3 which could

indicate sediment supplied to the floodplain from headward erosion of the AK-3 sediments. A combination of a poorly drained substrate (50.2% silt/clay) and high organic matter content (bromine: 21.8 ppm) have probably resulted in ferrimagnetic dissolution and diamagnetic effects reducing overall susceptibility.

Unit D indicates a moderate-strong ferrimagnetic signature (χ_{LF} = 59). As this unit is characterised by modern overbank sediments, it may be taken as an analogue of the magnetic properties of the sediment transported by the modern channels. Some interesting points relating to source can be drawn here. The only other documented source exhibiting comparably high S_{-100}% (25.9%) is the eroding dolerite intrusion upstream of AK-3. The remanence parameters are intermediate between the maagnetite dominated sediments of AK-2 (units A and E) and AK-3 unit B1, both of which display evidence of fresh bank erosion after ephemeral channel flows. It is therefore likely that the magnetic signature on the floodplain reflects a combination of these two different sediment sources.

The low concentrations of remanence carrying ferrimagnets exhibited by the inset grey fills compared to units A, B and D at AK-4, implies that ferrimagnetic dissolution has occurred consistent with a poorly drained environment such as a wetland. In this case, the S_{-300}% (2.6%) likely reflects goethite. The proportion of remanence carriers that are SD in size is higher (0.49) and the χ_{FD}% indicates high proportions of pedogenic SP grains. Even in light of the factors proposed as probable diluters of ferrimagnetic concentration, all concentration-parameters are much weaker than the floodout sediments at AK-2 (Table 5.11). It follows that sediment from the upper slopes (AKH – AK-2) was not supplied to this reach, most likely due to the dolerite barrier.

Table 5.11 – selected magnetic parameters for the palaeosol reported at 1) AK-2 floodout system and 2) inset channel deposits reported at AK-4.

Outcrop and unit	X_{LF}	$X_{FD\%}$	X_{ARM}	IRM_{1T}	χ_{ARM}/IRM_{1T}	S_{-100}%	S_{-300}%
AK-2 E	142.6	8.1	1057.3	1483.5	0.71	11.6	0.9
AK-4 Inset: -10cm	42.1	7.27	301.1	376	0.8	13.8	2.65
AK-4 Inset: +10cm	43.8	6.2	262.5	532.9	0.49	12.5	0

5.2.7a: AK-5 analysis

Log AK-5 was obtained from a 2.8 m gully exposure approximately 1029.2m downstream of the headwaters on the left bank (Fig. 5.1, 5.41 and 5.42). The exposure is immediately downstream of sandstone rock step 4 (see Fig. 4.4 – Ch. 4.2).

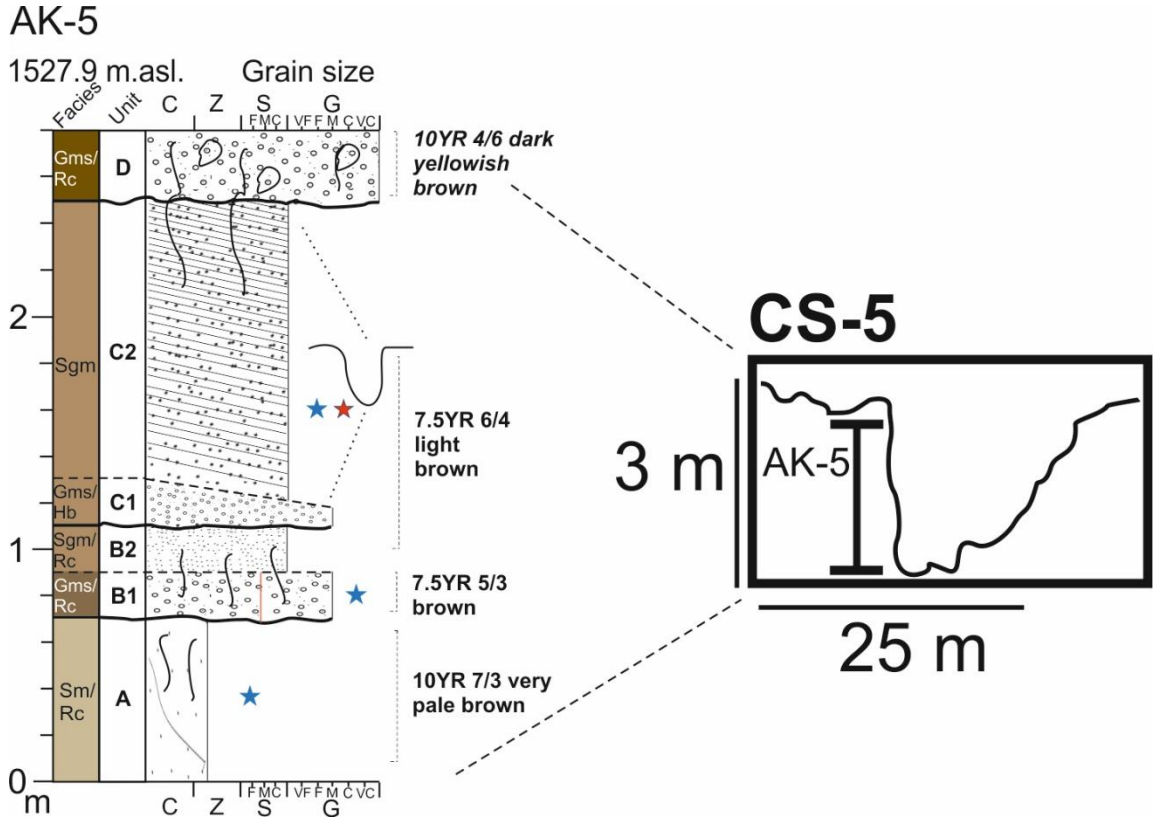

Figure 5.41 – sedimentary log AK-5 and cross section.

All sedimentary units exhibit sharp bedding contacts. Unit A consists of a cohesive, very poorly sorted matrix of mud (silt/clay – 78%) and a small peak in the fine-medium sand range (21.9% - see Fig 5.43a). This unit exhibits relatively high moisture and soil organic matter content (2.42% and 2.14% respectively - Table 5.12) relative to sampled units above. Colour is 10YR 7/3 very pale brown.

Unit B1 unconformably overlies unit A consisting of matrix-supported, predominantly fine-medium gravels (6-8 mm) but with local very coarse gravels and cobbles. The matrix is poorly sorted, consisting of 59.5% medium to coarse sand and is negatively skewed with 21.4% silt/clay (75-85 cm – Fig. 5.43b). Grain D_{50} is 351µm – medium sand (Fig 5.43, unit B1). Colour is markedly different to unit A: 7.5YR 5/3 brown. Unit B2 consists of a poorly sorted matrix of sandy silt, hosting local fine gravels. The unit

is friable with a weakly developed blocky structure. Root channels are common. Unit C1 cuts into unit B2, and is coarser with medium-bedded matrix-supported medium gravels. Unit C2 grades to thickly-laminated to thinly-bedded sandy silts and fine gravels which laterally grade to coarse gravels.

Figure 5.42 – photograph of outcrop AK-5.

Table 5.12 – percentage loss on ignition data and bromine content (ppm) for sampled horizons at AK-5.

Unit	Height (cm)	Loss on ignition (%)	Bromine (ppm)
C2	155-165	1.11	1.4
B1	75-85	1.84	3.2
A	35-45	2.14	2.9

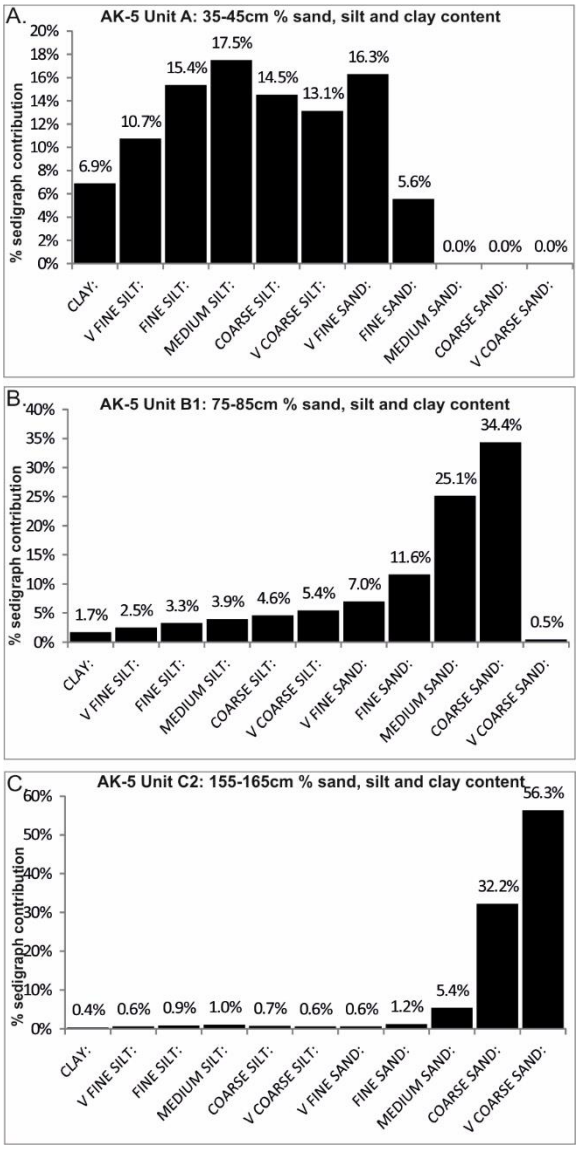

Figure 5.43 – % sand, silt and clay content derived from Coulter grain size analysis on samples collected from outcrop AK-5.

Gravels are predominantly subrounded (50%). The matrix for the sandy beds consists of a moderately-well sorted coarse to very coarse sand (88.5% collectively), with a fine tail to the distribution (7.2% fine-medium sand; 4.2% silt/clay – see Fig 5.43c). Laminae/beds have local lenses (few cms in diameter) of fine gravel and sand to the left. Colour is 7.5YR 6/4 light brown. Loss on ignition, bromine and moisture content are lowest in this unit (Table 5.12).

The contact between units C2 and D is sharp and undulating. Unit D consists of a very poorly sorted mix of subangular clast-supported gravels ranging from medium to coarse and local cobbles. Matrix support is variable, consisting of poorly sorted sandy silts where it does occur. Root channels are common.

Magnetic susceptibility decreases with depth. The basal unit (A) is distinctively weaker in terms of concentration-related proxies (χ_{LF} = 42), but no substantial variations in other properties occur (Fig. 5.44a).

5.2.7b: AK-5 interpretation

The very poorly sorted silty sands are virtually identical in terms of grain size distribution compared to AK-4 unit A and similarly exhibit low soil organic matter content. The presence of root channels infilled with silt attests to illuviation. The pale colour of AK-5 unit A is attributed to poor drainage due to it overlying bedrock.

The sharp undulating contact separating unit A from the laterally discontinuous matrix-supported gravel unit (B1) indicates an unconformity. Unit B represents channel deposits deposited under upper flow regime conditions (B1), with the massive sands above (B2) indicating flow cessation. The crumb structure exhibited by unit B2 in concert with root channels indicates bioturbation and soil formation. Unit C is an infilled palaeochannel carved into unit B sediments, which is subsequently incised again but this time by sediments deposited under high energy flow conditions. The very coarse nature of these deposits (unit D) in concert with the poorly sorted matrix indicates emplacement by debris flows. As the terrace (CS-5 – Fig. 5.41) slopes toward the modern channel, this palaeochannel must have originated from slopes to the west. The sediments immediately upstream of AK-5 are characterised by smaller scale ‘cut and fill’ features (Fig. 5.45).

Unit A is characterised by a relatively weak ferrimagnetic signature compared to the above units due to the poorly drained nature of the unit inducing dissolution of magnetite and formation of paramagnetic iron sulphides (Torrent et al., 2006). Given the evidence for bioturbation in the form of root channels, it is likely that the relatively high SP/SD content may be due to illuviation of grains.

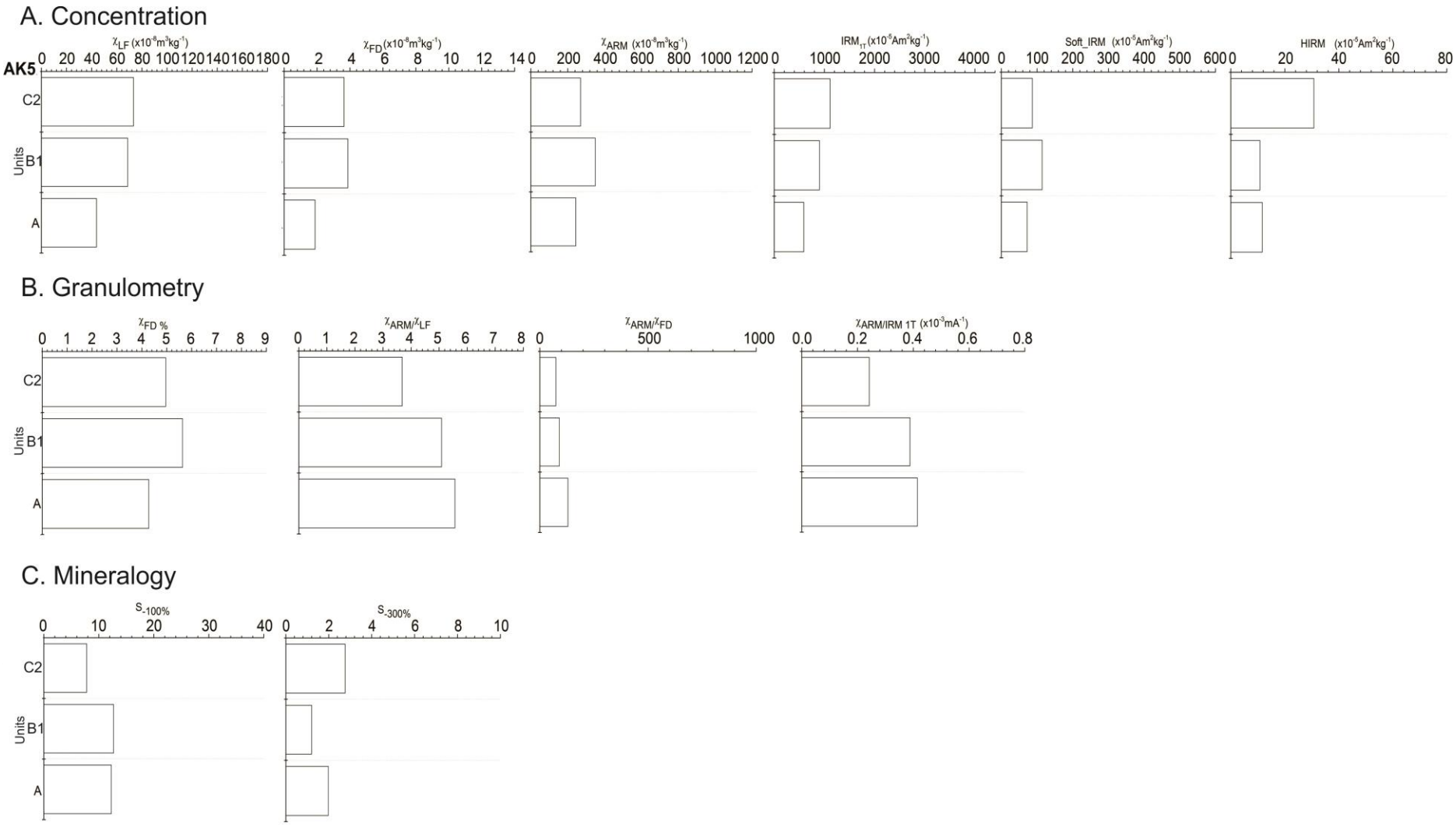

Figure 5.44 – mineral magnetic parameters from outcrop AK-5.

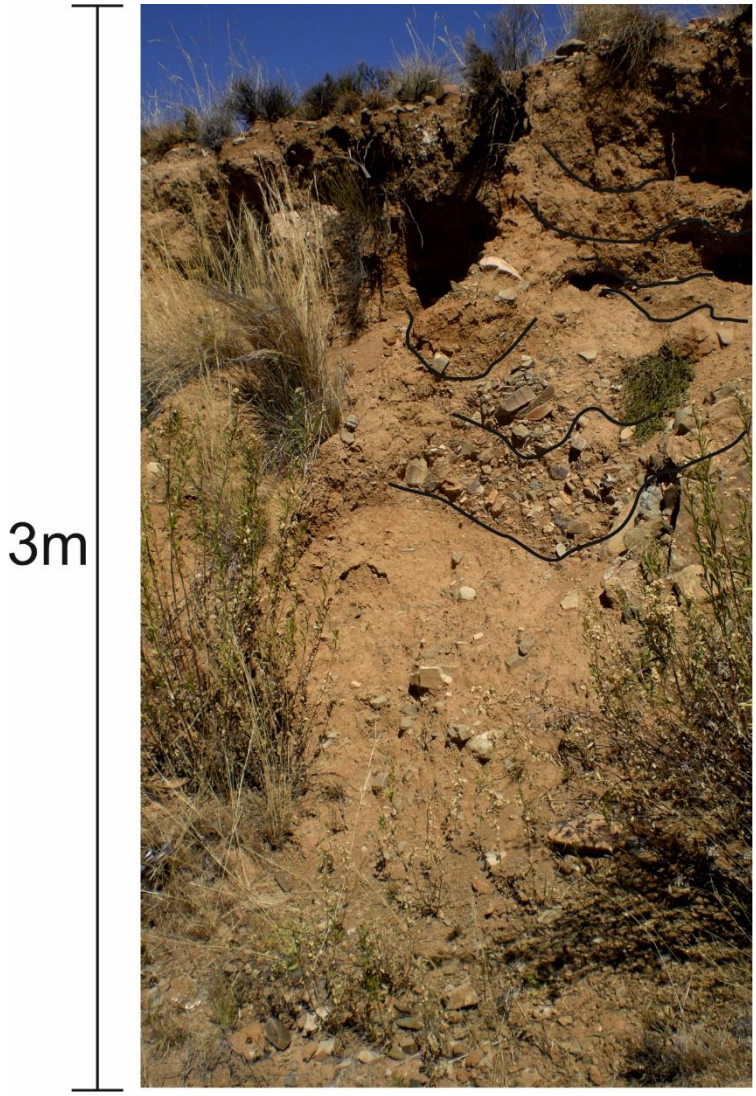

Figure. 5.45 – small scale ‘cut and fill’ architecture reflected in left-bank sediments adjacent to outcrop AK-5

Subunit B1 exhibits relatively high concentrations of SP/SD ferrimagnetic minerals, probably magnetite and plots inside the pedogenic envelope (Oldfield, 2007). Subunit C2 exhibits slightly higher concentrations of ferrimagnetic minerals with slightly lower concentrations of SP/SD grains. The similitude in ferrimagnetic concentration between B1 and C2 indicates that i) no intervening phases of soil development occurred and ii) there was no change in sediment source.

5.2.8a: AK-6 analysis

Log AK-6 is the first log obtained from terrace fills in the second order channel, recorded from a 3.4 m channel exposure on the left bank 1246.5 m downstream from the headwaters (Fig. 5.1, 5.46 and 5.47).

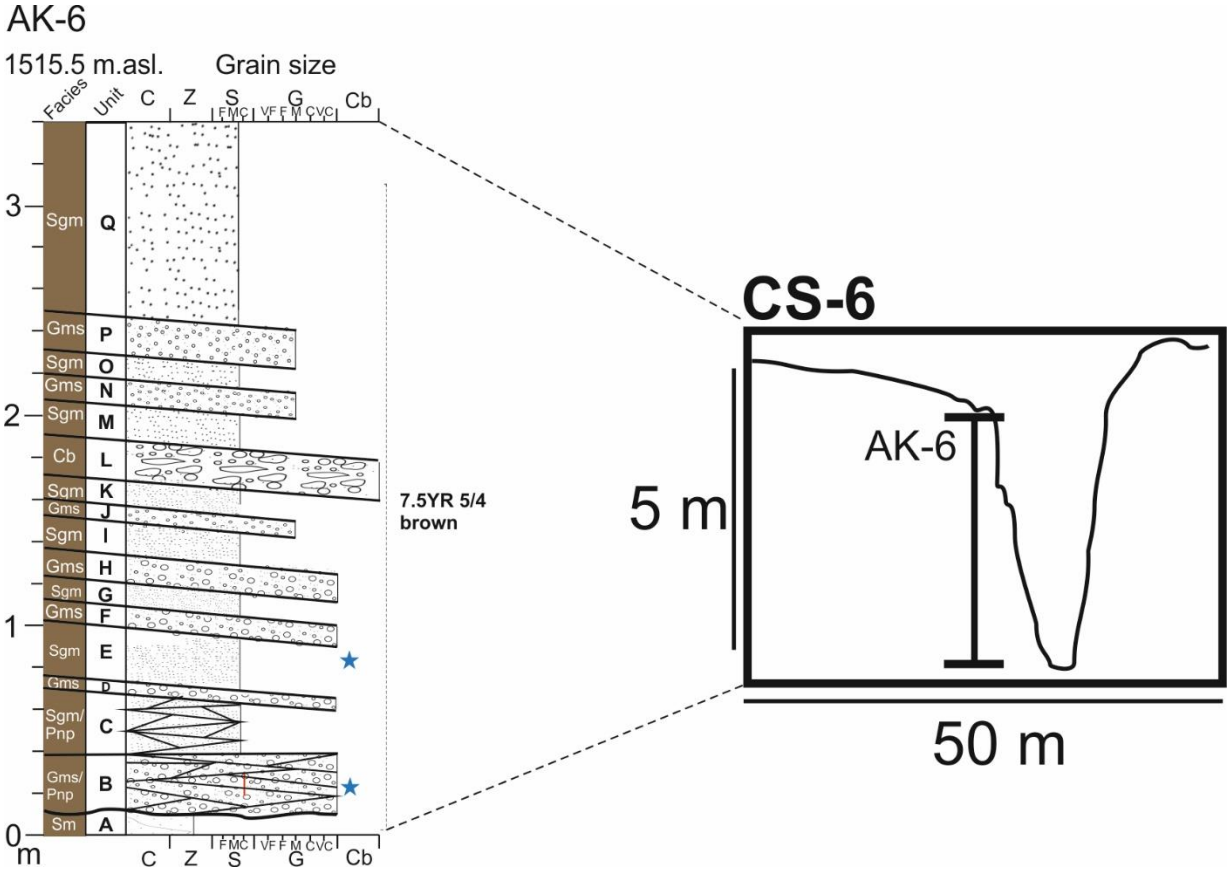

Figure 5.46 –sedimentary log AK-6 and cross section.

Unit A consists of poorly sorted, cohesive silty clays, which are overlain by thin-medium, planar-non parallel bedded, laterally discontinuous, very coarse gravels (unit B). The beds exhibit lateral coarsening from matrix supported gravel to clast-supported very coarse gravel. Total susceptibility is high (χ_{LF} = 87) Unit B is moderate-poorly sorted, consisting of coarse to very coarse sand (76.3%), negatively skewed toward finer grain sizes (10.8% silt and clay – Fig. 5.48a) which exhibits planar non-parallel cross bedding. Colour is 7.5YR 4/4 strong brown.

Table 5.13 – percentage loss on ignition data and bromine content (ppm) for sampled horizons at AK-6.

Unit	Height (cm)	Loss on ignition (%)	Bromine (ppm)
B	35-45	4.3	2.7
E	90-100	-	1.4

Figure 5.47 – photograph of outcrop AK-6.

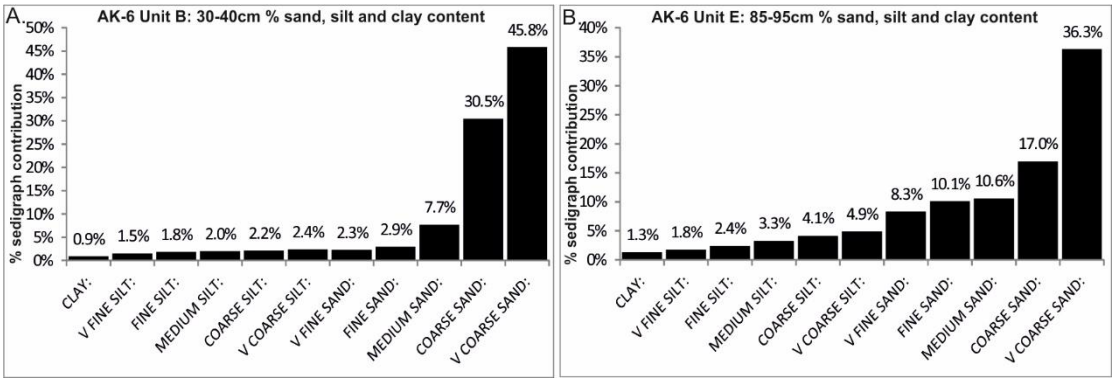

Figure 5.48 – % sand, silt and clay content derived from Coulter grain size analysis on samples collected from outcrop AK-6.

Units D-P comprise alternating massive beds of coarse sand and clast supported gravels or cobbles. The beds are laterally discontinuous with coarsening to the right of the logged section, with all units exhibit sharp, planar contacts. Unit E exhibits higher remanance values than B (Fig. 5.49a) as well as χ_{ARM}/χ_{LF} despite no increase in $\chi_{ARM/IRM1T}$ (Fig. 5.49b). Unit Q is massive and relatively clast poor, with a matrix dominated by medium-coarse sand.

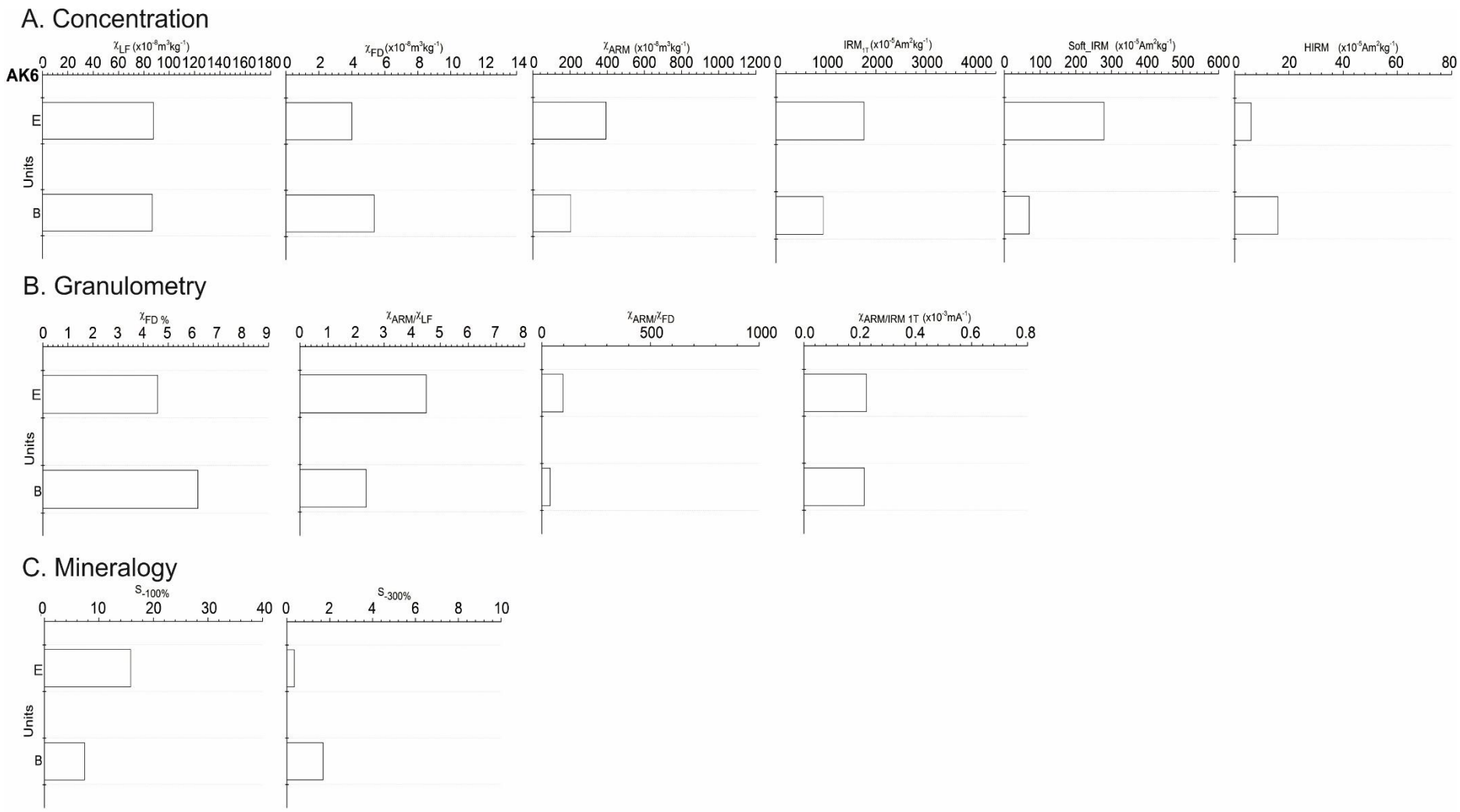

Figure 5.49 – mineral magnetic parameters from outcrop AK-6.

5.2.8b: AK-6 interpretation

The fine grained silty sand (unit A) is akin to that described for unit A of AK-4 and 5 representing slopewash facies. The rest of the succession (units B – Q) consists of infilled palaeochannel deposits confirmed by the 'channel' like structure carved into slopewash sediments and discontinuous beds of cobbles, gravels and sands.

Both sampled units (B and E) exhibit comparable total ferrimagnetic signatures, although unit B is predisposed towards higher SP compared to SD grains, whilst the reverse is true for unit E. The similitude in magnetic parameters between units implies a uniform source. The higher χ_{FD}% for unit B likely reflects illuvial concentrations of SP grains within clays and silts.

5.3 Central Valley: AK-7 – AK-14

5.3.1a: AK-7 analysis

Log AK-7 was obtained from a 4.2 m high channel exposure on the left bank directly overlying dolerite bedrock 1410 m downstream from the headwaters (Fig. 5.1, 5.50 and 5.51). Cross section 7 was obtained in closer proximity to AK-6 than AK-7, but is reported in association with AK-7 because it faithfully represents the inset 'grey' fills within rubified coarse deposits (Fig. 5.51).

Unit A directly overlies dolerite bedrock and consists of calcretised, clast-supported very coarse gravels. Unit B is markedly coarser, with weakly horizontally bedded cobbles and very coarse gravels. Any pockets of matrix consist of very poorly sorted sandy silt. Some clasts are orientated vertically within this matrix. Clasts are predominantly subrounded (44%) and subangular (36%) with a mixture of unweathered and deeply weathered dolerite clasts which display solution pits and and iron oxide coatings. Total magnetic susceptibility is higher than the overlying units (χ_{LF} = 91), but notably, there is not a hard remanence component (HIRM and S_{-300}%). S_{-100}% is lower than the overlying units (9% of applied remanance unreversed – Fig. 5.53).

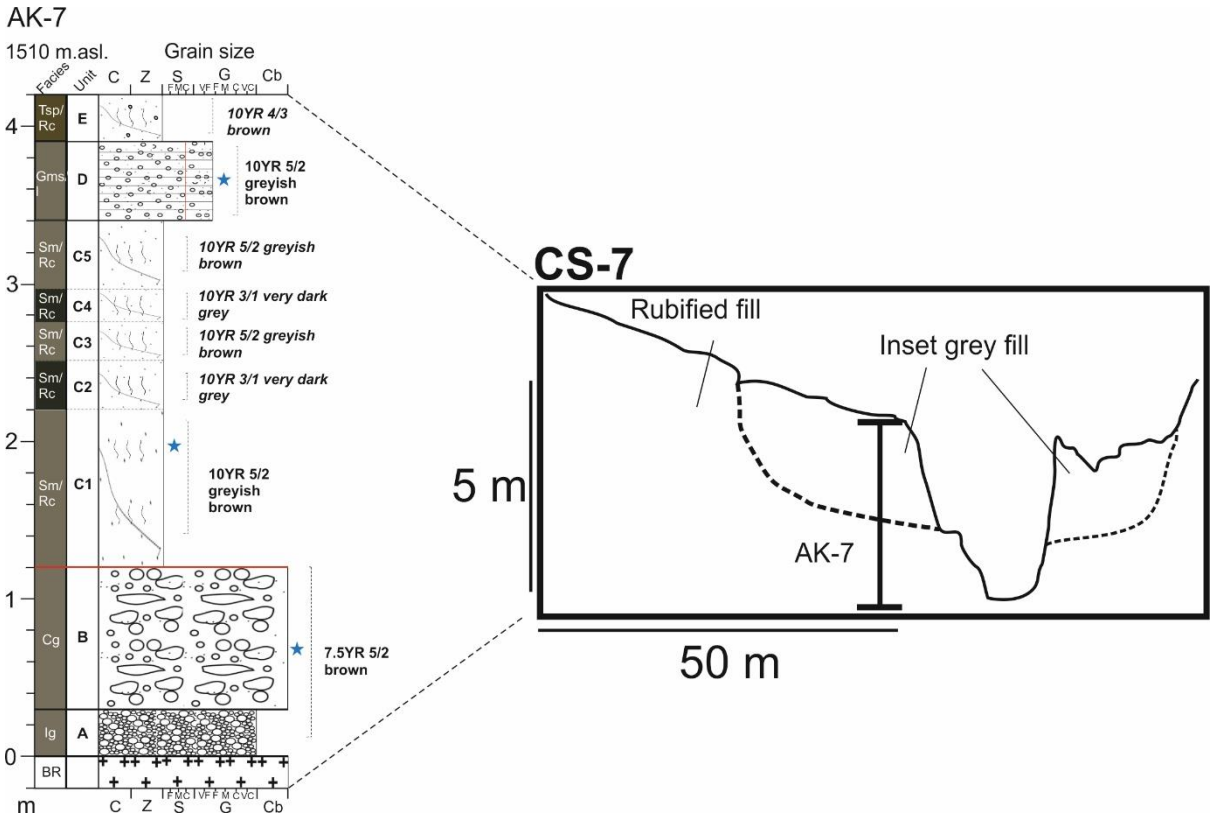

Figure 5.50 – sedimentary log AK-7 and cross section.

Unit C consists of silty sand with subtle variations in colour alternating between 10YR 3/1 very dark grey (subunits C2 and C4) and 10YR 5/2 greyish brown (subunits C1, C3 and C5). Unit C1 is dominated by silts and clays (52.6% combined- see Fig. 5.52a) but with subordinate fine doleritic gravels with darkened, smooth surfaces. This subunit also displays higher bromine content (9.7 ppm) but lower LOI (1.4%) than unit B below (4.1 ppm and 4.2%, respectively - Table 5.14). Concentration and granulometric magnetic proxies are typically much lower than for unit B – in particular the χ_{ARM} (3.83 – Fig. 5.53a) and χ_{FD}% (3.6%- Fig. 5.53b). S values are slightly higher than unit B (Fig. 5.53c).

Table 5.14 – percentage loss on ignition data and bromine content (ppm) for sampled horizons at AK-7.

Unit	Height (cm)	Loss on ignition (%)	Bromine (ppm)
B	60-70	4.2	4.1
C1	195-205	1.4	9.7
D	365-375	2.4	6.1

Figure 5.51 – photograph of exposure AK-7.

Unit D consists of thickly laminated sands (73.7% coarse to very-coarse – Fig. 5.60b) and fine gravels. The gravels are predominantly doleritic with 10% showing rubified surfaces akin to those noted for unit B. Bioturbation (root channels) has modified the sediment to the extent that it was not possible to determine precise lamination thickness, or other sedimentary structures. The fundamental difference in terms of magnetic properties for unit D is the relatively large χ_{ARM} (355) and HIRM (26), the latter corroborated with the higher S_{-300}% values (2.7% applied remanance unreversed- Fig. 5.53c).

5.3.1b: AK-7 interpretation

CS-7 shows the juxtaposition of inset 'grey' fill within coarse rubified deposits. On the right bank, the geomorphic evidence indicates the remains of a small channel network approximately 3.7 m above the elevation of the modern channel, incised into the underlying sediment (Fig. 5.50). At AK-7, the basal partially calcified clast-supported gravels (unit A) are interpreted as indicating gully-floor sediments deposited under upper-flow regime conditions. It was reported in section 5.2.5 that in doleritic reaches, calcite rich runoff is supplied as groundwater flow causing local accretion of $CaCO_3$, although the role of in situ weathering and release of Ca^{2+} ions

from clasts in situ must also be considered, particularly for sediments dominated by igneous grains.

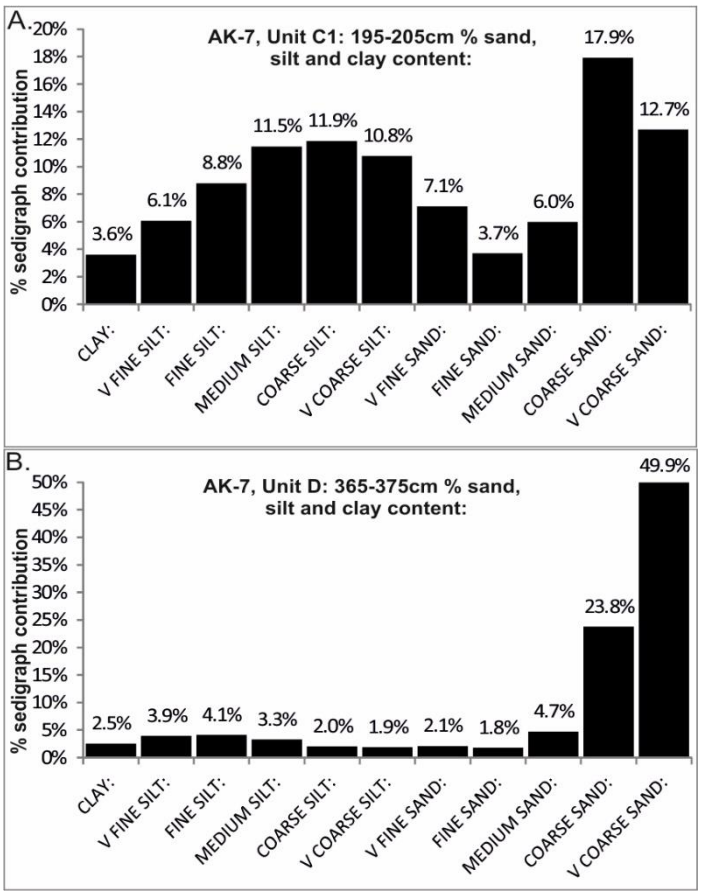

Figure 5.52 – % sand, silt and clay content derived from Coulter grain size analysis on samples collected from outcrop AK-7.

The overlying matrix-supported cobbles (unit B) are interpreted as debris flow deposits. This is because of the poorly sorted nature of the matrix (sandy silt) and the clast fabric, as well as the fact that many large gravel clasts are not horizontally bedded – but rotated vertically, implying (in the absence of micro-palaeochannel structures or lenses with clear boundaries) movement under very high energy flow conditions whereby blocks of sediment could be moved intact and unsorted. This thick (0.9 m) bed is typical of the facies in this reach although in places they are up to 1.1 m thick, lack cobbles and exhibit lateral discontinuities (Fig. 5.54). These deposits are distinguished from in situ rock break-up, reported as a possible analogue in Chapter 4 (Table 4.14: analogue 2).

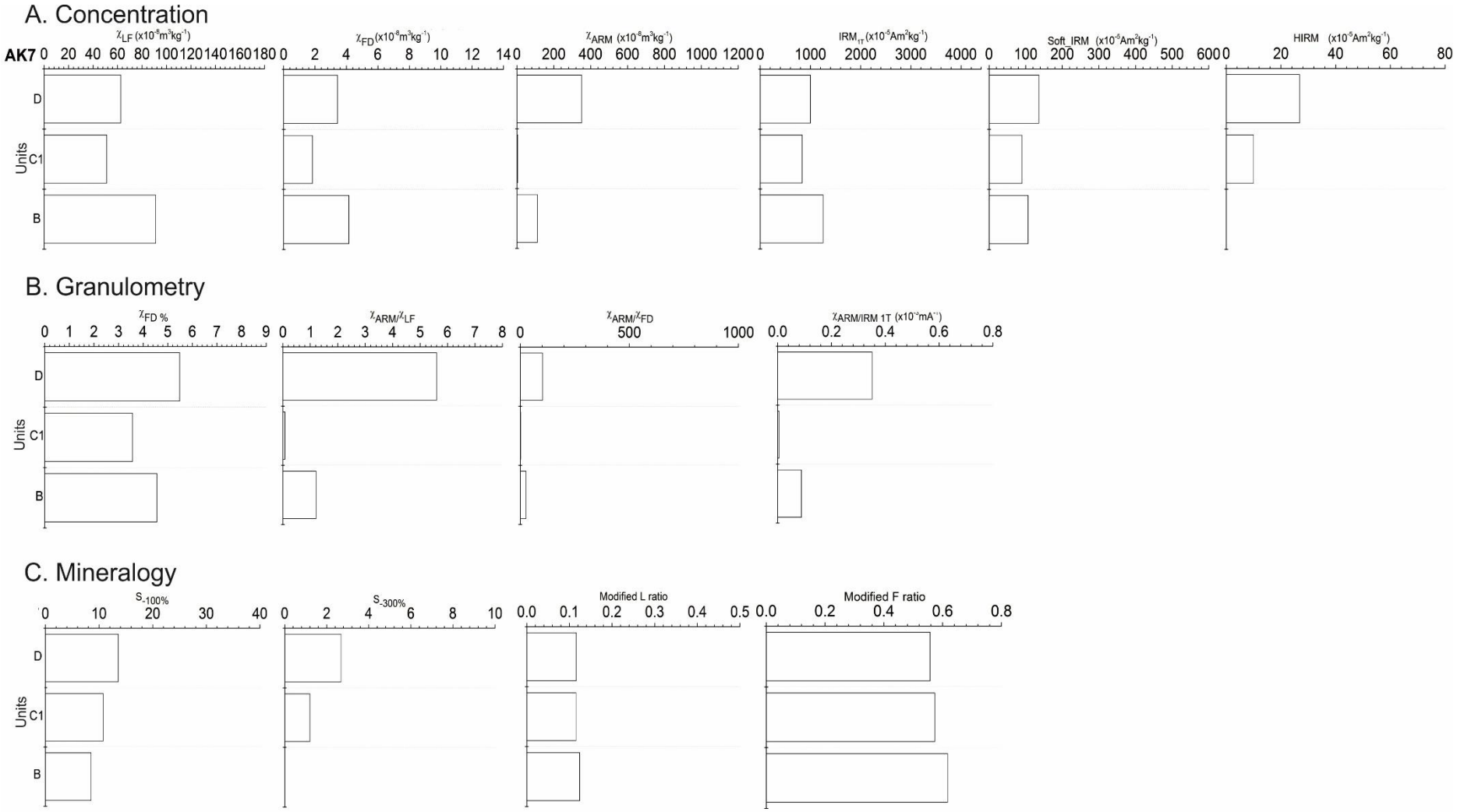

Figure 5.53 – mineral magnetic parameters from outcrop AK-7.

Table 5.15 – selected mineral magnetic parameters from 2 particle size fractions compared to the bulk (0-63 μm) fraction for unit B.

AK-7: Unit B.	**X_{LF}**	**X_{FD}%**	**X_{ARM}**	**IRM_{1T}**	**Soft_IRM**	**HIRM**	**X_{ARM}/X_{LF}**	**X_{ARM}/X_{FD}**	**$X_{ARM/IRM1T}$**	**S_{-100}%**	**S_{-300}%**
0-4	87.1	10.6	334.5	351.4	44	22.3	3.84	36.4	0.95	12.5	6.3
32-63	97.4	2	149	700.1	0	0	1.53	75.8	0.21	0	0
Bulk	91.2	4.6	110.1	1250.3	106.5	0	1.21	26.5	0.09	8.5	0

Figure. 5.54 – thick matrix-supported gravel units directly overlying dolerite bedrock in the reach immediately downstream of outcrop AK-7. Thinner units of coarse gravel are found at higher elevations in the terrace fill along the right bank.

The origin of these debris flow deposits are slopes of dolerite draining a nearby ridge and tor (Fig. 5.63a). Several coarse terminal palaeogullies are represented in terrace fills downstream of AK-7 (Fig. 5.54 and 5.55a) as laterally discontinuous gravel units, which similarly reflect debris-flow cascades. The deposits represented in unit B (AK-7) exhibit low concentrations of soil organic matter (bromine – 4.1 ppm). Thus, the deep 'orange' colour of the sediment primarily reflects inheritance from the eroding dolerite slope, rather than significant in situ bioturbation and weathering. The high χ_{LF} (91) also conforms to published susceptibility values for dolerite (Rowntree et al., 2012) and is distinctive compared to the above sampled units. When the clay fraction (0-4 μm) is considered, the bulk measurements underestimate pedogenic SP content by over 50%. A distinct hard component is also evident which may indicate pedogenic haematite also concentrated in the clay fraction. Similarly SD-size magnetite is underestimated in the bulk sample, ($\chi_{ARM}/_{IRM1T}$ = 0.09) reflecting a distinct lithogenic (doleritic) input of MD magnetite in the 32-63μm fraction confirmed in the highest susceptibility values here (97.4).

The sharp, planar contact between unit B and C1 signifies an unconformity. The massive, very-fine grained, friable overlying silty sands indicate low energy conditions of transport in a channel, rather than as slopewash from the hillslopes (see contact CS-7 – Fig. 5.58). The dark colour (10YR 3/1 very dark grey to 10YR 5/2 greyish brown), high bromine content (9.7ppm) and abundant root channels, indicates a gleyed wetland environment. Compared to the underlying debris flow deposits (unit B), total susceptibility is relatively weak (χ_{LF} = 52) which is likely to be

due to 1) diamagnetic dilution by vegetation and 2) ferrimagnetic dissolution under waterlogged conditions.

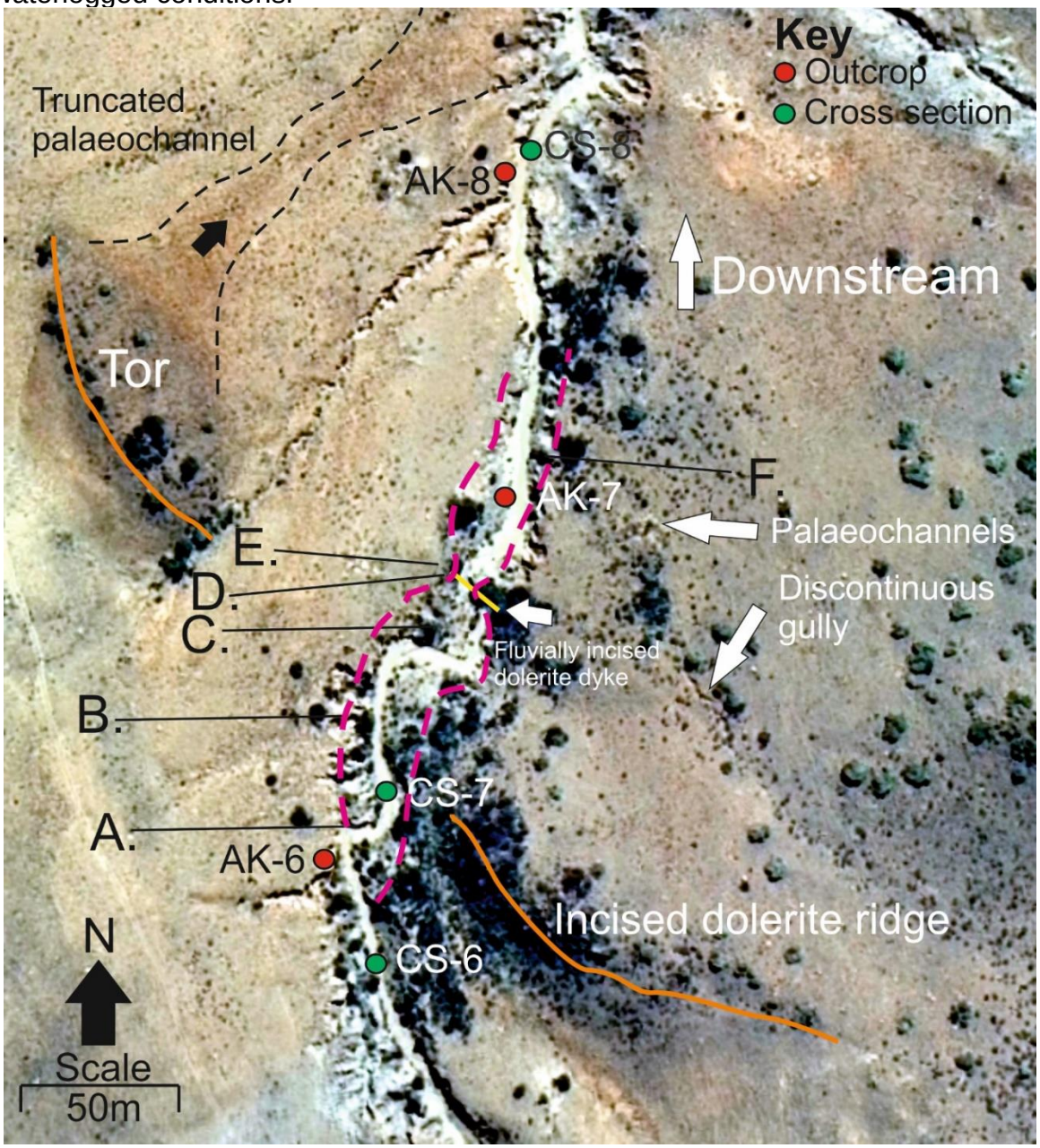

Figure 5.55a – digitized aerial photograph of segment of valley encompassing deposits represented in sediment logs AK-6 to AK-8. Note: 1) the incised dolerite ridge crossing the current channel perpendicularly and the abrupt changes in channel course, 2) The purple dashed line just after AK-6 (left bank) indicating the limits of the grey deposits (AK-7: units C and D), 3) The palaeochannels feeding in from the south-east in the vicinity and downstream of AK-7 and 4) The big infilled palaeochannel connecting the dolerite tor in the western extremity of the map with the central valley just downstream from AK-8 discussed in next section. See Fig. 5.55b (next page) for explanation of lettered annotations.

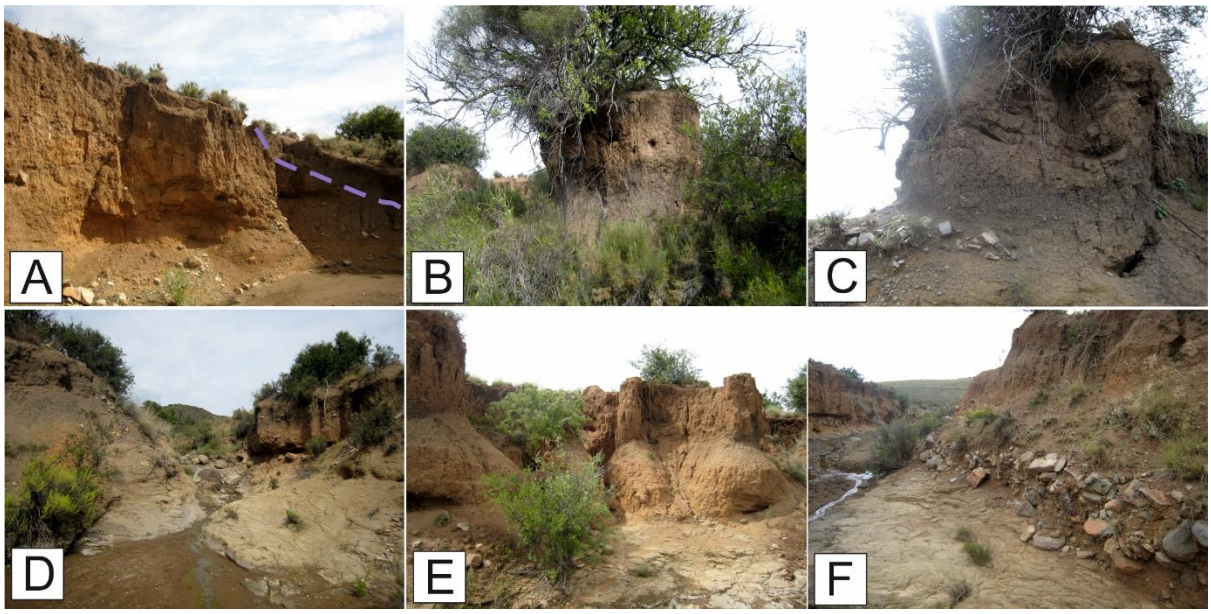

Figure 5.55b – photographs corresponding to lettered annotations in Fig. 5.55a – A) Note purple dotted line indicating erosional contact cut into relatively rubified deposits associated with AK-6 which marks the transition to, B) Tri-partite deposits with relatively rubified basal sandy gravels and grey palaeosol characterised by weakly developed blocky structure capped by laminated sands. C) Note the progressive thinning of the grey, organic horizon and the development of a sharp, undulating erosion surface with brown sands that exhibit curved bedding. D) View looking upstream of the partially breached dolerite dyke where the grey palaeosol horizon has virtually pinched out altogether – but note the continuity of the laminated brown sands going over the top of the dolerite barrier. E) The development of bank gullies that have eroded headwards into the sediments within which the tripartite deposits represented in A-D) are inset and F) Debris flow deposits (as described in text) in the right terrace bank opposite AK-8.

The bulk granulometric proxies indicate a predominantly multi-domain ferrimagnetic signature, with negligible SD content negligible ($\chi_{ARM/IRM1T}$ 0.01), but these should be viewed with caution in the light of the particle-size magnetic components identified earlier.

Two distinct phases of vegetation growth and soil development are reflected in subunits C2 and C4 with relatively lower organic content in units C3 and C5 on account of their lighter, colour (10YR 5/2 greyish brown). These wetland deposits are analogous to those located in low gradient, perennial channel reaches reported in Chapter 4 (Table 4.14: Analogue 3).

The thickly laminated fine gravels and sands capping the organic deposits (unit D) evidence overbank deposition in association with the small palaeochannel preserved in CS-7 (Fig. 5.50). The substantially higher χ_{ARM} of this unit (350) is very similar to samples reported from AK-5 and AK-6 which typically exhibited χ_{ARM} values between

2-400. This implies there was connectivity between these sediment sources. Although the χ_{LF} of unit D is much weaker than the AK-6 units (62 compared to 86 respectively), bromine values of 6.1 ppm in concert with root channels and surface vegetation may indicate some diamagnetic dilution.

AK-7 fine-grained sediments (unit C) start just after AK-6 (Fig. 5.55a – purple dashed line, Fig 5.55b – photo A and B), the boundary of which indicates an erosion surface associated with a former channel, rather than hillslope deposits laterally impinging on the channel as discussed for AK-7 unit B. The inset channel deposits pinch out temporarily at the dolerite barrier, but re-appear downstream where AK-7 is located. The continuity of these inset channel deposits implies a continuous channel system which was forced through the constriction dictated by the morphology of the dolerite barrier. The fact that this palaeochannel only partially carved into the underlying hillslope sediments (AK-7 unit B) implies that this was the former base level (i.e. 1 m above the contemporary channel surface). This grades to the top of the barrier represented in Fig. 5.55b (photo D). The bedrock topography and characteristics were thus probably identical during these phases of sedimentation and erosion to what is exposed in the contemporary system.

The sharp undulating contact between the grey fills and overbank deposits further downstream (Fig. 5.55b – photo C and B respectively) likely reflects hummocks formed in a previously vegetated wetland with small channels episodically reworking sediment.

5.3.2a: AK-8 analysis

Log AK-8 was obtained from a 4 m channel exposure on the left bank, 1506.9m downstream of the headwaters and 120 m north-east of a deeply weathered dolerite tor (Fig. 5.1, 5.56 and 5.57).

Unit B consists of thinly horizontally bedded, matrix-supported coarse gravels. The matrix consists of massive, coarse to very-coarse sands (43.8%), with a secondary peak in the fine sand range (25%), subordinate silts (23.4%) and minor clay (1.5%) (Fig. 5.58a). These are overlain by poorly sorted sandy silts (subunit C1). The colour of these subunits is 10YR 6/4 light yellowish brown.

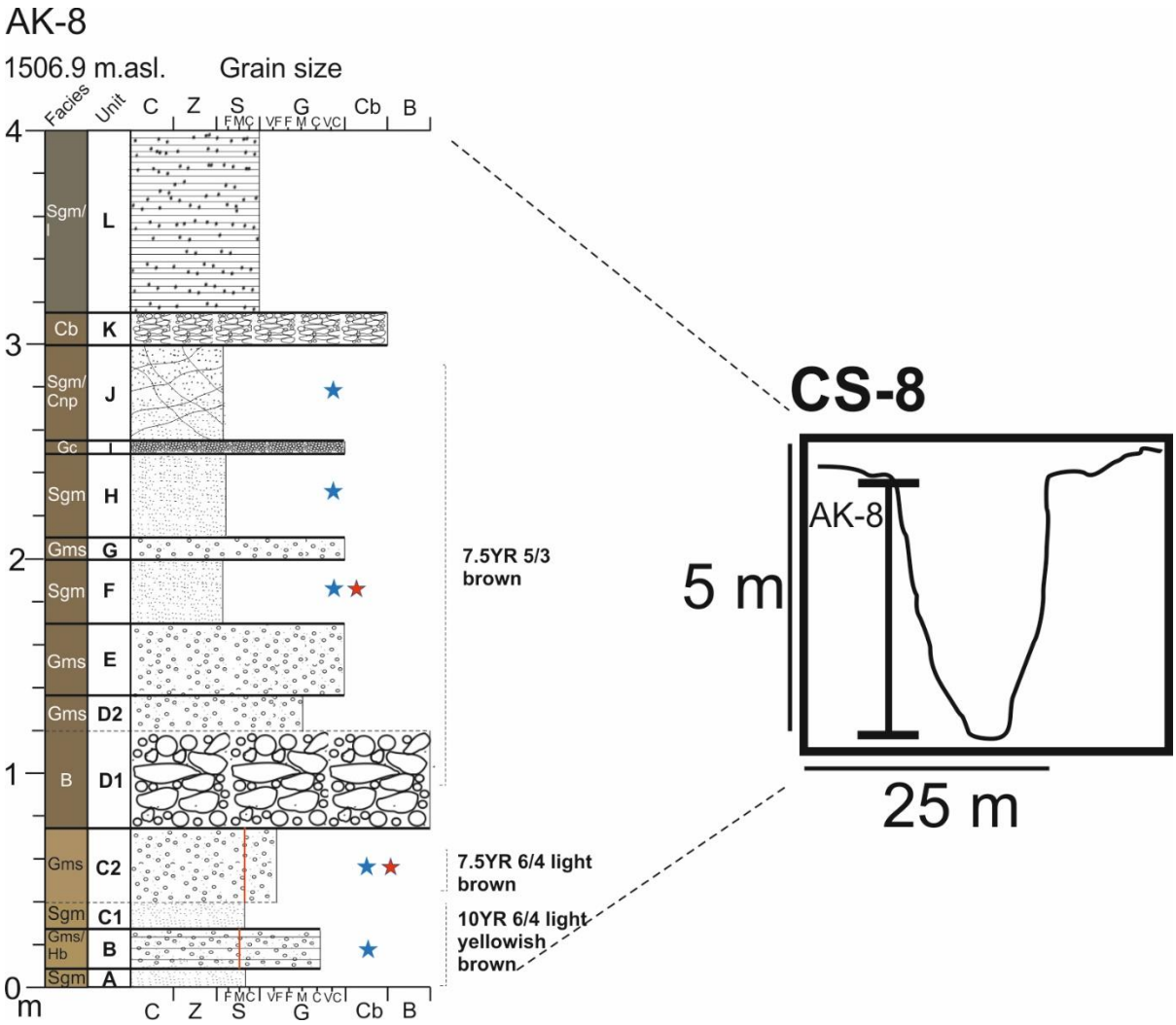

Figure 5.56 – sedimentary log AK-8 and cross section.

Unit C2 consists of poorly sorted matrix-supported gravels. The matrix grain size distribution is negatively skewed with two distinct modes at 1092 µm (50.8% coarse to very coarse sand) and 116.4 µm (21.8% fine sand - Fig. 5.58c). Median grain size of the matrix is 517.4 µm.

Unit D1 consists of faintly bedded sub-angular dolerite boulders (b axis up to 44 cm), with cobbles and lenses of gravel. The unit grades to massive, very poorly sorted, matrix-supported medium gravels (D2). Unit E consists of horizontally bedded very coarse gravels with occasional cobbles. The matrix consists of coarse silt to fine sand, with lenses of well sorted very coarse sand.

Figure 5.57 – photograph of outcrop AK-8.

Table 5.16 – percentage loss on ignition data and bromine content (ppm) for sampled horizons at AK-8.

Unit	Height (cm)	Loss on ignition (%)	Bromine (ppm)
B	25-35	3.7	1.4
C2	55-65	3.4	0.9
F	185-195	3.2	2.2
H	225-235	-	1.4
J	275-285	-	6.2

Units F-K alternate between massive sands and gravels but are uniform in colour: 7.5YR 5/3 brown. Unit F is poorly sorted dominated primarily by fine-medium sand (58.9%), but with subordinate silts and clays (35.2% combined- Fig 5.58c). This sand unit is separated by matrix-supported gravels which exhibit faint trough cross-beds. Unit G represents a single, thin bed (see Table 3.4 for classification of bed thickness) of very coarse matrix-supported gravel. Unit H is a thick, very poorly sorted,

predominantly fine sand unit (median grain size: 139.2µm) although there is more coarse to very-coarse sand (30.7% - Fig. 5.58d) than unit F (5.9% - Fig 5.58c). Unit I is a very thin bed of clast-supported very coarse gravels. Unit J is characterised by bimodal sands and silts which exhibit curved, non-parallel cross-bedding. Silt content is higher than previous units (42.6% silt and clay - Fig. 5.58e) and soil organic matter content relatively high compared to the other sampled units (Table 5.16). Unit K consists of a single medium bed of clast-supported cobbles, which are overlain by thickly laminated very coarse sands and very fine gravels (unit L). Root channels are common.

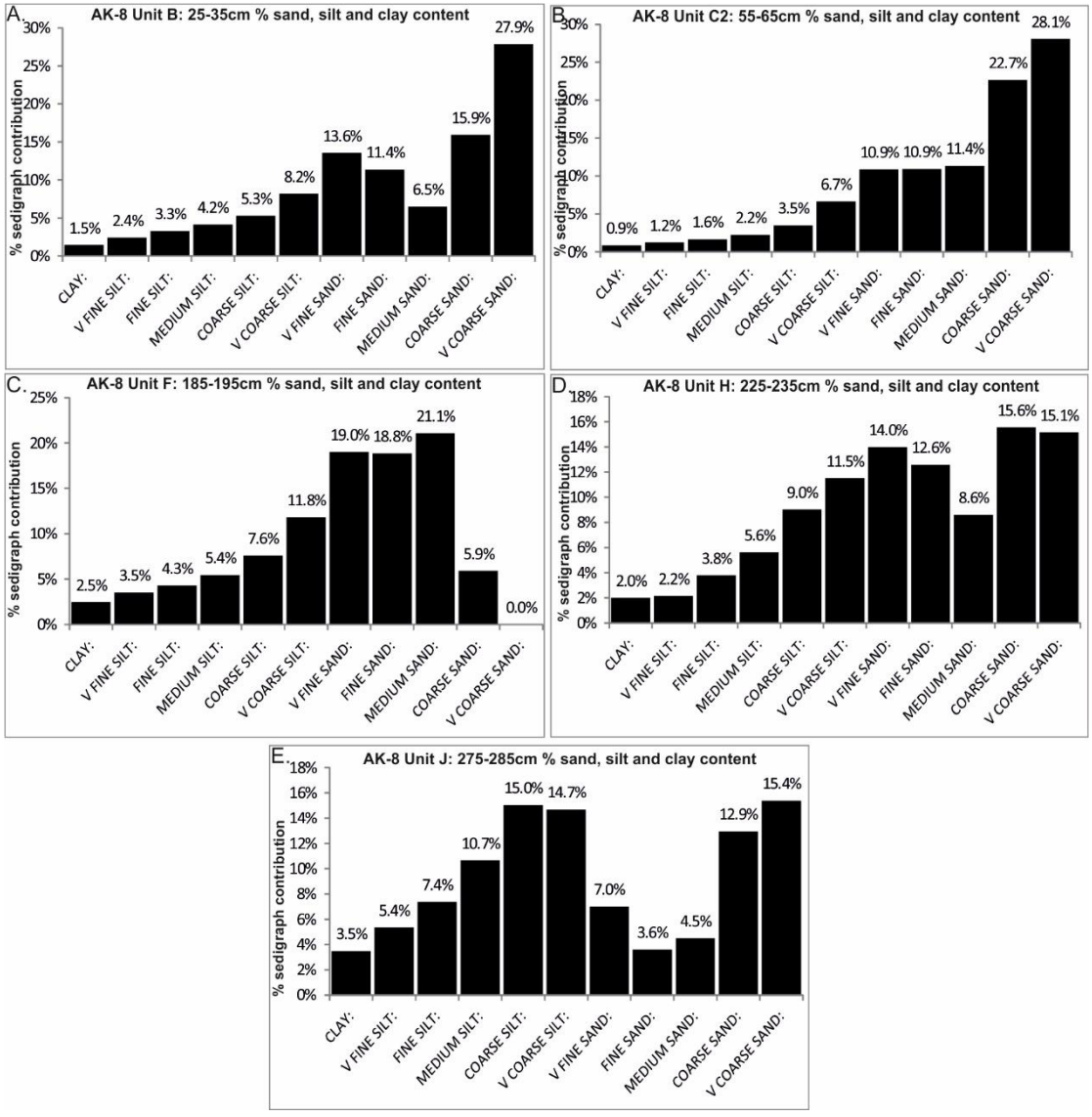

Figure 5.58 – % sand, silt and clay content derived from Coulter grain size analysis on samples collected from outcrop AK-8.

Magnetic susceptibility shows an inverse relationship with depth with χ_{LF} and χ_{ARM} both peaking at unit J (Fig. 5.59a). χ_{FD}% is less straightforward, exhibiting two

distinct peaks for unit F and J, but only the latter is accompanied by an increase in χ_{ARM}/χ_{LF} and $\chi_{ARM/IRM1T}$ (Fig. 5.59b). Further, S_{-100}% increases slightly up-profile, from a minimum of 90% reversal for unit B to a peak of 85% for unit H, and this is typically mirrored by declining S_{-300}% values (Fig. 5.59c).

5.3.2b: AK-8 interpretation

The sediments at the base of the succession (units A-C) indicate emplacement by current flow under varying energy conditions. The relatively pale colour (7.5YR 6/4 light brown to 10YR 6/4 light yellowish brown) indicates leaching via lateral movement of groundwater considering the basal unit is just above dolerite bedrock.

The very poorly sorted boulder/cobble unit (D1) reflects deposition under high energy conditions, probably debris flows originating from the dolerite tor to the south west. The sharp, planar contact between unit C and D indicates an unconformity, with incision into unit C sediments (Fig. 5.56 and 5.60). The valley cross section shows a surface dipping north east toward the contemporary channel (Fig. 5.56). This suggests that the tor 120 m to the south-west was the primary supplier of sediment to the valley floor at this point. In the previous section (5.3.1b), an infilled palaeochannel linking the dolerite tor to the valley floor terminating as a lobate sediment body was presented (Fig. 5.55a). On average, there are less boulders and cobbles reflected in terrace fills just downstream of AK-8 towards the next major knickpoint through sandstone, which is interpreted to indicate alluvial fan progradation with distal fining characteristics.

The gravel unit (D2) overlying unit D1 indicates flow cessation and deposition of finer material. The alternating beds of sand and gravel reflect event driven phases of deposition on the fan, with the overall reduction in grain size reflecting the aggradation of the fan surface and reduction of local slope (units E-I). The sharp undulating contact at 138 cm and the laterally discontinuous nature of the matrix-supported gravels (unit E) is interpreted to indicate small channel entrenchment, incising into unit D2 under upper-flow regime conditions, depositing locally sourced coarse gravels, with flow cessation (and possibly loss of confinement as the channel filled) reflected in the capping sands (unit F).

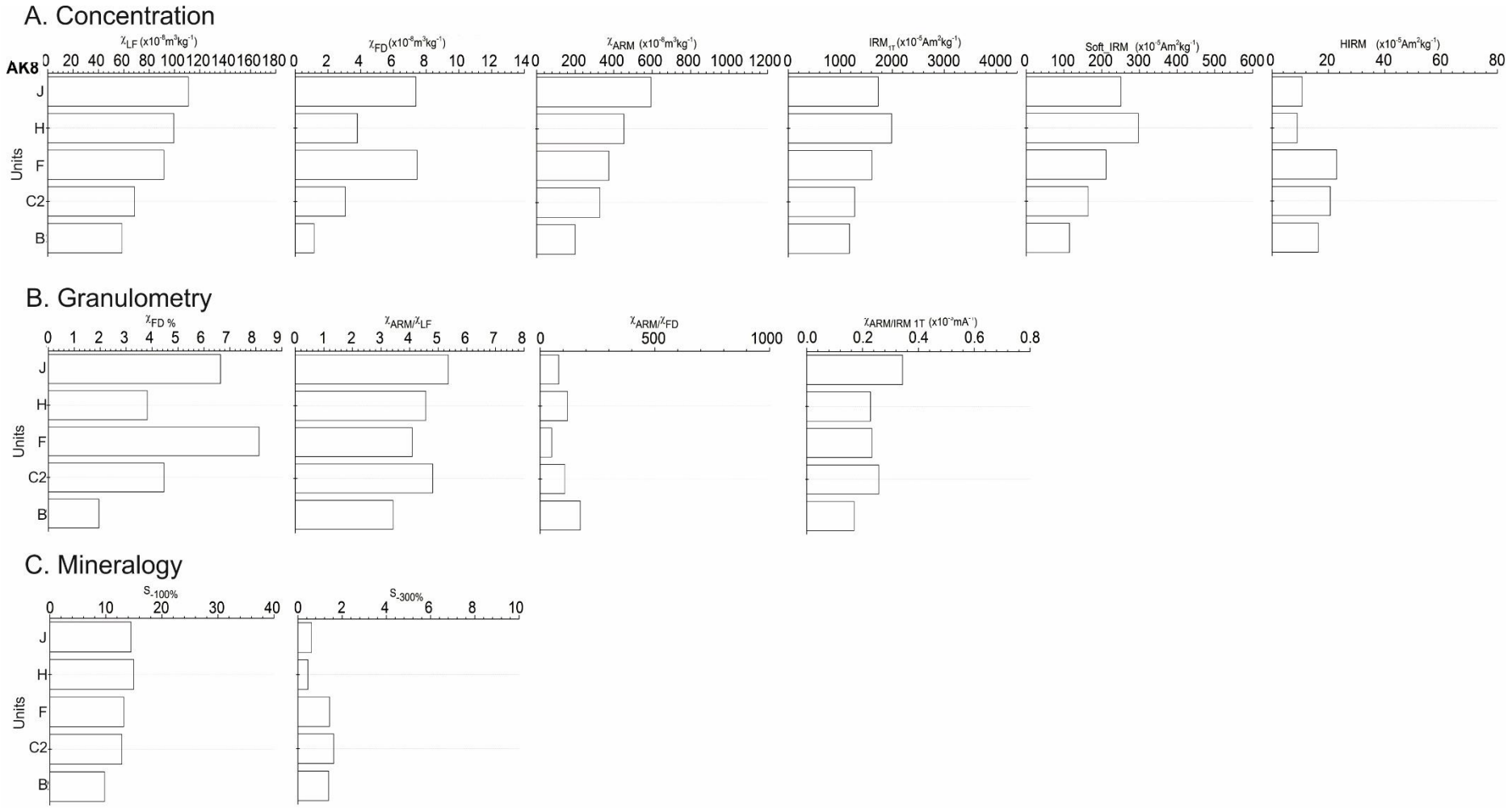

Figure 5.59 – mineral magnetic parameters from outcrop AK-8.

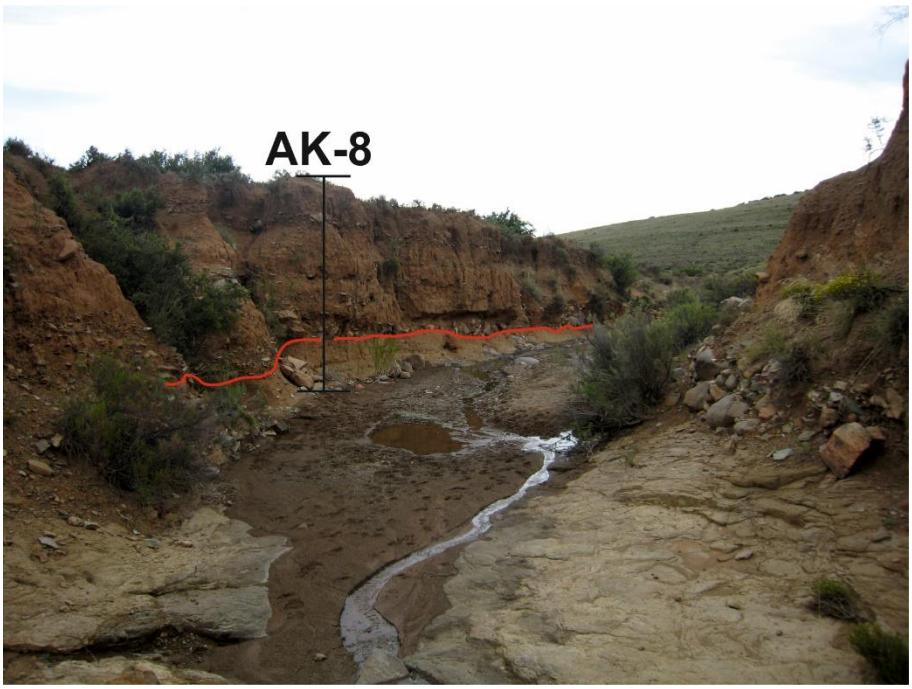

Figure. 5.60 – photograph showing outcrop AK-8 in context of the local channel reach. In the foreground is actively eroding dolerite flanked by debris flow deposits described for AK-7 (unit B) on the right bank. The red line drawn indicates the erosional contact between the relatively well sorted, fine grained sediments of AK-8 unit A-C and the very poorly sorted, mudflow deposits sourced from hillslopes to the left.

The fine sands exhibiting curved-non parallel bedding (unit J) are interpreted as being low energy channel deposits, probably laid down in a small laterally mobile fan channel. The very coarse cobble deposits above probably represent debris flow deposits. The thinly laminated very coarse sands (unit L) are incongruous with the underlying succession. These sands were traced from AK-7 and reflect overbank deposition in association with the wetland channel (AK-7 unit D). The absence of grey fills from this reach (Fig. 5.60) is most likely due to their having been reworked.

All units shows high to very high (χ_{LF} = 60-112) concentrations of ferrimagnetic minerals, with increasing concentrations of SD remanence carrying ferrimagnetics with elevation above the modern channel. Each successive phase of deposition from the slope injects a fresh supply of magnetite/maghemite hence the incremental increases in χ_{LF} and χ_{ARM}. From the S_{-100}%, freshly delivered sediment from the hillslopes contains more high coercivity (hard) magnetite compared to that which has been altered post-depositionally.

The χ_{FD}% values are more variable. As fine-grained SP ferrimagnets tend to be concentrated in the 0-4 µm clay/very fine silt fractions (Hao et al., 2008b), it follows

that higher silt/clay contribution to the sedigraph may enhance the SP signal, although this may not hold true for all depositional settings.

Table. 5.17 – amalgamated organic, soil magnetic and Coulter grain size proxies for sampled units at AK-8.

Unit	Height (cm)	Bromine (ppm)	0-4 μm %	X_{FD}%
B	25-35	1.4	3.9	1.95
C2	55-65	0.9	2.1	4.46
F	185-195	2.2	6	8.12
H	225-235	1.4	4.4	3.82
J	275-285	6.2	8.9	6.64

In this case however, the concentration of SP grains is highest for units F and J which exhibit the largest 0-4 μm fraction (6 and 8.9% respectively). Units B and C2 do not conform to this pattern, with X_{FD}% exhibiting an inverse association with %0-4 μm (Table 5.17). However, these units have been subjected to leaching by groundwater. Considering the sedimentological interpretation of unit J (a laterally mobile, fan channel), it is possible that sediment from relatively stable areas of the fan or slope could have been reworked and delivered to the valley floor, which underwent further in situ weathering (AK-8). The relatively high bromine value (8.9 ppm), yet no macro-sedimentological evidence for bioturbation or soil development could be a signal that a new soil source on the slope was being eroded. Alternatively, though not exclusively from the previous submission, the %0-4 μm concentration reflects changing supply of fine sediment from the hillslope which would be contingent on weathering rates as much as connectivity with new soil sources. An outstanding question remains: could the X_{FD}% and higher %0-4μm not reflect in situ weathering? Notably, the higher S_{-300}% for unit F could be a signal for the ageing of magnetite to haematite, especially considering that the measured hard component above (units H and J) is miniscule. But the issue of eroding soil sources delivering haematite to the valley floor is as probable a driver affecting S_{-300}% as the inheritance of SP magnetite, especially as no change in soil Munsell colour, or a distinct palaeosol, was found. The prospect of in situ transformations of magnetite to AF minerals (probably goethite) at the base of the succession is at least reconcilable with the evidence quoted for leaching by groundwater, facilitating the production of a bigger hard IRM component. This is further reinforced by the relatively dilute (though

still strong) χ_{LF} (61-74) reflecting the increased AF mineral concentration at the expense of magnetite.

5.3.3a: AK-9 analysis

Log AK-9 was obtained from a 5 m channel exposure on the right bank, 1688.5m downstream from the headwaters (Fig. 5.1, 5.61 and 5.62).

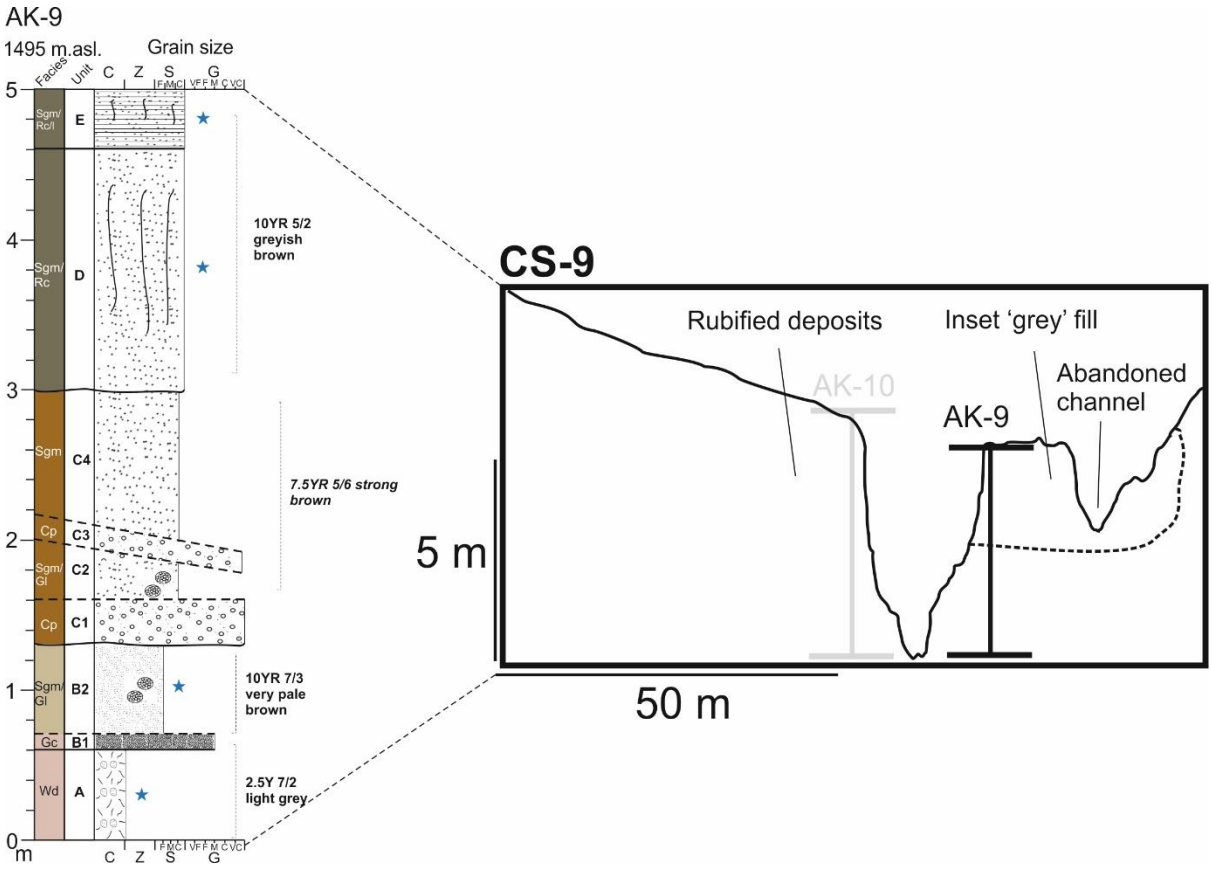

Figure 5.61 – sedimentary log AK-9 and cross section.

Unit A consists of massive, poorly sorted silty clays (61.2% combined) with subordinate sands (38.8% - Fig 5.62a) which is overlain by laterally discontinuous (3-4 m), clast-supported medium gravels (subunit B1). Subunit B2 is predominantly sand (58.6%) but with significant silt/clay content (41.4% - Fig 5.62b). There are mottled iron concentrations in places as well as lenses (1-2 cm diameter) of very coarse sand. Colour is significantly different (10YR 7/3 very pale brown) compared to unit A (2.5YR 7/2 light grey).

Figure 5.62 – photograph of exposure AK-9.

Unit C consists of laterally discontinuous (10-15 m), alternating beds of matrix-supported gravel and massive sand with local lenses. Subunit C3 is inclined relative to the modern channel surface. A sharp, undulating contact separates unit C from D. Unit D is characterised by friable, predominantly coarse-very coarse sand (59.2%) with subordinate silts and clays (32.7% - Fig. 5.63c) and abundant root channels. Colour is 10YR 5/2 greyish brown. A sharp planar contact punctuates units D and E, the latter consisting of laminated, predominantly very coarse sand (53.3%) with a minor silt/clay component (21.5% - Fig. 5.63d) and root channels. Both units D and E are characterised by highest soil organic content relative to below (Table 5.18).

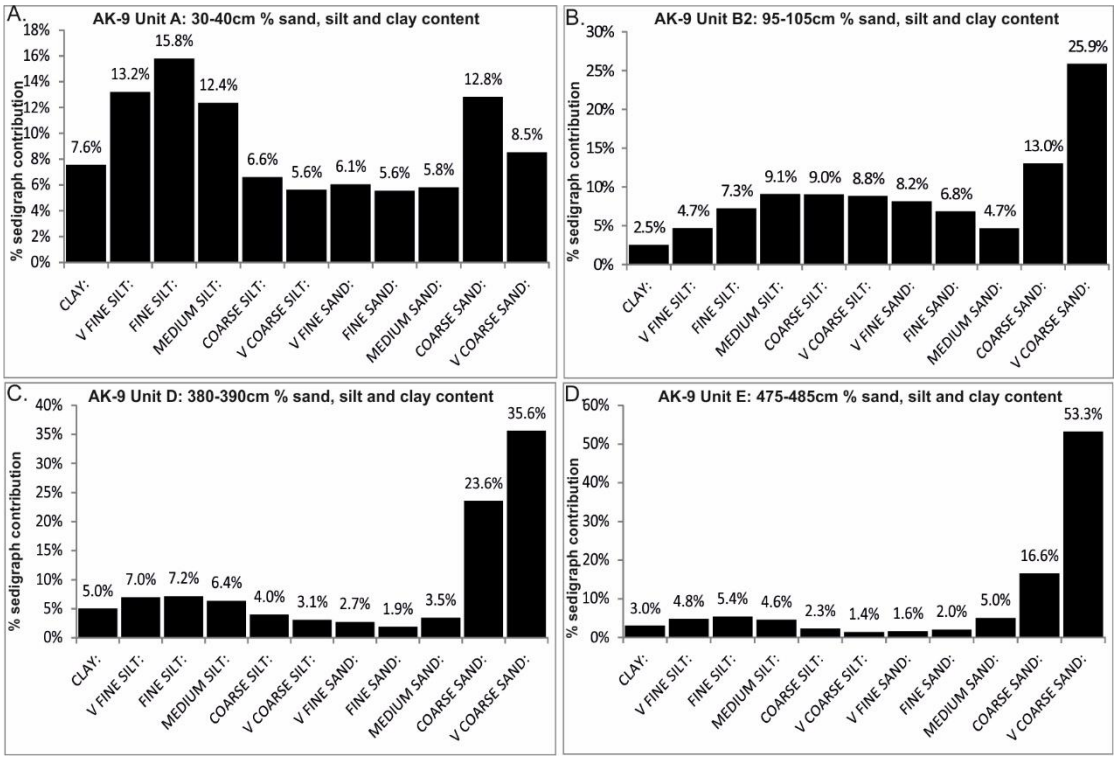

Figure 5.63 – % sand, silt and clay content derived from Coulter grain size analysis on samples collected from outcrop AK-9.

Table 5.18 – percentage loss on ignition data and Bromine content (ppm) for sampled horizons at AK-7.

Unit	Height (cm)	Loss on ignition (%)	Bromine (ppm)
A	30-40	2.3	1.3
B2	95-105	2.1	1.4
D	380-390	3.4	6.8
E	475-485	3.1	6.6

The concentration-related magnetic properties of AK-9 exhibit an inverse relationship with depth, although susceptibility is much weaker than AK-8 (Fig. 5.59a and 5.64a). χ_{FD}% is much higher for units D and E, which is matched by higher $\chi_{ARM/IRM1T}$ (Fig. 5.72b). The S_{-300}% shows a progressive decline with depth. For example, the basal dolerite soil shows 7% of the applied remanence unreversed (unit A), but unit E lacks a measurable hard component (Fig. 5.72c).

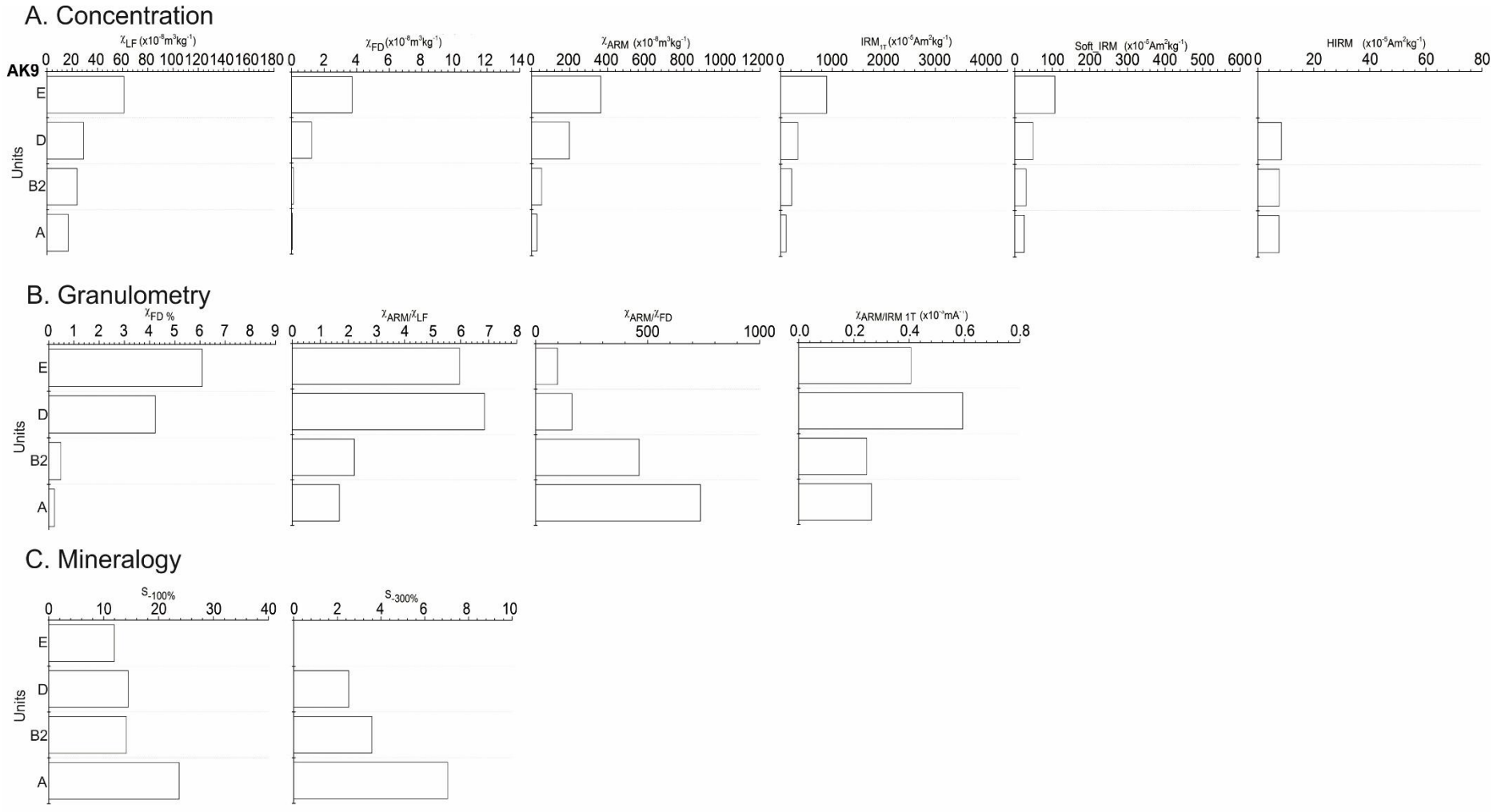

Figure 5.64 – mineral magnetic parameters from outcrop AK-9.

5.3.3b: AK-9 interpretation

The basal unit is deeply weathered dolerite similar to that reported at AK-3. The laterally discontinuous matrix-supported gravels may reflect the remnants of a medial bar deposited in a channel, with the overlying sands reflecting deposition under low energy flow conditions. The very pale brown colouration (10YR 7/3) indicates the unit is intensively leached by groundwater, sourced from a nearby seepage zone. The presence of the coarse sand lenses at unit B2 may reflect three processes: 1) illuviated sands and 2) scour and filling of the gully floor. The first process is unlikely as there is no evidence for root channels and the organic content is very low (Br = 1.4 ppm), which corroborates the evidence for waterlogging and leaching. During flow recession, the streamflow in the modern channels bifurcates into smaller channels up to several cms across. This is advanced as the most probable process generating this lenticular architecture for unit B2.

Unit C is interpreted as a palaeochannel. The sharp, undulating contact between units B and C signifies incision and the laterally discontinuous, channel shaped arrangement of very coarse gravels which fine upwards are similar to the facies analysed for AK-6. The stronger brown colour (7.5YR 5/6) reflects the greater additions of organic matter, confirmed by the abundant root channels infilled with well sorted sands. The overlying sandy silt package (unit D) represents facies deposited in a low energy channel. The relatively high bromine (6.8 ppm), abundant root channels, the blocky soil structure and greyer colouration (10YR 5/2) indicates stabilisation by vegetation. However, does the organic content reflect in-channel vegetation under a slow rate of infilling or soil profile development post-infilling due to reduction of local slope gradient and colonisation by surface vegetation? If the facies reflected a low energy, vegetated channel, mud-drapes or clear alternating minerogenic/organic laminations may be expected, but no such architecture was found. This could be due to bioturbation relating to surface vegetation colonisation and the development of soil blocks, but overall silt/clay content remains low relative to sand (32.7%). Given that in-channel vegetation has been shown to promote sedimentation of fines due to flow attenuation (Sandercock et al., 2007), the organic content here pertains to post-depositional overprinting. The section is capped by overbank sediments (unit E), associated with the abandoned channel which has partially incised the underlying inset grey fills (see Fig. 5.61 – AK-9 and CS-9).

The decline in susceptibility and magnetic remanence with depth beneath the terrace surface is a clear indication of ferrimagnetic dissolution and formation of paramagnetic minerals under waterlogged conditions. The increase in S values with depth is most likely representative of goethite over haematite.

The floodplain sediments (unit E) indicate high concentrations of remanence carrying ferrimagnets, but attest to a sandstone rather than doleritic signature, similar to the overbank succession reported for AK-7. The pocket-like appearance of these wetland fills, abandoned channel and its floodplain, may reflect reworking by erosion as these are friable compared to the rubified terrace fills. If so, this implies a continuous channel system at least as far upstream as AK-7.

5.3.4a: AK-10 analysis

Log AK-10 was obtained from a 5.4 m channel exposure on the left bank 1703.9 m downstream (Fig. 5.1, 5.65 and 5.66).

Unit A consists of horizontally bedded, matrix-supported medium gravels. The matrix is very poorly sorted with a significant coarse to very coarse sand component (39.2%) and a secondary peak in the fine-medium silt range (19.3% collectively - see Fig 5.67a). A sharp, planar contact punctuates unit A and B, the latter consisting of clast-supported cobbles with pockets of matrix and smaller gravels in places. Units A and B are distinct from the overlying units on the basis of colour (10YR 7/4 very pale brown).

Unit C consists of relatively well sorted, clast poor silts which abruptly transition to alternating horizontally bedded fine gravels and sands (Unit D). Unit E consists of two subunits. E1 consists of matrix-supported coarse gravels which grade to E2, predominantly clast-poor, very poorly sorted, massive medium-coarse sands (Fig 5.67b). A final burial age of 17 ± 2.5 ka (1σ) was obtained for unit E2 (Fig. 5.65 and Table 5.20).

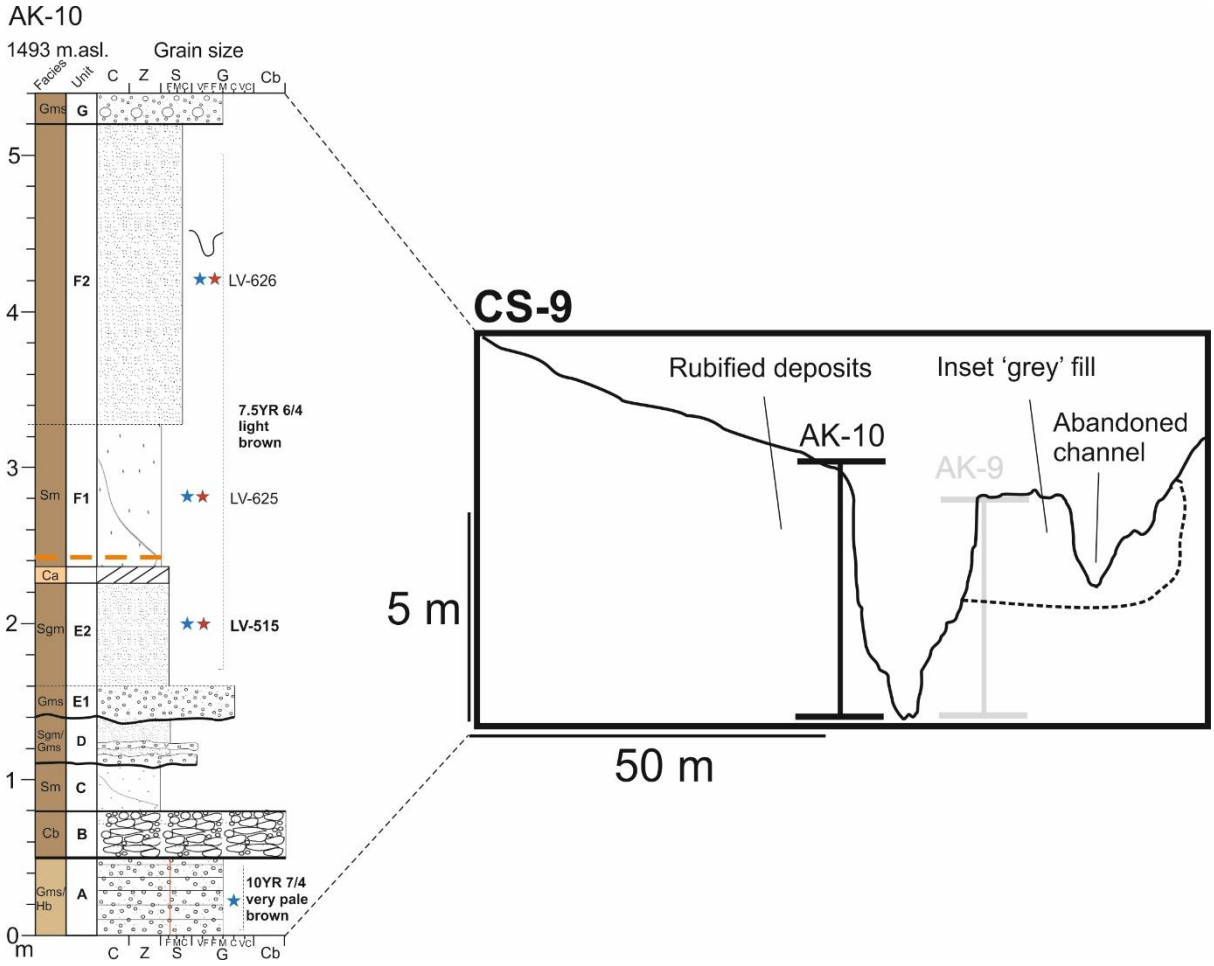

Figure 5.65 – sedimentary log AK-10 and cross section.

Figure 5.66 – photograph of outcrop AK-10.

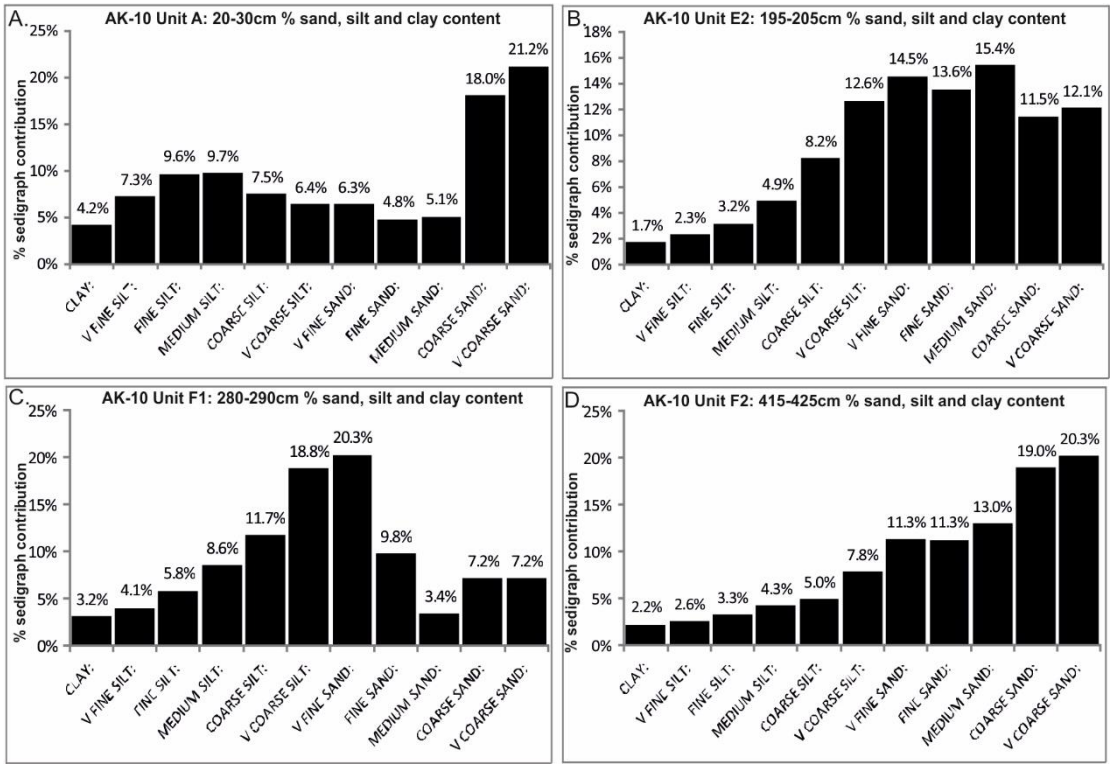

Figure 5.67 – % sand, silt and clay content derived from Coulter grain size analysis on samples collected from outcrop AK-10.

The top of the unit is overprinted by a thin band of carbonate cement, not described in detail here. The overlying dashed orange line (Fig. 5.65) indicates the boundary between a rubified surface which is sharply bounded above by the sediments of unit F. Subunit F1 is silt dominated (52.2%- Fig 5.67c) whereas F2 is sand dominated (74.8%), exhibiting a negatively skewed distribution (Fig 5.67d). All sampled units exhibit very low LOI% and Br values (Table 5.19).

Table 5.19 – percentage loss on ignition data and bromine content (ppm) for sampled horizons at AK-10.

Unit	Height (cm)	Loss on ignition (%)	Bromine (ppm)
E2	195-205	1.4	1.1
F1	280-290	1.4	0.5
F2	415-425	1.8	2.8

At 420-430cm (unit F2) set back from the main channel a larger channel feature is incised into the sandy unit (Fig. 5.68). The succession is capped by a very poorly sorted gravel matrix-supported gravel unit (unit G; Gms - Fig 5.68). The colour of units C-F is homogeneous 7.5YR 6/4 light brown.

Figure. 5.68 – localised matrix-supported coarse to very-coarse gravels incised into the coarse sands of unit E4, setback from AK-10 exposure in modern bank gully.

Total magnetic susceptibility is variable for this outcrop; units A and E3 are weak (χ_{LF} = 25-36); units E2 and E4 are strongly magnetic (χ_{LF} = 62-80) – the former also exhibiting relatively large soft_IRM and HIRM (Fig. 5.69a). χ_{FD}% and $\chi_{ARM}/_{IRM1T}$ peaks for unit E4 (Fig. 5.69b). The S_{-300}% parameter increases up the profile, peaking at 3.2% (units E3 and E4 – Fig. 5.69c).

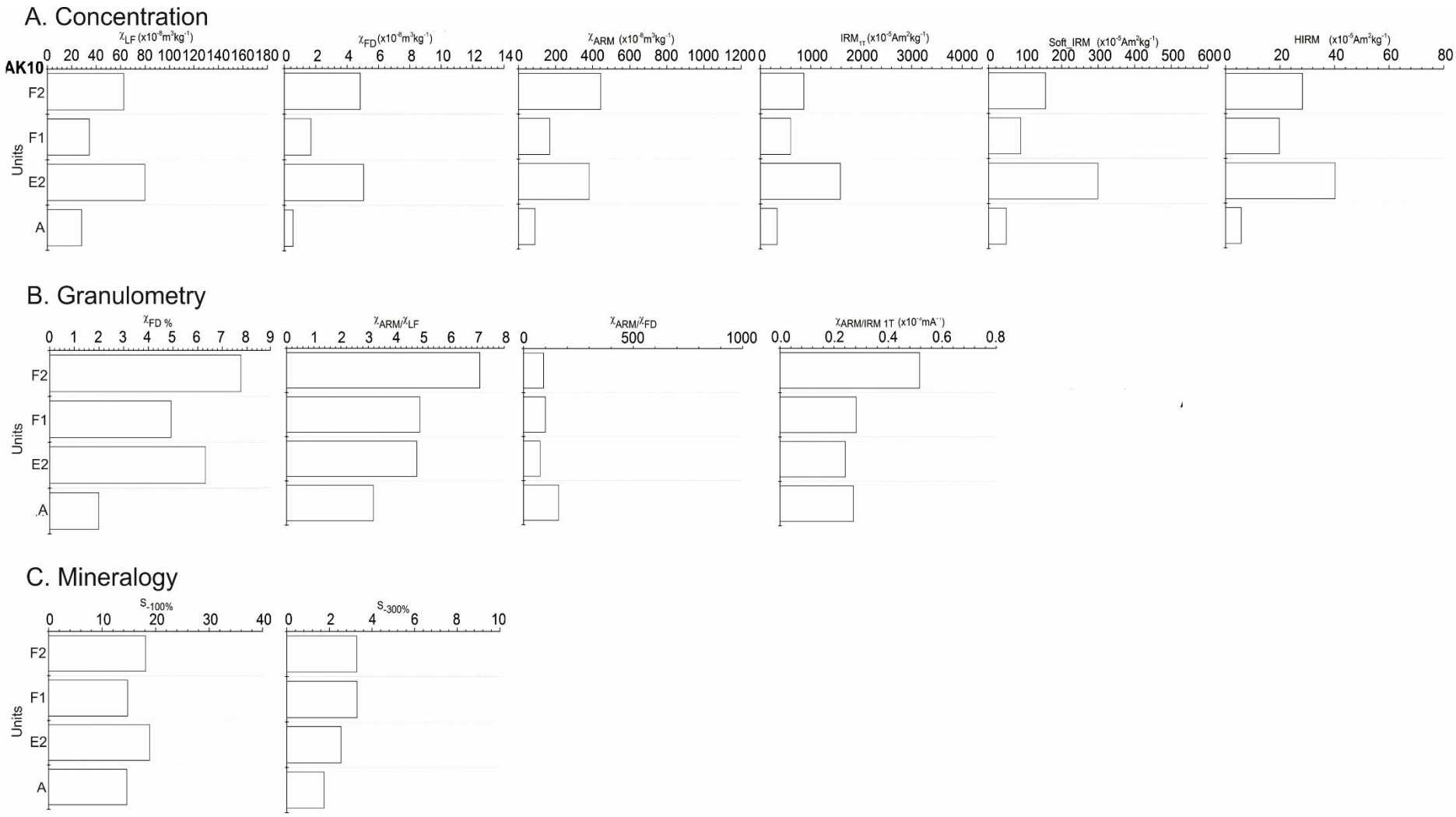

Figure 5.69 – mineral magnetic parameters from outcrop AK-10.

Table 5.20 – age modelled D_e values, D_r values and calculated age for sample **LV515**. Overdispersion, skewness and standardised kurtosis parameters are also provided. Note associated error bar on final age is quoted to 1σ . *Cosmic dose value was obtained for northern hemisphere equivalent latitude. [a] Water content measured from field sample. [b]Estimated average long-term water content accounting for saturation prior to terrace incision, on which final age is based.

Sample	**n**	**D_e (Gy)**	**Water content (%)**	**K%**	**Th (mg/g)**	**U (mg/g)**	***Dcosmic Gy/Ka**	**Skew of lnDe *c***	**Standardised Kurtosis *k***	**Overdispersion σ (%)**	**Age model**	**Final age (ka) (1 σ)**
LV515	61	54 ± 5.4	[a]2.3 [b]**15±5**	2.1 ± 0.05	11.83 ± 0.21	2.55 ± 0.06	0.17 ± 0.01	0.05	0.67	27	CAM	17 ± 2.5

5.3.4b: AK-10 interpretation

The local topography here favours sedimentation on the valley floors rather than away from it. The modern channel at this point has been deflected by the inset palaeosol/channel sequence (AK-9) into the orange sediments (AK-10) that mantle the slopes to the south west.

The basal gravels indicate emplacement under upper flow regime conditions. The overlying doleritic cobble/gravel bed appears to have incised into the gravels of unit A as reflected in the sharpness of the bed contact. Their matrix-supported nature indicates emplacement by debris flow. The abrupt transition to silty sand (unit C) could reflect overbank deposition in a channel. The laterally discontinuous (few dms), thin beds of gravel (unit D and E1), are interpreted as channel reactivation surfaces with localised bar deposition with sand subsequently deposited during recessional phases of flow (E2). The absence of laminae reflects the intense weathering of the terrace. In either case, an aggradational regime is indicated. The calcrete at 225-235 cm is not analysed in detail here, but is stratigraphically coeval with that reported in section 5.3.6 (AK-12). The rubified horizon immediately above (though poorly defined at AK-10 compared to AK-12) is interpreted as a palaeogeomorphic surface. Sedimentation terminated some time in the deglacial period (17 ± 2.5 ka – Table 5.20). Although measured water content for sample LV515 was 2.3%, its location beneath the calcrete means that water content since burial of unit E2 will have likely been higher. This means the true burial age is probably closer to the Last Glacial Maximum than Holocene. Increasing water content in increments of 5% results in approximately 0.9 ka difference (Table 5.21). Overdispersion is lower (27%) compared to LV509 (37%) and likely reflects better bleaching of the OSL signal.

Table 5.21 – sensitivity of final OSL age to moisture content. [a]Error bar given to 1σ. [b] Moisture content value obtained from field sample.

Moisture content %	[a]Resulting age (ka)
[b]2.3	14.9 ± 2.6
10	16.2 ± 2.5
15	17 ± 2.5
20	17.8 ± 2.5

The overlying inversely graded thick units of silt (F1) and sand (F2) are most likely to be slopewash deposits sourced from the hillslope to the west. The local lenses of gravel (up to 10 cm thick) probably represent infilled rills. Similarly, the deposits reported in Fig. 5.68 represent a small bank gully carved into the slopewash sediment. These patterns of filling by slopewash and entrenchment by minor bank gullies probably reflect channel entrenchment through slopewash sediments capping the calcrete. Formation of a shallow gully draining the valley would have provided the impetus for such incision by lowering the local base level.

The basal unit (A) exhibits paramagnetism consistent with other reported examples of gleyed deposits overlying bedrock. Unit E2 in contrast exhibits high concentrations of fine-viscous SP particles (see X_{FD}%) consistent with a high degree of pedogenic magnetite formation, yet juxtaposed with a distinct MD signature derived from the dolerites (see $X_{ARM/IRM1T}$).

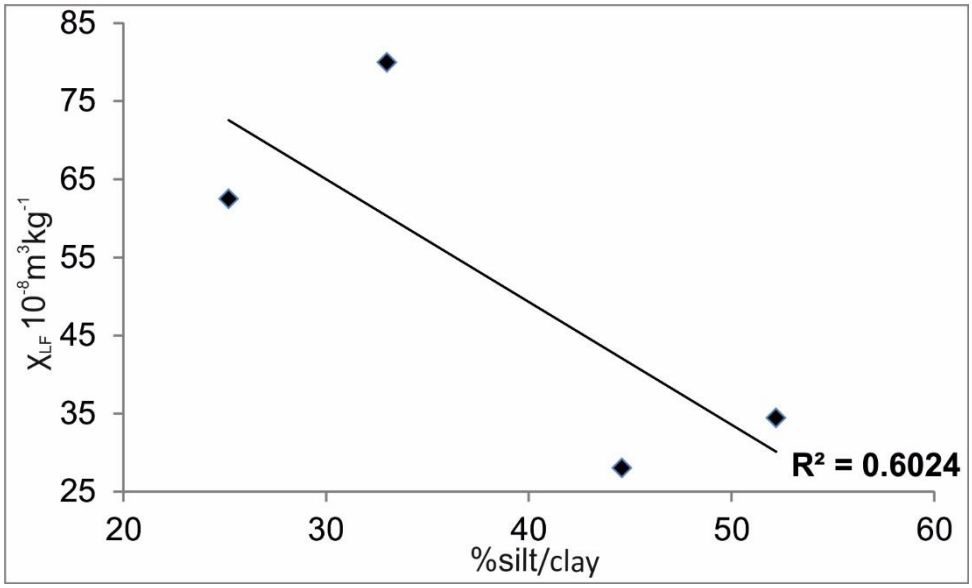

Figure. 5.70 – bi-plot showing %silt/clay content versus low frequency magnetic susceptibility for sampled units from AK-10.

Unit F1 exhibits paramagnetism reflected in the low concentration-based proxy values, whereas F2 exhibits ferrimagnetism. The reason for these differences requires further discussion. Soil texture was found to explain 60% of the variation in X_{LF} (Fig. 5.70). The high silt/clay content of unit F1 means it is less well drained than the bracketing sand units and thus conducive to paramagnetic mineral formation as reflected in the supressed magnetic remanence properties (Fig. 5.69a). Notably, the

strongest ferrimagnetism was exhibited by unit E2, which was interpreted as either an aggrading channel floor or overbank deposit. X_{LF} values > 80 conclusively indicates a doleritic source, and on the basis of the facies, likely inherited from upstream (AK-7 and 8). Further, this value should be taken as a conservative representation of ferrimagnetic intensity at time of deposition because this sample comes from beneath the calcrete horizon, which as will be demonstrated in section 5.3.6, is of the rhizogenic variety which forms at the capillary fringe (interface between phreatic and vadose zone). This means that unit F2 would have been waterlogged during time of calcrete fixation and subject to ferrimagnetic dissolution processes.

In contrast, the ferrimagnetic properties of F2 closely relate to those reported for sandstone (Rowntree et al., 2012), thus attesting to inputs via wash processes from the proximal slopes. Since the unit is free draining and above the influence of palaeo-water table height, the values of X_{LF}, X_{ARM} and IRM_{1T} may be taken as approximately representative of original source. The high X_{FD}% attests to a strong pedogenic overprint, but this likely represents several phases of soil formation under different palaeoclimatic conditions.

5.3.5a: AK-11 analysis

Log AK-11 was obtained from a 4.2 m channel exposure on the right bank 1782.7 m downstream (Fig. 5.1, 5.71 and 5.72).

Unit A consists of poorly sorted very coarse sands with subordinate silt and minor clay with occasional cobbles (A1), punctuated by a thin, laterally discontinuous bed of clast-supported very coarse gravels (A2), which is then overlain by massive, predominantly coarse to very coarse sands (57.7% combined- Fig 5.73) and very fine gravels. Organic content is low (bromine - 3.4ppm).

The sediment package is characterised by moderately strong magnetic susceptibility (χ_{LF} =41) and S values are typically low with 14% and 3% of the applied remanence unreversed at -100mT and -300mT (Fig. 5.74c).

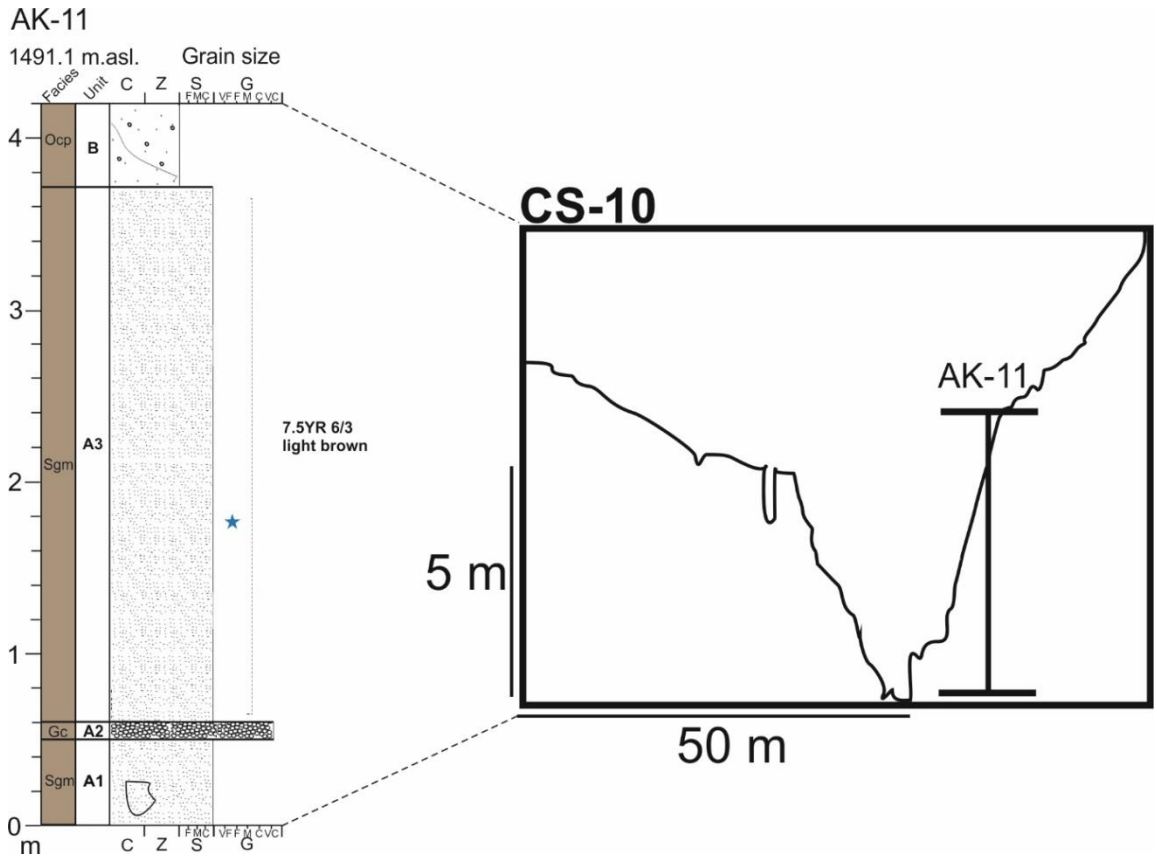

Figure 5.71 – sedimentary log AK-11 and cross section.

Figure 5.72 – photograph of outcrop AK-11.

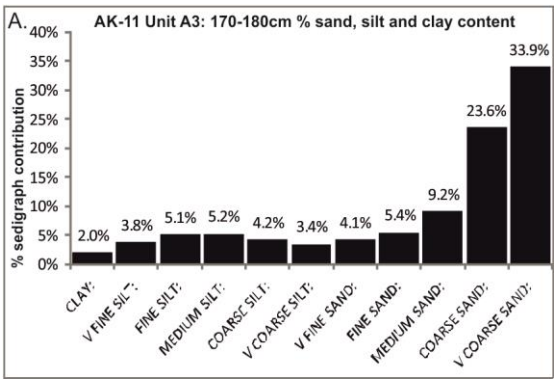

Figure 5.73 – % sand, silt and clay content derived from Coulter grain size analysis on samples collected from outcrop AK-11.

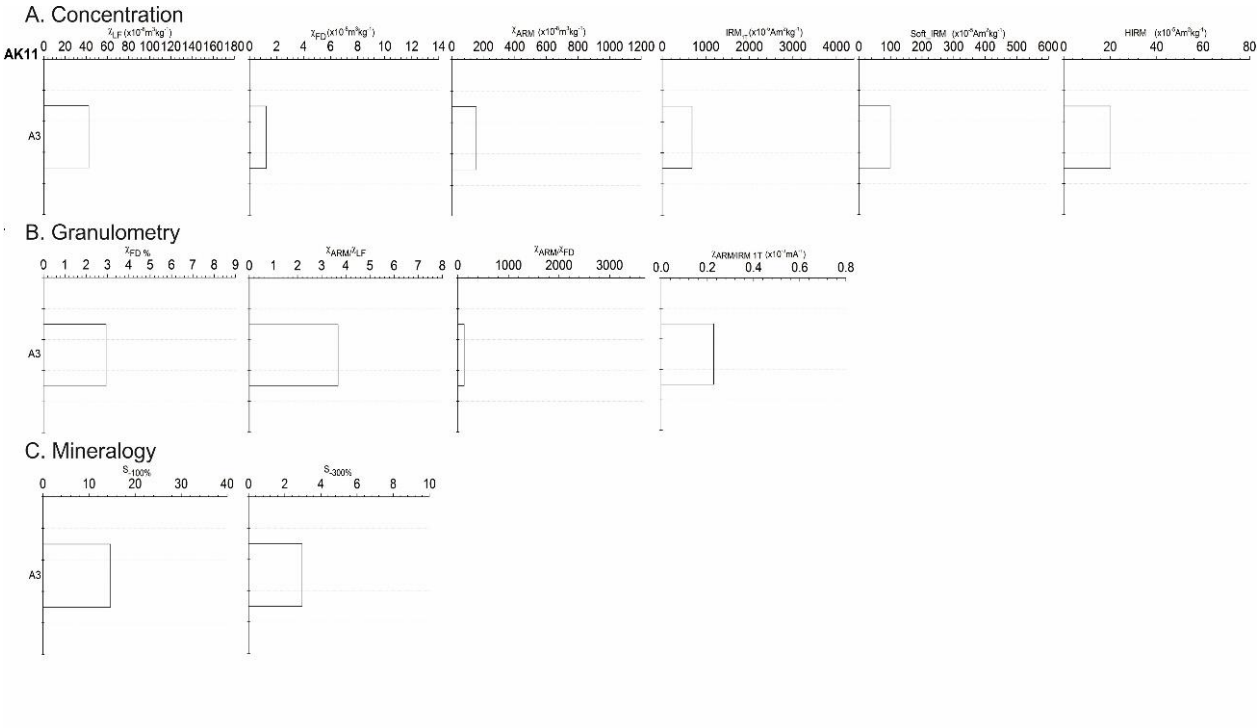

Figure 5.74 – mineral magnetic parameters for AK-11 unit A3.

5.3.5b: AK-11 interpretation

The sediments at AK-11 are sourced from the steep sandstone/mudstone slope to the right of the channel (Fig. 5.71). The occasional cobble-sized clasts reported at the base (A1) are very angular, derived from the eroding valley rock-wall and subsequently buried by slopewash (coarse sands- unit A3) deposits. The discontinuous clast-supported very-coarse gravel unit (A2) is interpreted as a small infilling of the palaeo-surface topography.

The predominance of sand over silt/clay (Fig. 5.73) indicates free-draining soil texture, so the relatively low susceptibility is not likely to be due to ferrimagnetic

dissolution (Fig. 5.74). Rather, the relatively weak ferrimagnetic signature (χ_{LF} = 41) with high concentrations of MD grains ($\chi_{ARM/IRM1T}$ = 0.2) reflects inputs from sandstone and mudstone rather than dolerite (Rowntree et al., 2012).

5.3.6a: AK-12 analysis

Log AK-12 was obtained from a 4.6 m exposure in an adjoining first order tributary draining a dolerite slope approximately 1783 m downstream from the Africanders Kloof headwaters (Fig. 5.1 and 5.75).

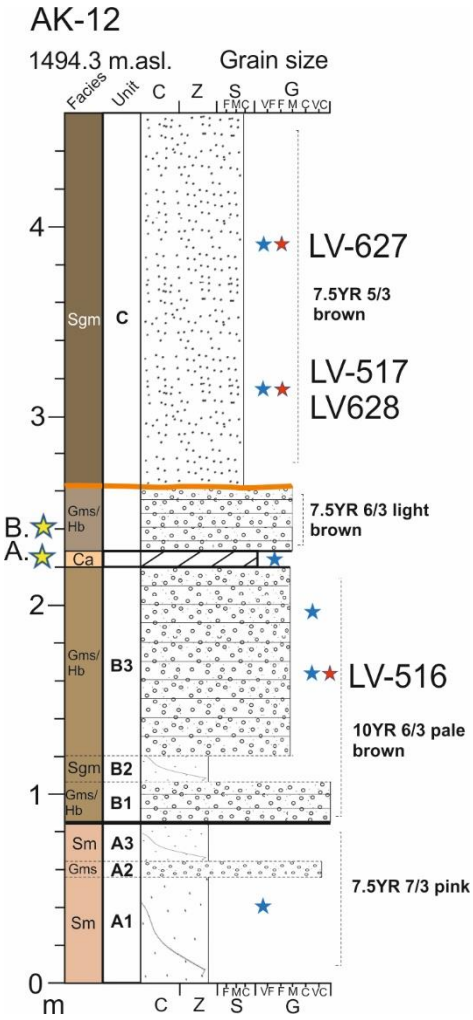

Figure 5.75 – sedimentary log of outcrop AK-12. Note yellow stars to left denoting locations of thin section A and B reported in text.

Unit A typically consists of structureless silty sands punctuated by a thin bed of very coarse gravel. Subunit A1 is dominated by a clast poor, very poorly sorted matrix consisting predominantly of silts and clays (50.7% combined). The sand component is predominantly very coarse (23.3% - Fig 5.76a). All concentration related magnetic

proxies are low relative to above units (Fig. 5.81a). χ_{FD}% is still high (4.5%), but the $\chi_{ARM}/_{IRM1T}$ is very low (0.32) (Fig. 5.81b).

The matrix exhibits a colour change at 85 cm from 7.5YR 7/3 pink to 10YR 6/3 pale brown. Unit B is dominated by medium-bedded, medium gravels. Some gravel occurs as lenses a few cm in diameter. Compared to the basal unit, the matrix at 170-180 cm is relatively enriched in sand (predominantly very coarse - 31.3%) compared to silt/clay (collectively 35.7% - Fig. 5.76b). Total magnetic susceptibility is high relative to unit A1 (χ_{LF} = 63-67). There is a slight enhancement in IRM_{1T}, Soft_IRM and HIRM at 195-205 cm (Fig. 5.81a). Conversely, $\chi_{ARM}/_{IRM1T}$ is very low (0.32) compared to 170-180 (Fig. 5.81b). The $S_{-100\%}$ is markedly higher at 195-205 cm with 19% of the applied remanence unreversed at -100mT (Fig. 5.81c).

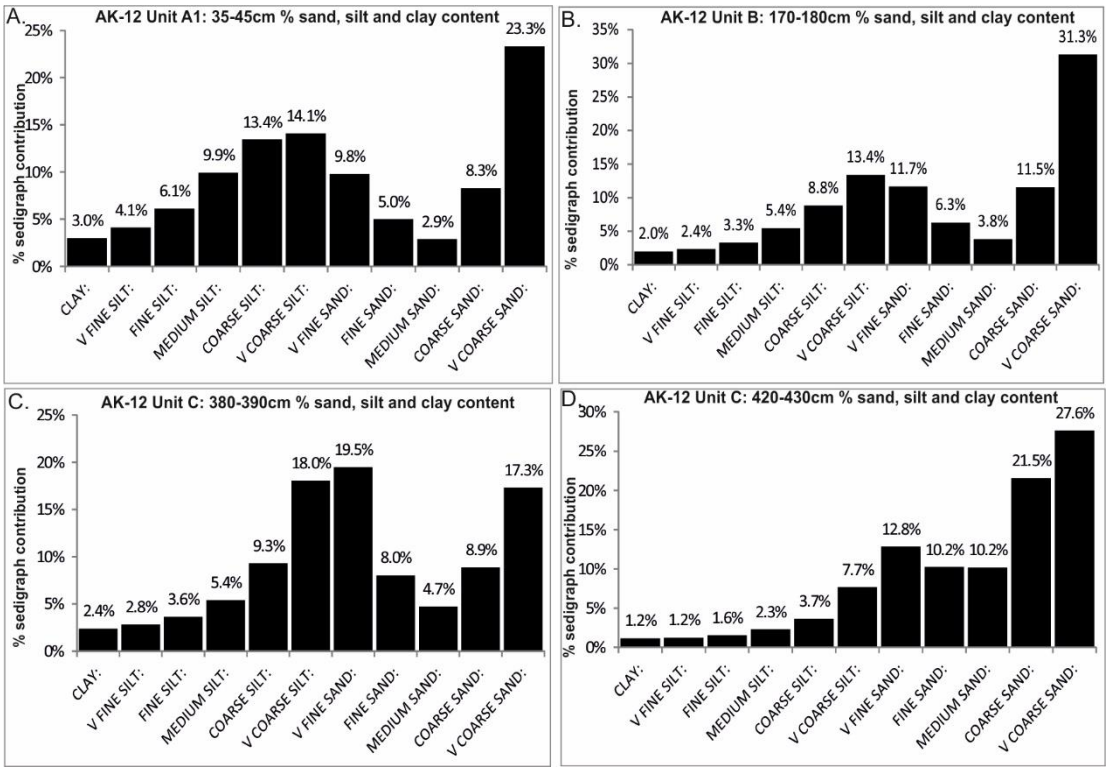

Figure 5.76 – % sand, silt and clay content derived from Coulter grain size analysis on samples collected from outcrop AK-12.

The top of the subunit (220-240 cm) is characterised by carbonate cements which are herein described based on field observation and micromorphological investigation via thin-section analysis under both scanning-electron and cross-polarised microscopy.

Thin section A spans a relatively thin horizon of calcrete (220-227 cm), characterised by sharp contacts with the underlying and overlying non-cemented sediment (Fig. 5.77). The sediment directly underneath the calcrete is characterised by moderate-well sorted silts with local doleritic fine sand grains. Localised and channel-like voids are common. The contact between the soil and calcrete is abrupt as evidenced by an abrupt colour change from light to dark brown (Fig. 5.78a). There is evidence that this contact may be erosional, evidenced by a wavy bed contact between the two distinct groundmasses (Fig. 5.78b). The cemented groundmass shows evidence of lamination and also slight variations in colour.

The host skeleton of the calcrete consists of moderately sorted grains ranging from silts to very coarse sand. Detrital grains are typically sub to well-rounded. At the macroscopic scale, the calcite cements appear ‘nodular’ due to their coalescence around lithic grains (Fig. 5.79a). Calcite has also accumulated as tube-like structures (Fig. 5.79b).

Despite being apparently densely cemented (Fig. 5.77c), there are zones of uncemented carbonate. Calcium carbonate content is variable depending on where sampled, but 18% (total % weight of bulk sample) was obtained using the acid soluble weight-loss method. Concentration of mobile elements (Na, S and Ca) all peak compared to other horizons (Table 5.22).

At the microscopic level, the calcrete horizon is dominated by a dense accumulation of carbonate coated detrital grains and rounded grains of secondary carbonates fixed within sparite cement (Fig. 5.80a and b). The carbonate that comprises the coated and rounded grains is micrite/microspar and contains evidence of a weakly laminated structure within the grain coatings (Fig. 5.80c). The coated grains are up to 1 mm at most in diameter. The voids between these grains that have become infilled with spar (Fig. 5.80d) are relatively small (<10 µm). The uncemented zones are characterised by a series of channel-like voids which are frequently lined with clay coatings that sometimes display laminations (Fig. 5.80e). In summary, the principal characteristics of the carbonate cements are:

1) Minimal fabric expansion indicating host sediment grains are cemented together rather than pushed apart by calcite growth.

2) Coated grains and grains of secondary carbonate.

3) Root traces.

4) No evidence for grain etching or quartz replacement by calcite.

Total magnetic susceptibility for this horizon remains high (χ_{LF} = 51.5), although the IRM_{1T} is relatively low (573) and the Soft_IRM and HIRM parameters much lower than the bracketing units (Fig. 5.81a). The calcrete unit is also characterised by very high χ_{FD}% (9.2) and relatively high $\chi_{ARM}/_{IRM1T}$ (0.64 – Fig. 5.81b). S values are also lower than the bracketing units, with 15% and 0.4% of the applied remanence unreversed at -100mT and -300mT respectively.

The unconsolidated sediment represented in thin section B (227-234 cm – Fig. 5.77c) that overlies the calcrete (5 cm above) is characterised by moderately sorted sediments ranging from silt to coarse sand. Grains are predominantly sub-rounded. Channel-like pores are common, most of which are lined by calcite hypo-coatings, but also inset laminated clays (Fig 5.79c and d; Fig 5.80f). Voids exhibit micro-erosional features such as detached, fragmented clay coatings that appear to have been washed into channel-shaped pores as *geopetal* accumulations in concert with detritus and fragments of carbonate.

Table 5.22 – percentage loss on ignition data, bromine, sodium, sulphur and calcium (ppm) content for sampled horizons at AK-12.

Unit	Height (cm)	Loss on ignition %	Br (ppm)	Na (ppm)	S (ppm)	Ca (ppm)
A1	35-45	-	0	4,700	140	14,350
B3	170-180	2.0	0.9	5,700	153	14,500
B3	195-205	1.8	7.5	9,200	151	57,880
B3	220 -225 (Calcrete)	-	5.4	16,800	281	228,170
C	380-390	1.8	10.7	5,100	206	14,680

Above the calcrete horizon (top of unit B), thinly bedded matrix-supported gravels predominate, but colour is markedly different to below: 7.5YR 6/3 light brown. Unit A is then discontinuity bounded above by massive, predominantly coarse sands (Fig. 5.76) that constitute unit B. Colour changes to 7.5YR 5/3 brown. Total susceptibility at the top (380-390 cm) is very high (χ_{LF} = 94), although IRM_{1T} exhibits a more modest increase (1230 – Fig. 5.81a). χ_{FD}% is very high (8% ~), but the $\chi_{ARM}/_{IRM1T}$ still relatively low (0.43) compared to the calcrete sample (Fig. 5.81b). S values are

slightly higher than the calcrete horizon with 17% and 2.2% of the total applied remanence unreversed at -100 and -300mT respectively (Fig. 5.81c).

5.3.6b: AK-12 interpretation

The facies of unit A are consistent with emplacement by current flow, the bedded gravels (A2) representing deposition as sheets. The doleritic gravels are locally sourced from an actively eroding intrusion 30 m upstream (Fig. 5.86a). The basal subunits (A1-A3) exhibit the strongest indications of gleying reflected in the colour (7.5YR 7/3 pink). Furthermore, soluble elements such as Na, S and Ca are low relative to above, indicating their loss in solution to groundwater. The very poorly sorted matrix of unit A1 is attributed to in situ weathering and clast break-up, expressed locally in the form of lenticular (1-2 cm) very coarse sands. The concentration-related magnetic proxy values are consistent with a gleyed environment, where ferrimagnetic dissolution and paramagnetic mineral formation have reduced susceptibility. Notably, susceptibility peaks in the 0-4 μm rather than the 32-63 μm, probably reflecting loss of the lithogenic magnetic component due to the deeply weathered nature of the sediment. In concert with the evidence for gleying, the S_{-300}% undoubtedly reflects goethite. The relatively high susceptibility above (170-180 cm) may be related to the coarser texture of the sediment (64.6% sand) such that ferrimagnetic dissolution was less intense under better drained conditions. This is confirmed in the lower S_{-300}% values of the finest and coarsest grades respectively (Table 5.23).

The sharp, near-planar contact at 262 cm separating units A and B indicates a distinct unconformity above the relatively rubified horizon overlying the calcrete (7.5YR 6/3 light brown). The overlying massive coarse sands with lenticular fine gravels are interpreted to be slopewash deposits, with local re-working of the sediments by rilling. The unconformity (262 cm) between units B and C signifies a hiatus in sedimentation and a period of prolonged exposure permitting soil development (reflected in the distinct reddening).

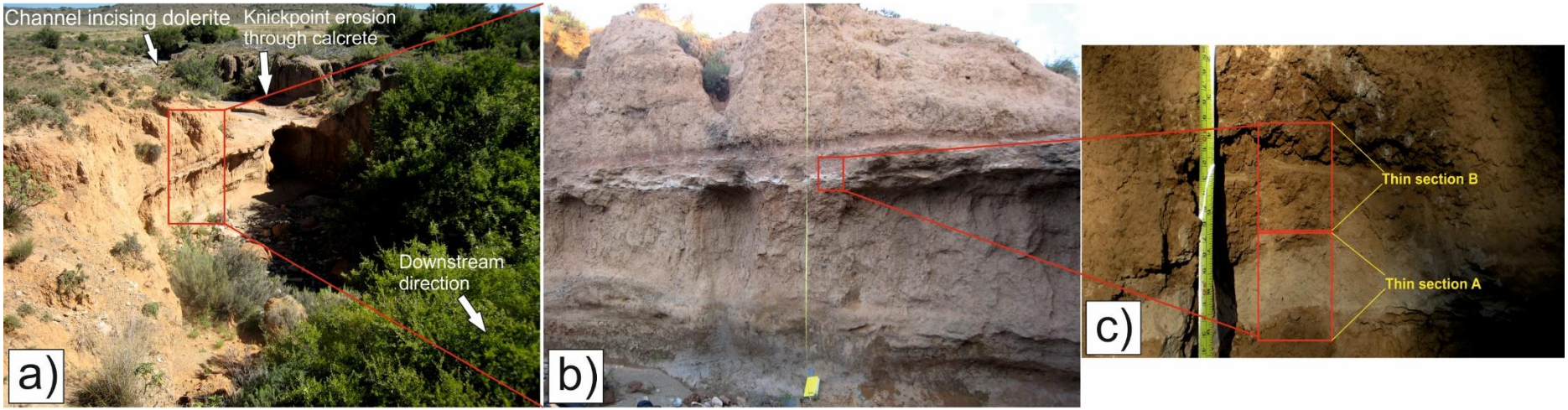

Figure 5.77 – photographs of outcrop AK-12 – a) view upstream establishing context for sampled outcrop (highlighted in red) , b) AK-12 outcrop, c) sampling locations for thin sections A and B (220-227 and 227-234 cm, respectively).

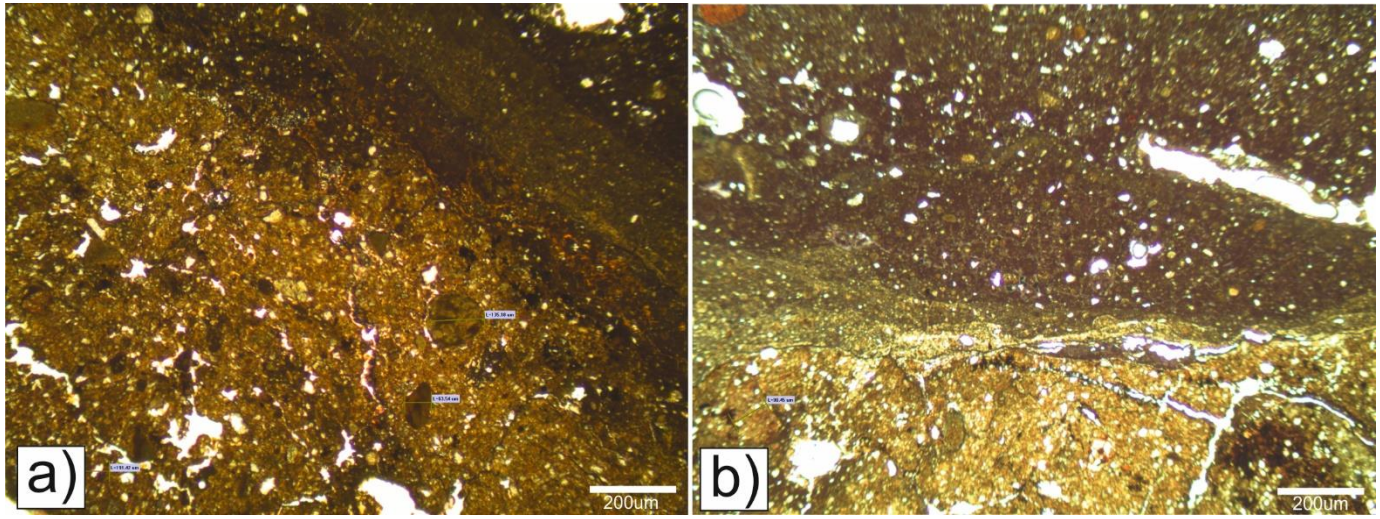

Figure 5.78 – photomicrographs of thin section A (220-227 cm) – a) note the abrupt transition in groundmass colour from light to dark brown, b) contact between underlying soil and calcrete, note the abrupt undulating contact.

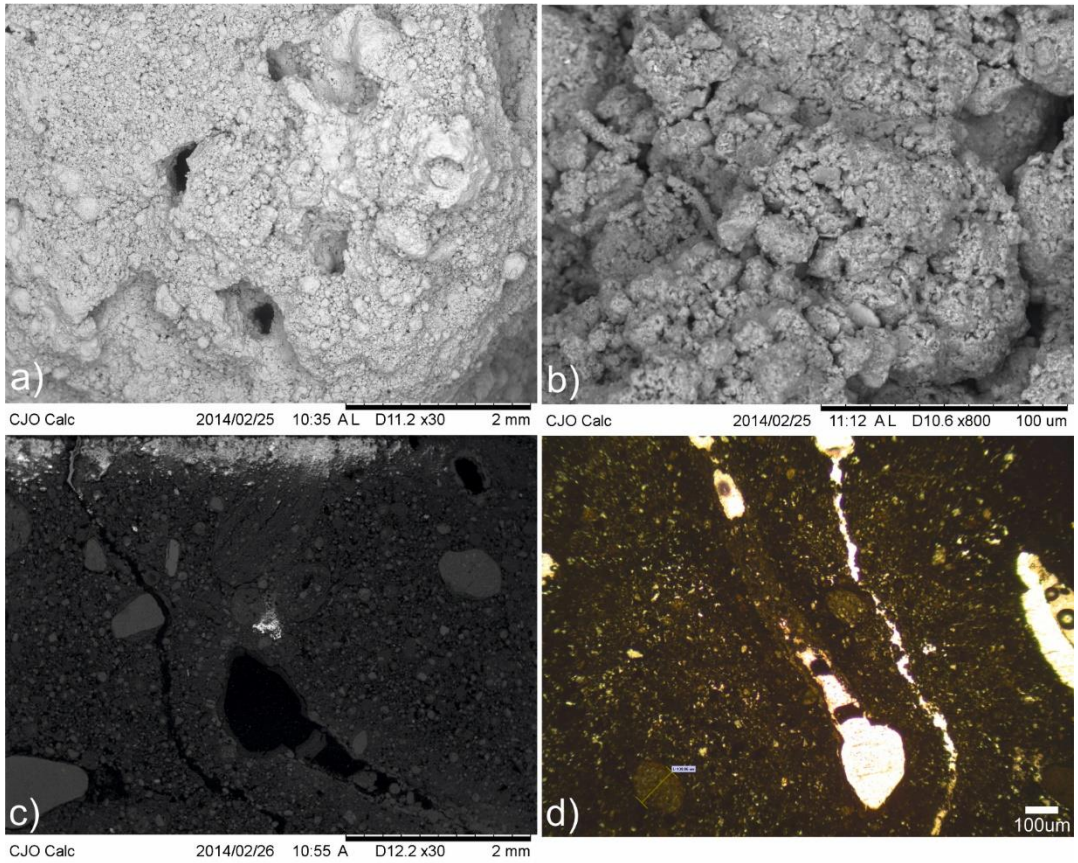

Figure 5.79 – photomicrographs of AK-12 calcrete and soil taken from scanning-electron (a-c) and cross-polarised light microscopy (d). A) macrostructure of sands and carbonate cement from bulk sample (correspondent to 220-227 cm), note the tubular channel structures and nodular cements, b) microstructure of calcrete fabric from bulk sample, note calcite accretion on silt size grains and elongated tubular structures, c) thin section B (227-234 cm), note laminated clay coatings in large void inset within calcite hypo-coating and in some cases, voids completely infilled by moderately sorted accumulations of silt and fine sand, d) thin section B (227-234 cm), clay coating in void - note distinct brown colouration associated with the calcite hypo-coatings flanking the channel structure.

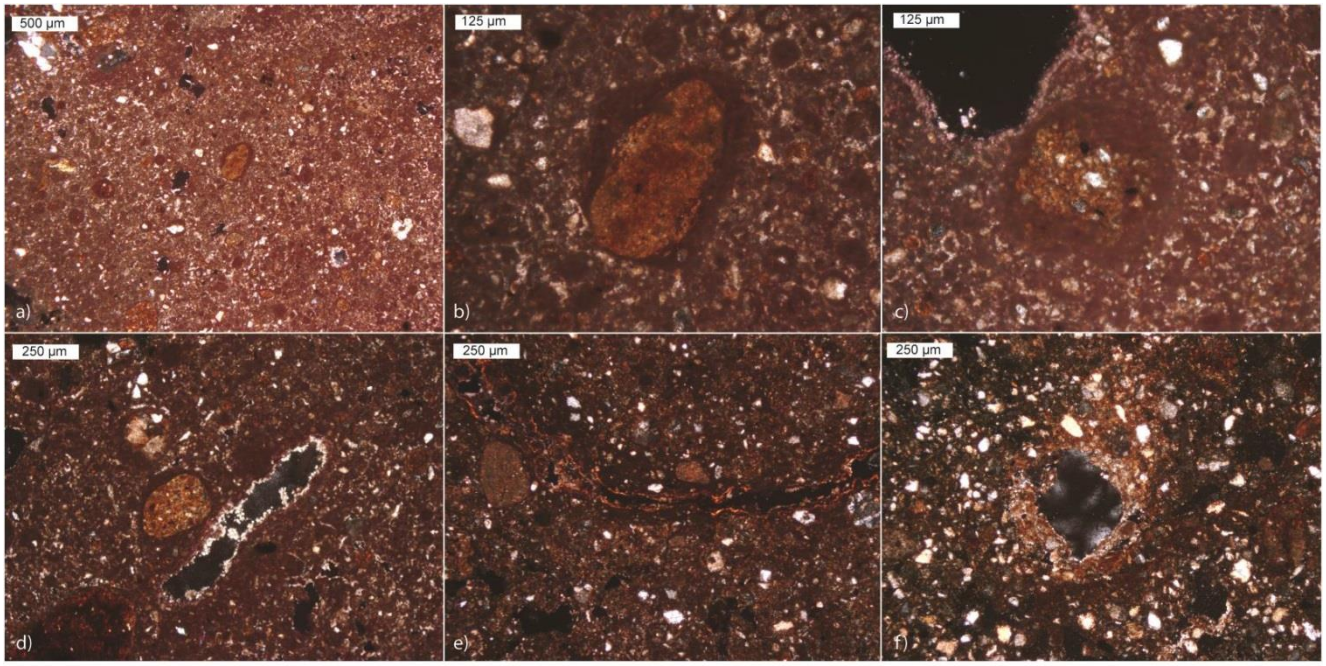

Figure 5.80 – photomicrographs of thin sections A (a-e) and B (f) taken under cross-polarised light – a) microstructure of the calcrete (x2), b) a carbonate coated dolerite grain (x10), note the smaller rounded carbonate grains (<50µm) observable in the groundmass, c) a carbonate coated dolerite grain (x10), note the weakly developed laminations within the grain coating. Radial voids can be observed between coated grains that have bright colours due to the presence of spar cement within them, d) a coated dolerite grain next to a spar lined channel (x4), e) a clay lined pore within the uncemented zones of the calcrete (x4), f) a calcitic hypo-coating from the sediments overlying (thin section B) the calcrete horizon (x4).

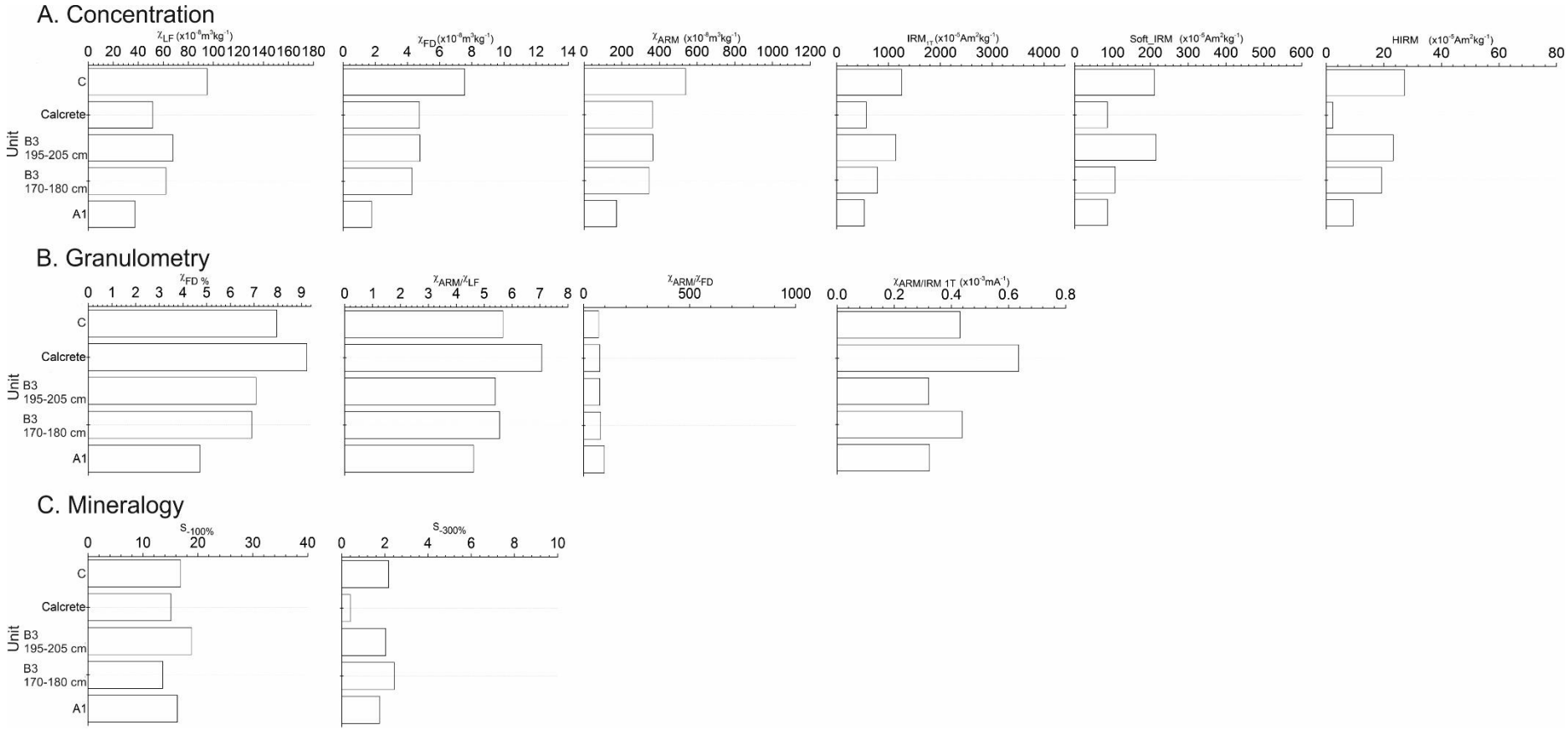

Figure 5.81 – mineral magnetic parameters from sampled horizons at outcrop AK-12.

Table 5.23. Magnetic parameters obtained for two particle sized fractions and bulk samples from units A1 and B3 at outcrop AK-12.

AK-12: Unit A1.	**X_{LF}**	**X_{FD}%**	**X_{ARM}**	**IRM_{1T}**	**Soft_IRM**	**HIRM**	**X_{ARM}/X_{LF}**	**X_{ARM}/X_{FD}**	**$X_{ARM/IRM1T}$**	**S_{-100}%**	**S_{-300}%**
0-4 μm	46.3	7.8	142.8	132.4	19.5	7.1	3.08	39.3	1.08	14.7	5.4
32-63 μm	36.3	2.5	88.7	879.5	160.9	48.6	2.44	96.5	0.10	18.3	5.5
Bulk	37.3	4.7	172.5	533.2	86.6	9.4	4.62	98.0	0.32	16.3	1.8
AK-12: Unit B3*	**X_{LF}**	**X_{FD}%**	**X_{ARM}**	**IRM_{1T}**	**Soft_IRM**	**HIRM**	**X_{ARM}/X_{LF}**	**X_{ARM}/X_{FD}**	**$X_{ARM/IRM1T}$**	**S_{-100}%**	**S_{-300}%**
0-4 μm	61.1	6.7	450.6	563.6	65.5	15.2	7.37	109.8	0.80	11.6	2.7
32-63 μm	52.8	2.3	96.9	1254.1	191.7	35.2	1.84	80.2	0.08	15.3	2.8
Bulk	62.1	6.9	344.9	787.7	107.0	19.2	5.55	80.4	0.44	13.6	2.4

The massive nature of unit C implies conditions of relatively rapid overbank sedimentation with no intervening phases of soil development.The magnitude of the ferrimagnetic concentration proxies and $X_{ARM/IRM1T}$ clearly attests to a doleritic source – most likely the dolerite outcrop upstream (Fig. 5.77a). The X_{FD}% (8%) indicates high concentrations of pedogenic (SP) magnetite, uncompromised by dissolution as was the case for units A and B. Notably, the higher HIRM compared to below attests to greater contributions from hard AF minerals, probably haematite over goethite.

Thin section A: Calcrete micromorphology - 220-227 cm.

In soil environments, coated and rounded grains of secondary carbonate in concert with root traces are typically associated with dense root mats. These rounded grains occur where fungal communities associated with the rhizome metabolise in contact with lithic grain surfaces (Calvet and Julia, 1983).

This calcite microfabric lacks fractured grains, grain replacement, “exploded” fabrics (i.e. calcite growth which pushes lithic grains apart) consistent with ‘alpha fabrics’, which are the products of inorganic precipitation controlled by evaporation and/or CO_2 degassing (Machette, 1985). Although the calcrete exhibits a weakly laminated structure, this tends to occur at the base rather than at the top of the horizon, implying that it is not a depositional feature in response to underlying deeply cemented impermeable carbonate cements. Therefore, the micromorphological features are consistent with the ‘beta fabric’ (biologically dominated) calcrete variety (Wright, 1990; Renaut, 1993). The formation of such calcrete types occurs in association with phreatic root systems that are accessing a deep or near-surface water table. Where the root networks come into contact with the water table, they spread laterally and subsequent calcification, dominated by biological fixing, generates a thin but laterally extensive calcrete horizon (Wright et al., 1995). The fact that 63% of the iron oxide content is represented by goethite on the calcrete horizon further supports the notion of poorly drained soil conditions, although this goethite signature was only found to make a small contribution to the amount of unreversed IRM at -300mT% (Fig. 5.81c). The relatively subdued ferrimagnetic signature of the calcrete compared to the underlying sediment is undoubtedly due to diamagnetic dilution by the calcite itself as evidenced by the high ppm concentration (228,170 – Table 5.22).

The maturity of the AK-12 calcrete horizon is classified as stage 2 of Wright et al's (1995) classification scheme for rhizogenic calcretes on the basis of two lines of evidence: 1) >50% of the horizon consists of carbonate sheets or stringers, but there are still places where the intervening matrix is visible, giving it the distinctive band-like appearance (see Fig. 5.77b and c); and 2) grain coatings are continuous and firm carbonate nodules are common. This is broadly concordant with stages I and II of Machette's (1985) classification of pedogenic calcretes.

The referenced zones of uncemented sediment within the calcrete are interpreted as evidence for localised decalcification reflected by the occurrence of illuviated clay coatings in voids and channels. This process is incompatible with carbonate fixing conditions because dissolved Ca^{2+} within the soil water causes clay particles to flocculate rendering them immobile (Kemp, 1985a and b; Rose et al., 2000). The evidence for calcrete dissolution and clay mobilisation thus indicates a shift in soil conditions (Yaalon, 1997). In light of the strong evidence that calcite accretion was driven by position of the water-table, this is interpreted to reflect a drop in groundwater levels allowing vadose water to drain freely through soil, resulting in clay translocation, carbonate leaching and some associated brecciation and reworking of sparite cements. Further evidence for leaching of the carbonate cement is reflected in the relatively high Ca content immediately below the calcrete horizon (57880 ppm – 195-205 cm). Low susceptibility values χ_{LF} is attributed to the diamagnetic effect of calcite, ferrimagnetic dissolution and paramagnetic mineral formation. The latter is indicated by the distinctly low IRM_{1T} compared to bracketing units. Similarly, the very low HIRM and S_{-300}% is likely due to diamagnetic effects from the calcite. The very high χ_{FD}% (9.2) of the calcrete is related to the accumulation of SP grains contained within illuviated clays derived from the uncalcified soil above (227-262 cm).

Thin section B: Overlying soil - 227-234 cm.

The relative abundance of calcite hypocoatings implies a return to calcite fixing within the sediment column after the aforementioned phase of clay translocation (Kemp, 1995). This implies that there was a drying out of the sediment column, possibly associated with a lower water-table, such that localised calcite hypocoatings were fixed by evaporitic processes along pre-existing root channels.

Two distinct horizons of calcrete are found to the left of the modern channel approximately 150 m downstream (Fig. 5.82). This indicates that the water-table lowered after the formation of the first (top) rhizogenic calcrete. The lack of expression of this 'double calcrete' here at AK-12 and elsewhere downstream, is probably due to leaching of Ca.

Although evidence has been identified to indicate the calcic soil is polygenetic due to changing groundwater levels, it is likely that progressive reduction of Ca^{2+} supply from the in situ weathering of the host sediment also constrained maturation of the calcrete also. Without any radiometric ages from the soil itself and the capping sediments (unit B), it is impossible to determine the length of time between the respective phases of aggradation and geomorphic stabilisation. The lack of well-dated modern analogues of rhizolitic calcrete formation make it very difficult to estimate rates of formation of such profiles, but Klappa (1980a) reported living roots with calcareous sheaths implying that their formation is likely to be rapid compared to 'alpha fabric' pedogenic calcretes (Candy and Stewart, 2009).

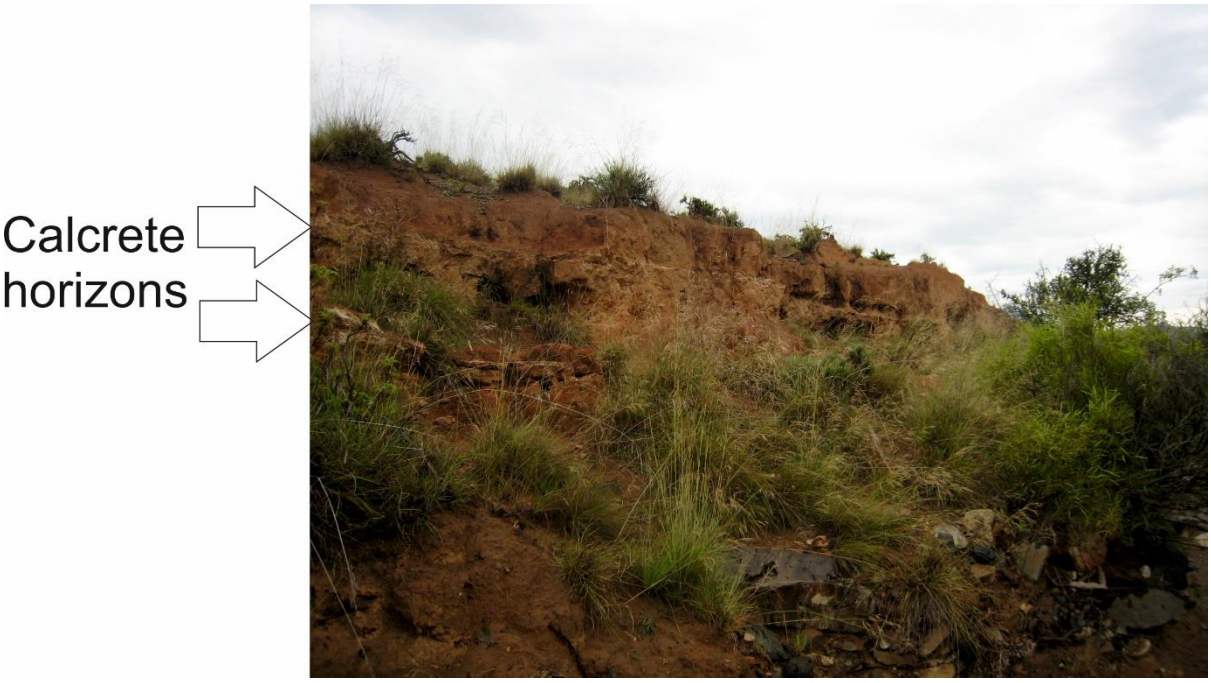

Figure. 5.82 – photograph showing outcrop to left of main tributary where two distinct horizons of thin (5-7 cm), laterally continuous calcrete occur. The top calcrete corresponds with the AK-12 unit along with the overlying rubified soil exhibiting a discontinuity with the overlying sediment.

The drivers of these changes in groundwater levels are ambiguous. Two possible scenarios are presented accounting for the changes reflected in the soil conditions.

1) Both calcrete units (Fig. 5.82) reflect seasonal fluctuations in the water table, i.e. the basal calcrete (summer: hot and dry) and the top calcrete horizon associated with late summer rains causing the groundwater level to rise. Considering the relatively rapid rates of formation of rhizogenic calcretes, successive cycles could theoretically produce similar morphological characteristics. However, if there were several annual cycles of wet-dry-wet associated with seasonal precipitation change, this would likely produce a legacy of successive clay illuvation and re-cementation phases, as well as localised leaching of iron oxides from the groundmass. This does not corroborate the micromorphological evidence which attests to one dominant phase of inset clay coatings.

2) Reduced groundwater level could have been a response to aridification, although the timing and magnitude of such a change is unknown. If climate did become drier, a lowering of the water-table could have led to clay illuviation down the profile with brecciation and reworking of the calcic cements. Drying of the climate could have also provided the impetus for sedimentation from hillslopes to continue (unit C). This would have buried the palaeosol (262 cm), but also provided fresh sediment, from which extra Ca^{2+} ions were derived and fixed as second generation calcite hypocoatings at 227-234 cm. This implies a more strictly 'pedogenetic' rather than 'rhizogenic' origin. The lower calcrete portrayed downstream (Fig. 5.83) could be coeval with the second generation hypocoating phase at AK-12 after incision of the palaeosol and re-activation of hillslope sediment sources.

Estimating aggradation rates in ephemeral channel settings is complicated by the fact that rates are non-linear due to sedimentation episodes being event driven particularly by flash-flooding. Although AK-12 lacks the very thick (40-50 cm), very coarse (gravel-cobble) units that imply extremely high energy rapid sedimentation events identified further upstream (AK-8 and 10 for example), it is feasible for 2-3 m of alluvium under conditions of steadier aggradation (on the basis of thinner beds of gravel lacking clear erosion structures) to occur within several decades. As shown in chapter 4, an old check dam (c. 1973) at Wilgerbosch filled up to capacity (2 m) with backfilling approximately 250 m upstream and whilst the exact date the capacity of the dam was reached is unknown, it must have been less than 40 years. As a result, re-structuring of the local hydrology here at AK-12 (ephemeral gully changing to sub-surface dominated flow) probably occurred rapidly.

5.3.7a: AK-13 analysis

Log AK-13 was obtained from a 2.6 m exposure opposite AK-12 described previously (Fig. 5.1, 5.83 and 5.84).

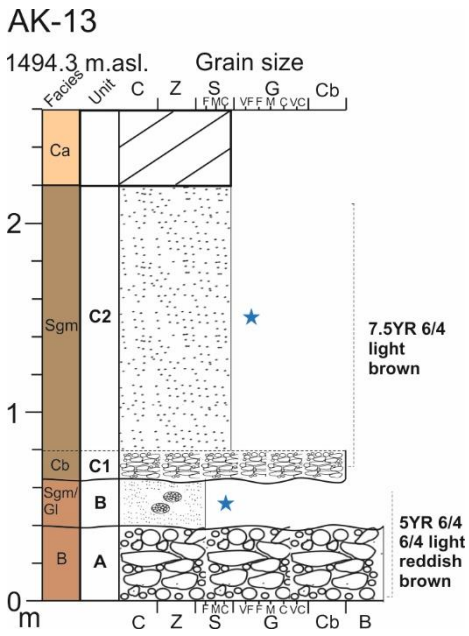

Figure 5.83 –sedimentary log of outcrop AK-13.

Unit A consists of a very poorly sorted assemblage of laterally discontinuous boulders, cobbles, gravels within a poorly sorted matrix of silty sand. Clast rounding varies from rounded to subangular. Unit B consists of minerogenic (Table 5.24) very poorly sorted sands (72%) with subordinate silts and clays (28% - Fig 5.85a). There are local small (several cm wide) lenses of very coarse sand and very fine gravel. Matrix colour changes from 5YR 6/4 light reddish brown (units A and B) to 7.5YR 6/4 light brown at subunit C1, which is a laterally discontinuous bed of poorly sorted cobbles and gravels. Subunit C2 is composed of predominantly coarse-very coarse sands (52% - Fig 5.85b) and contains negligible soil organic matter (Table 5.24). The succession is capped by the same calcrete horizon described at AK-12.

Total susceptibility is comparable with AK-12 for both sampled units, the base (B) exhibiting weaker χ_{LF} (58 – Fig. 5.86a). S_{-300}% declines from subunits B to C2 with 3.5% and 0.4% unreversed respectively at -300mT (Fig. 5.86c).

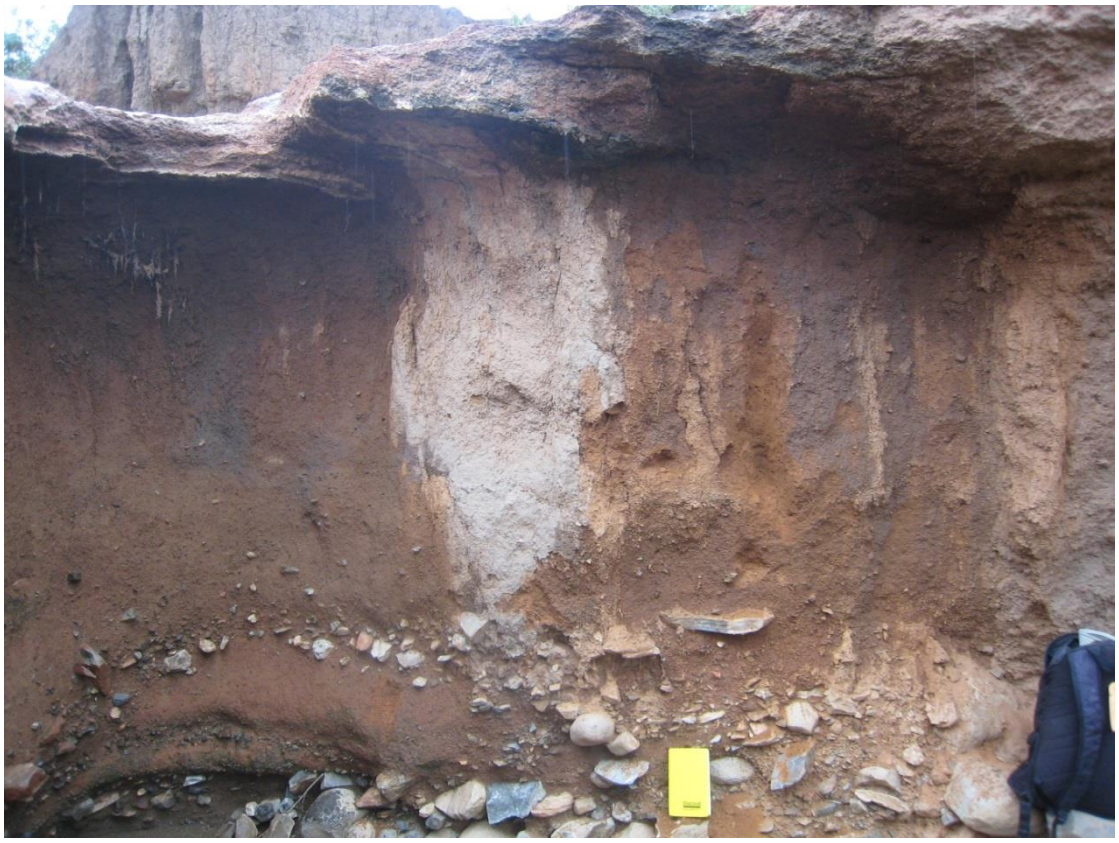

Figure 5.84 – photograph of outcrop AK-13.

Table 5.24 – percentage loss on ignition data and bromine content (ppm) for sampled horizons at AK-13.

Unit	Height (cm)	Loss on ignition (%)	Bromine (ppm)
B	45-55	3.55	1.8
C2	150-160	1.34	0.7

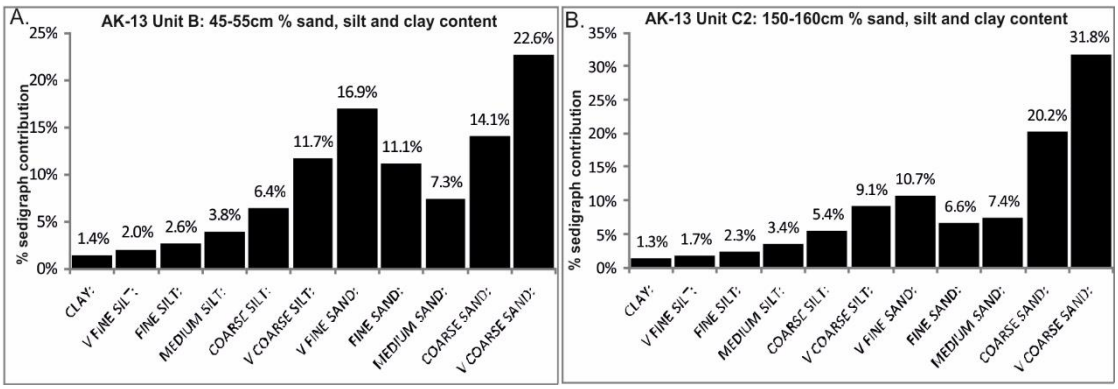

Figure 5.85 – % sand, silt and clay content derived from Coulter grain size analysis on samples collected from outcrop AK-13.

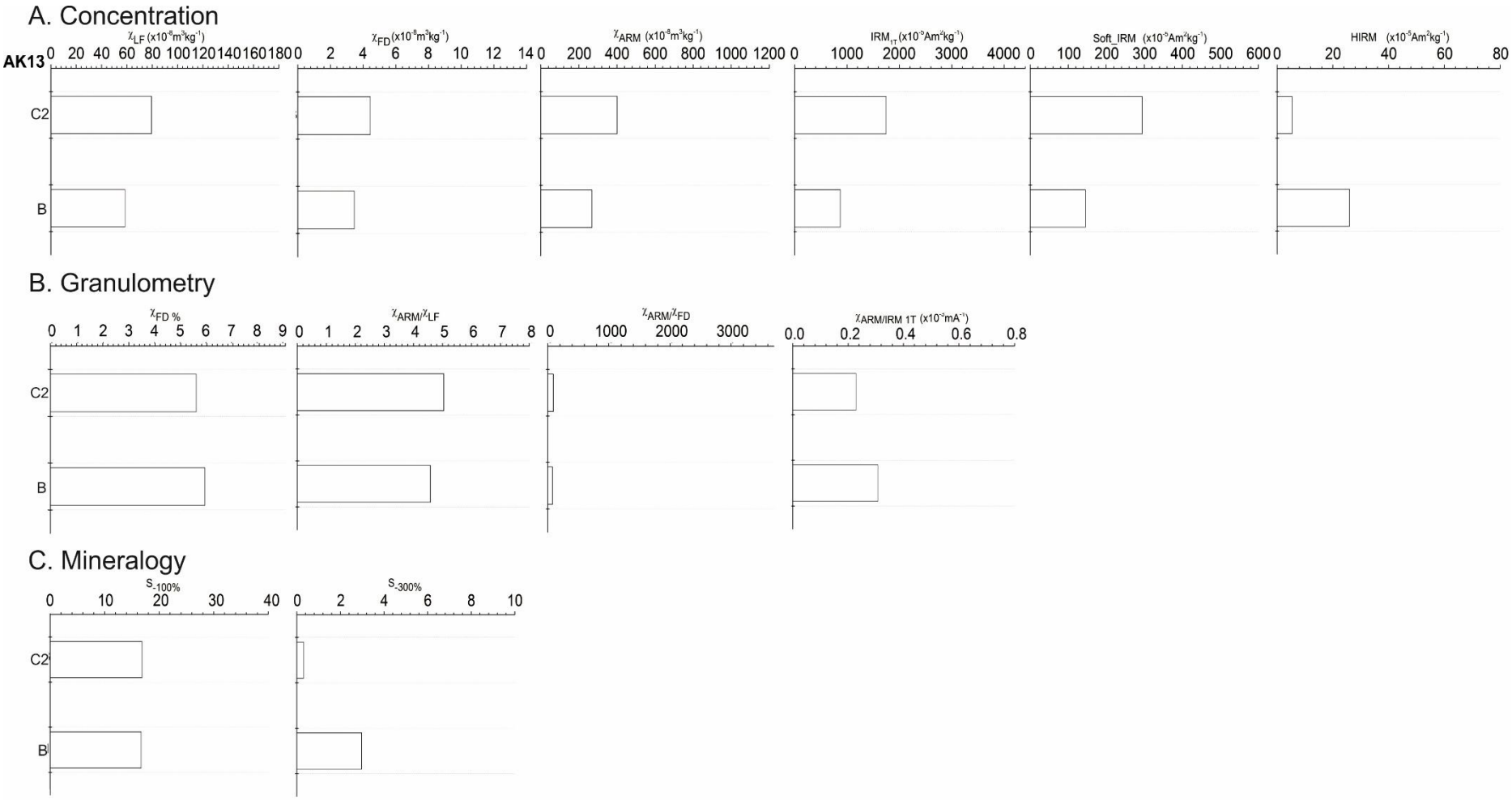

Figure 5.86 – mineral magnetic parameters from sampled horizons at outcrop AK-13.

5.3.7b: AK-13 interpretation

The basal coarse unit (A) indicates high energy transport by current flow. The laterally discontinuous nature of the deposit as well as the 'U' shaped appearance in relation to the finer grained sediment implies an infilled channel with debris flow deposits considering the very poorly sorted nature of the facies. The lenticular gravels within a matrix of sand (unit B) are interpreted as sheetflood deposits with dissection by small rills. χ_{LF} values of 58 indicate moderate-high concentrations of ferrimagnetic minerals and whilst the $\chi_{ARM/IRM1T}$ indicates that only a small (30% ~) amount of the remanence carriers are in the SD range, the high χ_{FD}% (6) implies high concentrations of pedogenic SP grains. This high concentration is probably due to illuviation of pedogenic clays following the drop in water-table (see AK-12 for full discussion). The locally 'redder' colour (5YR 6/4) in concert with the distinctively higher S_{-300}% (3.1%) indicates haematite rather than goethite dominating the AF magnetic signature.

The sharp undulating contact between unit B and C1 implies an erosion surface associated with channel incision, with the overlying massive sands (unit C2) reflecting infilling of this palaeochannel. The poorly defined bedding is probably related to bioturbation reflected in the root channels and weakly developed blocky structure of the soil. The higher concentration-related proxies indicate larger contributions remanence carrying ferrimagnets, though most of these appear to be carried by pedogenic SP grains as before (χ_{FD}% = 5.6%).

5.3.8a: AK-14 analysis

Log AK-14 was obtained from a 4.4 m outcrop 2143 m downstream from the headwaters on the right bank (Fig. 5.1, 5.87 and 5.88).

The sediment package represented in log AK-14 occurs in close proximity to the hillslope to the east with a minimum distance of 30 m to the base of the slope. The sediment package slopes steeply down toward the contemporary channel (see CS-12 - Fig. 5.88).

Unit A1 is characterised by massive, very coarse sands with very fine gravels overlying dolerite bedrock. Unit A1 grades to lenticular, matrix-supported medium gravels (A2).The matrix is composed of very poorly sorted sands (86.7%) and minor

silt and clay (13.3% - Fig. 5.89a). The soil exhibits a friable, blocky structure with blocks up to 30 cm in diameter. Root channels are abundant throughout the entire profile with localised slumping present.

Figure 5.87 – photograph of sediments to the right bank of the channel represented in log AK-14 (Fig. 5.88).

Table 5.25 – percentage loss on ignition data and bromine content (ppm) for sampled horizons at AK-14.

Unit	Height (cm)	Loss on ignition (%)	Bromine (ppm)
A2	125-135	0.83	1.6
A2	185-195	0.99	5.6

There is a change in colour from 10YR 7/3 pale brown to 7.5YR 5/4 brown above 1.45 m. Sorting improves above (185-195 cm) with the matrix consisting of primarily coarse to very coarse sand (77.5% - Fig. 5.89b).

Total magnetic susceptibility for both sampled units is very high (χ_{LF} = 119-141) with the IRM_{1T} exceeding all other samples measured (up to 4341 – Fig. 5.90a). Both samples are also characterised by extremely low χ_{FD}% and $\chi_{ARM/IRM1T}$ values (Fig 5.90b).

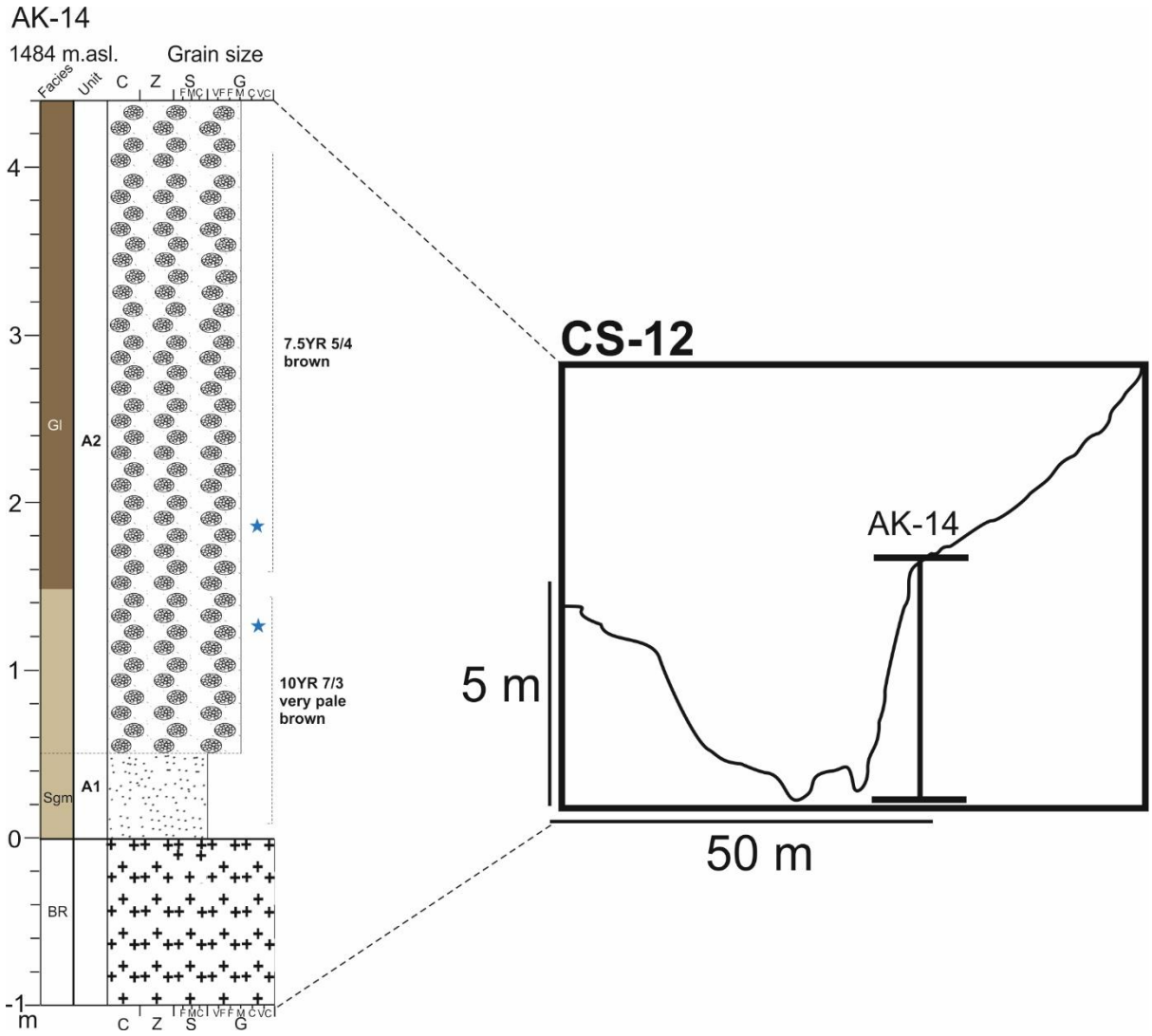

Figure 5.88 – sedimentary log AK-14 and cross section.

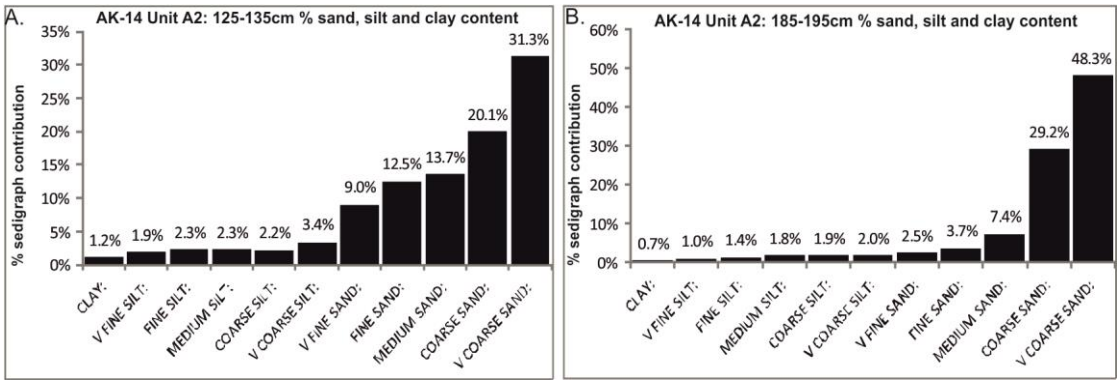

Figure 5.89 – % sand, silt and clay content derived from Coulter grain size analysis on samples collected from outcrop AK-14.

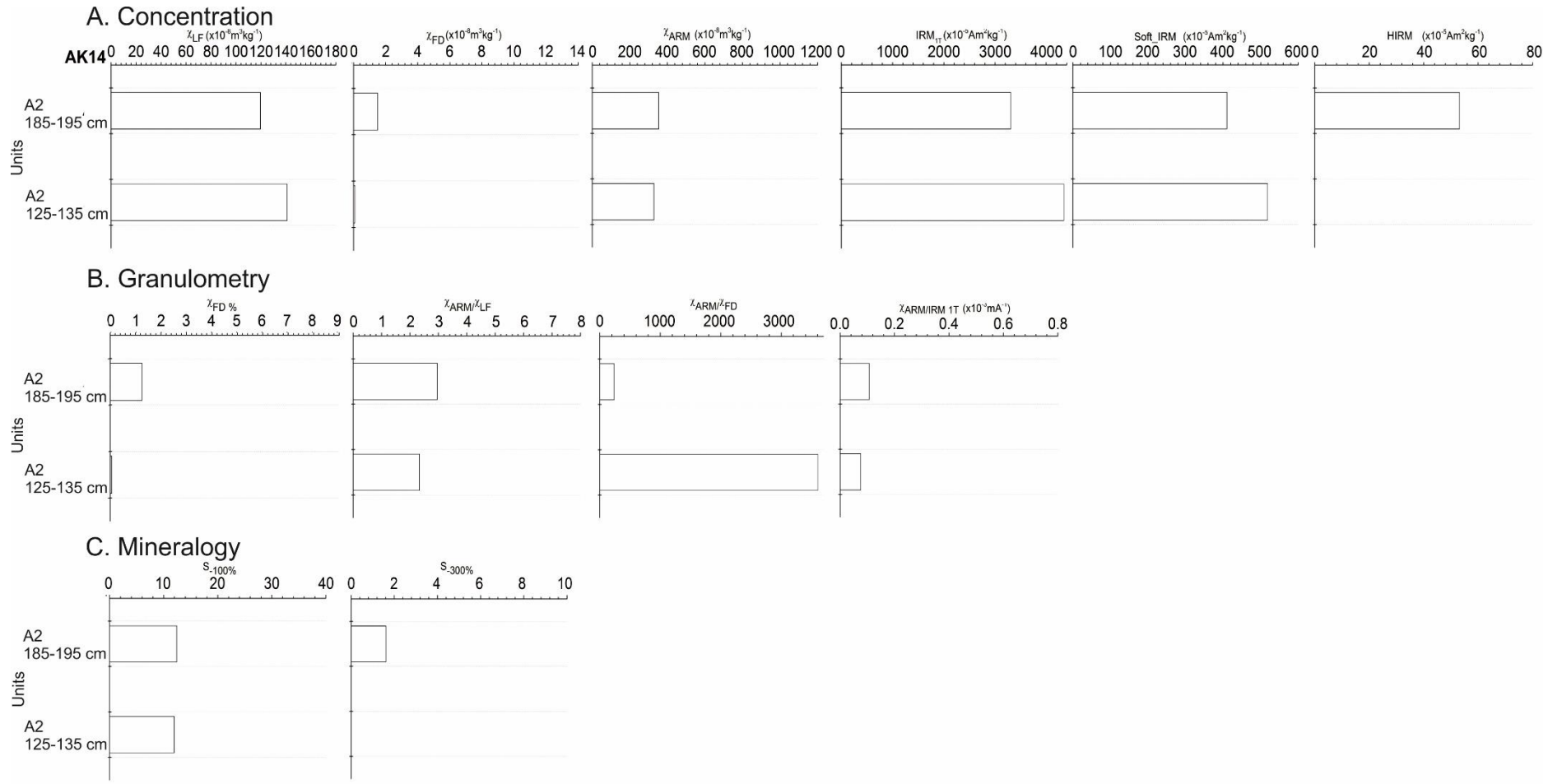

Figure 5.90 – mineral magnetic parameters from sampled horizons at outcrop AK-14.

5.3.8b: AK-14 interpretation

The steeply sloping sediment package indicates probable deposition from the hillslope rather than a channel delivering sediment from upstream. Aerial imagery reveals a partially infilled gully extending up the slope to the north. dGPS survey of the top bank of the right hand terrace indicates that the AK-14 sediments exhibit convex lateral topography. The deeply bioturbated nature of the sediments make it difficult to firmly identify diagnostic structures that imply mode of deposition. However, weakly bedded matrix-supported gravels dissected by lenticular clast-supported gravels may represent the latter stages of sheet-flow consistent with unconfined flow possibly after the terminus of a gully. The fact that the weakly developed planar non-parallel crossbeds dip in an upstream direction (i.e. at right angles to the long axis of the sediment body) may indicate flow deposition radiating laterally downstream of the point of loss of confinement, although any proximal-distal fining is hard to identify. The morphology and facies are similar in character to some of the sediment units in the floodout sequence on the upper slopes (AK-1B), although distinct coarse beds are lacking. This could be due to the lack of coarse sediment supply (gravels), or that the point of sampling is capturing the distal margins of the floodout, where distal fining has resulted in accumulation of sediment no coarser than medium gravels. The relative enrichment of very fine-medium sands as well as slightly higher silt/clay at 125-135 cm may reflect a combination of two processes: 1) illuviation down-profile, 2) preferential transport of finer material from the hillslope first (125-135 cm) followed by coarse sands (185-195 cm) as fine sediment supply became exhausted to produce slight inverse grading.

The χ_{LF} values (119 and 141) indicate very high concentrations of ferrimagnetic minerals comparable only with the headwater floodout (AKH–AK-2) draining slopes of deeply weathered dolerite. The very low S_{-300}% values (unit A2 – 185-195 cm) indicate a very low contribution of AF minerals, but these may be masked by the huge ferrimagnetic signature (Fig. 5.90c). However, IRM_{1T} values of up to 4341 (185-195 cm) indicate extremely high concentrations of remanence carrying ferrimagnets – the highest reported for the study region. Yet, the relatively very small χ_{ARM} and χ_{FD}% indicate that most of the remanence carrying grains are in the PSD or MD grain size window, confirmed by the extremely small $\chi_{ARM}/_{IRM1T}$. The constant S_{-100}% indicates no change in the coercivity of magnetite. In combination with the

geomorphological evidence, this demonstrates sufficiently that the sediments are sourced from a nearby hillslope capped by dolerite, probably representing a small floodout sequence that has subsequently been truncated as the valleys incised.

5.4 Lower valley (AK-15 - AK-18)

5.4.1a: AK-15 analysis

Log AK-15 was obtained from a 5.5 m outcrop 2568.4 m downstream from the headwaters on the right bank (Fig. 5.1, 5.91 and 5.92). This sediment package occurs at the base of a large headcut (2 m) through sandstone.

Figure 5.91 – photograph of outcrop log AK-15.

Unit A consists of a single, medium-thick bed of matrix-supported gravel, the matrix being composed of predominantly coarse to very coarse sand (69% - Fig. 5.93a). The unit exhibits low LOI% (1.5) and Br content (4.4 ppm – Table 5.26). The contact between units A and B is planar, sharp. Unit B comprises an upward fining sequence from matrix-supported gravels (B1) to very poorly sorted sandy silt (B2 – Fig. 5.93b) and then silts with lenses of very coarse sand and infrequent very fine gravels (B3).

The unit exhibits low LOI% and Br values (Table 5.26). Colour is subtly different to unit A: 7.5YR 6/4 light brown. This is then capped by very coarse matrix-supported gravels (unit C).

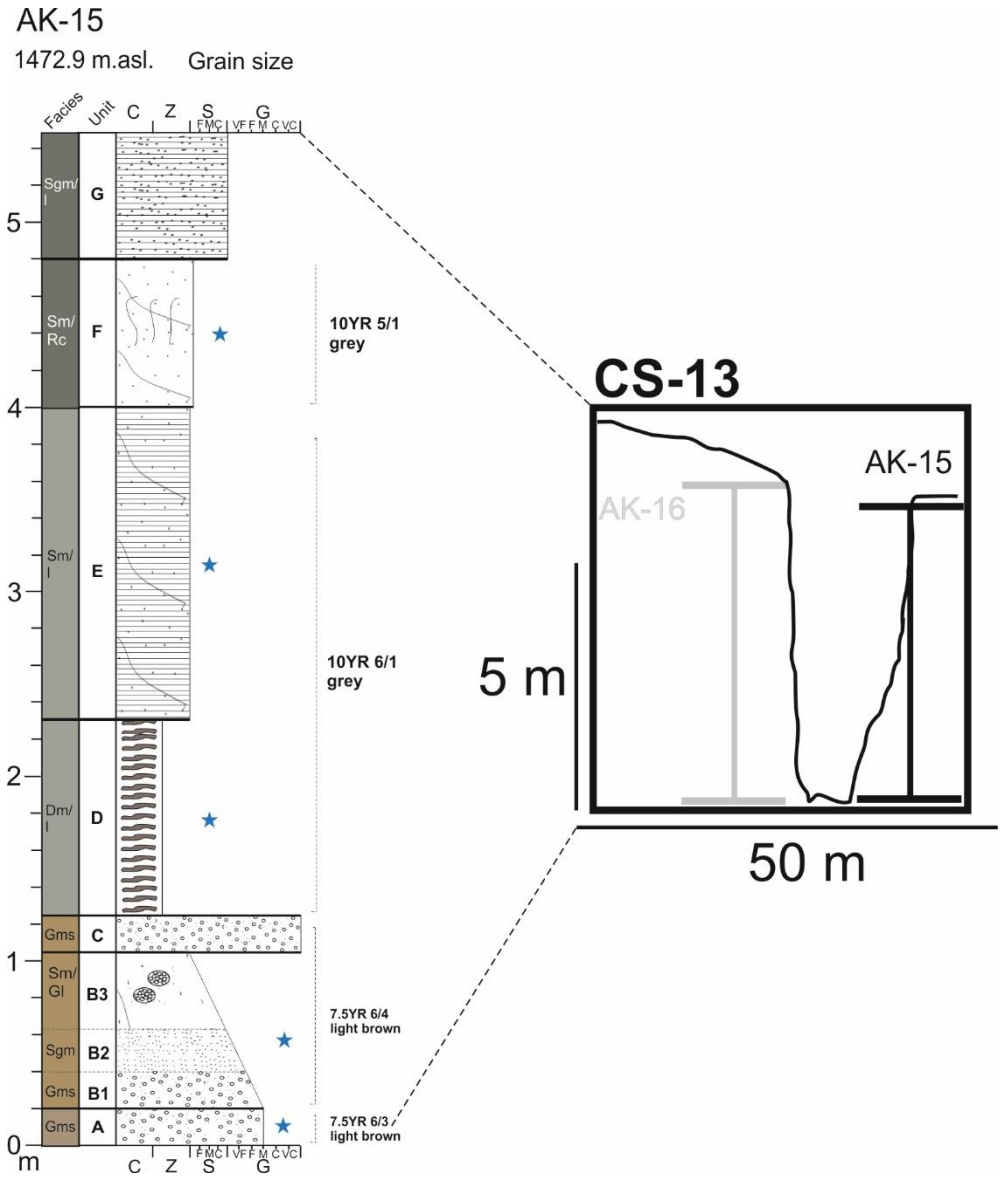

Figure 5.92 – sedimentary log AK-15 and cross section.

Unit D is composed of alternating, thick cross-laminations (3-10 mm) of very fine sand and mud-drapes (up to 3 cm thick), with some concentrated lenses of organic matter (Fig. 5.92 and Table 5.26) which are different in colour to the brown sand matrix (10YR 6/1 grey). Sampling resolution exceeded stratigraphic resolution in the cases of units D and E, so the sedigraph (Fig. 5.93c and d) reflects an aggregation of laminae of different particle sizes.

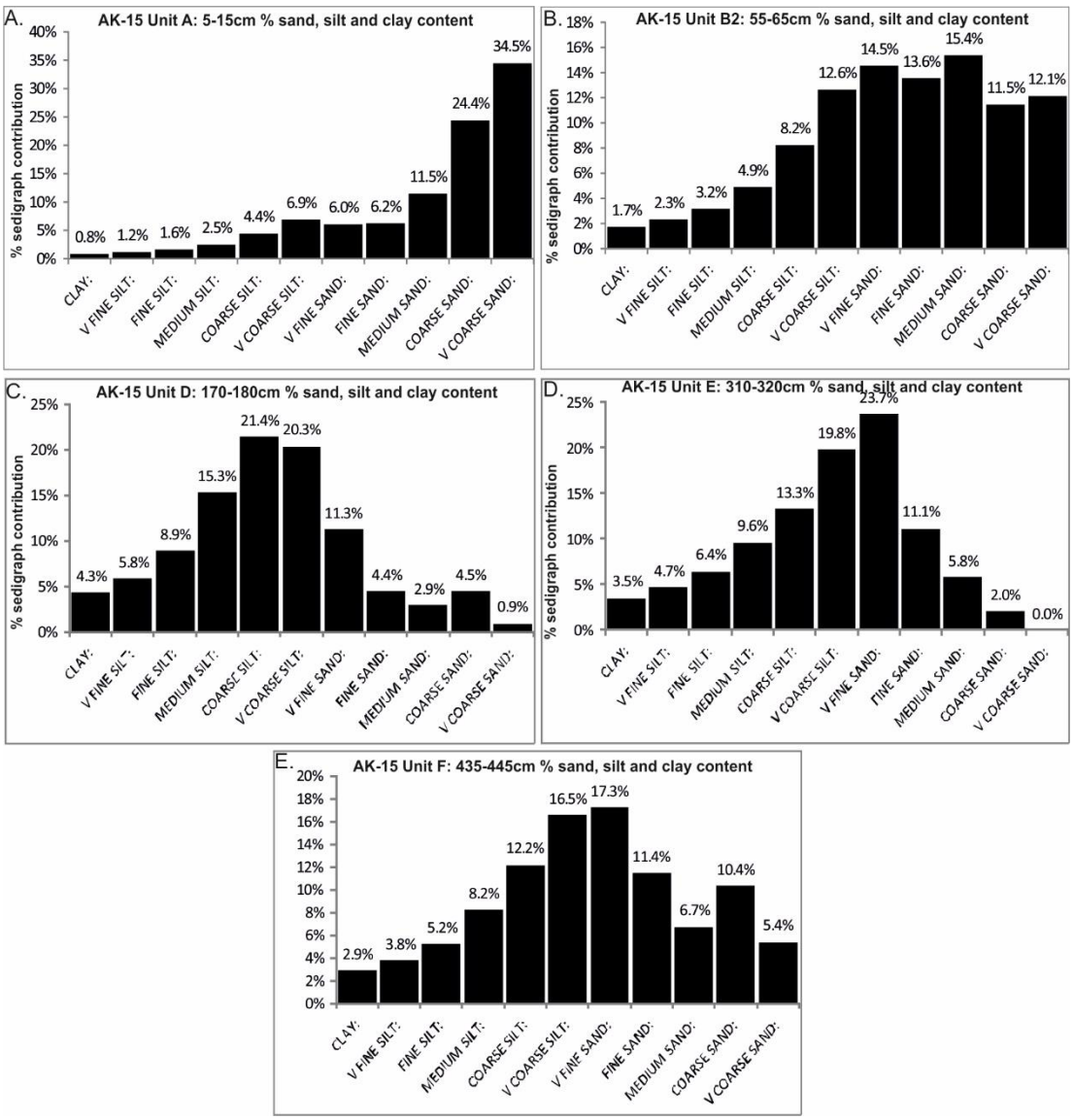

Figure 5.93 – % sand, silt and clay content derived from Coulter grain size analysis on samples collected from outcrop AK-15.

Table 5.26 – percentage loss on ignition data and bromine content (ppm) for sampled horizons at AK-15.

Unit	Height (cm)	Loss on ignition (%)	Bromine (ppm)
A	5-15	1.5	4.4
B	55-65	1.4	2.6
D	170-180	3.2	7.2
E	310-320	2.6	6.2
F	435-445	3.1	6.8

Figure 5.94 – photograph of AK-15 unit D showing mud-drapes and fine sand lenses.

Unit E is composed of organic rich, thickly laminated, silty sands (Fig. 5.93d). LOI% and bromine values are comparable to unit D and colour is the same. Unit F consists of massive silty sands with abundant root channels (Fig. 5.93e). Organic matter content is comparable to units D and E but colour is slightly different – 10YR 5/1 grey (Table 5.26). The succession is capped by well defined, thickly laminated coarse to very coarse sands (unit G).

Concentration-related magnetic proxies are consistently higher for units A and B, whilst D-F exhibit typically weak magnetism (Fig. 5.95a). χ_{FD}% peaks for units B and D, the latter accompanied by highest values of $\chi_{ARM/IRM1T}$ (0.38 – Fig. 5.95b). S values increase inversely to depth for units A-E, the latter showing 20% and 3.2% of the applied remanence unreversed at -100mT and -300mT respectively (units A – E Fig. 5.95c).

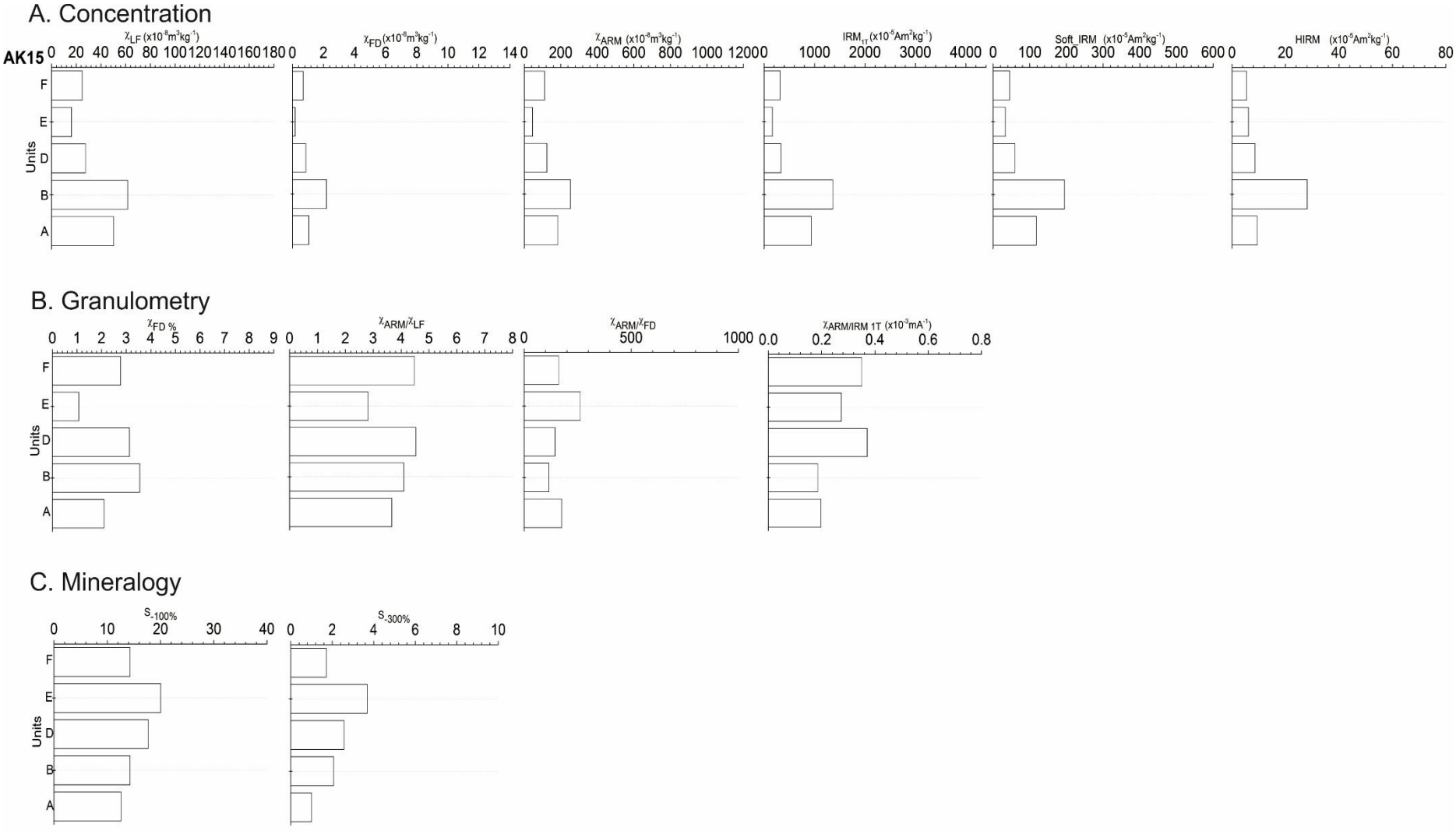

Figure 5.95 – mineral magnetic parameters from sampled horizons at outcrop AK-15.

5.4.1b: AK-15 interpretation

The basal units (A and B1) are interpreted as channel bar deposits. The sharp, planar contact separating the two units indicates a reactivation surface. The normal grading from gravels to sands and silts (unit B1-B3) reflects aggradation of the channel floor. The lenticular sands likely represent incision of the channel surface during flow recession, concentrating coarser sand into lenses. This feature was observed in the contemporary channel bed (Chapter 4 analogue 2). The contact between units B3 and C signifies a channel reactivation surface, with emplacement of bar deposits (unit C), probably representative of a single storm event.

The cross-bedded sands and organic-rich mud-drapes (unit D) indicate continued aggradation with a reduction in stream power to the extent that vegetation colonised the channel bed. The contact between units D and E is a major unconformity signifying a change from the underlying brown sediments, to homogeneous organic rich, wetland deposits with extensively gleying (units E and F). Similar wetland settings were reported earlier in Chapter 4, at the base of major knickpoints in low energy, perennial reaches (Table 4.3: Analogue 3). The unconformity between units E and F implies a hiatus in sedimentation such that a palaeosol (unit E) formed.

The massive silty sand above (unit F) indicates renewed but slow aggradation (wetland environment) as before. The soil exhibits extensive bioturbation evidenced by root channels and development of blocky structure. The deeper grey (10YR 5/1) is probably related to enhancement organic input from surface vegetation cover, although the differences in Br and LOI% between this and unit E are only negligible (Table 5.26). The capping unweathered, laminated sands (unit G) are identical in characteristics to the sands reported earlier (AK-7-9), constituting overbank deposits in association with a channel in a wetland.

Units A and B exhibit moderate concentrations of remanence carrying ferrimagnetic minerals. X_{LF} values likely reflect inputs of sediment derived from the sandstone knickpoint 15 m upstream, but with some ferrimagnetic dissolution due to conditions of poor drainage. Notably, unit B exhibits the highest total concentrations of AF minerals (HIRM), probably goethite.

Units D-F are dominated by paramagnetism, consistent with other palaeo-wetland fills analysed in this chapter. S_{-300}% explains 38% of the variance in χ_{LF} indicating hydration of magnetite to goethite (Fig. 5.96A). Soil texture was found to be the most significant driver of χ_{LF} (r^2 = 0.53 - Fig. 5.96B). Trapping of fine sediment in vegetated wetlands enhances waterlogging and thus ferrimagnetic dissolution.

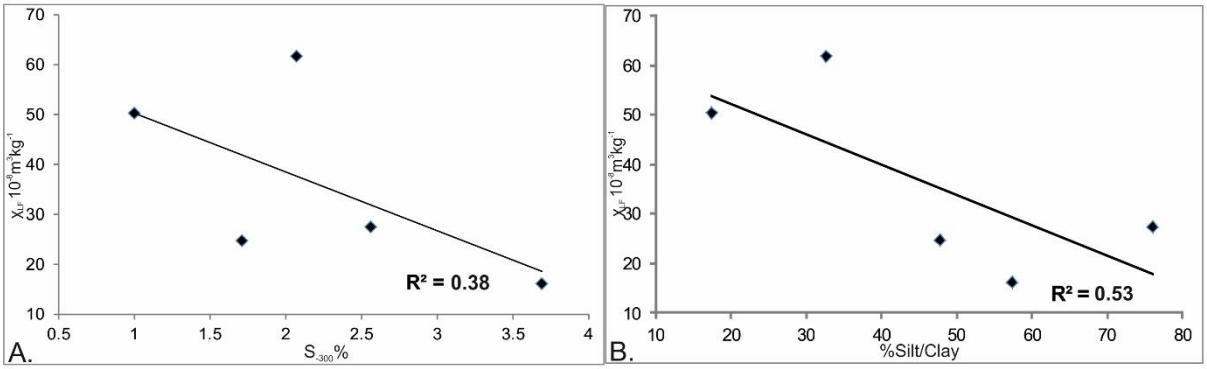

Figure. 5.96 – biplots showing A) S_{-300}% vs. X_{LF}; B) % silt/clay vs. X_{LF}.

The spike in S_{-300}% for unit E indicates goethite is the dominant AF mineral. The lower S_{-300}% for unit F indicates a 'softer' hard component relative to E, but only slightly lower total concentrations of hard magnetic minerals (HIRM – Fig. 5.104). As both units exhibit comparable pedogenic overprinting, the unconformity between E and F does not signify a prolonged hiatus. Rather, differences in S_{-300}% are controlled by changing hydrological conditions with haematite likely being more significant for unit F than E.

5.4.2a: AK-16 analysis

Log AK-16 was obtained from a 6.4 m outcrop on the left bank opposite AK-15 (Fig. 5.1, 5.97 and 5.98).

Unit A consists of poorly sorted minerogenic, matrix-supported cobbles (Fig. 5.97; Table 5.27). The matrix consists of interstitial gravels and predominantly coarse to very-coarse sands (77.5% - Fig. 5.99a). Unit A is capped by a single medium-thickness unit of matrix-supported gravel (unit B). This is overlain by matrix-supported, very poorly sorted cobbles (unit C). The rest of the succession consists of organic poor (Table 5.27) massive units of matrix-supported gravels (E and G) and sands (D, F, H, J and K) of varying thickness (0.1 m - 2.55 m). The composition of the sand units is variable: unit D consists of predominantly medium-very coarse sand

(51.9% - Fig 5.99b); unit H is composed of 33.6% coarse to very coarse sand but with a secondary mode of very coarse silt and very fine sand (33.8% combined – Fig 5.99c); and unit J in contrast is well sorted, with a distinct very coarse sand peak (70.3% - Fig. 5.99d).

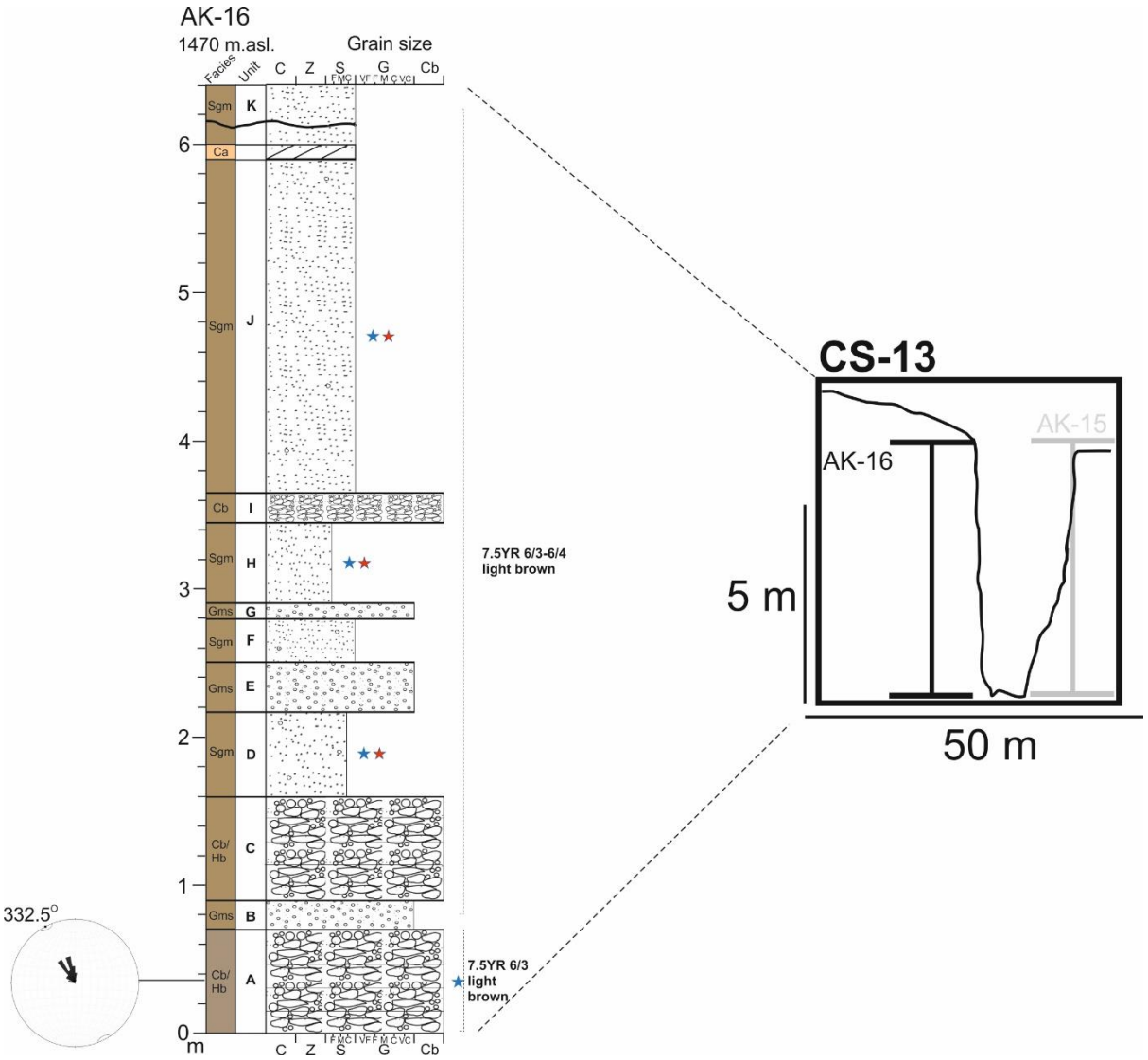

Figure 5.97 – sedimentary log AK-16 and cross section.

A 5-6 cm thick and continuous calcrete horizon occurs at 5.95-6 m, similar in composition and characteristics to that identified and described at AK-12 and 13. A sharp, wavy contact separates units J and K with slight reddening at the very top of J.

Total magnetic susceptibility for this outcrop is typically high (χ_{LF} = 55-70), except unit H (χ_{LF} = 42) which also has low χ_{ARM} and IRM_{1T} (165 and 580 respectively - Fig.

5.100a). χ_{FD}% peaks distinctively for unit J (9%), but only a modest increase in $\chi_{ARM}/_{IRM1T}$ (0.34- Fig 5.100b). Unit J also exhibits distinctively high S_{-100}% and S_{-300}% (18% and 3.8% unreversed respectively) compared to the underlying units (Fig. 5.100c).

Figure 5.98 – photograph of outcrop AK-16.

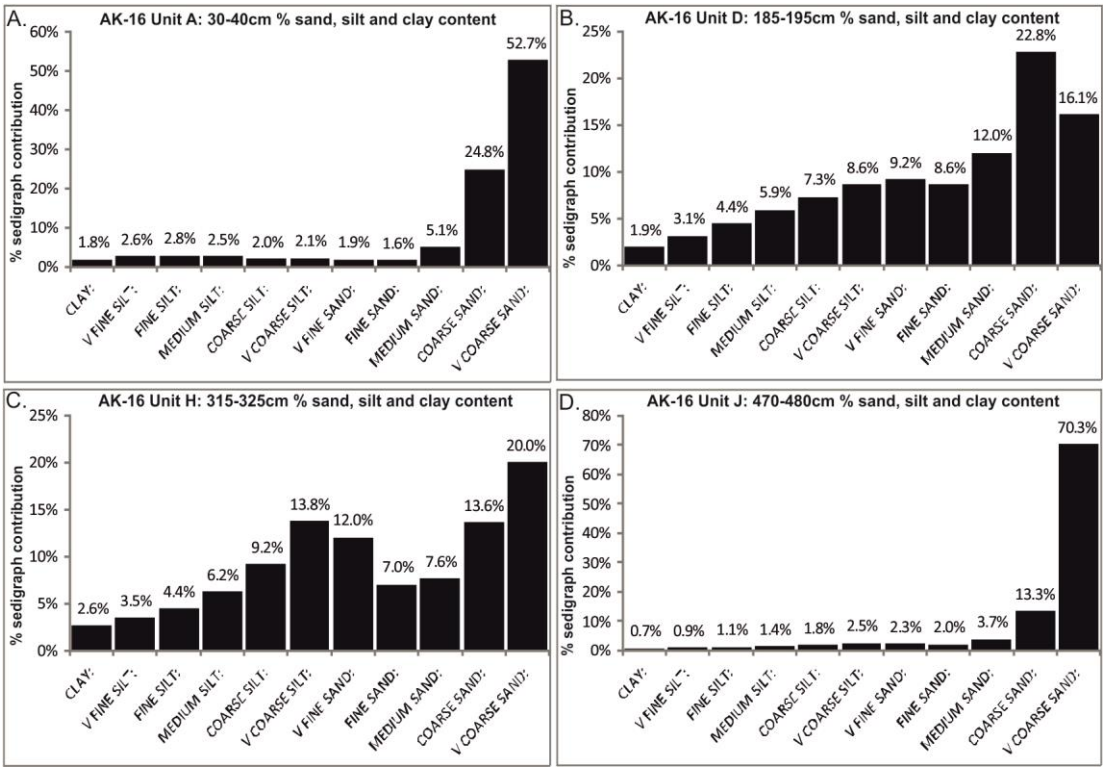

Figure 5.99 – % sand, silt and clay content derived from Coulter grain size analysis on samples collected from outcrop AK-16.

Table 5.27 – percentage loss on ignition and bromine content (ppm) for sampled horizons at AK-16.

Unit	Height (cm)	Loss on ignition (%)	Bromine (ppm)
A	30-40	1.8	2.2
D	185-195	1.5	2.0
H	315-325	1.8	1.0
J	470-480	1.5	0.7

5.4.2b: AK-16 interpretation

The horizontally bedded gravels and cobbles (units A-C, E, G and I) are channel bar deposits. Clasts comprising the unit A bar (b axis = 332.5^{o}) are orientated parallel to the modern channel implying that the deposits are not sourced from the flanking slopes**.** The bedded sands (units D, F and H) reflect recessional phases of flow. Alternating coarse and fine deposits occur in the modern channel systems reflecting individual flood events (Ch.4: Table 4.3 – analogue 5). The reduction in clast size up-profile may imply that a lack of coarse material was available to transport. The top of unit J is overprinted by the same rhizogenic calcrete and overlying rubified palaeosol as was described for AK-12/13 and various other locations along the western margins of the central valley. The extensiveness of this calcrete/rubified Bw horizon indicates a catchment wide phase of soil development and higher groundwater.

The basal units of AK-15 and 16 exhibit comparable ferrimagnetism (Table 5.28). The S_{-300}% for AK-15 is to do with goethite. This has slightly diluted susceptibility (see section 5.4.1) caused by perennial seepage from the nearby sandstone knickpoint. These results demonstrate that the basal units are stratigraphically coeval (Table 5.28).

Table 5.28 – selected magnetic properties for comparison between AK-15 and 16.

Magnetic susceptibility parameters	AK-15 / A	AK-15 / B	AK-16 / A1	AK-16 / D
X_{LF} ($10^{-8}m^3kg^{-1}$)	50.3	61.7	68.0	65.6
X_{FD} ($10^{-8}m^3kg^{-1}$)	1.1	2.2	3.6	2
X_{ARM} ($10^{-8}m^3kg^{-1}$)	184.3	252.9	293.1	258.0
IRM_{1T} (10^{-5} Am^2 kg^{-1})	936.4	1363.3	1061.1	1240.2
S_{-300}%	1	2.1	0.4	0

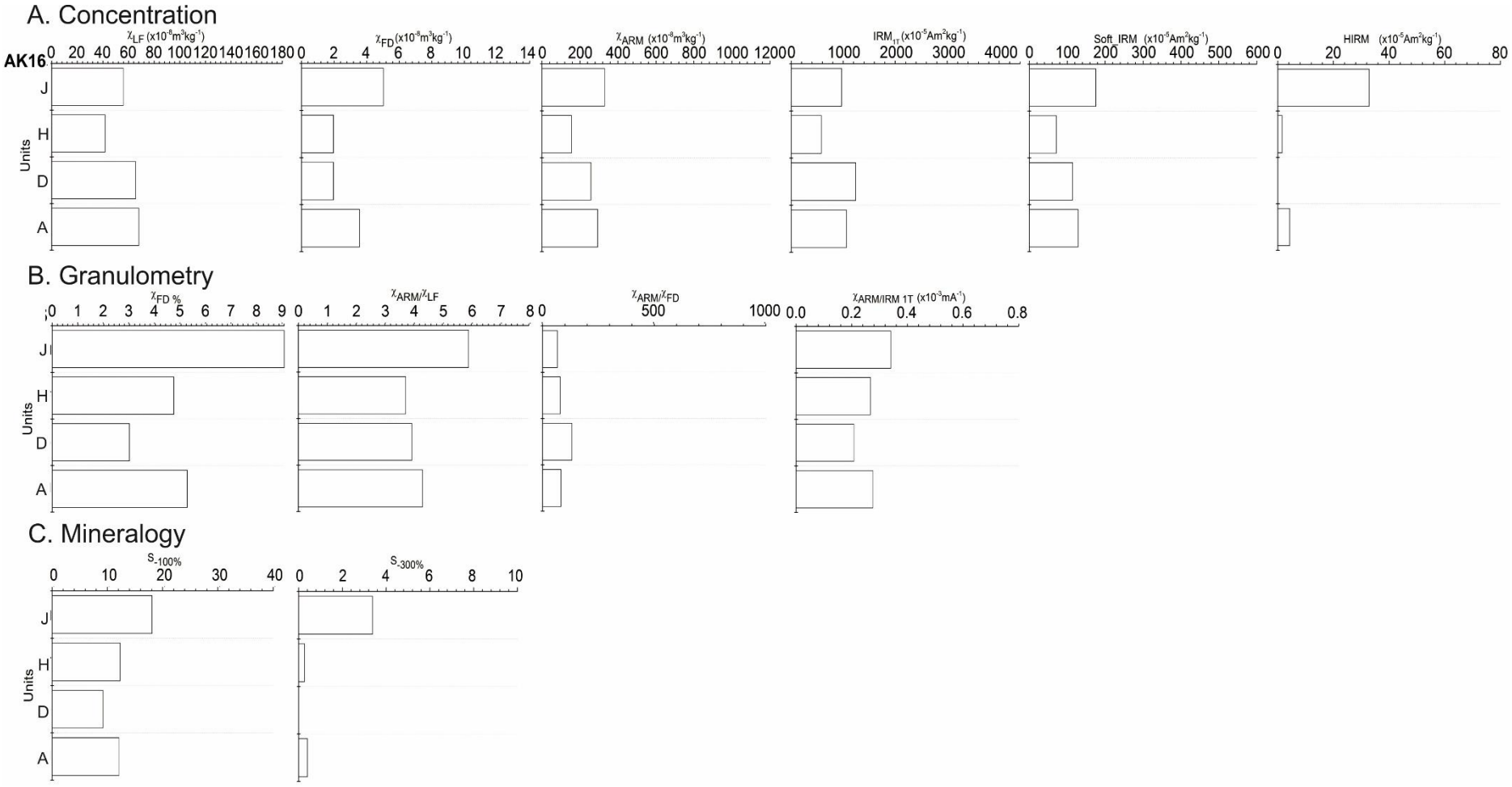

Figure 5.100 – mineral magnetic parameters from sampled horizons at outcrop AK-16.

AK-16 units D and H exhibit coarser-grained ferrimagnetism reflected in the smaller $\chi_{ARM/IRM1T}$ and χ_{FD}% compared to unit A. Reduction of this fine-grained component explains diminishing susceptibility χ_{LF}. The higher silt/clay content of these units (Fig. 5.99) may have facilitated dissolution of the fine-grained ferrimagnetic component.

In contrast, unit J has: 1) high total proportions of ferri and anti-ferro magnetic minerals (Soft_IRM and HIRM) and 2) higher concentrations of pedogenic SP grains (χ_{FD}% = 9%) - distinguishing it from the underlying units (Fig. 5.100). Notably, this unit is currently well drained with little clay/silt (Fig. 5.99). The concentration of hard minerals likely reflects goethite – fixed during the period of elevated groundwater (see section 5.3.6 for explanation of process), but also subsequent oxidation to haematite following the drop in water-table and resumption of oxidising conditions. The soils overprinting these channel deposits are polygenetic (section 5.3.6) meaning that it is not possible to link magnetic properties specific phases of soil development.

5.4.3a: AK-17 analysis

Log AK-17 was obtained from a 5.5 m outcrop 2950.9 m downstream from the headwaters on the right bank (Fig. 5.1, 5.101 and 5.102). Major lithostratigraphic units are characterised by sharp bed contacts.

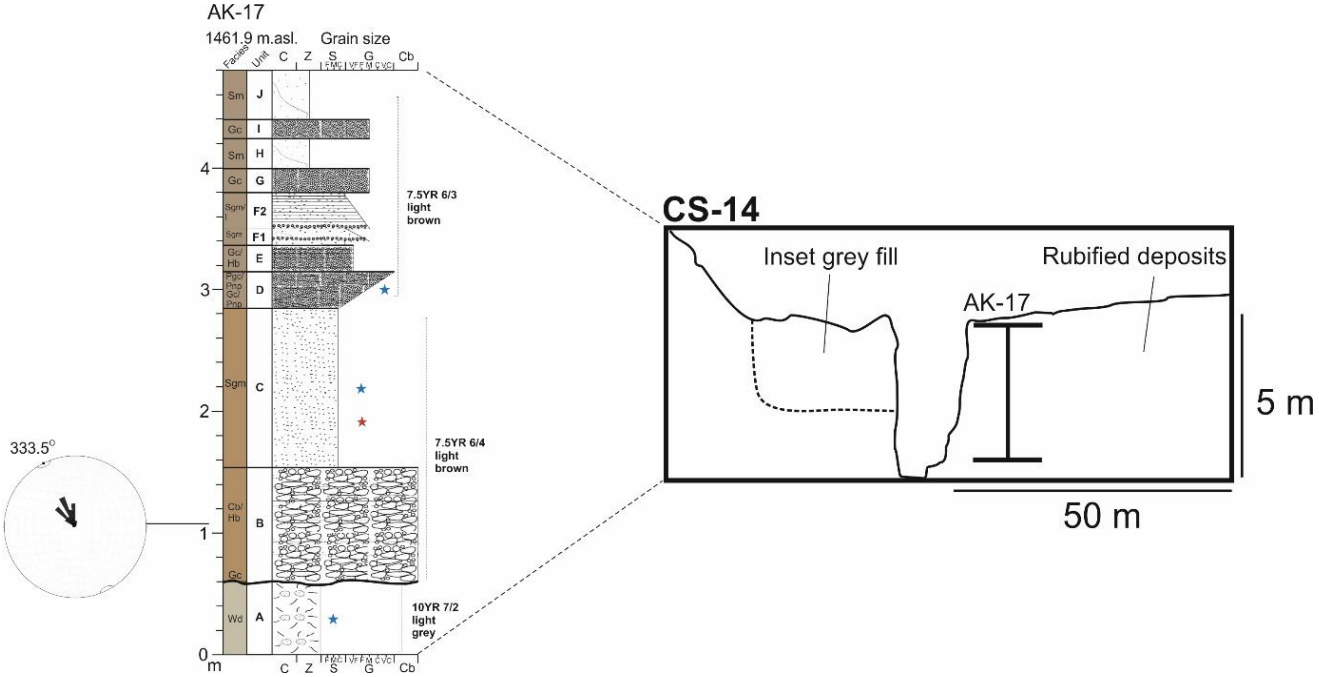

Figure 5.101 – sedimentary log AK-17 and cross section. Note the inset grey fill in the left terrace bank

Figure 5.102 – photograph of outcrop AK-17.

Unit A consists of very poorly sorted sandy silts (Fig. 5.103a), with sands concentrated into lenses (several cm wide) in places. These are overlain by a thick bed of matrix-supported cobbles (unit B) orientated parallel to the modern channel (333.5^{o} - unit B). Unit C is characterised by a thick (1.4 m) bed of cemented, massive, poorly sorted sands (81.6%) with subordinate silts and clays (18.4% - Fig 5.103b).

Unit D consists of friable clast-supported gravels that grade from medium to very-coarse. Colour also changes to 7.5YR 6/3 light brown. Any matrix present consists of very poorly sorted sandy silt (Fig. 5.103c). This is capped by a single, thick horizontal bed of clast-supported gravel (unit E).

Unit F consists of two distinct, normally graded units which start with a single, distinct lamination of coarse gravel that grades to sand; the fundamental difference between subunit F1 and F2 being that for the latter, sands were deposited as distinct medium-thickness laminae. The top of the section is characterised by alternating thick units of massive, clast-supported gravels and massive, clast-poor silts (units G-J).

Table 5.29 – percentage loss on ignition data and bromine content (ppm) for sampled horizons at AK-17.

Unit	Height (cm)	Loss on ignition (%)	Bromine (ppm)
A	25-35	1.6	0
C	215-225	1.2	2.3
D	295-305	1.2	2.4

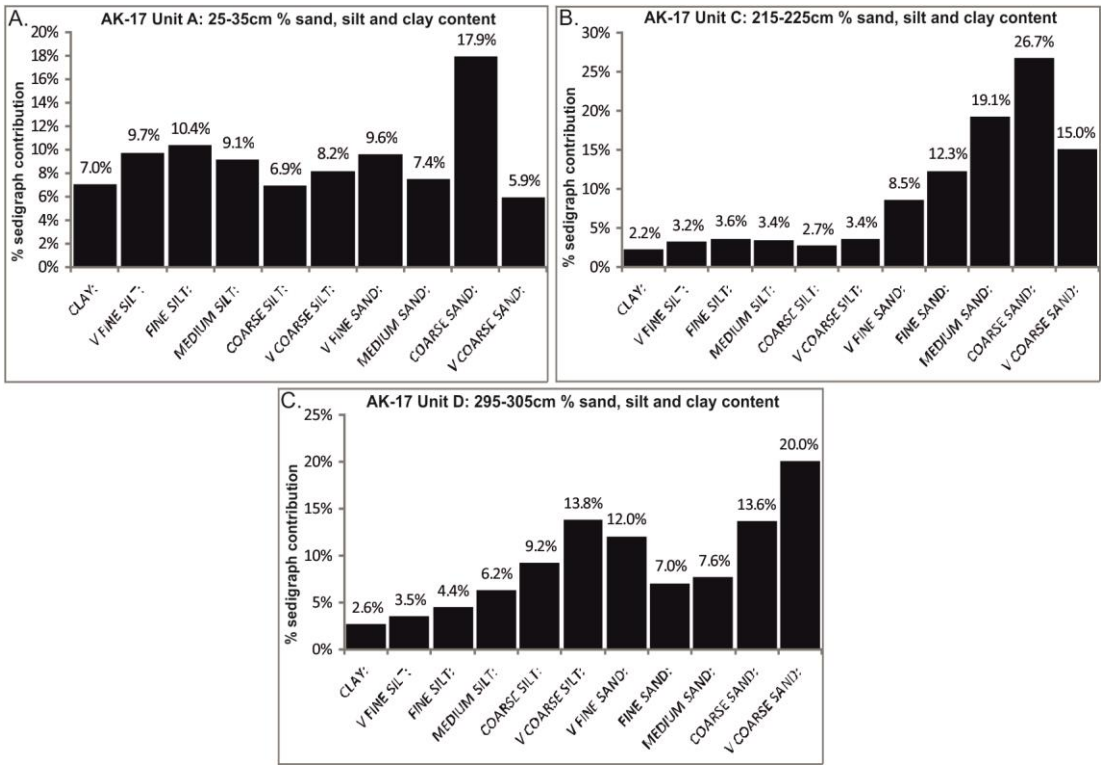

Figure 5.103 – % sand, silt and clay content derived from Coulter grain size analysis on samples collected from outcrop AK-17.

Unit A is characterised by very low magnetic susceptibility (χ_{LF} = 18), but extremely high S values with 22% and 5.7% of the applied remanence unreversed at -100mT and -300mT respectively (Fig. 5.104). Contrastingly, unit E has very high χ_{LF} (85) and IRM_{1T} values (2040 - Fig. 5.104a), but χ_{FD}% and $\chi_{ARM}/_{IRM1T}$ are small (Fig. 5.113b). Furthermore, unit E lacks a measurable hard component (S_{-300}%) and the S_{-100}% is lower (14% - Fig. 5.104c). Unit D in contrast exhibits slightly lower concentration related proxies, but χ_{FD}% is much higher (4.9% - Fig. 5.104b).

5.4.3b: AK-17 interpretation

The local topography gently slopes toward the channel at CS-14. There is an abrupt change in gradient to the left of the channel (Fig. 5.101), indicating a junction between the slope and terrace. The basal unit is a deeply gleyed (10YR 7/2 grey) soil formed on dolerite comparable to that identified upstream (AK-3 and AK-9). Consistent with this observation is the very minimal concentration of remanence carrying ferrimagnets (Fig. 5.104a), reflecting breakdown of the lithogenic magnetic constituents. This high S values attest to high concentrations of goethite (Fig. 5.104c).

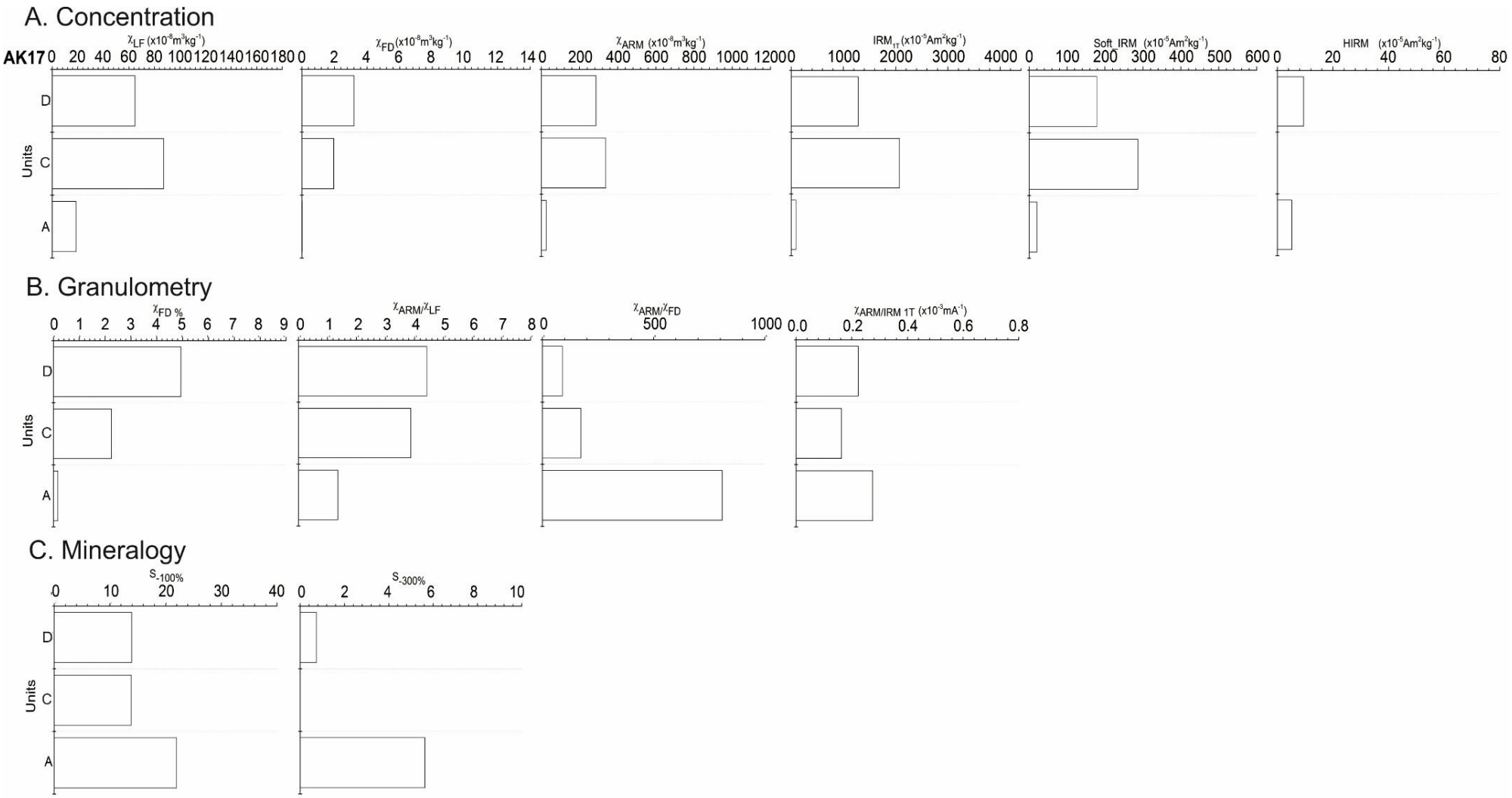

Figure 5.104 – mineral magnetic parameters from sampled horizons at outcrop AK-17.

The sharp, undulating contact between the soil and unit B indicates the soil has been incised rather than merely 'capped' by sediments. The facies of unit B attest to high energy conditions of emplacement. The vertical orientation of clasts 'floating' within a rubified matrix indicates emplacement by debris flow. The laterally discontinuous nature of the deposits (350 m) in the right bank indicates that flow originated from the dolerite ridge to the north-east (Fig. 5.105). Debris flow deposits also occur in the left bank and based on the direction of bedding perpendicular to the modern channel, these originated from the slope to the left (Fig. 5.105). Downstream, this coarse bed (unit B) thickens in the left bank, displaying imbrication indicating deposition of a channel bar (Fig. 5.106). This indicates probable reworking of the debris flow deposits upstream by fluvial processes. These debris flow and bar deposits are unconformably buried by inset grey fills (Fig. 5.101, 5.105 and 5.106) and brown laminated sands comparable to those analysed earlier (AK-7, 9, 15).

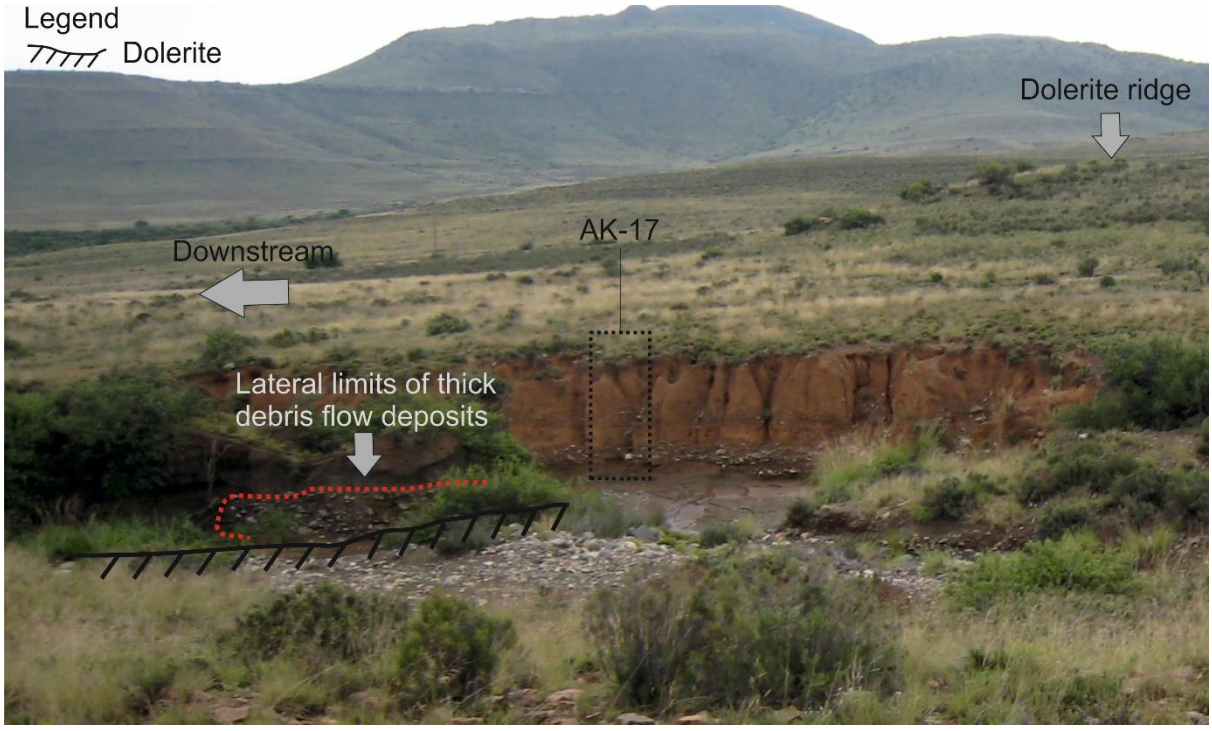

Figure 5.105 – photograph of lower valley showing contemporary meander bend and channel bar deposits. Note location of log AK-17 (black box) and dashed red line demarcating lateral extent (left of main channel) of cobble/boulder deposits coeval with those reported for unit B (AK-17).

The overlying sands (AK-17 unit C) indicate low energy sedimentation. The high concentration of multi-domain remanence carrying ferrimagnets for this unit attests to a doleritic source (Rowntree et al., 2012). Therefore, the deposits are slopewash sourced from the nearby ridge (Fig. 5.105). The comparatively low χ_{FD}% probably

reflects dissolution of the fine-grained pedogenic component. The low bromine content indicates minimal soil organic matter content remaining, though this is likely due to rapid oxidation and leaching.

The overlying inversely graded gravels that (unit D) is interpreted as a bar with cross beds reflecting low angle lateral accretion surfaces associated with lateral channel migration. The friable nature of these channel deposits is unlike any of the cemented fills discussed upstream (AK-10, 12, 15 and 16), implying a relatively unweathered, younger deposit. The weaker ferrimagnetic signature (χ_{LF} = 64) attests to dilution compared to unit C, by inputs of sandstone from upstream vindicating the proposition that these are channel rather than locally sourced slope deposits. High concentrations of fine-viscous SP grains (χ_{FD}%: 4.95) compared to below likely reflect conditions of better drainage.

Figure 5.106 – photograph of succession exposed in left bank opposite AK-17. Note: a) the greater thickness of the coarse bed (1.1–1.2 m) b) the imbricated, rather than matrix-supported characteristics and c) the fine-grained grey and then laminated brown sands on top very similar to the succession recorded at AK-7.

The switch to normally graded bedded gravels and sands (unit E-J) are interpreted as channel deposits. Alternating beds of gravel and sand can be produced by a migrating single thread channel, as observed in the modern channel system.

5.4.4a: AK-18 analysis

Log AK-18 was obtained from a 2.8 m outcrop on the right bank just after the confluence between Africanders Kloof and a tributary from the east (Fig. 5.1 and 5.107). This outcrop is approximately 200 m upstream from a sandstone rock step.

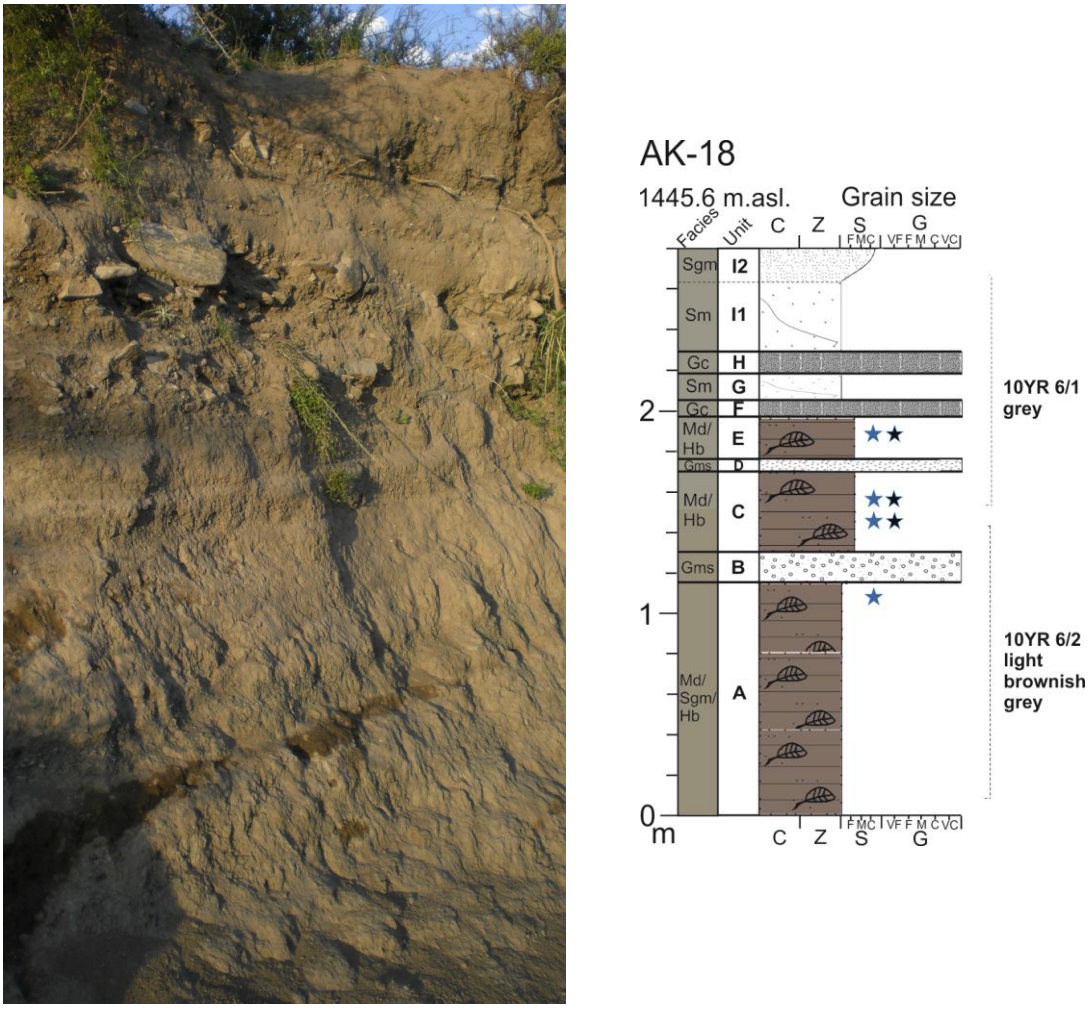

Figure 5.107 – sedimentary log and photograph of outcrop AK-18.

Unit A consists of thinly bedded silty sands and fossilised plant stems. The top of the unit is composed primarily of silt and clay (62.6%) with subordinate, primarily very fine-fine sand (26.9% - Fig 5.108a). Unit B is a medium bed of matrix-supported, very coarse gravels, which is capped by thinly bedded sandy silts (unit C- Fig 5.108b and c) that show similar LOI% values to unit A (Table 5.30). Freshwater bivalves

were also found at 140-150 cm under low powered microscopy. Colour changes slightly from 10YR 6/2 light brownish grey to 10YR 6/1 grey at 150 cm. The organic rich muds are punctuated by a single, thin bed of minerogenic matrix-supported, very coarse gravels, before returning to organic-rich sandy silts (unit E - Fig. 5.108d). The upper part of the succession is characterised by alternating beds of clast-supported, very coarse gravels and massive coarse silts (units F-I). The succession is capped by inversely graded coarsening sands (subunit I2).

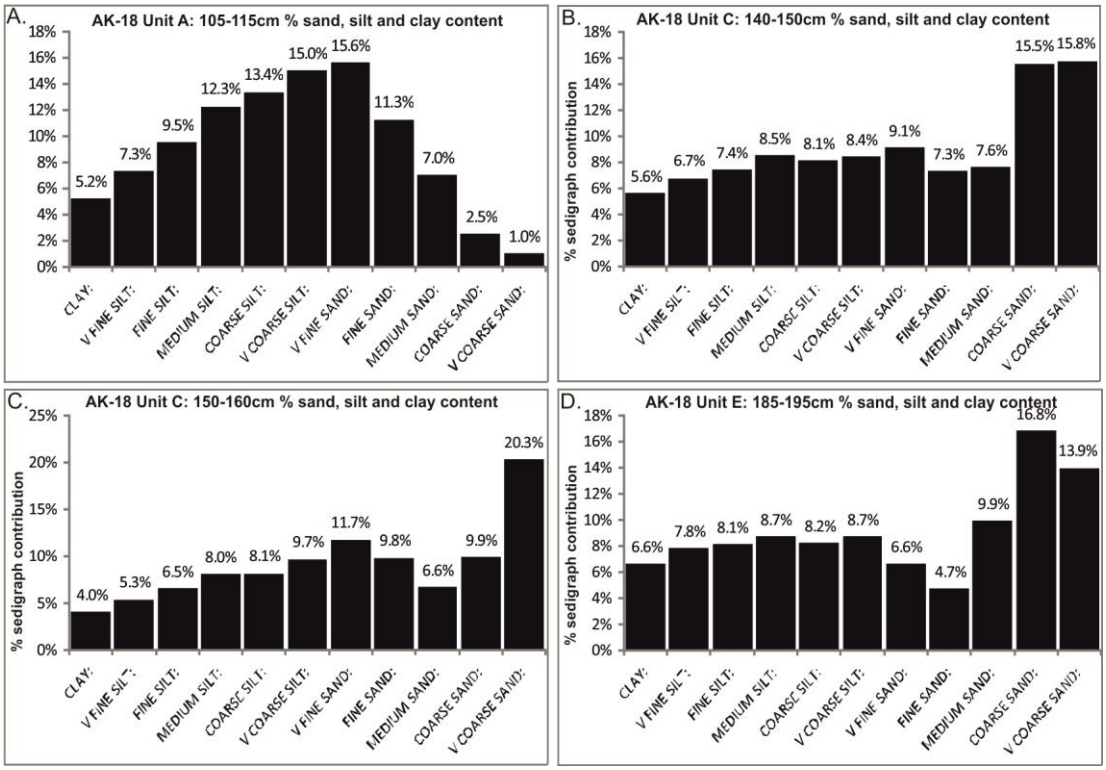

Figure 5.108 – % sand, silt and clay content derived from Coulter grain size analysis on samples collected from outcrop AK-18.

Concentration-related magnetic proxies are typically high (unit C) but declines at 185-195 cm (χ_{LF} = 45 - Fig. 5.109a). This is accompanied by lower χ_{FD}% relative to unit C (7% - Fig. 5.109b). S values are slightly higher for unit E with 17% and 3.6% of the applied remanence reversed at -100mT and -300mT (Fig. 5.109c).

Table 5.30 – percentage loss on ignition and bromine (ppm) data for sampled horizons at AK-18.

Unit	Height (cm)	Loss on ignition (%)	Bromine (ppm)
A	105-115	4.36	-
C	140-150	3.28	15.9
C	150-160	2.98	24
E	185-195	2.61	18.1

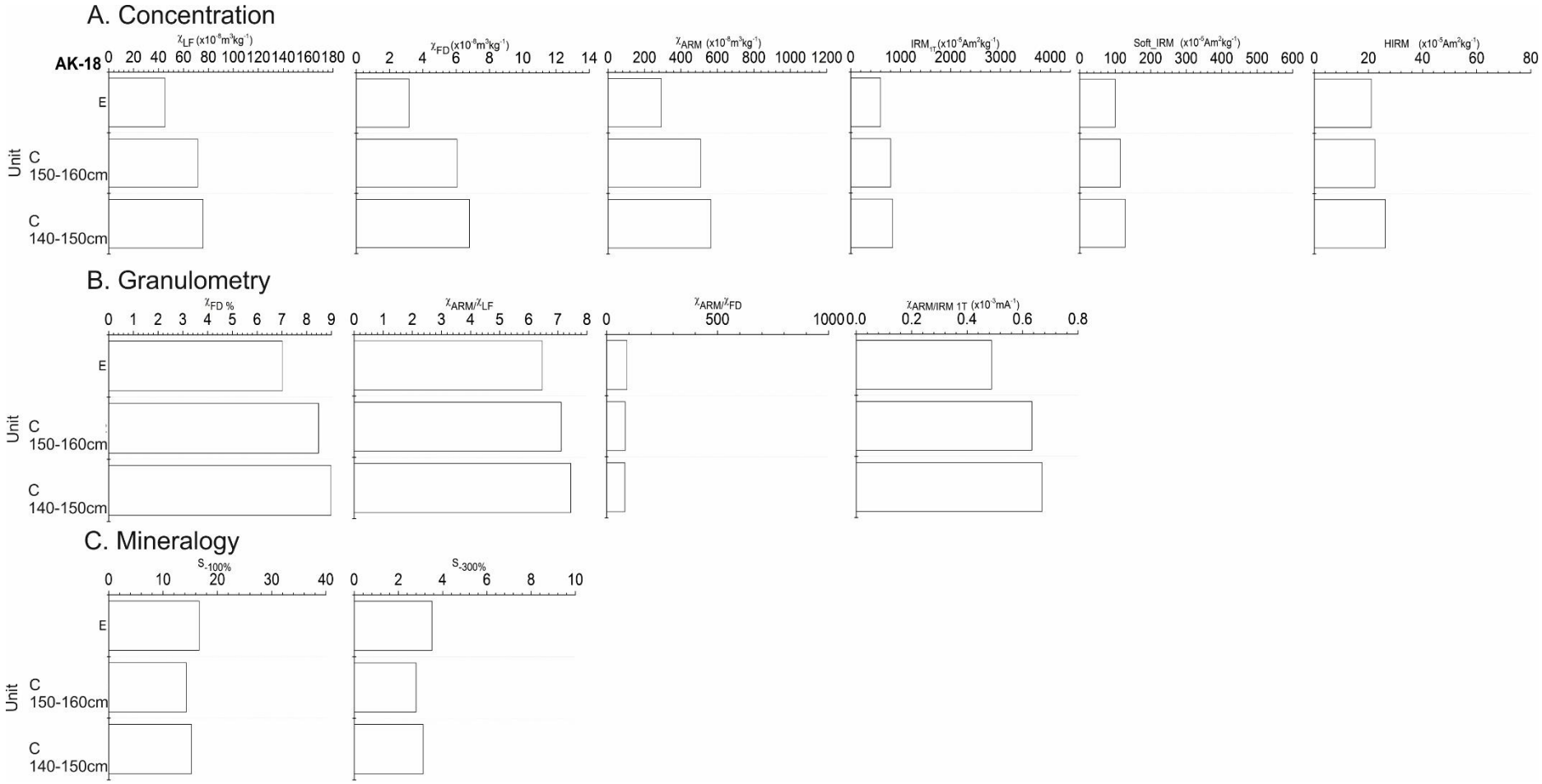

Figure 5.109 – mineral magnetic parameters from sampled horizons at outcrop AK-18.

5.4.4b: AK-18 Interpretation

The fine-grained, organic rich deposits with bivalves reflect deposition in an aggrading wetland environment (units A, C and E). The minerogenic, very coarse gravel beds (units B, D, F, H) reflect individual flood events of a magnitude sufficient to connect coarse sediment through the reach (Table 4.3: analogue 4). The minerogenic silty sands at the top of the exposure (unit I) reflect overbank deposits.

Crucially, these grey wetland terrace fills directly overlie bedrock rather than burying the rubified deposits. The rubified fills and calcrete are preserved at the valley margin here and thus the grey deposits (AK-18) are as before, clearly inset (Fig. 5.110).

Fig. 5.110 – rubified terrace fills at valley margin opposite AK-18 overprinted by band-like rhizogenic calcrete.

Compared to the palaeowetlands upstream, the magnetic properties here differ markedly. The co-increase in χ_{LF} with χ_{FD}% and $\chi_{ARM/IRM1T}$ indicates that susceptibility

is controlled primarily by SP/SD remanence carriers and thus, both unit C samples plot inside the pedogenic envelope discussed earlier (Fig. 5.7). This implies relatively large quantities of sandstone rather than dolerite – the latter exhibiting consistently stronger, MD-dominated ferrimagnetism. Increasing quantities of goethite are indicated by the increasing HIRM with depth. The lack of ferrimagnetic dissolution and paramagnetism implies different soil conditions to those reported upstream. This would mean that anoxic conditions conducive to reduction of iron oxides to sulphides were not sustained to the same degree as upstream (AK-4, 7, 9, 15). The modern wetlands reported earlier are characterised by alternating fine-coarse deposits, reflecting minor braiding and channel avulsions, with fines deposited in zones of slackwater. This pattern conforms to the alternating fine-coarse beds at AK-18. Although phragmites and Juncus are common, so are non-wetland species such as Willow trees and Karroid shrubs. In this respect, the combination of evidence attests to periodic wetting and drying – conditions that are ideal to the formation of pedogenic magnetite (Maher, 1988), rather than prolonged phases of groundwater-driven ferrimagnetic dissolution as witnessed upstream.

5.5: Summary

The upper Africanders Kloof (AKH-AK-2) is mantled by four major floodout deposits with two major palaeosols established through soil magnetic analyses. Deposition of these sequences was shown to be a complex response to a dolerite barrier separating AK-2 and 3. The extremely high magnetic susceptibility values obtained from the floodouts compared to terrace fills downstream reflects two main factors: 1) deeply weathered dolerite regolith from slopes and 2) diversion of groundwater and runoff toward the valley margins due to the morphology of the floodout. As a result, processes of ferrimagnetic dissolution did not act to reduce susceptibility. The termination of floodout depositional units, the change in terrace morphology downstream (surfaces sloping towards gully) of the dolerite barrier and the radically reduced susceptibility of the slopewash sediments (AK-3) even above the limits of the palaeo-water table was a clear indication that the proximal sandstone slopes rather than dolerite-rich sediment from upstream was deposited in this reach.

The presence of inset grey fill within the slopewash sediments (AK-3 and AK-4) upstream of a major sandstone rock step may be indicative of a wetland at a terminal

channel due to loss of slope gradient and confinements. Notably, the lack of high energy fluvial deposits observed further downstream (AK-6, 9, 10, 12) upstream of this rock step may imply that other phases of cut and fill did not propagate this far up the valley, due to the blocking effect of the step on channel headcutting (Jones et al., 2010). In the central and lower valleys, the same sequences essentially persist: slopewash deposits incised by palaeochannels and inset well cemented, rubified channel deposits. The wetland deposits (inset grey fill) occur as pockets. This evidence, in concert with the deep knickpoints through sandstone and breached dolerite barriers, may mean that these terrace fills reflect catchment-wide changes in geomorphic conditions, rather than compartmentalised filling (see chapter 4.6). The micromorphological analysis on the calcrete and palaeosol (AK-12) indicated soil polygenesis controlled by fluctuating water-tables. The possible palaeoclimatic significance of this was ambiguous, since the reconstructed elevation of the palaeo-water table was shown to be a feedback of valley aggradation (Boardman, 2014) and thus, a drop in water table could reflect base level lowering downstream. The fact that soils were polygenetic means that the soil magnetic data need to be interpreted with caution, since the various parameters reflect the integrated signals contingent on multiple alternating phases of oxidation, reduction and possible iron sulphide formation. Finally, the progressive dilution of ferrimagnetism downstream was a function of two processes: 1) Increasing inputs of magnetically weaker sandstone and mudstone and 2) increasing water content due to seepage zones. The synthesis of this evidence with respect to testing the trajectories of landscape response as outlined in Chapter 4.6, are presented in Chapter 8.2.

Chapter 6: Results iii: Sedimentology and pedology of valley fills – Wilgerbosch Kloof

6.1 Introduction

The following section reports on the sedimentology, pedology and magnetic properties of valley fills from Wilgerbosch Kloof. 11 sediment logs are reported, the locations of which are indicated in Figures 6.1 and 6.2.

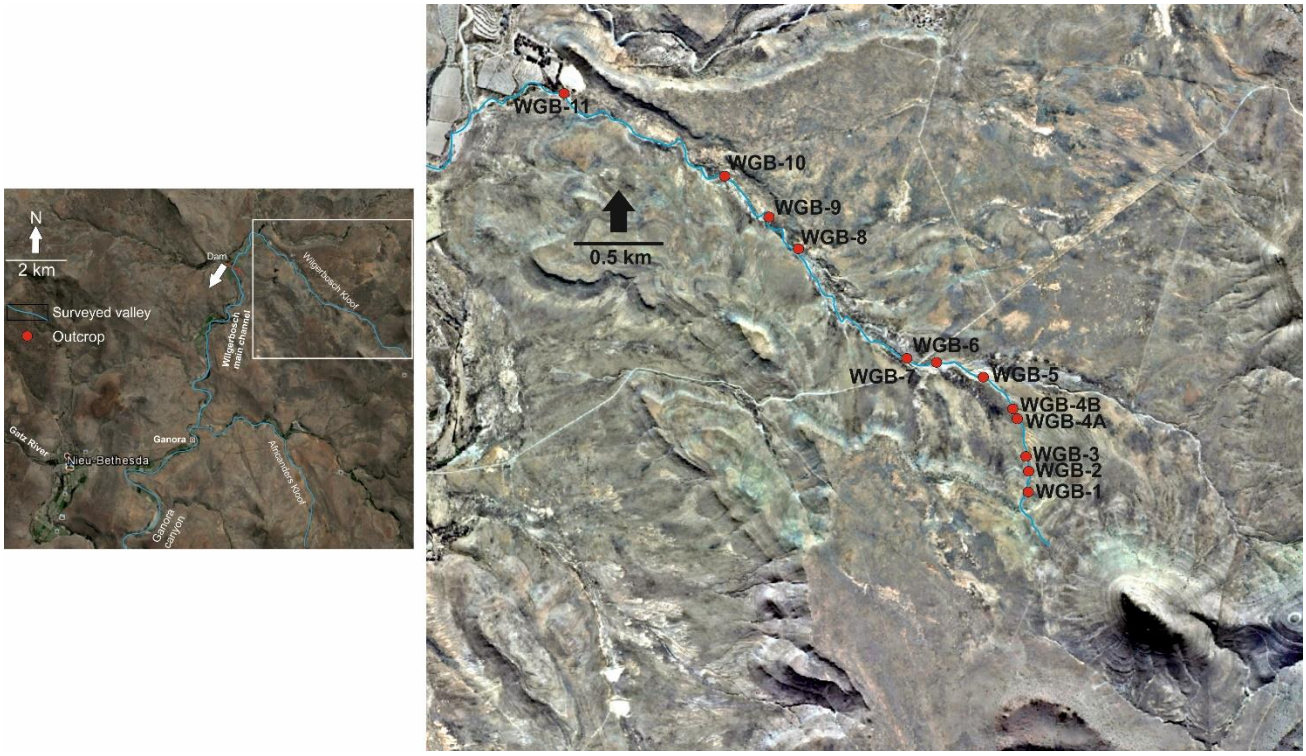

Figure 6.1 – Google Earth image (left) and digitised aerial photo of Wilgerbosch tributary in the north of the study region.

Wilgerbosch Kloof tributary is approximately 4 km long (Fig. 6.2). The catchment lithology is dominated by Beaufort group mudstone and sandstones. Compared to Africanders Kloof, there is little dolerite exposed at the present day surface. Channel gradient is lower and there are comparatively abrupt transitions from narrow headwater valleys (25-50 m wide) to alluvial plains (up to 300 m across). The thickness of alluvium ranges from 2-3 m in unconfined zones to 5 m in segments of narrow valley.

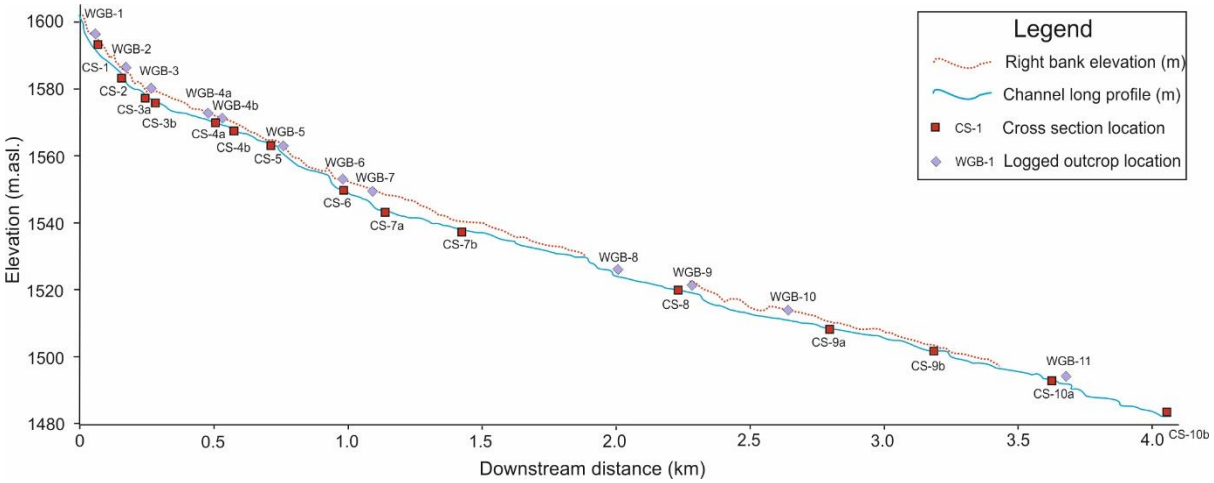

Figure 6.2 –Wilgerbosch Kloof long profile, bank elevation and location of logs and cross sections.

6.2a: WGB-1: analysis

Log WGB-1 was recorded from a 3.7 m sediment exposure directly overlying sandstone bedrock approximately 40 m downstream of a major break in slope where the definable channel commences (Fig. 6.3 - 6.6). The local valley slope is steep (0.24 m/m). Above this break in slope, a pediment buffers this channel (WGB-1) from a large mesa (Figure 6.3). Two soil samples were collected: WGB-91 from this pediment; WGB-92 from sediment mantling the steep (0.024 m/m) sandstone slope and another sediment package downstream of WGB-1 (WGB-93) in addition to the 8 samples collected from outcrop WGB-1.

A weakly developed soil crumb structure occurs throughout the whole profile, with little if any soil horizonation. The base of the succession at WGB-1 is characterised by medium-thick beds of matrix-supported gravel (units A1 and A2). The matrices are typically sandy with little silt/clay (Fig. 6.7a and b). LOI% declines slightly for A2, but bromine increases (Table 6.1).

Subunit A3 consists of thinly bedded gravels, containing the highest coarse to very coarse sand content observed thus far for WGB-1 (83.8% - Fig. 6.7c), whilst bromine content is comparable to A2 (Table 6.1). In contrast, subunit A4 exhibits relatively high silt/clay (49.3% - Fig. 6.7d), lacks a gravel component and exhibits higher LOI% and bromine values (Table 6.1).

Subunit A5 exhibits a subtle change in colour (10YR 6/3 pale brown), with thinly-bedded medium gravels contained within a relatively well sorted matrix of coarse to

very-coarse sand (Fig 6.7c). Bromine values fall sharply compared to below (Table 6.1).

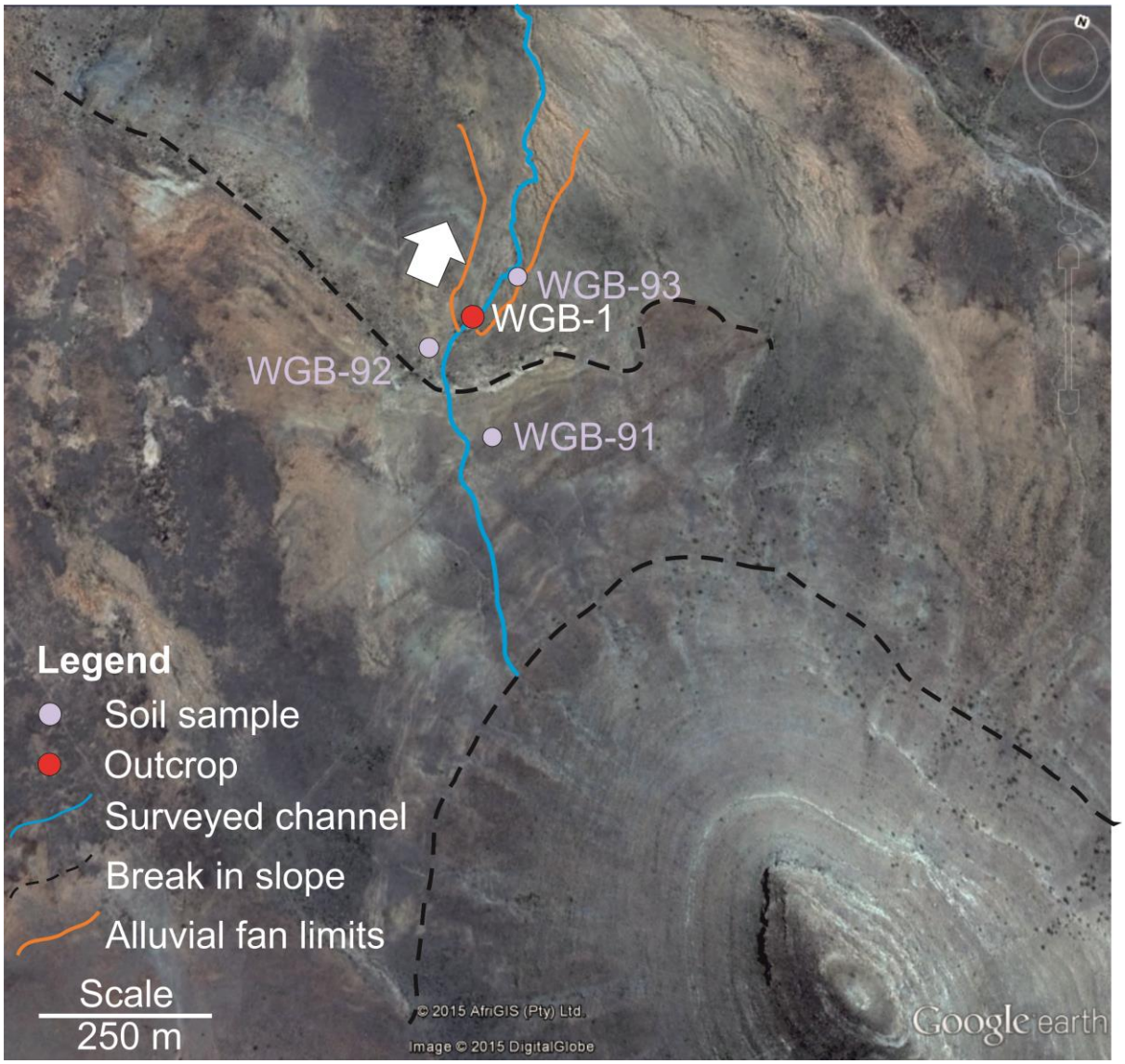

Figure 6.3 – Google Earth image showing soil sampling locations above (WGB-91) and below (WGB-92 – 93) the major break in slope.

Root channels are abundant and bromine peaks at 110-120 cm (Table 6.1) whilst colour is the most distinctive for the entire profile (7.5YR 5/4 brown) before returning to 10YR 6/2 light brownish grey.

The top of the profile is characterised by thinly-bedded gravels, the matrix of which is composed of predominantly medium to very coarse sand (85.9% - Fig 6.7h). Both LOI% and bromine are the lowest for this profile Table 6.1).

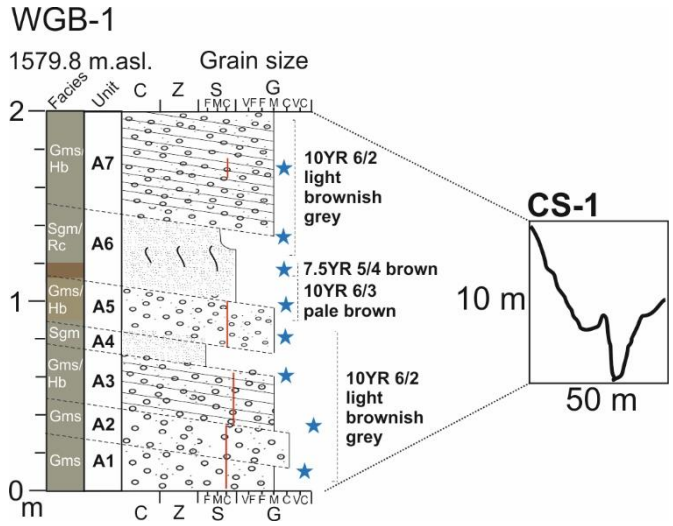

Figure 6.4 –sedimentary log of outcrop WGB-1. Note inclined beds dipping into the channel.

Table 6.1 – % loss on ignition and Bromine (ppm) data for sampled horizons at WGB-1 and soil samples (WGB-91 – 93).

Unit	Height (cm)	Loss on ignition (%)	Bromine (ppm)
A1	10-20	2.64	8.3
A2	35-45	1.56	15.9
A3	60-70	1.69	14.8
A4	75-85	2.74	17.3
A5	95-105	2.98	9.4
A6	110-120	2.47	27.8
A6	130-140	3.22	7.9
A7	165-175	1.89	7.2
WGB-91	-	4.1	26.1
WGB-92	-	1.82	3.1
WGB-93	-	2.38	10.3

Total magnetic susceptibility (χ_{LF}) for this profile typically ranges from 53-59 with high χ_{ARM}, $_{IRM1T}$ and $\chi_{FD\%}$. $\chi_{ARM}/_{IRM1T}$ declines steadily up-profile but has a distinct minimum at unit A6-1 (110-120 cm), which interestingly, exhibits lowest concentration-based magnetic values and lacks a measurable hard (S_{300}%) component (Fig. 6.9). The surface horizon (A7) possesses slightly subdued concentration-related values compared to the rest (except A6-1 – 110-120 cm). Table 6.2 shows that for unit A3, susceptibility is dominated by the clay rather than coarse silt grade, despite the latter possessing an unusually high $\chi_{FD\%}$ signature (4.7%).

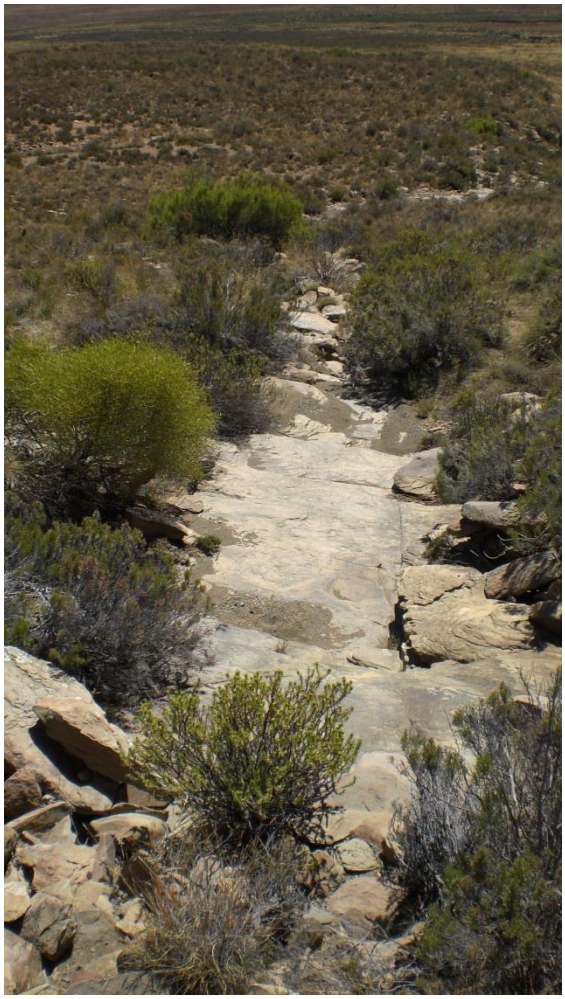

Figure 6.5 – upper sandstone slopes looking downstream towards WGB-1.

Figure 6.6 – photograph of outcrop WGB-1

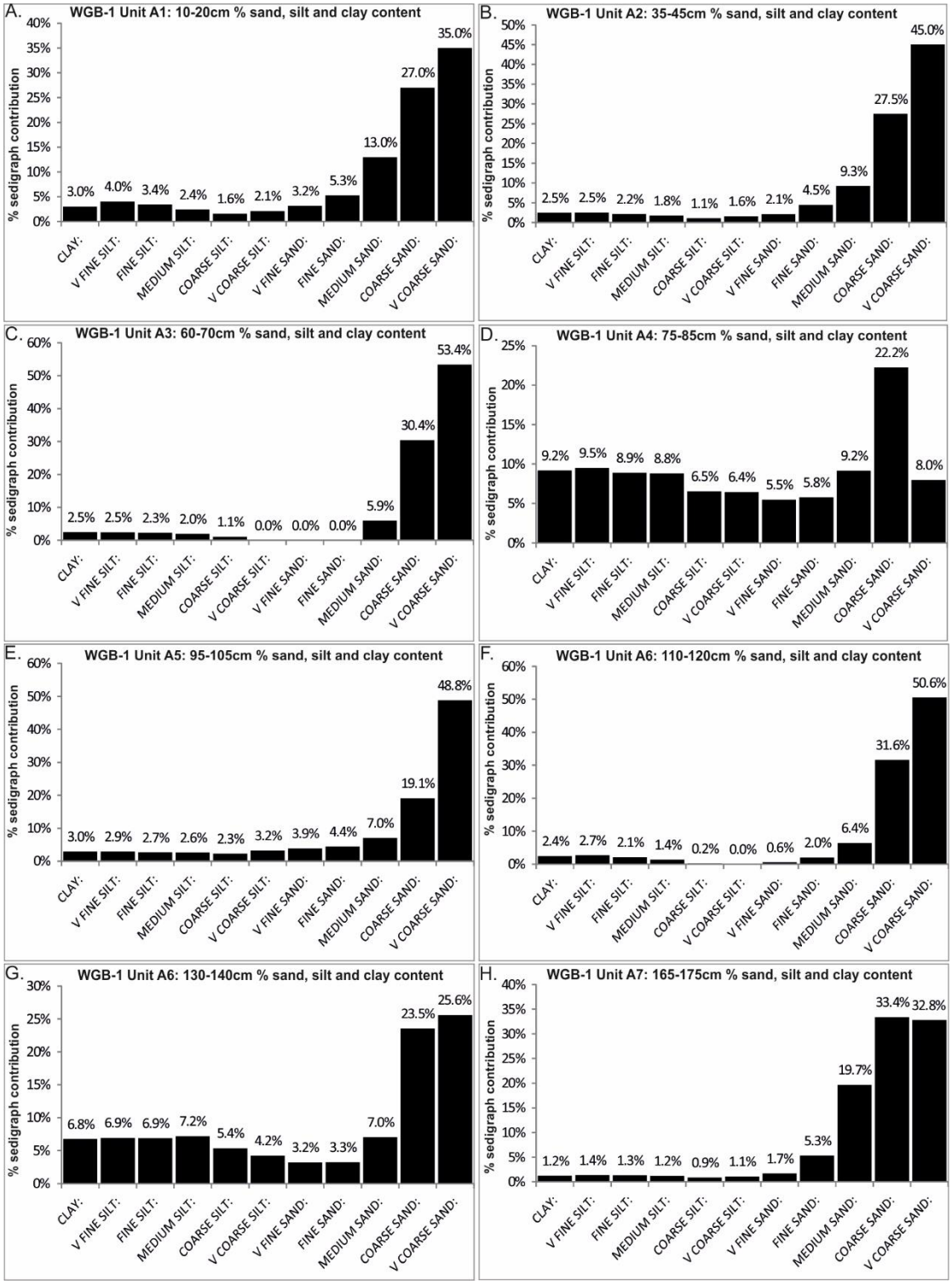

Figure 6.7 – % sand, silt and clay content derived from Coulter grain size analysis on samples collected from outcrop WGB-1.

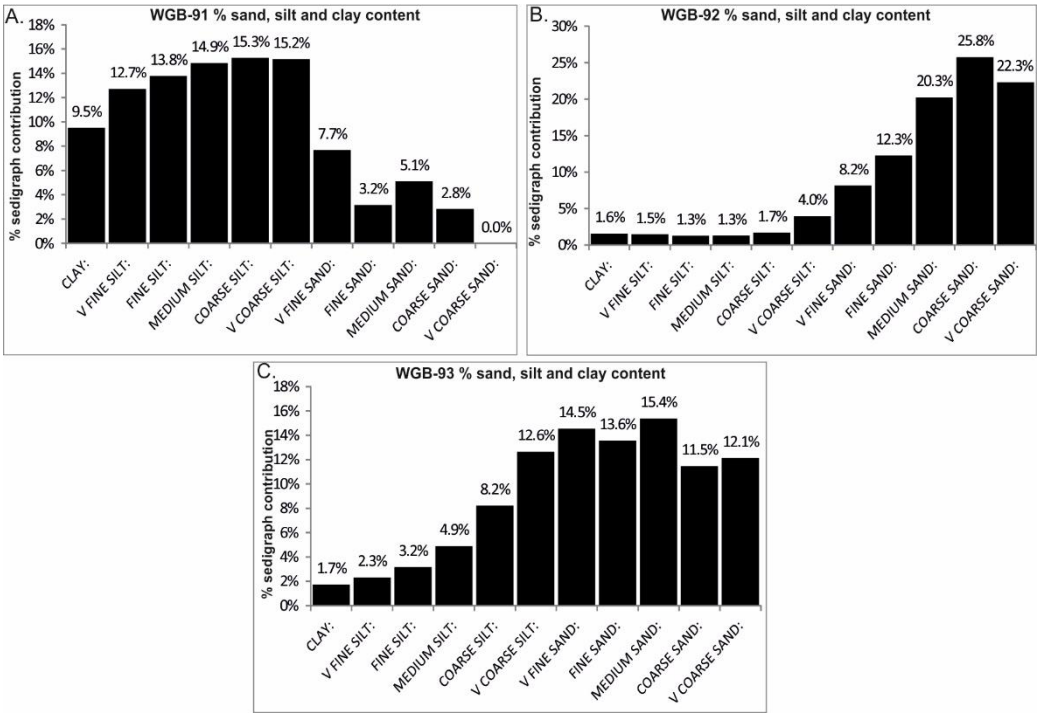

Figure 6.8 – % sand, silt and clay content derived from Coulter grain size analysis on WGB91-93 soil samples.

The two surface soil samples upstream of WGB-1 (WGB-91 and 92) exhibit contrasting grain size distributions (Fig. 6.8). WGB-91 is predominantly composed of silt and clay (55.6% combined – Fig 6.6a), the D_{50} of which is 42.3 µm. LOI% and bromine content is high compared to the other soil samples (Table 6.1). WGB-92 is predominantly sand (88.7%- Fig. 6.8b). WGB-93 is very poorly sorted, but primarily sand (67% - Fig. 6.8c).

For WGB-91, all concentration-related magnetic proxies are low, although total susceptibility is substantially higher than WGB-93 (χ_{LF} = 29) (Fig. 6.10a). By contrast χ_{FD}% is high (6.9%) and $\chi_{ARM}/_{IRM1T}$ high (0.52) relative to the other samples (Fig. 6.10b). Unlike the particle-sized magnetic signatures obtained from WGB-1 (A3), χ_{LF} peaks in the coarsest fraction for this sample (Table 6.2).

WGB-92 exhibits slightly higher concentration-related proxies, accompanied by a notable increase in S_{300}% (6% - Fig. 6.10c). WGB-93 exhibits extremely low concentration-related magnetic proxies. However, S values are strikingly high, with just 47% and 19% of the applied remanence unreversed at -100mT and -300mT respectively.

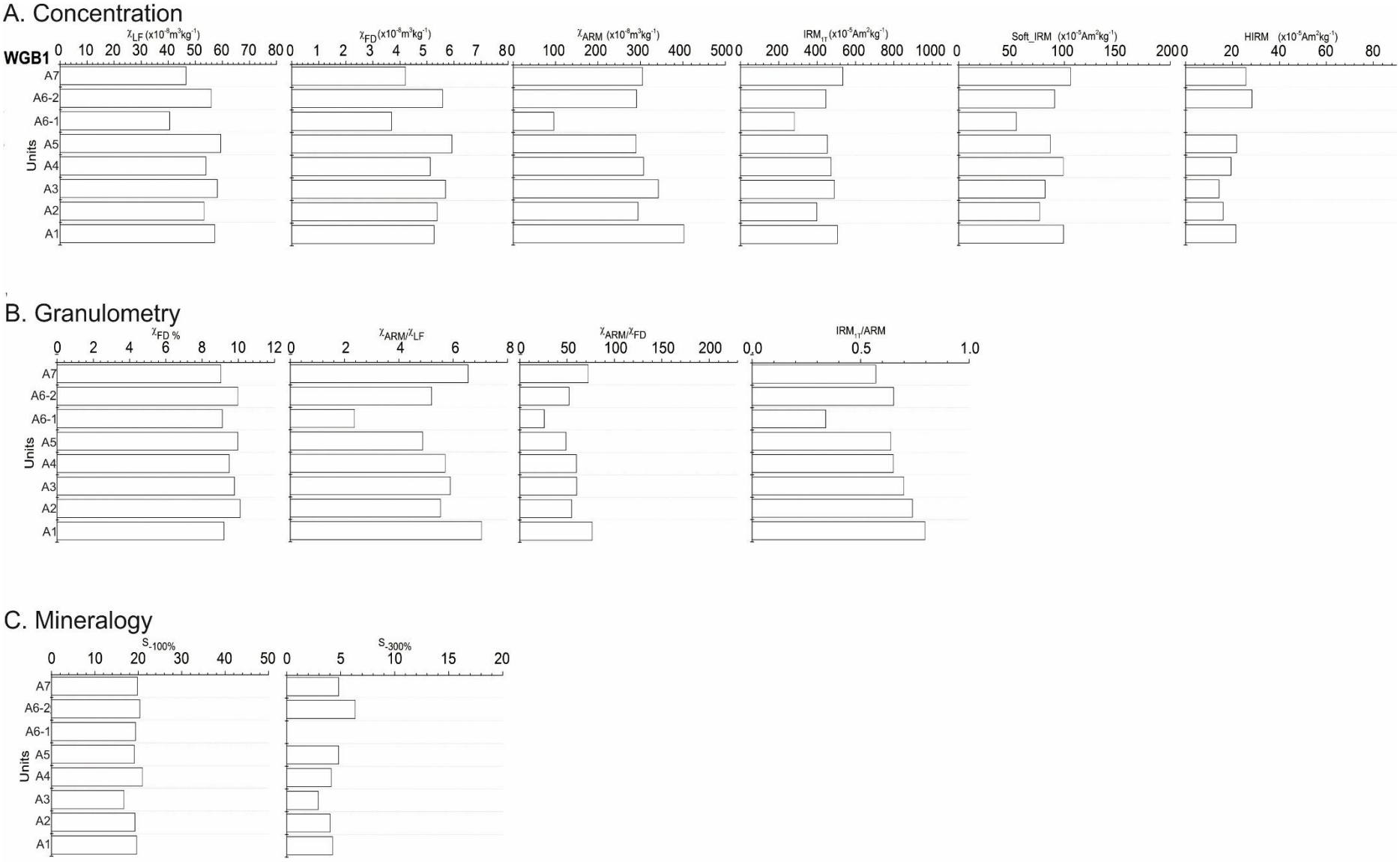

Figure 6.9 – mineral magnetic parameters from outcrop WGB-1.

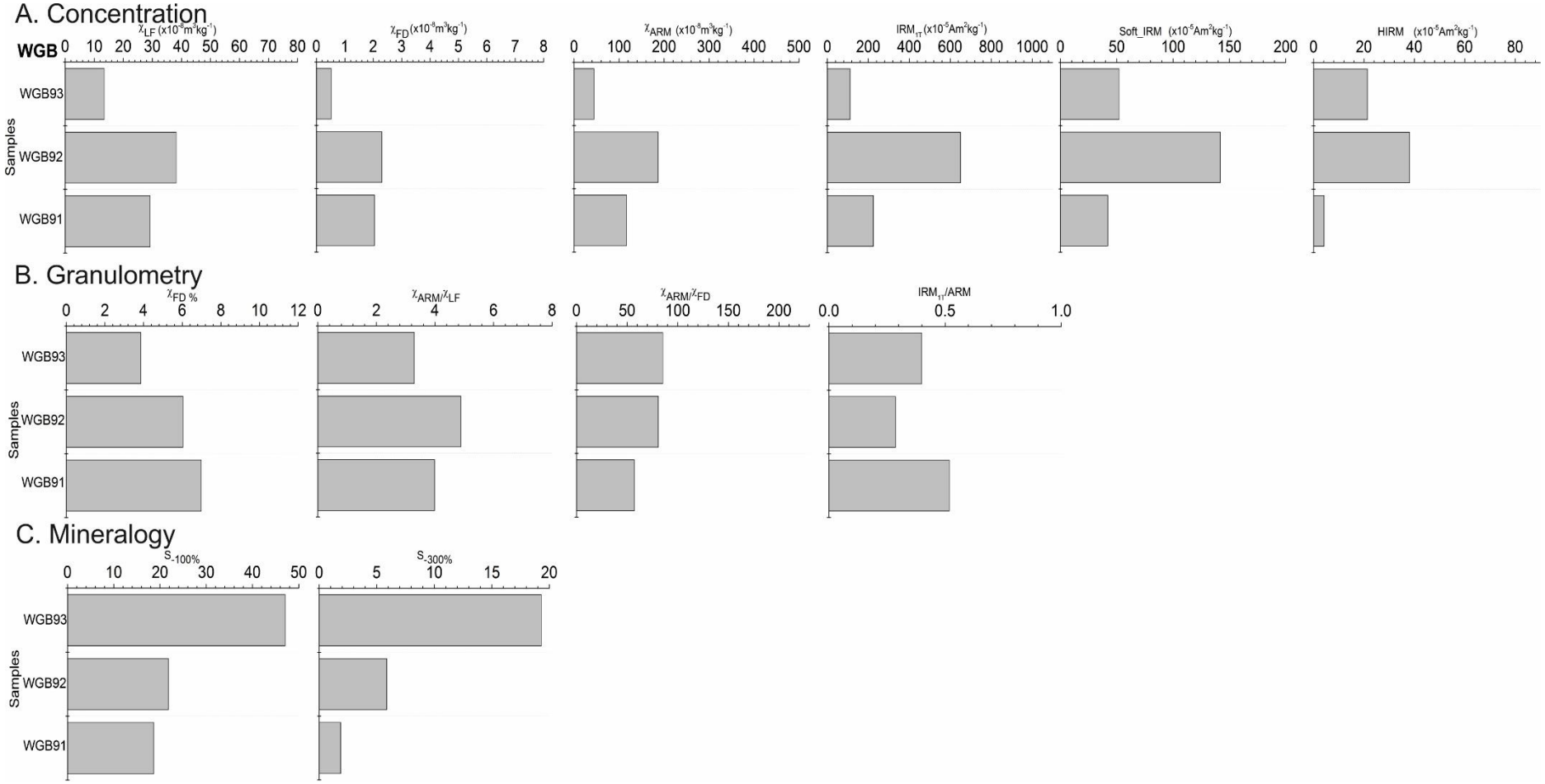

Figure 6.10 – mineral magnetic parameters from soil samples WGB91-93.

Table 6.2 – mineral magnetic parameters from 5 particle size fractions compared to the bulk (0-63 µm) for the pediment soil sample and WGB-1 unit A3.

WGB-91 Soil sample	**X_{LF}**	**X_{FD}%**	**X_{ARM}**	**IRM_{1T}**	**Soft_IRM**	**HIRM**	**X_{ARM}/X_{LF}**	**X_{ARM}/X_{FD}**	**$X_{ARM/IRM1T}$**	**S_{-100}%**	**S_{-300}%**
0-4 µm	28.8	7.8	129.1	131.9	34.7	11.2	4.5	57.6	1.0	26.3	8.5
32-63 µm	24.3	2.8	55.2	431.7	51.7	0.0	2.3	82.3	0.1	12.0	0.0
Bulk	29.3	7.0	116.7	225.2	42.0	4.2	4.0	57.1	0.5	18.7	1.9
WGB-1 A3	**X_{LF}**	**X_{FD}%**	**X_{ARM}**	**IRM_{1T}**	**Soft_IRM**	**HIRM**	**X_{ARM}/X_{LF}**	**X_{ARM}/X_{FD}**	**$X_{ARM/IRM1T}$**	**S_{-100}%**	**S_{-300}%**
0-4 µm	70.9	10.5	350.0	382.6	55.1	14.9	4.9	47.0	0.9	14.4	3.9
32-63 µm	28.8	4.7	68.8	359.9	51.9	0.4	2.4	50.5	0.2	14.4	0.1
Bulk	53.9	9.5	307.4	471.9	98.9	19.4	5.7	60.0	0.7	21.0	4.1

6.2b: WGB-1: interpretation

The abrupt transition from confined to unconfined on the sandstone slope is conducive to the formation of fans. The limits of the gravels and sands of WGB-1 which constitute a phase of fan aggradation were mapped. The massive, poorly sorted calibre of the gravel units (A1 and A2) indicates high energy conditions of transport consistent with mass movement processes. The low silt/clay content rules out mudflow processes as defined by Bull (1964a & b) and Varnes (1978). Debris flows typically include <50% fine sediment (0-2 mm), thus being coarser than mudflows (Varnes, 1978). The relative % of fines (0-2 mm) and gravel was not calculated, but the low concentrations of silt/clay (as a % of the 0-2 mm sedigraph) for unit A may reflect exhaustion of supply of finer grain sizes during runoff events. Consequently, the matrix-supported nature of the gravels most likely reflects emplacement by debris flows following the definition of Vardnes (1978). These mass-flows likely cascaded off the pediment, with stream power boosted by the steepness (0.24 m/m) of the sandstone slope.

Units A3, A5 and A7 reflect lower energy conditions of deposition. Although such gravel sheets can evidence flow spreading associated with channel termini, the surface is normally associated with lenticular reworked gravels during the latter stages of flow, but no such architecture is evident here.

The friable, weakly developed crumb structure and unlithified nature of the soil implies limited weathering and soil development, but this is evaluated more fully in the magnetics subsection. The browner colour in concert with high bromine values and silt-impregnated root channels at 110-120 cm depth may indicate a smaller illuvial horizon.

Compared to Africanders Kloof headwaters (section 5.2), ferrimagnetic concentration at WGB-1 is modest, though still high with the exception of unit A6-1 (110-120 cm). The strikingly high χ_{FD}% values indicate a large concentration of pedogenic SP grains. Furthermore, the lower IRM_{1T} indicates lower overall concentrations of MD remanence carrying ferrimagnets. The high $\chi_{ARM}/_{IRM1T}$ indicates large concentrations of SD carrying ferrimagnets relative to the fan deposits at AK. Additionally, canted anti-ferromagnetic mineral contribution is higher reflected in the ‘S’ values. As distinct palaeosol horizons are absent and sedimentation seems to have been

continuous at this location (WGB-1), any haematite content is likely sourced from eroding soil upstream and/or erosion of sandstone bedrock.

As the soil is well-drained (WGB-1), it follows that the χ_{ARM} reflects SD magnetite formed under conditions of progressive wetting and drying. Unit A6 (110-120 cm) is a clear exception reflected in the low concentration of SD ferrimagnetic minerals and hard minerals (S_{300} = 0%). This may reflect changing sediment source inputs from the pediment upstream.

The very weak susceptibility carried in the coarse (32-63 μm) grade (unit A3) (χ_{LF} = 28.8) attests to a comparatively subdued lithogenic magnetic signature reflecting absence of dolerite (Table 6.2). The high $X_{ARM/IRM1T}$ exhibits bulk values (0.7) most closely tracking the 0-4 μm (0.9) fraction. Bulk susceptibility is thus controlled primarily by concentrations of pedogenic SP rather than lithogenic MD magnetite. The unusually high χ_{FD}% signature in the coarse grade most likely relates to imperfect dispersion of aggregates (Lyons et al., 2010).

Figure 6.11 – Beaufort group sandstone outcropping on the upper slopes above WGB-1.

The soil sample collected upstream from the pediment (WGB-91) reveals very low concentrations of ferrimagnetic grains. Whilst its bulk properties (Fig. 6.9) are considerably different to most of the horizons at WGB-1, the magnetic signature of the coarse grade compares very well with unit A3 indicating a distinct resurgence of SP grains. This similitude implies a common lithogenic origin: eroding sandstone

bedrock on the nearby slopes. However, very different pedogenic signatures are evidenced by the very low concentration-related proxies for WGB-91. Since the bulk magnetic properties faithfully track the clay fraction, which has been demonstrated elsewhere as being a common depository for secondary ferrimagnetic minerals formed by pedogenesis (Hao et al., 2008b), there are not problems of dilution in this respect compared to use of the $X_{ARM/IRM1T}$ parameter – 50% lower for the bulk than 0-4 μm (WGB-91).

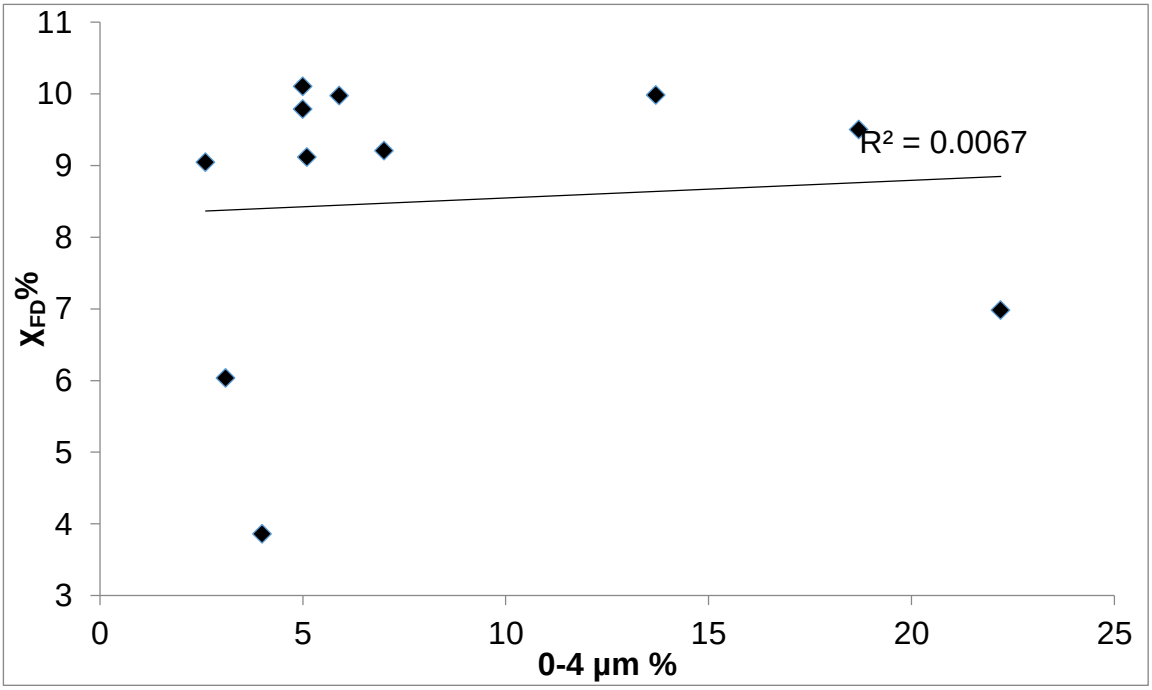

Figure 6.12 – bi-plot of %0-4 μm fraction versus χ_{FD}% for soil samples and WGB-1.

χ_{FD}% of the clay fraction remains high between WGB-91 and WGB-1 unit A3, in spite of the large difference in χ_{LF}. In contrast, the χ_{ARM} is much higher (350) at unit A3 and probably the main driver of the high susceptibility in the fine grade. This is because susceptibility follows a power law relating to magnetic grain size (Evans and Heller, 2003). There are two possible hypotheses regarding the nature of the consistently high χ_{FD}% which is unrelated to χ_{LF}: 1) Since χ_{FD}% typically resides in the clay and very fine silt fraction (Table 6.2), size selective transport of fines may be responsible for concentrating clays and silts such that the SP signature is enhanced. Fig. 6.12 indicates that this is not the case. 2) χ_{FD}% pertains to eroding catchment soil from upslope as well as in situ pedogenic transformations (WGB-1). Although total concentration of remanence carrying ferrimagnets for WGB-91 is lower than WGB-1, the relative proportions of SP grains remains the same. Regardless, it is clear from

the particle size data, that the χ_{ARM} is a more useful discriminator of weathering and pedogenesis than χ_{FD} alone on these upper slopes.

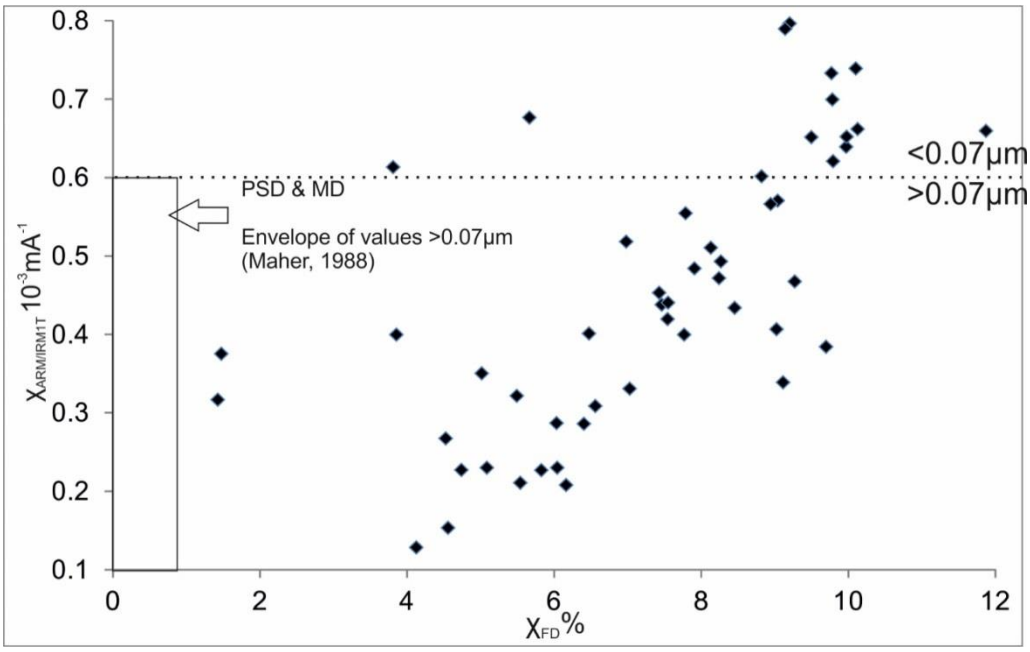

Figure 6.13 – bi-plot of χ_{FD}% versus $X_{ARM/IRM1T}$ for Wilgerbosch Kloof dataset.

With the reduced emphasis on a lithogenic component dominating the bulk magnetic signature, the granulometric quotients are more widely usable (n = 13/51) as a proxy for weathering than at AK (Fig. 6.13 and 6.14).

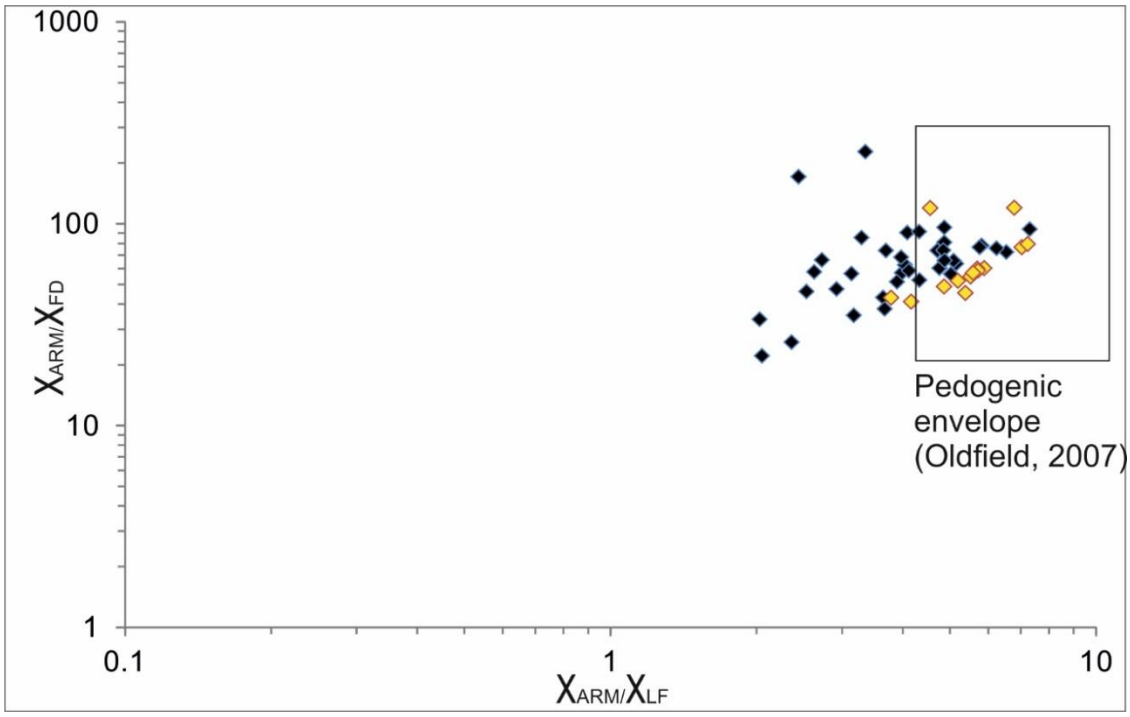

Figure 6.14 – bi-plot of χ_{FD}% versus χ_{ARM}/χ_{LF} versus χ_{ARM}/χ_{FD} for Wilgerbosch Kloof dataset. Yellow diamonds represent samples which exhibited $X_{ARM/IRM1T}$ >0.6x10^{-3} mA^{-1} as shown in Fig 6.13.

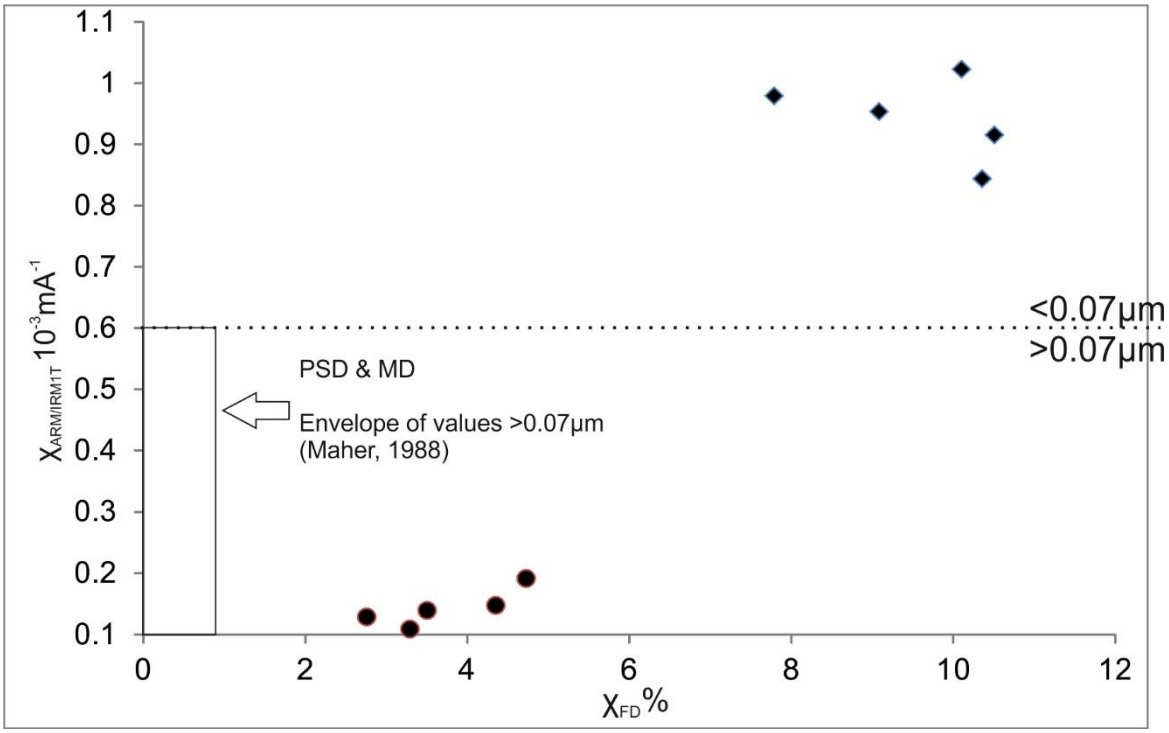

Figure 6.15 – bi-plot of χ_{FD}% versus $X_{ARM/IRM1T}$ for particle sized extract (diamonds = 0-4 µm; circles = 32-63 µm) from a subsample of the Wilgerbosch dataset (n = 5).

There is very good discrimination between the clays and coarse silts (Fig. 6.15), with the latter showing consistently higher χ_{FD}% values than at Africanders Kloof reflecting the predominance of sandstone over dolerite.

In summary, given the weaker lithogenic magnetic component compared to that identified at Africanders Kloof, higher susceptibility values may be taken as a more robust indication of in situ pedogenic transformation where this is supported by macro-pedological evidence. The absence of macro-pedological soil features at WGB-1 implies only incipient soil development overprinting these fan sediments. The magnetic properties analysed and discussed are therefore reflecting mainly subtle changes in the source of eroding soil from the pediment and interfluve slope upstream.

6.3a: WGB-2: analysis

Log WGB-2 was recorded from a 2 m exposure on the right hand side of the channel approximately 145 m downstream of the pediment (Fig. 6.1, 6.2, 6.16 - 6.18).

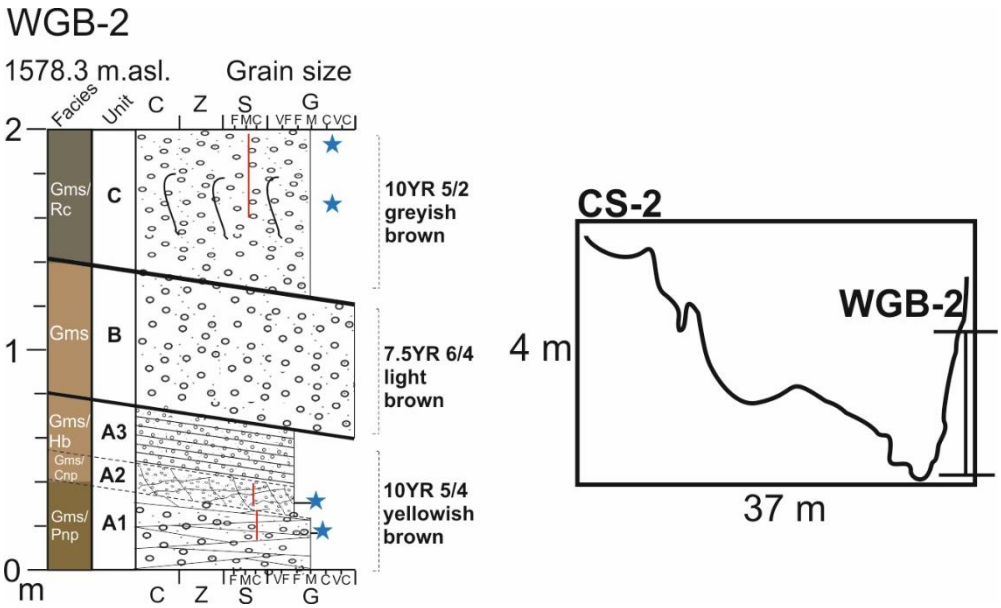

Figure 6.16 – sedimentary log of outcrop WGB-2 and cross section 2 (50 m upstream). Note inclined strata, dipping into the channel.

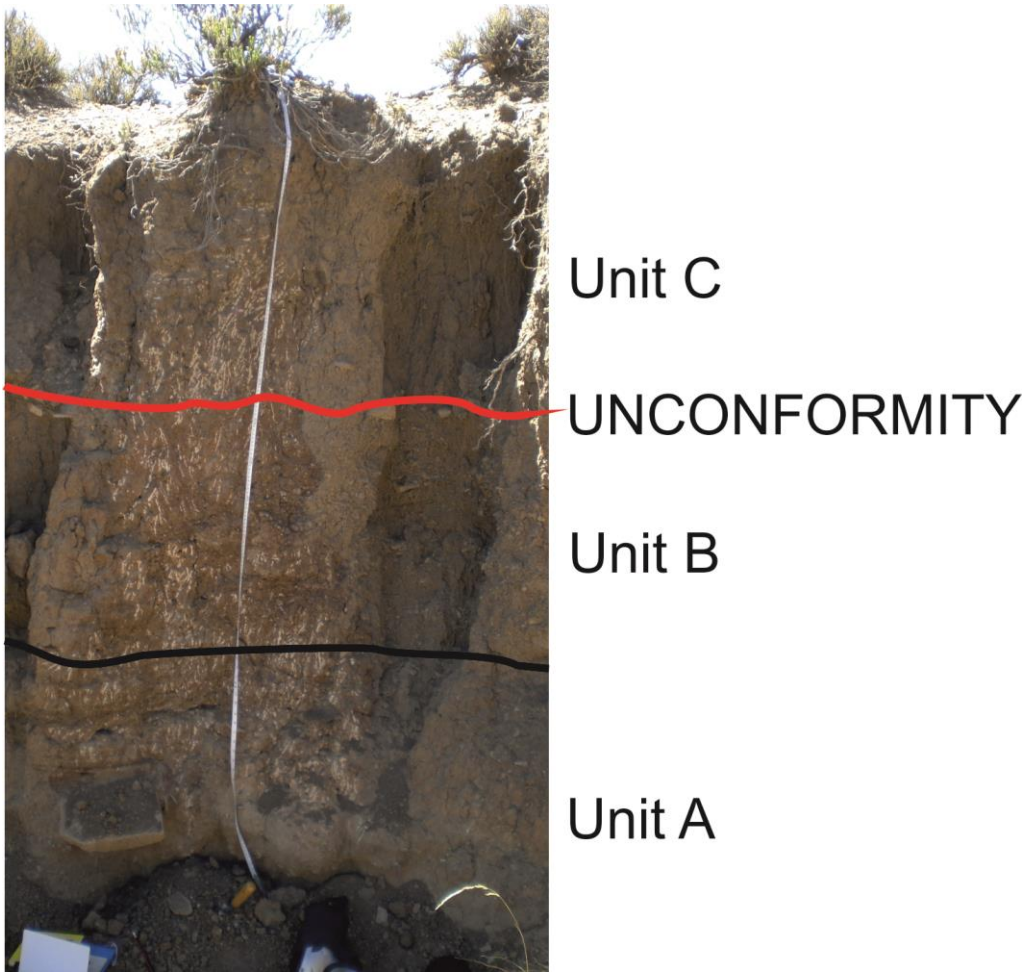

Figure 6.17 – photograph of outcrop WGB-2. Note abrupt contact (red line) between brown and grey sediment ¾ of way up profile.

Figure 6.18 – photograph taken from WGB-2 looking upstream toward the upper sandstone slopes. Note the 'grey' fill draped over the brown sediments of WGB-2 and the cobble/boulder deposits exhumed within the channel itself.

The contemporary channel at this point is roughly 25 m wide (Fig. 6.16) compared to just 5 m at WGB-1 (Fig. 6.4). Erosion has exhumed the coarse deposits forming part of the local succession, the base of which is characterised by matrix-supported medium gravels that exhibit thin, planar non-parallel cross bedding (A1 – Fig. 6.16). These grade to matrix-supported very fine gravels (subunit A2) which exhibit curved non-parallel cross bedding. Colour also changes to 7.5YR 6/4 light brown and bromine content is small (3.6 ppm) compared to A1 (Table 6.3). The matrix of both subunits is dominated by coarse to very coarse sand (Fig. 6.19a and b).

Subunit A3 is composed of thinly horizontally bedded fine gravels, which are then sharply overlain by clast-supported very coarse gravels with any weak matrix present showing no differentiation in colour (unit B).

Table 6.3 – % loss on ignition and bromine (ppm) data for sampled horizons at WGB-2.

Unit	Height (cm)	Loss on ignition (%)	Bromine (ppm)
A1	15-25	2.29	6.6
A2	40-50	2.16	3.6
C	160-170	2.34	12.4
C	190-200	2.80	12.9

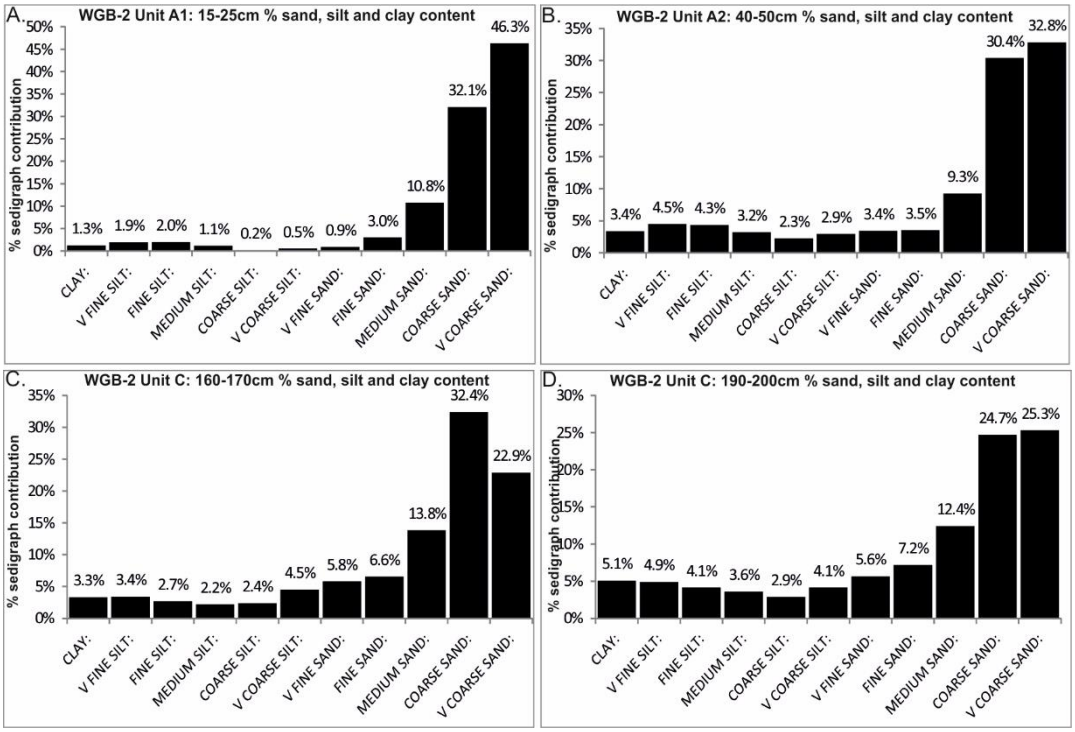

Figure 6.19 – % sand, silt and clay content derived from Coulter grain size analysis on samples collected from outcrop WGB-2.

Unit C sharply overlies B, exhibiting a significant change in colour to 10YR 5/2 greyish brown. The sediments consist of massive, matrix-supported medium gravels with abundant root channels. The matrix at 160-170 cm is characterised by a distinct coarse sand mode (32.4%) and subordinate silt/clay (18.5% - Fig 6.19c), but silt/clay content increases (24.7% - Fig. 6.19d) at the top (190-200 cm). Bromine values are typically double or more than the previous units (Table 6.3).

The basal subunits exhibit low concentration-related magnetic properties (χ_{LF} = 33-35) compared to the overlying sediment although IRM_{1T} is no different (Fig. 6.20a). Total magnetic susceptibility is substantially higher for unit C (χ_{LF} = 55-59) as are the χ_{FD} and χ_{ARM} parameters comparing well with the grey sediment reported at WGB-1 (Fig. 6.4 and 6.9). χ_{FD}% is higher (9.7-10.1%) for unit C than A, as is the ($\chi_{ARM/IRM1T}$: 0.66 - 0.73 – Fig. 6.20b). The S and HIRM for unit C are both lower than A, in particular the $S_{300\%}$ which shows 3.8 - 4.5% of the applied remanence unreversed at -300mT (unit C) compared to 6-7% (unit A – Fig. 6.20c).

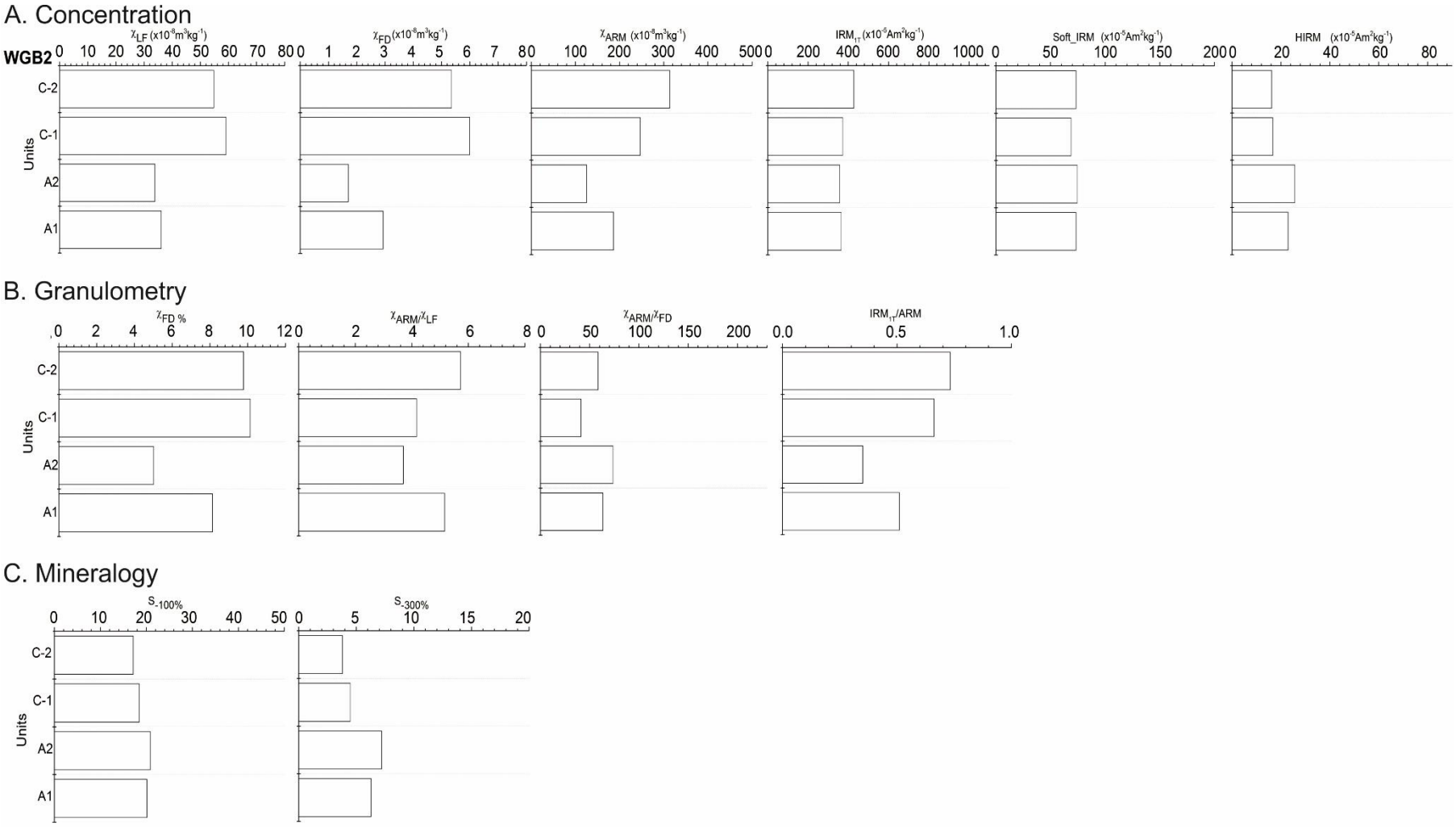

Figure 6.20 – mineral magnetic parameters from outcrop WGB-2.

6.3b: WGB-2 interpretation

The basal gravels at WGB-2 are characteristic of sedimentation in an alluvial fan channel. Unit A1 is interpreted as indicating low angle dunes. The transition to dunes of shorter wavelength and higher angle above (unit A2) in concert with reduced grain size indicate flow recession, with lower plane bed deposition resulting in gravelly sands deposited as horizontally bedded sheets (unit A3). Ripple cross laminations are uncommon in sediments above 0.6 mm, accounting for their absence here (Allen, 1982a).

The overlying matrix-supported gravels are at the same elevation as the coarse cobbles/boulders exhumed within the active gully system (Fig. 6.16). This upward coarsening is interpreted as a progradational feature of the palaeofan rather than a channel bar. Furthermore, their finer calibre (very coarse gravel) relative to the sediments preserved in the centre of the valley attest to proximal-distal fining associated with a hyper-sediment saturated flow, probably debris flow surging down the steep slopes upstream (0.24 m/m). The absence of this succession at WGB-1 is undoubtedly due to the very low preservation potential for sediment on the steep upper sandstone slope. The overlying gravels (unit C) are similar in character to those analysed at the base of WGB-1 (unit A1 for example), 100 m upstream. Their friable nature attests to relatively little in situ weathering compared to the indurated units below (A and B). It follows that the sharp, planar contact between units B and C is an unconformity, with WGB-1 sediments being stratigraphically younger than WGB-2 (A and B), the former representing reactivation of sedimentation on the fan surface following a period of soil development.

The basal units (A1 and 2) exhibit low concentrations of ferrimagnetic minerals but high contributions of SP grains reflected in $\chi_{FD}\% > 4.5$. The low susceptibility relative to WGB-1 sediments is related to the production of antiferromagnetic minerals, probably haematite considering the rubified nature of the deposits ($S_{300}\%$ - 6-7%).

The litho- and magneto-stratigraphic evidence thus indicates that sedimentation on the upper slopes halted for a period of time sufficient to allow haematite soil to develop as indicated by the rubified soils of units A and B which exhibit this spike in S_{300}. The magnetic properties of unit C closely resemble those at WGB-1 (Fig. 6.9), attesting to a magnetite-dominated assemblage, which on the basis of the friable

nature of the sediments, reflects the early stages of pedogenetic transformation through progressive oxidising and reducing conditions of the soil surface, rather than deep rubification, iron mottling and cementation as observed for units A and B (WGB-2). In summary, the evidence so far shows at least one prior distinctive phase of fan aggradation and soil development followed by a distinct incision phase and subsequent episode of aggradation (WGB-1). Considering that the valley is narrow at WGB-2 (approximately 60 m), this is probably reflective of soil development on the entire fan, rather than part of it, as can be the case in wider, larger fan settings.

6.4a: WGB-3: analysis

Log WGB-3 was recorded from a 3.8 m exposure on the left hand side of the channel approximately 280 m downstream of the pediment (Fig. 6.2, 6.3, 6.21 and 6.22). Valley cross section morphology slopes away from the contemporary gully (CS-3), in spite of close proximity to the hillslopes (Fig. 6.1).

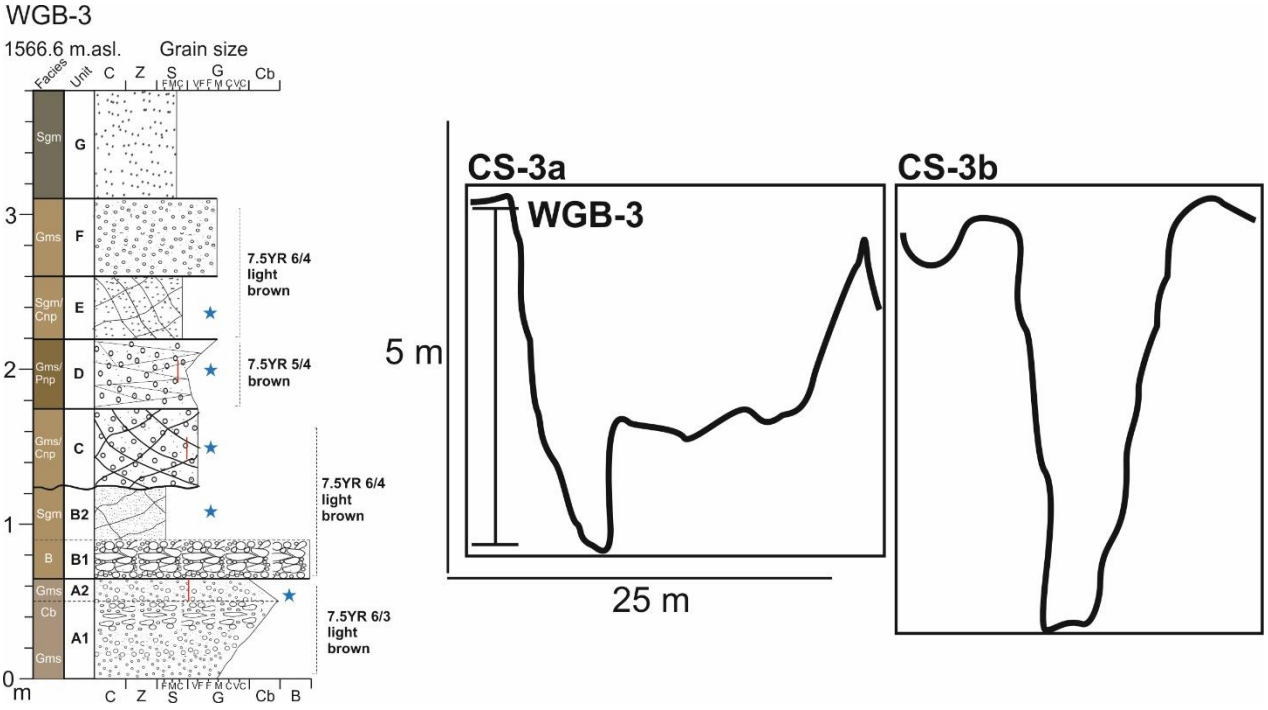

Figure 6.21 –sedimentary log of outcrop WGB-3 and cross sections 3a and b.

Unit A consists of inversely graded matrix-supported medium to then very coarse gravels and then cobbles (subunit A1) before fining to predominantly very coarse matrix-supported gravels (subunit A2). The matrix of A2 is moderately sorted (79.6% coarse to very-coarse sand – Fig. 6.23a). Total magnetic susceptibility is low (χ_{LF} = 28) as are the remanence parameters (Fig. 6.24a), but χ_{FD}% is relatively high (6.4%-

Fig. 6.24b). The S_{100}% parameter is relatively high showing 18% of the applied remanence was unreversed (Fig. 6.25c). The colour of this unit is 7.5YR 6/3 light brown.

Figure 6.22 – photograph of outcrop WGB-3.

Unit B sharply overlies A, consisting of a thick bed of matrix-supported, very poorly sorted mix of boulders (up to 53 cm in diameter), cobbles and gravels (B1), which is capped by very poorly sorted sandy silts (Fig. 6.23b – unit B2). This unit and C are slightly lighter in colour: 7.5YR 6/4 light brown.

Concentration-related magnetic proxies are high relative to unit A (Fig. 6.25a) whilst the granulometric proxies are only slightly higher (Fig. 6.25b). S values peak for this unit with 21.5 and 5.5% of the applied remanence unreversed at -100mT and -300mT respectively (Fig. 6.25c). The contact between units B and C is sharp undulating. Unit C consists of trough cross bedded, matrix-supported, fine gravels. The matrix at 130-140 cm consists of well sorted, predominantly coarse to very-

coarse sands (92.1% - Fig. 6.23c). Concentration related magnetic proxies are comparable to unit B although the Soft_IRM and HIRM exhibit lower values (Fig. 6.25a). Conversely, granulometric parameters are relatively high, especially the χ_{FD}% (12%), χ_{ARM}/χ_{LF} (5.5) and $\chi_{ARM}/_{IRM1T}$ (0.68 - Fig. 6.25b).

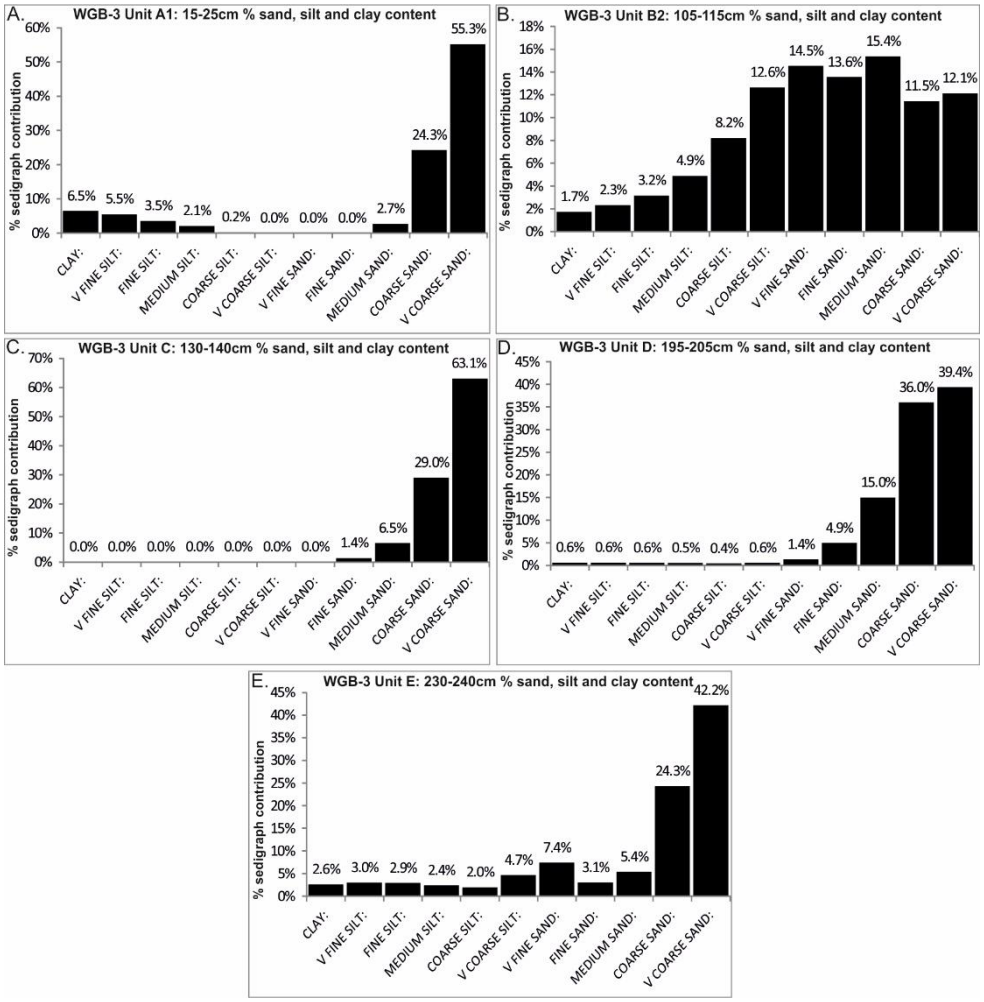

Figure 6.23 – % sand, silt and clay content derived from Coulter grain size analysis on samples collected from outcrop WGB-3.

Table 6.4 – % loss on ignition and bromine (ppm) data for sampled horizons at WGB-3.

Unit	Height (cm)	Loss on ignition (%)	Bromine (ppm)
A2	50-60	2.93	2.7
B2	105-115	2.10	3.4
C	145-155	2.23	3.3
D	195-205	1.76	14.9
E	230-240	1.83	3.5

S values are much lower than unit B, with 7.5% and 1.2% of the applied remanence unreversed at -100mT and -300mT respectively (Fig. 6.25c).

A sharp, planar contact separates units C and D and there is a change in colour to 7.5YR 5/4 brown. Unit D consists of planar-non parallel bedded, matrix-supported alternating fine-medium gravels. Bromine values peak in this unit (Table 6.4). Matrix sorting is poorer than unit C, although still dominated by coarse to very-coarse sand (75.4% - Fig. 6.23d). Compared to unit C, the χ_{FD} and χ_{ARM} parameters are much lower, as is χ_{FD}% (6%), χ_{ARM}/χ_{LF} (2) and the $\chi_{ARM/IRM1T}$ (0.23 – Fig. 6.25b), whereas the mineralogical proxies are virtually the same (Fig. 6.25c).

Unit E sharply overlies D and is composed of moderately sorted mainly coarse to very-coarse sands (66.5% - Fig. 6.23e) that exhibit curved-non parallel bedding. Concentration related magnetic proxies are high relative to unit D, with the IRM_{1T} and Soft_IRM in particular exhibiting the highest values found for this outcrop (525 and 112, respectively – Fig. 6.25a). The S values are relatively high with 21.5% and 3.8% of the applied remanence reversed at -100mT and -300mT respectively (Fig. 6.25c). The succession is capped by two thick units of matrix-supported medium gravels (unit F) and then very coarse sand with sharp contacts (unit G).

This succession has been incised by palaeochannels up to a depth of 1 m on the eastern side of the valley (Fig. 6.24a) which are characterised by unconsolidated, very poorly sorted matrix-supported gravels that exhibit poorly defined bedding (Fig. 6.24b). The reconstructed limits of this palaeochannel indicate it originated from the slopes to the south-east cross-cutting the long axis of the valley.

Figure 6.24 – A. Palaeochannel carved into previously reported succession – note photo is of right terrace bank. B. Matrix-supported, poorly gravels sharply overlie the sediments reported for WGB-3.

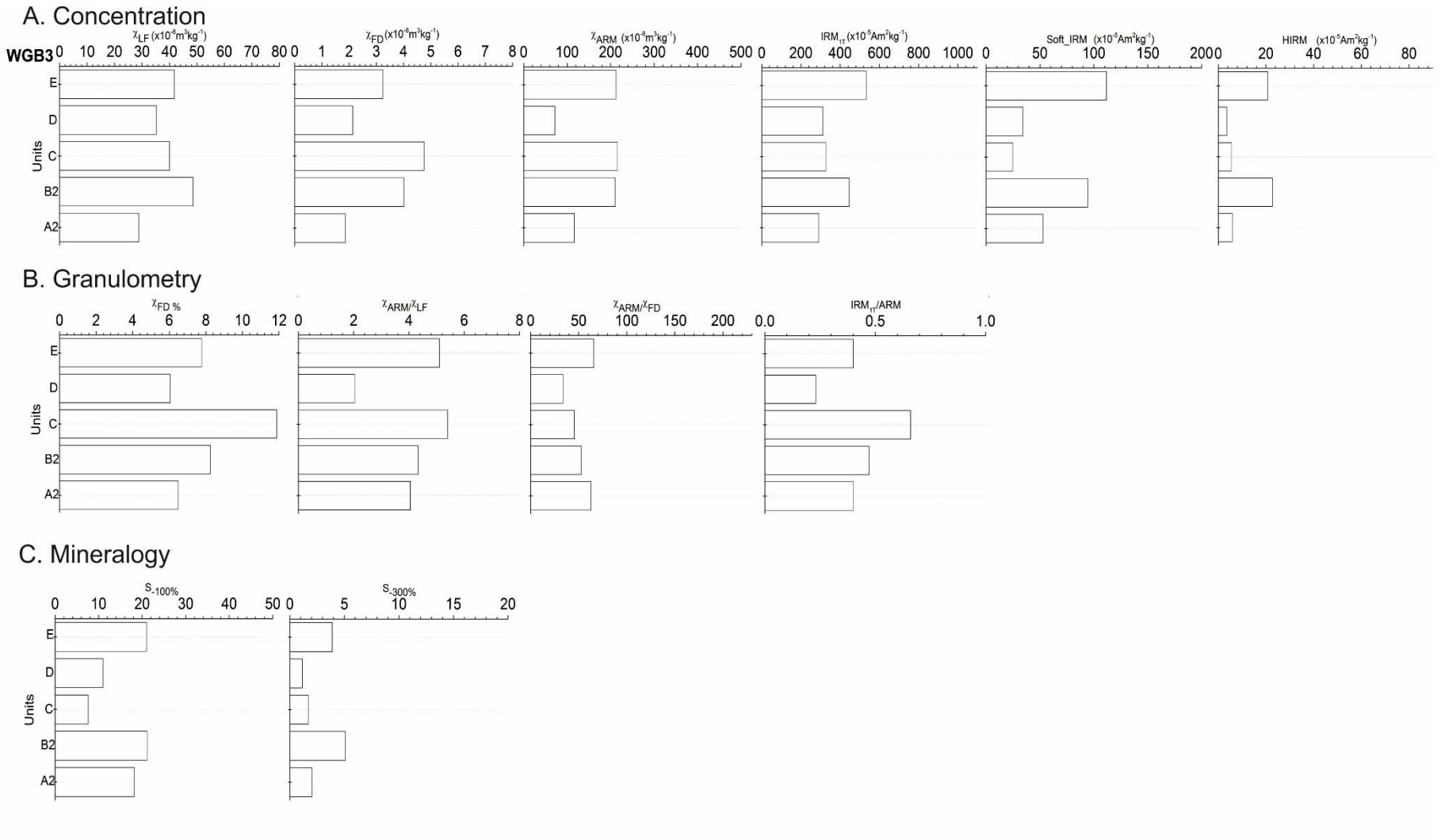

Figure 6.25 – mineral magnetic parameters from outcrop WGB-3.

6.4b: WGB-3: interpretation

The local fan morphology favours sedimentation away from the contemporary gully (Fig. 6.21) despite the narrow valley.

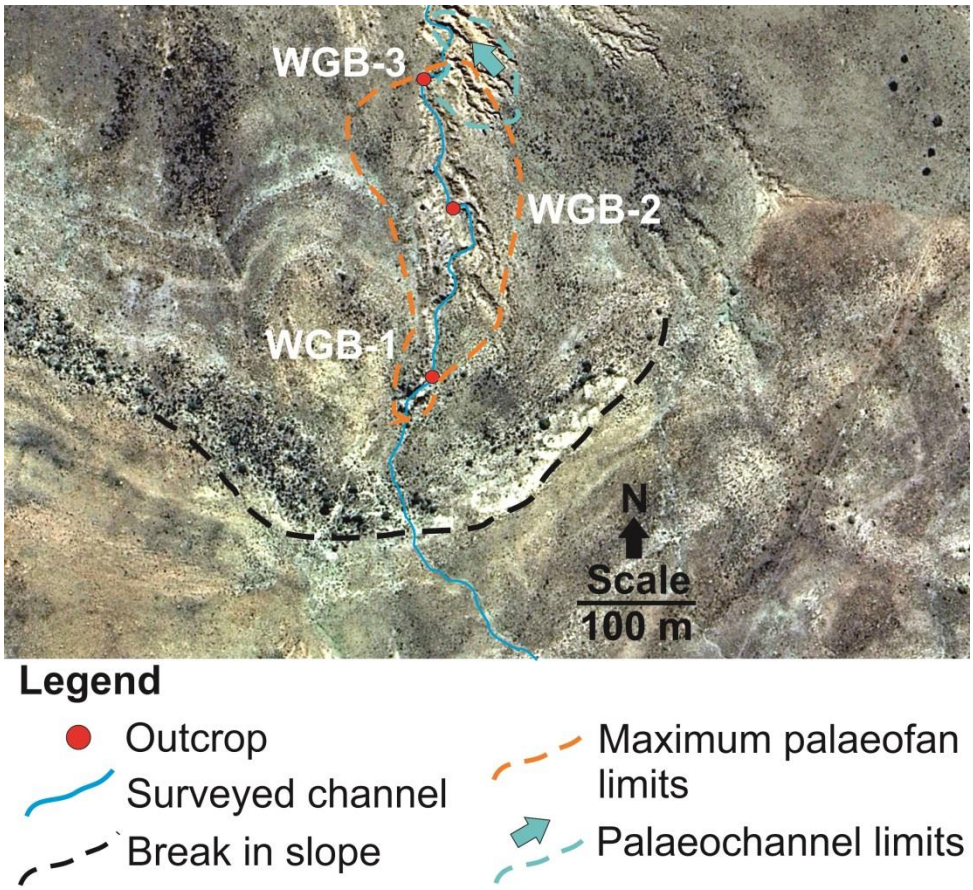

Figure 6.26 – digitised aerial photograph showing mapped maximum limits of headwater palaeofan extending from upper sandstone slope at WGB-1 to WGB-3. Note also the limits of the palaeochannel sourced from the hillslope to the east (blue dashed line).

The inversely graded gravels and cobbles are likely to be progradational features in association with the palaeofan identified at WGB-2 (Fig. 6.26). The top of this unit (A2) is characterised by a weak, relatively coarse-grained (MD) magnetic signature on the basis of analysed parameters. Since anti-ferromagnetic mineral concentration is modest compared to above (unit B2), an alternative explanation for diluted susceptibility is required. One possibility is that a relatively magnetically dilute soil source was eroded and supplied to the valley at time of deposition; in this case, the signature in question is syn-depositional. More probable however, and in light of previous experience at AK, is that in spite of being texturally 'coarser', the unit is close to bedrock, and therefore less well-drained than the sediments above (Fig.

6.23a). This can result in ferrimagnetic dissolution which dilutes susceptibility (Section 5.2.5). Under such conditions, a distinctive pedogenic signature which might hint at a sedimentation hiatus on the fan leading to soil development is difficult to infer confidently from available evidence: the sharp contact with overlying sediment is probably just a reactivation surface rather than an actual 'palaeogeomorphic' surface.

The overlying coarse cobble/boulder unit (B1) in association with the sharp bed contact is interpreted as debris flow deposits as they are matrix-supported and lie at approximately the same relative elevation as the inset cobble unit exposed at WGB-2. The overlying indurated sandy silts are conformable and represent the later stages of flow. Compared to unit A2 underneath, this sandy silt package exhibits a distinct ferrimagnetic signature (χ_{LF} = 48), although still relatively coarse-grained ($\chi_{ARM/IRM1T}$ = 0.46). The S values attest to a spike in haematite content for this horizon. The correspondence of this and the undulating, erosional contact with the overlying sediment implies there could have been a hiatus in local sedimentation for a period of time sufficient to permit pedogenesis to overtake aggradation. However, this would normally be accompanied by a change in soil colour, texture and degree of cementation (see ch.5). No such changes were noted. Therefore, this stratigraphic boundary is more likely to just be a reactivation surface. These haematite rich soils compare with the basal units at WGB-2 and upstream where this soil first crops out (WGBLP96 – Table 6.5) and are treated as coeval.

Table 6.5 – selected mineral magnetic parameters and munsell colour for units from WGB-2 and 3.

Outcrop/Unit	Height (cm)	X_{LF}	X_{arm}	IRM_{1T}	S_{-100}%	S_{-300}%	Munsell colour
WGB-2 / A1	15-25	36.1	186.2	364.8	20.1	6.3	10YR 5/4
WGB-2 / A2	40-50	33.9	125.2	357.4	20.9	7.2	7.5YR 6/4
WGBLP96	45-55	45.7	173.2	287.9	20.0	6.9	7.5YR 6/4
WGB-3 / A2	50-60	28.8	116.7	290.9	18.2	2.0	7.5YR 6/3
WGB-3 / B2	105-115	48.6	210.5	446.4	21.1	5.1	7.5YR 6/4

The overlying trough cross-bedded, fine gravels are interpreted as fan channel deposits, signifying a renewed phase of channelized incision into the fan surface (unit C), dissecting unit B. Compared to below, this unit (C) exhibits a distinct SP/SD ferrimagnetic rather than anti-ferromagnetic signature. The SP signature is likely inherited from the upper sandstone slopes, in which case the χ_{FD}% will reflect both eroded soil and in situ pedogenic transformation, which, on the basis of the

accompanying high $\chi_{ARM,}$ reflects SD magnetite. The units above further evidence a 'pulsed' sedimentation regime in a fan channel with minor phases of soil development in between reflected in discrete, rather than gradational, subtle changes in colour and minor progradational features where inverse grading occurs (unit D). Unit D possesses a distinctively more 'lithogenic' signature, evidenced by the very small $\chi_{ARM/IRM1T}$ (0.68). This may be indicative of reworked, pedogenically unaltered fan material from upstream, or additions from actively eroding bedrock. The colour change of this unit (D) and the sharp, planar contact with unit C implies that this is a palaeogeomorphic surface – a phase of geomorphic inactivity which allowed a soil to develop underneath (unit A-C). Therefore, the strong SP ferrimagnetic signature of unit C may pertain to a former surface horizon, with pedogenic magnetite formation. The reason for lack of magnetic enhancement relative to other reported cases for topsoils (see ch.5), is probably due to downward illuviation of remanence carrying ferrimagnets, collecting in unit B2. This supposition is supported by the relatively high silt/clay content of the latter (Fig. 6.23b).

Unit E, which lies above another sharp bed contact (2.2 m), exhibits a pedogenic haematite signature albeit weaker than unit B2. Notably, the facies here are similar to unit B2. Upward fining sequences in floodouts can represent the retrogradation of the system (Grenfell et al., 2012), in which case sedimentation rates at the margins can be relatively low and conducive to soil formation. However, the low $\chi_{ARM/IRM1T}$ (0.39), attests to a relatively strong lithogenic rather than pedogenic signature. This signature may therefore signify erosion of different soil sources from upstream. Unit F shows a return to progradation of the fan. The contact between units F and G represents an unconformity, the latter unit corresponding stratigraphically to the grey sediments capping WGB-2. These are coeval with those reported for WGB-1, indicating the last preserved phase of fan accretion prior to incision and fan terrace abandonment associated with incision of the contemporary gully.

6.5a: WGB-4A and B: analysis

Log WGB-4a was recorded from a 2.4 m exposure on the left hand side of the channel approximately 495 m downstream of the pediment and 250 m downstream from WGB-3 (Fig. 6.2, 6.3 and 6.27 and 6.28).

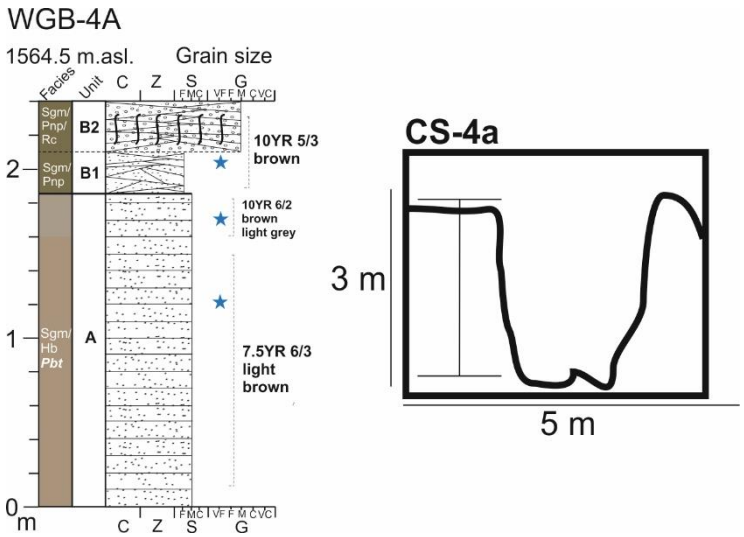

Figure 6.27 – sedimentary log of outcrop WGB-4A and valley cross section.

Unit A consists of medium-bedded sands and local very fine gravels. The sands are poorly sorted with subordinate silts and clays (25.6% and 28.8% at 120-130 and 170-180 cm respectively – Fig. 6.30a and b). Colour grades from 7.5YR 6/3 light brown (120-130 cm) to 10YR 6/2 light grey (170-180 cm) and bromine values peak (table 6.6). Magnetic susceptibility is enhanced at 170-180 cm (χ_{LF} = 68) as well as the χ_{FD} and the χ_{ARM} in particular (Fig. 6.31a). χ_{FD}% is very high (10%) as is the χ_{ARM}/χ_{LF} (5.5) and the $\chi_{ARM/IRM1T}$ (0.64) relative to 120-130 cm (Fig. 6.31b). By contrast, mineralogical proxies are typically constant between 120-130 and 170-180 cm, but the latter exhibits lower S_{300}% indicating only 2.5% of the applied remanence was unreversed at -300mT.

A sharp, planar contact separates units A and B. 50 m upstream, unit B first appears exposed in the left bank (Fig. 6.29a) and lies at the same elevation as a series of infilled palaeochannels in the right bank (Fig. 6.29b).

Table 6.6 – % loss on ignition and bromine (ppm) data for sampled horizons at WGB-4A.

Unit	Height (cm)	Loss on ignition (%)	Bromine (ppm)
A	120-130	1.69	11
A	170-180	1.84	12.4
B1	200-210	1.02	6.4

Figure 6.28 – photograph of outcrop WGB-4A.

Colour changes to 10YR 5/3 brown and bromine values are reduced by 50% (table 6.6). Subunit B1 consists of very poorly sorted sandy silts (Fig. 6.30c) which exhibit planar-non parallel cross bedding. Total magnetic susceptibility is lowest for this unit (χ_{LF} = 48) with χ_{FD} and χ_{ARM} much smaller than for unit A (170-180 cm), but the IRM_{1T} and Soft_IRM are relatively high (Fig. 6.31a).

The granulometric proxies are also generally much lower, in particular the $\chi_{ARM/IRM1T}$ (0.21 - Fig. 6.31b). The magnetic mineralogical proxies are typically invariable (Fig. 6.31c). The succession is capped by matrix-supported sandy gravels with abundant root channels that exhibit similarly low-angle planar non-parallel cross beds.

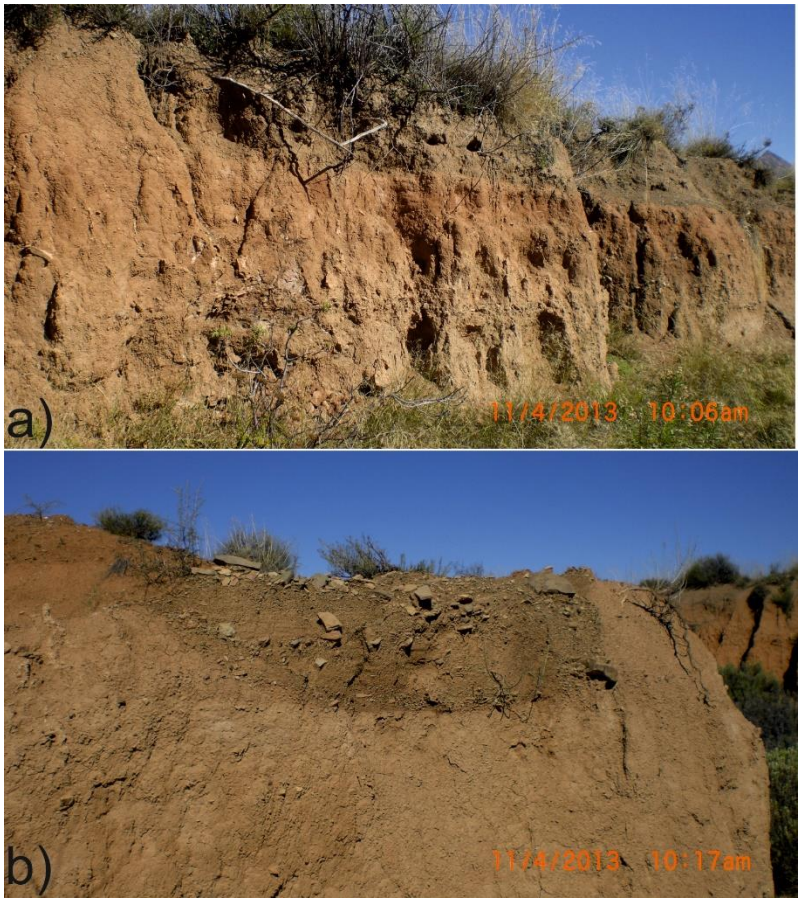

Figure 6.29 – photographs showing a) commencement of brown sands (unit B) and b) palaeochannel architecture in right bank at same stratigraphic elevation.

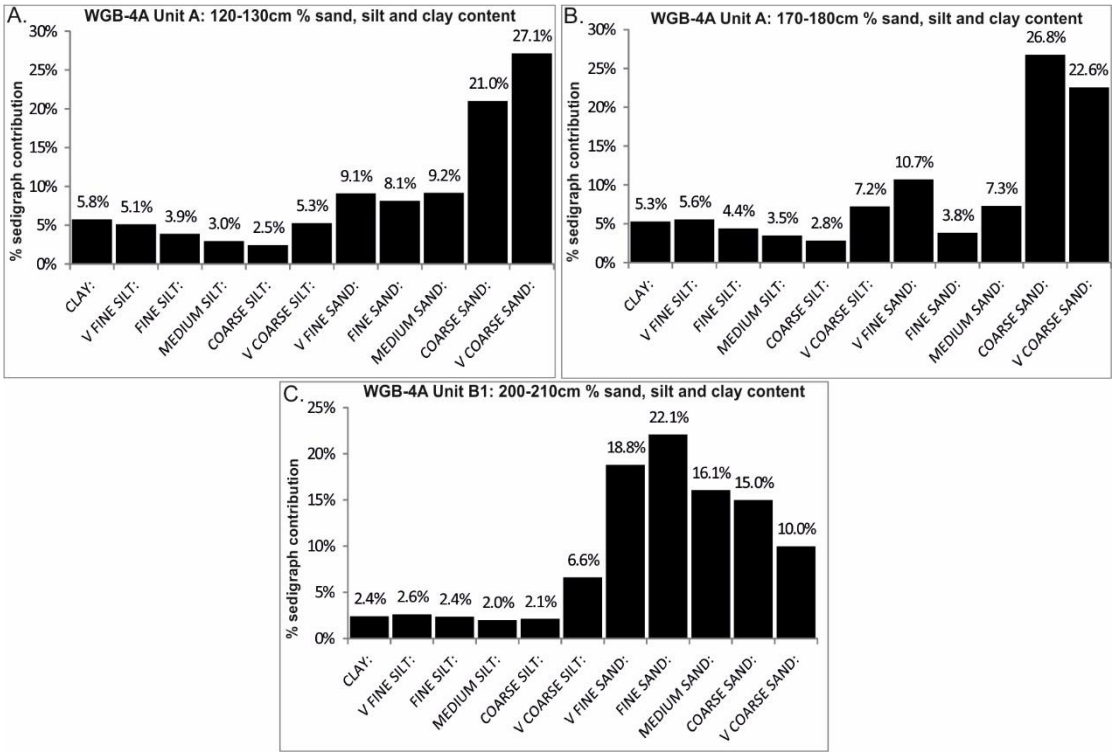

Figure 6.30 – % sand, silt and clay content derived from Coulter grain size analysis on samples collected from outcrop WGB-4A.

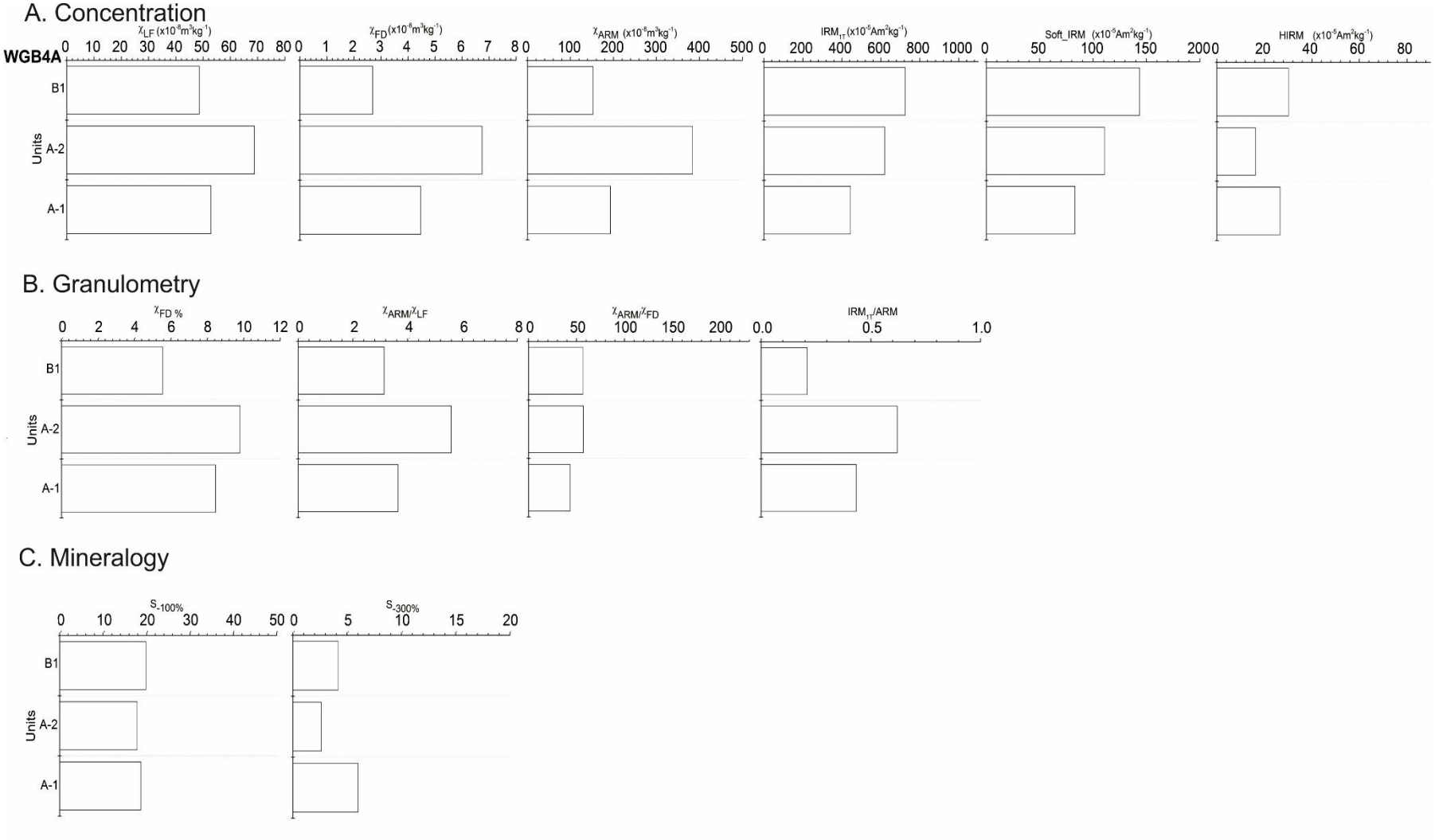

Figure 6.31 – mineral magnetic parameters from outcrop WGB-4A.

Log WGB-4B was obtained approximately 30 m further downstream of 4A (Fig. 6.1, 6.32 and 6.33). This section was logged and sampled to test for continuity of the surfaces and facies examined at 4A.

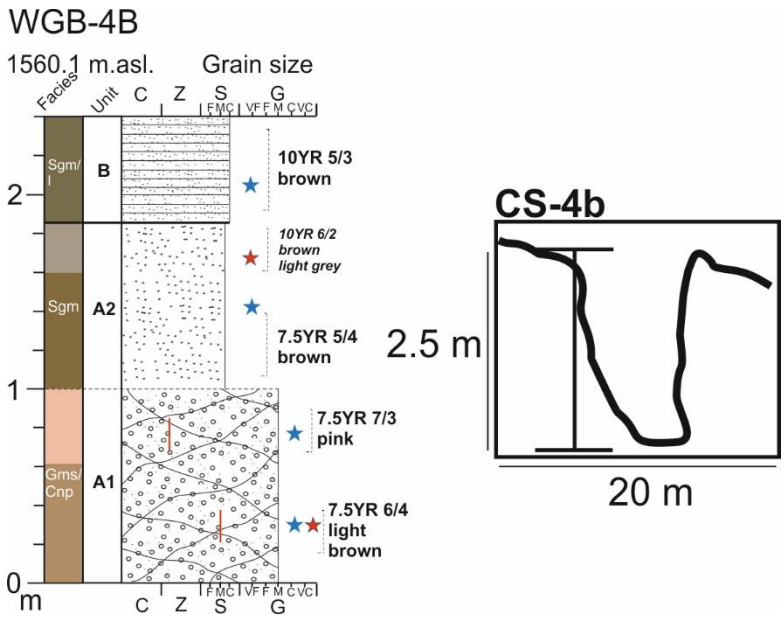

Figure 6.32 – sedimentary log of outcrop WGB-4B and cross section.

Figure 6.33 – photograph of outcrop WGB-4B.

Compared to WGB-4A, unit A consists of two distinct facies. A1: matrix-supported gravel package which exhibits curved parallel cross-bedding. The particle size distribution of the matrix changes dramatically from coarse to very coarse sands (52.4%) at 25-35 cm to very poorly sorted silty sands (80.5% silt/clay) above (Fig. 6.34a and b). This transition to a finer matrix is accompanied by a switch in colour to 7.5YR 7/3 pink and a slight increase in bromine values from 1.3 to 4.3 ppm (Table 6.7).

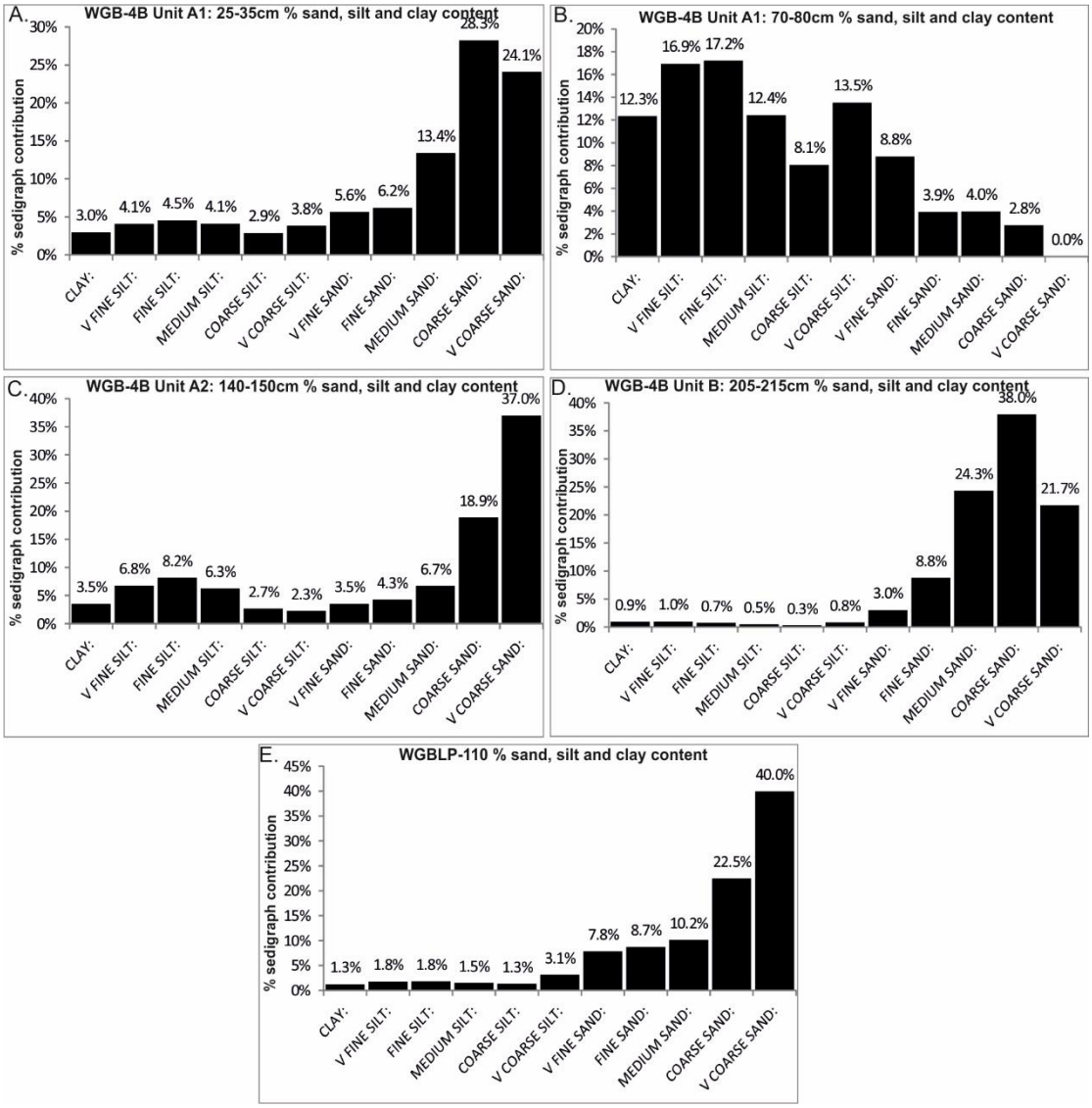

Figure 6.34 – % sand, silt and clay content derived from Coulter grain size analysis on samples collected from outcrop WGB-4B.

All concentration related magnetic proxies fall at 70-80 cm (Fig. 6.35a) compared to 25-35 cm, but ferrimagnetic granulometry is identical (Fig. 6.35b) and of the mineralogical proxies, S_{300} is very slightly lower (Fig. 6.35c).

Table 6.7 – % loss on ignition and bromine (ppm) data for sampled horizons at WGB-4B.

Unit	Height (cm)	Loss on ignition (%)	Bromine (ppm)
A1	25-35	0.97	1.3
A1	70-80	0.93	4.3
A2	140-150	1.83	11.7
B	205-215	1.37	5.1
WGBLP110	-	-	5.8

A2 consist of a single massive, bed of moderately sorted sands with a small subordinate clay/silt fraction (Fig. 6.34c), the colour of which changes to 10YR 6/2 at the top (160-185 cm) as was the case at WGB-4A (Fig. 6.27 and 6.30). Bromine concentration (11.7 ppm – Table 6.7) compares well with that reported at WGB-4A (12.4 ppm – Table 6.6). Similar to the top of WGB-4A unit A, this unit exhibits a spike in concentration-based and granulometric magnetic properties (Fig. 6.35a and b), with S_{300} values intermediate (3.4%) between those recorded in the middle and top of WGB-4A unit A (Fig. 6.31c and 6.35c).

Unit B, unlike at WGB-4A, consists of very thinly horizontally bedded sands, which exhibit increased sorting (84% medium to very coarse sand – Fig. 6.34c). Rilling of this surface set further back from the channel has reworked this surface material at WGBLP-110 resulting in higher concentrations of coarse to very coarse sand (Fig. 6.34e). Bromine values are identical (Table 6.7) and compare closely with the 6.4 ppm value obtained at WGB-4A (Table 6.6). Concentration related magnetic properties for unit B are higher than those obtained at WGB-4A unit B, whilst the granulometric proxies are nearly identical (Fig. 6.31, 6.35a and b) and the S values smaller (Fig. 6.31 and 6.35c). Interestingly, sampled WGBLP-110 compares better with WGB-4A in terms of concentration related values (Fig. 6.31 and 6.35a).

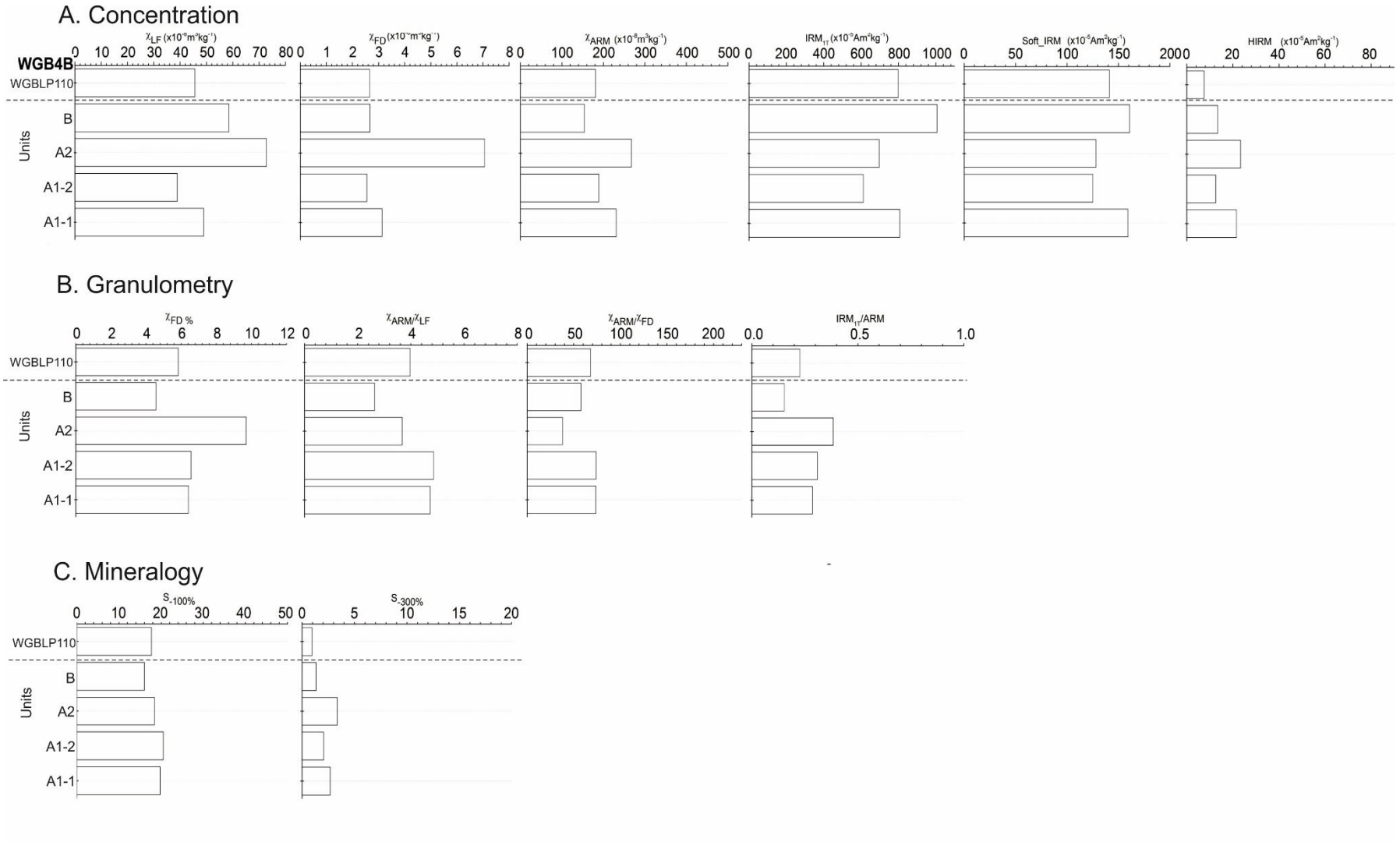

Figure 6.35 – mineral magnetic parameters from outcrop WGB-4B.

6.5b: WGB-4 interpretation

i. WGB-4A

The horizontally bedded sands are interpreted as overbank deposits in association with a channel system. The fine calibre of this sediment compared to the upstream palaeofan is attributed to the abrupt change in valley morphology from a confined (0.1 km) sandstone slope (WGB-1 and 2) to a relatively broad, alluvial plain (0.4 km). Bromine values >10 ppm at both sampled horizons indicates relatively high organic matter content compared to the haematite rich palaeofan soils analysed upstream. The magnetic proxies indicate a similar haematite component for 120-130 cm, corroborated by the relatively rubified soil compared to the top of the unit. Concentration-related proxies are similar to WGB-3 unit B2 indicating, in concert with haematite, a relatively large ferrimagnetic component.

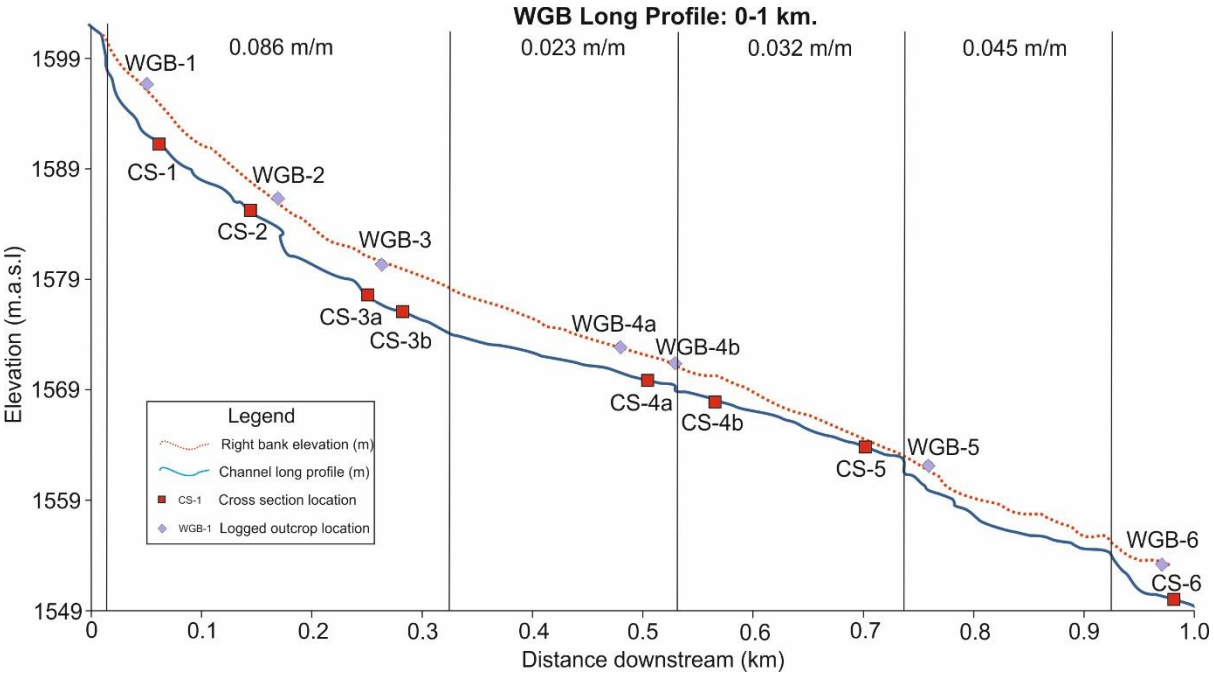

Figure 6.36 – valley long profile segment (0-1 km) showing changes in gradient for: a) the reach mantled by the palaeofan (0 – 0.32 km), b) the wide, relatively flat alluvial plain (0.32 – 0.53 km) (note reach is delimited at 0.53 km by minor knickpoint through mudstone), c) steepening reach as contemporary channel erodes through dolerite on approach to d) major knickpoint through dolerite (1 m) upstream of WGB-5.

This palaeofan would have been the main supplier of sediment to the valley floor though it appears only fine sediment (i.e. sand or less) was connected to WGB-4A due to the wider valley (up to 300 m). Compared to the valley floor mantled by the palaeofan (0-0.32 km), gradient from 0.32 – 0.53 km is also relatively low (0.086 m/m and 0.023 m/m respectively – Fig. 6.36).

The gradational transition to a greyer hue (10YR 6/2) at the top of the unit is interpreted as a palaeogeomorphic surface. Unlike the underlying haematite soil (120-130 cm), this grey horizon is characterised by a distinct ferrimagnetic signature with susceptibility exceeding that of other documented soils thus far at Wilgerbosch (χ_{LF} = 69). The high χ_{FD}% and $\chi_{ARM/IRM1T}$ values attest to high concentrations of SP/SD grains. Such enhancement is common for soil surfaces (Maher et al., 1988). Though the drivers of magnetic enhancement are still contested, Torrent et al., (2006) have suggested the paragenetic formation of magnetite and haematite associated with progressive oxidising/reducing conditions. The grain size characteristics of this ferrimagnetic assemblage closely resemble that of WGB-3 unit C (see section 6.4b). This indicates two things: 1) sediment supply from the palaeofan by a connecting channel and 2) that the top of these units form a continuous palaeogeomorphic surface. This is because soil properties and formation are controlled by both the host substrate and time (Jenny, 1941).

The capping sandy gravels are interpreted as gully rather than overbank deposits. The inversely graded nature of the sediments is comparable with marginal channel deposits located in the Wilgerbosch main channel (see ch.4.4) with emplacement under bankfull discharge. The planar non-parallel cross beds are interpreted as dunes. In contrast to unit A, this sediment package exhibits little if any pedogenic overprinting. The evidence is that the headwater fan (WGB-1 – 3) did not supply these sandy gravels. Rather, the palaeochannel (Fig. 6.29b) from the slopes to the south-east provided the supply, confirmed in the sharp, erosional contact into the underlying palaeosol (Fig. 6.29a). Furthermore, whilst χ_{LF} compares with WGB-1, the total concentration of remanence carrying ferrimagnets at WGB-4 unit B is much higher and, crucially, carried by predominantly MD rather than SD grains as determined from the extremely low $\chi_{ARM/IRM1T}$ (0.2). Whilst χ_{FD}% at WGB-4 is still moderate, it is much lower than WGB-1. This further attests to a lithogenic magnetite origin inherited from a different source to that of the upper fan.

ii. WGB-4B

The deposits at WGB-4B form part of the same terrace sequence, with some subtle shifts in depositional environment indicated. Instead of floodplain (WGB-4A), the basal gravels here indicate a channel bar with cross beds representing accretion

faces. The up-unit reduction in matrix grain size is consistent with bar aggradation and flow recession. Sand and silt grains appear to be interstitial, deposited during recessional phases of flow when the bar was submerged. The wide valley would have facilitated aggradation by lateral channel movement, a supposition supported by the preservation of lateral accretion faces. As a result, palaeo-channel migration and diversion of the thalweg away from the palaeo-bar permitted it to remain stable (i.e. not reworked). Increased bromine values indicate high organic matter content relative to the base of unit A1 probably relating to vegetation colonisation of the bar after formation and incipient soil development. This may account for the change in colour (7.5YR 7/3). The magnetic properties of the top and bottom of the palaeo-bar exhibit a predominantly coarse-grained ferrimagnetic signature ($\chi_{ARM/IRM1T}$ = 0.25 – 0.3), but χ_{FD}% (6%) indicates a distinct pedogenic SP component. The top of the palaeo-bar, where a minor phase of soil development is postulated indicates lower overall concentrations of both ferrimagnetic and anti-ferromagnetic minerals compared to below on the basis of Soft_IRM and HIRM. The fact that there is no spike in χ_{FD}% and S values confirms that soil development was minimal prior to burial of the bar by the overlying sands (unit A2).

This sandy unit, though lacking clear bedding, is interpreted as floodplain deposits similar to WGB-4A. High bromine content attests to former vegetation on this floodplain, which indicates that the local fluvial environment was stable enough to permit formation and slow aggradation. Similar to WGB-4A (170-180 cm), susceptibility is dominated by a strong ferrimagnetic signature with very high concentrations of SP grains (χ_{FD}%), but a more modest contribution to overall remanence by SD carriers ($\chi_{ARM/IRM1T}$ = 0.4). Haematite content peaks at this location compared to subunit A1 (S_{300} = 3.4%) – which compares more closely to 170-180 cm height at WGB-4A. Crucially, the same geomorphic surface reported at WGB-4A occurs here, manifesting as a greyer surface horizon unconformably buried by sand (unit B). In this case, the capping sands represent strictly floodplain deposits, again exhibiting very minimal pedogenic overprinting, confirmed in the very low values of ($\chi_{ARM/IRM1T}$ = 0.15).

iii. Summary of WGB-1 – WGB-4.

From the available lithostratigraphic and magnetostratigraphic evidence, there appear to have been several alternating phases of fan progradation and retrogradation (WGB-1–3). This palaeofan acted as the primary supplier of sediment to the alluvial plain (WGB-4 unit A).

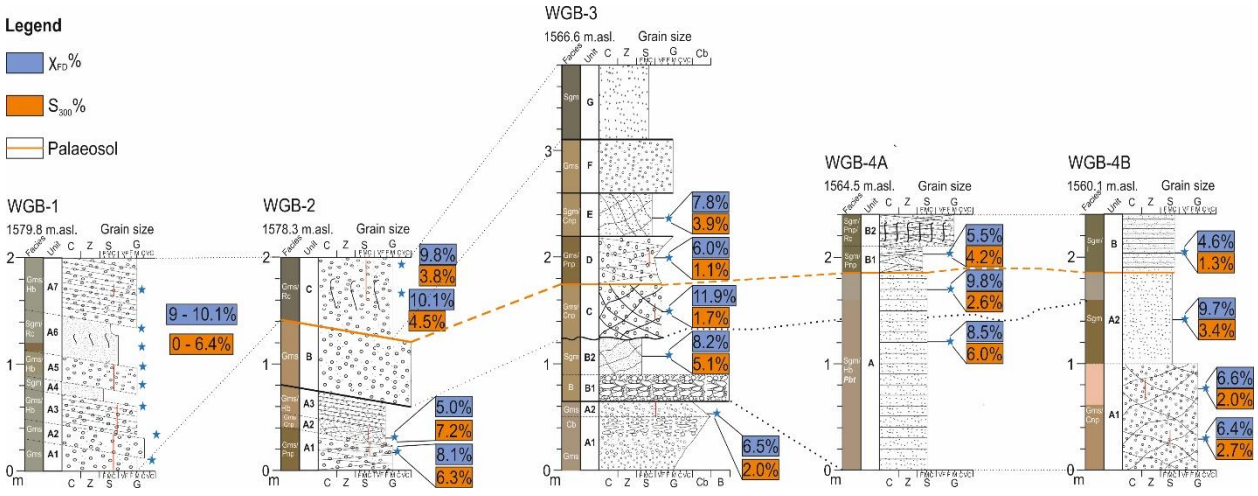

Figure 6.37 – sediment logs WGB-2 to 4b showing preliminary lithological and magnetostratigraphic relations. Note: 1) the secondary dashed black lines to indicate concordance between haematite concentration (S_{300}%) and intensity of ferrimagnetic weathering (χ_{FD}%) and 2) dashed orange lines to indicate palaeogeomorphic surface.

Figure 6.37 and 6.38 demonstrate the continuity of the haematite rich soils (WGB-2 unit A; WGB-3 unit B; WGB-4A and 4B unit A) down the valley, which are overlain by a distinct SP/SD magnetite enriched horizon which occurs below an unconformity and which likely represented a former land-surface when palaeofan and associated gully outlet sedimentation halted. This unconformity appears to extend all the way from these upper slopes (WGB-2) to the alluvial plain (WGB-4- see Fig. 6.38b – orange dashed line). Reactivation of fan sedimentation represented by the sediments of WGB-1 extends as far as WGB-3 (Fig. 6.37 and 6.38a) and did not supply the alluvial plain at WGB-4. Rather, these channel and floodplain deposits (WGB-4 unit B) were sourced from the palaeochannels draining hillslopes to the southeast (Fig. 6.38c).

The episodic cut and fill character of the palaeofan is attributed to the steep gradient of the upper sandstone slope, having primed this area to more frequent erosion by gullying. It follows that such regular cut and fill phases are absent in fills mantling the valley floor due to attenuation of flow by the broad valley.

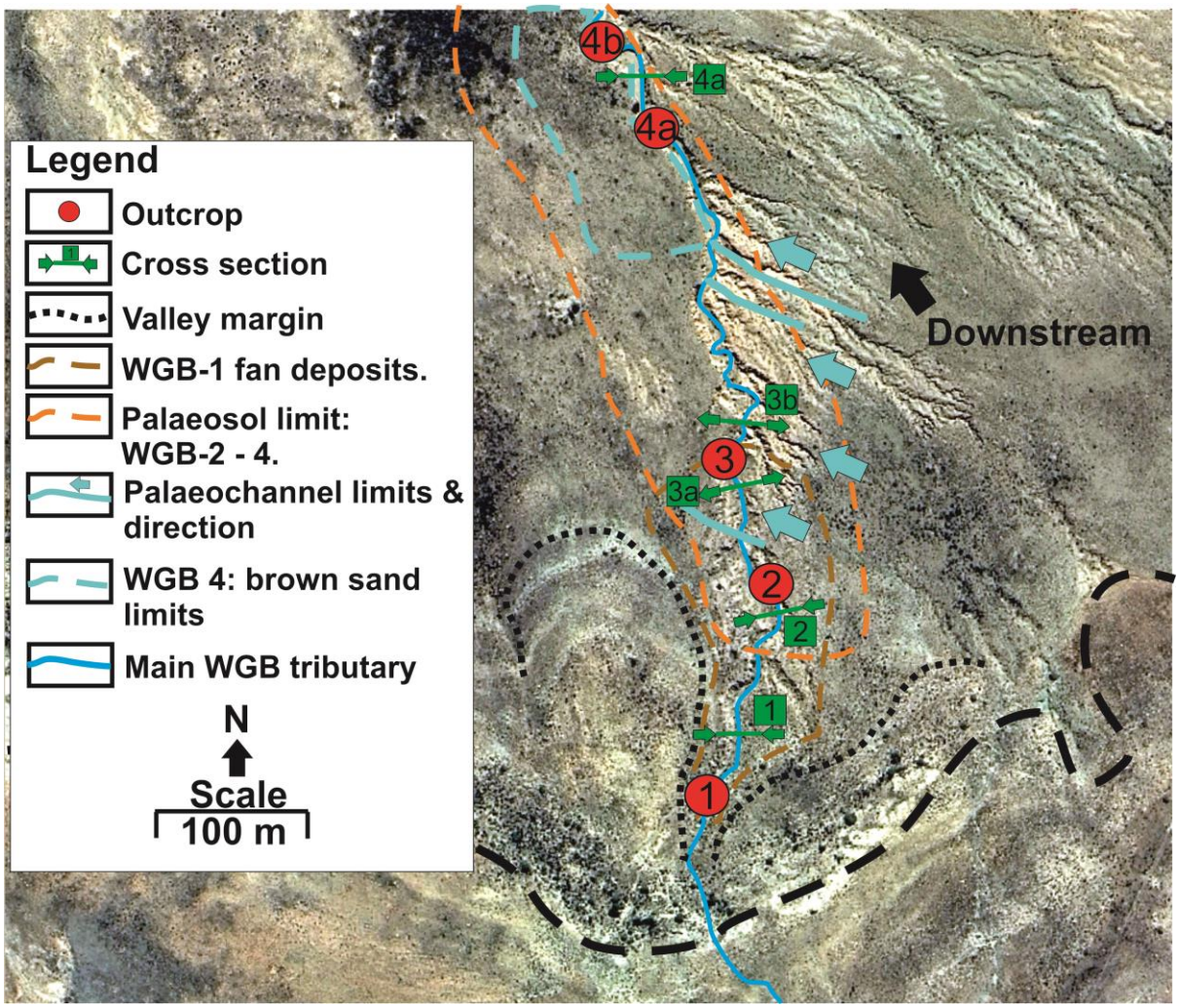

Figure 6.38 – digitised aerial photograph showing surveyed spatial limits of primary deposits (WGB-1 – 4). a) The brown line indicates limits of most recent fan deposits (WGB-1). b) The orange line represents the palaeogeomorphic surface outlined in Fig. 6.32, which is represented at logs WGB-2–4. c) Infilled palaeochannels (light blue line) sourced from the slopes to the south east. Note the dashed blue line linked to the northern-most palaeochannel which signifies the brown sands identified at WGB-4 (unit B).

Although ambiguity exists in relation to clarifying the extent to which the magnetic proxies for pedogenic magnetite and haematite represent in situ pedogenesis versus inheritance from eroding soil sources, in concert with logged lithostratigraphic boundaries and notation of soil features, there is strong evidence for a phase of geomorphic stability in this upper part of the catchment. However, downstream of the fan (WGB-3), the abrupt loss of valley confinement resulted in the accumulation of fine sediment (WGB-4) due to flow attenuation. As a result, aggradation and subsequent soil development could be a local autogenic response controlled by valley morphology (loss of confinement triggers backfilling causing channel upstream to aggrade) rather than an allogenic driver such as climate (Schumm, 1977).

6.6a: WGB-5 analysis

Log WGB-5 was recorded from a 2 m exposure on the right hand side of the channel approximately 760 m downstream of the pediment (Fig. 6.2, 6.3, 6.39 and 6.40). The sediments analysed occur as a wedge against an eroding dolerite slope (Fig. 6.41).

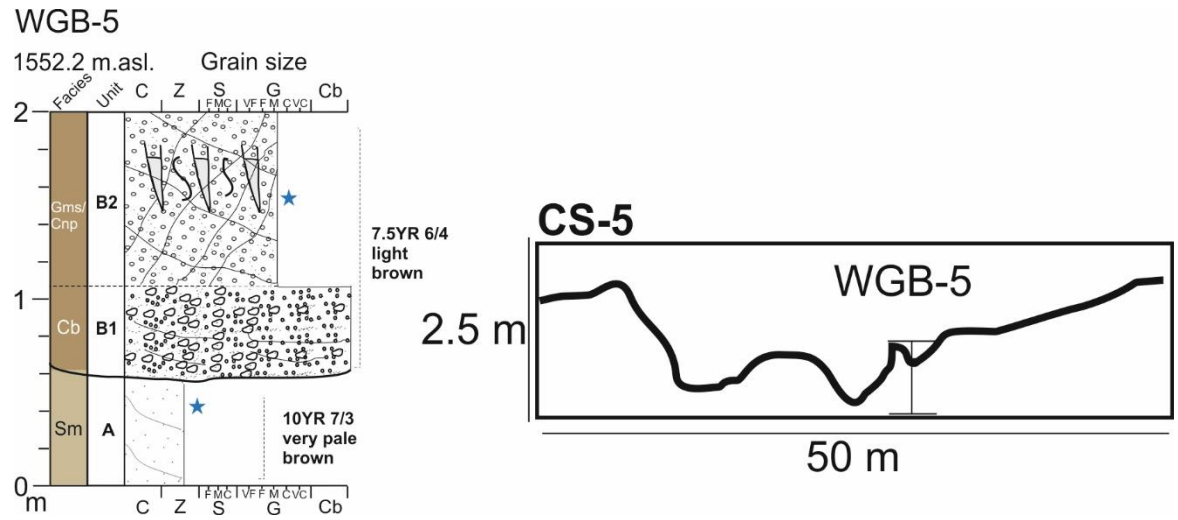

Figure 6.39 – sedimentary log of outcrop WGB-5 and cross section.

The base of the succession is characterised by very pale brown (10YR 7/3) silty sands which directly overlie dolerite bedrock (Fig. 6.42b). A repeat sample taken from the same horizon just upstream reveals a slightly coarser texture (Fig. 6.42a) and higher bromine values (Table 6.8). Both samples exhibit extremely low concentration-related magnetic proxies (Fig. 6.43a) and strikingly high S values (37.5 and 15.5% of applied remanence at -300 and -100 respectively unreversed- Fig. 6.43c).

Figure 6.40 – photograph of outcrop WGB-5.

Figure 6.41 – photograph showing junction between sediments (WGB-5) and eroding dolerite.

A sharp, undulating bed contact separates these silts from the very poorly sorted cobbles and coarse gravels above (unit B1) which exhibit a marked colour change (7.5YR 6/4 light brown). This coarse subunit grades to matrix-supported medium gravels which exhibit curved, non-parallel bedding (B2). The matrix is relatively well sorted, consisting of coarse to very-coarse sand (73.4% - Fig. 6.42c). Root channels and dessication cracks are present. The dessication cracks are infilled with silt and a 'whitish' deposit. Compared to unit A, bromine and calcium peak in this unit, yet sodium is lowest (Table 6.8). Magnetic susceptibility is much higher χ_{LF} (37) and the S values are much lower compared to unit A (Fig. 6.43c).

Table 6.8 – % loss on ignition, bromine, calcium and sodium (ppm) data for sampled horizons at WGB-5.

Unit	Height (cm)	Loss on ignition (%)	Bromine (ppm)	Calcium (ppm)	Sodium (ppm)
WGBLP116	25-35	1.15	6.3	10,690	5,800
A	45-55	1.60	0.8	18,260	8,700
B2	160-170	2.82	3.8	20,830	5,400

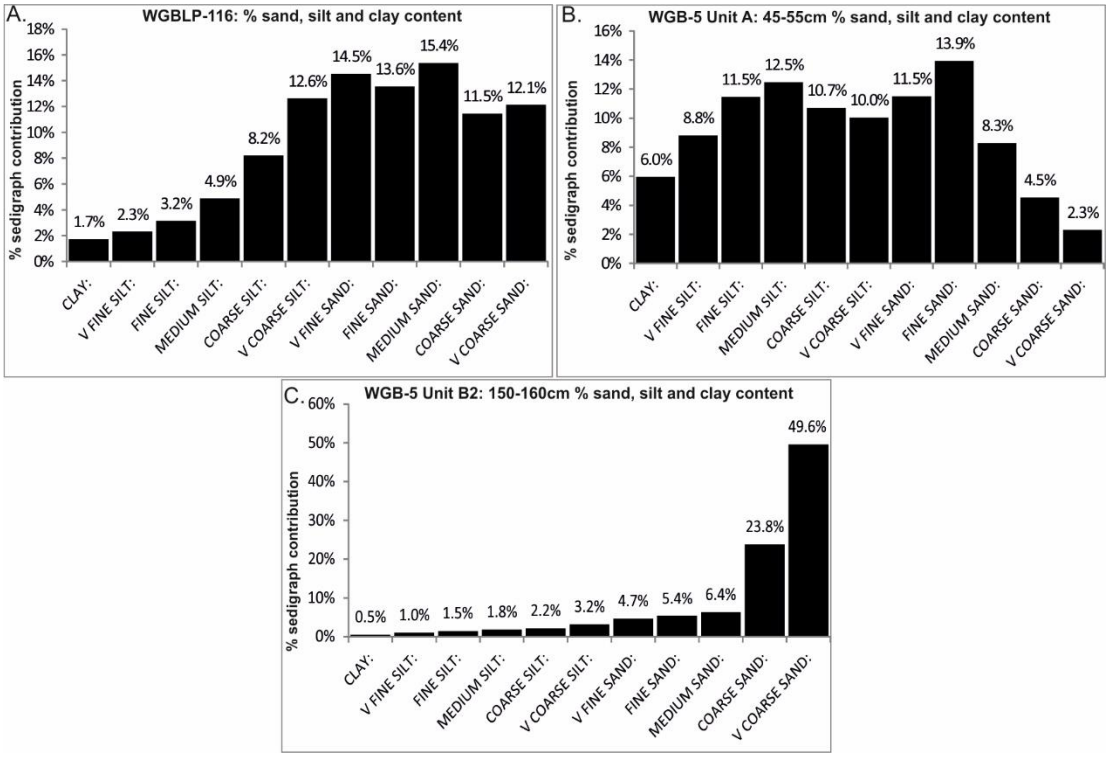

Figure 6.42 – % sand, silt and clay content derived from Coulter grain size analysis on samples collected from outcrop WGB-5.

6.6b: WGB-5: interpretation

The basal sandy silts indicate low energy fluvial deposition. The grey colouration attests to conditions of poor drainage. The magnetic properties of this unit indicate paramagnetism consistent with other gleyed environments reported in the last chapter. The ferrimagnetic grain size signature is predominantly multi-domain and probably reflects the dissolution of SP/SD pedogenic magnetite. The extremely strong anti-ferromagnetic signature (S values) for both samples reflect goethite formation. This is the first occurrence of strictly gleyed, magnetically depleted soils at Wilgerbosch and, notably, corresponds to the point at which the valley begins to cross a dolerite sill (Fig. 6.44) with an associated seepage zone. Furthermore, these soils are inset within the haematite soils upstream (WGB-4) and localised to a 250 m stretch exposed in the right bank (Fig. 6.44). The depositional environment is analogous to the infilling modern wetlands reported in Chapter 4 (Table 4.3: Analogue 1).

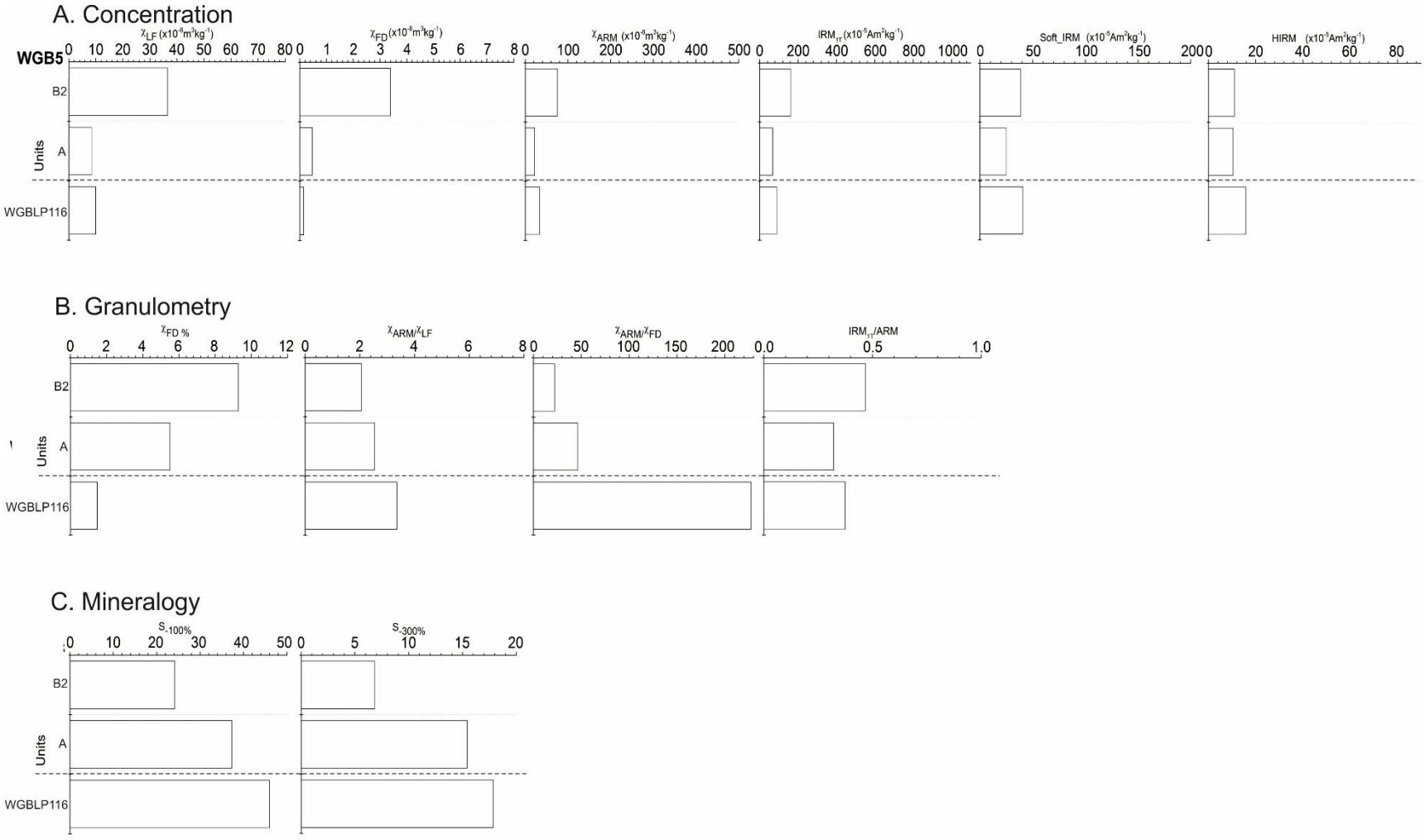

Figure 6.43 – mineral magnetic parameters from outcrop WGB-5.

The boundary between unit A and B signifies an unconformity. Whilst the angle of dip perpendicular to the modern channel of this bed contact is unknown, the cross section morphology clearly indicates a distinct surface dipping toward the contemporary gully (Fig. 6.39). This signifies that it was sourced from the east. The overlying sediments are a palaeochannel deposit. In spite of a local doleritic source, magnetic susceptibility is extremely modest compared to Africanders Kloof and must reflect dilution by sandstone as well as diamagnetism by calcite, as confirmed in the high calcium values (Table 6.8) and probable ferrimagnetic dissolution due to poor drainage. Low sodium content means this whitish deposit is not halite. Rather, calcium values of 20830 ppm indicate that it is $CaCO_3$.

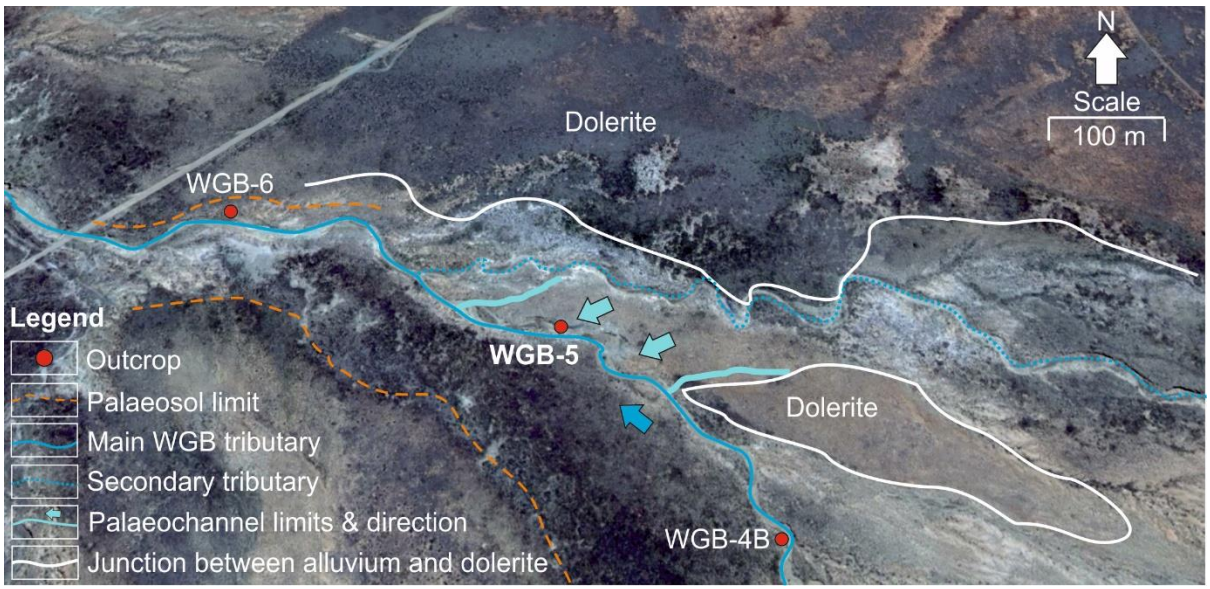

Figure 6.44 – Google Earth imagery of Wilgerbosch upper valley where the tributary crosses a dolerite sill. Note 1) The approximate limits of the geomorphic surface (orange line) noted at WGB-3 and 4, 2) The extent of the palaeochannel and abrupt junction with the subaerially exposed sill, 3) The switch in channel configuration from straight, low sinuosity, wide (4-5 m) gullies to highly sinuous, poorly defined channels (see thin blue dashed line) when crossing the sill on approach to the confluence with the main tributary (solid, thick blue line).

Although not analysed in detail, the characteristics of the calcium carbonate overprinting unit B2 are ‘pedogenic’ rather than ‘rhizogenic’ as discussed in the previous chapter. The ‘powdery’ texture of the $CaCO_3$ and its discontinuous nature implies it is very immature. The relatively rubified colour of this unit implies that haematite is likely to contribute to unreversed remanence more than goethite. Magnetic grain size is still predominantly MD, but with a definitive increase in the proportions of SD carrying ferrimagnets ($\chi_{ARM/IRM1T}$). Previous experience of a strong lithogenic bias in magnetic signatures derived from dolerite host sediment residing in

the coarse silt grade could be reducing this ferrimagnetic weathering signature, however. In any case, the high S values and secondary carbonate accumulations attest to prolonged weathering relative to the brown sands opposite (WGB-4B) and are clearly stratigraphically 'older'.

6.7a: WGB-6: analysis

Log WGB-6 was recorded from a 3.3 m exposure on the right hand side of the channel approximately 975 m downstream of the pediment (Fig. 6.3, 6.45 and 6.46).

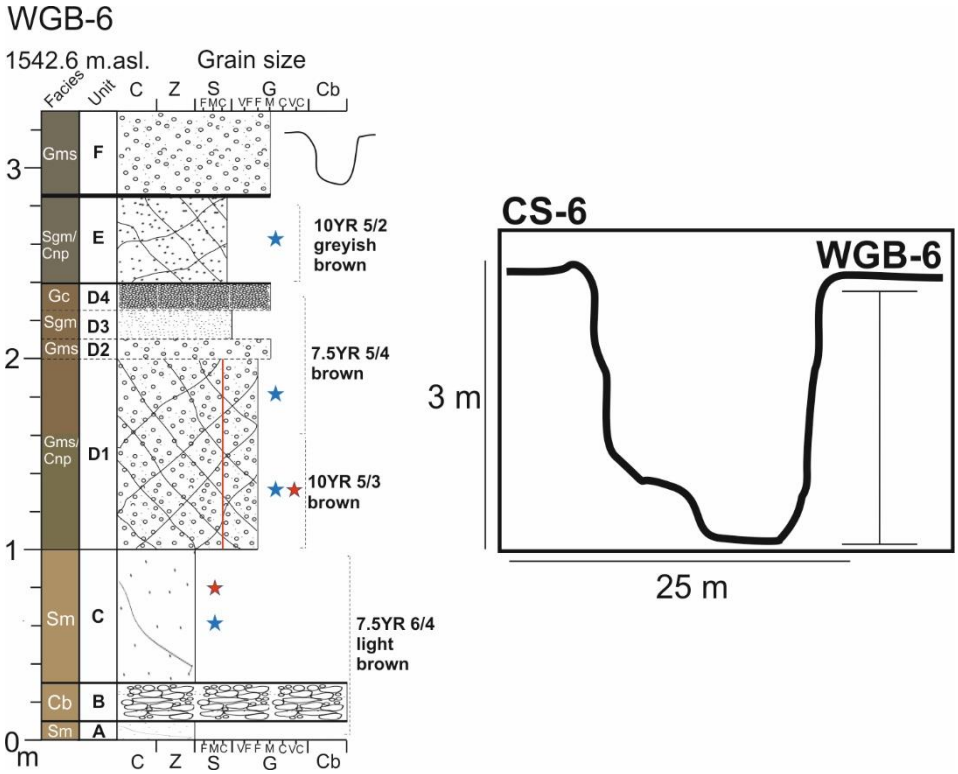

Figure 6.45 – sedimentary log of outcrop WGB-6 and cross section.

The base of the succession is characterised by two units of massive silty sands (A and C – see Fig. 6.47a) separated by a single bed of clast-supported cobbles and gravels (unit B). The sediments exhibit a weakly developed crumb structure. χ_{ARM} and IRM_{1T} magnetic parameters peak in unit C compared to units above whilst the granulometric proxies are typically very similar compared to other units (Fig. 6.48a and b).

Unit D sharply overlies C and consists of a thick unit of matrix-supported fine gravels with curved non-parallel bedding (C1) and then alternating thin beds of gravel and

sand (D2-D4). The matrix of D1 is better sorted at the base (125-135 cm) where 88.2% of the sedigraph is dominated by coarse to very coarse sand (Fig 6.47b), compared to the top (180-190 cm) which shows higher silt and clay (11.9% - Fig. 6.47c). Bromine content increases to 7.9 ppm at 180-190 cm (Table 6.9).

Figure 6.46 – photograph of outcrop WGB-6.

Table 6.9 – % loss on ignition and bromine (ppm) data for sampled horizons at WGB-6.

Unit	Height (cm)	Loss on ignition (%)	Bromine (ppm)
C	55-65	1.34	1.6
D1	125-135	1.39	4.1
D1	180-190	1.83	7.9
E	260-270	-	14.3

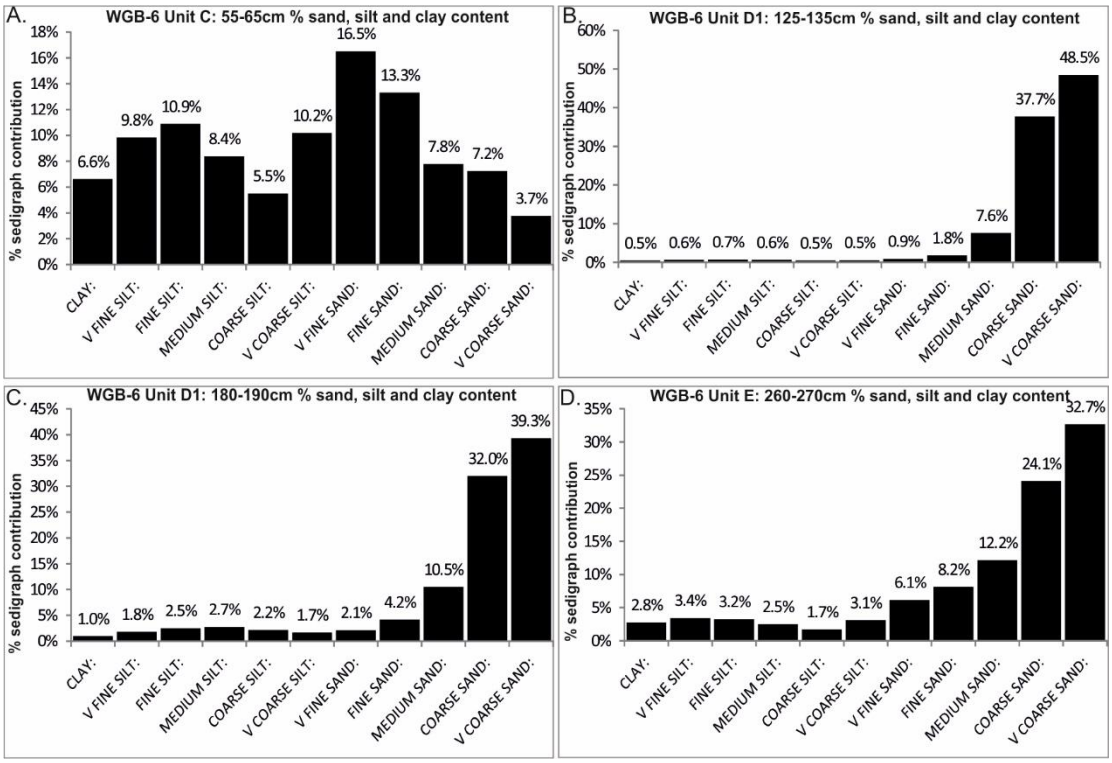

Figure 6.47 – % sand, silt and clay content derived from Coulter grain size analysis on samples collected from outcrop WGB-5.

Total magnetic susceptibility is stronger at the top of unit D1 (χ_{LF} = 64) as is χ_{FD}% (9) and $\chi_{ARM/IRM1T}$ (0.4 – Fig. 6.48b). S_{-300}% is also relatively high with 93.5% of the applied remanence reversed at -300mT (Fig. 6.48c).

Unit E sharply overlies D, exhibiting a colour change to 10YR 5/2 greyish brown. The facies consist of poorly sorted sandy silts (Fig. 6.47d) that exhibit curved non-parallel bedding. Bromine peaks (14.3 ppm) for this unit (Table 6.9). Concentration related magnetic parameters are relatively low (Fig. 6.48a). χ_{FD}% is still high (7.9%) and is $\chi_{ARM/IRM1T}$ highest for this unit (0.49- Fig. 6.48b). S_{100}% is highest for this unit with 23.5% of the applied remanence unreversed at -100mT (Fig. 6.48c).

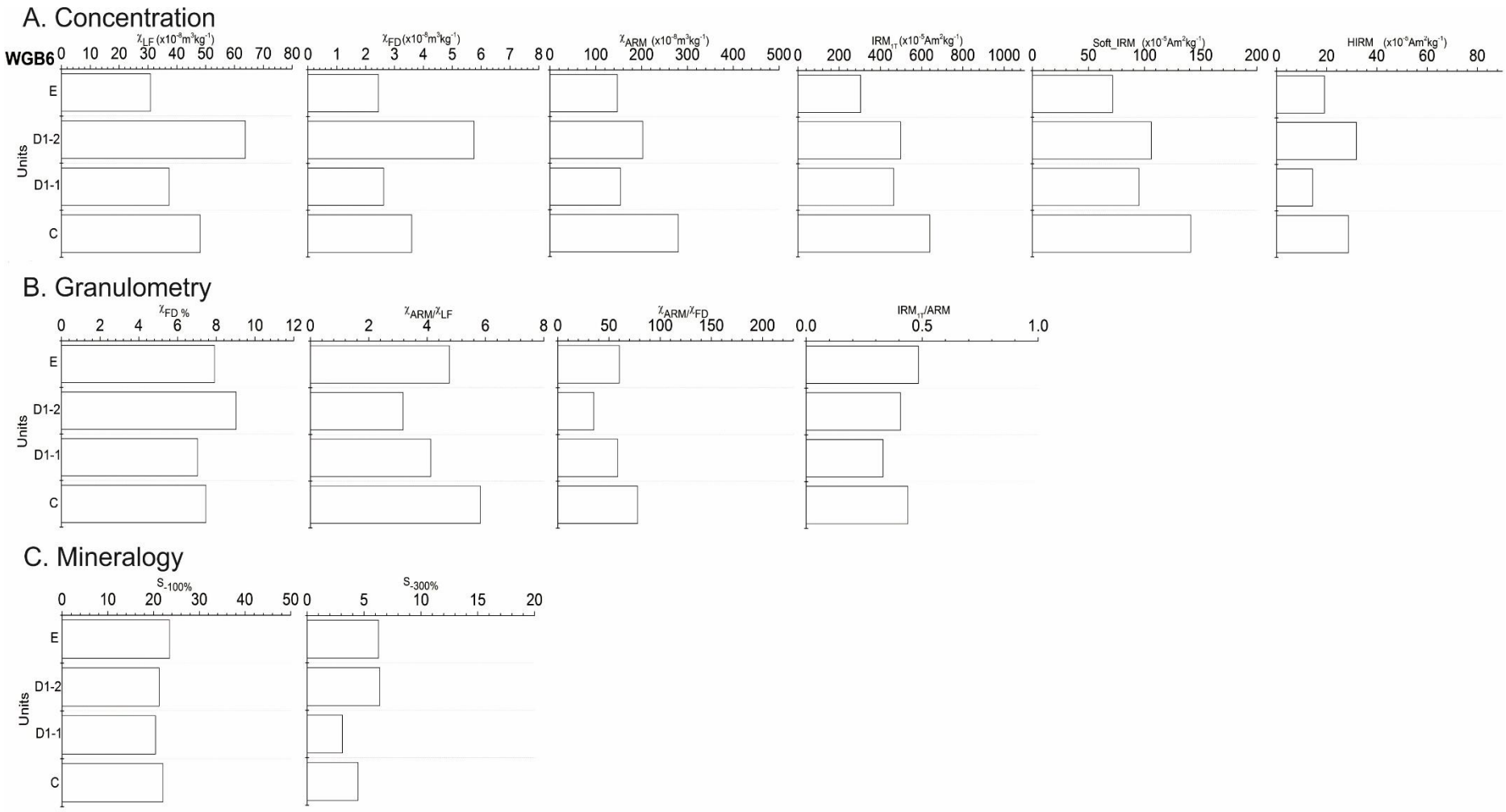

Figure 6.48 – mineral magnetic parameters for samples collected from WGB-6

6.7b: WGB-6: interpretation

The basal silty sands indicate low energy fluvial sedimentation. These deposits must either be floodplain or channel. In order to be floodplain, the former channel would have had to be at a lower elevation than the present one. This is unlikely as the present channel is very close to dolerite bedrock and there is no evidence that the channel has incised deeply into it. As discussed earlier, a migrating single thread channel may produce alternating fine and coarse deposits in this fashion, particularly for channels with comparatively unrestricted lateral mobility. These sediments are characterised by low-moderate concentrations of SP-sized ferrimagnetic minerals and overprinted by a distinct AF signature. The poorly-drained texture of this unit in concert with its proximity to bedrock would have likely facilitated goethite production, though not as intense as at WGB-5. The enhanced ferrimagnetic signature compared to above (unit D) in concert with the depleted clay content could signify inherited illuvial accumulations of iron oxides.

The high angle cross-bedded gravels (unit D) indicate channel deposits. The poor preservation of the bed structures prevents definitive inference of fluvial environment, but could be representative of either 1) dunes formed in the upper-flow regime or 2) channel bar migration. Organic matter content increases toward the top of this unit (180-190 cm) reflected in bromine values of 7.9 ppm. Unit D1-1 (125-135 cm) possesses a weak, coarse-grained ferrimagnetic signature. The pale colour at the base of this unit (10YR 5/3) attests to probable leaching as mentioned before, and appears not to be related to production of goethite as S_{300} is lower than unit C. Above (unit D1-2 – 180-190 cm), ferrimagnetic mineral concentration is much higher, with concomitant increases in SP/SD grain contributions. This magnetic signature is comparable with that exhibited by the palaeosol reported at WGB-4, though slightly coarser grained. The relatively rubified nature of the soil relative to 125-135 cm in concert with the higher S_{300}% (6.5) probably reflects haematite. Both the mapped continuity of these deposits and the similitude in magnetic characteristics with the red palaeosol at WGB-4 implies this is the same surface as shown in figure 6.44.

The nature of the sharp bed contact separating units D from E in concert with abrupt change in colour implies that this is a major discontinuity (Fig. 6.49).

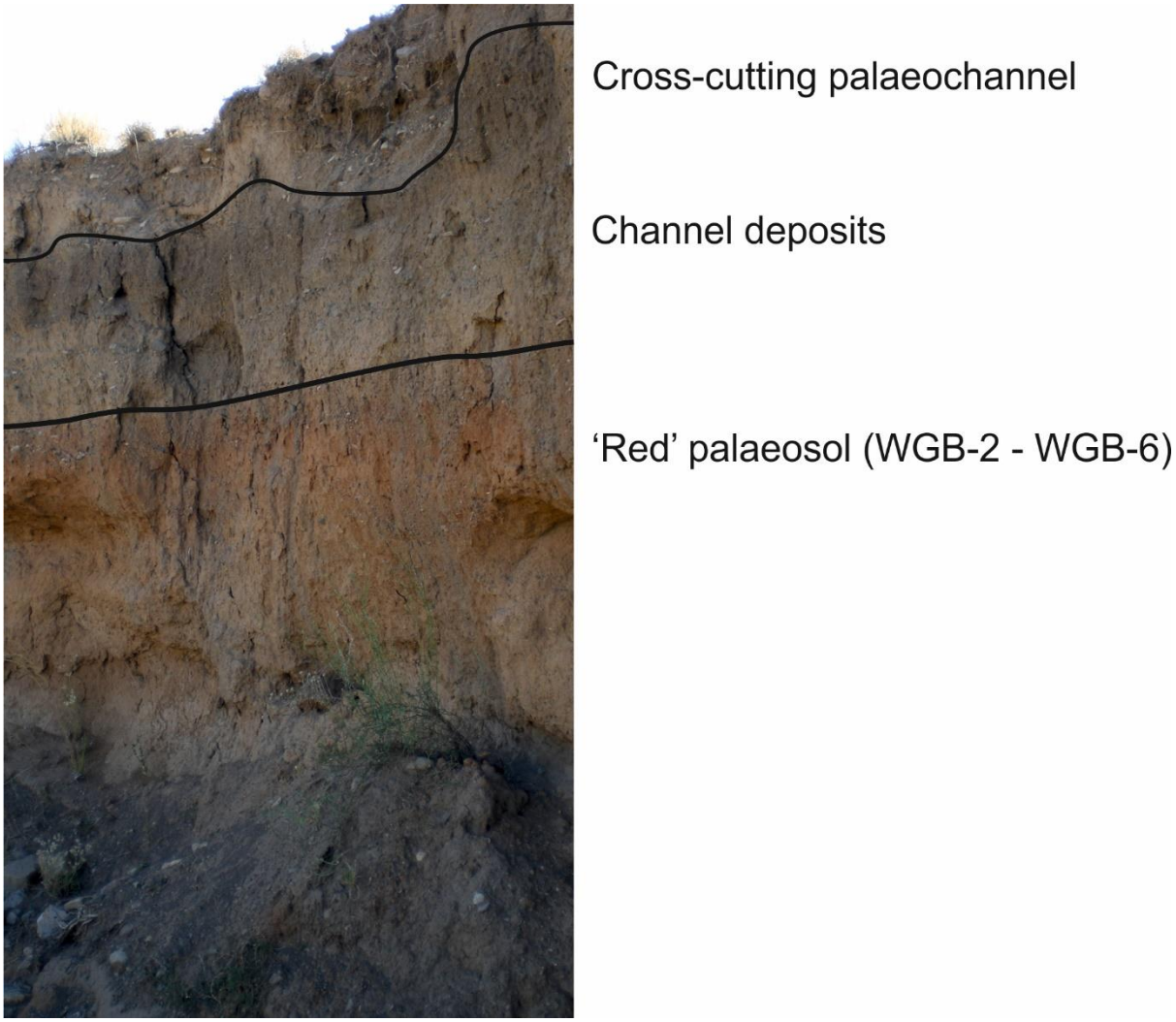

Figure 6.49 – photograph showing abrupt junction between rubified palaeosol (units A-D) and overlying 'grey' fill (unit E) which has been incised again.

The cross-bedded sands of unit E imply formation of high angle dunes in a palaeochannel bed. The grey colouration in concert with high bromine values (14.3 ppm - Table 6.9), indicates that after deposition, the channel bed was colonised and stabilised by vegetation. This is supported further by the relatively fine-grained ferrimagnetic signature of the sediment, implying a distinct pedogenic SP/SD contribution. The comparably high S_{300} with unit D (180-190 cm), in light of the greyer colouration may reflect higher proportions of goethite, formed due to the less well-drained texture of this unit. This lithostratigraphic unit is at the same relative elevation as WGB-7 unit D discussed in the next section.

The overlying gravelly sands (unit F) are part of a palaeochannel which cross-cuts the channel deposits of unit E (see Fig. 6.45). The evidence is that this palaeochannel drained south-east, as the right bank slopes away from the contemporary channel (see CS-6 – Fig. 6.45). These deposits are relatively unweathered, with weakly developed granular structure and are at the same elevation as WGB-7 unit E discussed in next section.

6.8a: WGB-7: analysis

Log WGB-7 was recorded from a 4 m exposure on the left hand side of the channel approximately 1095 m downstream from the pediment and 100 m downstream of WGB-6 (Fig. 6.2, 6.3, 6.50 and 6.51). This reach is characterised by deep incision into underlying sandstone bedrock, the modern channel experiencing perennial discharge supplied from a nearby aquifer.

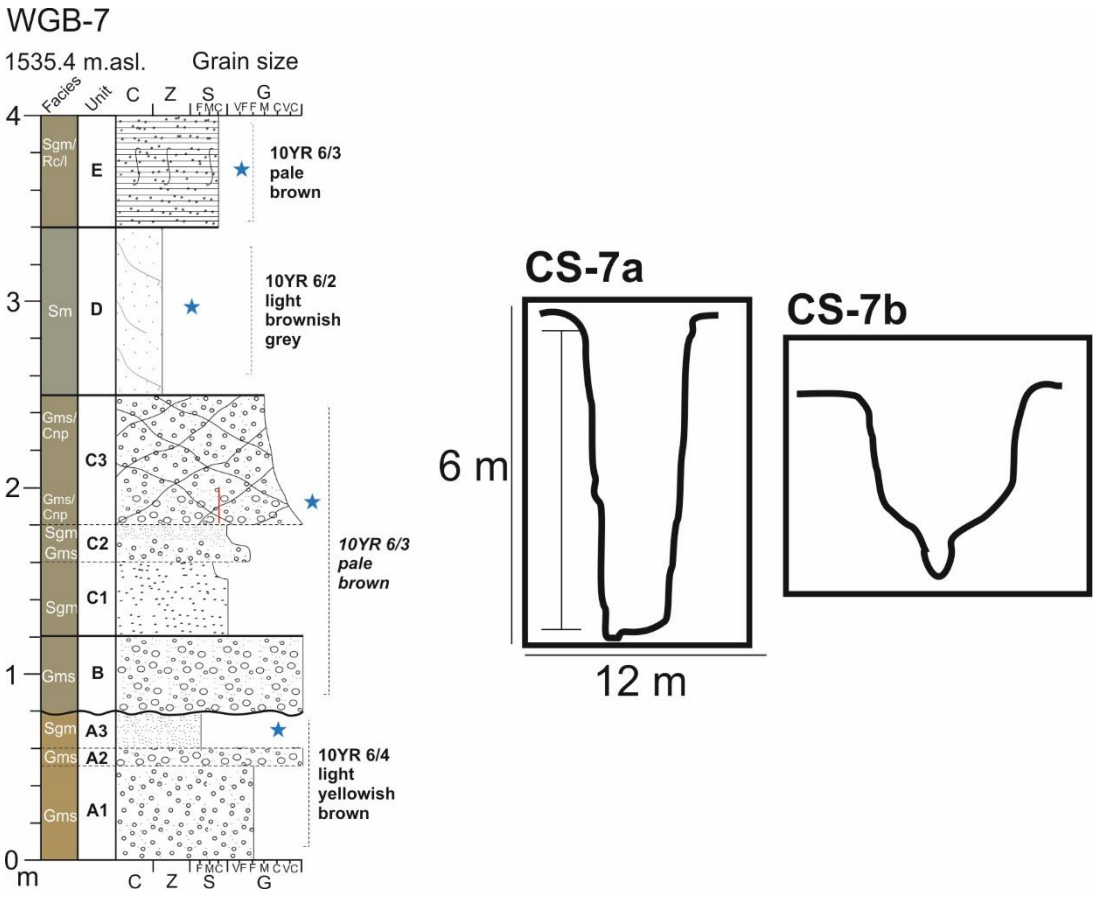

Figure 6.50 – sedimentary log of outcrop WGB-7 and cross sections. Note cross sections 7-A and B are 50 and 350 m downstream of outcrop WGB-7 respectively.

The succession is characterised by matrix-supported gravels (A1) that locally coarsen to very coarse gravels (unit A2) but are then capped by gravel poor, poorly

sorted sandy silts (subunit A3 - Fig. 6.52a) that exhibit low bromine content compared to above. This subunit exhibits the second lowest concentration-related proxy values for this outcrop (Fig. 6.53a). χ_{FD}% and $\chi_{ARM}/_{IRM1T}$ are particularly low relative to above (Fig. 6.53b). Crucially, S_{300}% is relatively small compared to above (Fig. 6.53c).

The sharp, undulating contact dividing units A and B is accompanied by a subtle change in colour to 10YR 6/3 pale brown, the facies becoming predominantly very coarse, matrix-supported gravels.

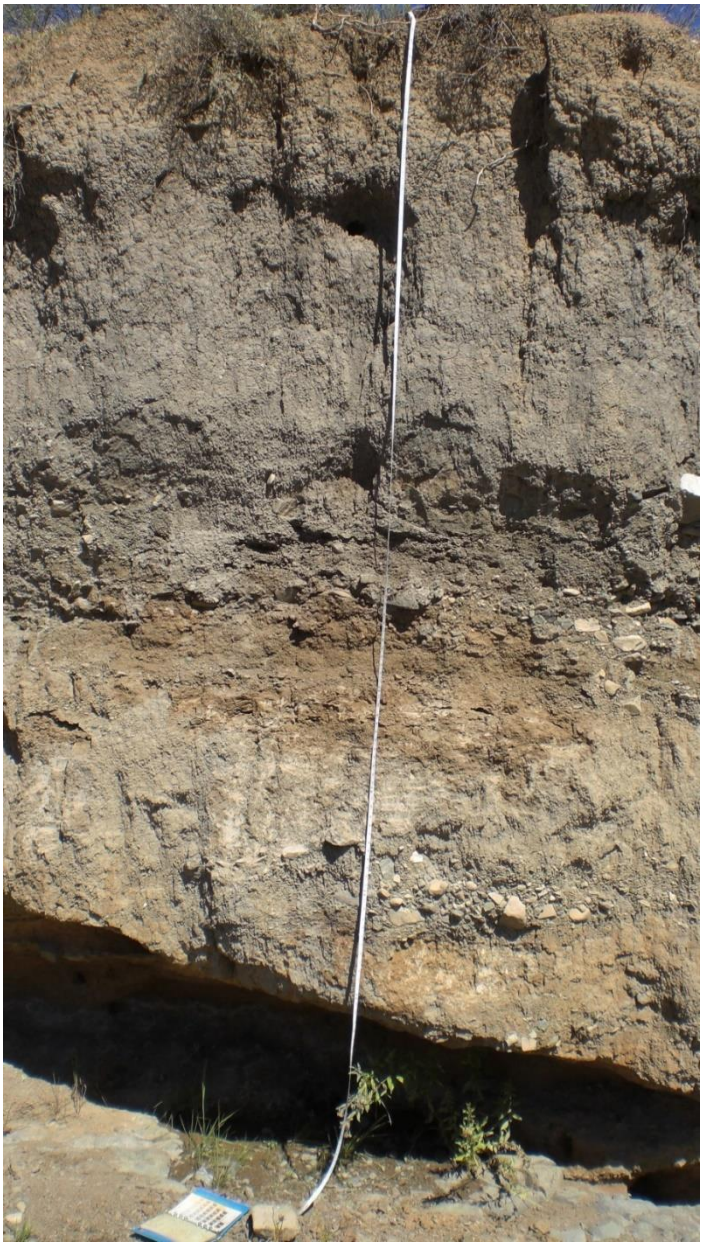

Figure 6.51 – photograph of outcrop WGB-7.

Unit C comprises three distinct subunits which exhibit normal grading. C1 displays a transition from very coarse to medium sands; the base of C2 is characterised by gravels which fine to very-coarse sand and C3 is a much thicker unit of matrix-supported gravel that exhibits low angle curved, non-parallel cross bedding. The matrix of C3 is well sorted: 83.7% coarse to very-coarse sand (Fig. 6.52b). It exhibits slightly higher bromine concentration compared to unit A1 (Table 6.10) and typically higher concentration-related magnetic proxies – except for the IRM_{1T} and Soft_IRM (Fig. 6.53a). Crucially, χ_{FD}% and $\chi_{ARM}/_{IRM1T}$ are relatively high compared to unit A3 (Fig. 6.53b), as is the S_{300}% (Fig. 6.53c).

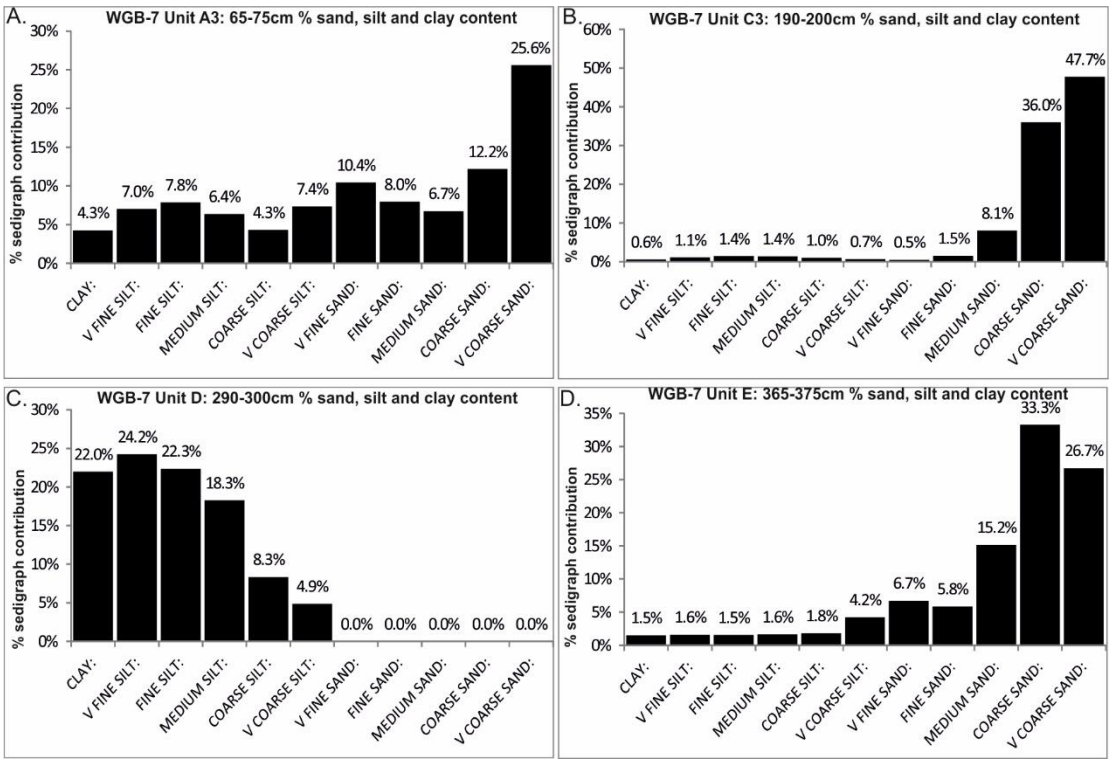

Figure 6.52 – % sand, silt and clay content derived from Coulter grain size analysis on samples collected from outcrop WGB-7.

Table 6.10 – % loss on ignition and bromine (ppm) data for sampled horizons at WGB-7.

Unit	Height (cm)	Loss on ignition (%)	Bromine (ppm)
A3	65-75	1.4	5.1
C3	190-200	1.4	8.7
D	290-300	3.5	11.7
E	365-375	1.5	2.1

Unit D sharply overlies C, exhibiting a greyer colour (10YR 6/2) and crucially, the highest bromine values for this outcrop (Table 6.10). The texture of this unit is silty clay: no sand is present (Fig. 6.52c) and sedimentary structures are absent. This unit is magnetically distinct from the rest of those sampled: All concentration-related proxies are extremely low (Fig 6.53a), whilst with the exception of χ_{FD}%, granulometry proxies are high (Fig. 6.53b). In particular, both S parameters are distinctively high compared to the bracketing units (Fig. 6.53c).

Unit E sharply overlies D, consisting of thickly laminated predominantly coarse to very coarse sands (Fig. 6.52d). LOI% and bromine content is lower than the underlying units (Table 6.10). χ_{ARM}, IRM_{1T} and Soft_IRM peak for this unit and χ_{FD}% and χ_{ARM}/χ_{LF} remain high (Fig. 6.53a and b). Despite higher Soft_IRM, the S_{100}% is comparatively modest compared with unit D with 22% of the applied remanance unreversed at -100mT (Fig. 6.53c).

6.8b: WGB-7 interpretation

The basal gravels (unit A1-A2) are consistent with channel deposits reported elsewhere, with the capping sands reflecting overbank sedimentation (unit A3). The lighter colour of this unit implies probable effects of translocation of iron oxides through groundwater flow. This is because the unit directly overlies sandstone bedrock and is downstream of a seepage zone (see section 6.8). Magnetically, the sediment exhibits a weak ferrimagnetic signature, but this appears to be more related to the grain size of magnetite/maghemite rather than formation of paramagnetic minerals on the basis of the relatively high IRM_{1T} (390), but very low χ_{ARM} (105). This coarse grained (MD) signature likely reflects the dissolution of fine-grained ferrimagnets such that the weaker lithogenic component dominates overall susceptibility. In this case, χ_{FD}% = 4 may be taken as a diluted vestige of former pedogenic intensity, the implication being that this floodplain deposit was exposed at the former landsurface for long enough to allow pedogenesis to overtake aggradation. The S_{-300}%, while low compared to above, probably reflects goethite in this instance, attesting to predominance of reducing rather than oxidising soil conditions. It is unclear the extent to which there was an intermediate phase of haematite formed from pedogenic magnetite/maghemite punctuating reduction to goethite under conditions of high soil moisture content.

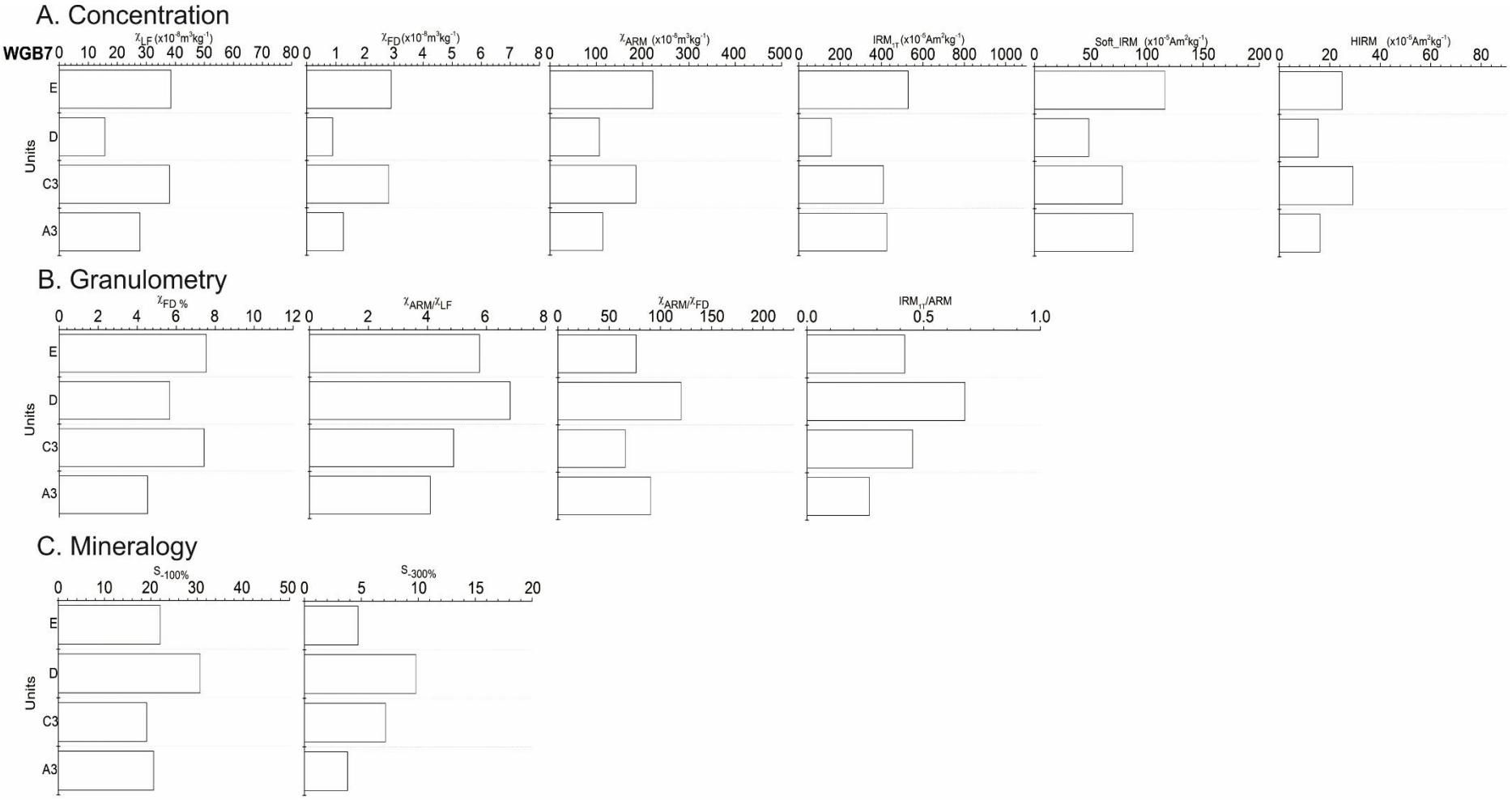

Figure 6.53 – mineral magnetic properties from samples collected from WGB-7

The sharp, undulating contact between units A and B implies a distinct erosion surface, with incision by a palaeochannel associated with the emplacement of very coarse gravel deposits (unit B). The alternating, normally graded sands and gravels of unit C imply two kinds of deposition respectively: 1) overbank sedimentation with upward fining reflecting the progressive aggradation of the floodplain and 2) deposition as channel bars during flooding, with upward fining characteristics reflecting bar aggradation. The matrix in this case reflects interstitial filling by finer material during periods of bar submergence. Notably, χ_{LF} is only 39 for the interstitial sediments of this bar deposit compared to 64 for the bar deposits at the same relative elevation (2 m) reported at WGB-6, where the distinct 'red' palaeosol surface traced from the upper slopes (WGB-2) was noted. In concert with the 'greyer' colour (10YR 6/3) of unit C3 compared to unit D1 of WGB-6, this calls into question whether the aforementioned palaeosol is present at WGB-7.

Compared to outcrops 4 and 6 upstream, the deposits of WGB-7 are also substantially coarser and thicker up to 2.5 m above bedrock (units A-C). The evidence from terrace fills thus far is that very little sediment coarser than fine-medium gravel was connected through the wide valley upstream and that this likely acted as a barrier to connectivity of bigger gravels, cobbles and boulders from the upper slope (WGB-1 -3). Two possible alternative origins for this coarse sediment are therefore proposed: 1) knickpoint erosion through the dolerite supplied coarse sediment to the channel; 2) the coarse deposits originate from the proximal hillslopes to the south. The first proposed origin may hold true for the basal unit (A), as this directly overlies bedrock. Although the evidence indicates this unit is partially leached relating to influence of groundwater, magnetic susceptibility is still much lower than many basal units at similar elevations above bedrock at Africanders Kloof. Given the distinctively strong magnetic signature of the Karoo dolerite, it appears its influence is at best secondary here. The overlying gravels of units B and C pertain to a phase of channel aggradation such that the bedrock surface now exposed in the modern channel would have been buried. As shown in Figure 6.54, the limits of the succession at WGB-7 extend part way up the valley directly to the south.

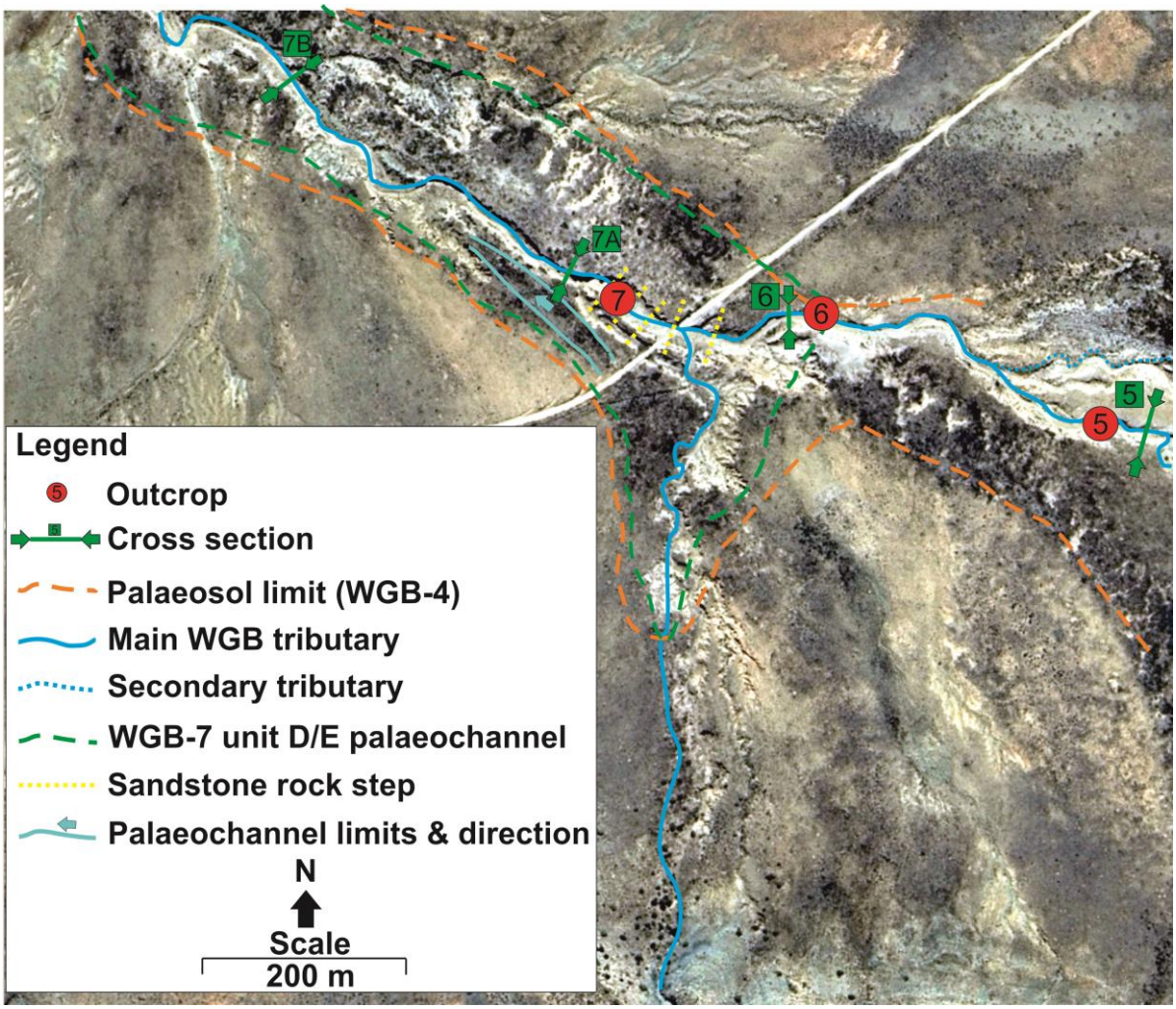

Figure 6.54 – digitally referenced aerial photograph showing relations and extents of the succession reported at WGB-7 (see Fig. 6.50). Note: 1) the continuity of the palaeogeomorphic surface downstream of WGB-7 and 2) the abandoned palaeochannel (light blue lines) running parallel to the contemporary gully.

This implies that the origin of the coarse material is the hillslope to the south, but fine sediment from the upper slopes (WGB-2 – 6) may have still fed through. The thicker beds of alluvium at WGB-7 may reflect higher water discharge due to the confluence between both tributaries just upstream. The 'greyer' colouration compared to WGB-6 is therefore likely due to enhanced channel vegetation cover due to increased water availability. As a result, reduced susceptibility is probably related to ferrimagnetic dissolution, an hypothesis supported by the reduced Soft_IRM (80) compared to WGB-6 (105), though ferrimagnetic remanence is only slightly lower. Another line of evidence in support of the postulation that the palaeosol surface of WGB-6 is present at 7 is the near-identical HIRM values – 30 ~. However, as the S_{300} is minutely higher for WGB-7 unit C (7%), this in concert with the grey coloration, implies greater amounts of goethite compared to haematite, whilst overall ferrimagnetic coercivity is again identical to WGB-6.

Unit D (WGB-7) is compositionally very different to the other parts of this succession. The silty clays imply a very low energy depositional environment, probably a floodplain. The high bromine values confirm that this was a vegetated surface.

These sediments exhibit very weak ferrimagnetism, with extremely low concentrations of remanence carriers (IRM_{1T}). Attribution of a substantial proportion of SP grains even though χ_{FD}% is high (5.6%) is unwise considering the very low overall susceptibility (χ_{LF} = 15) (Dearing, 1999). The very high S values imply a substantial contribution of AF minerals, probably responsible for reducing the ferrimagnetism of the unit, although the very low proportions of remanence carrying grains likely reflect paramagnets such as ferrihydrite. The extremely clayey texture probably facilitated conditions of waterlogging which would have generated ferrihydrite and goethite. Collectively, the strong evidence for waterlogging, vegetation and a low-energy depositional setting implies a wetland-like environment, reflected in unit D facies. Considering this outcrop occurs immediately downstream of a seepage zone supplied from doleritic aquifers, this is certainly feasible (see Table 4.3 analogue 4). This unit is in the same stratigraphic position as WGB-6 unit E, the continuity of which was traced and thus displayed in Fig. 6.54 (see green dashed line). WGB-6 unit E was found to be much coarser and exhibited cross bedding (Fig. 6.45 and 6.47d), though slightly enriched in overall ferrimagnetic concentration (see Fig. 6.48a and Fig. 6.53a).

Taken together, both units are related to the same phase of palaeochannel aggradation. Differences in sedimentology and waterlogging are related to a) WGB-7 overlying sandstone bedrock and therefore directly overlying a seepage zone, b) the position of the channel thalweg.

The lack of any obvious progradational features (i.e. longitudinal fining of unit – as reported in floodout setting in ch.5) indicates these facies were part of a channel system that was continuous upslope as indicated in fig. 6.54 (see green dashed line) rather than a terminal channel system and floodout.

The abrupt contact between units D and E indicates sudden burial of this former floodplain surface (unit D) by clastic, comparatively well sorted laminated sands (E). The strong comparability in terms of ferrimagnetic signature of units C3 and E implies that no change in sediment source (i.e. the slope to south) occurred. Had

these floodplain sediments been derived from the sands deposited on the alluvial plain (WGB-4), it would be expected that both 1) total ferrimagnetic susceptibility would be much higher (e.g. χ_{LF} = 45 – 65) and 2) IRM_{1T} values would be closer to 800 (see Fig. 6.31 and 6.35). Collectively, this implies that the sediments at WGB-7 were not supplied by the upper slopes (WGB-1 – 4). The extent of these fills downstream is discussed in later section.

6.9a: WGB-8: analysis

Log WGB-8 was obtained from a 2 m exposure set back from and to the right of the main contemporary channel approximately 2 km downstream of the headwaters and 0.9 km from WGB-7 (Fig. 6.1, 6.55 - 6.57). A modern infilling wetland partially disconnected from the main channel discussed in Chapter 4 buffers the sediments reported here from bank erosion by the main tributary (Fig. 6.56).

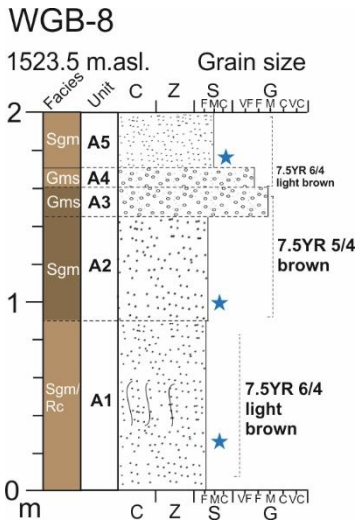

Figure 6.55 – sedimentary log of outcrop WGB-8.

The succession consists of predominantly thick (30-90 cm) units of massive sand with root channels (unit A1, A2 and A5) with two distinct thinner (10-15 cm) units of matrix-supported gravel (A3 and A4) that exhibit subtle changes in colour and no sharp bed contacts. The matrices of units A1, A2 and A5 exhibit a distinct very coarse sand mode but with varying silt/clay content (Fig. 6.58). Unit A1 (25-35 cm) shows the greatest silt/clay contribution (37.8% - Fig. 6.59a) and bromine concentration (37.5 ppm – Table 6.11).

Figure 6.56 – photograph of heavily incised alluvial fills at the eastern extremity of the valley, represented by log WGB-8. Note the mudstone barrier in the near-distance and abundant vegetation cover of the local valley floor.

This unit also exhibits the highest concentration-related and granulometric magnetic properties, which typically decline in a step-wise fashion above (Fig. 6.59a and b). S values peak for this unit too, with 23% and 5.8% of the applied remanence unreversed at -100mT and -300mT respectively (0.46- Fig. 6.59c).

Figure 6.57 – photograph of outcrop WGB-8.

Subunits A2 and A5 exhibit declining magnetic susceptibility (χ_{LF}) but the IRM_{1T}, Soft_IRM and HIRM parameters increase at the top again (Fig. 6.59a). The lowest χ_{FD}% and $\chi_{ARM/IRM1T}$ (6% and 0.2 respectively) occur at the top (A5- Fig. 6.59b), but bromine values resurge (19.2 ppm – Table 6.11).

Table 6.11 – % loss on ignition and bromine (ppm) data for sampled horizons at WGB-8.

Unit	Height (cm)	Loss on ignition (%)	Bromine (ppm)
A1	25-35	2.1	37.5
A2	95-105	2.2	8.9
A5	170-180	1.2	19.2

Micromorphological evidence from subunit A2 displays few well developed soil features with the exception small carbonate accumulations which make up less than 5% of the entire slide (Fig. 6.60). These form calcitic hypo- and hyper-coatings that have developed around a series of pores and elongated voids (Fig. 6.60b). Locally these have coalesced to form small nodule features that are rarely greater than 5 mm in diameter (Kemp, 1995).

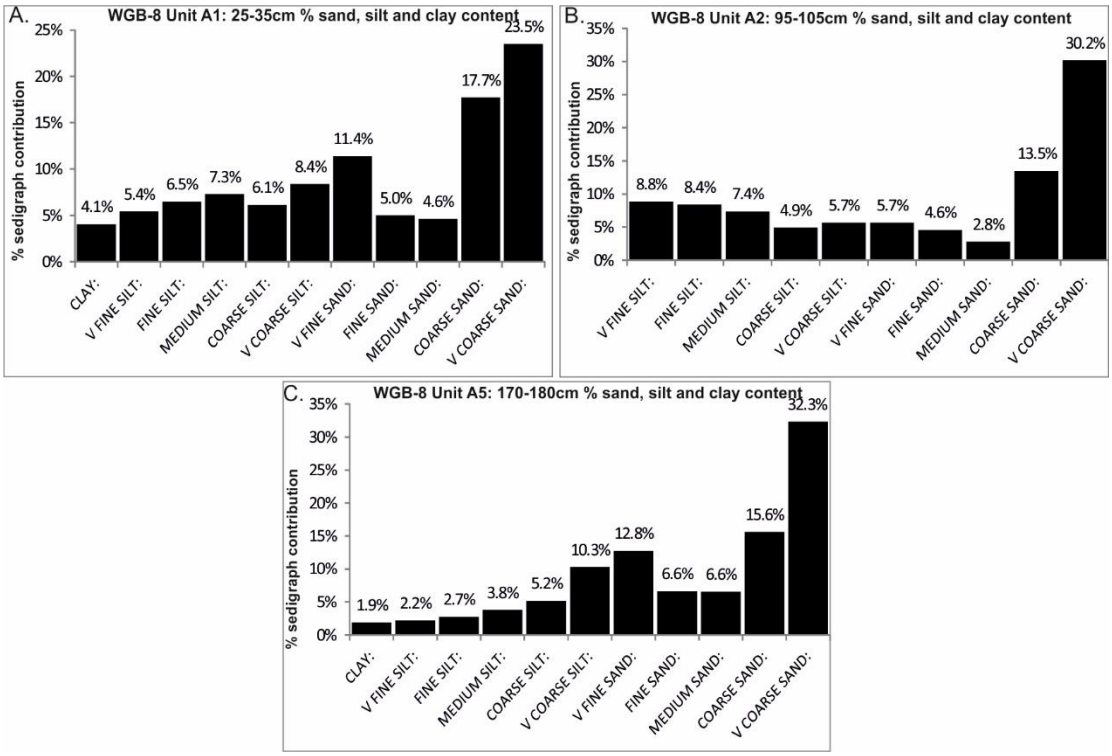

Figure 6.58 – % sand, silt and clay content derived from Coulter grain size analysis on samples collected from outcrop WGB-8.

These nodules consist of microspar/micrite texture calcite and are either; 1) homogeneous, or 2) contain circular/elongate calcite sheathes (Fig. 6.60b). Further, there are illuviated silts, clays and brecciated sparite cements inset within calcite hypercoatings (Fig. 6.60b). There are occasional concentric iron stains in the vicinity of deeply eroded lithic grains that have impregnated the groundmass (Fig. 6.60c).

6.9b: WGB-8 interpretation

The facies characteristics indicate deposition by slopewash as reflected by two distinct lines of evidence: 1) the fact that the deposits grade to the top of a sandstone ridge at the eastern valley margin; 2) The inversely graded nature of the sediments implying preferential removal of fines from nearby slopes followed by gravels. The absence of sharp bedding contacts implies near-continuous sedimentation, with no intervening distinct surfaces associated with palaeosol development.

Each of the sampled units exhibits strong pedogenic overprinting. Unit A1 for instance shows the highest concentrations of SP/SD grains and the strongest ferrimagnetic signature. In concert with the evidence for root channels and the high clay and bromine content of this subunit, illuviation processes have are likely responsible for concentrating weathering products in this horizon. This may also account for the slight reductions in ferrimagnetic intensity for unit A2. Crucially, bromine values of 37.5 ppm attest to a highly organic rich soil. The high S_{-300}% value (6%) probably indicates haematite over goethite since the colour of this unit (A1) is relatively rubified compared to the basal units upstream (WGB-7) and there is, on the basis of the strong ferrimagnetic remanence, little evidence for paramagnetic activity which would signify reducing conditions.

The carbonate features present in unit A2 are typical of carbonate cementation around roots, or rhizoliths (Kemp, 1995; Candy, 2002) and imply no more than incipient soil formation.

In contrast with the underlying units, A5 exhibits a distinctive MD ferrimagnetic signature reflected in the low values of $\chi_{ARM/IRM1T}$ (0.2). Although χ_{FD}% remains high, attesting to a strong SP pedogenic contribution, the absence of SD grains and that this occurs at the top (youngest) part of the succession implies likely inheritance from both soils and relatively unweathered regolith upslope.

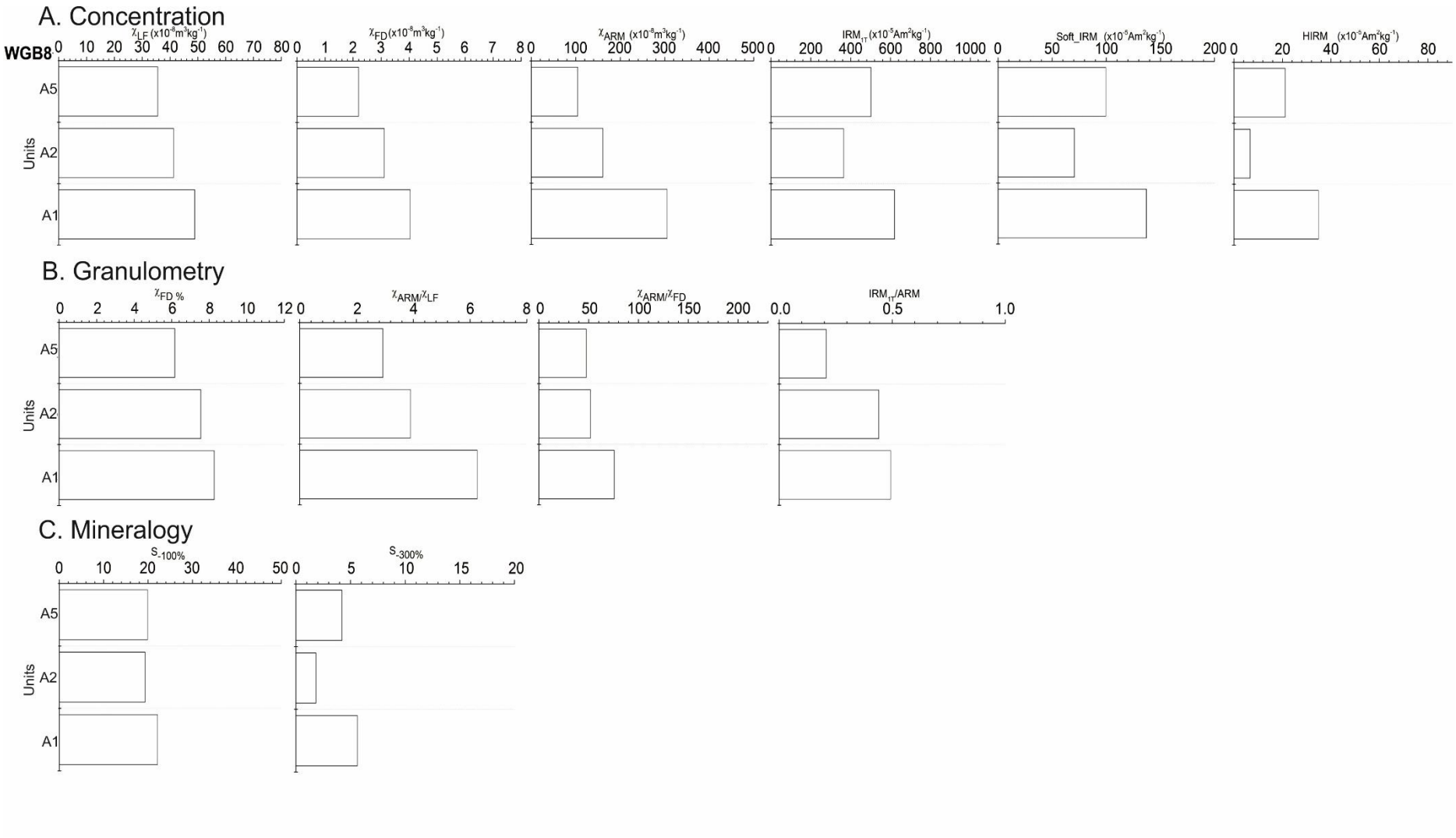

Figure 6.59 – mineral magnetic parameters from outcrop WGB-8.

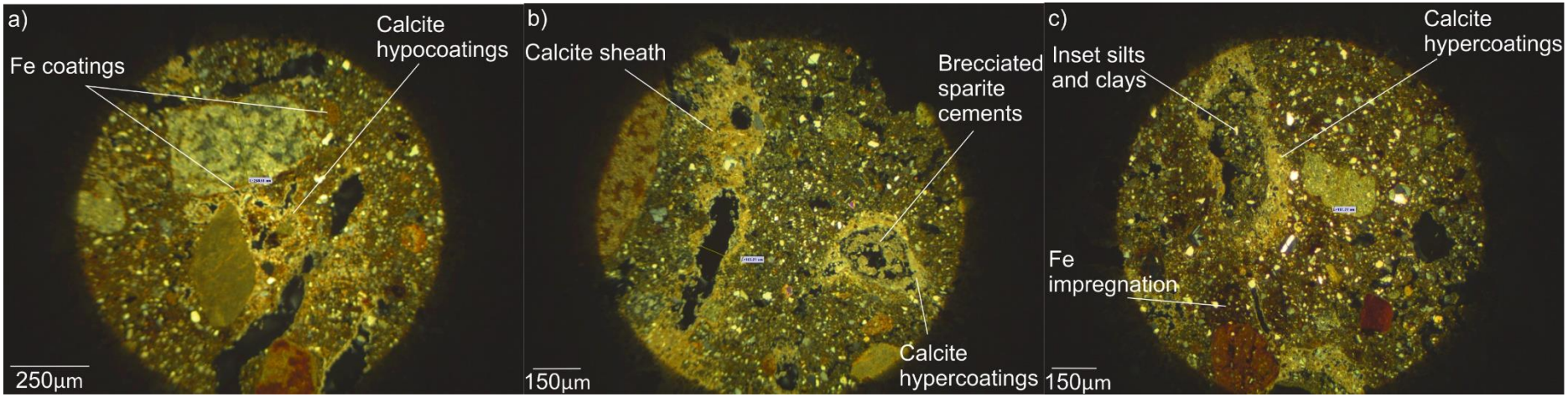

Figure 6.60 – thin section micrographs from WGB-8 unit A2, a) note clayey silt groundmass impregnated by calcite hypocoatings as well as distinct iron coatings around detrital grain, b) example of calcite hypercoatings and larger sheaths where these have coalesced with hypocoatings to form sheaths – notes the sharp contacts between the groundmass and sparite cement as well as inset brecciated sparite cements in the void to the bottom right, c) inset illuviated silts and clays within calcitic hypercoatings – note also impregnation of groundmass by concentric iron stains.

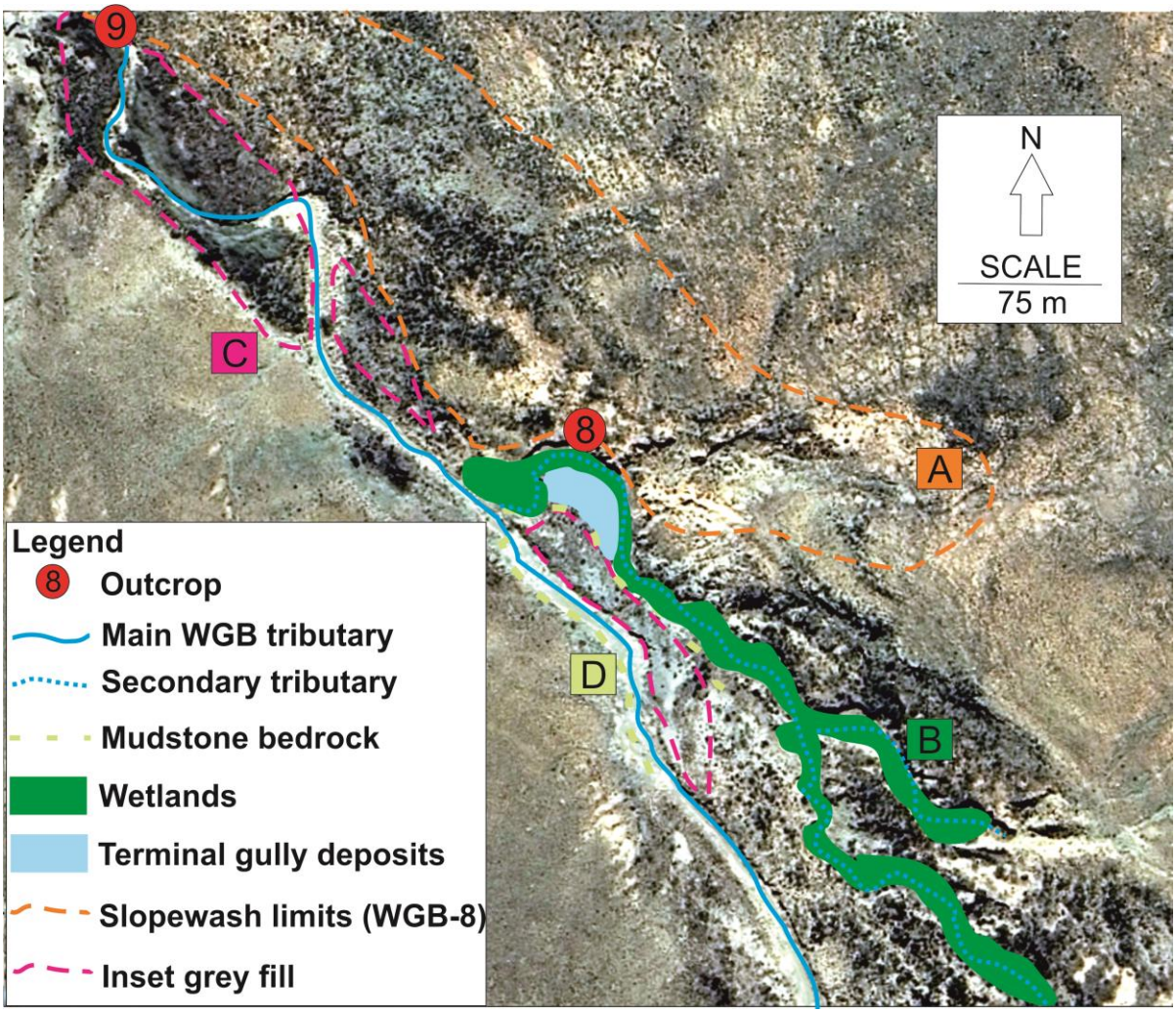

Figure 6.61 - digitised aerial photograph with surveyed limits of A) Slopewash fills (WGB-8), B) extent of contemporary wetlands in infilling secondary tributary, C) extent of grey fills which are inset from the slopewash deposits and mantle D) the mudstone bedrock through which a 0.6 m knickpoint is retreating up the main tributary, but is a major barrier disconnecting the secondary tributary adjoining from the east. Note also the terminal gully deposits inset between the contemporary wetland (B) and the brown fills (D).

These slopewash fills have largely been stripped, with only remnants remaining at the local valley margins. The local geomorphic setting means that the main channel has been and continues to be buffered by ongoing stripping of the remaining sediments and exposed regolith at the valley margins. This has been caused by the mudstone outcrop (Fig. 6.61d) disconnecting the tributary from the main channel. The extensive, modern wetlands in this area attest to local infilling and stabilisation, with only a small, low energy perennial channel (highly vegetated) diverted to the north by terminal gully deposits (Fig. 6.61 - blue infilled polygon). The evidence is that these terminal deposits accumulated here due to disconnectivity induced by the mudstone barrier. This has subsequently led to diversion of the tributary to the north,

exacerbating erosion of the slopewash fills (Fig. 6.61a), as reflected in the development of a small scarp face at WGB-8.

6.10a: WGB-9: analysis

Log WGB-9 was recorded from a 3 m exposure on the right hand side of the channel approximately 2,285 m downstream of the headwaters and 300 m downstream of WGB-8 (Fig. 6.1, 6.62 - 6.63).

The facies consist primarily of thick beds of homogeneous, poorly sorted sandy silts (Fig. 6.62 and 6.64) separated by very fine to very coarse beds of gravel of varying thickness (subunits A2 and B1). Bed contacts are typically planar diffuse with the exception of the contact between units A and B which is sharp undulating (Fig. 6.62).

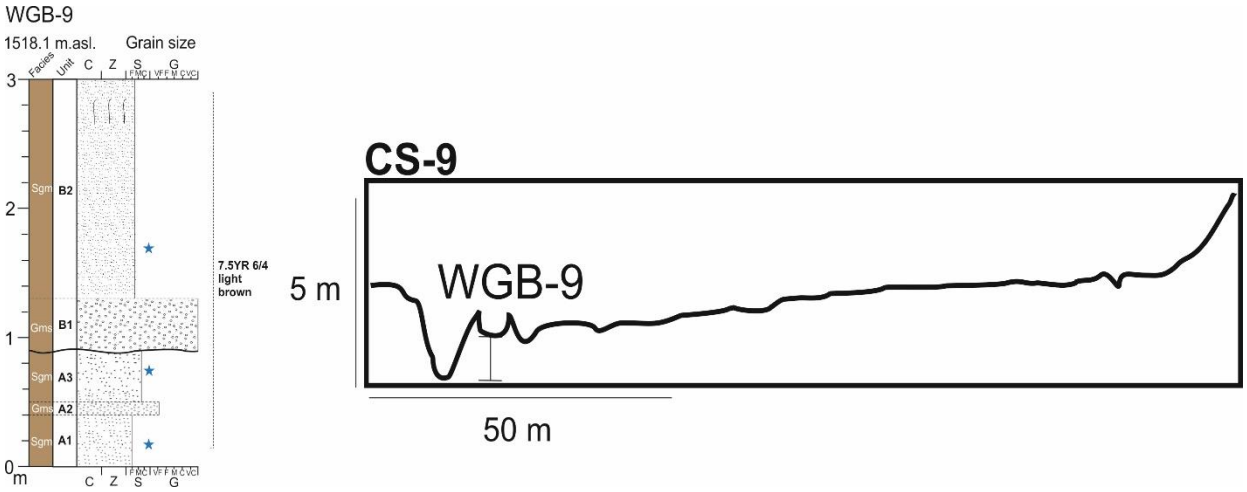

Figure 6.62 – sedimentary log of outcrop WGB-9 and cross section.

Table 6.12 – % loss on ignition and bromine (ppm) data for sampled horizons at WGB-9.

Unit	Height (cm)	Loss on ignition (%)	Bromine (ppm)
A1	10-20	1.30	1.6
A3	70-80	0.97	2.1
B2	165-175	1.08	2.5

However, colour does not change above this contact (7.5YR 6/4) and bromine content increases very slightly, whereas LOI% is variable (Table 6.12). The primary pedofeatures are void networks that are typically planar voids or channels which reach up to 2-3 cm in length for unit A1 (5-14 cm) and only 1 cm in length in unit A3 (52-61 cm). Concentration related magnetic proxies are typically constant between the three sampled units.

Figure 6.63 – photograph of outcrop WGB-9.

Crucially, the HIRM peaks for subunit A3 whilst the χ_{ARM} is relatively small compared to the other units (Fig. 6.65a) and this is accompanied by relatively small $\chi_{ARM/IRM1T}$ and $\chi_{FD\%}$ (Fig. 6.65b). Subunit A3 possesses a distinctive S_{300}% signature with 11% of applied remanence unreversed at -300mT (Fig. 6.65c).

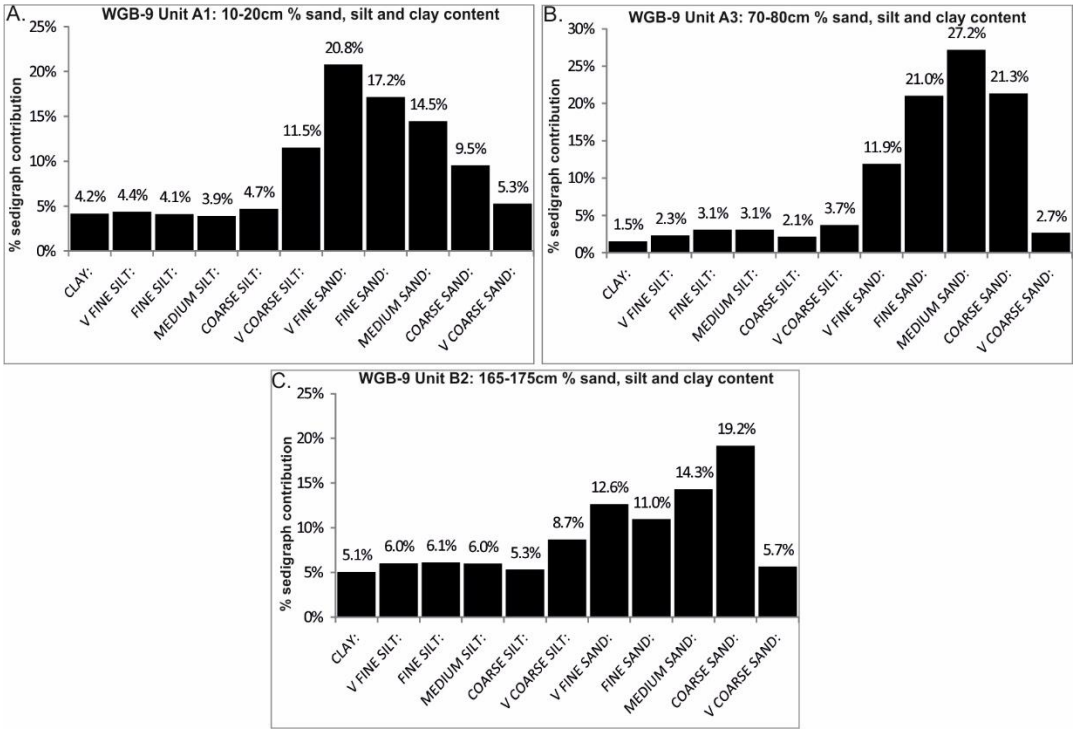

Figure 6.64 – % sand, silt and clay content derived from Coulter grain size analysis on samples collected from outcrop WGB-9.

6.10b: WGB-9 interpretation

The thick beds of sand evidence low-energy deposition. The modern bedload of the channel is sand, though there is some deposition of coarser gravels on small, poorly developed point bars along the insides of meander bends. The relatively wide valley compared to Africanders Kloof facilitates lateral channel movement and associated accretionary features. In this regard, the alternating beds of sand and gravel are interpreted as reflecting lateral movement of the stream, with emplacement of coarser lag deposits during conditions of high flow. These sediments exhibit typically minimal if any soil overprinting based on the micromorphological evidence. The void characteristics, at most, signify the very earliest stages of incipient soil development, in this case by root channels. Magnetically, low to moderate concentrations of ferrimagnetic minerals are indicated by total susceptibility, but crucially, the carriers of magnetic remanence appear to be predominantly PSD-MD on the basis of the very low $\chi_{arm/IRM1T}$ values.

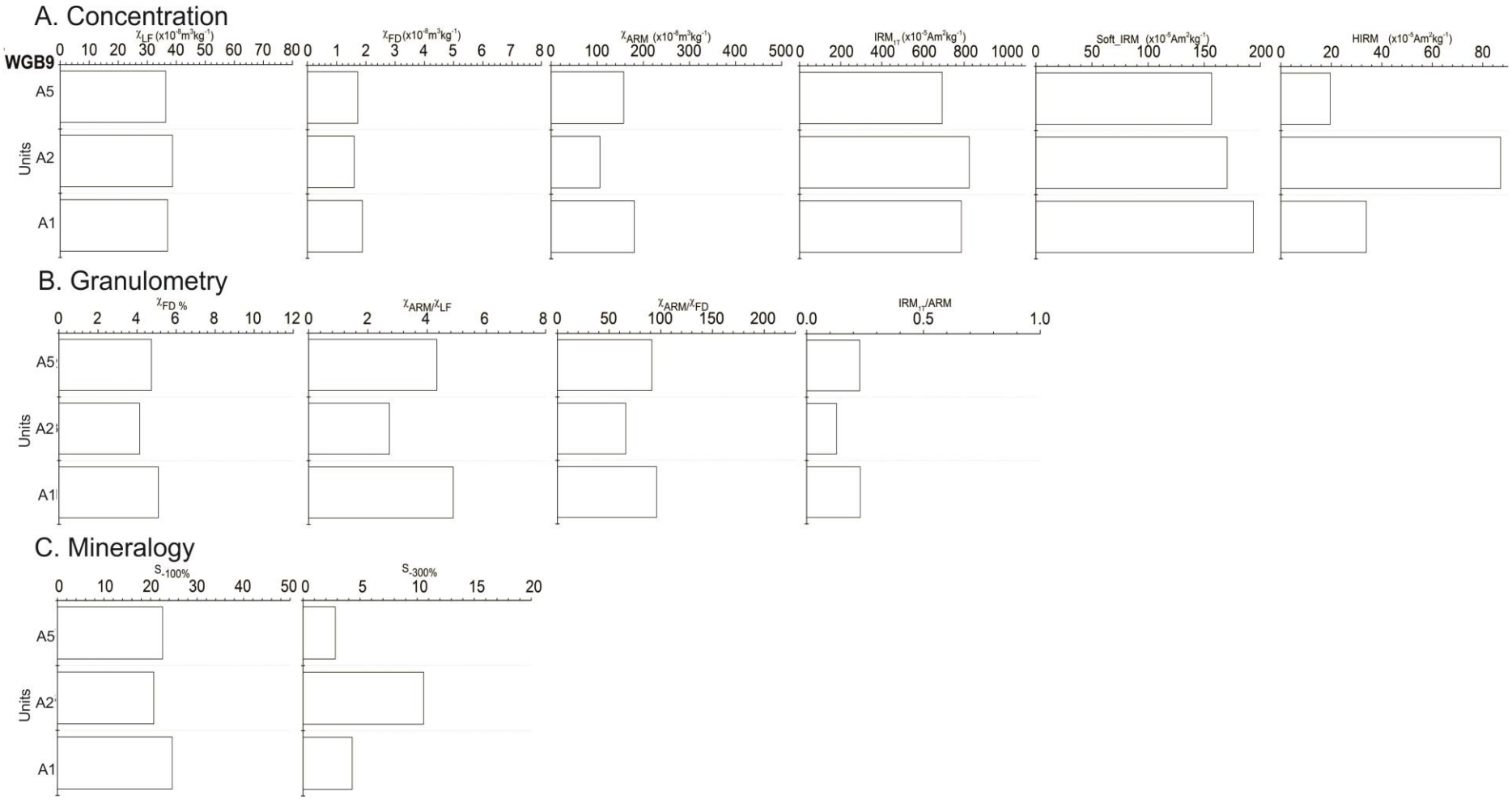

Figure 6.65 – mineral magnetic parameters from outcrop WGB-9.

On this basis, the sediments at WGB-9 are clearly discriminated from those at WGB-8, yet susceptibility and the total concentrations of soft and hard minerals (with the exception of WGB-9 unit A3) are strikingly similar to WGB-8. Furthermore, the moderate-high concentrations of SP grains indicated by the $\chi_{FD\%}$ values for WGB-9 must reflect inheritance, because of the lack of soil development. Similarly, the high HIRM and S_{300}% values for unit A3 indicating a surge in AF mineral concentration is undoubtedly inherited and could reflect weathering rinds coating lithic grains locally sourced from nearby hillslopes. It follows that the palaeochannel deposits of WGB-9 were probably supplied from the slopes at WGB-8, accounting for these similarities.

Thus the sharp undulating contact between units A and B is not a palaeosol, but rather a reactivation surface associated with a large flood event. This is confirmed in the very coarse nature of the overlying gravels (unit B1) which are interpreted as bar deposits emplaced under flood conditions. The overying massive sands are interpreted as overbank sediments, the magnetic signature of which is virtually identical to unit A1, implying no change in sediment source.

6.11a: WGB-10 analysis

Log WGB-10 was recorded from a 3 m exposure on the right hand side of the channel approximately 2630 m downstream from the pediment and 345 m downstream of WGB-9 (Fig. 6.1, 6.66 - 6.67). Two additional samples from another exposure 2955 m downstream (WGB-173) are also reported to compare and contrast depositional and pedogenic environments.

This outcrop consists of two principal lithostratigraphic units. A consists of friable, well sorted massive sands (A1) which grades to clayey silt (Fig. 6.68a) and exhibits high LOI% and bromine values compared to WGB-9 (Table 6.13).

Unit B, which is separated from A by a planar sharp contact, consists of very coarse, matrix-supported gravels which grade to medium gravels at the top of the subunit (2.3 m). The matrix consists of very poorly sorted silty sands (Fig. 6.68b). There is a subtle change to greyer colouration (10YR 5/1) above this contact and bromine and LOI% values are high relative to unit A2 (Table 6.13). Magnetically, both sampled units exhibit very weak concentration-based proxy values (Fig. 6.70a), but χ_{FD}% and $\chi_{ARM/IRM1T}$ are noticeably higher for unit B1 (Fig. 6.70b). Crucially, S values for both

units are very high, with over 30% and 10% of remanence applied at -100 and -300mT respectively unreversed (Fig. 6.70c).

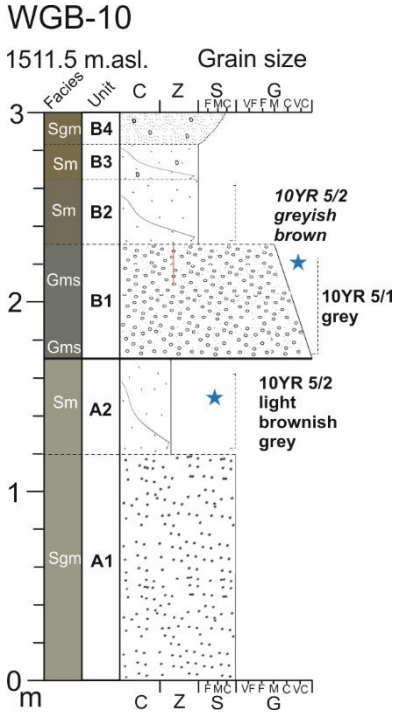

Figure 6.66 - sedimentary log of outcrop WGB-10.

Figure 6.67 - photograph of outcrop WGB-10.

The lithofacies above (unit B2-3) consist of silty sands with diffuse bedding structures. The top of the succession coarsens to predominantly coarse sand (unit B4).

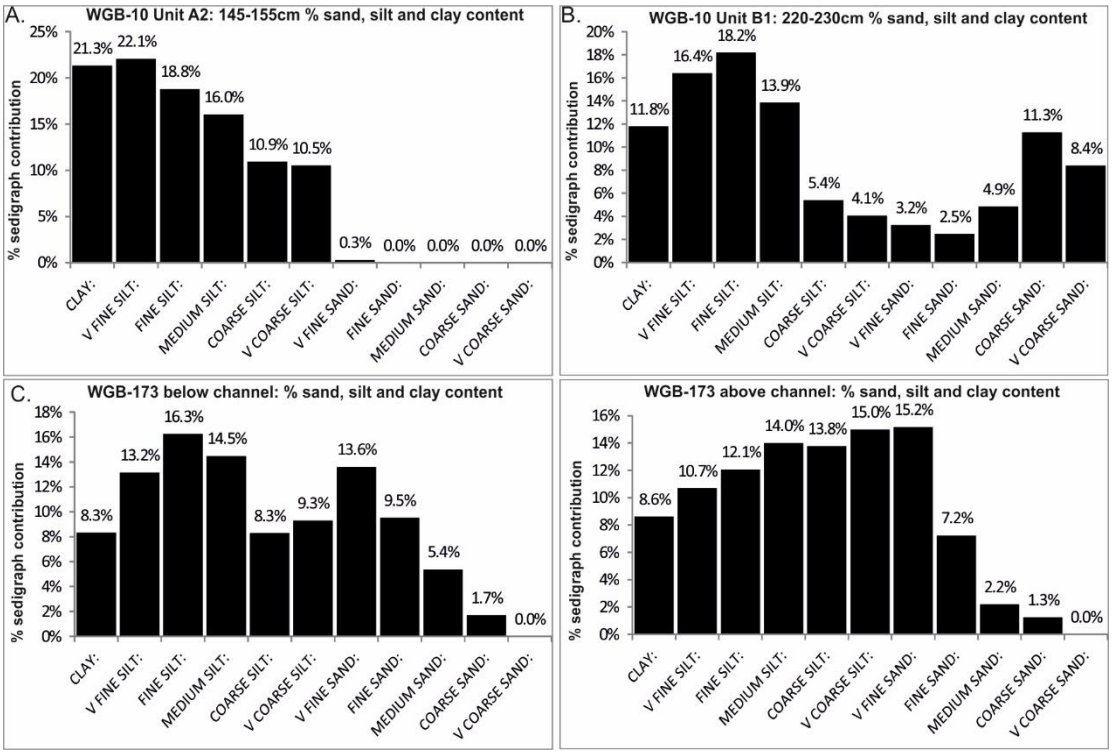

Figure 6.68 – % sand, silt and clay content derived from Coulter grain size analysis on samples collected from outcrop WGB-10 (A and B) and deposits at WGB-173 (C and D).

Table 6.13 – % moisture, loss on ignition and bromine (ppm) data for sampled horizons at WGB-10.

Outcrop/Unit	Height (cm)	Loss on ignition (%)	Bromine (ppm)
WGB-10 / A2	145-155	2.34	9.2
WGB-10 / B1	220-230	3.79	14.2
WGB-173 BC	-	-	2.6
WGB-173 AC	-	-	3.5

The samples collected from the 2 m exposure at WGB-173 (Fig. 6.69) exhibits similar texture to WGB-10 consisting of poorly sorted silty sands (Fig. 6.68 C and D), but colour differs (7.5YR 6/3 light brown) and bromine content is substantially lower (Table 6.13). Compared to WGB-10 samples, concentration-related properties are all significantly higher (Fig. 6.70a) as are their granulometric properties (Fig. 6.70b). Conversely, S values are dramatically lower with unreversed remanence values not exceeding 24% and 6% at -100mT and -300mT respectively.

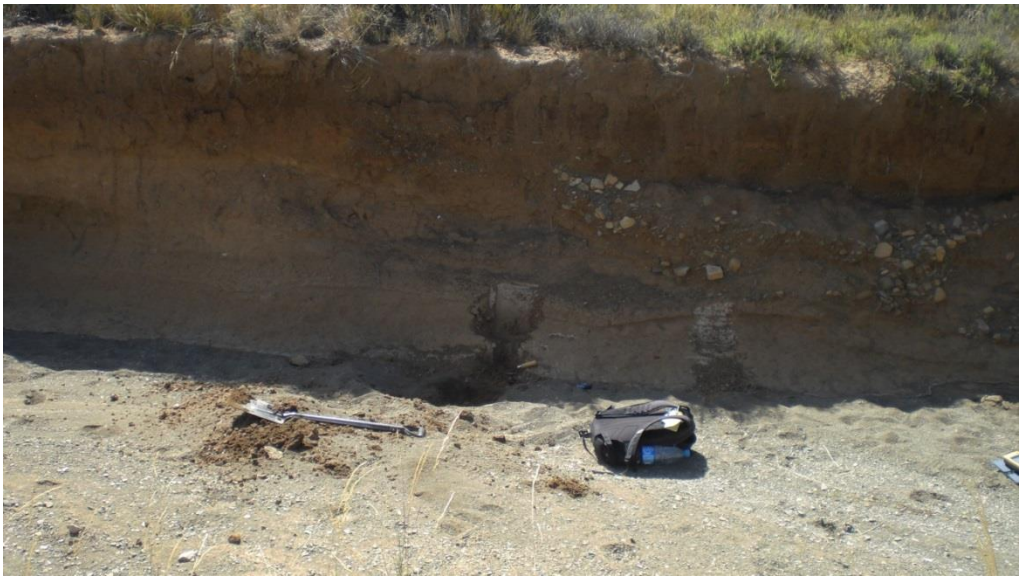

Figure 6.69 - photograph of exposure WGB-173.

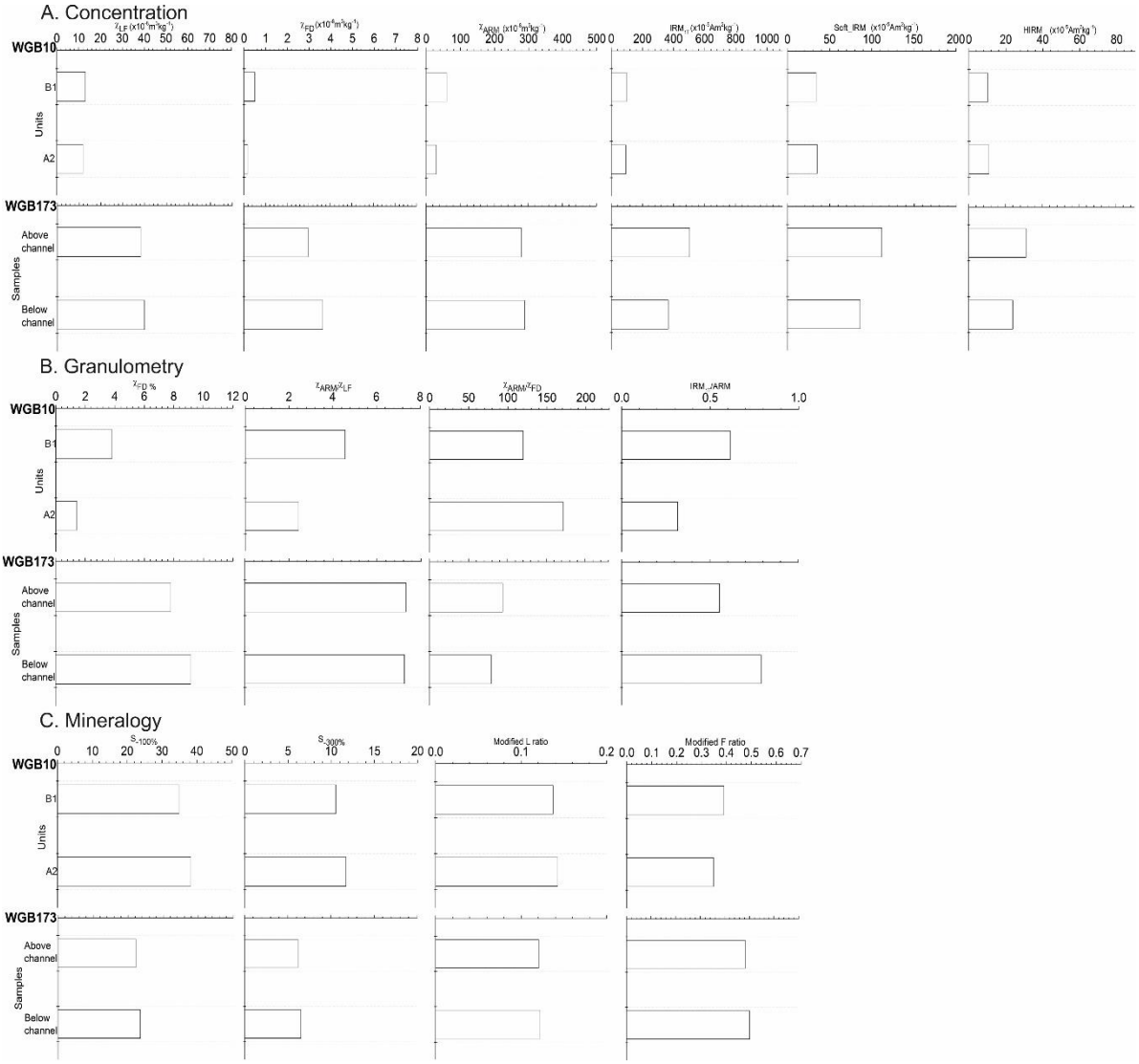

Figure 6.70 – mineral magnetic parameters from outcrop WGB-10 and two alluvial samples at WGBLP-173.

6.11b: WGB-10 interpretation

The sandy silts of subunit A1 are similar to those reported at the base of WGB-9, interpreted as migrating channel deposits. The capping clayey silts (unit A2) also evidence high organic content and gleying reflect in the grey colouration (10YR 5/2). The nature of the facies implies a vegetated, low energy environment which was poorly drained. X_{LF} of less than 15 indicates very low ferrimagnetic mineral concentration. The low remanence parameters are consistent with paramagnetic activity, whilst the high S values are probably representing goethite over haematite. The collection of evidence points to a wetland environment analogous to that reported in the modern system at WGB-8.

The sharp, planar contact and switch to very coarse gravels at WGB-10 is comparable with that reported at WGB-9 and may be stratigraphically coeval given their proximity to each other. The incision into the wetland at WGB-10 (unit A2) implies a major flood event reactivated this part of the valley floor after a period of stability by wetland vegetation. This is analogous to the very coarse deposits mantling vegetated silty sand deposits outlined in chapter 4. However, compared to WGB-9, the evidence is that conditions of high vegetation and gleying then persisted above the unconformity represented in the grey colouration (10YR 5/1–5/2) and high bromine values at the top of the gravel unit (B1) – 14.2 ppm. The magnetic characteristics imply paramagnetic mineral formation and goethite similar to unit A2. The overlying coarse silty sands (B2-B4) imply overbank deposition, but in a poorly drained setting.

There are several possible reasons as to why wetland may have been present at WGB-10 but not 9. Firstly, the valley is slightly wider at WGB-10: 150 m across compared to 100 m. As a result, local sediment storage potential is somewhat increased due to relative loss of confinement. Secondly, this part of the valley is fed by several small first-order tributaries draining slopes to the south. There is evidence for incision into the mudstone bedrock of these slopes. As a result, local water and sediment supply are likely to have been locally increased at this point. The dominance of fine sediment in these reaches is also conducive to vegetation formation in areas away from the channel thalweg. The stratigraphically coeval bedding of the major unit boundary raises a note of caution with respect to the use of

sediment magnetism for stratigraphic correlation purposes at Wilgerbosch. In this case, the magnetic properties are overridden by the effects of drainage which is clearly related to local valley morphology and position of the fills.

The absence of any progradational features or lenticular bedding means that the deposits are unlikely to signify a terminal channel, whereby loss of confinement can result in floodout deposition and wetland formation (Bull, 1997; Billi, 2007; Grenfell et al., 2014). The inset nature of these fills and their continuity since at least WGB-8 (see Fig. 6.61) implies a continuous channel system.

In contrast, the sediments sampled at WGB-173 exhibit a relatively strong ferrimagnetic signature, with little paramagnetism on account of high magnetic remanence values. Furthermore, the deposits exhibit a distinct pedogenic SP/SD signature based on $\chi_{ARM/IRM1T}$ and χ_{FD}% values > 0.5 and 7% respectively. The evidence for in situ soil development is minimal, comparable with WGB-9 and 10. In this regard, the magnetic pedogenic signature reflects incipient soil development at the very most. Furthermore, the proximity of these deposits to the eroding orange-brown fills on the slopes means that this eroded soil could have been supplied to the palaeochannel at this point. The S values still attest to a distinct AF mineral signature. This is likely to reflect inherited haematite from slopes but some goethite is likely relating to conditions of poor drainage post-deposition, though nowhere near as intense as reported for WGB-10.

6.12: Summary

The upper Wilgerbosch Kloof is mantled by palaeofan sediments with two distinct phases of emplacement, but lacks the stratigraphic complexity of the floodout at Africanders Kloof. Thereafter, terrace fills primarily consist of several generations of alluvial channel deposits with varying degrees of pedogenic overprinting. Notably, terrace fills between the fan and alluvial plain were shown to be continuous, implying that, in concert with the soil magnetic signatures that the fan was a major supplier of sediment downstream, contrasting with Africanders Kloof, where floodout units abruptly terminated at a major dolerite barrier. Reducing grain size of terrace fills with distance from the upper slope to the alluvial plain was attributed to partial loss of connectivity associated with the abrupt switch to an unconfined valley setting. Compared to Africanders Kloof, there is greater evidence for aggradation by lateral

rather than vertical accretion processes, this owing to the lithologically softer (mudstone), wider valley floors. The lack of slope deposits (with exception of WGB-1-3 and 8) is due to the lower relief of this catchment and greater distances between valley floor and hillslopes compared to Africanders Kloof. Finally, the deposits of WGB-9 appear to be intermediate in maturity (relative age) between the rubified alluvial fills (WGB-2–7) and the inset wetland (grey fills). This sequence was not found at Africanders Kloof and may be a feature of greater preservation potential in the Wilgerbosch Kloof, since the deposits do not evidence discontinuous channel and floodout sediment architecture.

Chapter 7: Results iv: Sedimentology and pedology of valley fills – Wilgerbosch River

7.1 Introduction

This chapter presents detailed analytical evidence of the sedimentological and pedological characteristics of the valley fills from 6 sampling sites on the Wilgerbosch main channel into which Wilgerbosch and Africanders Kloof drain, the locations of which are indicated in Figure 7.1.

Figure 7.1 – Wilgerbosch River, Africanders and Wilgerbosch Kloof study areas. Outcrop locations on the main channel are reported in the following section. Enhanced aerial photos and maps of the tributary study sites are provided at the beginning of their respective sections. Town of Nieu Bethesda and Ganora farm shown for reference. Image extracted from Google Earth (2015).

7.2a: WGW analysis

Log WGW was obtained from a 2 m tall sediment outcrop on the right channel bank immediately downstream of the large dam on the Wilgerbosch main channel (Fig. 7.1, 7.2).

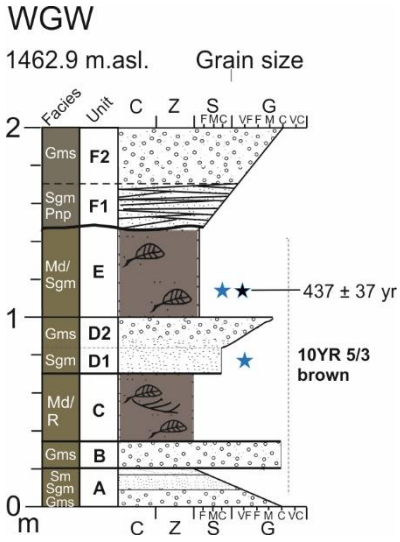

Figure 7.2 – sedimentary log of outcrop WGW.

Unit A (0-20 cm) consists of friable matrix-supported coarse gravels that fine to sand and then silt. The contact between units A and B is sharp planar. Unit B is a homogeneous matrix-supported gravel package which is overlain by much finer, clast poor, organic rich silts (unit C) which exhibit ripple cross lamination (Md/Rl). Unit D exhibits inverse grading from coarse sand to matrix-supported gravel.

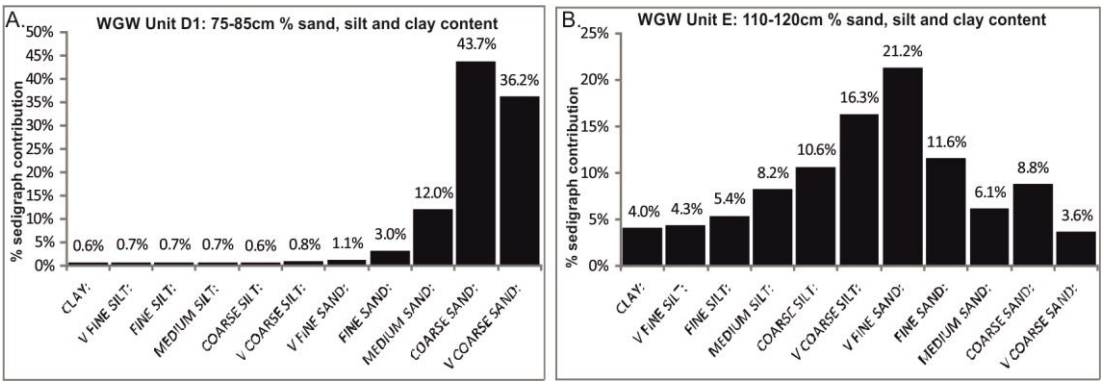

Figure 7.3 – % sand, silt and clay content derived from Coulter grain size analysis on samples collected from outcrop WGW.

The sand subunit (D1) is massive and dominated by coarse to very coarse sand (79.9%) with negligible clay and silt content (4% - see Fig 7.3a) and very low LOI (1.7% - Table 7.1). Total magnetic susceptibility is low (χ_{LF} = 27) but the HIRM and Soft_IRM parameters are relatively high (Fig. 7.5a). χ_{FD}% is high (4.8) (Fig 7.5b). S values indicate that 21% and 5.8% of the applied remanence was unreversed at -100mT and -300mT respectively (Fig. 7.5c).

Unit E consists of very poorly sorted, massive sands and silts (Fig 7.3b), which exhibit high LOI (5.8%) and bromine values (12.6 ppm – Table 7.1). An AMS radiocarbon date was obtained from fossilised *Juncus* stems: 437 ± 37 yr (Fig. 7.4).

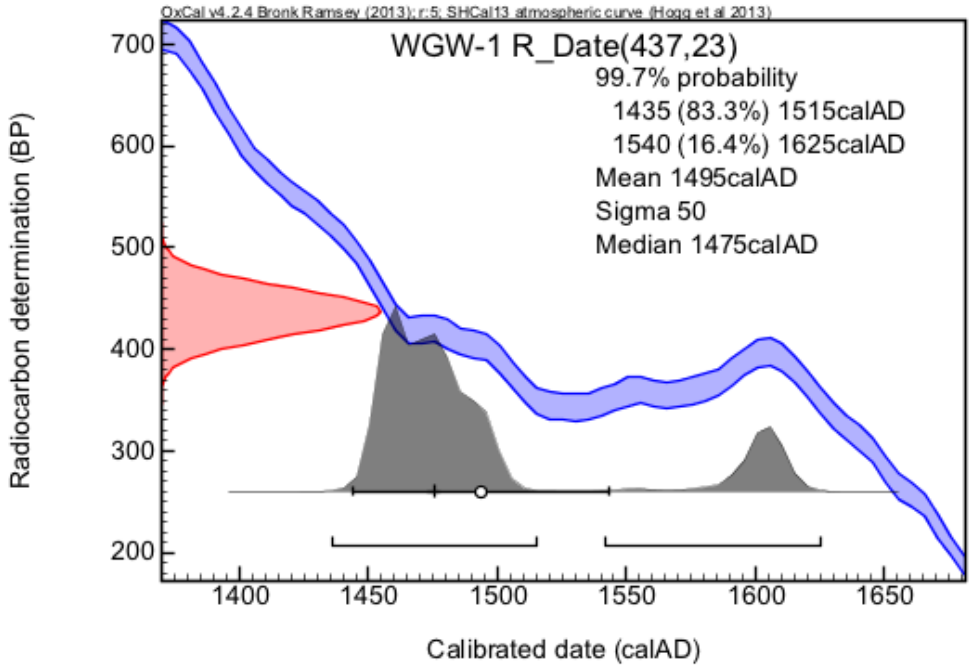

Figure 7.4 - Radiocarbon calibration curve and probability distribution plot for sample WGW-1. OxCal v4 2.4. SHCal13 atmospheric curve used (Hogg et al., 2013).

Total magnetic susceptibility is very low (χ_{LF} = 19) and the other concentration-based proxies are very low (Fig. 7.5a). Compared to unit D1, χ_{FD}% is very low (1.3) but the χ_{ARM}/χ_{FD} relatively high (220) and the $\chi_{ARM}/_{IRM1T}$ slightly lower (0.2 - Fig. 7.5b). The S values are relatively high indiciating 27% and 6.8% of the applied remanence was unreversed at -100mT and -300mT respectively. Units A to E are very similar in colour: 10YR 5/3 brown.

A sharp undulating contact punctuates units E and F. The latter is characterised by friable, inversely graded sands and matrix-supported gravels. Subunit F1 exhibits planar non-parallel bedding, whilst F2 is massive.

Table 7.1 – % loss on ignition and bromine (ppm) data for sampled horizons at WGW.

Unit	Height (cm)	Loss on ignition (%)	Bromine (ppm)
D1	75-85	1.7	-
E	105-115	5.8	12.6

7.2b: WGW interpretation

The depositional setting for sediments at WGW is the inside of a meander bend (right bank) where the modern channel is actively eroding mudstone bedrock along the outer left bank. The inside of the bend is characterised by a modern vegetated point bar deposit. The fining upward sequence (unit A) from gravels to very fine sands reflects flow cessation at the top of a palaeo-point bar. The matrix-supported gravels (unit B) indicate emplacement on top of the bar under conditions of high flow. The intervening organic-rich silty sand and sandy silt units (C and E respectively) indicate deposition in the later phases of a receding flood confirmed by the presence of climbing ripple cross-laminations (unit C). Organic rich, muddy sediments can occur in swales associated with scroll bars – where each scroll bar of a point bar represents the results of channel migration during a flood. However, they are characterised by lenticular-shaped sandy units embedded within the muds due to periodic inundation by floods. Inwashed plant remains are common too (Sundborg, 1956). Typically, they are associated with large rivers and can be several decimetres deep (Fisk, 1947 – Mississippi River, USA; Sundborg, 1956 – Klarälven River); for smaller rivers or streams, point bars are simpler depositional features (typically 1-3m) on the convex sides of meanders which dip gently toward the channel (Collinson, 2003). Thus, the organic accumulations at WGW are interpreted as in situ vegetation growth at the margins of the formerly active channel on the basis of: 1) fine grained, medium-thick beds of well sorted silty sand/sandy silts; 2) the absence of coarse sand/gravel lenses in association with allochthonous fossilised plant remains; 3) the modern analogues of vegetation growing in fine-grained sediment straddling the modern channels and floodplains.

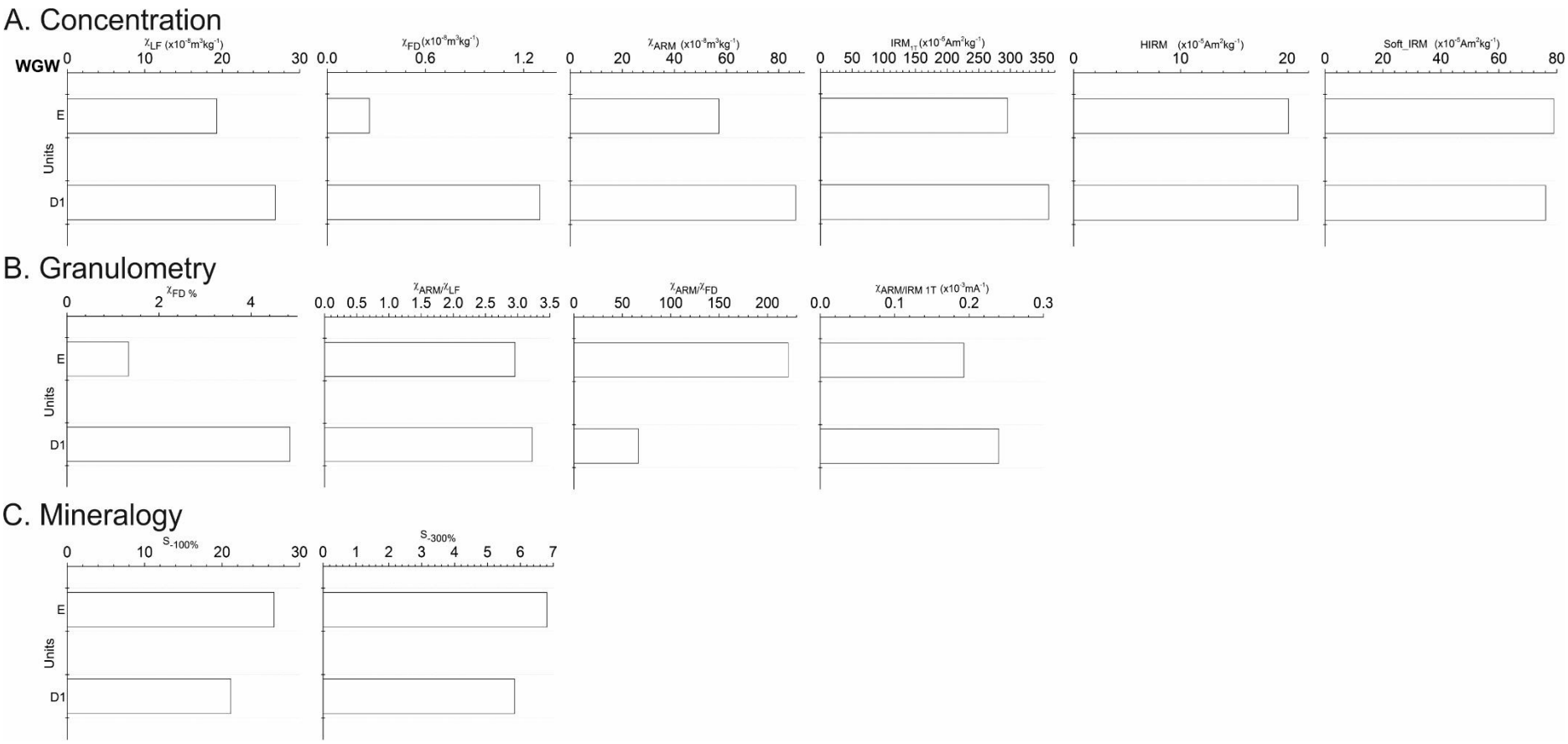

Figure 7.5 – mineral magnetic parameters from sampled horizons at outcrop WGW.

Given the nature of the facies and organic characteristics of unit E, it follows that the AMS radiocarbon date is representing the age of in situ plant death rather than inwashed plant material of unknown source. Nevertheless, this age needs to be treated with caution, as there were only enough usable fossilised plant remains to produce one AMS date. The ideal would have been to have obtained several dates on the same horizon to test for repeatability. At best, it is possible to say that the vegetated point-bar in question remained stable until at least 437 ± 37 yr. Considering the sedimentological and geomorphological evidence for aggradation in this reach, this age may be taken (tentatively) as a maximum age for the incision of the modern channel to its current base level. However, at this stage it is not possible to state whether the inferred phases of aggradation and incision are a local phenomenon related to barrier effects downstream.

It follows that the bracketing minerogenic sands and coarse-gravels (units D and F) reflect large floods sufficient to cause sedimentation at the channel margins and obliterate the former vegetation cover. This is particularly evident for unit F, with a sharp, undulating contact signifying an erosional reactivation surface incising the vegetated surface (unit E). This recurrent pattern of inverse grading in ephemeral channels has been attributed to deposition of coarse material on bars at the margins of the active channel (Hooke, 2004). The facies characteristics and spatial context within the valley is also analogous to the upward-coarsening patterns associated with bars at the margins of the active channel just upstream reported in Chapter 4 (Table 4.3 - analogue 5). The pattern reflected at unit F is not consistent with a typical point-bar sequence. Whilst low angle, planar cross beds can evidence lateral bar migration, these are typically accompanied by an upward fining sequence as the channel migrates away from the opposing meander bend leading to deposition of fines (akin to floodplain) on top of the sequence (Collinson, 2003). The erosion surface is more consistent with a large flood truncating the underlying bar/wetland sequence. In this case, the low angle cross beds probably reflect deposition as channel dunes. Furthermore, evidence from aerial photographs shows corridors of unvegetated alluvium on the inside of the meander bend which are not parallel to the modern active channel. As reported in Chapter 4, flood marks (woody debris) were found attached to small dead trees up to 2 m above the channel margin in

association with the 2009 flood. Therefore, the evidence points to modern cross-cutting flow through the palaeo-point bar/wetland sequence.

Both sampled units exhibit low concentrations of remanence carrying ferrimagnets and the relatively high S_{-300}% indicates a substantial contribution from AF minerals particularly for unit E. This may reflect seasonal wetting and drying which would favour goethite formation. Since the wetland was destroyed and incised by the modern channel, lower local moisture will now favour oxidation of goethite to haematite.

7.3a: WGM-1 analysis

Log WGM-1 was recorded from a 3.7 m exposure on the right hand side of the channel directly overlying mudstone bedrock (Fig. 7.1, 7.6). The geomorphic context differs from log WGW, with outcrop WGM-1 representing alluvial sediments inset within material being washed off the slopes to the north by gullying. As shown in Figure 7.6, units A-E appear to be inset within the overlying grey deposits (units F-I). This section reconstructs the phases reflected in terrace fills and addresses whether units A-E truly constitute an inset terrace or are part of the same terrace as units F-I.

Unit A grades from fine to medium sands preserving fossilised stems and roots. There is a substantial silt contribution to the sedigraph (38.8% - Fig. 7.7a) and organic content is high (Table 7.2). This unit exhibits weak magnetic susceptibility (χ_{LF} = 18), although χ_{FD}% is relatively high (4%) and both S values exceed above sampled units with only 33% and 11% of the applied remanence unreversed at -100mT and -300mT respectively (Fig. 7.8c). Unit A is sharply bounded by clast-supported medium gravels that comprise unit B (Gc). Unit C consists alternating thinly bedded organic and clastic sediment (64.7% sand - see Fig 7.7b) and is sharply bounded above by minerogenic, matrix-supported gravels (unit D - Gms). Unit C exhibits comparably weak magnetic susceptibility to unit A (χ_{LF} = 22). S values are considerably lower with 25% and 7% of the applied remanence unreversed at -100mT and -300mT respectively (Fig. 7.8c).

Unit E consists of entirely silt and clay (99.8% - Fig 7.7c) and soil organic matter content is high (Table 7.2) despite apparent absence of plant macrofossils. Total magnetic susceptibility peaks (χ_{LF} = 33) compared to other sampled units as well as

the χ_{FD}, $\chi_{ARM,}$ IRM_{1T} and HIRM values (Fig. 7.8a). The S values are relatively low with 20% and 5% of the applied remanence unreversed at -100mT and -300mT respectively (Fig. 7.8c).

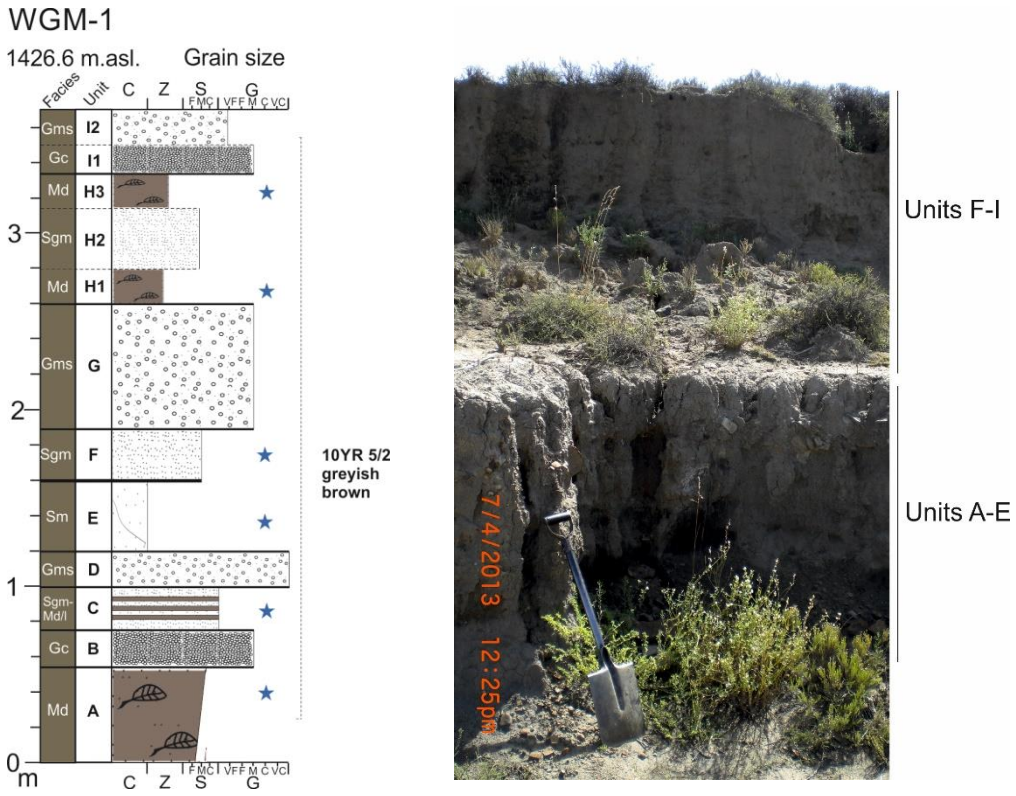

Figure 7.6 – photograph and sedimentary log of outcrop WGM-1.

A sharp, planar contact separates units E and F, the latter exhibiting increased sorting and substantially coarser material (65.4% coarse to very-coarse sand- Fig 7.7d) with substantially lower bromine and LOI values (Table 7.2). Total magnetic susceptibility is slightly lower (χ_{LF} = 25), whilst χ_{FD} and χ_{ARM} are both much lower and IRM_{1T} remains high (400) and the HIRM and Soft_IRM are very slightly smaller (Fig. 7.8a). The granulometric quotients are significantly smaller with the exception of the χ_{ARM}/χ_{FD} (280 - Fig. 7.8b). The proxies for mineralogical composition are nearly identical to unit E (0.47 – Fig. 7.8c). Unit G consists of matrix-supported medium gravels, constituting the thickest alluvial unit of the outcrop (70 cm). Unit H consists of two distinct organic beds (H1 and H3) separated by a relatively thick (35 cm) and minerogenic coarse sand unit.

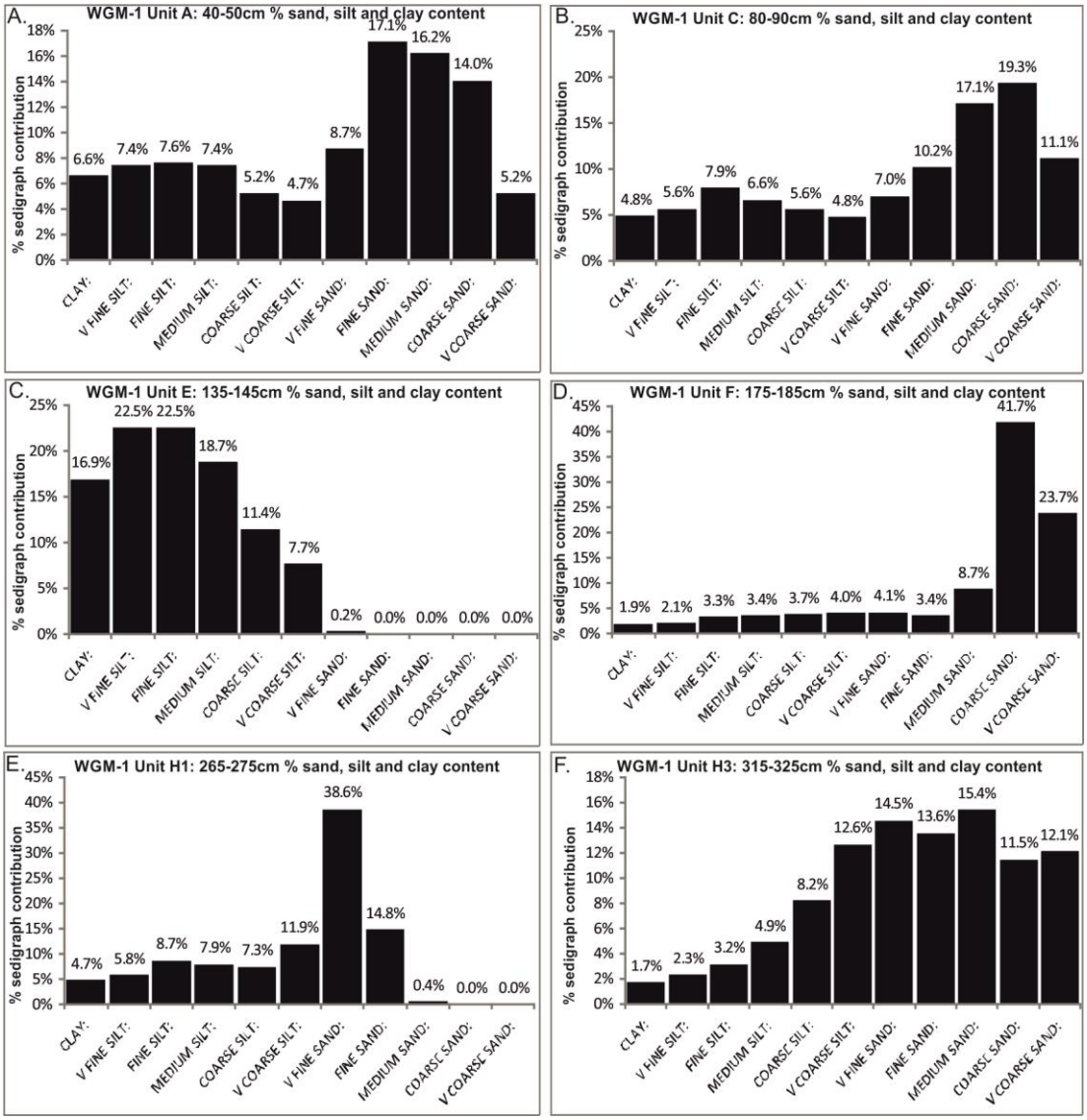

Figure 7.7 – % sand, silt and clay content derived from Coulter grain size analysis on samples collected from outcrop WGM-1.

Subunit H1 consists of predominantly very fine-fine sands (53.4% combined), but with a large silt/clay component (46.6% - Fig 7.7e) and local plant macrofossil fragments. Total magnetic susceptibility is very slightly lower than unit F (χ_{LF} = 21), as are the χ_{ARM} (60) and IRM_{1T} (350) and Soft_IRM (88), whilst χ_{FD} and HIRM are both slightly higher (Fig. 7.8a). The granulometric quotients are nearly identical to unit F (Fig 7.8b). S values are slightly higher than unit F with 25% and 7% of the applied remanence unreversed at -100mT and -300mT respectively (Fig. 7.8c).

Table 7.2 – % loss on ignition and bromine (ppm) data for sampled horizons at WGM-1.

Unit	Height (cm)	Loss on ignition (%)	Bromine (ppm)
A	40-50	2.92	50.5
C	80-90	1.98	27.4
E	135-145	3.31	41.6
F	175-185	1.41	12.1
H1	265-275	1.94	7.2
H3	315-325	2.43	15.4

Subunit H3 is substantially coarser (67.1% sand - Fig 7.7f). Bromine concentration is doubled (15.4 ppm) compared to unit H1 (7.2 ppm) with a slightly higher LOI% (2.43% - Table 5.2). Total magnetic susceptibility is slightly higher (χ_{LF} = 24) than H1 as are the other concentration-related proxies albeit the HIRM, which is slightly lower (20 – Fig 7.8a). Similarly, the granulometric proxies are slightly higher – the largest difference occurring in the χ_{ARM}/χ_{FD} quotient (245 – Fig. 7.8b). The S values on the other hand are both slightly lower with 23% and 4.7% of the applied remanence unreversed at -100mT and -300mT respectively (Fig. 7.8c).

Unit I unconformably overlies unit H consists of clast-supported medium gravels (Gc) which grades to matrix-supported very fine gravels. The colour of sampled units is invariable: 10YR 5/2 greyish brown.

7.3b: WGM-1 interpretation

The fine-grained sediments of unit A indicate deposition under low energy conditions Bromine content indicates very high concentrations of organic matter (50.5 ppm – Table 7.2), confirmed by the presence of abundant plant macrofossils. This unit also has the highest contribution of AF minerals (S_{-300}% = 10.4), probably goethite considering indicated conditions of poor drainage. The small amount of remanence carrying ferrimagnets will be related to their dissolution and to the formation of paramagnetic minerals under waterlogged conditions. Chapter 4 outlined the relations between fine grained sediments and dense accumulations of vegetation even in central channel positions where the channel crosses bedrock. In such settings, it was documented in Chapter 4 how a veneer of coarse clast-supported gravels cap the vegetation, implying that exchange of very coarse material through such reaches may only occur during the highest flows due to the attenuating effect of vegetation on streamflow. The association between the organic rich sands (A) and clast-supported gravels (unit B) indicate this sequence (Table 4.3; analogue 4).

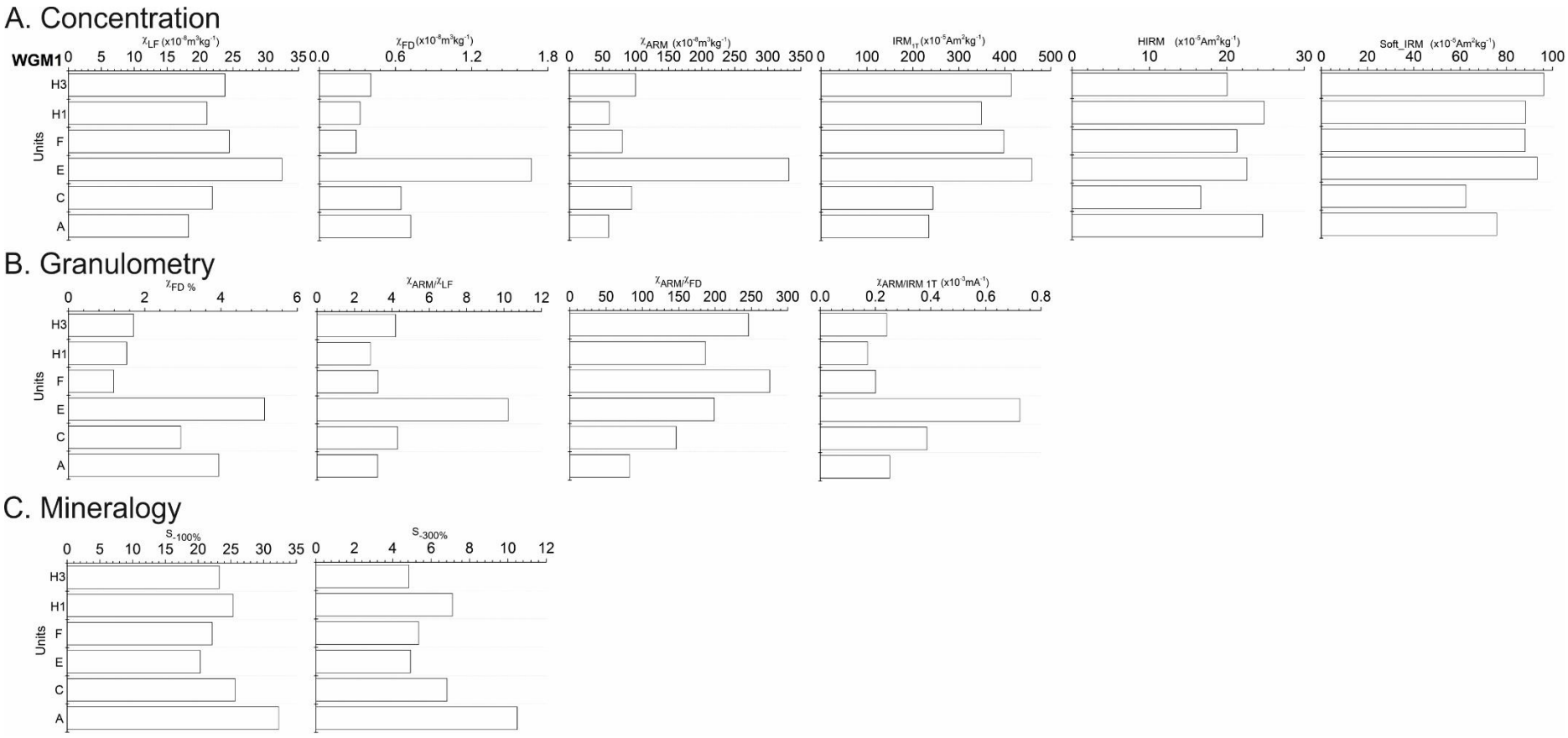

Figure 7.8 – mineral magnetic parameters from sampled horizons at outcrop WGM-1.

The overlying alternating sands and muds of unit C reflect shorter alternating phases of local vegetation growth in the channel which have then been incised by high energy flood deposits (unit D) as reflected in the sharp, undulating bed contact. The very poorly sorted matrix of these gravels, in concert with basal scour structures and a reduction in clast frequency (right to left) implies that the mode of deposition could have been a channelized debris flow. The overlying silty clays (unit E) indicate low energy deposition probably at the margins of the active sedimentation zone (floodplain), with abundant organic matter content evidenced by the high Br content (41.6 ppm – Table 7.2). This unit exhibits the highest concentrations of remanence carrying ferrimagnets that are SD and SP size compared to the underlying units (Fig. 7.8). As the deposits are palaeofloodplain, this undoubtedly relates to incipient soil development and formation of pedogenic magnetite.

In contrast, unit F exhibits comparatively low organic matter content (Br = 12.1 ppm) and much lower indications of weathering reflected in the very low values of χ_{FD}% and χ_{ARM} which indicate a predominantly multi-domain ferrimagnetic assemblage, though the total proportions of the hard and soft magnetic minerals is only slightly lower than unit E (see HIRM and Soft_IRM respectively). This abrupt switch to a 'lithogenically' dominated magnetic assemblage implies the junction of unit E and F is a true unconformity rather than mere activation surface. Furthermore, as intensity of weathering (partially dependent on time) is considerably lower, this implies that units F-I are part of the same fluvial terrace rather than A-E representing an inset deposit (Fig. 7.6).

The coarser facies of unit F evidence higher energy conditions of transport, but whether this represents channel or floodplain sediments is a matter for further consideration. In order for the original floodplain surface to aggrade either: 1) a larger flood would be required to inundate the floodplain and lay down coarse sands; and/or 2) the original channel aggraded such that either floodplain sedimentation could continue or the channel infilled completely and the former floodplain surface became the channel bed.

The inverse grading from the sands of unit F to the overlying matrix-supported gravels with poorly defined bedding (unit G) probably reflects infilling of the original

channel to the level of the palaeofloodplain (unit E), such that bar deposits then buried this.

The overlying organic-rich unit (H) is interpreted as wetland vegetation at the margins analogous to that found in the modern channels in the vicinity of rock barriers (discussed previously), although the contemporary analogues are situated only just above the bedrock surface. The very fine calibre of sediment expressed here may reflect the channel thalweg having migrated to a greater distance from this part of the palaeovalley, such that inundation only occurred during times of high flow, with low energy conditions created by residual ponding after flow recession allowing silts and clays to drop out of suspension. In this regard, the thick, comparatively coarse sand unit (H2) could reflect increasing proximity of the channel thalweg once again, or reflect a high energy flow which activated the entire channel such that coarser material could be delivered buring the vegetated surface expressed in H1. The organic silts at H3 indicate a return to low energy conditions and high vegetation cover.

Notably, the ferrimagnetic grain size signature of units H1 and H3 (like unit F) is multi-domain, with very low contributions of SP/SD grains. This implies that any incipient soil development that could have produced pedogenic ferrimagnets has been removed by gleying. Nevertheless, the Soft_IRM and IRM_{1T} for both units H1 and H3 imply that paramagnetic activity is subordinate to ferrimagnetism, implying that waterlogging was not of sufficient duration to produce ferrihydrite. The increase in HIRM and S_{300} indicates increasing contributions of 'hard' minerals, probably goethite which, being an AF mineral, is likely the major culprit responsible for reduction in ferrimagnetic intensity χ_{LF}. The unconformable gravels (unit I) likely represent a big flood emplacing coarse deposits at the channel margin capping the wetland deposits.

7.4a: WGM-2 analysis

Log WGM-2 was obtained from a 6.3 m gully exposure on the left bank opposite WGM-1 (Fig. 7.1 and 7.9).

Unit A consists of imbricated cobbles and boulders up to 30 cm in diameter. It is capped by a thin, laterally continuous (4-5 cm) calcretised horizon. Unit B consists of

minerogenic (Table 7.3) thinly bedded, predominantly coarse to very coarse sands (63.9% - Fig. 7.10a), which exhibit mottled iron concentrations around grains.

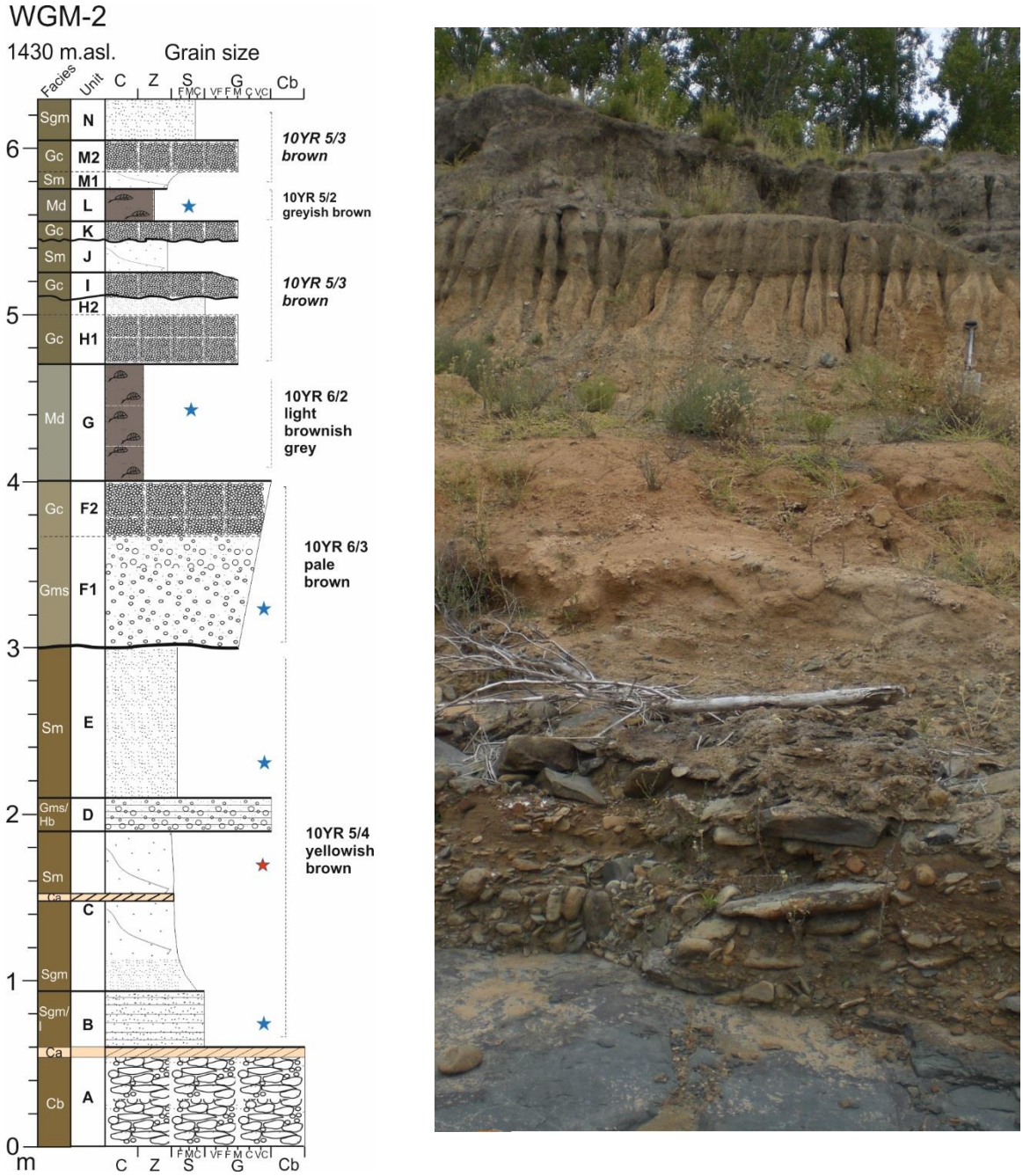

Figure 7.9 – photograph and sedimentary log of outcrop WGM-2.

Total magnetic susceptibility is relatively high (χ_{LF} = 33), but χ_{FD} and χ_{ARM} relatively low (0.65 and 75 respectively). The IRM_{1T} is high (466) and the Soft_IRM larger relative to the HIRM compared to the other units (Fig. 7.12a). In terms of magnetic granulometry (Fig. 7.12b), χ_{FD}% is low (2%) In terms of mineralogical proxies (Fig. 7.12c), the lowest S values are found for unit B with 18% and 1% of the applied

remanence unreversed at -100mT and -300mT respectively. A sharp, planar contact separatess units B and C, the latter grading from coarse sand to very coarse silt. The remnants of a thin calcrete horizon were found at 150 cm (unit C), which appears to have been deeply eroded (Fig. 7.11).

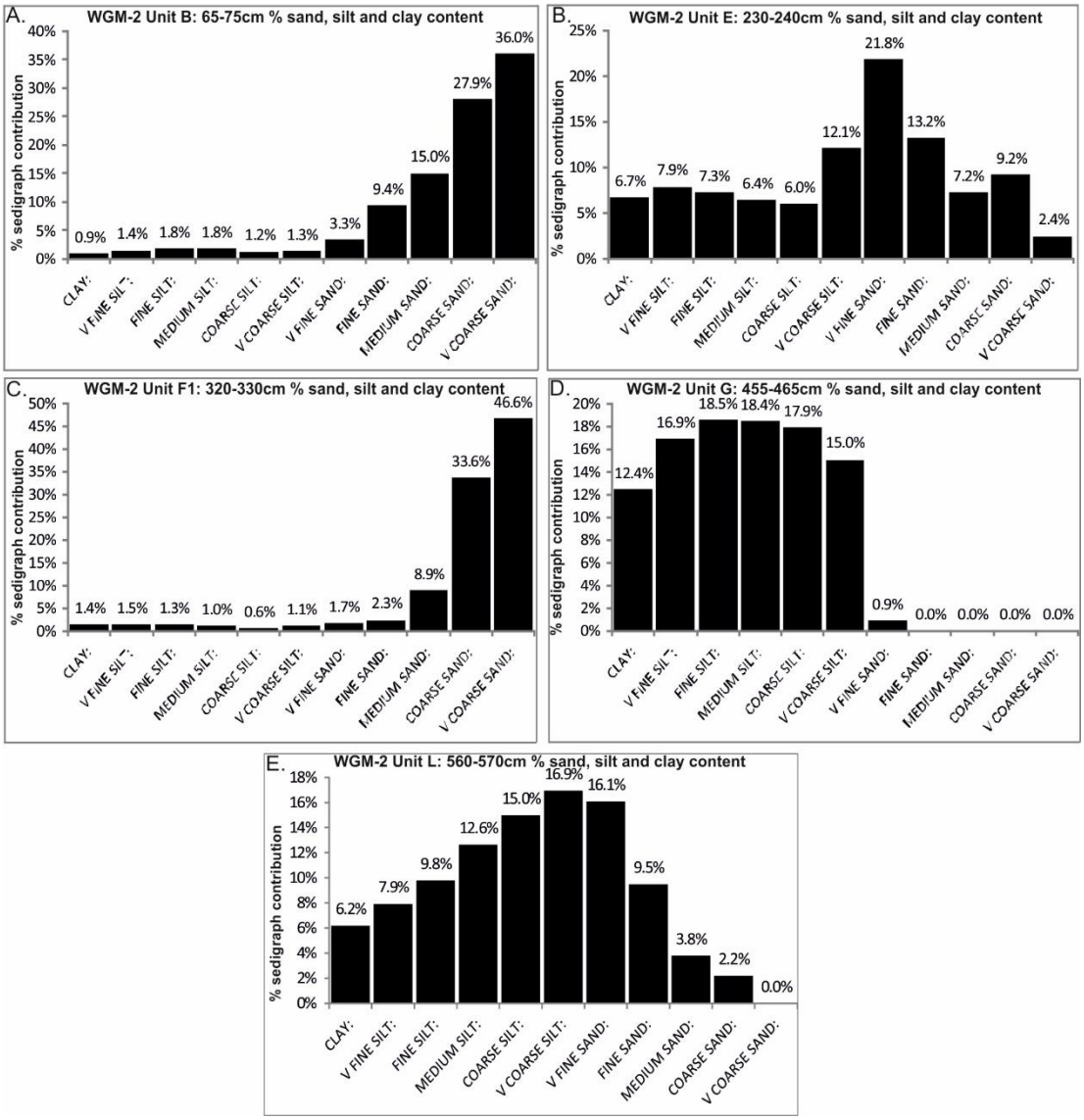

Figure 7.10 – % sand, silt and clay content derived from Coulter grain size analysis on samples collected from outcrop WGM-2.

Unit D consists of thinly bedded matrix-supported gravels and is capped by massive very poorly sorted sands that comprise unit E (Fig. 7.10b). Unit E exhibits the strongest magnetic susceptibility values for the entire outcrop (χ_{LF} = 42~) and all other concentration-related proxies with the exception of the HIRM exhibit the highest values relative to other sampled units (Fig. 7.12a). χ_{FD}% is similarly high (4%), although the quotients are modest by comparison (Fig. 7.12b). S values are slightly higher relative to unit B (Fig. 7.12c).

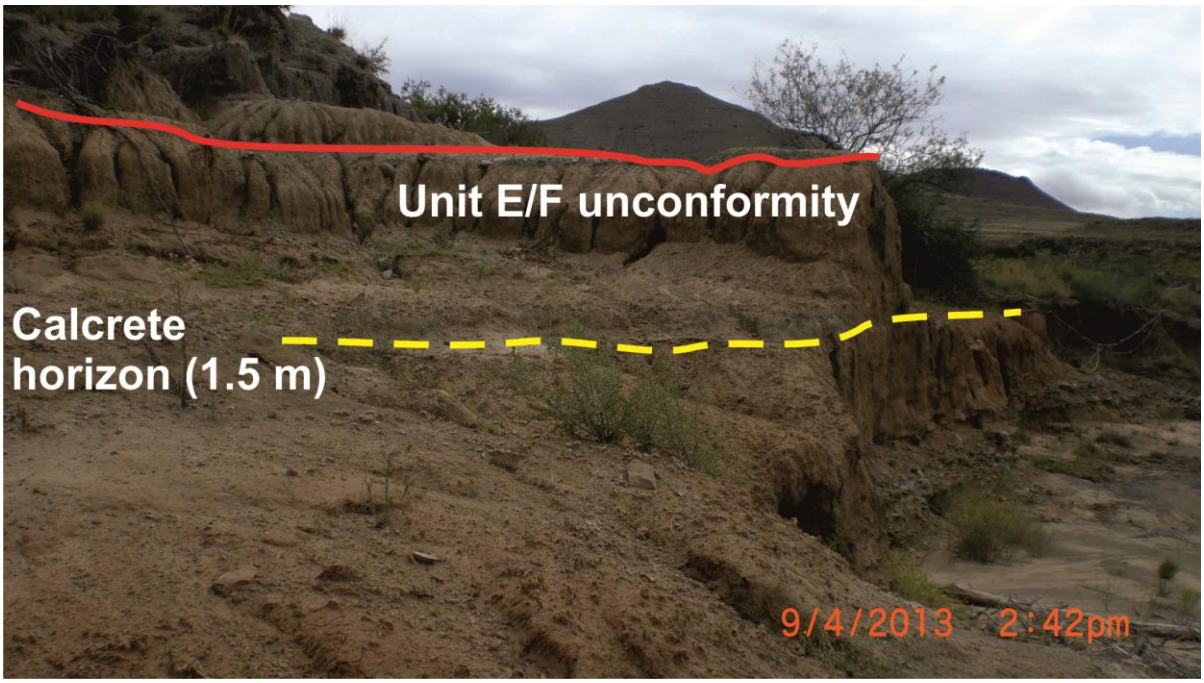

Figure 7.11 – photograph of WGM-2 highlighting the remnants of a thin calcrete horizon similar in macro-morphology to that identified at 55-60 cm. Above, the stratigraphic unconformity is highlighted between units E and F.

A wavy, sharp contact separates units E and F with a colour change from 10YR 5/4 yellowish brown (units A-E) to 10YR 6/3 pale brown. Unit F is a matrix-supported medium gravel package (subunit F1) which grades inversely to clast-supported very coarse gravels (subunit F2). The matrix of subunit F1 is moderately-well sorted consisting primarily of coarse to very coarse sand (80.2% - Fig. 7.10c). Total susceptibility is much lower than unit E (χ_{LF} = 23) as are the other concentration-based proxies except the HIRM, which is slightly higher (30 – Fig. 7.12b). Crucially, the S_{-300}% proxy is substantially higher indicating only 10.6% of the applied remanence was reversed at -300mT (Fig. 7.12c).

A sharp planar contact separates units F and G, the latter being comparatively very fine-grained consisting of predominantly clays and silts (99.1% - Fig 7.10d) which house fossilised plant remains. Bromine and LOI% values are higher relative to preceeding sampled units (Table 7.3) and soil colour is greyer (10YR 6/2). Unit G also exhibits very weak magnetic susceptibility (χ_{LF} = 11), but HIRM is still relatively high (19 – Fig. 7.12a). The granulometric proxies are, with the exception of χ_{FD}% (1.8), relatively high; for example the $\chi_{ARM}/_{IRM1T}$ (0.36 - Fig. 7.12b). The S values are markedly higher compared to the other units with 47% and 18% of the applied remanence unreversed at -100mT and -300mT respectively.

Unit H consists of clast-supported gravels overlain by a single medium-thickness bed of massive, minerogenic sand. The contact between unit H and I is sharp, undulating.

Table 7.3 – % loss on ignition and bromine (ppm) data for sampled horizons at WGM-2.

Unit	Height (cm)	Loss on ignition (%)	Bromine (ppm)
B	65-75	1.38	-
E	230-240	1.58	4.8
F1	320-330	1.48	2.7
G	450-470	2.58	6.4
L	555-575	2.4	13.3

The clast-supported gravels above (unit I) are laterally discontinuous with subtle changes in clast size from medium gravel to a thin veneer of very fine gravel (see Fig. 7.9). Unit J is a massive medium thickness (0.2 m) bed of silt, which is unconformably overlain by clast-supported medium gravels (unit K). Collectively, the colour for units I-K is 10YR 5/3 brown. Unit L is a fine-grained (53.4% fine-very fine sand; 46.2% silts and clays - Fig 7.10e) package with abundant fossilised plant remains and is greyer (10YR 5/2). The highest bromine values are found for this unit (13.3 ppm - Table 7.3). Total magnetic susceptibility is somewhat higher (χ_{LF} = 21.5), whilst the χ_{FD} and χ_{ARM} are much higher compared to unit G (Fig. 7.12a). χ_{FD}% is the highest recorded for this outcrop (5.4%) as is the $\chi_{ARM}/_{IRM1T}$ (0.45 - Fig. 7.12b). S values are lower than unit G, comparing well with subunit F1 (Fig. 7.12c). Unit M sharply overlies L, consisting of silt which grades to sand and then clast-supported medium gravels. The top of the succession (unit N) consists of massive coarse sands and, like unit L, the colour is 10YR 5/3 brown.

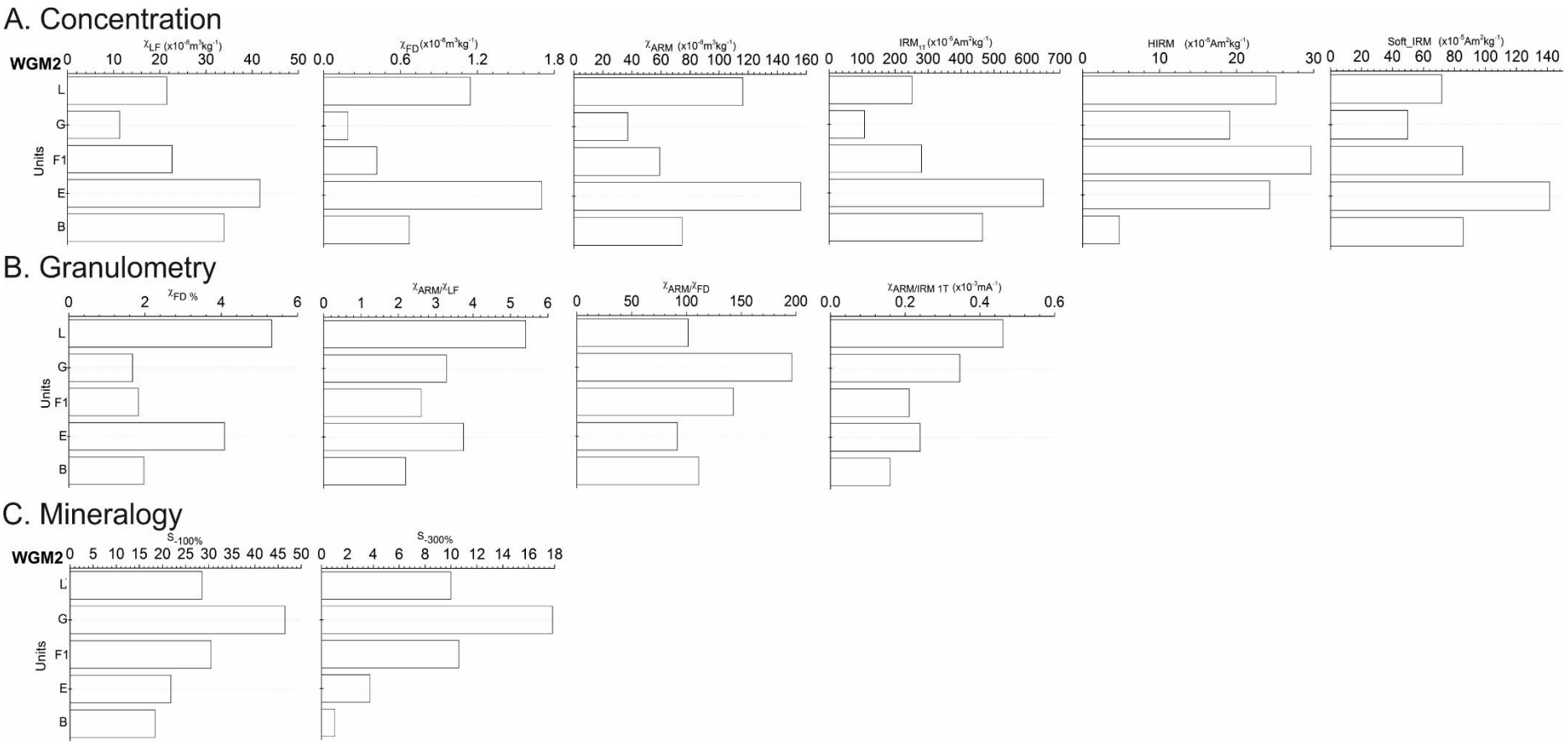

Figure 7.12 – mineral magnetic parameters from sampled horizons at outcrop WGM-2.

7.4b: WGM-2 interpretation

Units A-E reflect channel bar and floodplain aggradation evidenced by the upward fining sequence, with coarser beds of gravel (unit D) reflecting larger flood events. Soil organic matter content reflected in the LOI% is low, particularly for unit B. The massive nature of units A, C and E indicate that aggradation may have been rapid. The thin, laterally continuous calcrete horizon (55-60 cm) has the macroscopic characteristics of an immature rhizogenic calcrete formed by biological processes associated with root channels resulting in lateral accretion of calcite in the phreatic soil zone just above the water table (Wright et al., 1988). The fact that this sediment package is so close to bedrock would, under an aggrading channel regime, favour a raised water table which, assuming sufficient vegetation cover and supply of Ca^{2+} ions, result in a rhizogenic calcrete forming. It is not possible to infer in detail the characteristics of the thin, calcrete horizon identified above at 1.5 m (Fig. 7.11) because it has been significantly eroded and leached. Before any inference is made concerning the probable nature of the second calcrete layer (1.5 m), it is necessary to consider other evidence that may (not) indicate groundwater movement.

The presence of mottled iron stains around sand grains in unit B likely indicates groundwater-driven saturation, although S_{-300}% (1.2%) values indicate only a small contribution from AF minerals and the IRM_{1T} is still relatively high (460) indicating that paramagnetic minerals are not dominant. Nevertheless, χ_{LF} is lower for unit B (33) compared to E (42) which probably indicates some groundwater related dissolution of magnetite/maghemite irrespective of degree of paramagnetic mineral formation (Grimley and Arruda, 2007). In concert with the yellowish brown (10YR 5/4) colour, this reinforces that the lower part of the succession in particular has been subject to changing groundwater level. Therefore, the remnants of the calcrete at 150 cm probably relate to changing groundwater conditions. These characteristics attest to a raised water table which could not exist if the channel were incised as it would drain into the channel to form concentrated streamflow (Boardman, 2014).

Units B and E exhibit higher concentrations of remanence carrying ferrimagnetic minerals than the base of WGM-1 with low to moderate contributions from SP/SD grains (Fig. 7.12). In concert with the relatively lithified nature of WGM-2 sediments, this evidence indicates the two sediment packages are not stratigraphically coeval.

The sharp, undulating contact between units E and F indicates incision into the relatively indurated, compacted sediment of unit E. The fact that unit E exhibits higher concentrations of SP grains (χ_{FD}% = 4%) below this unconformity, indicates that a period of pedogenesis must have taken place prior to channel entrenchment and the deposition of the friable unit F-N sediments. In summary, units A-E constitute a distinct lithostratigraphic 'member' according to 1) bar/floodplain facies and 2) distinct pedogenic overprinting indicating concentrations of pedogenic magnetite, soil compaction and induration, and $CaCO_3$ deposition by groundwater and leaching at the base.

Unit F1 is interpreted as marginal channel bar facies similar to those described at WGW and WGM-1 (see also Table 4.3, analogue 5) and exhibits very low organic matter content (2.7 ppm – Table 7.3), which implies that aggradation of these deposits was rapid enough to prevent significant colonisation by vegetation and/or soil development. Unit F also exhibits much lower concentrations of remanence carrying ferrimagnetic minerals compared to unit E, as well as a much higher contribution from AF minerals reflected in the high S_{-300}% (10.5%). Figure 7.13 indicates that sediment texture is an important driver of anti-ferromagnetic mineral concentration (R^2 = 0.49), but unit F1 is an outlier.

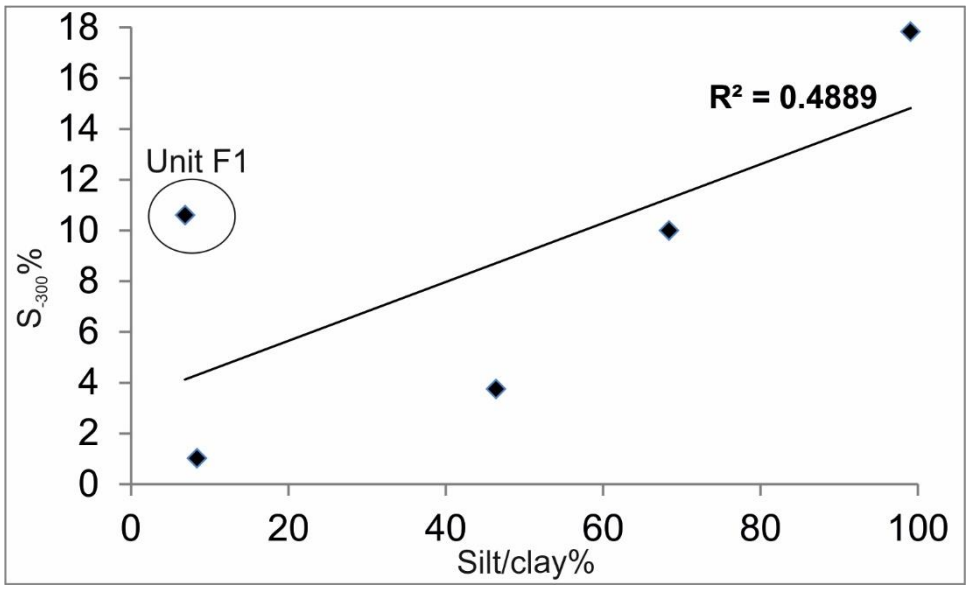

Figure 7.13 – bi-plot showing S_{-300}% versus %silt clay for sampled units from WGM-2.

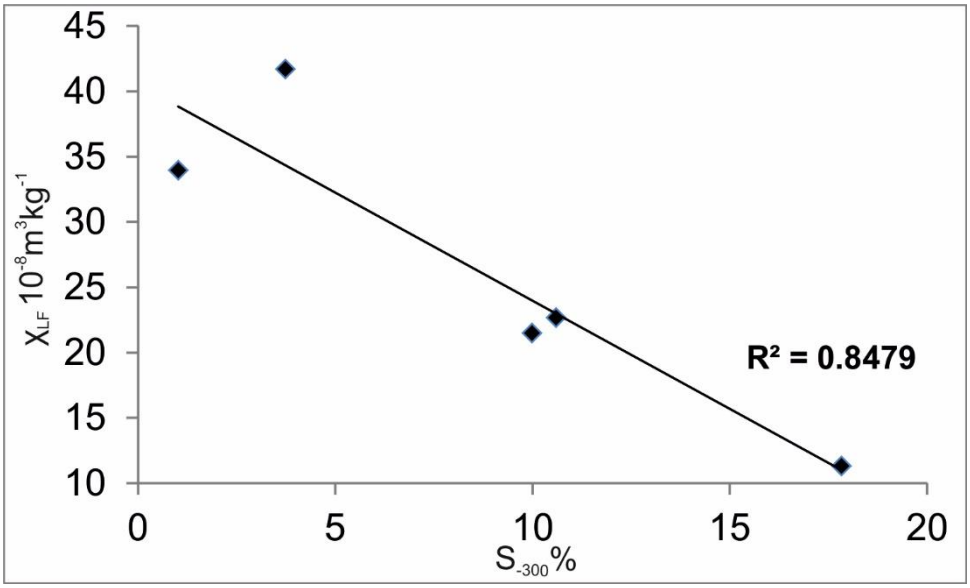

Figure 7.14 – bi-plot showing S_{-300}% versus low frequency magnetic susceptibility for sampled units from WGM-2.

This could be due to two factors: 1) the AF signature is inherited from reworked sediment from upstream; 2) soil moisture content was high due to the relatively poorly drained underlying unit E. The nature of the facies indicating channel entrenchment, with deposits laid down under high energy conditions favours the first hypothesis.

If unit F1 is removed from the dataset, $R^2 = 0.924$, indicating that for the other units, texture is the principal driver of AF mineral concentration, which is itself related to the low-energy depositional environment of the units above.

The overlying muds (unit G) are interpreted as wetland facies, with deposition of silt/clay (99.1% - Fig 7.10d) under low energy conditions. Bromine values although relatively high (6.4 ppm) compared to below (2.7 ppm – unit F1) do not indicate substantial amounts of soil organic matter. The association between coarser flood deposits (unit F, H, J, M) and these mud deposits (G, L) is interpreted as reflecting a laterally migrating, aggrading channel akin to that described for WGM-1. On the basis of these facies associations, units F-M are classified as lithostratigraphic member B.

Unit G is dominated by a canted anti-ferromagnetic signature. The very low Soft_IRM of this unit implies low total concentrations of ‘soft’ ferrimagnets relative to the other units, though on the basis of the high S_{100}% the existing ferrimagnets

probably reflect a ‘hard’ form of magnetite, though inherited pedogenic haematite from eroding upland catchment sources cannot be ruled out (Liu et al., 2015). Further, the magnetic remanence proxies (χ_{ARM} and IRM_{1T}) indicate a paramagnetic contribution to the overall magnetic assemblage, though it has already been established that AF mineral concentration is the main driver of susceptibility (R^2 = 0.848 – Fig. 7.14). These magnetic properties attest to different conditions of magnetic mineral formation than those reported for units B, E and F1. Given the pale colour and high moisture conditions (10YR 6/2), goethite is most likely to be the dominant anti-ferromagnetic mineral (confirmed by high S_{300}) rather than haematite, since the latter preferentially forms in dry, oxidising conditions (Lyons et al., 2010).

The laterally discontinuous, sharply bound gravels (unit I and K) are interpreted as a localised channel bar infilling scour troughs with silty sands deposited during recessional phases of flow or in low energy settings (unit J). Unit L exhibits the highest concentrations of organic matter (Br = 13.3 ppm). The Soft_IRM for this unit indicates slightly higher concentrations of ‘soft’ ferrimagnets, with slightly higher proportions of SP/SD grains as compared to the preceeding units (G and F1). This increased fine-grained ferrimagnetic component is probably due to weak illuviation associated with successive phases of vegetation growth on the contemporary terrace surface, which may partially account for the higher Br values relative to unit G. Notably, the higher remanence parameters attest to a reduced paramagnetic influence indicating better drained conditions relating to the coarser texture of this unit (Fig. 7.10e). The relatively large HIRM compared to unit G implies higher contributions of AF minerals, probably goethite. The inversely graded sands and gravels (unit M) capping the wetland facies (unit L) probably represent fresh bar deposition at the former channel margin sufficient to bury the former wetland vegetation. The massive, unweathered sands capping the succession likely represent overbank sediments. This sequence of alternating coarse-fine deposits is analogous to the contemporary wetlands in bedrock reaches reported in Chapter 4 (Table 4.3; analogue 4).

7.5a: WGM-3 analysis

Log WGM-3 was obtained from a 4.9 m exposure on the right bank approximately 100 m downstream of WGM-1. The sediments extend all the way up slope as far as

(Fig. 7.15) an actively eroding knickpoint through sandstone representing the side of the valley. Erosion through bedrock has produced a local 'ampitheatre' into which these sediments have been deposited. The deposits of WGM-3 locally have a 'fan-like' form (Fig. 7.15), but the limits of this deposit extend downstream and have been truncated by the deposits of WGM-4 which forms a distinct inset terrace surface (discussed in section 7.6). The sediments of WGM-3 are deeply eroded with badland topography, dendritic gullying and rilling (Fig. 7.15 and 7.16) and as a result, discerning a clear junction between what could hypothetically be a fan (Fig. 7.15) from other deposits sourced from proximal slopes was not possible.

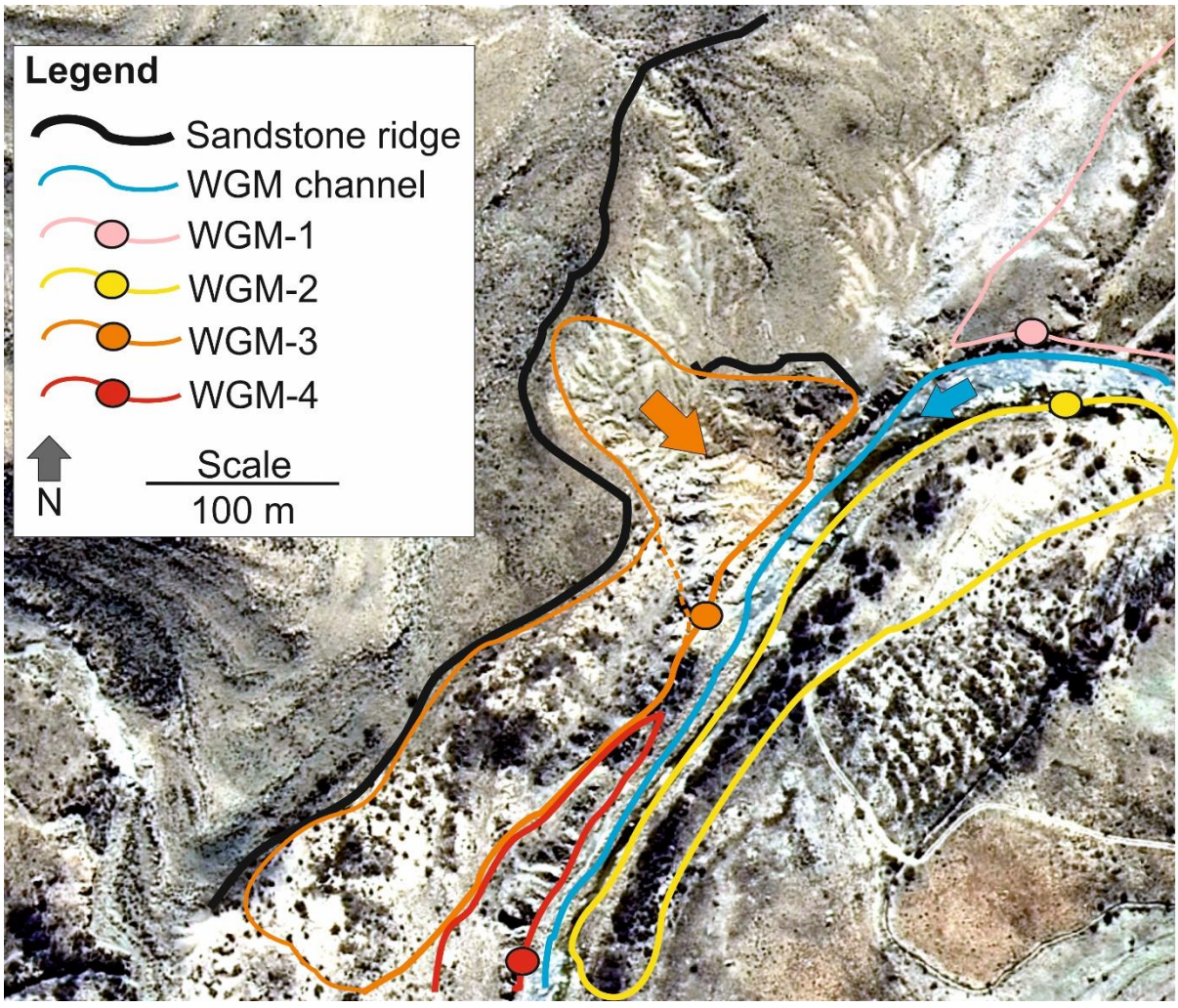

Figure 7.15 – digitally referenced aerial photos of WGM channel showing surveyed limits of each unique stratigraphic succession as portrayed in logs WGM-1 -4.

Unit A consists of massive poorly sorted very fine-medium sands (collectively 75.8% - see Fig. 7.16 and 7.17a) and directly overlies mudstone bedrock. A colour change from 7.5YR 5/4 brown to 7.5YR 6/3 light brown occurs at 40 cm marking the

transition between units A and B (Fig. 7.16). Total magnetic susceptibility peaks in unit A (χ_{LF} = 42) and the other concentration related proxies (except χ_{FD}) are high (Fig. 7.18a). Conversely, the granulometric and mineralogical proxies are all relatively low (Fig. 7.18b-c). Subunit B1 inversely grades from sandy silt (51.8% sand; 48.2% silt/clay - Fig. 7.17b) to deeply weathered, matrix-supported medium sandstone gravels (subunit B2).

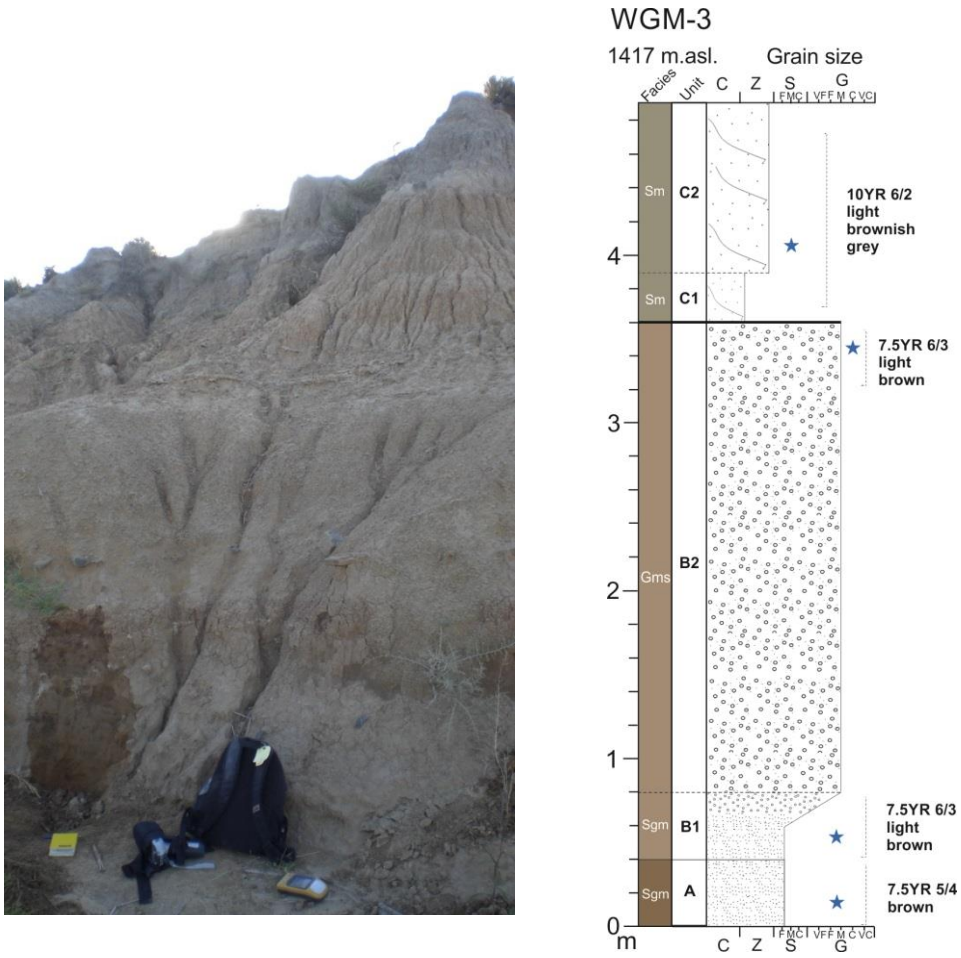

Figure 7.16 – photograph and sedimentary log of outcrop WGM-3.

Some sandstone clasts have broken up in situ to form 'exploding lenses' which exhibit local mottling (10YR 6/4 light yellowish brown). Bromine and LOI% are substantially higher than units A and B1 (Table 7.4). The sample obtained from 340-350 cm (subunit B2) shows the sedigraph to be silt/clay dominated (98.3% - Fig. 7.17c). Taken together, magnetic susceptibility declines from B1-B2, whilst χ_{FD} and χ_{ARM} peak (1.28 and 116 respectively), and both the Soft_IRM and IRM_{1T} drop by over 50% (Fig. 7.18a). Subunit B1 exhibits very large χ_{ARM}/χ_{FD} (400), whereas B2

has high χ_{FD}% and $\chi_{ARM}/_{IRM1T}$ (Fig. 7.18b). S values increase incrementally (Fig. 7.18c).

A sharp, planar contact separates units B and C, the latter displaying a significant colour change to 10YR 6/2 light brownish grey and contains the highest concentrations of organic matter (Table 7.4). Unit C consists of clast poor, very fine silty clay, which coarsens above (subunit C2 - 47.3% sand; 52.7% silt/clay - Fig. 7.17d). Total magnetic susceptibility is lowest for this unit (χ_{LF} = 16) along with the other concentration-based proxies except the HIRM (Fig. 7.18a). The χ_{ARM}/χ_{FD} values are relatively high (240) compared to unit B2 and χ_{FD}% is very small (1 – Fig 7.18b).

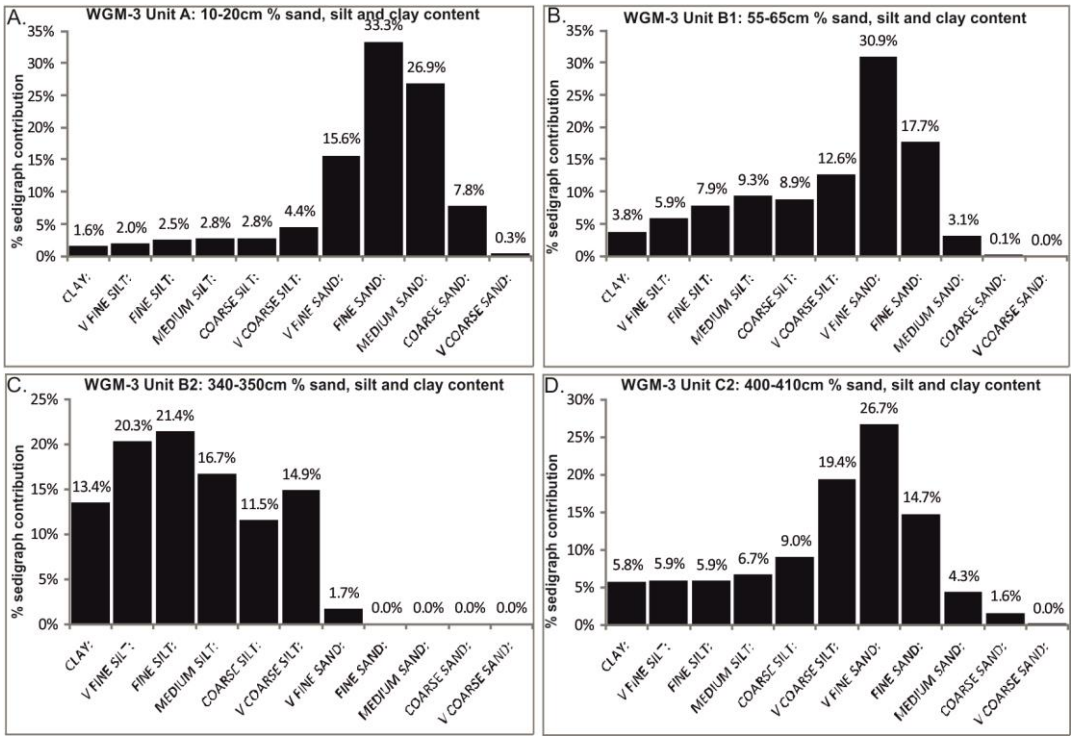

Figure 7.17 – % sand, silt and clay content derived from Coulter grain size analysis on samples collected from outcrop WGM-3.

Table 7.4 – % loss on ignition and bromine (ppm) data for sampled horizons at WGM-3.

Unit	Height (cm)	Loss on ignition (%)	Bromine (ppm)
A	10-20	0.98	2.7
B1	55-65	-	4.5
B2	340-350	2.57	46.1
C2	400-410	1.8	53.4

The S values peak compared to the other units with 33% and 10.3% of the applied remanence unreversed at -100mT and -300mT respectively (Fig. 7.18c).

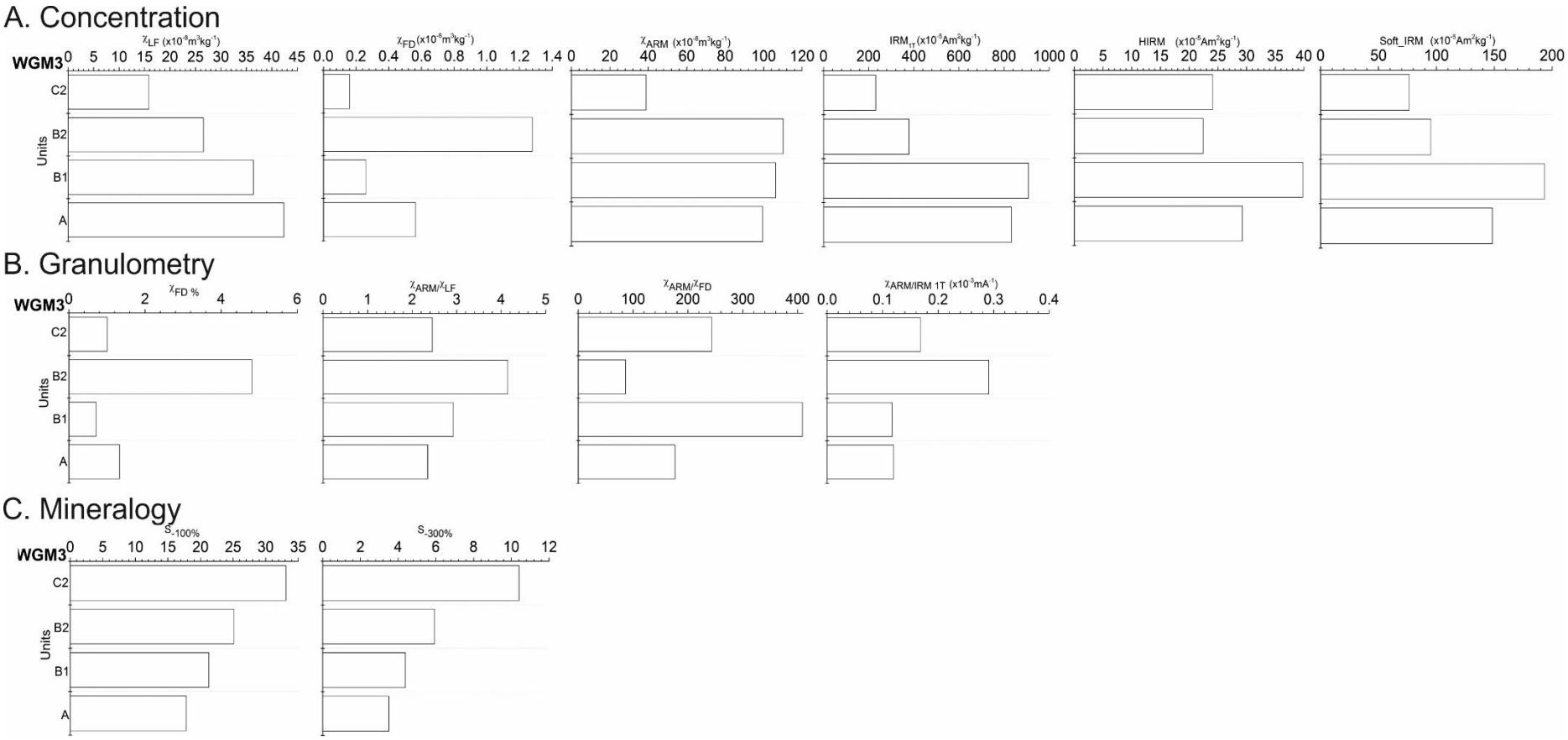

Figure 7.18 – mineral magnetic parameters from sampled horizons at outcrop WGM-3

7.5b: WGM-3 interpretation

The geomorphic evidence is that these deposits are sourced from the slope to the north having been deposited in a natural amphitheatre created by tributary headcutting through a major sandstone ridge upslope.

The basal units (A and B1) indicate low energy deposition. Soil organic matter content for both units A and B1 is low. Furthermore, the χ_{FD}% is very low for both units, indicating little in situ pedogenesis. The χ_{ARM} values (99-108), indicate, in concert with the very low χ_{FD}%, that most of the fine-grained ferrimagnets lie on the SD side of the narrow viscosity band, but the very low $\chi_{ARM}/_{IRM1T}$ indicates a predominantly MD ferrimagnetic assemblage. This attests to a strongly 'lithogenic' signature no doubt derived through erosion of the sandstone ridge as well as upslope soils. The inverse grading to gravels (unit B2) is consistent with other reported case studies of fan progradation (see Chapter 6.3).

Figure 7.19 – photograph taken overlooking slope deposits reported for zone A2 in the text with the sediments contained within outcrop WGM-2 to the left (upstream) and WGM-3 to the right (downstream).

The very fine-grained silt-clay matrix at the top (340-350 cm) exhibits very high organic content (Br = 46.1 ppm – Table 7.4). The χ_{ARM} and the χ_{FD}% in particular peak for this unit indicating moderate-high concentrations of pedogenic SP/SD grains, although the overall total concentration of ferrimagnetic remanence carrying minerals is less than 50% of that exhibited by unit B1. S_{300}% is relatively large (4%)

at the top of this unit indicating higher contributions of haematite. The fact that χ_{LF} decreases as S_{300}% increases implies that susceptibility is controlled by increasing concentrations of AF minerals. Collectively, this evidence indicates a highly vegetated palaeofan surface (340-350 cm).

The sharp, undulating contact separating units B and C indicates an unconformity. The overlying silty sands (C) exhibit very high concentrations of organic matter (Br = 53.4 ppm), but unlike the top of unit B (340-350 cm) show very low concentrations of SP/SD remanence carrying ferrimagnets. Rather, the magnetic signature is dominated by hard AF minerals on the basis of the relatively very high S values (Fig. 7.18c). The fine-grained nature of the facies indicates low energy deposition. Considering that this unit pinches out several metres up the slope perpendicular to the modern channel, the sediments were probably laid down as floodplain sourced from a channel not the hillslope. If the deposits were the product of incision upslope and deposition as a floodout, there would be evidence of distal fining or other progradational features (inverse grading, lenticular bedding). The evidence is that following deposition, this floodplain surface was stabilised by abundant vegetation cover.

In summary, 3.6 m of vertical fan aggradation (units A and B) in this setting could only occur in response to rising base level on the main Wilgerbosch channel. The massive nature of unit B with no intervening depositional hiatuses implies that this phase of aggradation was rapid and probably a response to the backfilling of the main valley.

7.6a: WGM-4 analysis

Log WGM-4 was obtained from a 5 m exposure on the right bank approximately 150 m downstream of WGM-1 (see Fig. 7.15 and Fig. 7.20).

This outcrop is characterised by medium-thick alternating beds of medium-coarse matrix and clast-supported gravels (unit A), whilst above are thick units (up to 1.1 m) of moderate to well sorted sands (unit B – 78.8% coarse to very-coarse sand- Fig. 7.21a) which typically display curved-non-parallel bedding, except for subunit C3 where the sands are massive (72.8% coarse to very coarse sand – Fig. 7.21b). Unit B exhibits large soil columns (up to 40 cm in diameter).

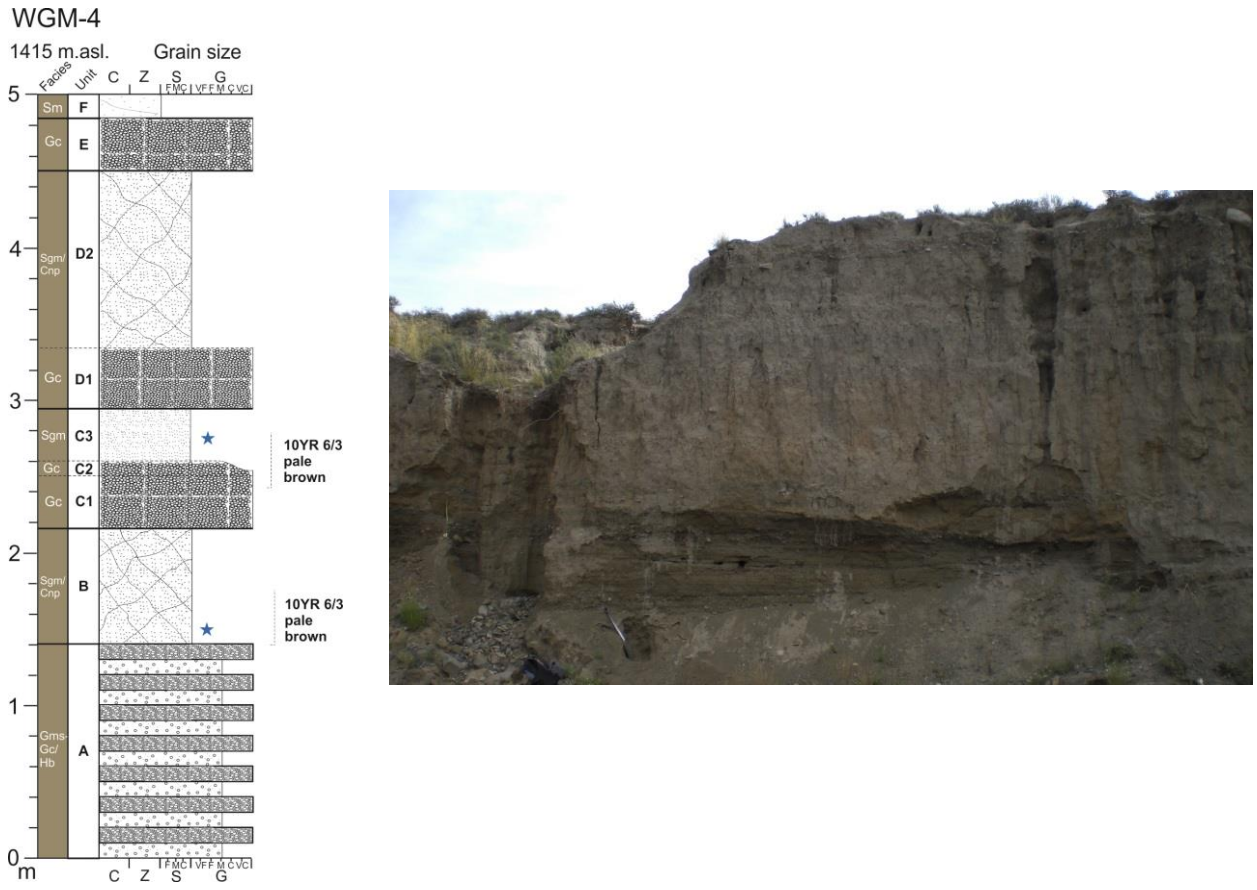

Figure 7.20 – photograph and sedimentary log of outcrop WGM-4.

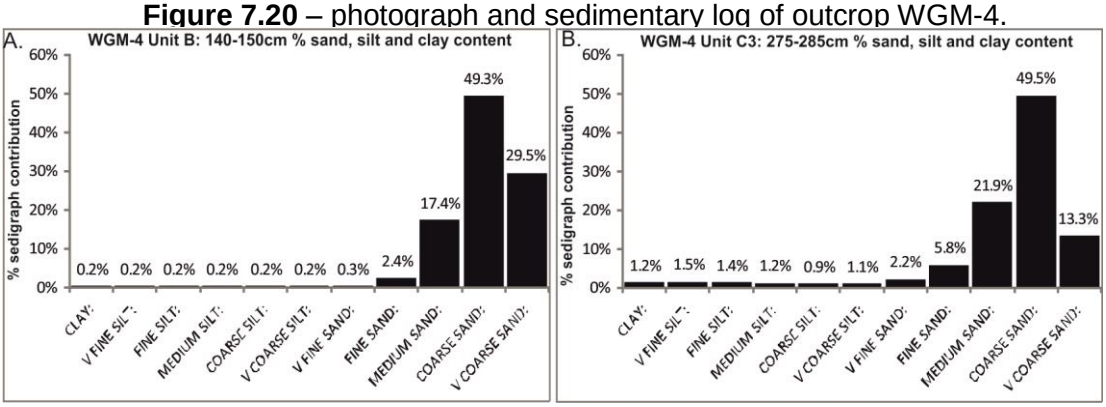

Figure 7.21 – % sand, silt and clay content derived from Coulter grain size analysis on samples collected from outcrop WGM-4.

Unit B exhibits strong total magnetic susceptibility (χ_{LF} = 50 and IRM_{1T} **=** 800 – Fig. 7.22a). The granulometric proxies are all low (Fig. 7.22b), but the $\chi_{ARM}/_{IRM1T}$ parameter is particularly small (0.124). The S values are relatively low with 13.5% and 4% of the applied remanence unreversed at -100mT and -300mT respectively (Fig. 7.22c). In contrast, unit C3 exhibits low total susceptibility (χ_{LF} = 28), a much smaller remanance (IRM_{1T} – 344) and lower HIRM and Soft_IRM (Fig. 7.22a). Both the granulometric and mineralogical proxies are all slightly higher than unit B; in particular, the $S_{-100\%}$ indicates 20.5% of the total applied remanence unreversed at -100mT (Fig. 7.22 b and c).

Table 7.5 – % loss on ignition and bromine (ppm) data for sampled horizons at WGM-4.

Unit	Height (cm)	Loss on ignition (%)	Bromine (ppm)
B	140-150	0.81	0.6
C3	275-285	1.41	1.8

The exposure was too vertical to sample units D & E. Therefore, visual observations are reported. Clast-supported gravels (subunit D1) are overlain by curved non-parallel cross bedded sands (subunit D2), whilst unit E exhibits a sharp contact with D2, again characterised by clast supported gravels. The surface of the terrace is characterised by coarse silt (unit E).

7.6b: WGM-4 interpretation

The very coarse facies of unit A indicate high energy channel deposits. The couplets of horizontally bedded, clast-supported, very coarse gravels and matrix-supported medium gravels are interpreted as stream bedload sediment, with the latter facies signifying flow recession with interstitial filling of the gravels by fine sediment.

These facies associations are subtly different to those reported upstream. Instead of discontinuity-bounded inversely graded units of sand and gravel, these exhibit basal sharp, planar contacts bracketing beds of clast-supported gravel (Units C1, C2, D1) which grade ‘normally’ to either massive sands or sands with curved non-parallel cross bedding (units B, C3, D2). The presence of dessication cracks manifested through large soil columns for unit B (up to 40cm in diameter) indicates seasonal wetting and drying. The former facies at WGW and WGM-2 were interpreted through cross-referencing with appropriate literature and modern system analogues (Section 4.5) as representing very coarse bars at the channel margins under a net valley aggradational regime. In this case, the deposits appear to represent deposition as bedload in the central channel, with the sands representing phases of flow cessation. The bed contacts in this represent flow-reactivation surfaces during individual, high energy flood events. The horizontally bedded gravels imply plane-bed deposition, but the sands with curved non-parallel bedding likely dunes under receding flow conditions. The succession of inversely graded fine then coarse beds is analogous to modern channel deposits reported in Chapter 4 (see Table 4.3; analogue 5).

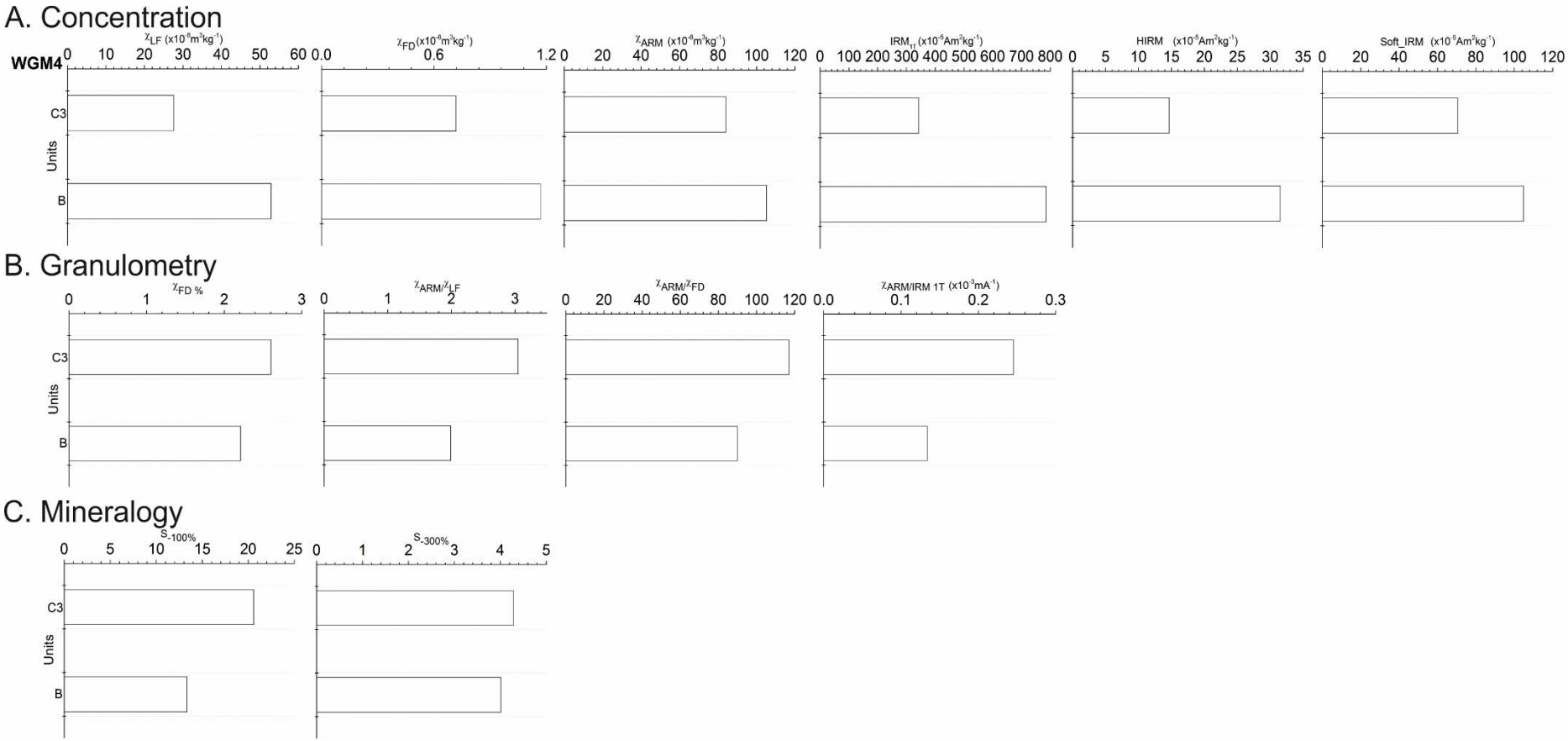

Figure 7.22 – mineral magnetic parameters from sampled horizons at outcrop WGM-4

Both sampled sand units exhibit very low organic matter content (Table 7.5). Unit B exhibits high proportions of remanence carrying ferrimagnetic grains, although on the basis of the very low χ_{FD} and χ_{ARM} relative to the high IRM_{1T} indicates a predominantly MD ferrimagnetic assemblage. Subunit C3 in contrast exhibits much lower concentrations of ferrimagnetic grains but a distinct change to higher coercivity ferrimagnetic properties is indicated by the higher (20.8% - Fig. 7.22c) S_{-100}% values. The virtually identical Br content and grain size distribution indicate that diamagnetic dilution or differential drainage (controlled by texture) are not driving the changes in susceptibility observed. The comparable S_{300}% values indicate a strong AF mineral contribution – probably goethite considering the 'pale brown' (10YR 6/3) colouration associated with greater extremes of oxidation and reduction that would not favour haematite production.

7.7a: GG-1 analysis

This section reports on the sediments just upstream of the Ganora canyon, whilst Section 7.8 reports on GG-2 near the canyon outlet.

Log GG-1 was obtained from a 5.2 m exposure on the right bank approximately 2.5 km downstream of the confluence between Africanders Kloof and the Wilgerbosch main channel (Fig. 7.1, Fig. 7.23–7.25). This exposure occurs at a relatively wide part of the valley (0.5 km) 1 km upstream of the canyon representing the first intact valley fills since upstream of the Africanders Kloof tributary at Ganora (see Fig. 7.1 and 7.23).

Unit A consists of a thick, homogeneous bed of very coarse, matrix-supported, subrounded, predominantly gravels (Fig. 7.25). The contact between unit A and B is sharp planar; unit B consisting of a single, thick, massive bed of silty (62.5%) sand (37.5% - Fig. 7.26a). Total magnetic susceptibility is moderately high (χ_{LF} = 40) as are the other concentration-related proxies, except the χ_{FD} (1.95 – Fig. 7.28a). The $\chi_{ARM}/_{IRM1T}$ is very low (0.34 - Fig. 7.28b). The S values are slightly higher than other sampled units, with 21% and 3.4% of the total applied remanence unreversed at -100mT and -300mT respectively (Fig. 7.28c).

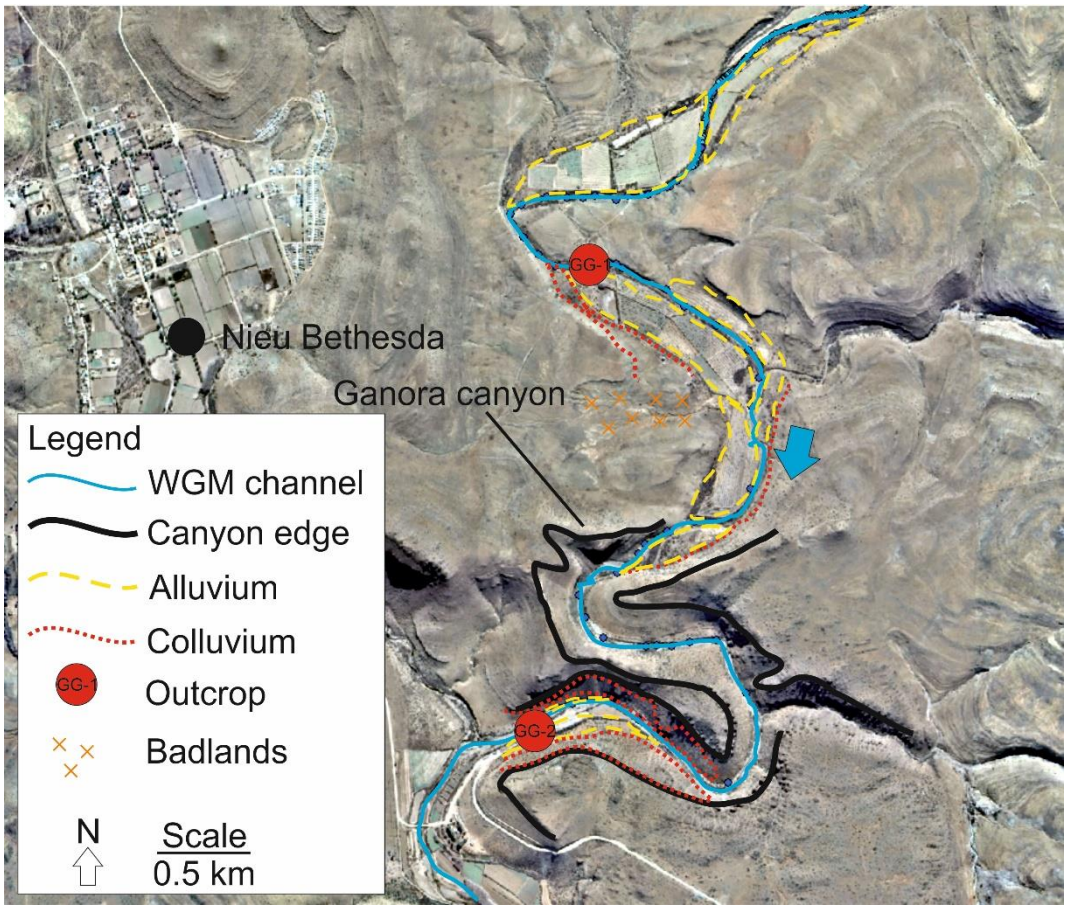

Figure 7.23 – digitised aerial photograph showing location of outcrop GG-1 approximately 1 km upstream of the Ganora Canyon.

Unit C consists of a thick bed of matrix-supported, very coarse gravel. This is capped by a thick bed of cobbles (subunit D1) that exhibits a sharp, undulating contact with unit C, as well as a slight change in colour from 7.5YR 6/4 light brown to 7.5YR 6/3 light brown. The coarse cobble unit (D1) is laterally discontinuous, but this is attributed to contemporary bank erosion having reworked the sediment, evidenced by small talus accumulations at the base of the profile straddling the edge of the modern channel.

Figure 7.24 – photograph showing valley context for outcrop GG-1.

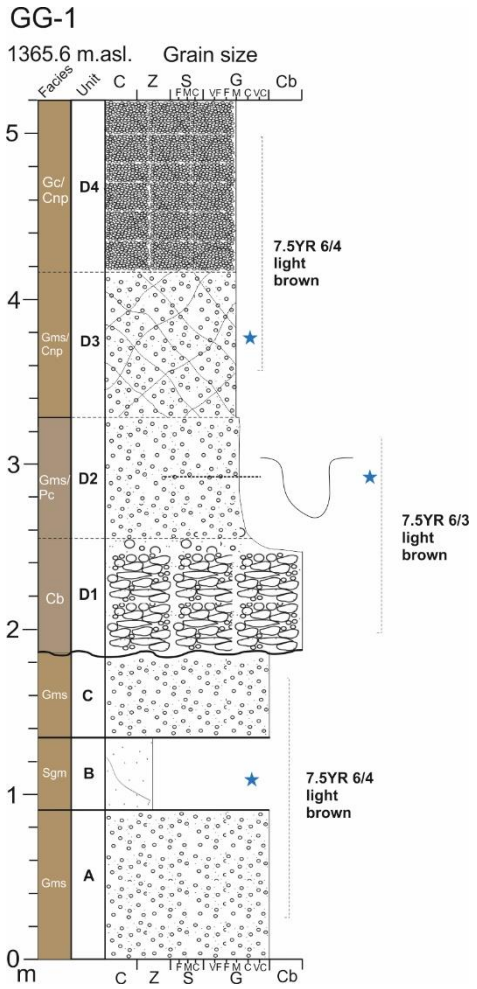

Figure 7.25 – sedimentary log of outcrop GG-1.

Subunit D1 grades to medium, matrix-supported gravels which make up subunit D3, the matrix of which is characterised by predominantly coarse-very coarse sand

(79.7% - Fig. 7.26b). Total magnetic susceptibility is comparable with unit B (χ_{LF} = 43~) as are the other concentration related proxies (Fig 7.28a). χ_{FD}% is slightly higher (6) (Fig. 7.28b) than unit B. S values are smaller with 17.5% and 2.3% of the total applied remanence unreversed at -100mT and -300mT respectively (Fig. 7.28c).

Subunit D3 is texturally similar to D2, but exhibits curved non-parallel bedding, and the colour is subtly different (7.5YR 6/4 light brown). The matrix is also slightly finer, with more silt and fine sand, but still a distinct very coarse sand mode (45.4% - Fig 7.26c). Concentration related magnetic susceptibility proxies are almost identical to unit D2, however in terms of magnetic granulometry, χ_{FD}% is higher (6.9%) and the χ_{ARM}/χ_{FD} smaller (63). S values are intermediate between previously referenced values for units B and D2 (Fig. 7.28c).

Table 7.6 – % loss on ignition data for sampled horizons at GG-1 and adjacent slope deposit reported in Fig. 7.27.

Unit	Height (cm)	Loss on ignition (%)
B	110-120	1.64
D2	295-305	1.41
D3	375-385	1.96
Slope	-	1.83

The succession terminates with clast-supported medium gravels that also exhibit curved non-parallel bedding (subunit D4).

The deposits reported at GG-1 occur in juxtaposition with more deeply rubified deposits (5YR 6/4 reddish brown) set behind and which grade to the valley edge (Fig. 7.27) forming a separate local terrace. These deposits are diamictic consisting of very poorly sorted, matrix-supported, very angular, sandstone gravel-cobble clasts and have low LOI% (Table 7.6).

Their concentration-related magnetic signature is distinct compared to that exhibited by the sediments at GG-1, with particularly high χ_{LF}, χ_{FD} and χ_{ARM} (Fig. 7.28). Crucially, the deposits of GG-1 are inset within these rubified diamictic fills forming a distinct terrace.

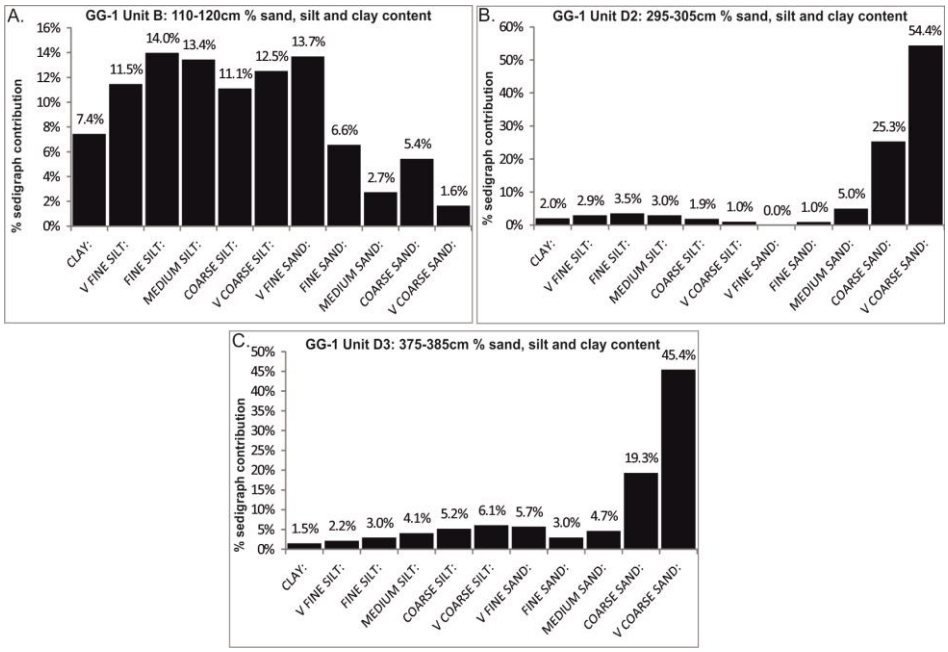

Figure 7.26 – % sand, silt and clay content derived from Coulter grain size analysis on samples collected from outcrop GG-1.

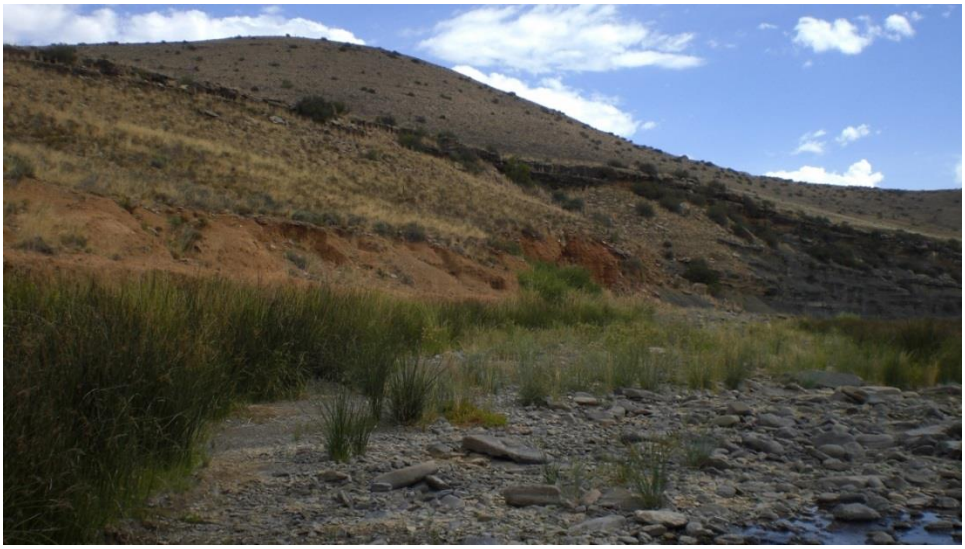

Figure 7.27 – photograph showing rubified deposits in close proximity to the adjacent sandstone ridge sloping steeply toward the valley centre.

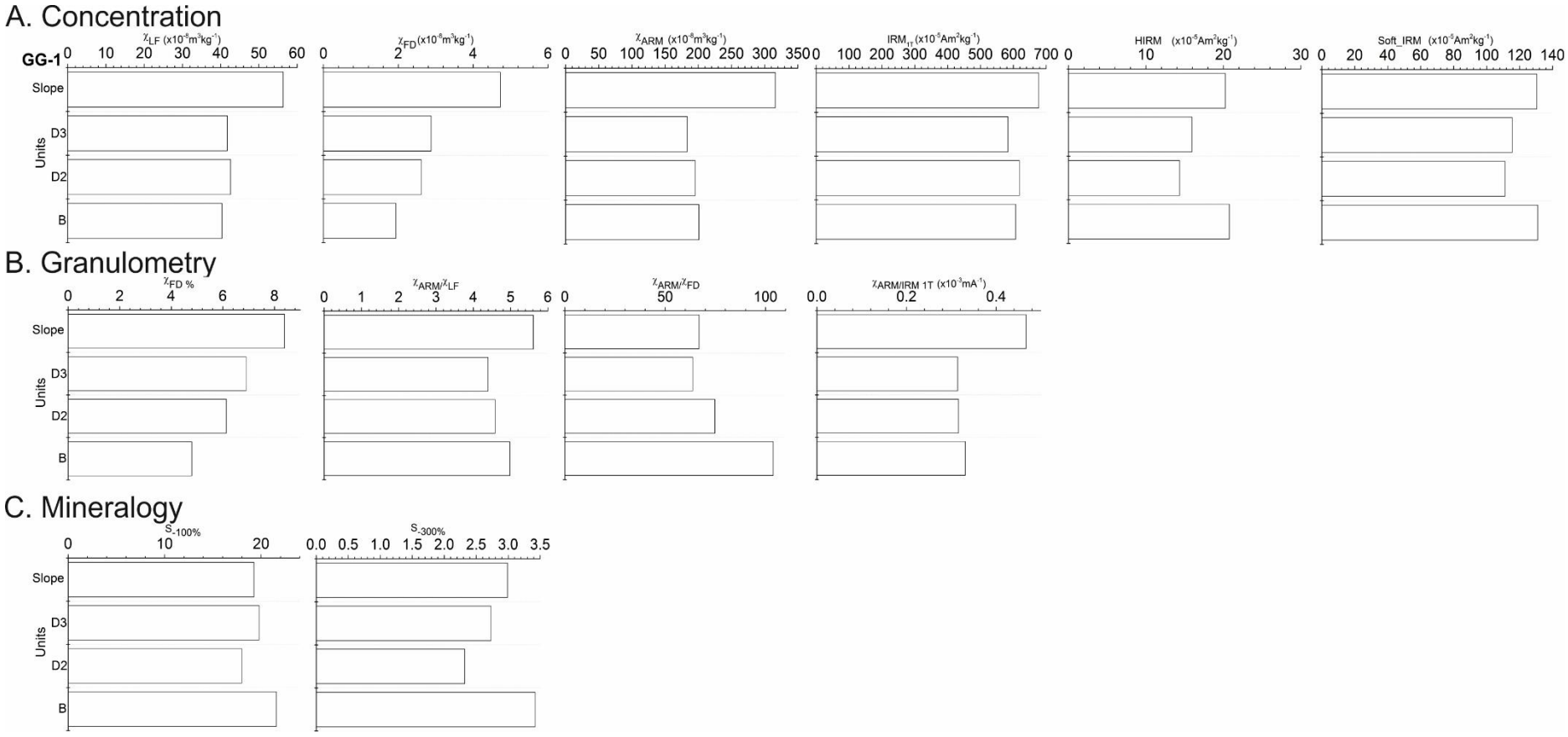

Figure 7.28 – mineral magnetic parameters from sampled horizons at outcrop GG-1.

7.7b: GG-1 interpretation

The thick deposits (up to 0.9 m) of very coarse gravels to cobbles are interpreted to reflect an aggrading channel bar sequence (unit A), with the fine-grained unit (B) reflecting overbank deposition. The sharply bedded very coarse gravels above (unit C) are interpreted as channel bar deposits, probably in association with an infilling channel, such that the original floodplain (unit B) was buried.

The sharp undulating contact between units C and D is an erosional surface, indicating channel incision of the underlying bar deposits. Notably, unlike elsewhere on the WGM channel (WGM-2 for example), the overlying deposits are coarse with low organic content. The nature of this deposit is analogous to very coarse deposits that occur in the active, contemporary channel margins (see chapter 4). The switch to gravel with curved non-parallel bedding (unit E) may represent a channel bar sequence. Although units D-F collectively represent an upward fining sequence, unit E does not exhibit lenticular deposits and there is no reduction in bed thickness upwards commonly found in point-bar sequences (McGowen and Garner, 1970). There is also no evidence of a fine-grained veneer of sediment capping any of the units, although this is commonly eroded prior to further deposition (Allen, 1965), nor are there muddy lenses associated with small-scale swales. Loss on ignition values are very low (1.41-1.96%) implying negligible contribution of organic matter. Therefore, the weak cross bedded nature of the deposits probably indicates lateral accretion facies associated with channel bar migration (unit E and F). The matrix of these deposits reflect interstitial filling by sands and finer gravels during the recessional phase of flow. The implication of this is that the former channel was laterally mobile, cross cutting underlying bar deposits (D1) that once marked the margins of the active channel, inundated only during periods of high flow. A key question emerges, could the local valley morphology permit lateral mobility of a channel? At this point in the system, the valley transitions from a relatively confined bedrock dominated reach with high slope-channel coupling, to a relatively wide valley floor with up to 270 m of former floodplain and probably, on the basis of the facies at GG-1, channel and bar deposits flanking the contemporary channel (Fig. 7.25). Deeply weathered slope deposits occupy the valley margin (right bank) before this transition and once probably extended all the way to the valley floor (Fig. 7.27).

The remarkably consistent χ_{LF}, χ_{ARM} and IRM_{1T} values for sampled units at GG-1 indicate similar proportions of remanence carrying ferrimagnets, although overall susceptibility is weak compared to the signatures obtained in the upper headwater regions at Africanders Kloof. Total concentration of both soft and hard ferrimagnets declines slightly at unit D2 and 3 compared to B, the latter showing the clearest evidence of haematite content (see S_{300} and HIRM). All three sampled units, like the base of WGM-2 (see Section 7.4), exhibit a distinct multi-domain signature ($\chi_{ARM/IRM1T}$ = 0.32) despite the fact that the soil (particularly units A-C) is partially lithified implying a long period of stabilisation. The increasing χ_{FD}% with height above the modern channel implies that any remaining pedogenic ferrimagnets occur on the SP side of the narrow viscosity band. The reason as to why χ_{FD}% is relatively low at the base is unclear, but could be due to time-dependent ageing of pedogenic magnetite to haematite. Groundwater-related ferrimagnetic dissolution cannot be ruled out either, but such an effect appears at best to be secondary here, as there is little macropedological evidence of gleying and the magnetic remanence parameters do not indicate paramagnetism.

In spite of the unconformity between units C and D, ferrimagnetic properties are strikingly similar at GG-1, contrasting with the big stratigraphic junction reported for WGM-2 between the relatively 'orange' basal deposits (units A-E) and the gleyed, organic rich sands and gravels above (units F-N) where magnetic susceptibility dropped by >50% (see section 7.4). This indicates that GG-1 unit D is not stratigraphically coeval with WGM-2 units F-N, implying a separate, intermediate phase of cut and fill between time of emplacement of the thick, orange alluvial deposits and their dissection by fine-grained, organic rich channel facies expressed at WGM-2 and in the Africanders Kloof tributary.

The magnetic signature of GG-1 sediments is distinct from the slope deposit sampled upstream (Fig. 7.27) which exhibits relatively high concentrations of SP/SD remanence carrying ferrimagnets reflected in the high $\chi_{ARM/IRM1T}$ and χ_{FD}% (0.47 and 8.2% – Fig. 7.28b and c). This implies the soil has been very deeply weathered to produce this magnetic grain size distribution, and in light of the geomorphic evidence, indicates the deposits pre-date the fluvial deposits at GG-1.

7.8a: GG-2 analysis

The succession at GG-2 consists of a 1.5 m inset sediment package at the base, characterised by calcretised, imbricated cobbles, boulders and gravels (unit A1) capped by predominantly sand with some gravel (unit A2). Clasts are predominantly subrounded-rounded (Fig. 7.29 – T2). 30 m downstream, this succession is more completely preserved with an extra 2 m of sand or sandy gravel and calcrete deposits near the top (see Fig. 7.30) in a similar fashion to that reported at AK-12 (Section 5.3.6).

Figure 7.29 – photograph of GG-2 exposure along the right bank.

At GG-2, above the inset 1.5 m of sediment, there are 3 m of weakly bedded matrix-supported gravels punctuated by a single, distinct bed of clast-supported gravels (unit B2 - Fig. 7.29). Unit B1 is subtly different to unit B3 in that platy gravel clasts are vertically orientated within a poorly sorted matrix of sandy silt. The matrix is relatively rubified compared to the inset deposits underneath (T2). Clast lithology is dominated by angular sandstone regolith rather than mixed, rounded clasts. Furthermore, unlike for T2 (Fig. 7.30), there are no accumulations of calcium carbonate.

Figure 7.30 – photograph of terrace 2 inset fill 30 m downstream of exposure shown in Fig. 7.29. Note the leached calcrete deposts toward the top of the profile overprinting fine-grained sediment.

7.8b: GG-2 interpretation

7.8.1 Terrace 1

The facies of unit B1 are very different to some of the other coarse deposits examined so far in this thesis. The angular to subangular sandstone gravels indicate the sediments have been locally derived, are immature and therefore most likely sourced from the canyon walls. The lack of weathering rinds on the clasts implies they have been derived through processes of physical weathering, probably frost-shattering along bedding planes and joints. The vertical orientation of the clasts within a poorly sorted matrix attests to mass movement processes. If the deposits represented a debris flow, there would likely be a far greater range of clast sizes ranging from gravel to boulder.

The deposits could therefore have been produced by solifluction, a type of mass movement which can occur on slope angles as low as 1^{o} in periglacial settings (Summerfield, 1991). *Gelifluction* is a type of solifluction, but occurs due to waterlogging induced by underlying frozen ground, such that the overlying soil melts during spring and moves ‘en masse’ over the permafrost to form a distinct bedding plane (Benedict, 1976; Summerfield, 1991). Obstruction of the base of T1 by the inset cobbles (unit A) precludes evaluation of the underlying deposits and any bed

contacts. Given the strong seasonal differences in moisture for the Sneeuberg, gelifluction deposits are more probable than solifluction. Vertical alignment of clasts can be produced by the upward movement of particles with the expansion and melting of ice lenses (Ballantyne and Harris, 1994; Lowe and Walker, 1997).

The overlying clast-supported gravels (unit B2) appear to be more consistent with water-lain deposition. However, two lines of evidence argue against this being a channel bar: 1) homogeneous, angular clasts that are mono-lithologic; 2) lack of well defined, continuous imbrication; and 3) laterally discontinuous. However, the deposits are too coarse to infer emplacement by slopewash. The deposits (unit B2) may therefore be remnants of a debris flow. The absence of any matrix could reflect seasonal melting and winnowing of fines by slopewash, such that the larger clasts ended up in contact with each other. On the dolerite slopes at Africanders Kloof, debris-flow deposits exhumed by erosion were left as isolated cobbles and boulders devoid of any matrix owing to contemporary winnowing of fine sediment by slopewash.

The weakly bedded nature of the overlying gravels (B3) with locally concentrated lenses implies emplacement by current flow, probably as slopewash. In this case, the lenses could reflect rilling of the surface during periods of rainfall. The absence of vertically orientated clasts implies that the deposits were probably not subject to the same intensity of freeze thaw as was implied for unit A.

In summary, the facies of terrace 1 indicate periglacial processes driven by a much colder climatic regime reflected in evidence for gelifluction deposits and large amounts of frost-shattered regolith in the section. The slopewash deposits imply a large amount of angular regolith was available on the slopes, but the mode of emplacement was fluid flow, rather than mass-wasting implying a possible recovery of climate. These events took place within the context of an aggrading valley regime, likely facilitated by the generation of large amounts of regolith from the canyon walls under a much colder climate than that which currently prevails (Holmes et al., 2003).

7.8.2 Terrace 2

The inset terrace deposits are clearly fluvial in origin and the preponderance of weathered dolerite in concert with sandstone attests to a phase of connectivity with

the upper tributaries such as Africanders Kloof (see Ch. 5). The ‘stacked’ nature of the deposits implies deposition on an aggrading channel bar. The capping sands probably represent the former floodplain associated with this channel. Further downstream where this outcrop is preserved in its entirety, the presence of a thin calcrete overprinting fine-grained alluvium in the mid-section is comparable with that reported at Africanders Kloof (see Chapter 5.3.6).

7.9: Summary

In relative stratigraphic order, the deposits preserved within the Wilgerbosch Main Channel include: 1) Periglacial and slopewash deposits in the Ganora Gorge, 2) Thick beds of inset alluvium overprinted by calcium carbonate similar to AK and the base of WGB, 3) inset grey fills, specifically an aggrading, migrating single thread channel producing alternating coarse-fine deposits analogous to those expressed in the current channel. The presence of two distinct grey palaeosol horizons at WGW, WGM-1 and 2 may be of wider environmental significance, since two such palaeosols were also noted at AK-7 and AK-15. The stratigraphic relationship of the alluvial fan (WGM-3) in relation to the other sequences is unclear from the present evidence and is treated fully in Chapter 8.4. Finally, the repetition of the sequences analysed and discussed in the central and lower Africanders Kloof valley, and to some degree, the Wilgerbosch Klof valley, may evidence extensive catchment-wide geomorphic changes in response to allogenic rather than autogenic forcing (Schumm, 1977; Erkens et al., 2009). In this case, it may be that base level changes in the lower order Wilgerbosch River primarily drove patterns of cutting and filling in the tributaries, thereby favouring the backfilling trajectory of landscape response shown in Fig. 4.20 (Section 4.6).

Chapter 8: Synthesis and Discussion

8.1: Introduction

This chapter amalgamates the lithostratigraphic relations portrayed in the sediment logs, their associated magnetic properties, grain size data, surveyed continuity and spatial limits in the context of a morphostratigraphic framework of terrace relations. Each component of the system is discussed in turn following the order of the three major results Chapters (5–7).

The extent of cutting and filling as portrayed in terrace fills and the number and characteristics of different environmental phases within each major facies or pedological association are discussed and their drivers evaluated. These relations are established and demonstrated through a combination of: 1) digitised aerial maps with surveyed limits and junctions of fills mapped in relation to both rock barriers and steps (where relevant); 2) enhanced channel long profile showing terrace elevation and sediment logs with correlation lines to show longitudinal limits of fills downstream (note, relevant long profiles are divided into 3-4 graphs so as to capture in detail variations in stratigraphy); and 3) synthesis of mineral magnetics data, with data points grouped according to terrace number as determined from 1-2 to evaluate similitude in terms of ferrimagnetic and antiferromagnetic mineral concentration.

The chapter concludes with a regional stratigraphic model of terraces demonstrating the extent to which various environmental phases were transmitted, registered and preserved in each part of the study area and the drivers. This combination of evidence is compared against the conceptual model of trajectories of valley filling (Chapter 4.6) and used to reconstruct the palaeoconnectivity of the system within each palaeoenvironmental phase. The established patterns of cutting and filling and their environmental significance are compared to the regional and wider literature.

8.2: Longitudinal Correlation of Terrace Sequences i: Africanders Kloof

8.2.1 AKH – AK-2.

The sediments at these outcrops occur at the base of a hillslope which is capped by deeply weathered dolerite. Four local morphostratigraphic members are represented in terrace fills between AKH–AK2 (Table. 8.1).

Table 8.1 – summary of morphostratigraphic members, their associated units, facies and interpretation.

Member	Log/Unit	Facies	Interpretation	Section
A	AKH - A	Gms/Hb/Rc Gl	Distal headwater floodout at or near gully terminus. Palaeogeomorphic surface with pedogenic haematite formation.	5.2.1
B	AKH – B AK1A – A-E AK1B – A AK2 – A-D	Gms, Sgm/Gl/Rc, Gms/Gl, Sgm, Gc/Hb.	Floodout distributary channel and overbank sediments.	5.2.1 – 5.2.4
C	AK1A – F AK1B – B AK2 – E	Sgm/Rc, Ocr/Rc, Gms, Sm/Rc.	Infilled shallow palaeogully carved into underlying sediments terminating as a floodout. Palaeogeomorphic surface at margins with pedogenic magnetite formation.	5.2.2 – 5.2.4
D	AK2 – F	Sgm, Gms/l, Ocr/Rc.	Infilled small palaeogullies associated with renewed floodout deposition.	5.2.4

In summary, four stages of local floodout evolution can be reconstructed from the sedimentological and geomorphic evidence analysed and discussed in Chapter 5.

Stage 1: the base of the local morphostratigraphic succession is characterised by terminal gully deposits in association with a floodout extending all the way back to the footslopes (member A). The top of the member is delimited by a palaeogeomorphic surface implying that floodout sedimentation halted for a period of time sufficient to permit soil formation. Although exact thickness of fill above bedrock was not determined, it is unlikely to have been greater than 1 m at most, as evidenced by the frequent intersection of the contemporary channel with sandstone (rock steps 1-3 – Fig. 8.1). This surface does not crop out at AK-1A meaning that soil development here was localised to the upper 200-300 m of the valley (Fig. 8.1).

The factors controlling the supply of sediment from hillslopes to valley floors are inter-related and complex. Botha (1996) emphasised the role of regolith derived from specific bedrock types in pre-disposing hillslope colluvium in certain areas to gully erosion. This is particularly exacerbated in zones of runoff convergence and/or where large contrasts in permeability of colluvial horizons occur (Rienks et al., 2000). Oversteepening of footslopes by successive phases of low-energy sedimentation can trigger incision through the effect of increasing slope on discharge (Patton and Schumm, 1981), but this co-varies with vegetation cover, which is known to stabilise

surfaces and ‘absorb’ extrinsic perturbations to geomorphic systems such as rainfall magnitude, particularly in dryland catchments (Sandercock et al., 2007).

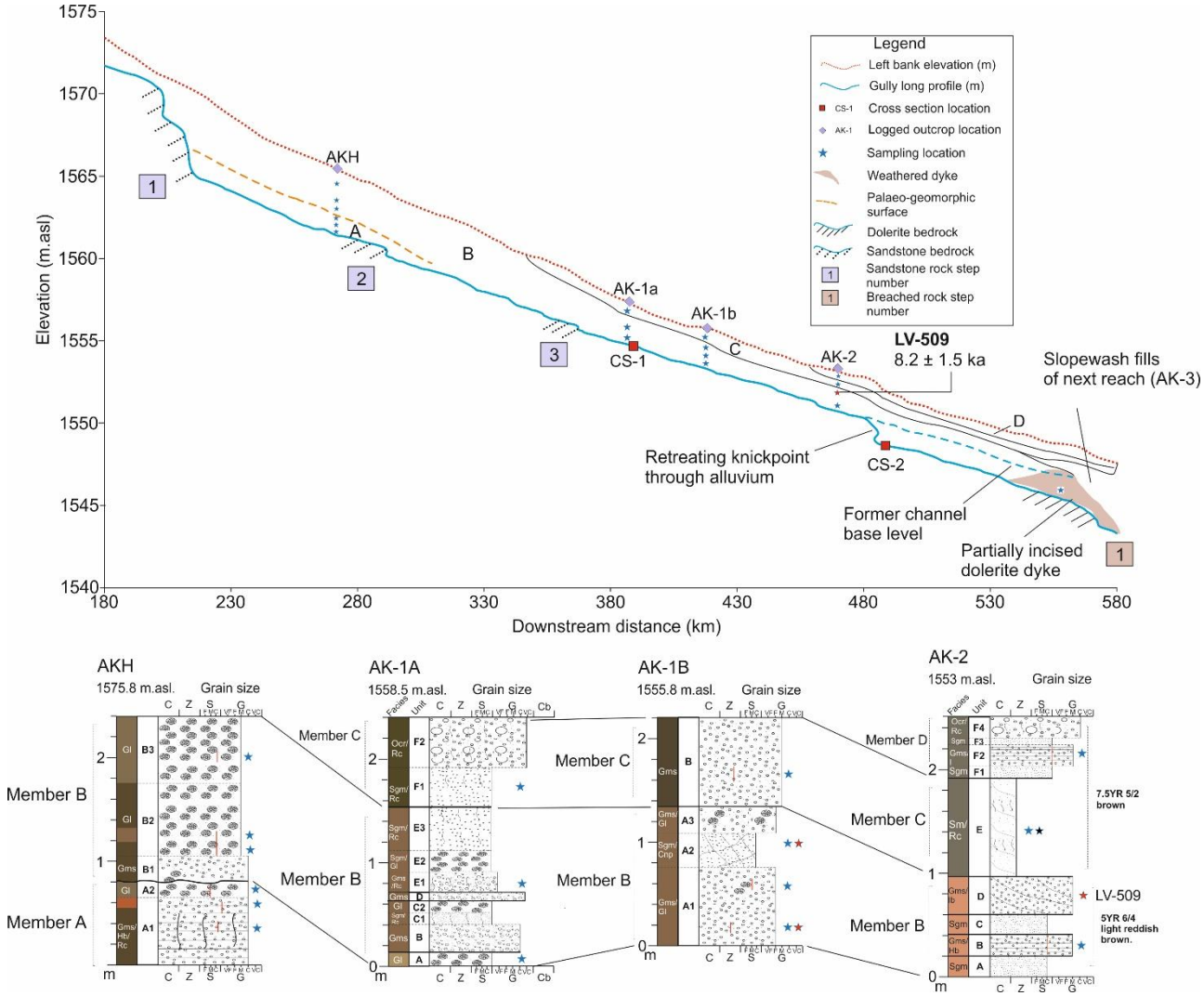

Figure 8.1 – Enhanced long profile for reach spanning 180-580 m downstream of the headwaters. Note lettering system used on long profile to indicate vertical and lateral extent of stratigraphic members A-D reported in Chapter 5 and summarised in the text of this section. A dotted line is given for member A, as exact limits of palaeogeomorphic surface are unknown. These correspond to graphed lithostratigraphic correlations between sediment logs AKH-AK-2 reported below.

Even in low gradient slope settings, partial or complete removal of vegetation cover can thus sensitise the landsurface to gullying assuming the sediment store in question is not blanketed by some armouring layer (Rienks et al., 2000; Fryirs et al., 2007).

Working on successions of colluvial deposits in eastern South Africa, Clarke et al. (2003) posited that accumulations of thick sandy colluvium required an initial humid phase of weathering of bedrock and regolith which was then stabilised by vegetation.

Thus, during climatic aridification this material is then available to transport to valley floors as a result of lower vegetation cover. This model is too simplistic for several reasons: 1) loss of vegetation cover can clearly be driven by processes such as natural fire, grazing (natural or anthropogenically induced) and changing seasonality. 2) Changing seasonality of precipitation may mobilise large amounts of sediment e.g. if flashfloods occurred in the winter months when vegetation cover is low. 3) Hence, although oversteepening of footslopes, vegetation cover, precipitation and temperature are all valid potential forcings in their own right controlling initial weathering and subsequent transport, they clearly co-vary with one another to produce non-linear, threshold driven geomorphic responses. As a result, patterns of landscape behaviour are spatially and temporally complex and evidence of direct climate change hard to reconstruct from hillslope colluvial sedimentation and phases of release to valley floors. From the present evidence, it is not possible to unequivocally demonstrate the role of each in triggering sedimentation to the valley floor (AKH).

Since floodouts restructure local topography and distribution of water and sediment by diverting them away from the former valley centre toward the floodout margin, therein lies the potential for periods of prolonged sediment inactivity in relatively discrete, small regions of the floodout surface near the apex (Grenfell et al., 2012). Given the depositional environment in which this soil has formed, it is not likely that this palaeosol reflects a catchment wide response to climate.

Stage 2: this palaeosol was incised by a distributary channel with rapid emplacement of up to 1.6 m of coarser sediments (member B), extending as far as the now incised dolerite barrier (no.1) 550 m downstream (member B – Fig. 8.1, 8.2 and Fig. 8.3). A 1 m knickpoint through this alluvium has developed and is actively migrating upstream: 480 m on long profile (Fig. 8.1). The top of this knickpoint is below the height of the breached dolerite barrier (no. 1 – Fig 8.1). Therefore, contemporary knickpoint retreat through member B alluvium is likely a response to the incision of the barrier. The limited OSL dating evidence places aggradation of these distributary channel sediments (member B) at 8.2 ± 1.5 ka. This date is a maximum limiting age for the incision of the barrier.

Stage 3: due to oversteepening of the local valley surface upstream of AK-1A (see Section 5.2.2), the infilled distributary channel deposits (member B) were incised by a gully which then terminated as a floodout (member C – see CS-1 and 2 – Fig. 8.2). Deposition was probably facilitated by the reduced valley gradient induced by the dolerite barrier at 550 m on the long profile, prior to its incision (Fig. 8.1). This implies that the dolerite had not been incised to present-day level by stage 3 of floodout evolution. The evidence is that this floodout surface was then vegetated and a soil formed with extremely high concentrations of pedogenic magnetite (see Ch. 5.2.3). Resulting soil formation and stabilisation of this surface was an autogenic feedback to disconnectivity in response to the reduction of valley slope and loss of confinement.

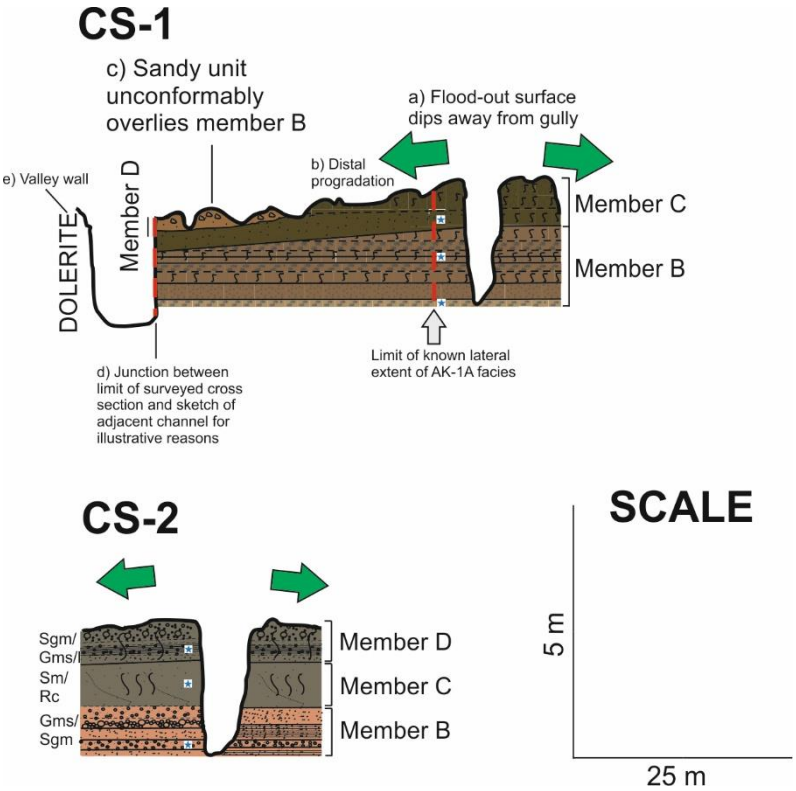

Figure 8.2 – valley cross sections obtained on the upper slopes. See Fig. 8.1 for exact position on long profile. Member B represents distributary channel deposits reported in the text; C represents burial of the distributary channel deposits by a floodout, then vegetated and overprinted by a magnetite-rich soil; D represents incision of the floodout surface by a series of palaeochannels. Note how the terrace surface dips away from the contemporary gully.

Stage 4: at the distal margins of the floodout, this palaeosol was then incised by a series of palaeochannels (member D). The impetus for the incision of this palaeosol may have been due to three key processes. 1) Fire removing vegetation on surface,

2) knickpoint recession working upstream from the lower slopes and 3) autogenic incision relating to valley morphology and base-level adjustment (Fig. 8.4). There are several possible permutations to this.

1) Evidence for firing of this surface was identified in Chapter 5 (p.141). This is a key factor by which vegetation can be removed, priming slopes for incision.

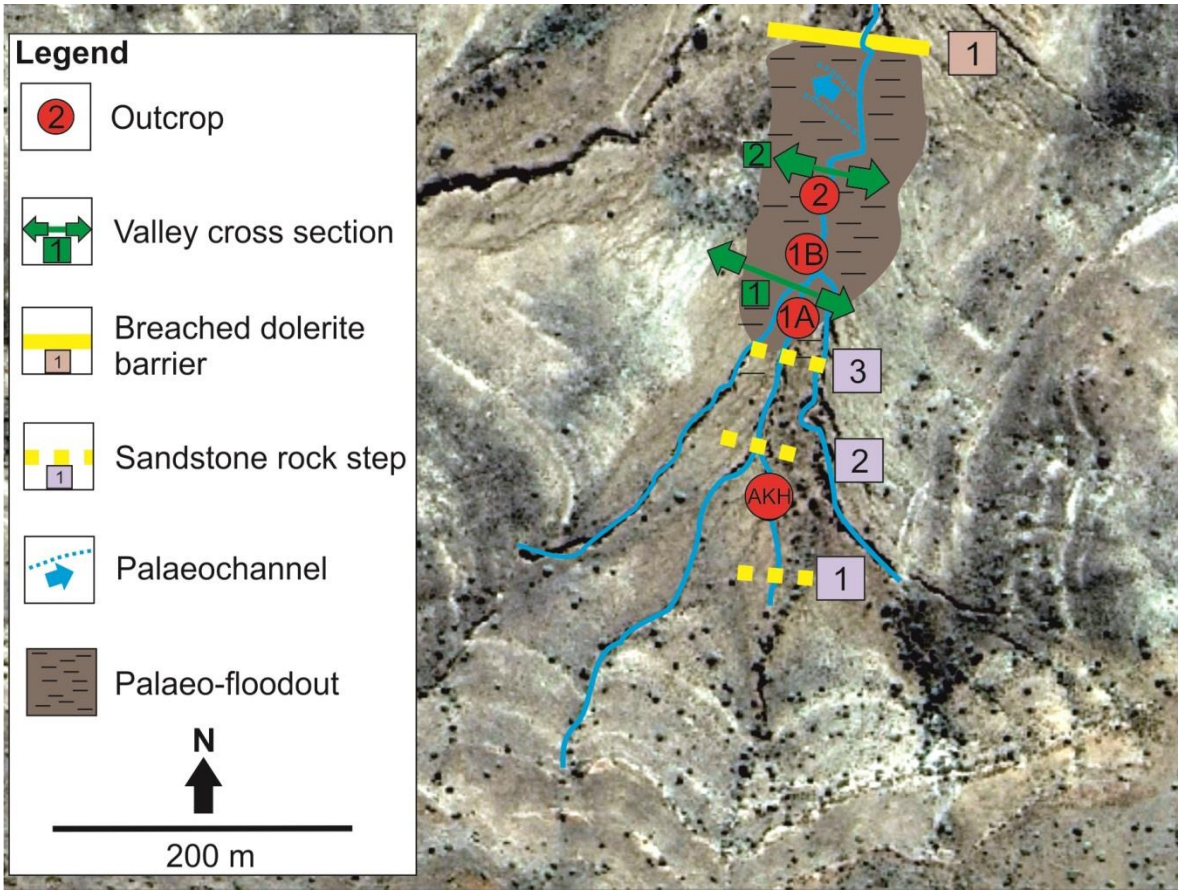

Figure 8.3 – digitised aerial photograph of headwater floodout area upstream of the dolerite dyke (solid yellow line). Member C sediments which appear upstream of AK-1A terminate at the dyke. Note green arrows which correspond to cross-sections 1 and 2 (Fig. 8.2) and the palaeochannel downstream of AK-2 dipping away from the modern gully.

2) Successions of bank gully and palaeochannel deposits downstream of the big dolerite barrier (no.1 - Fig. 8.1 – 560 m) indicate cutting and filling (Fig. 8.4 and Ch.5: Sections 5.2.5-5.2.8). However, the soil magnetic characteristics of sediments downstream of the floodout (i.e. AK-3 – see Ch.5. Fig. 5.2.5) does not support the idea of sediment connectivity between that reach and AKH–AK-2. 3) Localised autogenic 'cut and fill'' is more likely than 1-2. Runoff is preferentially diverted to the valley margins due to convex topography intrinsic to the floodout (see Fig. 8.4A). Runoff convergence at the margins most likely provided impetus for incision (Fig.

8.4B). Removal of vegetation cover on floodout surface would lower the geomorphic threshold for incision (Fig. 8.4C).

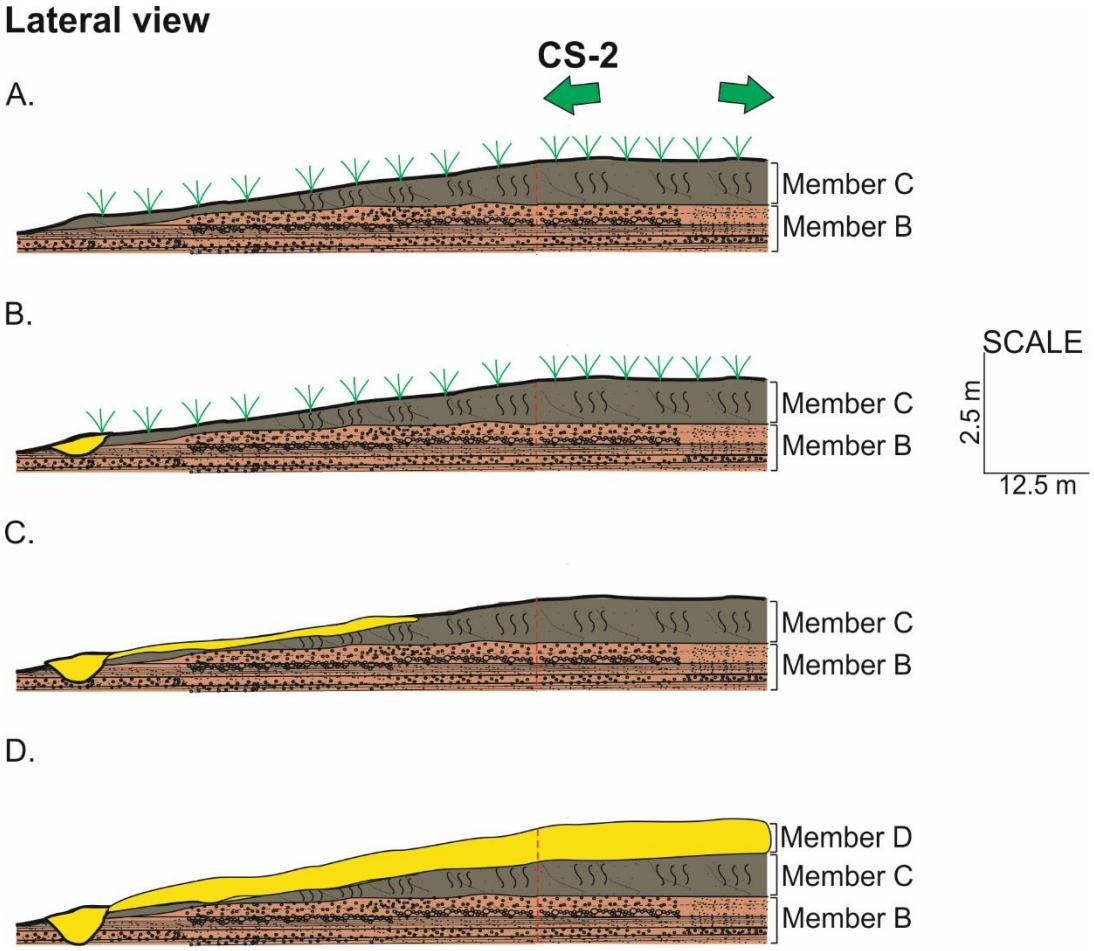

Figure 8.4 – morphostratigraphic model accounting for emplacement of member D sediments capping floodout member C. A) The floodout surface (member C) is stabilised by vegetation cover. B) Channel entrenchment at the local valley margin occurs due to either i) base level adjustment downstream or ii) response to coalescence of overland flow supplied from floodout surface. C) Deepening of this channel in concert with partial or complete removal of vegetation triggers channel incision of the floodout surface that propagates up-slope (to the right). D) Incision of the floodout surface at advanced stage with small gully and associated floodplain generating the 'brown sands' that constitute member D. Note the dashed red line indicating junction between surveyed cross section and sketch of valley surface and deposits.

Incision in the form of small gullies perpendicular to the long axis of the member C floodout then worked back upslope (Fig. 8.4D). The fact these gullies filled and there is no evidence that the strongly magnetic sediment of the floodout reached AK-4 400 m downstream, implies the channel portrayed in the far left of the diagrams (Fig. 8.4) likely terminated in a floodout elsewhere than the long axis of the contemporary valley, such that the associated feeder gullies backfilled.

In summary, it appears that prior to the incision of the dolerite dyke (Fig 8.1 and 8.3 and Ch.5. Fig. 5.2.2), the upper slopes were largely unresponsive to changes in base-level elsewhere in the catchment. Cut and fill phases preserved in the trunk river (see Ch.7), were not transmitted this far into the headwaters. Therefore, the morphostratigraphic units defined here are treated separately from those identified in the following sections for lower segments of the valley.

8.2.2 AK3 – AK-6.

Three morphostratigraphic units are recognised in the succession from 0.6-1.3 km downstream (Table. 8.2). T3 is restricted to the central and lower valley and discussed later on. Note that units T1, T2 and T4 here are not coeval with members A-D discussed in the previous section.

Table 8.2 – summary of local [1]morphostratigraphic units, their associated [2]lithostratigraphic units, facies and interpretation for logs AK-3 – AK-6.

Unit[1]	**Log/Unit[2]**	**Facies**	**Interpretation**	**Section**
T1	AK-3 – A and B AK-4 – A AK-5 – A AK-6 – A	Gc, Sgm, Gms/l, Sm/Rc	Fine-grained slopewash deposits derived from flanking hillslopes.	5.2.5 – 5.2.8
T2	AK-6 – B-Q	Gms/Hb/Rc, Sgm/Rc, Sm.	First generation bank gullying with coeval with inset debris flow deposits in second order channel.	5.2.8
T4	AK-3 – C AK-4 (inset fill) AK-4 – C and D AK-5 – B-D	Sgm Sgm/Rc/l, Sgm, Sm Sm/Rc	Second generation bank gullies, palaeochannels and their associated floodplain deposits.	5.2.5 – 5.2.7

In summary, three distinct terraces can be reconstructed from the sedimentological and geomorphic evidence analysed and discussed previously (Table 8.2).

Terrace 1: slopewash deposits sourced from the flanking hillslopes rather than the upper floodout (AKH-AK-2) have filled the valley, forming a distinct inversely graded sequence (AK-3 and AK-4) pertaining to the preferential erosion of fine sands and silts on hillslopes first, before coarser material was transferred to the valley floor (Table 8.2 and Fig. 8.5). These slopewash deposits are best preserved at the valley margins (CS-3 – Fig 8.6) and run continuously over sandstone rock steps 4 and 5 between CS-4 and 6 (Fig. 8.6). The deposits of this terrace contrast markedly with those of T2 discussed next. A slow aggradational regime is indicated, punctuated by

minor incisional events reflected in bank gullies (see 0.7 km on long profile – Fig. 8.5). T1 deposits, except where overprinted by calcrete which formed following major infilling of T2, lack any gleying and are minerogenic. Therefore, the prevailing environmental conditions associated with T1 aggradation were likely cold and dry relative to T2. The lenticular gravels of T1 may reflect freeze-thaw processes. The lack of coarse, frost shattered regolith compared to that found in the Ganora Gorge relates to the weaker slope-valley floor coupling at Africanders Kloof. There appear to have been as many as two generations of incision into these slopewash deposits.

Terrace 2: The major evidence for this terrace is restricted to downstream of sandstone rock step 5 (Fig. 8.5). Firstly, there are thickly bedded debris flow deposits deposited in a bedrock channel as a wedge against rock step 5 which appear to be inset within the slopewash deposits of T1 (see Fig. 8.5 – 'T2' for position on long profile and Fig. 8.8c for photo). Secondly, there is a large palaeochannel incised into the slopewash deposits that indicates emplacement under high energy conditions (see AK-6 at 1.25 km on long profile – Fig. 8.5). The absence of T2 above rock step 5 (Fig. 8.5), as indicated in cross sections 3 and 4 (Fig. 8.6) where only T1 and T4 occur (Fig 8.7), requires further discussion. Small infilled bank gullies within 100 m of AK-3 and then again at AK-5 (Fig. 8.5 and 8.9) do imply a phase of incision into T1 that *could* be linked to that reflected in the inset debris flow deposits and palaeochannel (AK-6) downstream.

However, sandstone rock step 4 at 1 km is not incised (Fig. 8.5 and 8.8a), whereas at 1.1 km, there is deep fluvial incision and knickpoint retreat to the extent that a small bedrock channel has formed (Fig. 8.5 and 8.8b). The relatively limited incision of the rock wall that constitutes the local base level for the Africanders Kloof tributary (Fig. 8.7) implies comparatively minimal erosion by water sourced from this part of the catchment. What little erosion has occurred is in response to the base level set by the deep erosion of the flanking tributary (Fig. 8.7 and 8.8).

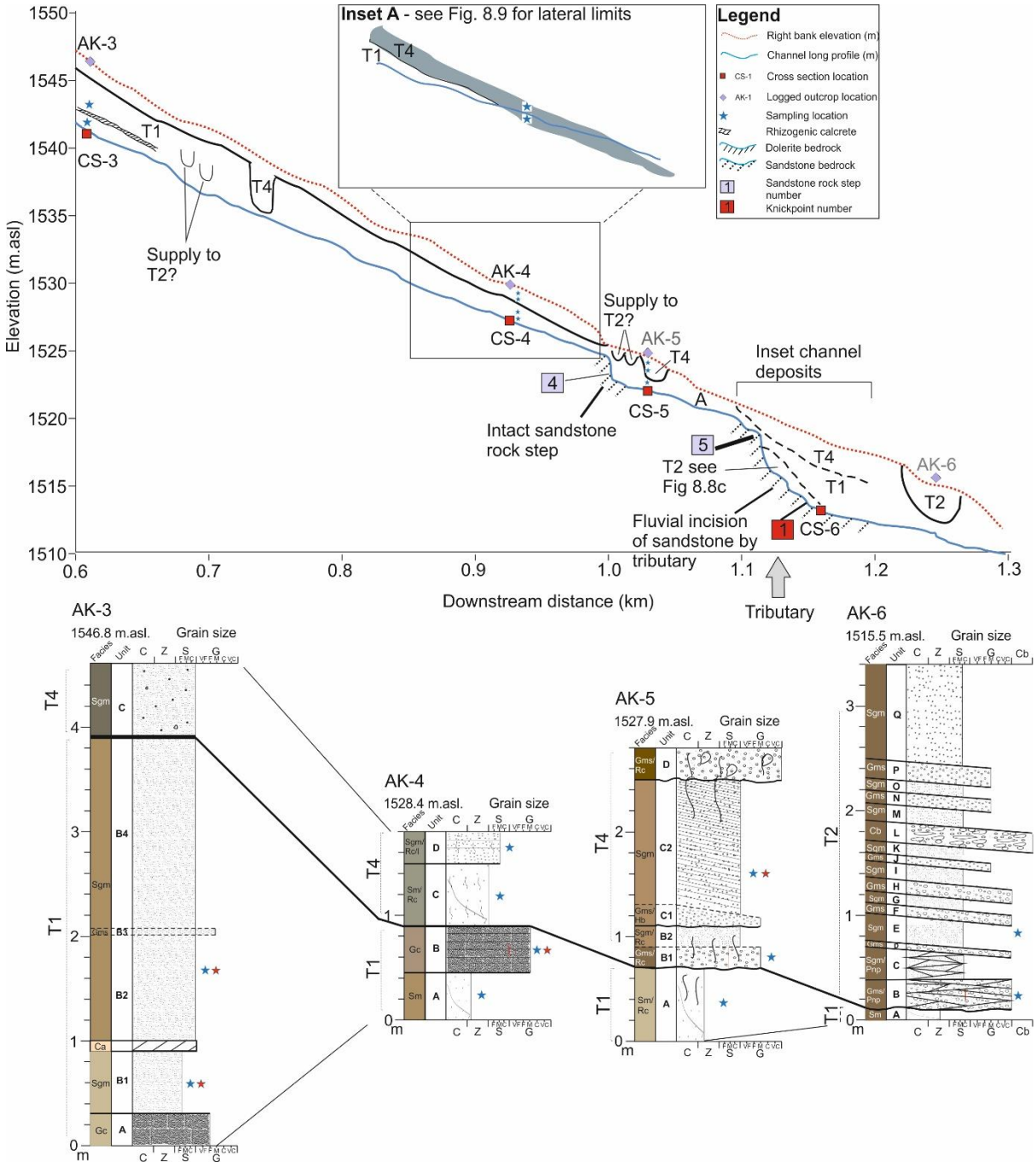

Figure 8.5 – long profile for reach spanning 600 and 1300m downstream of the upper headwaters. Note lettering system used on long profile to indicate vertical and longitudinal extent of T1, T2 and T4 reported in Table 8.2 and summarised in text of this section. Also note inset A showing channel deposits (T4) inset within T1 and T2 sediments. A dashed line is used to indicate where this inset sequence re-emerges at 1.1 km.

As a result, the upper slopes (AK-3–AK-4) may have remained largely unresponsive to cut and fill phases expressed in these deeply incised reaches further downstream. If so, could T1 in these upper reaches (AK-3–4) represent a filling phase that is offset from T1 below rock step 5 at 1.1 km (Fig. 8.5)?

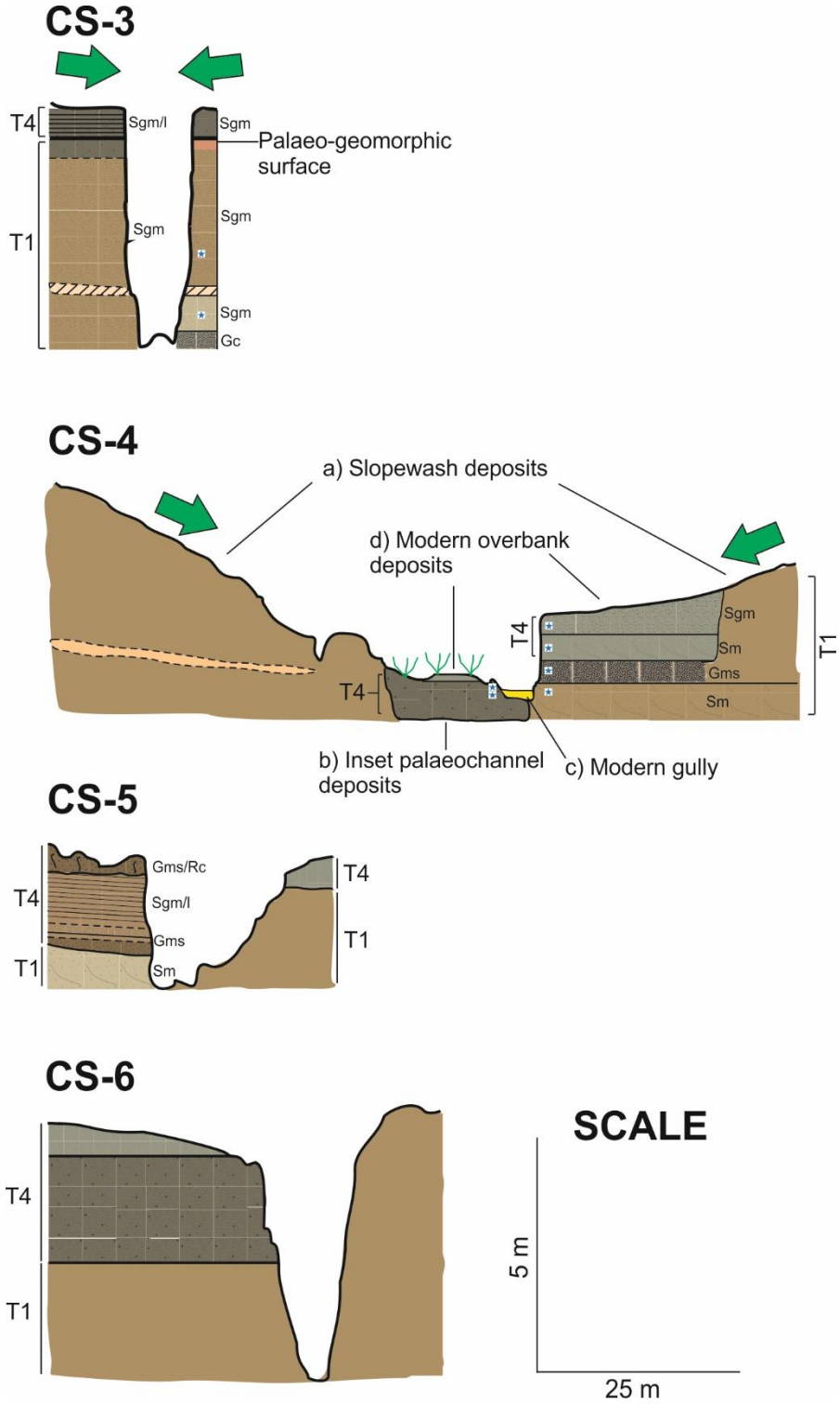

Figure 8.6 – surveyed valley cross sections (CS-3 – 6) showing the relations of different terraces annotated accordingly. See Fig. 8.5 for position on long profile. CS-3 shows thick slopewash deposits associated with T1, overprinted by a rhizogenic calcrete horizon and buried by floodplain sediments of T4. CS-4 shows the first clear example of the gleyed T4 palaeochannel facies inset within T1 upstream of the dolerite (Fig. 8.8a). CS-5 shows a feeder tributary for T4 palaeochannel carved into T1 fills, whereas CS-6 displays the re-emergence of the T4 palaeochannel itself. The distribution of T2 in relation to these fills is shown in Fig. 8.5.

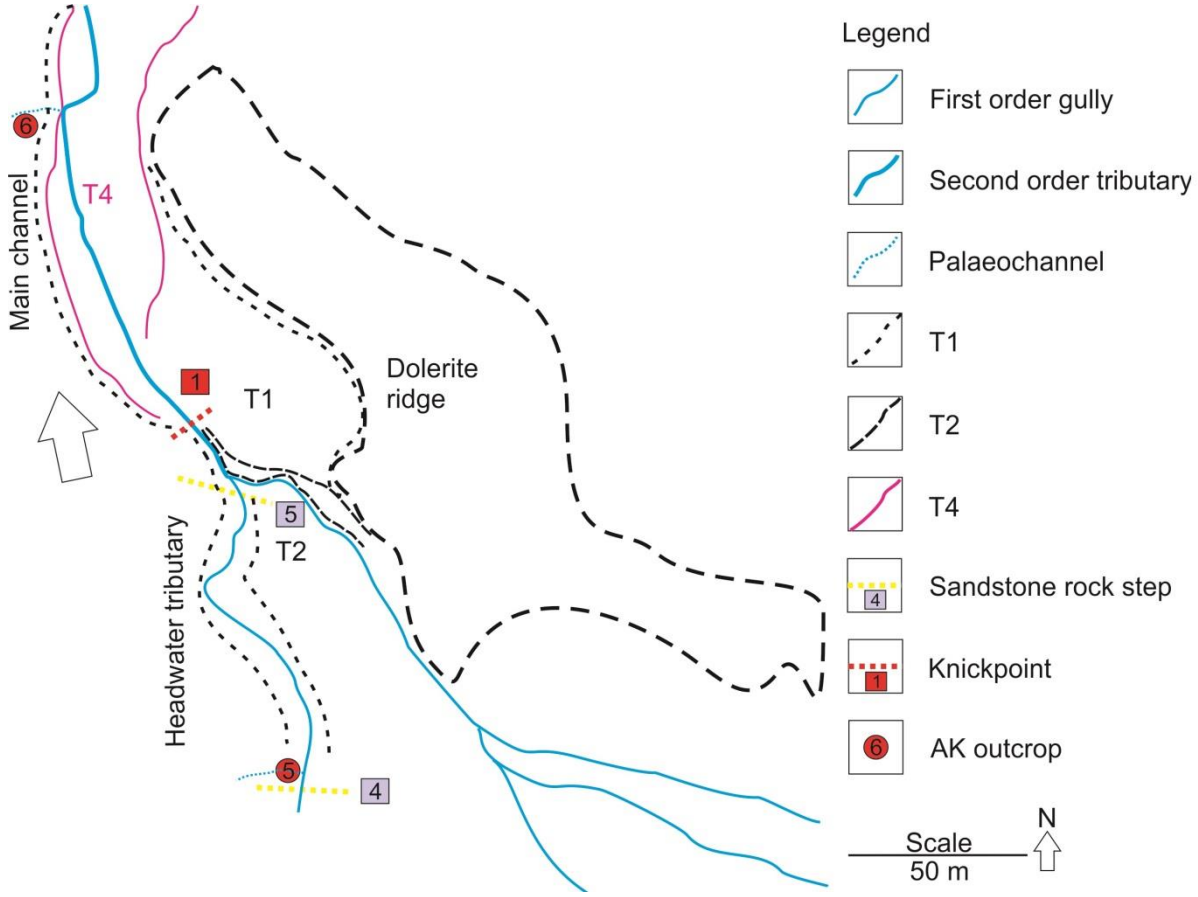

Figure 8.7 – geomorphic map showing mapped limits of morphostratigraphic units T1, T2 and T4 in relation to rock steps at 1 and 1.1 km (Fig. 8.5). Note the position of T2 inset within T1 at the confluence between the AK tributary and deeply incised bedrock channel coming in from the south-east.

The elevation of the debris flow deposits in relation to the rock step implies that this was a former channel surface (Fig. 8.8c). These thick channel deposits could therefore have provided the impetus for back-filling expressed in the thick alluvial deposits (up to 5 m) of AK-3–AK-5. In this case, the slopewash deposits (T1 – Fig. 8.8c) may represent a graded long profile in response to this base level adjustment as portrayed in schematic 1 (Fig. 8.9).

However, the T2 debris flow deposits are inset within the fine-grained fill (T1) which is continuous down the valley past AK-6. It follows that these debris flow deposits are a vestige of a former channel otherwise poorly represented except indirectly in the palaeobank gullies (AK-6) preserved in terrace fills discussed previously.

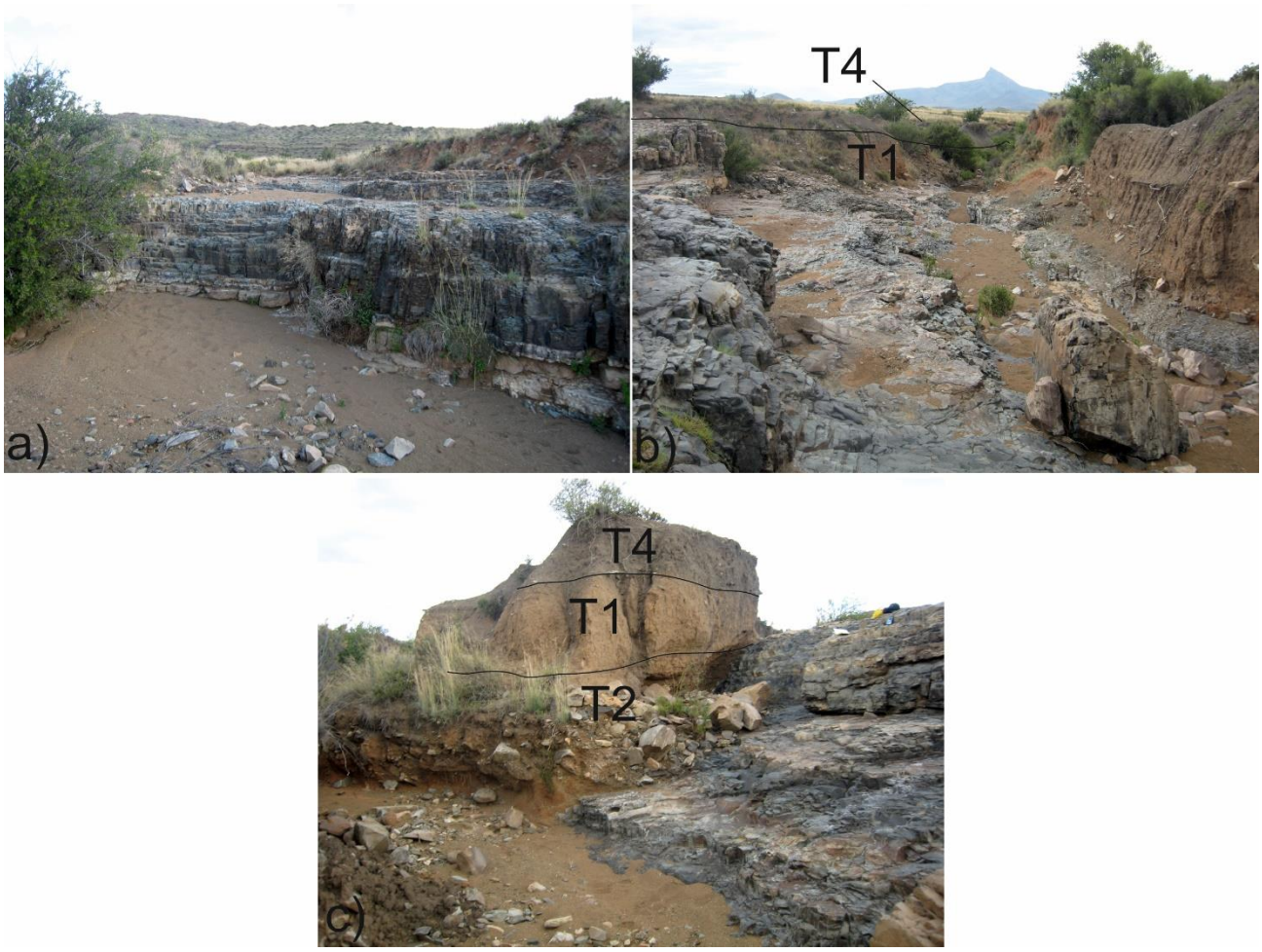

Figure 8.8 – photographs of sandstone rock steps (4 and 5) and associated fills: a) Rock barrier just upstream of AK-5 showing little incision (photo looking upstream of tributary – Fig. 8.8), b) incised bedrock channel has developed as part of the adjoining tributary to the right (looking downstream), c) view looking upstream showing postulated inset debris flow (T2) deposits within slopewash fills (T1), the latter overlain by T4 sediments. Note the continuity of T4 sediments over the rock barrier which dips downstream, inset within and overlying the slopewash deposits (T1).

The evidence thus compares best with model 2 (Fig. 8.9) where slopewash deposits have accumulated (T1), channel entrenchment has occurred, later filled by debris flow deposits (T2). In light of this, the possible significance of the small bank gullies reported within T1 needs to be clarified. Crucially, they are only up to 0.3 m deep compared to the large palaeochannel of AK-6 (3 m deep). When viewed in the context of a slow aggradational regime, under a cold, dry climate where freeze-thaw processes were likely prevalent, these bank gullies probably reflect minor incisional events associated with rainfall and/or runoff associated with seasonal snowmelt.

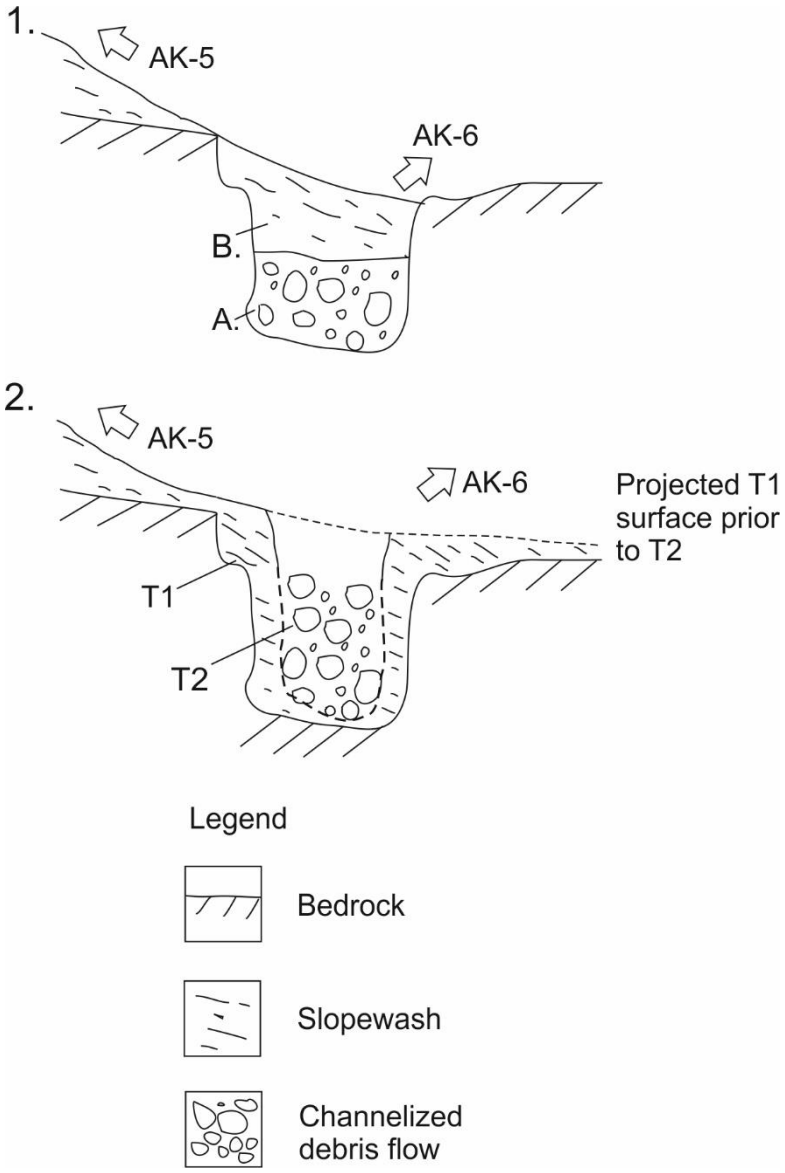

Figure 8.9 – sketched cross section of junction between surveyed AK tributary and channel joining from east (see Fig. 8.7). Two hypothesised morphostratigraphic sequences are presented: 1) channelized debris flow deposits sourced from tributary occur at the base of the succession (A) and are capped by slopewash deposits sourced from AK-3 – AK-5 (B). 2) fine-grained slopewash deposits (T1) are incised by a channel with inset debris flow deposits (T2). The original surface elevation of T1 is projected across.

Following the valley alluviation associated with T2, aggradation slowed sufficiently to allow a soil to form, expressed as a palaeogeomorphic surface. At the valley margin, this occurs as a rubified Bw horizon (AK-3 - 3.9 m- Fig. 8.6), but in the centre, the palaeosol is polygenetic, reflecting organic inputs from the contemporary soil surface (see CS-3 – Fig. 8.6). In theory, this surface could be coeval with that found at AKH upstream (see Section 5.2.1 and Fig. 8.1), but the uppermost valley section appears to be dominated strongly by localised floodout related ‘cut and fill’ dynamics rather

than incision and infilling driven by changes in the base level of the trunk Wilgerbosch River (see Section 8.4).

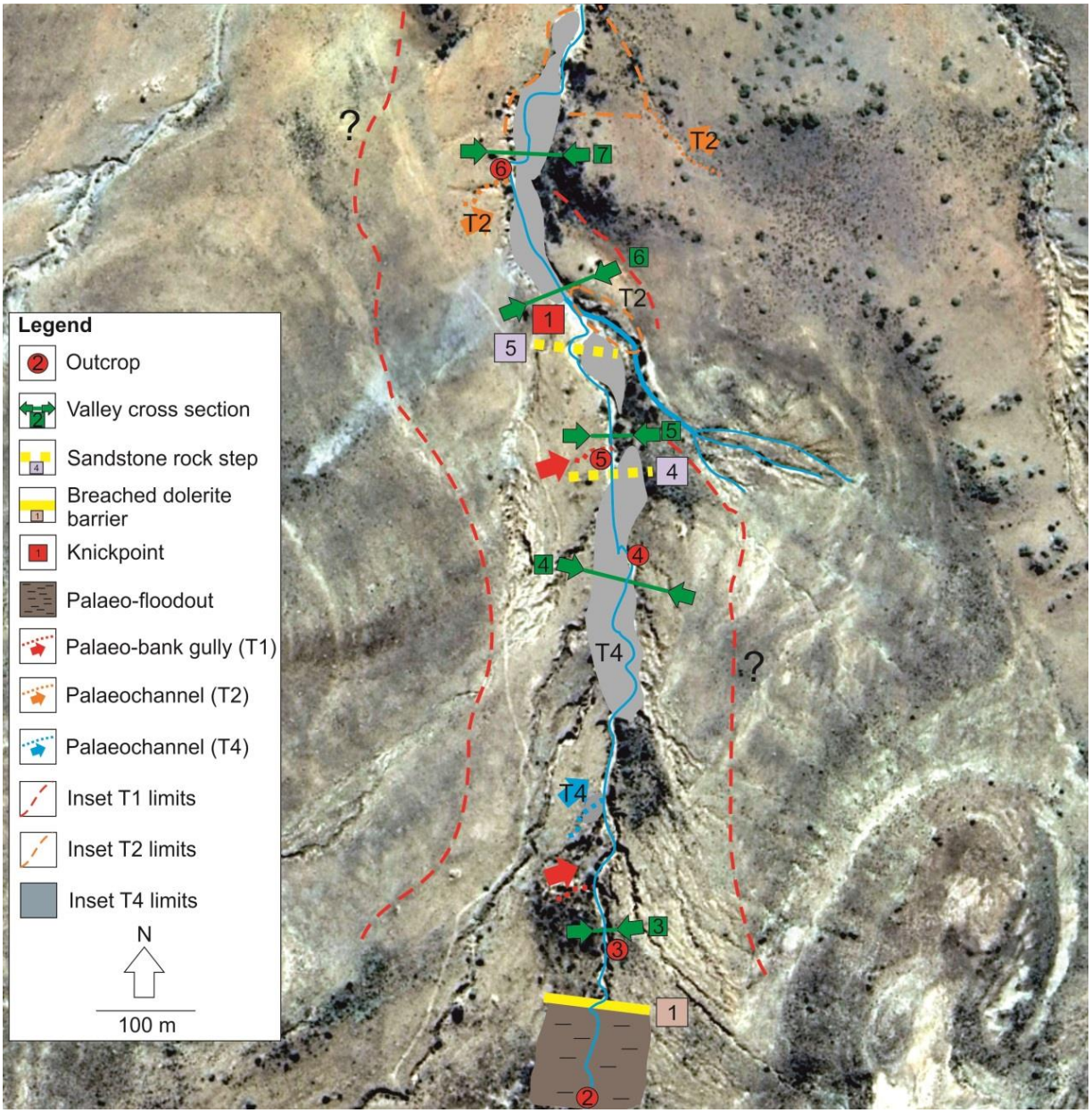

Figure 8.10 – digitised aerial photograph of the upper slopes of Africanders Kloof showing the longitudinal and lateral limits of major terrace fills: 1, 2 and 4. The locations of palaeobank gullies associated with minor incision of T1 are given (red arrows). The position of larger palaeochannels as reported in the text and long profile are given with the appropriate morphostratigraphic designation, i.e. orange lines are 'T2'; grey are 'T4'. The locations of intact rock steps (4-5) and partially breached dolerite barriers (1) are indicated corresponding to Fig. 8.5.

Rhizogenic calcrete occurs in association with T1 and T2 at the valley margins (CS-3 and 4), but is absent from the inset channel deposits (T4) discussed next. It follows that after emplacement of T1 and 2, the valley had a raised water table. No modern analogue for laminar calcrete formation in the contemporary gullied environment has

been found. It follows that such secondary accumulations of carbonate are indicative of an aggraded valley system. This is because such a feature would be unlikely to form if the valley were actively being incised, since groundwater would be preferentially diverted into channels, changing the local soil hydrology (Boardman, 2014).

Terrace 4: the sediments of T4 are represented by a second generation of infilled palaeochannels carved into T1 sediments and a vestige of inset organic-rich channel fill preserved (Fig. 8.5; CS-4-6 – Fig. 8.6; Table 8.12). The combination of stratigraphic and mineral magnetic evidence (see Ch. 5: Table 5.19) indicates that this channel did not erode headward as far as breached dolerite barrier 1 (Fig. 8.1 and 8.10- see limits of T4), but rather appears to have originated somewhere to the south-west of the contemporary gully (see T4 tributary – Fig 8.10). The mapped limits of this channel indicates that it did not terminate at rock step 4 associated with local widening of the valley (Fig. 8.5 and 8.10), but was continuous downstream into the central valley. Downstream of rock step 5 where the valley widens, this channel fill reappears, clearly inset within the hillslope derived sediments (CS-6 – Fig. 8.6, 8.7, 8.8b and 8.10). The floodplain associated with this palaeochannel (T4) buries the associated organic rich facies, or caps the deposits of T1. CS-3 and CS-4 illustrate these relations (Fig. 8.6). On the basis of the morphostratigraphic and mineral magnetic evidence, re-connection of the uppermost slopes (AKH–AK-2) occurred following the incision of T4 by the contemporary gully via incision of the barrier (no.1) at 0.55 km (Fig. 8.5).

8.2.3 AK7 – AK-14.

The complete alluvial succession represented by all four terraces is preserved in the central valley between 1.3 and 2.38 km.

Similar to upstream (AK-3–AK-6), the base of the succession is characterised by fine-grained slopewash deposits which exhibit inverse grading structures (T1 - Fig. 8.11, 8.12 – CS-9). However, at AK-9 and AK-10, the facies were found to indicate low-energy sedimentation in a channel (Table 8.3). Exactly how far upstream this channel extended is unclear. No fine-grained deposits that were the product of channelized flow and aggradation were found on the upper slopes (AK-3–AK-6). Crucially, these low energy channel sediments associated with T1 are inset within a

highly degraded remnant of T1 slope deposits expressed at AK-11 (see Fig. 8.11 and 8.12 – CS-10). The absence of calcrete from AK-11 undoubtedly reflects intense subsequent leaching due to enhanced runoff from the proximal dolerite slope (Fig. 8.14).

Regarding the T1 gully sediments (AK-9/10), fingerprinting sediment source-sink relations (i.e. whether the slopewash fills upstream were reworked by fluvial action and transmitted to AK-9/10) for these basal units is problematic.

Table 8.3 – summary of local [1]morphostratigraphic units, their associated [2]lithostratigraphic units, facies and interpretation for logs AK-7 – AK-14.

Unit[1]	Log/Unit[2]	Facies	Interpretation	Section
1	AK-8 A – C *[1]AK-9 – B *[2]AK-10 – A AK-11 AK-12 – A	Sgm, Gms/Hb Sgm/Gl Gms/Hb Sm/Gms	Sediments deposited by slopewash as sheets. *[1]Overbank sedimentation from gully system. *[2]Low-energy sedimentation in channel.	5.3.2 – 5.3.6
2	*[1]AK-7 A – B *[1]AK-8 D – K *[2]AK-9 – C *[3]AK-10 B – E *[2]AK-12 – B	Ig, Cg B, Gms, Sgm/Cnp Gms, Sgm/Gl, Sgm Cb, Sm, Sgm, Gms Gms/Hb	Cut-phase. *[1]Debris flow deposits in association with laterally-impinging fan systems. *[2]Infilled bank-gully and palaeochannel facies. *[3]Channel bar and floodplain deposits laid down in an aggrading gully.	5.3.1 – 5.3.4 and 5.3.6
3	AK-10 F – G AK-12 – C	Sm, Sgm, Gms Sgm	Sedimentation by slopewash and rilling.	5.3.4 and 5.3.6
4	*[1]AK-7 – C *[1]AK-8 - L *[1]AK-9 – D – E *[2]AK-14 – A	Sm/Rc Sgm/Rc Sgm, Gl	*[1]Low-energy channel and overbank facies in a wetland. *[2]Laterally impinging fine-grained alluvial fan deposits.	5.3.1 - 5.3.3 and 5.3.8

Table 8.4 – selected mineral-magnetic parameters and munsell colour for basal in situ slopewash deposits (AK-3, 4, 5, 8, 12) and reworked slopewash deposits by gullying (AK-9 and 10).

Outcrop/Unit	Height (cm)	X_{LF} ($10^{-8}m^3kg^{-1}$)	IRM_{1T} (10^{-5} Am^2 kg^{-1})	S_{-300}%	Munsell colour
AK-3 / B1	55-65	23.8	310.6	3.4	10YR 7/3
AK-4 / A	20-30	111.9	1359.8	2.1	7.5YR 5/4
AK-5 / A	35-45	43.9	588.7	2.0	10YR 7/3
AK-8 / B	15-25	58.6	1178.9	1.4	10YR 6/4
AK-9 / B2	95-105	23.8	213.7	3.6	10YR 7/3
AK-10 / A	20-30	28	329.6	1.7	10YR 7/4
AK-12 / A1	35-45	37.3	533.2	1.8	7.5YR 7/3

With the exception of AK-4, the other basal lithostratigraphic units exhibit predominantly low concentrations of fine-grained ferrimagnets due to ferrimagnetic dissolution under gleyed conditions (Anderson and Rippey, 1988; Roberts and Turner, 1993; Foster et al., 1998). AK-3, 5, 9, 10 and 12 in particular are all similar in terms of X_{LF} and colour (Table 8.4). Their apparent similitude is due to ferrimagnetic dissolution and production of goethite erasing any distinct magnetic signature of lithogenic significance that could have been used as a basis for reliable correlation in terms of source. At this stage, it thus remains inconclusive as to how far upstream gullying through T1 sediments proceeded and what sources were tapped into and transmitted to AK-10 and 12. In the absence of any other distinct 'cut and fill' features that would imply a preceding phase of incision and sedimentation in the central valley compared to the upper slopes, the channel sediments (AK-10 and 12) are herein treated as T1 – coeval with the supply to the valley floors from the hillslopes at AK-8 (Table 8.4; Fig. 8.11 and 8.12).

These basal deposits (T1), similar to AK-3–AK-6, are deeply incised – stripped completely in some areas (AK-7 – Fig. 8.11; CS-8 – Fig. 8.12) - and capped by cobble to boulder deposits and/or accumulations of gravel (AK-7, 8, 9 and 10) that constitute several different landforms ranging from alluvial terraces to truncated fans (Table 8.4). These attest to a phase of deep cutting of the valley and rapid sedimentation. This is because there are no palaeogeomorphic surfaces punctuating these lithostratigraphic units that would indicate a prolonged hiatus in the sediment cascade. The impetus for dissection of T1 slopewash fills on this scale would have to have been a major drop in base level on the valley floors associated with the entrenchment of a channel, a supposition supported by two lines of evidence: 1) the channelized debris flow deposits inset within T1 slopewash fills at rock step 5, 2) the thick beds of channel alluvium preserved at AK-10 (units B-E – Fig. 8.11). The absence of a generation of calcrete formation which pre-dated the incision of T1 could be related to issues of preservation, but more likely to do with different climatic conditions compared to T2, discussed earlier. Aggradation of T2 terminated around 17 ± 2.5 ka (see AK-10, Figure 8.11). Without the blanketing effect of calcrete, deep incision of T1 colluvium likely propagated up the flanking slopes, re-establishing connectivity with deep stores of highly weathered regolith.

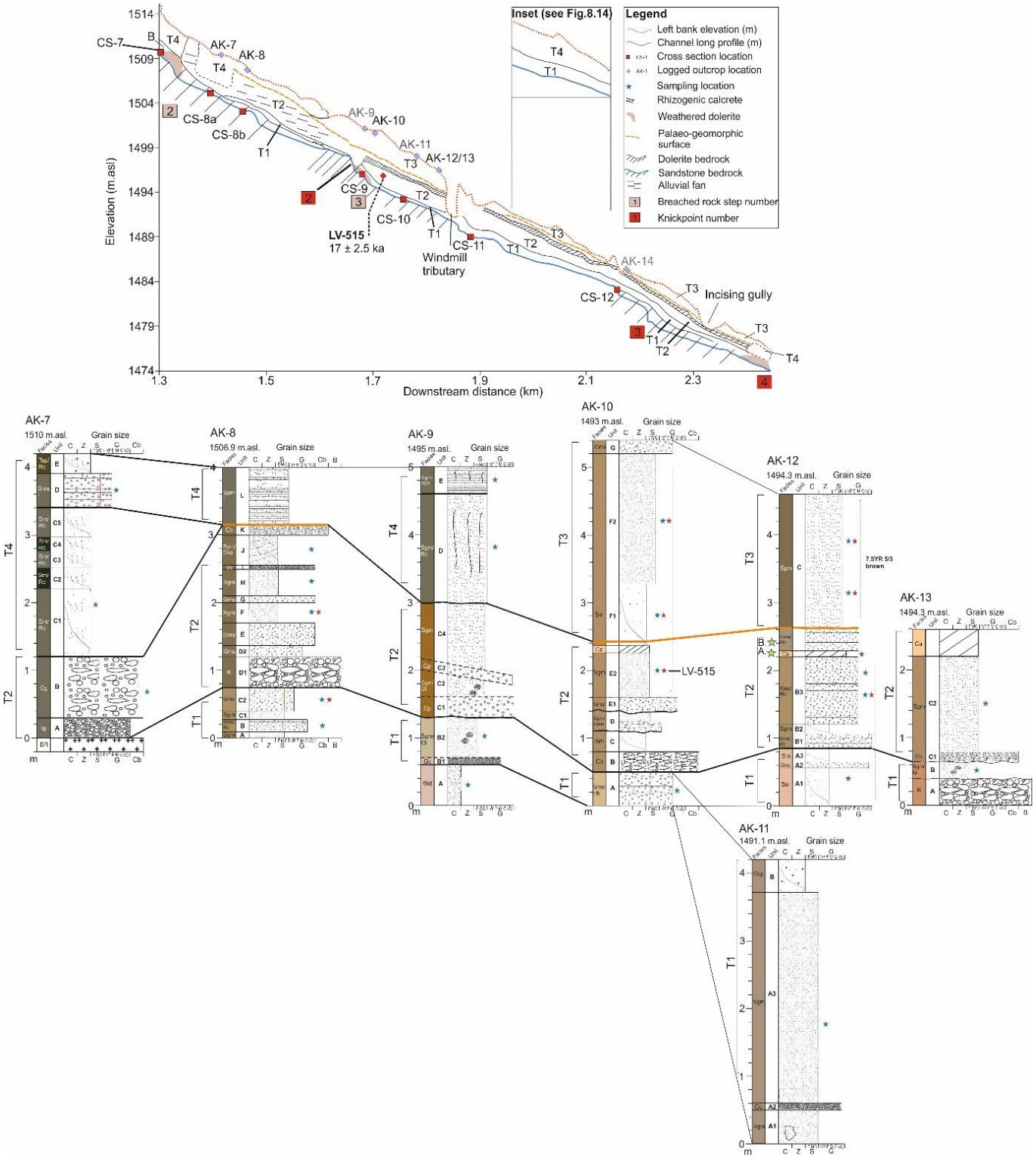

Figure 8.11 – long profile for the central valley region (1.3–2.38 km). The vertical and longitudinal limits of terraces 1-4 are indicated. Only the elevation of the left surveyed bank is presented: log codes (i.e. AK-9, 11 and 14) are coloured grey indicating they were obtained from the right bank. Note 1) the continuity of the palaeogeomorphic surface (orange dashed line – pedostratigraphic member (A) along the valley margins, 2) the inset palaeochannel succession (T4) from 1.35–1.45, 1.95–2.15 and 2.35–2.4 km (see Fig. 8.13 for exact spatial limits), 3) the position of knickpoints and breached rock steps and 4) OSL date LV515 from AK-10 unit E2.

The maturity of weathering rinds on dolerite clasts sourced from tors at Africanders Kloof (see Section 5.3.1 & 5.3.2) implies an extended period of weathering under

humid conditions that probably predated the LGM (Clarke et al., 2003; Holmes et al., 2003). These sediments were transmitted to the valley floors through palaeochannels (AK-6 and AK-12), in some cases terminating as fans (AK- 8). Mode of emplacement was predominantly debris flow, depositing in these fans (AK-7 and 8), but also as channel bars (AK-10). Initial impetus for incision may have been rainfall and vegetation being out of phase (Knox, 1972).

Resultant aggradation of T2 was partly an autogenic response to re-connection with these deep stores of sediment. The associated conveyance of large quantities of cobbles and boulders confirms that the predominantly fine-grained nature of T1 does not attest to a supply-limited system during its formation, but rather a transport-limited one consistent with the notion of a relatively cold, dry climate. At AK-8, AK-10 and AK-12, sedimentation associated with the emplacement of T2 deposits halted for a period of time sufficient for a soil to form – labelled 'pedostratigraphic member A' (see Fig. 8.11 and 8.12 – orange dashed lines and the limits of the rhizogenic calcrete). Since aggradation of T2 terminated in the deglacial period (17 ± 2.5 ka), subsequent soil development probably occurred in the late Pleistocene rather than early Holocene.

The evidence indicates that this palaeosol is pervasive across the upper slopes (AK-3 – Section 8.2.2) and central valley, characterised by haematite formation, confirmed in the 'redness' of the soil as well as a spike in AF mineral proxies (AK-12). The maximum thickness of this palaeogeomorphic surface was recorded at AK-12 (25 cm). The rhizogenic calcrete, thickest in the central compared to upper valley reaches, reflects a raised water-table associated with vegetated, aggraded valleys and slopes. Recently, Chase et al. (2015) demonstrated using a new hyrax midden record in SW Africa that a westward expansion of the SRZ occurred around 18 ka. In theory, the combined evidence for enhanced moisture, vegetation and development of a soil overprinting T2 implies climatically warmer, wetter conditions relative to T1. However, Lyons et al. (2014) working along the Modder River, central South Africa, found that rainfall declined from 28 ka but was lowest between 18 and 15.5 ka (100-200 mm/yr) seemingly contradicting Chase et al. (2015). The distribution and dynamics of the WRZ and SRZ are still incompletely understood (Stone, 2014). One reason for the apparent discrepancy could be that the SRZ did not expand as far north as the Modder River from 18-15.5 ka. As the Sneeuberg is farther south, it may

have been subject to SRZ dominance at an earlier stage, hence the pre-17ka incision of T1 along the Wilgerbosch River.

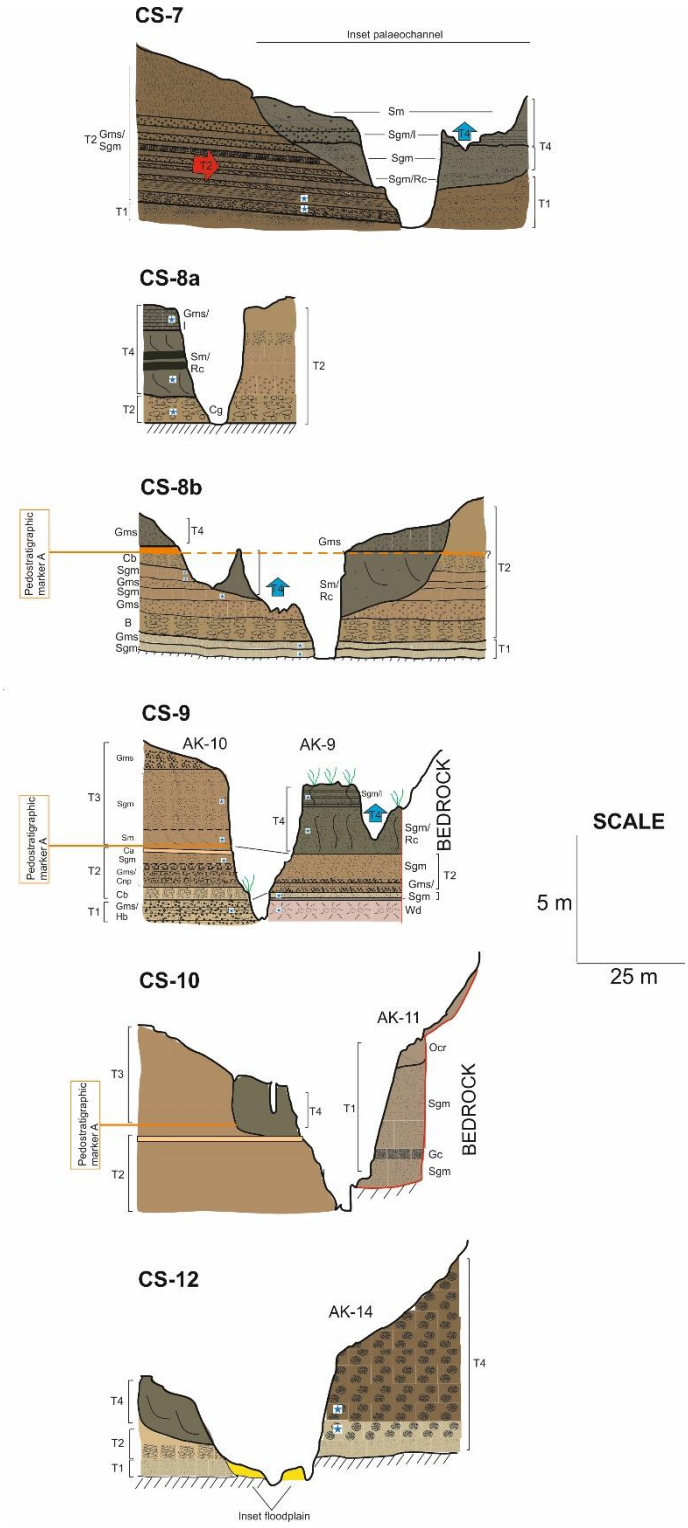

Figure 8.12 – surveyed valley cross sections (CS-7, 8, 9, 10 and 12) showing the relations of terraces 1-4. See Fig. 8.11 for cross section locations on long profile. Note facies codes are provided only for sections logged in detail, i.e. CS-7–12 (AK-6–10).

Complexity is added however because the Sneeuberg is also influenced by frontal rains from the south Atlantic (Chase and Meadows, 2007) and thus T1 incision could have occurred without an expansion of the SRZ. With respect to soil formation and calcrete development (T2), since this occurred after 17 ± 2.5 ka, it is reasonable to hypothesise that summer-dominated rainfall (Chase et al., 2015) presided. Reduced drought stress would have been conducive to vegetation expansion and, in concert with infilling valleys, a raised water table.

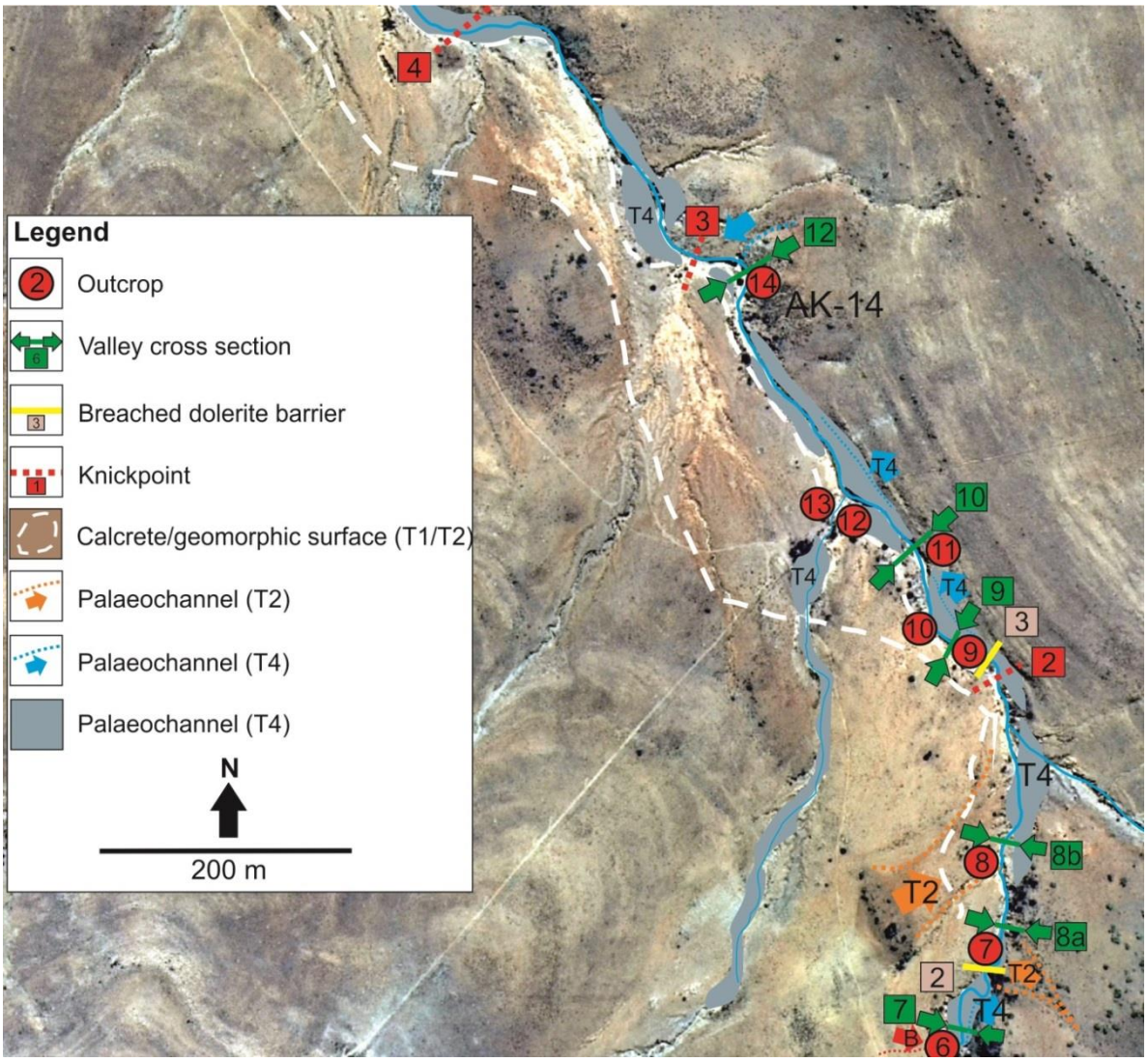

Figure 8.13 – digitised aerial photograph of central valley region spanning from AK-6 to the breached dolerite barrier no.2 (dashed red line - top of map) just upstream of AK-15 (discussed in next section). Note 1) the limits of the rhizogenic calcrete (dashed white line) which is taken as a surrogate for pedostratigraphic member A (see Fig. 8.12). 2) Two generations of palaeochannels are indicated (T2 and T4) – see blue dashed line. At AK-6 this is a bank gully (red dashed line). 3) The lateral and longitudinal limits of the inset palaeochannel sequence are presented (T4). Note the location of cross-sections (green) which are presented in Fig 8.12.

Following soil formation, there was a phase of incision, probably related to climatic aridification reflected in micromorphological evidence for lowering of the water-table (see Section 5.3.6 for full account). The absence of macro-scale brecciation and incision of the rhizogenic calcrete across the valley implies that this acted as a base-level anchor and that the incision phase was not of sufficient magnitude and/or duration to cut through it.

A switch to an aggradational valley regime is indicated in the sediments that comprise **T3** (Table 8.4). This terrace is thickest at AK-10 and 12 (2-3 m) whereas downstream it is much thinner (0.3–0.4 m thick). This is attributed to varying proximity to the hillslopes. AK-10 and 12 are particularly close to actively weathering and eroding dolerite slopes. Further downstream, the valley floors are buffered from the hillslopes. As there is no clear palaeosol horizon at the top of T3, this implies that the later shift to catchment-wide gully incision (T4 - discussed next) occurred relatively rapidly.

The sediments of **T4** (Table 8.4) are associated with the next **preserved** phase of 'cut and fill' in the valley. This morphostratigraphic unit constitutes the clearest example of ‘fill within fill’ reflected as inset terrace deposits (CS-7–12 – Fig. 8.12). The deposits are gleyed with varied grain size and bromine content (Table 8.5). These differences require further explanation in relation to local valley morphology.

Table 8.5 – consolidation of grain-size and bromine data for all sampled T4 lithostratigraphic units at Africanders Kloof.

T4 lithostratigraphic units	Median (μm)	% sand	% mud (silt + clay)	Br (ppm)
AK-4 below channel	6	2.7	97.3	-
AK-4 / C	60.8	49.7	50.3	21.8
AK-7 / C	52	47.4	52.6	9.7
AK-9 / D	749.6	67.3	32.7	6.8
AK-15 / E	49.9	42.7	57.3	6.2
F	65.4	51.2	48.8	6.8
AK-18 / A	35	37.3	62.7	-
C	92.3	55.3	44.7	15.9
C	102.4	58.3	41.7	24
E	72.8	51.9	48.1	18.1

The AK-4 (T4) sample comes from a reach immediately upstream of sandstone rock step 4 (Fig. 8.5), where the valley loses confinement compared to upstream (see CS-4, Fig. 8.6). AK-7 (T4) occurs immediately downstream of a partially breached

dolerite barrier (no.2 – Fig. 8.13). The geomorphic evidence is that the T4 channel was forced through the breached barrier (no.2), reappearing in the terrace legacy immediately downstream (p. 177-179). These two locations have one crucial factor in common: abrupt change from confined to unconfined setting. AK-18, discussed fully in section 8.2.3, occurs in a similarly unconfined zone at the end of a relatively confined, straight reach. Grain size, with the exception of the AK-4 'below channel' sample, is remarkably consistent ranging from 35–102.4 μm whilst bromine content is consistently higher compared to AK-9 and 15 (Table 8.5). AK-9 is much coarser (749.6 μm) and bromine relatively low (6.8 ppm), but this occurs downstream of the second major knickpoint through sandstone where local valley slope steepens (Fig. 8.11 and 8.13). AK-15 (discussed later) occurs in a similar setting to AK-9: the base of knickpoint 5 (forthcoming Fig. 8.16). No preserved T4 palaeochannel occurs here (Fig. 8.17) unlike AK-9 (CS-9).

Figure 8.14 – photograph of knickpoint 3 through dolerite bedrock crossing channel at the bottom of the central valley 2.2 km downstream from the headwaters (see Fig. 8.11 and Fig. 8.13).

The evidence indicates that in unconfined zones upstream of sandstone rock steps, T4 grain size is typically lower, whilst organic content is higher. This implies increased ponding in these zones compared to areas downstream of knickpoints. The characteristics of T4 closely resemble the mid-late Holocene wetlands ('vleis') reported by Holmes et al. (2003) on the Klein Seekoi River, though a review of Boardman et al. (2014, their Fig. 3) seems to show poorly defined 'cut and fill' boundaries with the underlying and flanking colluvium compared to T4 wetlands at Africanders Kloof where distinct lateral and vertical sharp contacts occur (Fig. 8.12).

Neville (1996) reported how the Klein Seekoi River was formerly a chain of pools prior to becoming an incised gully, whilst Grenfell et al. (2014) submit that these pools occupied small hollows upstream of floodouts. Whilst increased ponding upstream of dolerite rock steps is indicated due to loss of confinement and valley gradient, the facies and terrace morphology do not obviously attest to terminal channel processes. Rather, at several locations a palaeochannel associated with T4 is preserved (max. depth 1 m – see CS-9, Fig. 8.12) implying active fluvial sedimentation. Furthermore, T4 is continuous over: a) the rock steps and b) knickpoints as shown in Fig. 8.11. This implies that the palaeo-wetlands were not strictly localised to sections of valley immediately upstream of rock steps where confinement and gradient reduced. Furthermore, the depth of incision of the dolerite (Fig. 8.14) indicates several cycles of erosion which probably predates the preserved cut and fill terrace legacy. As a result, during deposition of T4, it is assumed that the dolerite had been already incised to its current base level and was filled in by sediment. Given the inherently resistant properties of Karoo dolerite to erosion (Tooth et al., 2004; Neuumann et al., 2011), it follows that incision of bedrock to this depth probably pre-dates the maximum age of terrace fills preserved in the valleys. With the exception of breached barrier 1 after the floodout (AK-2), there is little evidence to indicate major knickpoint retreat resulting in reconnection with formerly impounded sediment sources.

8.2.4 AK15 – AK-18.

The outcrops sampled in the lower valley represent terraces 2 – 4, as the slopewash deposits are set back from the valley (Table 8.6, Fig. 8.15).

Table 8.6 – summary of local [1]morphostratigraphic units, their associated [2]lithostratigraphic units, facies and interpretation for logs AK-15 – AK-18.

Unit[1]	Log/Unit[2]	Facies	Interpretation	Section
2	[1]AK-15 A – D [2]AK-16 A – J [3]AK-17 B – J	Gms, Sgm, Sm/Gl, Dm/l Cb/Hb, Gms, Sgm, Cb/HB, Sgm/l, Sm, Gc,	[1]Channel and overbank deposits in a vegetated, aggrading channel system. [2]Bar deposits at channel margins and overbank deposits. [3]Debris flow deposits from nearby dolerite slope. Switch in conditions above to migrating single-thread channel.	5.4.1 – 5.4.3
3	AK-16 K	Sgm	Slopewash deposits	5.4.2
4	AK-15 E – G AK-18 A – I	Sm/l/Rc Md,Hb, Sgm/Hb, Gms, Gc, Sm	Low energy channel system with wetlands.	5.4.1 and 5.4.4

T2 is represented by palaeochannel deposits at the logged sections rather than truncated laterally impinging fans as was the case in the central and upper valley. The nature of the facies at AK-15 is unlike those reported at outcrops upstream (see Section 5.31). This raises the question as to how justifiable it is to correlate the thick bar and clastic floodplain deposits (AK-16) exposed in the left bank with the relatively fine-grained, organic rich muds on the right at AK-15 (Fig. 8.16 and 8.17).

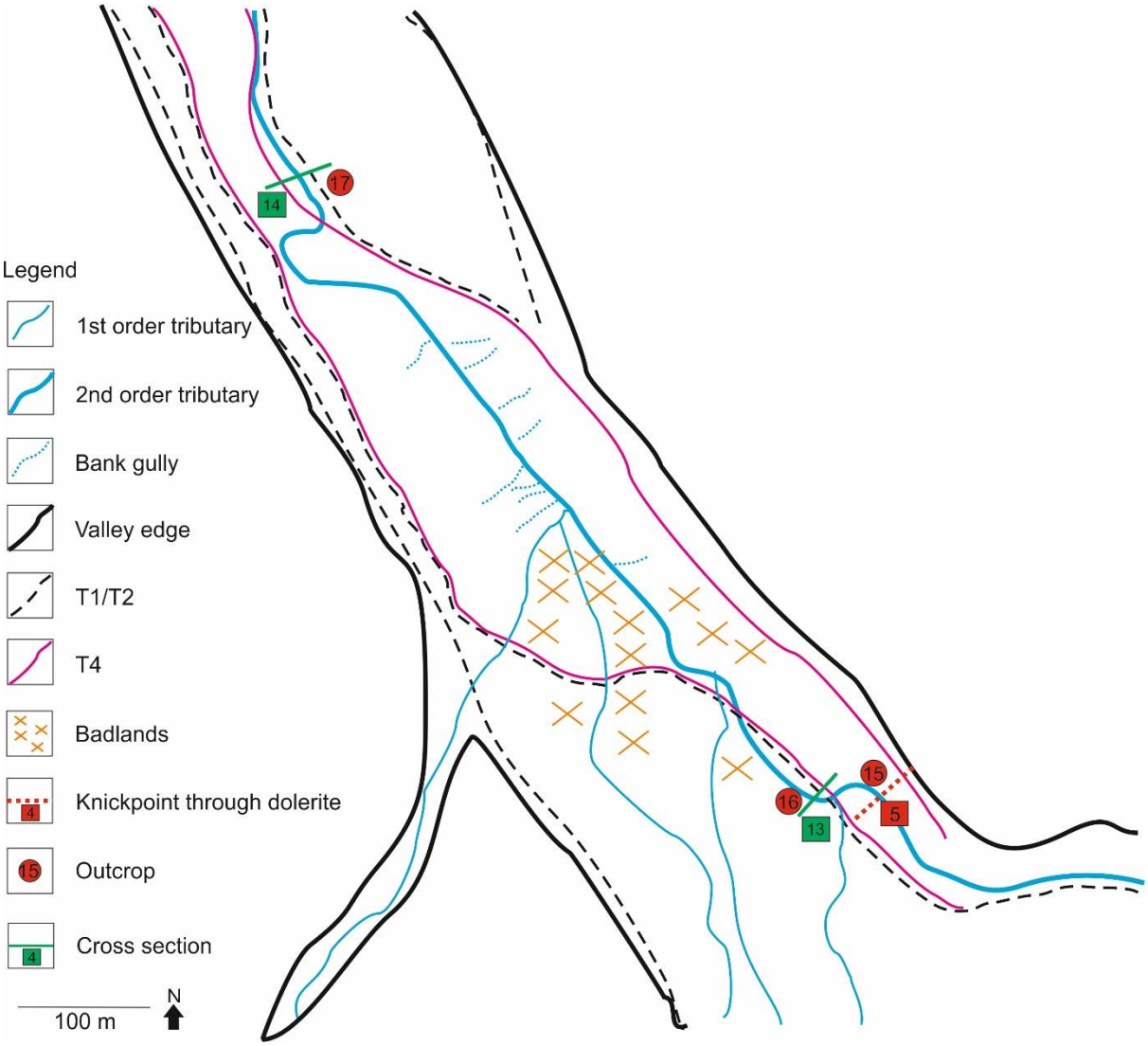

Figure 8.15 – map of stretch of channel from AK-15 – AK-17 showing extent of terraces 1-2 and 4. Note: 1) the location of AK-15 immediately downstream of dolerite knickpoint 2, within the limits of T4 and 2) the distribution and occurrence of bank gullies and badlands which have formed primarily within T4 sediments.

AK-15 lies immediately downstream of sandstone knickpoint 5, which is also a seepage zone for aquifer fed groundwater (Fig. 8.15 and 8.16). Up to 5 m of incision through sandstone attests to multiple phases of incision that predates those represented in the terrace legacy. Furthermore, the geomorphic evidence so far indicates that the present depth of channel incision has not occurred since the major incision phase associated with T1 abandonment in the deglacial period and the subsequent fluvial phase represented by T2. The proximity of AK-15 to this seepage zone likely provided the impetus for low energy sedimentation as a feedback response to dense vegetation cover in this part of the valley within the context of an aggradational (fill) regime, especially if the system was backfilling in response to base level rise of the trunk Wilgerbosch River.

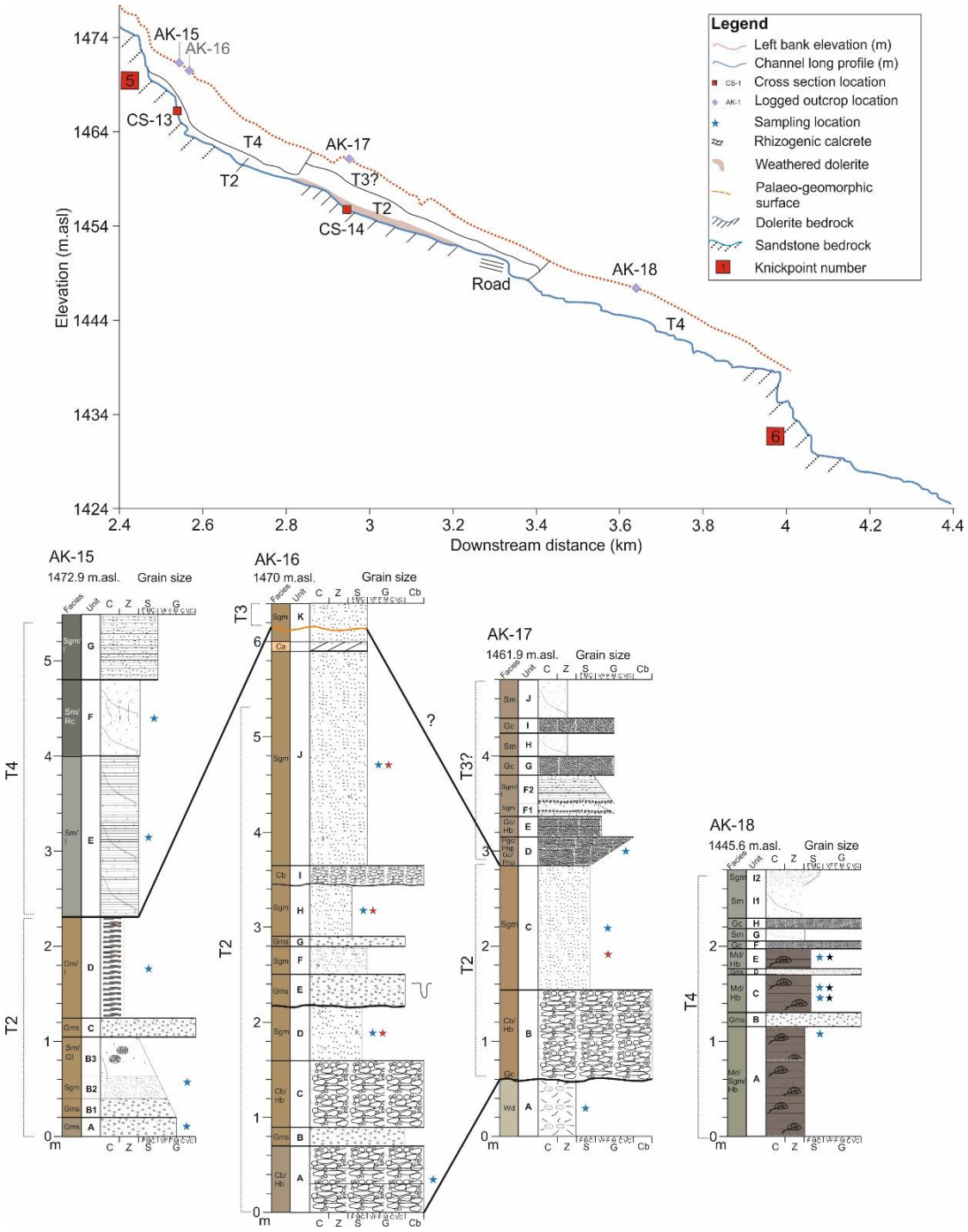

Figure 8.16 – enhanced long profile for the lower valley (2.4 – 4.4 km). The vertical and longitudinal limits of terraces 2-4 are indicated.

Magnetically, both AK-15 and 16 were found to be similar, but with slightly subdued ferrimagnetic susceptibility at AK-15 (see Section 5.3.1). This can readily be explained by conditions of poor drainage relative to AK-16 inducing ferrimagnetic dissolution. Therefore, these relatively fine-grained sediments are probably contemporaneous with the thick bar deposits at AK-16 (CS-13, Fig. 8.17). This would be analogous to the lateral relations of single-thread channel deposits in the contemporary channels described in Chapter 4 (Table 4.3, analogue 4). At AK-16,

the same stratigraphic sequence as that described for AK-10 occurs, with 6 m of thickly bedded fluvial deposits.

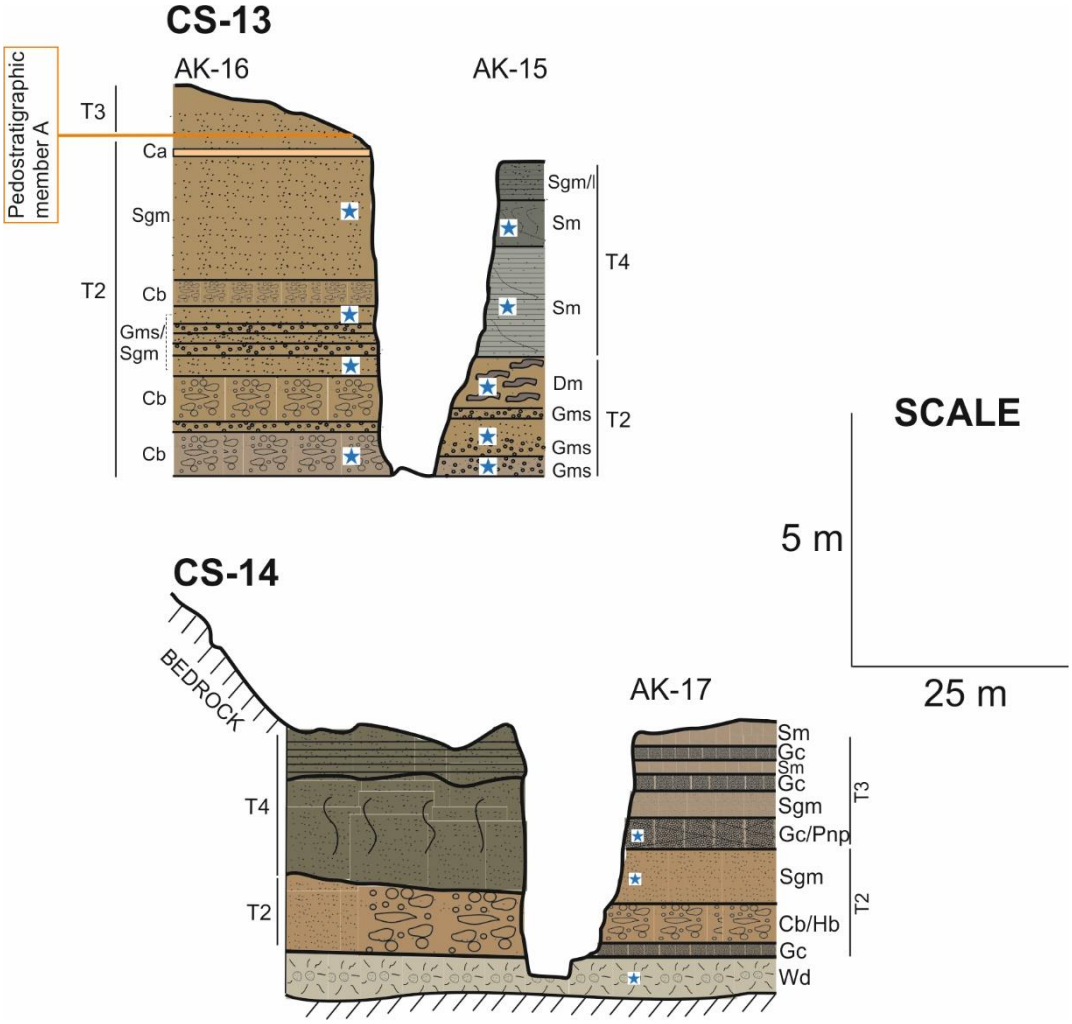

Figure 8.17 – surveyed valley cross sections (CS-13 and 14) showing the relations of terraces 2-4. See Fig. 8.17 for cross section locations on long profile.

The same rhizogenic calcrete horizon as that reported at AK-10 and 12 is present at the top, beneath a rubified palaeosol and thus the sequence represents T2 – the limits of which are indicated in Fig. 8.18. T3 is represented here by a thin horizon of indurated sand, corresponding to T3 described at AK-10 and 12 (Fig. 8.11 and 8.16). The organic deposits of T4 unconformably bury those of T2 at AK-15 (see Fig. 8.17), which are part of a palaeochannel sequence that runs all the way downstream past the road (Fig. 8.18).

At CS-14, this T2/T4 unconformity is clearly expressed again in the left bank. In the right bank, the basal bar and floodplain deposits (AK-17 units B and C – see Fig. 8.17) are buried unconformably by relatively friable, coarse-grained channel

deposits. The pedostratigraphic marker horizon and calcrete are absent from the top of this profile.

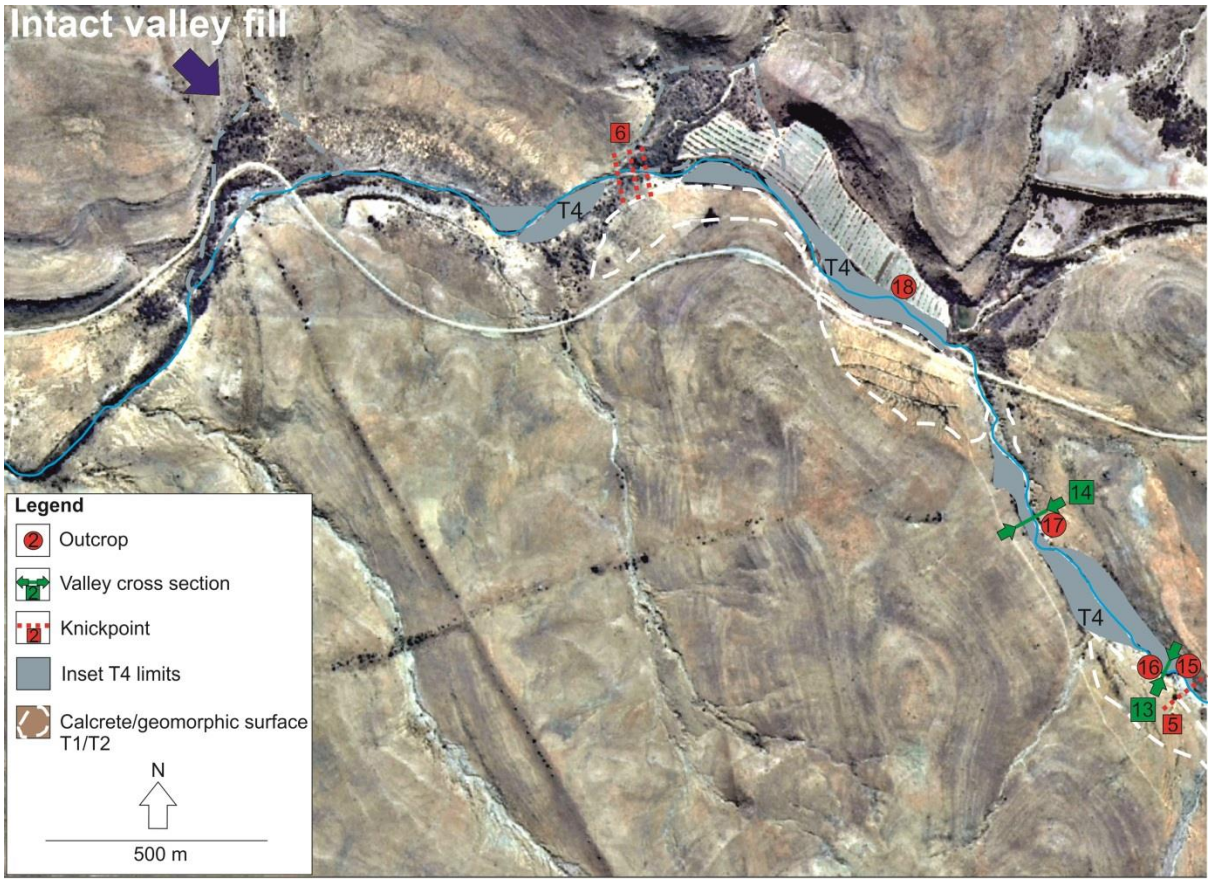

Figure 8.18 – digitised aerial photograph of lower valley region from AK-15 all the way to the base of the tributary past AK-18. Note: 1) the blue arrow indicating a vestige of intact valley fill disconnecting a small tributary from the modern gully, 2) the white dashed line indicating extent of calcrete/palaeogeomorphic surface of T1/T2.

The minerogenic, coarse calibre of units D-J at AK-17 (Fig. 8.16) mean that this is not T4, implying an intermediate phase of incision and aggradation that postdates emplacement of T2, but pre-dates T4. Since climatic aridification has been established following soil development at T2 elsewhere (AK-12 for example), it follows that these intermediate deposits (AK-17) may be coeval with T3 mantling the palaeosol surface at AK-10, 12 and 16 upstream. The apparent absence of the calcrete at this location may be due to two factors: 1) this is an example of a location where the calcrete was successfully incised following climatic aridification; 2) the calcrete was not incised at time of emplacement of T3 at AK-17, but has subsequently been removed by generations of leaching and erosion (AK-10 for example – the calcrete was hardly visible). However, the absence of the palaeosol surface associated with T2, lends credence to the first postulation, though there is little or no evidence to suggest that incision of the calcrete overprinting T2 during this

phase of aridification went further upstream. Rather, the response of the landscape is comparatively muted to between 0.5 - 2.8 m (AK-16 and AK-10 respectively) of aggradation burying the T2 palaeosol and these do not represent high energy deposits.

Figure 8.19 – thickening deposits of laminar rhizogenic calcrete at the valley margins 200 m downstream of AK-18 exposed in the left bank next to sandstone knickpoint 6 (see Fig. 8.18).

The only other documented occurrence of this stratigraphic relation is at outcrop GG-1 on the trunk Wilgerbosch channel discussed in forthcoming section 8.4. Whilst the relative morphostratigraphic sequence of ‘cut and fill’ may correspond, the absence of radiometric dates again precludes an evaluation of degree of synchronicity.

Immediately after the road (3.4 km downstream – see Fig. 8.16) at the confluence between the AK main channel and tributary joining from the east (Fig. 8.18), the right bank of the modern channel is T4, but it is crucial to note that terraces 1 and 2 with the calcrete and palaeosol succession alternate at the valley margins as indicated in Fig. 8.18 and 8.19.

8.2.5: Summary

The synthesis of surveyed channel, terraces and their intrinsic facies and soil characteristics have revealed a minimum of three cut and fill phases. The base of the succession is characterised by slowly aggraded sediment sourced primarily from hillslopes with little preserved evidence for high energy fluvial activity (T1).

These deposits are deeply incised by large channels and fans at least as far upstream as AK-5. The extent of incision and re-establishment of connectivity with the central valleys and deeply mantled slopes accounts for why so much sediment could be subsequently deposited and the valleys overloaded to the extent that aggradation of T2 occurred. Since this pattern is continuous across the catchment (with the exception of the AK headwaters), this incision may signify a rapid climatic shift to wetter conditions, but the magnitude of response may imply that vegetation and rainfall were out of phase (Knox, 1972). The termination of this aggradation phase (T2) occurred in the deglacial period. The catchment wide formation of haematite soil and a substantially elevated water-table attest to conditions that were relatively humid compared to T1, though the raised water-table has been found to be partly a feedback response to valley infilling. Conversely, burial of this palaeosol – in one case incision and emplacement of relatively high energy channel deposits - implies, in concert with leaching of the calcrete, that the climate became drier. The axiomatic implication of this is that vegetation cover reduced, the geomorphic threshold lowered and aggradation of a third terrace occurred, though spatially, this response appears to have been heterogeneous due to the armouring effect of the calcrete. Similarly during aggradation of T4, only at one location does the calcrete appear to have been incised (AK-15 and AK-16): upstream the evidence is that it remained intact and prevented the full exhumation of terraces 1 and 2. Whilst the drivers of T4 are less well understood, the deposits attest to a predominantly waterlogged, low energy fluvial environment, but unlike for T2, plant coverage was restricted to corridors on the valley floors instead of extending far up the slopes as confirmed by the extensiveness of the calcrete associated with T2.

Therefore, patterns of sedimentation and incision from AK-5 downstream to the trunk Wilgerbosch channel at Ganora farm do not reflect localised, discontinuous channels and floodouts as have been reported elsewhere (Grenfell et al., 2014). The bedrock

morphology and degree of incision attests to multiple generations of cut and fill some of which predates the oldest (T1) terrace fills preserved.

8.3: Longitudinal Correlation of Terrace Sequences ii: Wilgerbosch Kloof

The local stratigraphy of terrace fills contained in the Wilgerbosch Kloof valley is herein presented and then compared with Africanders Kloof. Six semi-continuous major terrace units were identified across the valley (Table 8.7).

Table 8.7 – summary of local [1]morphostratigraphic units, their associated [2]lithostratigraphic units, facies and interpretation for logs WGB-1 – WGB-7.

Unit[1]	Log/Unit[2]	Facies	Interpretation	Section
FT-1	[1]WGB-2 / A and B [2]WGB-3 / A-F	[1]Gms/Hb/Cnp/Pnp [2]Sgm/Cnp, Gms/Cnp, Cb, B	Alluvial fan channel deposits.	6.3 – 6.4
FT-2	[1]WGB-1 / A [2]WGB-2 / C [3]WGB-3 / G	[1]Sgm/Rc, Gms/Hb [2]Gms/Rc [3]Sgm	Alluvial fan channel deposits.	6.2 – 6.4
T1	[1]WGB-4a / A [2]WGB-4b / A [3]WGB-6 / A-D [4]WGB-7 / A-C	[1]Sm, Sgm, Gms [2]Sgm, Gms/Cnp. [3]Sm, Sgm, Gms/Cnp, Gc [4]Sgm, Gms/Cnp	Channel and floodplain deposits.	6.5, 6.7 and 6.8
T2	[1]WGB-8 / A [2]WGB-9 / A-B [3]J-22 (junction)	[1]Sgm/Gms [2]Sgm/Gms [3]Sgm	[1]Slopewash deposits. [2 3]Laterally mobile channel deposits: point bars, medial bars and floodplain.	6.9 – 6.10
T3	[1]WGB-4a / B [2]WGB-4b / B [3]WGB-6 / E-F [4]WGB-7 / D-E [5]WGB-10 / A-B	[1]Sgm/Pnp [2]Sgm/l [3]Sgm/Cnp, Gms [4]Sm, Sgm/l [5]Sm, Sgm, Gms	Low-energy gleyed channel deposits and floodplain.	6.5, 6.7-6.8 and 6.11
T4	WGB-11	Sgm/Cnp/Pnp, Gms/Cnp, Cb, B	Channel sediments infilled behind dam.	4.3
T?	WGB-5 / A–B	Sm, Gc, Gms/Cnp	Low-energy gleyed channel deposits incised by palaeochannel.	6.6

The synthesis commences with a detailed stratigraphic analysis of fills in the upper part of the tributary (WGB-1–7) as this part is characterised by the most pronounced changes in valley morphology compared to downstream (see Section 6.1). This is followed by a morphostratigraphic analysis of deposits in the central and lower valley (WGB-8–10) and the continuity of terrace fills established.

8.3.1 Upper valley: WGB-1 – WGB-7

In these upper reaches, 4 terrace units are recognised: FT-1 and 2, T1 and T3 (Table 8.7). The occurrence of T2 is restricted to the central-lower valley and discussed later.

The upper headwaters are occupied by a small palaeofan which has episodically cut and filled. Two fan channel terraces were recognised: FT-1 and 2. Figure 8.20 - 8.22 show that **FT-1** is absent along the first 120 m of valley long profile. This is due to the valley being too steep and narrow. FT-1 extends from J-1 to J-2. WGB-3 was the last recorded instance of fan-channel deposits in the downstream direction, differentiated from non-fan alluvial channel deposits on the basis of progradational features and terrace slope perpendicular to the modern channel (see Section 6.4). Identification of the boundary between fan-channel (sensu stricto) and alluvial channel was difficult to establish, but likely lies somewhere between J-2 and J-3 where fining and sorting of deposits increases, later represented at WGB-4 (Section 6.5). The base of FT-1 terrace soils is characterised by haematite, but the palaeosol surface (i.e. the original fan surface upstream of J-2) is dominated by fine-grained magnetite, producing a distinctive magnetic signature (see Section 6.3). This constitutes a major pedo-stratigraphic boundary as shown by the orange correlation line in Fig. 8.20. FT-1 has been incised by high energy deposits sourced from a palaeogully on hillslopes to the south-east between J-2 and J-3 that are not stratigraphically coeval with FT-2.

FT-2 extends from the headwater pediment to WGB-3 and represents the final phase of palaeofan aggradation before incision of the fan by the contemporary gully (see limits: Fig. 8.21 - 8.23). Compared to FT-1, the soils of FT-2 are poorly developed and friable, with magnetic mineralogy driven largely by spatial variations in upland soil sources rather than in situ soil development and horizonation (see Section 6.2). Compared to FT-1, FT-2 soils are extensively prone to rilling and incision, having developed hummocky badland terrain as shown in Fig. 8.21.

Downstream of the palaeofan, two major alluvial terraces were identified: 1 and 3 (Table 8.7). **T1** facies are fine-grained relative to FT-1 upstream, characterised by well sorted sands (WGB-4A) and then cross-bedded gravels, then sands at WGB-4B (Table 8.7; Fig. 8.20). This fining relative to FT-1 intersects with the abrupt transition morphologically to an unconfined valley setting, which undoubtedly caused a break

in the connectivity of the system for sediment coarser than gravel (see Fig. 8.21 for footslope boundary and CS-4 – Fig. 8.22). The continuity of the red soils of FT-1 with no abrupt stratigraphic junctions between these and the red soils of T1 indicates that both terrace fills are stratigraphically concordant.

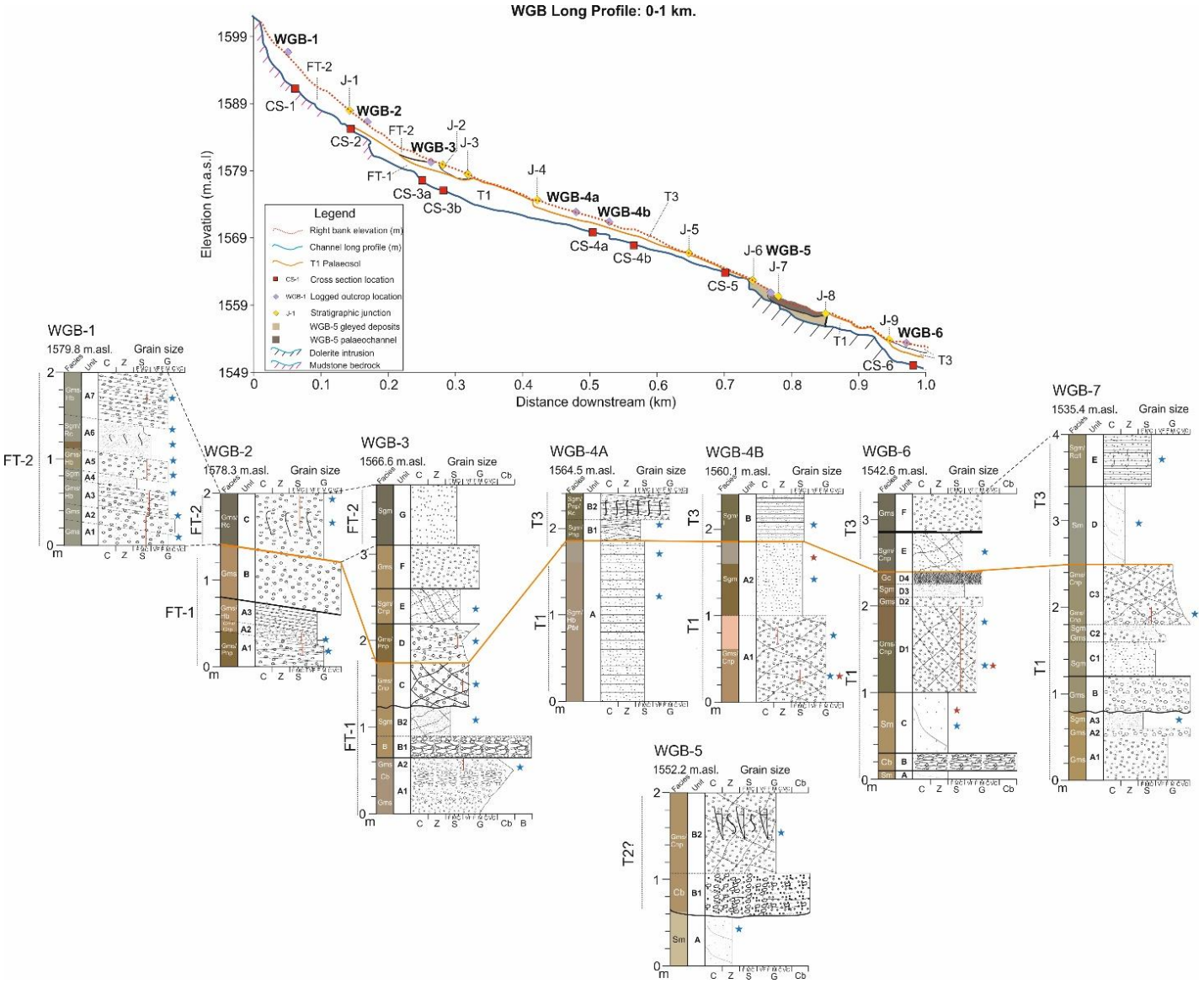

Figure 8.20 – enhanced long profile for upper headwaters of Wilgerbosch Kloof showing major stratigraphic junctions (J-1, 2 etc), the continuity of fan terraces 1 and 2 and alluvial terraces 1 and 3. Correlation lines between major pedo-stratigraphic unconformities are indicated between logs. Cross reference with Fig. 8.21 to see lateral and longitudinal limits of terraces. Note the dolerite intrusion after 0.7 km.

The distinctive ferrimagnetic-enriched palaeosol horizon identified at FT-1 is evident at WGB-4 and 6 indicated by the orange correlation line in Fig. 8.20. The underlying haematite rich soils at these outcrops imply comparable soil maturity from J-1 downstream. Therefore, the palaeofan (FT-1) was the main source of sediment to T1

mantling the alluvial plain. Since time is a crucial factor in maturation of soil (Jenny, 1941), the identical soil characteristics of FT-1 and T1 may be taken as evidence that the soils are approximately the same age and related to the same environmental phase.

T1 has been incised in two places: **1)** an infilled palaeochannel at J-4. This correlates stratigraphically with the unweathered sandy unit at WGB-4 (unit B) but this pinches out at J-5 (Fig. 8.20 and 8.21). Organic-rich, cross bedded sands bury the magnetite-rich palaeosol from J-9 onwards (see WGB-6), grading to clayey silt at WGB-7 (unit D – see Fig 8.20), capped by unweathered gravels at WGB-6 (unit E–F) and sand at WGB-7 (unit E). These deposits were ascribed to a low energy, migrating single thread channel only partially incised into T1 (see Table 8.7 for corresponding section). If this part of the succession at WGB-6 and 7 is coeval with the sand unit at WGB-4, why are the organic rich fills absent upstream of WGB-6? One explanation could be that the sands of WGB-4 are unrelated. Alternatively, it could be that the palaeochannel sediments represented at WGB-6 (units E-F) and WGB-7 (unit D) have been removed by erosion from J-4 – 9, such that only the floodplain associated with this palaeochannel has been preserved mantling T1 (WGB-4 unit B). Magnetically, WGB-4 unit B sands were found to exhibit far greater total susceptibility than WGB-6 and 7 sands, but the apparent discordance may be misleading for purposes of stratigraphic correlation in light of the fact that the sands of WGB-4 were clearly of reworked hillslope and possibly headwater fan-origin. WGB-7 sediments are at least partially sourced from hillslopes to the south with unit D exhibiting paramagnetism due to waterlogging, whilst E has been magnetically diluted, probably by higher density of vegetation due to the poorly drained underlying unit (see Section 6.8b for a full account). Therefore, the sands capping outcrops WGB-4, 6 and 7 are treated as being stratigraphically concordant and part of T3. In regard to T3, note the blue arrow and dashed lines at J-4 indicating the maximum south-eastern extent of this terrace (Fig. 8.21).

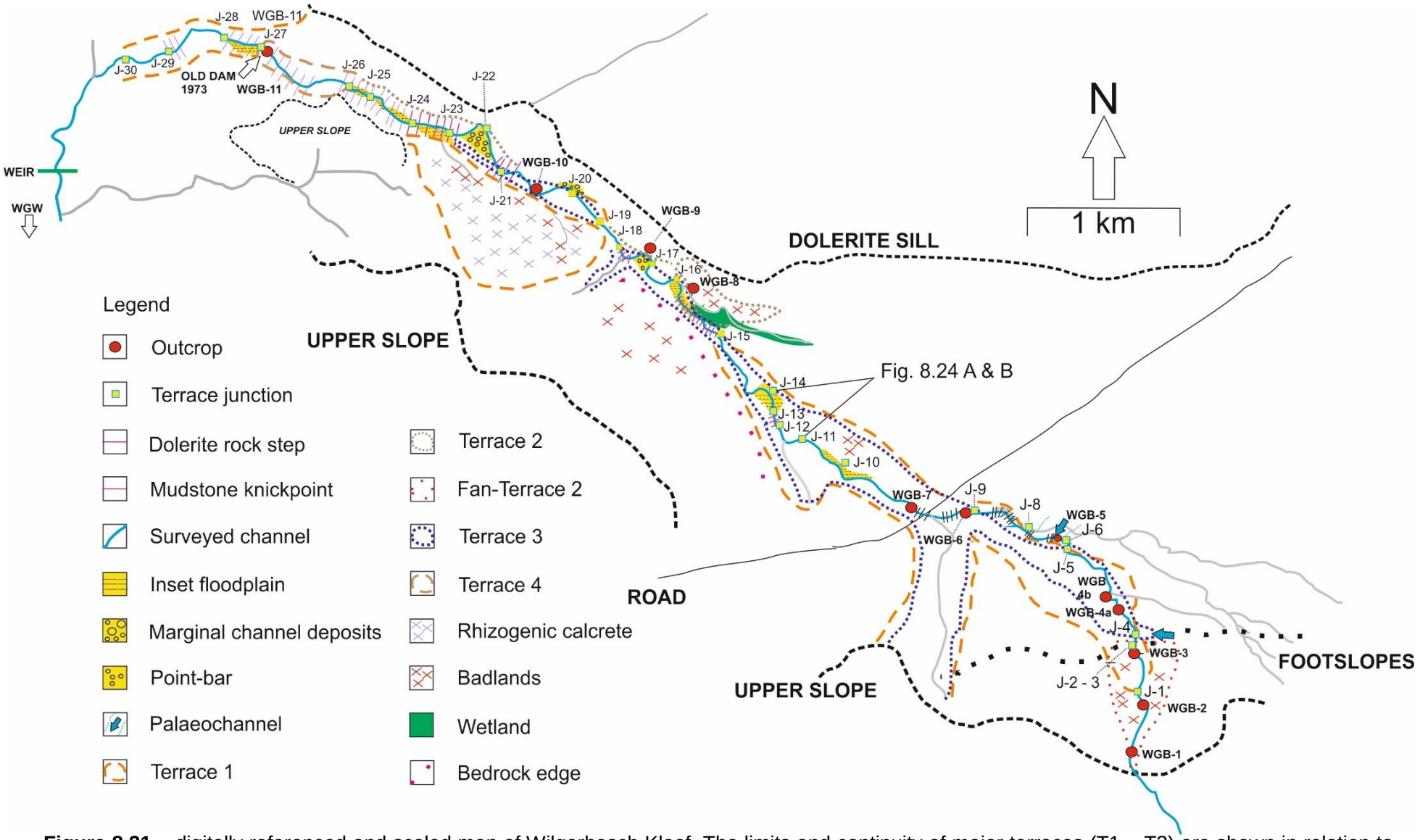

Figure 8.21 – digitally referenced and scaled map of Wilgerbosch Kloof. The limits and continuity of major terraces (T1 – T3) are shown in relation to the surveyed channel. Stratigraphic junctions are indicated. See Fig 8.20 (long profile) for longitudinal limits and junctions on upper slopes and central/lower valley respectively. Note, **FT-1** reported in the text and Fig. 8.20 is labelled as T1 (dashed orange line) here as they are stratigraphically coeval.

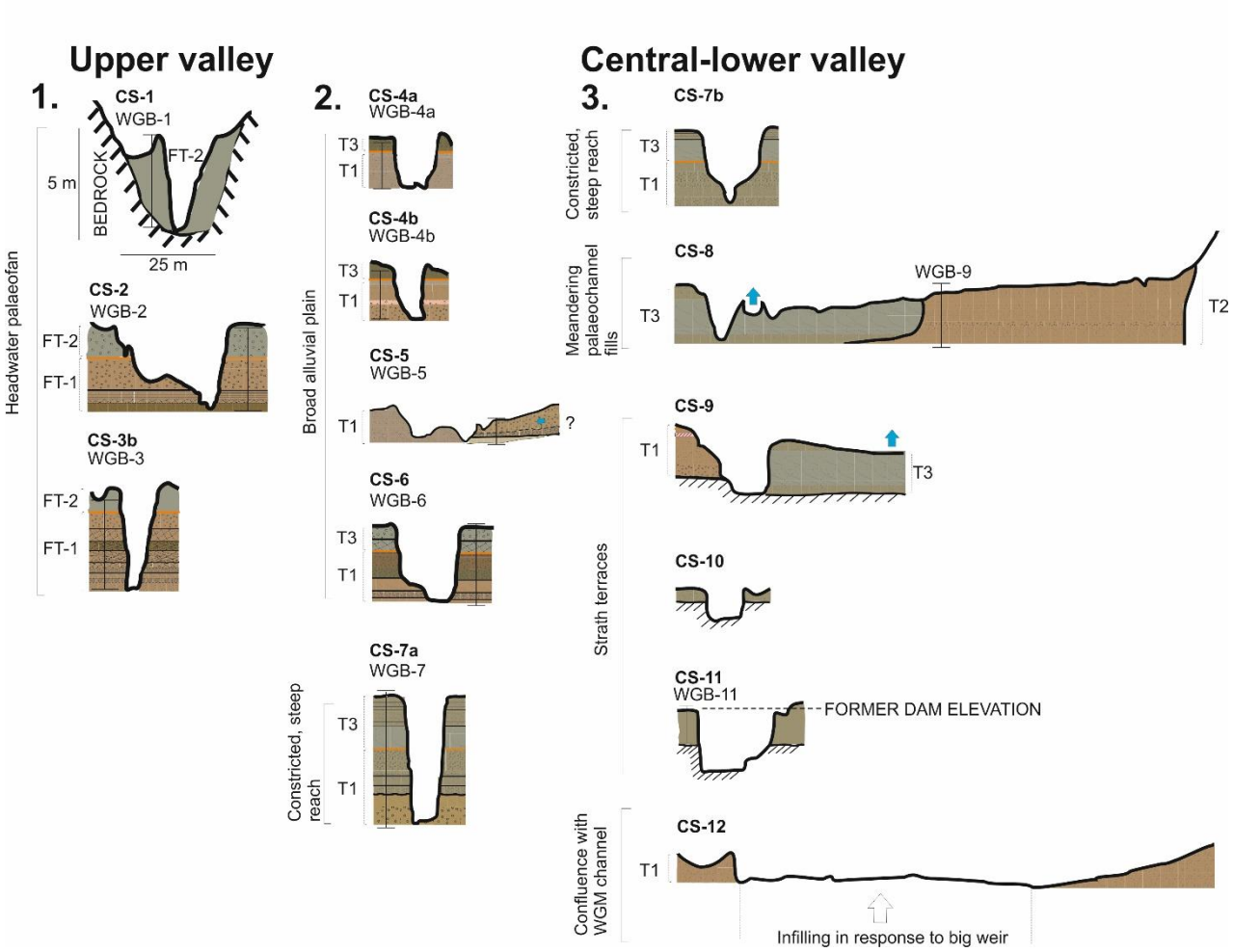

Figure 8.22 – surveyed valley cross sections: 1) CS-1 – 3 from the headwater palaeofan. Note the two preserved generations of fan emplacement: FT-1 and 2. 2) CS-4 – 7a from the alluvial plain as far as the beginning of the valley constriction at WGB-7. Note the shallower fills in the broad, flat alluvial plain (typically 2.4 m), relative to the depth in the steep, narrow reach (4 m – WGB-7). Also note the thickening of T3 with distance downstream. 3) CS-7b – 12 spanning the central to lower valley. Note the continuity of T1/T3 at CS-7b, but the absence of T1 from CS-8, replaced instead by T3 deposits overlying bedrock in the left part of the valley – but complete expression of meandering palaeochannel deposits (T2) to the right. At CS-9 note the re-appearance of T1 overlain by rhizogenic calcrete with T3 deposits inset to the right. Channel incision through bedrock increases from CS-9 – 11, CS-10 and 11 showing contemporary floodplain in direct contact with bedrock.

2) T1 has been incised by the gleyed palaeochannel deposits at WGB-5 (unit A) delimited by J-6 and 8. The abrupt contact between these gleyed deposits and T1 confirms that the former is an inset palaeochannel carved into T1 fills rather than T1 deposits that have undergone different soil forming processes due to local waterlogging. These gleyed channel deposits are incised again by a smaller palaeochannel overprinted by immature, vein calcrete (Ch. 6.6). Though no dating is available, these deposits are clearly more deeply weathered than those of T3 and

possess a distinct magnetic signature (see Ch. 6.6). Thus incision of T1 by the WGB-5 palaeochannel pre-dates emplacement of T3.

8.3.2 Central and lower valley: WGB-8 – WGB-11

Four alluvial terrace units are expressed in the central and lower valley (Table. 8.7: T1–T4). The continuity of **T1** downstream of WGB-7 is indicated in Fig. 8.23. The colour of T1 becomes increasingly grey particularly after WGB-7, but the change is gradational not abrupt. As a result, the relatively 'gleyed' fills displayed in Fig. 8.24a are T1, buried by the fine-grained palaeochannel deposits of T3 (see Fig 8.24b). The gleying of T1 reflects greater availability of moisture in the central valley due to increasing confinement of the valley within mudstone bedrock after J-10 and groundwater-flow supplied by the aquifer reported earlier upstream of J-9. T1 pinches out after J-15 (Fig. 8.21), with T3 directly overlying an incised segment of mudstone bedrock buffering the main channel from the modern wetland tributary between J-15 and 16. To the south-west of the channel between J-15 and 17, there are intensively incised valley fills exhibiting badland topography (Fig 8.21) which could have been T1.

At Africanders Kloof, the big fluvial terrace (local T2 – section 8.2) was overprinted by a continuous, discrete calcrete horizon. T1 reported at Wilgerbosch typically lacks calcrete. This absence of rhizogenic calcrete from logs WGB-2–6 upstream (J-1–9) is certainly related to negligible groundwater influence during phases of valley infilling, reflected in the dominance of haematite over goethite.

It is only after J-19 that rhizogenic calcrete matching characteristics of that documented elsewhere was found (Fig. 8.21; CS-9 – Fig. 8.22). The channel does not cross dolerite upstream of this point. Notably however, compared to upstream of J-15, the hillslope-channel coupling to the north-east with the intact dolerite sill is much stronger at J-19 (0.3 km compared to > 1 km – see Fig. 8.21) such that calcite rich runoff provided the supply for $CaCO_3$ fixation.

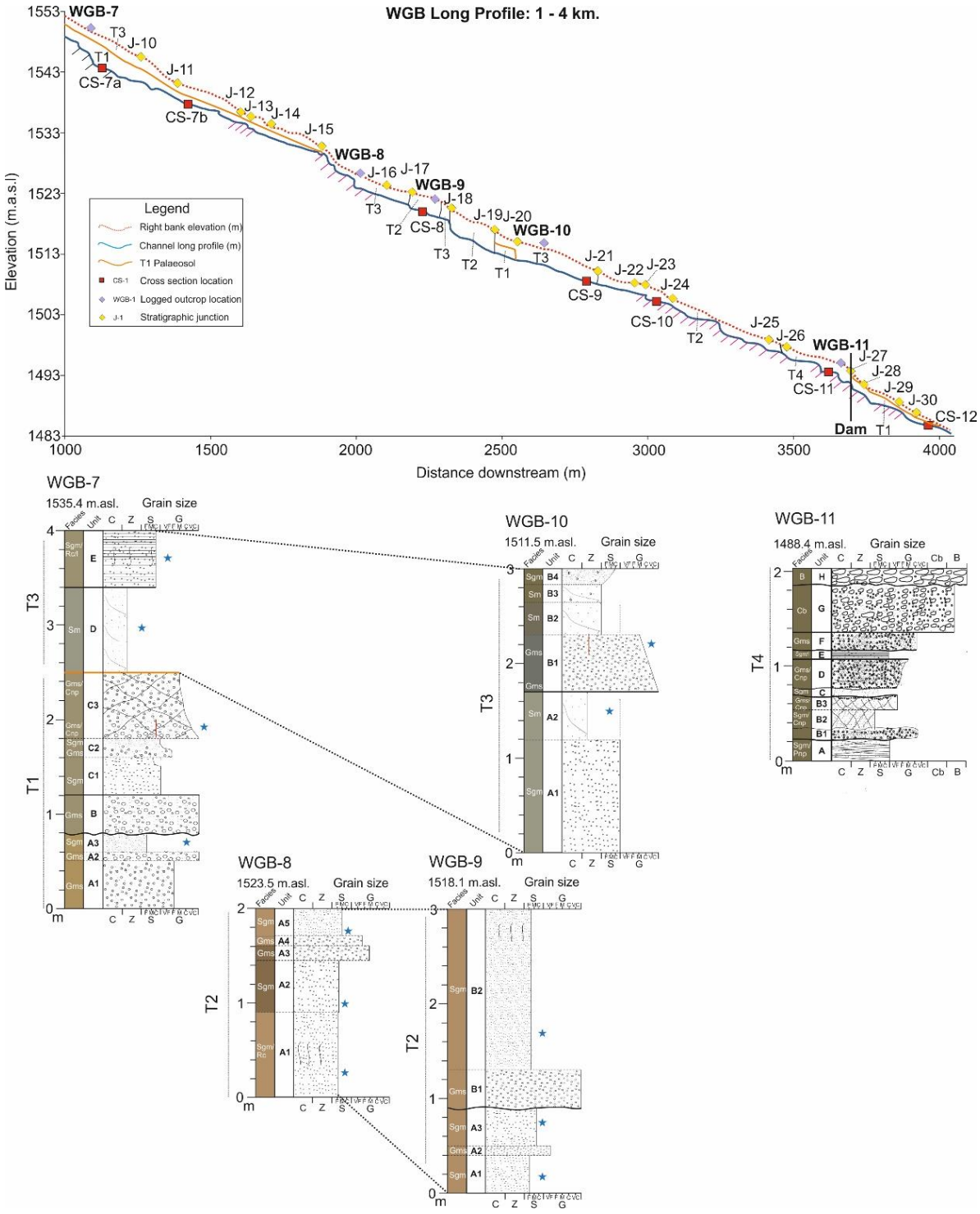

Figure 8.23 – surveyed valley long profile for central and lower Wilgerbosch valley as far as the confluence with the Wilgerbosch Main Channel at 4.1 km (see ch.7). Stratigraphic junctions and longitudinal continuity of T1 – T4 are shown. Note: T1 – T3 alternate after 2 km where the contemporary meandering channel has exhumed both the inset (3) and outset (1 and 2) terraces.

Additionally, the lack of calcrete between J-10-19 upstream could be partly a preservation issue: the calcrete at AK-10 (Section 5.3.4) was deeply eroded and leached with only remnants preserved. At Wilgerbosch, the dominance of sandstone and mudstone bedrock has facilitated lateral channel mobility, the creation of

relatively wide valley floors compared to the dolerite-dominated Africanders Kloof and strath terraces as knickpoint recession has occurred (Fig. 8.22 – CS-9–11).

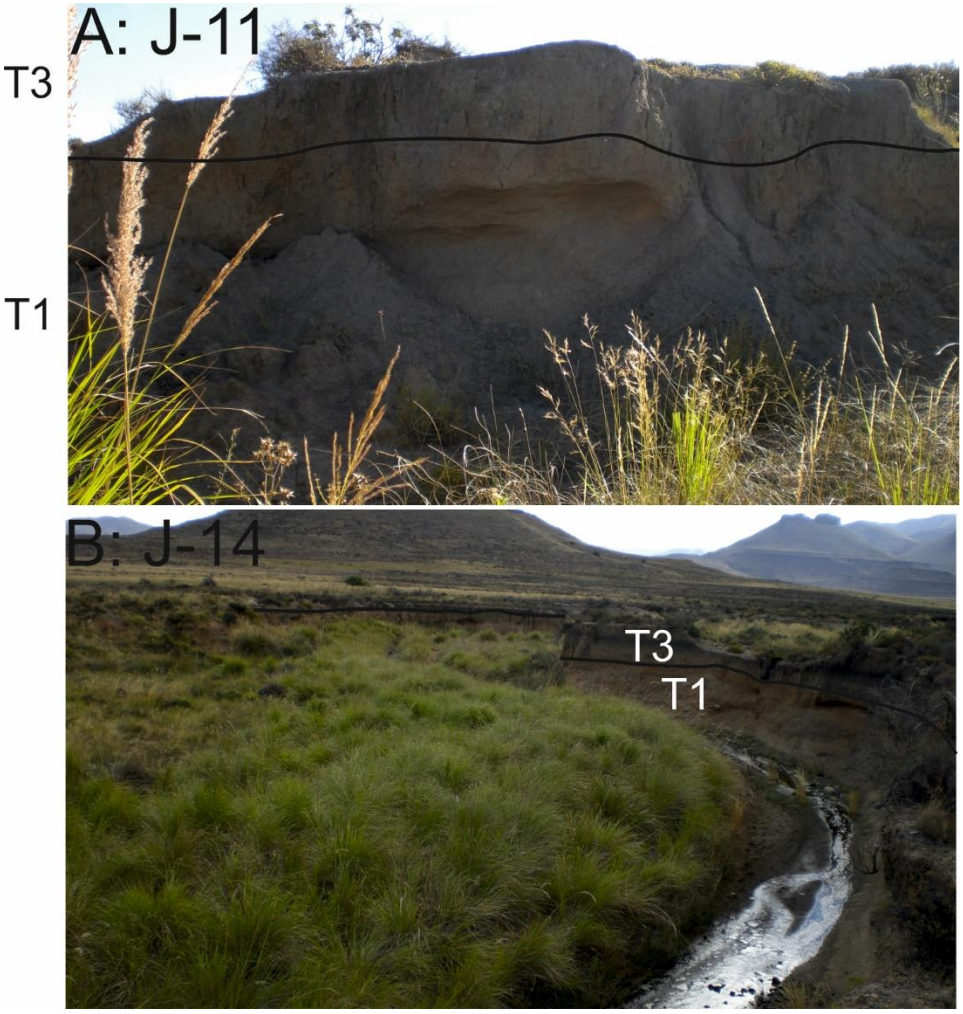

Figure 8.24 – A. Photograph of T1 and T3 along right bank at J-11 (Fig. 8.21). Note the greyer coloration of T1 compared to that reported at WGB-7 (Ch. 6.7). B. Photograph looking downstream at J-14 showing clear unconformity between T1 and T3 deposits. Note 1) that T3 thickens toward the centre of the valley and 2) the vegetated point bar in the near-distance – centre and left of photo.

The disappearance of T1 after J-24 correlates with the valley becoming relatively constricted by bedrock (Fig. 8.21), with longitudinally extensive wedges of modern floodplain inset against T2 as far as J-26. J-26 is the upstream limit for sediments that infilled behind the 1973 dam (Section 4.3). T1 then re-emerges, continuing as far as J-30. The apparent absence downstream of J-30 is likely to do with the infilling of the channel due to the large weir 0.6 km downstream of the confluence of the WGB tributary and WGM channel (Fig. 8.21; CS-12 - Fig. 8.22 and 8.23).

T2 comprises two distinct lithofacies: slopewash sediments (WGB-8) and channel deposits: point bars, medial bars and floodplain (WGB-9 and J-22 – see Table 8.7; CS-8 - Fig. 8.22; Fig. 8.23). Unlike T1 and T3, T2 is confined to between J-15–26 and absent from the upper and lower-most parts of the tributary. It is inset within T1 (see J-22 – Fig. 8.21).

The magnetic signature of the slopewash (WGB-8) and channel sediments (WGB-9) were found to be nearly identical, thus the channel associated with emplacement of T2 reworked these slope deposits (see Ch. 6.10b). The colour of this terrace, though superficially similar to T1, is inherited from reworked palaeochannel and slopewash deposits. It exhibits negligible pedogenic overprinting: at most, root channels and calcrete sheathes at WGB-8 (see Ch. 6.9a). T2 exhibits the narrowest range of χ_{LF} values, yet a wide range of IRM_{1T} values confirmed in the very large standard deviation (195 – see Table 8.8). As noted in Ch. 5 and 6, higher IRM_{1T} values are typically associated with the prominence of the lithogenic over pedogenic magnetic component. The wide range here further evidences the combination of reworked, old soils (T1 for instance), and relatively young, immature soils (WGB-8).

Table 8.8 – summary statistics for χ_{LF} (10^{-8} m^3 kg^{-1}) and IRM_{1T} (10^{-5} Am^2 kg^{-1}) for each terrace unit. Note T3 is divided up into 1) palaeochannel and 2) palaeofloodplain.

Terrace	Range X_{LF}/IRM_{1T}	Median X_{LF}/IRM_{1T}	St Dev. X_{LF}/IRM_{1T}	Median bromine (ppm).
FT-1	29-49 / 288-532	38 / 342	7 / 85	4
FT-2	40-58 / 282-534	55 / 450	6 / 73	13
T1	28-73 / 409-807	49 / 555	15 / 133	7
T2 – Slopewash	36-49 / 365-620	41 / 501	7 / 127	19
T2 – Channel	36-40 / 504-824	38 / 693	1.4 / 195	3
T3 – Floodplain	38-59 / 528-1006	47 / 762	8 / 197	5
T3 – Channel	12-31 / 92-304	14 / 127	9 / 99	13

T3 is the most continuously preserved alluvial terrace, extending all the way from J-4 to J-23. It is clearly inset within T1 and T2 (see CS-6–9 – Fig. 8.22). When viewed in long profile, the terrace fills alternate between T1-T3 after 2 km (Fig. 8.23) There are two major lithofacies: 1) channel deposits in the form of point bars and low energy channel deposits and 2) floodplain deposits (see Table 8.7). Unlike T2, average organic content is much higher: 13 ppm compared to 3 ppm (Table 8.8). This reflects a highly vegetated, low energy, channel complex (see Ch. 6.11). T3 channel sediments are the most distinctive magnetically with χ_{LF} ranging from just 12-31,

averaging 14. This terrace exhibits the lowest concentrations of remanence carrying ferrimagnets, averaging 127 (Table 8.8). Decomposition of organic matter within sediments has been identified as a causal factor in the dissolution of magnetite and formation of iron sulphides (Williams, 1992). The T3 floodplain sediments are much higher on average (47 and 762 - χ_{LF} and IRM_{1T} respectively) and reflect inherited soil from a range of sources, but crucially, have not been subject to gleying unlike T3 channel deposits.

The magnetic properties, colour, organic content and stratigraphic position relative to the palaeogeomorphic surface (locally T1) are virtually identical to the grey fills sampled on the main channel (WGM) and at Africanders Kloof (see sections 8.2 and 8.4). T4 represents the sediments infilled behind the former dam discussed in Chapter 4 and not referred to here.

8.4. Longitudinal Correlation of Terrace Sequences iii: Wilgerbosch River

This section synthesises the sedimentologic, pedologic and soil magnetic data from Chapter 7. This discussion section begins with a summary of the sequence of terraces as determined from analysis of sediment logs and their relations in Chapter 7 (Table. 8.9).

8.4.1: Terrace 1

T1, which constitutes the base of the stratigraphic succession across the entire study region, was logged at two locations: upstream of the Ganora Gorge (GG-1), and the outlet at the base of the gorge (GG-2), though thick accumulations (up to 6 m) of slope material persist as semi-continuous wedges against the canyon walls between these locations (Fig. 8.25 and 8.26). T1 is clearly setback from the alluvial deposits portrayed in Fig. 8.27 and its occurrence upstream of and within the gorge itself (established through visual observation – see Ch.3) may be indicative of a concordant phase of intense physical weathering (frost shattering in particular) and emplacement of gelifluction and slopewash deposits under a climatically colder regime.

Table 8.9 – summary of terrace morphostratigraphic units, associated lithofacies, interpretation and section.

Terrace	Log/unit	Facies	Interpretation	Section
1	[1]GG slope [2]GG-2 – B	Gms/Cb Gms, Gc	[1]Slope colluvium. [2]Gelifluction and slopewash facies.	[1]7.7
2	[1]WGM-2 – A-E [2]WGM-3 – A-B [1]GG-1 – A-C [1]GG-2 – A	Cb, Sgm/l, Sm, Gms/Hb Sgm, Gms Gms, Sm	[1]Thick channel and floodplain deposits. [2]Alluvial fan deposits.	[1]7.4 and 7.7 [2]7.5
3	GG-1 – D-F	Cb, Gms/Cnp, Gc/Cnp	Thick bar deposits in a migrating channel.	7.7
4	[1]WGW – A-F [2]WGM-1 – A-I [2]WGM-2 – F-N	[1]Gms, Sgm/Pnp, Sm, Md/R [2]Md/l, Sm, Sgm, Gms, Gc	[1]Point bar at channel margin. [2]Migrating single-thread channel deposits.	[1]7.2 [2]7.3 and 7.4
5	WGM-4 – A-F	Sm, Sgm/Cnp, Gms/Hb, Gc	Channel bedload deposits.	7.6

The angular sandstone talus fragments, particularly at GG-2, attest to physical weathering processes, probably frost shattering. The evidence for gelifluctate deposits at GG-2 (Table 8.9; Fig. 8.27) implies that palaeoclimatic conditions were likely much colder than today but still with some degree of seasonality (Lewkowicz, 1987a, 1987b). At present, these deposits occur at altitudes > 2765 m where mean annual air temperature (MAAT herein) is lower than 6^{o}C (Lewis, 2008a).

The absence of any accumulations of secondary carbonate in the context of an aggrading valley regime (T1) also implies a radically different palaeohydroclimate to that associated with the emplacement and pedogenic overprinting of terrace 2.

8.4.2: Terrace 2

The first mapped occurrence of **T2** is at outcrop WGM-2 (Fig. 8.28) and is characterised by thick beds of alluvium overprinted by two distinct rhizogenic calcrete horizons (Table 8.10; Fig. 8.30). T2 at WGM-2 is unconformably overlain by the organic deposits of T4 (Fig. 8.31), whilst at GG-1, T2 is incised and capped by further thickly bedded but clastic alluvial units (Fig. 8.27), but similarly to outcrop GG-2, is very clearly inset within the periglacial deposits of T1 (Fig. 8.25-8.27).

Furthermore, the correspondence between T2 at WGM-2 and GG-1 is remarkable in terms of total concentration of both remanence and non-remanence carrying ferrimagnets (Fig. 8.32). The only exception is WGM-2 unit B, which underwent ferrimagnetic dissolution when the palaeo-water table was high (see Ch. 7.4b).

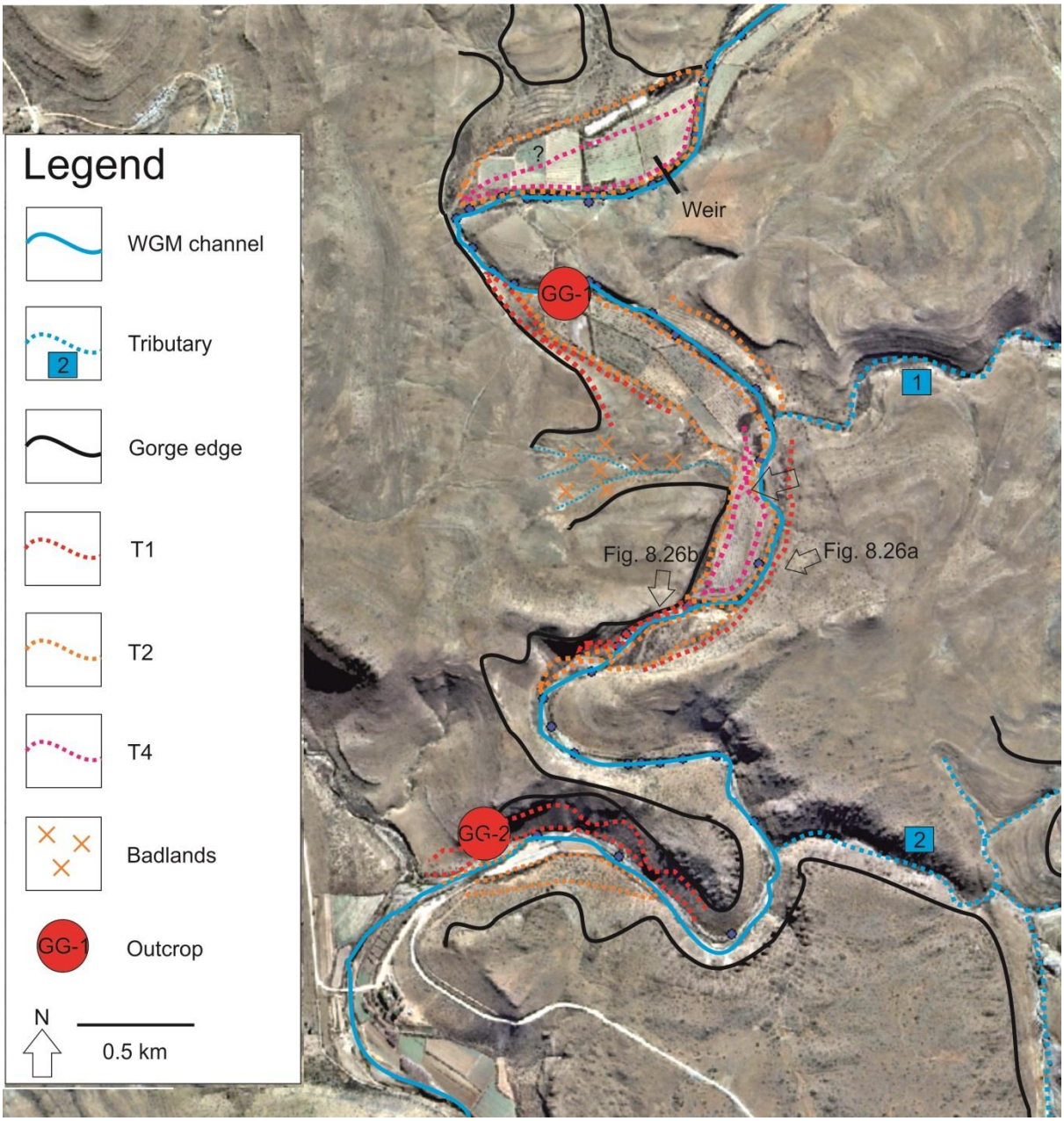

Figure 8.25 – digitised aerial photograph showing approximate limits of terraces 1, 2 and 4 upstream of and through the Ganora Gorge. With the exceptions of GG-1 and 2, the lateral continuity of terrace is estimated from field observations and photos. Note that the fills upstream of GG-1 in the vicinity of the weir are very highly degraded.

Lower total concentrations of soft and hard magnetic minerals at unit B evidence the same process, but otherwise, the similitude of T2 at both sampling sites is remarkable (Fig. 8.33). It is unclear as to whether the fan deposits at WGM-3 (Fig.

8.30) are concordant with the phase of filling reflected in the thick alluvial units of T2 or rather, are concordant with the periglacial deposits identified in the Ganora Canyon (T1).

Figure 8.26 – photos of a) 6 m thick colluvial deposits along the left bank and b) colluvial deposits exposed along the right bank (see Fig. 8.25 for locations of photos). Facies architecture is comparable with that analysed and discussed for the logged slope deposits GG-1 and GG-2 (T1 – see also Fig. 8.27).

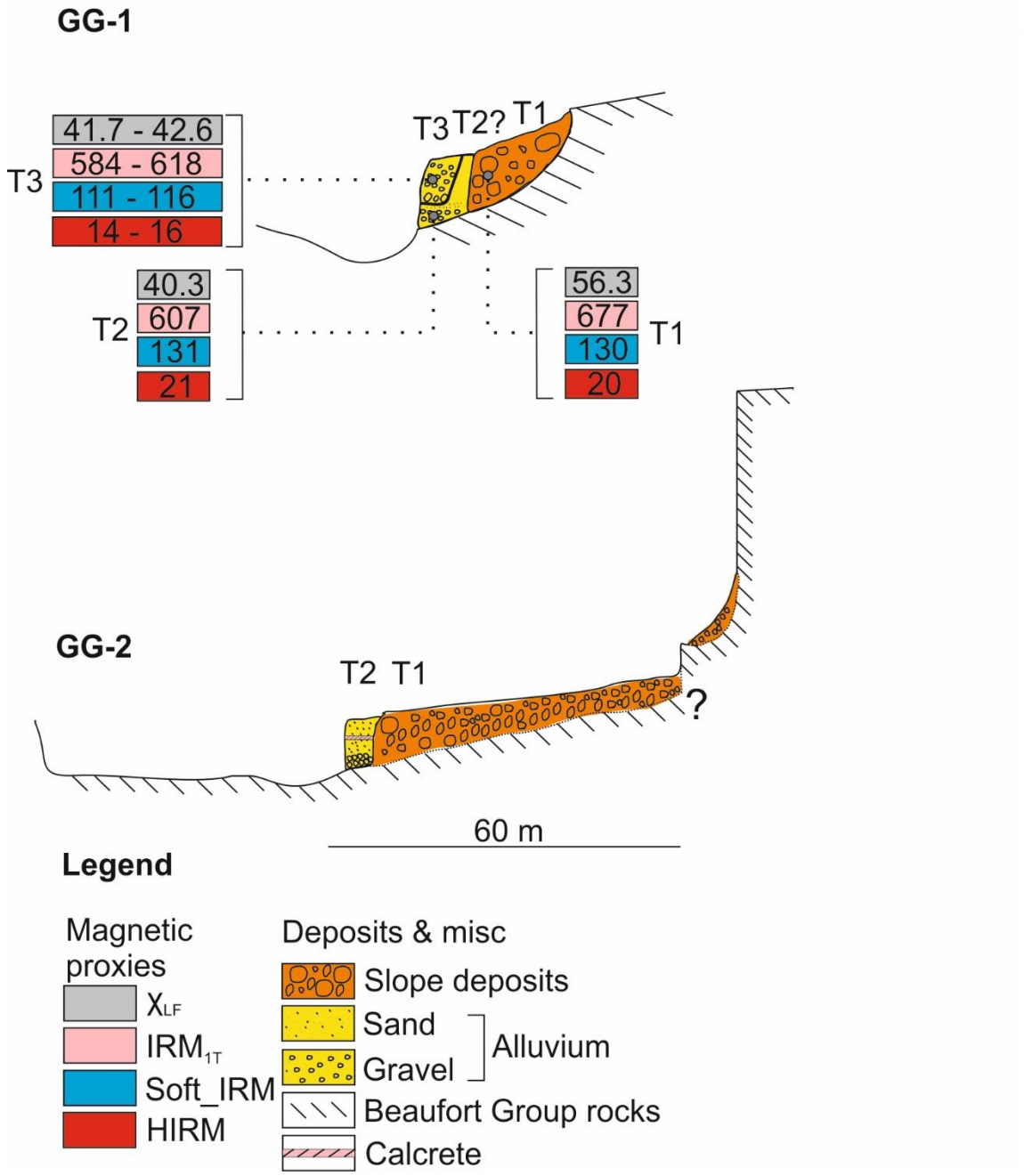

Figure 8.27 – field sketches, scaled based on calculated distances from digitised aerial photographs of valley, channel and width of pockets of alluvium and slope deposits at outcrops GG-1 and 2. 4 concentration-related magnetic proxies are quoted for comparative purposes at GG-1 to compare and contrast ferrimagnetic and anti-ferromagnetic intensities of the respective terrace sediments. Note scale applies to horizontal and vertical dimensions.

Since the periglacial deposits of T1 were truncated by subsequent fluvial activity (T2), and this associated big incision phase appears to have propagated at least as far upstream as WGM-2, it follows that if fan emplacement (WGM-3) was associated with aggradation of T1, there would be a distinct phase of fan incision in response to falling base level associated with subsequent T1 abandonment.

No successive phases of palaeofan incision and filling were found. Furthermore, although deeply weathered, the facies at WGM-3 lack any diagnostic periglacial features. Rather, iron mottlings and coatings around clasts attest to periodic conditions of oxidation and reduction – consistent with a relatively humid, seasonal climatic regime.

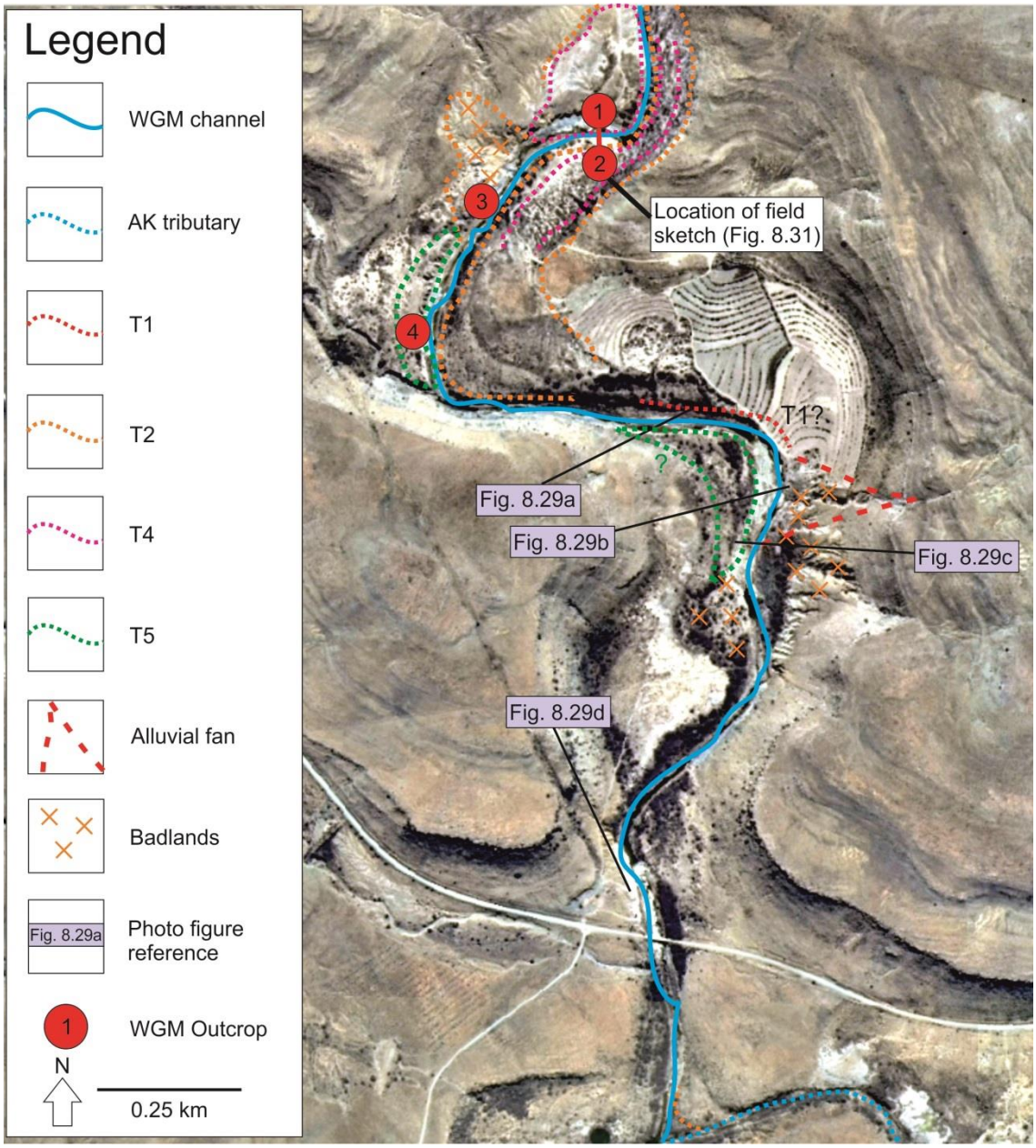

Figure 8.28 – digitised aerial photograph showing limits of T1, T2, T4 and T5 in the stretch of WGM channel upstream of Ganora and the confluence with Africanders Kloof. Note the occurrence of badlands overprinting the truncated laterally impinging alluvial fans (WGM-3) and downstream (see Fig. 8.29b).

As a result, the evidence for chemical over physical weathering of WGM-3 and absence of periglacial features, indicates fan aggradation was more probably a backfilling response to aggradation of T2, though this inference remains hypothetical

in the absence of radiometric dating of each terrace. The total concentrations of magnetic minerals (non remanence and remanence carrying / soft and hard minerals) are typically higher than T2 alluvium (WGM-2, GG-1), confirming the hillslope-dominated source, but crucially higher concentrations of pedogenic magnetite and haematite that reflect seasonal oxidation/reduction without groundwater influences (Fig. 8.32 and 8.33).

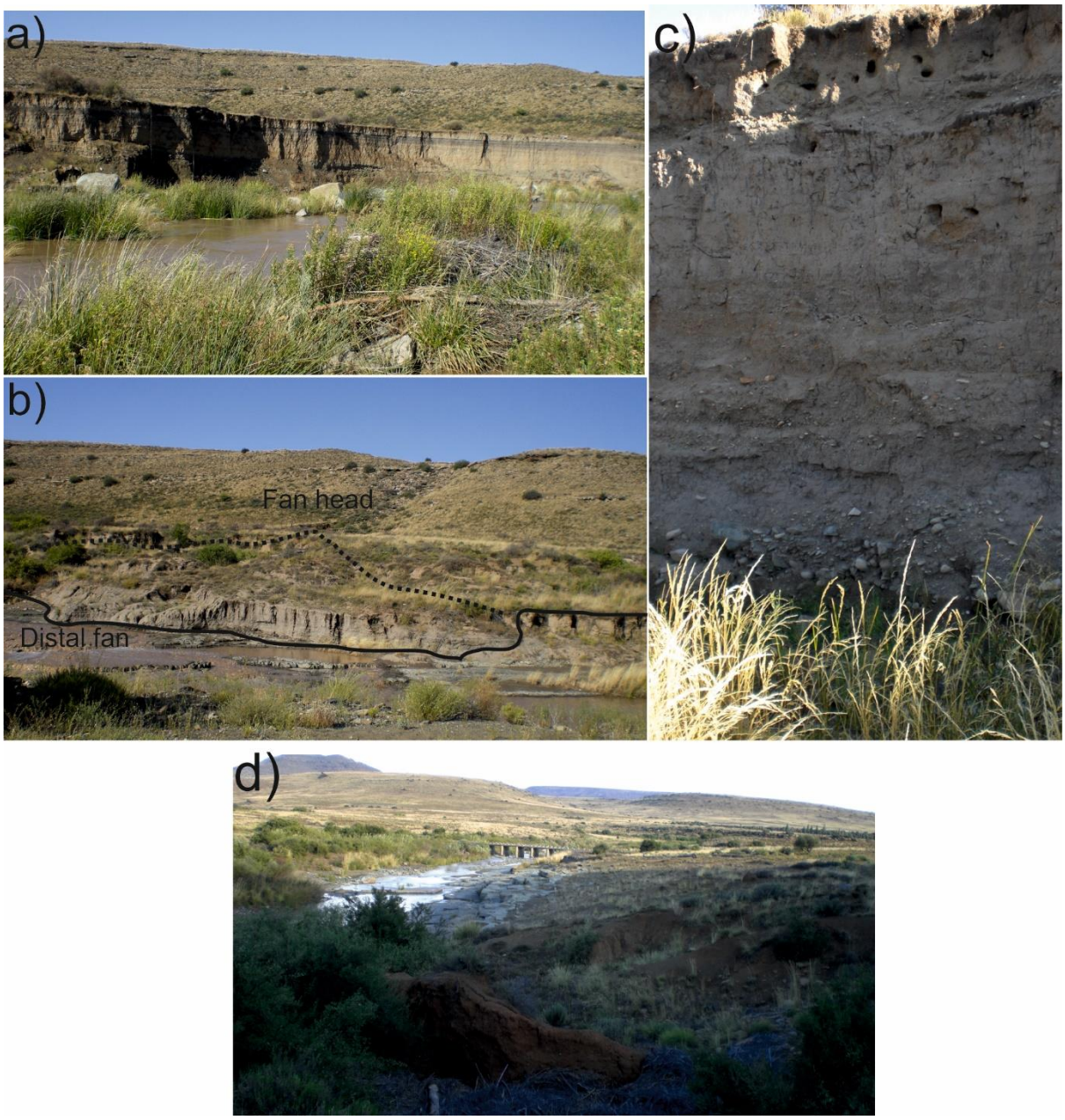

Figure 8.29 – photographs taken from stretch of valley downstream of WGM-4 extending as far as road upstream of confluence with Africanders Kloof: a) 5 m deposits along left bank consisting of fine-grained sediments, poorly defined bedding and a distinct grey palaeosol horizon at top, b) a truncated laterally impinging alluvial fan inset within (T2?) sediments, c) a 3 m stack of friable palaeochannel deposits from the right bank (T5?) and d) view looking downstream toward road immediately upstream of Ganora – note the highly degraded nature of the fills. See Fig 8.28 for locations.

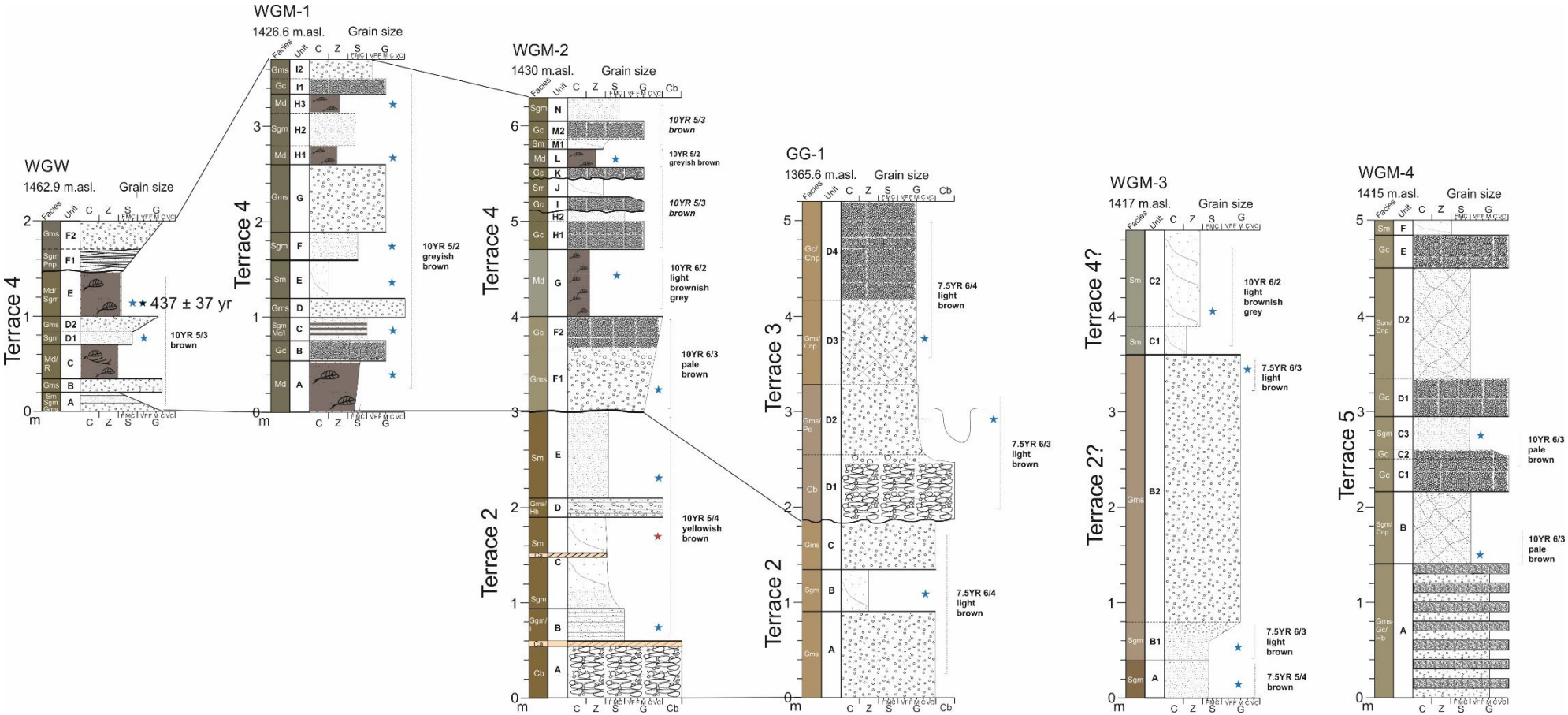

Figure 8.30 – correlation panel between different alluvial terrace units at logged locations. Note that the occurrence of terrace 3 is restricted to GG-1.

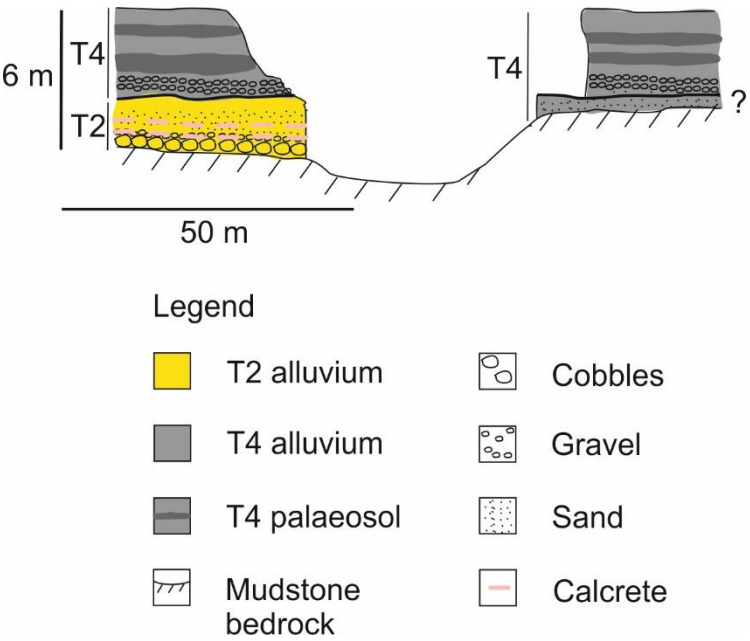

Figure 8.31 – field sketch of approximate elevation and lateral relations of T2 and T4, at locations indicated in Fig. 8.28.

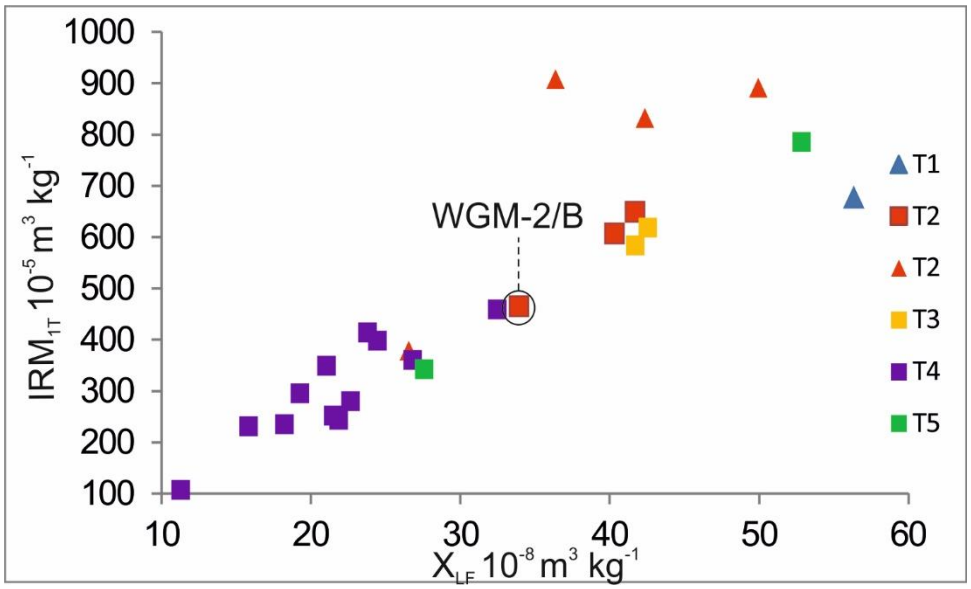

Figure 8.32 - χ_{LF} versus IRM_{1T} ferrimagnetic concentration proxies plotted for each terrace along the Wilgerbosch trunk river and Ganora Canyon. Note: triangles represent slope material whilst squares represent alluvium.

T2 compares with T1 only in terms of terrace height. The cold, dry climate associated with T1 precluded carbonate cementation via the rhizogenic pathway and whilst soil development was minimal, large volumes of regolith were generated by frost shattering. During channel entrenchment and abandonment of T1, these large accumulations of weathered material appear to have been the principal supply, particularly in the headwaters as the channels eroded headward (see Section 8.2). This need not necessarily have required a wetter climate than that which prevailed

during aggradation of T1 as a series of large floods could have initiated: 1) cutting on a catchment wide scale; 2) reworking of such a large volume of sediment; and 3) emplacement of high energy deposits in the newly cut channels. This proposition is reconcilable with the implication of arid conditions prior to 15.5 ka (Lyons et al., 2014), but the evidence for the SRZ having extended as far as the Western Cape around 18 ka means that flooding in the Sneeuberg could have been a feature of this large scale reorganisation of the meridional atmospheric circulation patterns (Chase et al., 2015).

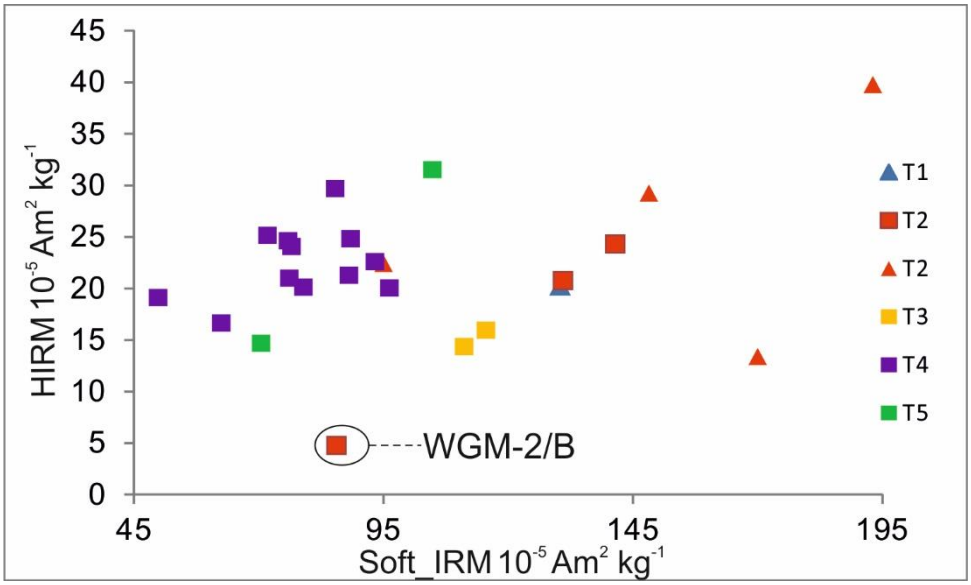

Figure 8.33 - Soft_IRM versus HIRM ferrimagnetic concentration proxies plotted for terraces 1-5 exposed along the Wilgerbosch River and Ganora canyon.

The maturity of the calcrete overprinting T2 in concert with haematite rich soil implies that wet, warmer conditions prevailed, though for how long is unknown. Compared to T4 in particular, organic content of T2 fills is low: LOI% ranging from 1 – 2.8% and bromine typically from 1.3–4.8 (Table 8.11) (excluding WGM-3 unit B2 (46.1 ppm), as this has been contaminated by illuviated material transferred from above the unconformity with T4 - see Fig. 8.30). The low LOI% is unsurprising, as any plant material associated with this stabilisation phase will have oxidised and disintegrated long ago: the same holds true for T3. The modest bromine values similarly will reflect leaching and illuviation of humic organic compounds out of the soil column and is thus not a faithful estimation of probable organic intensity during the palaeosol development after T2 aggradation ceased.

Table 8.10 – amalgam of all LOI% and bromine (ppm) data subdivided according to terrace number. Note dashed line to indicate gaps in dataset.

Terrace/outcrop	LOI%	Bromine (ppm)
T1		
GG slope deposit	1.8	-
T2		
WGM-2 / B	1.4	-
WGM-2 / E	1.6	4.8
WGM-3 – Slope	2.8	1.3
WGM-3 / A	1	2.7
WGM-3 / B1	-	4.5
WGM-3 / B2	2.6	46.1
GG-1 / B	1.6	-
T3		
GG-1 / D2	1.4	-
GG-1 / D3	2	-
T4		
WGW / D1	1.7	8.7
WGW / E	5.8	12.6
WGM-1 / A	2.9	50.5
WGM-1 / C	2	27.4
WGM-1 / E	3.3	41.6
WGM-1 / F	1.4	12.1
WGM-1 / H1	1.9	7.2
WGM-1 / H3	2.4	15.4
WGM-2 / F1	1.5	2.7
WGM-2 / G	2.6	6.4
WGM-2 / L	2.4	13.3
WGM-3 / C2	1.8	53.4
T5		
WGM-4 / B	0.8	0.6
WGM-4 / C3	1.4	1.8

The OSL date from Africanders Kloof (AK-10) indicated that aggradation of this terrace occurred in the Late Pleistocene (see section 5.3.4), but exactly how soon after the LGM is unclear due to the large error bar associated with this age and the lack of repeat dates. Similarly, it has not been possible to link the following phase of aridification reflected in the drop in palaeo-water table and burial of the haematite soil at Africanders Kloof to other documented palaeoclimatic archives due to absence of chronological control.

The continuity of these fluvial deposits (T2) along the WGM channel, Ganora Canyon and tributaries thus implies a catchment wide filling rather than pocket filling associated with reach-scale cut and fill (Grenfell et al., 2014).

8.4.3: Terrace 3

T3 was only noted at GG-1 (Fig. 8.30) and appears to signify an intermediate phase of terrace development which occurred between the emplacement of the thick alluvial deposits of T2 and the organic rich deposits of T4, though the spatial extent and relative timing is unclear (Table 8.9). The relative proportions of non-remanence and remanence carrying ferrimagnets are virtually identical to T2 (Fig. 8.32), but total concentrations of both soft and hard magnetic minerals are discernibly lower (Fig. 8.33). Since there is no evidence at GG-1 that the water-table inundated T3, the reduced soft and hard magnetic components respectively reflects a relatively immature pedogenic overprinting compared to T2, as confirmed in the macro-pedological evidence (see section 7.5b). This probably reflects the 'younger' age of T3. Further, it is clearly discriminated from T4 (Fig. 8.32 and 8.33).

The apparent absence of T3 at upstream sites (WGW–WGM-4) could be due to one of two factors: 1) T2 incision did not proceed that far upstream, 2) incision proceeded at least as far as WGW-WGM-4, but T3 has been eroded. The only other phase of geomorphic instability preserved in the alluvial stratigraphic record that occurs between emplacement of T2 and T4, occurs at Africanders Kloof, manifesting as a return to conditions of floodplain aggradation and burial of the haematite-rich soil which marks the terminus of T2 aggradation (see Section 5.3.6). It was proposed that calcite hypocoatings above the calcrete horizon in concert with brecciation of the original sparite cements and inset clay coatings indicated climatic aridification (see Section 5.3.6) and this was the probable driver of instability. Only at AK-17 do thicker channel deposits intermediate between T2 and T4 occur and these may be coeval with T3 at GG-1. The implication of this is that T3 was probably emplaced over a large spatial area, but its limited representation in the succession is partly a function of: 1) the degree of thickness of the underlying calcrete limiting incision; and 2) lack of subsequent alluvial preservation.

Regarding (1), if the development of T3 at GG-1 is related to this climatic aridification, then channel entrenchment in the Africanders Kloof tributary was clearly muted due to the armouring of the underlying sediment by the calcrete.

A similar effect is apparent at WGM-2: no erosional features (palaeochannel architecture) underneath the T2/T4 unconformity are present (Fig. 8.30) implying that

if T3 aggradation and incision propagated upstream this far, the calcrete at WGM-2 successfully prevented downcutting as far as bedrock. This association also reinforces the notion that calcite fixing was definitely associated with the palaeovegetation mantling the palaeo-T2 surface and not T4.

Regarding (2), valley confinement is known to be a key control on long-term preservation potential of terrace fills (Fryirs and Brierley, 2010 and Macklin et al., 2010). The sediments of GG-1 (T1 - T3) occur as a wedge along the right valley margin after a sharp, structurally controlled meander bend (Fig. 8.25), where the valley widens (0.5 km). The current channel is eroding into T2 deposits and fills sourced from the tributary to the east along the left bank (see Fig. 8.25 – tributary 1). As a result, alluvial storage potential along the right valley flank is enhanced relative to left, the latter preserving relatively intact valley fill with a cut and fill phase intermediate between T2 and T4. As has been highlighted earlier for T4 at Africanders Kloof, the 'patchy' occurrence of fills which are clearly of different age, appears to be a function of the inherent memory of the geomorphic system relating to valley morphology and location of the contemporary channel thalweg (Keen-Zebert et al., 2013).

This contrasts with the next reach associated with the start of the gorge, which is 0.25 km wide at most: T3 is absent, whilst T2 has been severely degraded and incised by T4 and T1 occurs only as a very thin wedge against the side of the gorge (See Fig. 8.25).

8.4.4 Terrace 4

T4 is clearly inset with T2 and is well represented at WGW downstream of the major weir (see Fig. 7.1), WGM-1 and 2 (Table 8.10; Fig. 8.28). The occurrence of what appeared to be inset 'grey fills' in the Ganora Canyon were noted.

T4 is clearly distinguished from T1-T3 on the basis of there being much lower concentrations of soft ferrimagnets rather than hard anti-ferromagnetic minerals (Fig. 8.32 and 8.33), though the dominant hard mineral here is probably goethite rather than haematite. The consistent discrimination from the other terraces implies, in concert with the combined litho- and morphostratigraphic evidence that T4 is continuous at least as far downstream as WGM-3 and appears to extend into the

canyon. These terrace fills are distinct from the others on the basis that they are gleyed and relatively organic rich: LOI% ranges from 1.4–5.8%, whilst bromine ranges from 2.7–53.4 ppm (Table 8.10).

T4 is much younger than T1-T3. The one radiocarbon date obtained from the last recorded 'organic phase' at outcrop WGW occurred in the very Late Holocene (437 ± 37 yr: Fig. 8.30). Though the dating evidence is weak, the preservation of organic remains and lack of significant oxidation of the sediment to haematite implies that the true age of the sediment is probably Late Holocene, though the timing of onset of T4 aggradation is unknown. The obtained radiocarbon age predates the onset of the 19th century European occupation of this region (Boardman, 2014).

8.4.5: Terrace 5

T5 is distinguished from the other terraces on the basis of there being very clear preservation of sedimentary structures, similar in clarity to those documented in the Wilgerbosch Kloof (see Section 4.5 – WGB-11). T5 occurs as a thin wedge inset within the fan sediments of WGM-3 (Fig. 8.28). Of the two samples obtained from this terrace, there are contrasting ferrimagnetic signatures, but in terms of overall concentrations of hard and soft minerals, T5 samples plot closest to T4 (Fig. 8.30 and 8.32). But unlike T4, T5 is very minerogenic with only tiny amounts of plant organic matter present (Table 8.10). T5 probably reflects backfilled sediments behind what is now a breached, old dam at Ganora farm.

8.4.6: Summary

From the morphostratigraphic evidence, it has been possible to reconstruct four cycles of terrace aggradation and incision. The start of the succession is characterised by periglacial deposits (T1) which, on the basis of limited OSL dating of T2 and other documented, dated periglacial deposits in the Eastern Drakensberg region, probably represents the Last Glacial Maximum in the Sneeuberg. The incision of T1 could be a response to the re-instatement of rain-bearing tropical easterlies in the deglacial period some time after 18 ka acting on a relatively cold, poorly vegetated landscape. Alternatively, the role of large floods in a cool dry post-glacial climate was discussed as a possible mechanism triggering incision. The aggradation of T2 may have occurred in response to either of these climate-based

scenarios, but also reinstated sediment connectivity with tributaries and slopes which flushed large volumes of sediment rapidly into the valleys, overloading them. As the valleys filled, the water-tables rose and calcite fixing occurred, signifying a low energy, highly stable and vegetated landscape. Climatic aridification and loss of vegetation cover appears to have provided the impetus for incision of T2 and emplacement of a third terrace, the response of which is muted in sections of channel where thick calcrete deposits occur. The organic rich, low energy facies of T4 attest to a migrating, aggrading channel as part of a wetland environment, which extend up the Africanders Kloof tributary as far as AK-4 (see Section 8.2) and the Wilgerbosch tributary as far as WGB-4 (Section 8.3). Although migrating single-thread channels can and do produce alternating coarse and fine deposits, this pattern appears to have been situated within a mode of aggradation which probably related to a humid climate, conducive to vegetation growth. These deposits are locally thicker in the vicinity of seepage zones and also upstream of rock steps where there is local loss of gradient and confinement. However, as noted earlier, in contrast to T2, vegetation appears to have been localised to corridors along the valley floor rather than extending up slopes as represented by the calcrete deposits.

8.5: Regional terrace development

To demonstrate the sequences of terrace aggradation, soil development and incision the three valley settings are depicted for each ‘cut and fill’ cycle in Fig 8.34. Four major cycles of ‘cut and fill’ are reflected in four semi-continuous terraces, the complete succession of which is expressed in the Wilgerbosch Main Channel, the Ganora Gorge and Africanders Kloof. At Wilgerbosch Kloof, only cycles 2 and 4 are represented, with an intermediate phase of deposition and aggradation from a meandering channel (local terrace 2 - WGB).

8.5.1 LGM (Bottelnek Stadial) valley fill (cycle 1)

Cycle 1 is characterised by slow aggradation of slopewash deposits which exhibit lenticular freeze-thaw structures in the Africanders Kloof headwaters, whilst in the Gorge, large amounts of frost shattered regolith are present, reworked by slopewash and gelifluction processes (Fig. 8.34). Similar deposits have been found in the Eastern Drakensberg above 1,800 m a.s.l and may indicate temperatures of at least 6^{o}C lower than present (Lewis, 2008). There is no minimum age for these deposits in

the Drakensberg, but maximum ^{14}C ages of 40, 37.2 and 26.2 ka have been obtained at different locations (Lewis, 1999; Hanvey and Lewis, 1990; Lewis, 2005 respectively) placing the genesis of gelifluctate fills at or close to the MIS3/2 boundary. The legacy of rock glaciers and potentially, glaciers, in the eastern Drakensberg have led authors to suspect these gelifluctate deposits represent 'less cold' climatic conditions subsequent to the growth of glaciers (Lewis, 2008).

The palaeoclimate of MIS3/2 in the Sneeuberg is less clear as no dated local deposits have been found that may be correlated to existing palaeogeomorphic archives across the South African subcontinent (Clarke et al., 2003; Lewis, 2008; Lyons et al., 2013; 2014). Additionally, the Ganora Gorge is only 1360 m.a.s.l – 600 m lower than the Drakensberg sites. It axiomatically follows that temperatures in this region were less subdued and geomorphic response in the form of glaciers (rock or ice) were absent. However, the evidence of cut and fill at the Sneeuberg sites discussed means that the preservation potential of terraces older than MIS3-2 seems unlikely: sites GG-1 and 2 are the only documented cases of deposits with an origin distinct from fluvial activity (Section 8.4).

Current palaeoclimate models show a coherent first-order pattern of drier conditions during the LGM in the east of southern Africa, probably related to subdued easterly trade winds (Stone, 2014). Quantified estimates of palaeoprecipitation during the LGM for the Sneeuberg are unavailable, but in the Drakensberg precipitation may have been 70% lower than present during the Bottelnek stadial (Lewis, 2008). A 70% reduction in the Sneeuberg would translate to a maximum of 104 mm a^{-1} precipitation compared to present (346 mm a^{-1} - Boardman et al., 2003), much of which likely occurred in winter (Chase and Meadows, 2007; Chase et al., 2015). The lack of moisture relative to the Drakensberg sites may also, in concert with the Sneeuberg being at a lower elevation, explain the absence of larger 'glacial' features (glaciers, rock glaciers) preserved in the Sneeuberg valleys.

As a result, fluvial activity was reduced during emplacement of regional T1, with filling of the various compartments in the valley primarily, though not exclusively, by colluvial rather than alluvial processes (Fig. 8.34). Widespread colluviation during the *Bottelnek* stadial has also been a feature of slopes and valleys in the KwaZulu-Natal (Clarke et al., 2003; Botha et al., 1994), though Temme et al. (2008) suggest

sedimentation suspended altogether in the Okhombe valley, contrasting with Clarke et al's (2003) colluvial record from the KZN, where up to four palaeosols were used to infer climate may have been fluctuating around the time of the LGM. This is a reasonable proposition considering the proximity of KZN to the Indian Ocean, but at our inland study sites, no distinct palaeosol surfaces punctuating T1 deposits were found. Evidence for low-energy channel activity at AK-10 however implies there could have been partial longitudinal connectivity and transmission of sediment downstream probably during the snowmelt season.

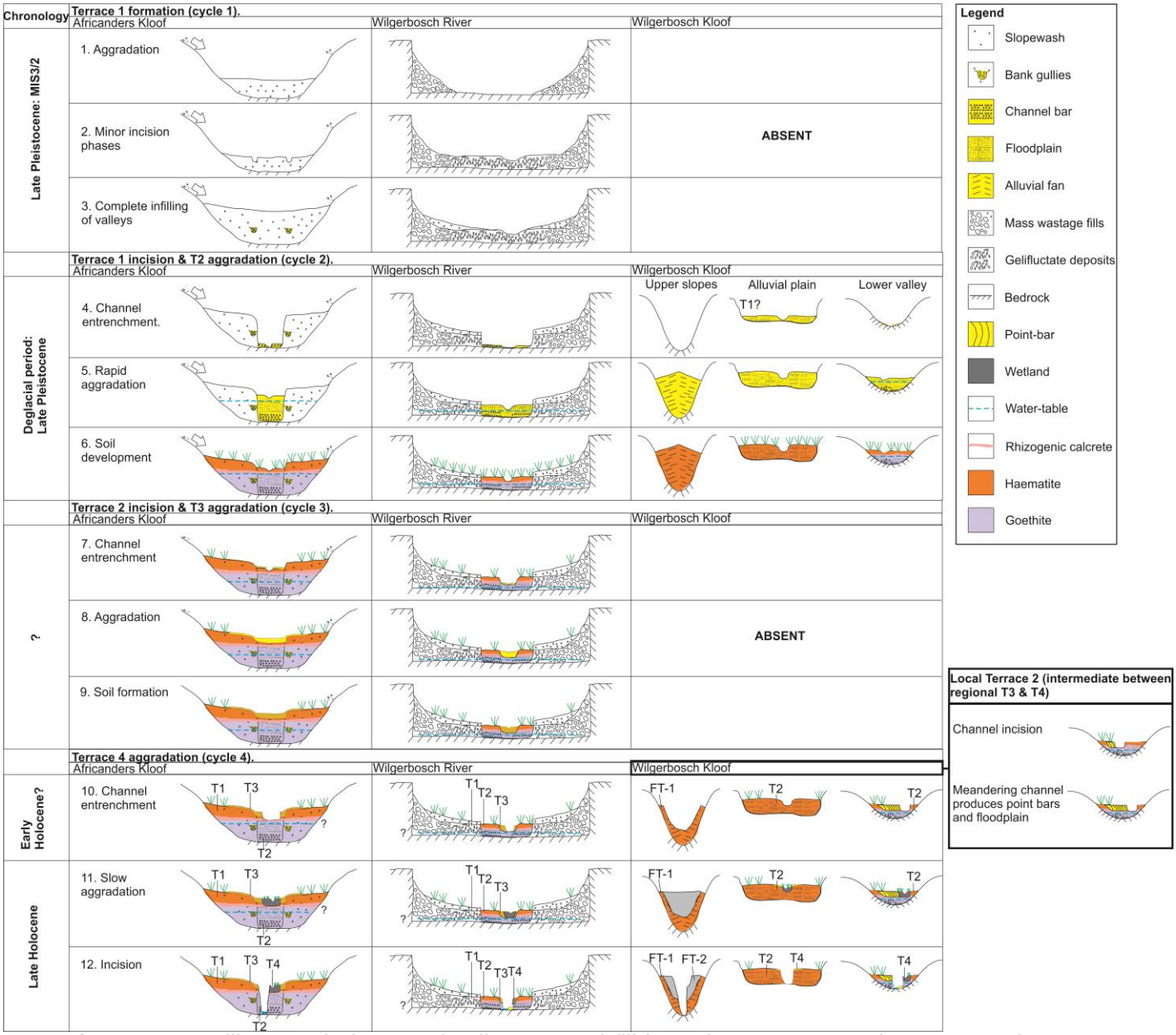

Figure 8.34 – illustrated phases of valley cut and fill based on representative type sections from Africanders Kloof, Wilgerbosch River and Wilgerbosch Kloof. T1 is proposed as having been deposited around the time of the LGM (MIS3/2) based on: 1) The periglacial nature of deposits; and 2) T2 having aggraded in the deglacial period (see date LV515). Age of T3 is unknown. Aggradation of T4 occurred in Late Holocene (see Section.7.2).

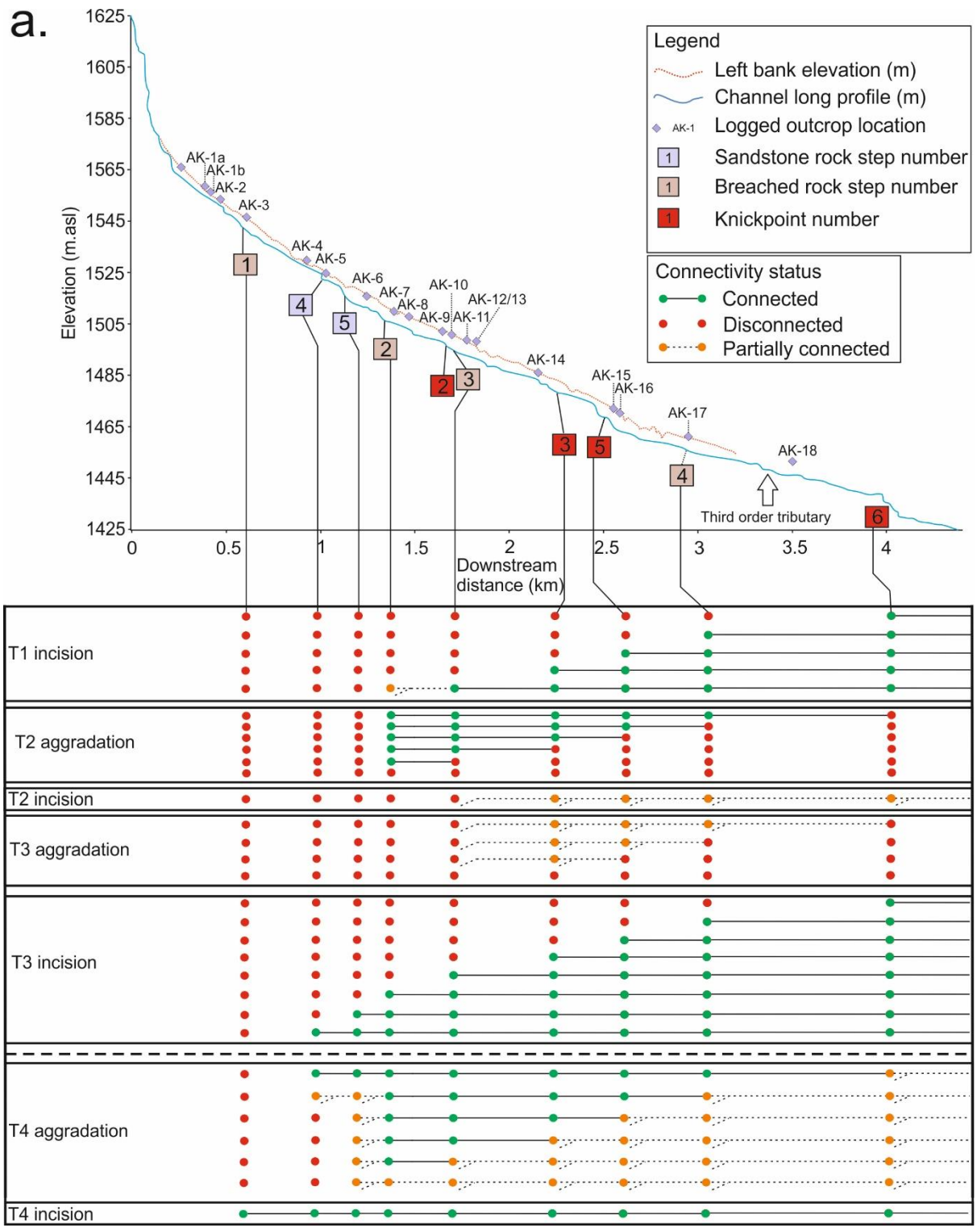
a.
Elevation (m.asl)
1625
1605
1585
1565
1545
1525
1505
1485
1465
1445
1425
0
0.5
1
1.5
2
2.5
3
3.5
4
Downstream distance (km)
AK-1a
AK-1b
AK-2
AK-3
AK-4
AK-5
AK-6
AK-7
AK-8
AK-9
AK-10
AK-11
AK-12/13
AK-14
AK-15
AK-16
AK-17
AK-18
Third order tributary
Legend
Left bank elevation (m)
Channel long profile (m)
AK-1
Logged outcrop location
1
Sandstone rock step number
1
Breached rock step number
1
Knickpoint number
Connectivity status
Connected
Disconnected
Partially connected
T1 incision
T2 aggradation
T2 incision
T3 aggradation
T3 incision
T4 aggradation
T4 incision

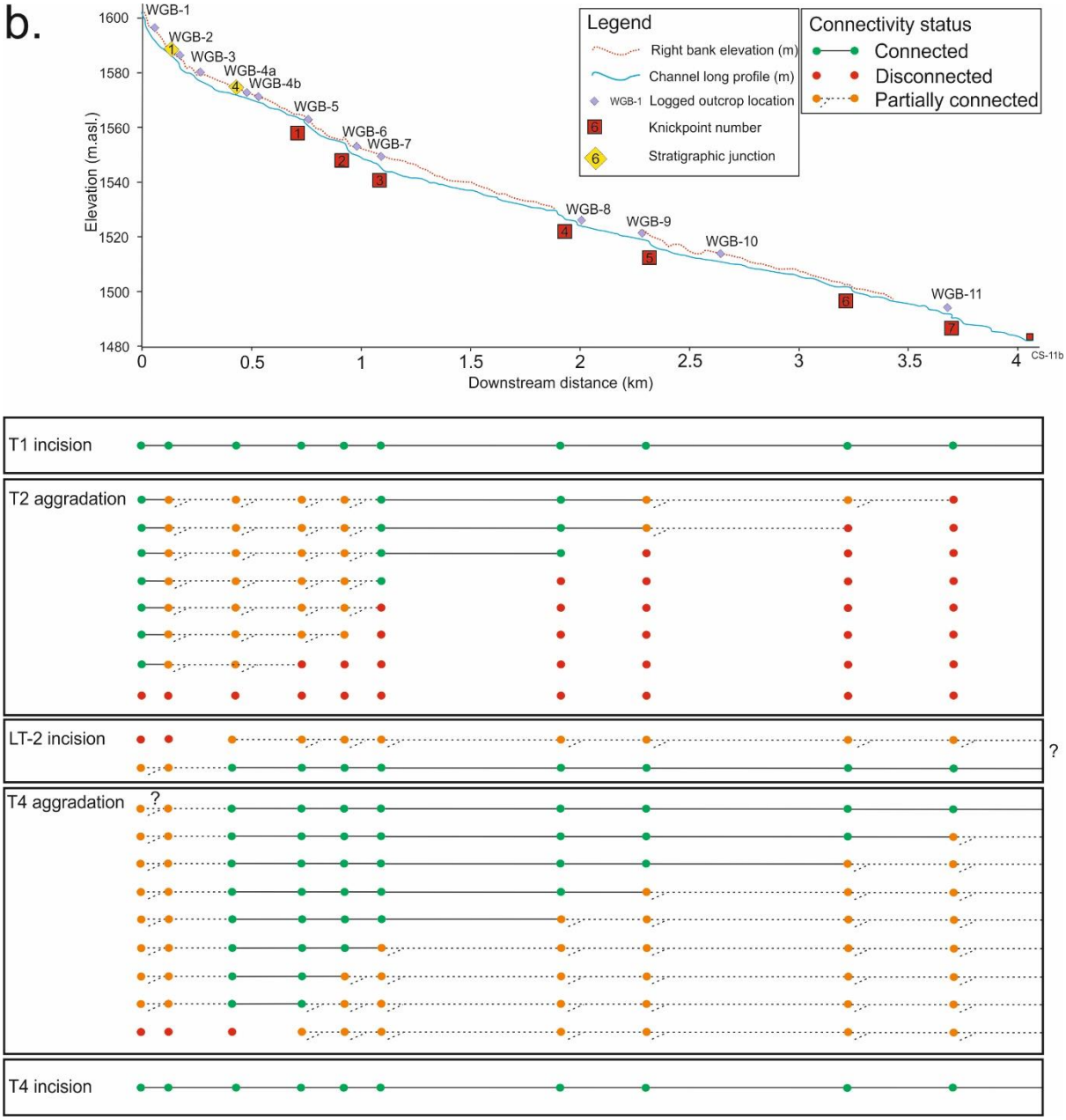

Figure 8.35 – a) Africanders Kloof and **b)** Wilgerbosch Kloof long profiles conceptualised in terms of longitudinal compartments for the storage of sediment, as determined by position of rock steps and knickpoints. The schematics show 'switches' between these compartments: red = disconnected, orange = partially connected, green = connected for each geomorphic phase as portrayed in Fig 8.34 and discussed in appropriate sequence in text.

The absence of T1 at WGB from the headwater fan was attributed to low preservation capacity of the upper valley. The sediments mantling the alluvial plain attest to fluvial activity associated with **T2** not T1. In theory, T1 sediments could be preserved at the margins of the plain, behind the younger T2 alluvium. Alternatively, most of the sediments of T1 could have been reworked during reinstatement of fluvial activity in the following deglacial period. In the central to lower Wilgerbosch Kloof valley, despite being wider than Africanders Kloof, T1 is absent. Badlands and gullies have stripped much of the soil from flanking slopes (Fig. 8.21). Soil formed on

mudstone-derived regolith has been shown to be more dispersible and 'erodible' (Rienks et al., 2000). Therefore, colluvial preservation potential may be limited at Wilgerbosch by the preponderance of mudstone over dolerite on the valley floor, accounting for why T1 is absent.

8.5.2: Post-LGM(?) incision phase (cycle 2)

The exact timing of channel entrenchment through T1 deposits is unclear. If Clarke et al's (2003) model of colluvial formation is correct, then channel entrenchment could, theoretically, have occurred during the LGM. However, the Sneeuberg is much farther inland than the KZN. Thus, it is unlikely that precipitation amounts, even impacting on a poorly vegetated landscape, were sufficient to trigger the scale of incision observed based on the lateral and longitudinal relations of T2 and T1. Working on the alluvial sediments and palaeosols of the Modder River (Erfkroon site), Lyons et al. (2014) using multi-proxy data proposed that climate conditions remained dry until 15.5 ka corresponding to Heinrich stadial 1 (Bond et al., 1997). The occurrence of high lake levels between 19.3–17 ka at Alexandersfontein 80 km west of Erfkroon may also reflect reduced evapotranspiration under cool, relatively 'dry' climatic conditions (Butzer et al., 1973; Butzer, 1984b). Furthermore, Chase et al's (2015) data suggesting a major westward expansion of the SRZ after 18 ka implies relatively moist conditions prevailed during HS1 (Bond et al., 1997), though the northward extent of this influence has yet to be conclusively demonstrated.

Channels were cut through colluvium as far as bedrock as shown by the occurrence of T2 fan and channel deposits mantling bedrock in all three valleys (Fig. 8.34). The early deglacial period (18-14.6 ka) was characterised by increasing humidity in the **Western Cape** region due to declining Atlantic Meridional Overturning Circulation (AMOC thereafter) and increasing SE Atlantic SSTs (McManus et al., 2004; Farmer et al., 2005), in spite of poleward migration of moisture bearing westerly storm-tracks.

Chase et al. (2015) have proposed that increased flow of warm Agulhas Current waters into the SE Atlantic and reduced northward heat transport in the AMOC favoured increasing advection of the tropical easterlies (from the Indian Ocean) in the SW Cape (Reason et al., 2006). This implies that even as far as SW South Africa, rainfall was concentrated in summer. If true, this large-scale expansion of the

summer rainfall zone has significant implications for the deglacial climate of the Sneeuberg, since it is much farther east (32^{o} N, 24.5^{o} E) compared to the De Rif midden site in the Cedarberg Mountains (32.5^{o} N, 19.2^{o}E - Chase et al., 2015) and therefore within this zone of expanded summer rainfall.

The implication of summer rather than winter dominated rainfall in the deglacial period would have been a significant reduction in drought-stress in the region. The depth and extent of the initial incision phase (T1 abandonment) may reflect the onset of increasing rainfall on a poorly vegetated periglacial landscape. However, a series of large floods without a major reorganisation of climate could also have triggered incision.

Propagation of incision from the trunk river up the tributaries likely occurred rapidly, especially if vegetation and rainfall were out of phase following the LGM (Knox, 1972). Furthermore, no calcrete was fixed in association with a raised water-table prior to incision of T1 due to climate having been cold and dry. Thus, T1 had no armour layer that would have retarded incision. Following initial channel incision in Wilgerbosch River, the newly cut channel would have been buffered from hillslopes and tributaries. As a result, the low sediment to discharge ratio would have likely favoured rapid reworking of colluvial stores mantling the valley through headward erosion.

8.5.3: Post-T1 incision: aggradational phase (cycle 2)

After T1 incision, the geomorphic evidence across the study region indicates a phase of high-magnitude fluvial activity manifesting in the form of: 1) extensive debris flow deposits (either channelized or as alluvial fans) in the Africanders Kloof, 2) channel bar deposits and 3) infilled, high energy deposits in aggrading tributaries. Channel and floodplain aggradation continued at a rate sufficient to overtake soil formation and, as a result, across the study area, no intervening palaeosols were noted. Up to 6 m of alluvium were deposited during this phase. Aggradation terminated some time after 17±2.5 ka.

At Wilgerbosch Kloof, the palaeo-connectivity of the system differed from Africanders Kloof as a result of abrupt changes in valley confinement. Before the effects of base level rise on the trunk Wilgerbosch River were ‘realised’ by the upper part of the

Wilgerbosch Kloof, the abrupt change from the confined upper slope to alluvial plain resulted in a partial loss of connectivity and sediment storage (Fig. 8.34 and 8.35b). The occurrence of high energy fluvial (bar) deposits intersects with increasing valley confinement in the central valley. Note in Fig. 8.34, that with the exception of the Wilgerbosch headwaters, T2 is overprinted by rhizogenic calcrete. This was attributed to the absence of seepage zones above WGB-6 and slopes dominated by sandstone instead of dolerite (see Section 8.3).

The longitudinal and vertical extent of this aggradation is likely a feedback response to channel incision propagating upslopes, having resulted in reinstatement of connectivity with deep stores of weathered material that had accumulated on footslopes and interfluves from the preceeding interstadial (MIS3) and glacial periods (LGM) (Clarke et al., 2003; Holmes et al., 2003). The volume of sediment injected into the sediment transport system overwhelmed the valleys, eventually resulting in a phase of disconnectivity (Fryirs, 2013). Fig. 8.35 shows progressive loss of connectivity at both Africanders and Wilgerbosch Kloof in response to aggradation in the trunk river. Sections of channel bracketed by major rock steps and knickpoints may have backfilled from the downstream end.

Differences in local lithology are likely to have affected the responses of tributaries to cutting and filling (McFadden and McAuliffe, 1997). Channel reaches and tributaries incised into mudstone (Wilgerbosch Kloof lower valley) would have generated higher sediment loads than those carved into dolerite. At these locations, rates of initial knickpoint retreat through T1 may have been locally lower as the newly cut channel was able to derive new sediment from eroding bedrock instead of purely reworking prior valley fills (T1) as was the case at Africanders Kloof. At Wilgerbosch Kloof, for instance, there has been comparatively deep incision and knickpoint retreat through mudstone relative to the major knickpoints formed on the more resistant sandstone at Africanders Kloof. Furthermore, even the most deeply weathered deposits of T2 on the Wilgerbosch River are very dilute with respect to ferrimagnetic intensity compared to the upper dolerite slopes of Africanders Kloof. For sedimentary units above the palaeowater table (limit of rhizogenic calcrete), this effect is maintained, reflecting inputs of magnetically weaker mudstone and sandstone derived sediment (Rowntree et al., 2012). In these respects, in association with morphological differences between the valleys, rates of geomorphic change are likely to have been

‘amplified’ by the steeper, narrower dolerite catchment (Africanders Kloof) and diluted by the relatively shallow, wider mudstone dominated catchment (Wilgerbosch Kloof) (Phillips, 2014a and b).

The patchy nature of T1 and T2 along the Wilgerbosch River and through the gorge is to do with subsequent reworking and thus an issue of preservation (Keen-Zebert et al., 2013). Therefore, the region-wide evidence for deep aggradation (T2) attests to major valley-floor adjustment. The timing of initiation of aggradation is unknown. Debris flow deposits imply there could have been a series of catastrophic floods but these may have occurred within a relatively cold, dry climate. Alternatively, the sedimentary sequences observed could reflect increasing wetness due to expansion of the summer rainfall zone (Chase et al., 2015). Heightened landscape sensitivity during major climatic transitions is a well known concept (Knox, 1972; Thomas, 2001; Woodward et al., 2008). The impetus for aggradation may have been amplified by rainfall and vegetation being out of phase around the time of or immediately after the LGM. Additionally, the absence of blankets (such as calcrete) disconnecting large stores of sediment during incision of T1 would have created a readily available supply of material that could be flushed into the valleys (Fryirs et al., 2007).

Nicholas et al. (1995) applied the term ‘superslugs’ to articulate major changes in sediment supply that produced basin-wide impacts (rather than segments of channel) and these can include a variety of sediment sources from channel (endoslugs) to slope (exoslugs). Examples of the drivers of superslugs on valley sediment cascades and fluvial behaviour vary from anthropogenic influences (Gilbert, 1917; Knighton, 1989) to Late Quaternary climate change (Knox, 1972; Church and Slaymaker, 1989). Aggradation rates of up to 15 cm a^{-1} have been reported where ‘superslugs’ have developed in the south-western USA in response to poor farming practices (Trimble, 1983). Without well-established chronological control, it is not possible to quantify aggradation rate of T2. Other examples from the literature of aggradation rates in dryland channels imply that this depth and extent of sediment could have accreted in less than a century, however (Leopold, 1976; Love, 1977; Hereford, 1986; Balling and Wells, 1990). In semi-arid environments, superslugs may be immobilised for long periods of time. The next sub-section, in part, will focus on this.

8.5.4 Post-T2 aggradation: soil development (cycle 2)

As part of a complex response to the emplacement of the sediment 'superslug', the watertable rose up to 2 m above present level in the tributaries, whilst on the main channel, a maximum of 1.5 m above bedrock was reached (Fig. 8.34 – see stage 6).

Floodplains and slopes were extensively colonised by vegetation, reflected in the occurrence of laterally and longitudinally continuous, calcified rootmats attaining maximum thickness (up to 20 cm) in the lower Africanders Kloof.

8.5.5 Post-T2 soil formation: cycle 3 incision

Micromorphological evidence from the calcified rootmat indicates a lowering of the watertable (see Sections 8.2.2 and 5.3.6). Furthermore, the haematite soil above the calcrete is buried by up to 3 m of alluvium at Africanders Kloof and 3.3 m at the start of the gorge (see Fig. 8.11 and 8.30).

Incision of T2 did not propagate further upstream than AK-10 due to the armouring effect and thus sediments upstream remained disconnected (Fig. 8.35a). There is no evidence indicating that this blanket was penetrated during incision neither at Africanders Kloof nor on the Wilgerbosch River (Fig. 8.34). The blanketing effect of the calcrete immobilised large quantities of sediment across the valleys, retarding incision due to elevation of the geomorphic threshold (Fryirs et al., 2007). Thus, the calcrete acted to 'desensitise' the landscape to major incision by acting as a base level anchor, attenuating the impact of flood events. Reduced vegetation cover on flanking slopes and possibly, infilled first order tributaries, supplied alluvium (T2) which was then deposited on the valley floors triggering a mode switch from "cut to fill". Though fragmentary, the morphostratigraphic relation of inset T3 sediments upstream of the gorge indicates that cutting and filling was a regional occurrence and that aggradation of T3 in the Africanders Kloof could have been a backfilling response similar to that documented for T2 (Fig. 8.35a).

Following aggradation, there is evidence that relatively dry conditions prevailed (see Section 5.3.6). As was the case for cycle 1, cycle 3 (T3) is absent from Wilgerbosch Kloof. Instead, a phase of cutting and filling which is intermediate (local terrace 2 – see Table 8.7) between regional T3 and T4 is recorded locally in the lower Wilgerbosch Kloof valley. The extent of connectivity with the upper reaches is

unclear, but for up to 3 m of alluvium to accrete (LT-2), this likely required supply from eroding upland sources (Fig. 8.35b). Based on the very low pedogenic overprinting of this locally occurring terrace (see Section 8.3.1) this must be much younger than T3 and is probably late Holocene. Nevertheless, the fact that a meandering channel form was maintained in the relatively wide, lower valley of Wilgerbosch Kloof, implies that channel discharge was sufficient to maintain equilibrium form. At Wilgerbosch, a seepage zone from a nearby dolerite sill (see Fig. 8.21) contributes to channel discharge such that the channels flow perennially.

8.5.6 Cycle 4

Cycle 4 is characterised by the slow infilling of valley floors by fine sediment and the development of wetlands both in the tributaries and the main Wilgerbosch channel and these sediments predate the European incursion (Neville, 1996; Boardman et al., 2003; Boardman, 2014). At Africanders Kloof, the geomorphic evidence implies that channels in the period between T3 (Late Pleistocene?) and Late Holocene (T4) had still not cut down to bedrock level upstream of AK-18 (see Fig. 8.17) due to the cemented nature of the fills. The fact that T4 was deposited on bedrock downstream of AK-18 may reflect increasing downstream discharge responsible for reworking T1-T3.

T4 is preserved farther upstream than T2 at Africanders Kloof, occurring between AK-3 and 4 (Fig. 8.35a), but connectivity with the upper headwaters (AKH–AK-2) had still not been established (Fig. 8.35a – 'T3 incision' phase). Although alternating minerogenic and very low energy, organic rich fills were noted in the Wilgerbosch River (WGW, WGM-1 and 2), caution is warranted in relation to assignment of a strictly climatic interpretation when a migrating single-thread channel can produce zones of low energy deposition, later colonised by vegetation. However, the occurrence of two discrete organic-rich 'palaeosols' at AK-7 (units C2 and C4) and AK-15 (units E and F) (see Fig. 8.11 and 8.16) and then again at WGB-10 (units A2 and B2) may imply an overriding climatic control. In this case, the dated second palaeosol at WGW (Fig. 8.30) implies that the last major phase of valley floor stability must have started by at least 437 ± 37 yr. Notably, this corresponds with the Little Ice Age (1600 AD) which has been implicated as the most likely driver of donga incision in the Blood River valley (Lyons et al., 2013). The unconformable burial of

the organic-rich low energy deposits by coarse gravels implied a phase of incision (see Section 7.2), but this was not dated. As discussed earlier, flood marks deposited in association with a 1 in 50 year flood that took place in 2011 as well as erosional features (scarp faces carved into terrace fills) along the Wilgerbosch River were clear indications of very recent geomorphic change. This coarse sediment overburden (evident elsewhere see Section 7.3a) could be dated in future to test whether the age of the gravels immediately postdates 437 ± 37 yr and if so whether the modern channels were cut prior to or following the European incursion (Boardman, 2014 and see Section 8.5.7).

Emplacement of T4 superseded the incision of LT-2 at Wilgerbosch Kloof. Incision extended at least as far as junction 4, upstream of WGB-4A (Fig. 8.21 – see blue dashed line indicating extent of local terrace 3 and 8.35b). It appears incision did not retreat as far as the headwater fan and thus the upper sandstone slope remained disconnected during aggradation of T4 (WGB-1–3 – Fig. 8.35b).

8.5.7 Modern incision phase

Gullies and channels up to 6 m depth through alluvium and colluvium are extensive in the Sneeuberg and typically form networks connected to higher order tributaries (Boardman et al., 2003). At Africanders Kloof, this most recent phase of incision appears to be unprecedented in terms of depth and spatial extent compared to those reconstructed from previous incisional episodes (Fig. 8.34 & 8.35a).

Both the timing and drivers of the present phase of incision in the Sneeuberg have attracted considerable attention and debate among researchers. In the last 9 years, there has been a growing consensus of opinion that the formation of gullies postdates the European occupation from the late 18th century onwards but as yet, the precise timing has not been quantitatively constrained (Boardman, 2014; Rowntree, 2014).

For instance, Boardman (2014) has convincingly demonstrated that gully incision must postdate the formation of ‘vlei’ deposits in the Klein Seekoi valley. The stability of terrace 4 deposits from at least 437 ± 37 yr on the Wilgerbosch River is a clear indication that incision here must have occurred in the very late Holocene, but whether it occurred in response to abrupt climate changes or anthropogenic impacts

is unclear (Section 8.5.6). Skead (2007) reported that all major rivers of the Eastern Cape contained hippopotamus when European settlers first arrived and quotes an example of drainage for agriculture causing a loss of vlei and hippos near Somerset East in the 1830s. This corroborates Neville's (1996) report regarding hippopotamus wallows (or chains of pools) on the Klein Seekoi River. Beinart (2003) attributed loss of grass and invasion of shrubs around Graff-Reinet (1810-1830) to significant overgrazing by sheep. This documented evidence in favour of an anthropogenic driver for incision is compelling, but Lyons et al. (2013) have demonstrated that donga incision in the upper Blood River catchment coincided with abrupt climate changes, namely the Medieval Climatic Anomaly (AD 900-1300) and Little Ice Age (1300-1800). As a result, incision of some valleys may well predate the European incursion and constitute natural responses to abrupt late Holocene climate changes.

8.6: Discussion

8.6.1: Comparison with conceptual model (Chapter 4.6)

The reconstruction of palaeoconnectivity (Fig. 8.35) indicates that aggradation of the tributaries was controlled by changing base level on the trunk river. The partial breaching of former geological barriers (breached rock step no. 2 and 4 – Fig. 8.35a) prior to the deposition of terraces 1-4 has amplified the sensitivity of the catchment to Late Quaternary climate changes (Phillips, 2014a; 2014b). The pocket-like appearance of fills (T4) relates to varied preservation potential controlled by residence time and degree of induration rather than floodout deposition with wetlands upstream of geological barriers (Tooth et al., 2004; Grenfell et al., 2014). There are two exceptions to this pattern: 1) The headwater floodout cut and filled episodically in response to a former barrier (no. 1 - Fig. 8.35a) and, based on morphometric evidence of bedding and soil magnetic data, exerted little influence on aggradation downstream. The second phase of floodout deposition (see Section 8.2.1) occurred in the early Holocene whereas aggradation of T2 in the central valley occurred in the Late Pleistocene. The younger age of the floodout sediment in spite of the discontinuity likely pertains to reworking and circumvention rather than overtopping of the barrier following the sequence outlined in Fig. 8.4. 2) Terraces 1 and 4 are represented upstream of sandstone rock steps 4 and 5. The sandstone steps likely acted to block headward erosion during the major incision of T1 (Fig.

8.34). As a result, the upper slopes were desensitised to changing sediment fluxes lower down the system.

Aggradation of the tributaries was thus a complex response to an initial climate change triggering rapid incision (T1), which via headcutting, reinstated connectivity with deep stores of colluvium that had accumulated slowly in the preceeding glacial phase, which caused the system to abruptly reset to an aggradational mode as valleys became overwhelmed by sediment. The resulting phase of widespread soil and wetland development was driven by the palaeohydrological conditions imposed by the aggraded state of the valleys. The sediment 'slug' associated with T2 aggradation was immobilised by subsequent development of an extensive blanket of calcrete, which acted to retard downcutting through the terrace alluvium, particularly in the tributaries. This further restricted accommodation space and, as a result, there is a large age gap between T2 and T4. The preservation of an intermediate terrace (LT-2 – Fig. 8.34) implies that there were other cut and fill cycles in the Holocene, but lack of representation reflects restricted preservation potential, as controlled largely by the dominance of T2 sediments.

No discernible terrace junctions at major drainage confluences implies that cycles of cut and fill were not controlled by autogenic mechanisms such as tributary impoundment (Brierly and Fryirs, 1999; Grenfell et al., 2008), loss of confinement triggering backfilling (Schumm and Hadley, 1957) or downcutting through rock barriers downstream (Tooth et al., 2004).

8.6.2: Comparison with regional records

Headwater tributaries of the Sundays River contain a terrace legacy signifying that there have been at least four major episodes of 'cut and fill' since the LGM. The presence of a second Late Holocene terrace in the lithologically softer and wider Wilgerbosch Kloof valley suggests there may have been 5 phases or more, but only four are widely expressed due to the limited 'memory' of this geomorphic system (Blong, 1970; Bull and Kirkby, 1997; Keen-Zebert et al., 2013).

These spatially extensive patterns of 'cut and fill' contrast with those reported in the nearby Klein Seekoi valley. The Sundays and Klein Seekoi headwaters are similar in that a major Late Holocene incision phase has occurred. In the Klein Seekoi, this has

been convincingly attributed to overgrazing and land mismanagement (Nesbitt, 1996; Holmes et al., 2003; Rowntree et al., 2012; Boardman, 2014; Rowntree, 2014), but the driver of incision in the Sundays Headwaters has not been unequivocally established (Section 8.5.7).

'Cut and fill' architecture in the Klein Seekoi tributary has been dominated by discontinuous channel processes that are strongly decoupled from palaeo-precipitation (Partridge et al., 1997; Grenfell et al., 2014). Upper tributaries here are infilled by mid-late Holocene alluvium (Sugden, 1989; Holmes et al., 2003). The imprecision associated with OSL date LV509 (8.2 ± 1.5 ka) from the basal floodout unit in the upper Africanders Kloof makes comparison with Holmes et al's radiocarbon date of 5790 ± 80 yr from a basal fill unit difficult. Further, as this is a ^{14}C date, this cannot be taken as reflective of the depositional age of the alluvium.

If the depositional age of the floodout alluvium stored in the Africanders Kloof headwaters is 'older' than that reported by Holmes – early Holocene or Late Pleistocene, this would be consistent with our reconstruction of palaeoconnectivity, which implies the upper-most slopes remained disconnected from second order tributaries by a geological barrier until the Late Holocene. This contrasts with the Klein Seekoi tributary, where the evidence indicates flushing through of sediment to valley floors, removing any pre-existing sediment – a situation similar to the headwater fan at Wilgerbosch Kloof where there is an associated absence of fine-grained (T1) colluvial deposits. However, the fact that headwater floodout deposits at Africanders are younger than those in the second order tributaries does imply more recent reworking, even if such episodes were not transmitted to the lower valleys.

The youngest ^{14}C date (2510 ± 50 yr) obtained by Holmes et al. (2003) from 'vlei' (wetland) sediments at the top of the local succession is much older than the radiocarbon date obtained from wetland deposits in the Wilgerbosch River (437 ± 37 yr). Since Grenfell et al. (2014) later attributed these 'vlei' fills to former 'ponds' filling upstream of floodouts, Holmes et al's date has probably captured a single 'vlei' formed following deposition of a floodout and has little wider palaeoenvironmental significance. Rather, it was established that the wetlands in the upper Sundays River were an ubiquitous feature of the valley floors in the Late Holocene and not related to a) isolated pockets of low-energy deposition in association with a migrating single

thread channel or b) localised ponds upstream of floodouts similar to those reported by Grenfell et al. (2014).

Debris-flow deposits are common at Africanders Kloof deposited on fans and in palaeochannels but infrequent in the Wilgerbosch River and absent at Wilgerbosch Kloof, probably due to their being relatively unconfined and possessing slightly shallower gradients. In the Klein Seekoi headwaters, Holmes et al. (2003) originally postulated that the debris-flow deposits preserved here were at least 125,000 years old (Last Interglacial Maximum), but significantly revised this on the basis of a preliminary OSL age (48.9 ± 5.9 ka – Boardman et al., 2005). Boardman et al. (2005) reported that the dolerite component had decomposed and the gravels were heavily calcretised: nowhere at our study sites has the dolerite component significantly decomposed and calcretisation is primarily a feature of changing groundwater hydrology. Therefore, the depositional age of the debris flow deposits at Africanders Kloof must postdate the LGM, associated with the aggradation of the second major terrace. However, the deep weathering rinds associated with dolerite clasts imply that they must have been subject to a long phase (or possible several) of in situ weathering on slopes prior to being flushed to the valley floors.

The matter as to why there are so many ‘cut and fill’ phases preserved in the Sundays headwaters, but not the nearby north-draining Klein Seekoi headwater valleys requires further discussion. In summary, fluvial behaviour in the Klein Seekoi valley is predominantly controlled by an intact dolerite outcrop which causes the channel upstream to lose confinement triggering floodout deposition. A channel reforms downstream of the discontinuity and, because the slope gradient is high relative to the floodout, incision into valley fill sediment and eventually bedrock occurs along the reformed channel course. Repetition of this cycle has created laterally planed but a longitudinally stepped valley long profile in both the headwaters and on the valley floor (Grenfell et al., 2014).

Both headwater tributaries (Africanders and Wilgerbosch Kloof) exhibit stepped long profiles, but crucially, knickpoints have developed in second and third order tributaries that attest to long term base level adjustment in response to the landward retreat of the Great Escarpment and the valleys are narrower (150-300 m) than the Klein Seekoi (400 m). Over geological timescales, progressive knickpoint retreat

through the dolerite has created accommodation space for terrace alluvium. Tooth et al. (2004) proposed in a comparative study of three incising mixed bedrock-alluvial rivers in the Free State, that partial or complete fluvial incision of dolerite sills may take > 10^4 years, but these are large valley floors compared to the Sundays headwaters. Incision in the Sundays is likely to have been comparatively rapid because of the narrow, steep configuration of the valleys. However, the abundant formation of in situ gleyed, illite clay soils on the dolerite imply that long term base level adjustment has likely been highly episodic, with the bedrock having been buried for long time intervals (> 10^3–10^4 years). For example, in spite of three cut and fill cycles post-dating aggradation of the major fluvial terrace (T2) at Africanders Kloof, incision down to bedrock in the 1st and 2nd order tributaries did not occur until after 437 ± 37 yr (post-T4). During such phases, fluvial incision of the bedrock cannot take place, though in situ breakdown of the dolerite has clearly been maintained, reflected in the illite clay soils. Such long term in situ weathering and pedogenesis then primes the dolerite to incision during phases of overlying terrace abandonment as evidenced by the breached rock steps at Africanders Kloof (Fig. 8.35a). Reaches formerly controlled by autogenic processes of cut and fill, such as the Africanders Kloof headwater palaeo floodout, became sensitised to major base level changes in 2nd - 4rd order tributaries – though in terms of future 'cut and fill,' this will be dependent on the magnitude-frequency dynamics of any catchment geomorphic changes (Bracken et al., 2015).

The steep, narrow configuration of the Sneeuberg valleys has acted to 'amplify' the sensitivity of response to Late Quaternary climate changes (Argobast and Johnson, 1994; McFadden and McAuliffe, 1997; Thomas, 2001; Phillips, 2014a, 2014b), though as discussed in Section 8.6.1, the nature and magnitude of 'cut and fill' has been equally contingent on antecedent conditions of sediment supply relating to the evolving connectivity of the system and subsequent duration and conditions of soil formation.

Palaeosols formed in alluvium (Lyons et al., 2014) and colluvium (Botha et al., 1994; Temme et al., 2008) have been investigated in South Africa and their significance as indicators of palaeoclimate evaluated. Using a combination of DRS, soil magnetism and OSL dating, Lyons et al. 2014 was able to convincingly demonstrate a relationship between the concentrations of ultra-fine SP pedogenic ferrimagnets from

the Modder River terrace palaeosols and spikes in the Tswaing rainfall record (Partridge et al., 1997). Demonstrating this linkage between climate and magnetism depends on our ability to constrain other soil forming variables such as topography, parent material and time (Jenny, 1941). Additional factors such as bioturbation and changes in water table may distort climatically-related signals (Lindquist et al., 2011; Tooth et al., 2013). The lack of chronometric data in this study has prevented tying distinct magnetic properties of terrace palaeosols to a distinct climatic forcing as well as establishing sedimentation rates to compare extent of soil magnetic enhancement with Lyons et al. (2014).

Magnetic properties of the terrace palaeosols were primarily subject to dissolution of the fine-grained (SP/SD) component under anoxic conditions (Maher, 1988) and preferential formation of goethite (Balsam et al., 2004) associated with the raised water table that followed aggradation of T2. Additionally, thin section analyses revealed the T2 palaeosol is polygenetic, controlled by water-table variability. Variations in water-table are related to both climate and depth of channel entrenchment (Boardman, 2014). As a result, the magnetic parameters reflect the integration of potentially multiple phases of oxidation and reduction, superimposed on variations in sediment source and bioturbation.

Magnetic susceptibility (X_{LF}) and remanence (X_{ARM} and IRM_{1T}) parameters were used to differentiate between sedimentary and igneous sources, assist in correlating terraces and establishing the connectivity between different components of the fluvial system. These parameters were generally successful except in cases where persistent reduction and iron sulphide formation (relating to waterlogging and/or dissolution of organic matter- Williams (1992) altered the inherited (source-related) magnetic composition.

The results of the particle size-magnetics data demonstrated that in settings proximal to or on dolerite, the ‘bulk’ samples are dominated by a lithogenic ferrimagnetic signature to the extent that the pedogenic fine-grained component is underestimated and the bi-logarithmic plots of X_{ARM}/X_{FD} and X_{ARM}/X_{LF} often used to assess degree of pedogenesis thus unsuitable (Oldfield, 1994; Oldfield and Crowther, 2007).

8.6.3 Comparison with other dryland fluvial records

Detailed investigations conducted on stratigraphic records along several arroyos in the SW USA indicate periods of 'cut and fill' cyclicity on centennial-millenial timescales. Rates of incision are known to be rapid in comparison to rates of arroyo filling, though these can vary from decadal (Love, 1977) to multi-centennial (Bull, 1997; Gellis et al., 2012) timescales. Frequency of arroyo cutting was found to increase throughout the Holocene, notably at 4000, 2500, 2000, 1000 and 500 yr in several watersheds (Waters and Haynes, 2001). Cut and fill cycles on the Colorado Plateau were generally synchronous, emphasising arroyo incision during the late 19th and early 20th centuries, but palaeoarroyo formation between 1–0.5 ka (Schumm and Hadley, 1957; Cooke and Reeves, 1976; Leopold, 1976; Webb, 1985; Hereford, 1986; Karlstrom and Karlstrom, 1987; Webb et al., 1991; Hereford et al., 1996; Hereford, 2002). Crucially, the palaeo-alluvial record in the SW USA does not predate the late Pleistocene (Harden et al., 2010), but the colluvial/alluvial stratigraphic record in comparatively small, narrow and steep South African headwater tributaries does.

The preservation of the Pleistocene terraces in the Sneeuberg was a complex response (Schumm, 1977) to the rapid aggradation of the valleys controlled by changing dynamics of connectivity. As a result, the 'geomorphic memory' of valleys that should, without the effects of a major armouring blanket, be low – was significantly enhanced. The restricted accommodation space imposed by the dominance of these terraces (T1 and 2) meant that sediments pertaining to more recent Holocene phases of "cut and fill" have been poorly preserved, if at all. The geomorphic behaviour of the Sundays headwaters has been, and to some extent continues to be, influenced by impacts of the last major valley floor adjustment which occurred following the LGM. As a result, it is crucial to contextualise phases of cut and fill with respect to the antecedent conditions of sediment supply and storage.

The Mediterranean region hosts some of the most well-developed and well-studied flights of Late Pleistocene and Holocene terraces in the world (Macklin et al., 2012). Since the first systematic regional evaluation of these deposits by Vita-Finzi (1969), major advances in ^{14}C, TL and OSL techniques have permitted detailed, high resolution chronologies of fluvial activity to be obtained. This has allowed the timing

of fluvial activity in the last glacial cycle in both tectonically active and stable regions to be compared against records of North Atlantic climate change (McManus et al., 1999; Petit et al., 1999; Benito et al., 2008; Woodward et al., 2008; Soria-Jáuregui et al., 2016).

Late Pleistocene river evolution in terms of major phases of aggradation and incision has been shown to be controlled primarily by both orbitally driven and sub-orbital scale climate variability – even between areas of varying tectonic uplift (Macklin et al., 2002; 2012). Aggradation has consistently taken place during climatically cold, dry phases (Petit et al., 1999; Macklin et al., 2002). Various authors have proposed that this has been achieved through the effect of climate on vegetation cover, enhanced mechanical weathering, rock breakdown and mass wasting producing major increases in sediment supply (Gil García et al., 2002; Woodward et al., 2008; Soria-Jáuregui et al., 2016). For example, stratified slope and periglacial deposits occur in the high summits of the Cantabrian Mountains (González-Amuchastegui and Serrano, 2013) produced during Pleistocene cold stages. Conversely, phases of incision and floodplain sedimentation commonly coincided with interglacial conditions as vegetation on slopes reduced sediment supply to channels. For example, on the River Ebro, Soria-Jáuregui et al. (2016) attributed the fine sedimentary composition of an early Holocene terrace (T5) to reduced sediment input from slopes and tributary valleys. The terrace sedimentology reflected individual flooding events resulting in deposition of fine sediment on vegetated floodplains. Macklin et al. (2002) proposed that the sensitivity of response of basins across the Mediterranean to climate, related to effective coupling between hillslopes and channels. However, the interplay between Pleistocene tectonism and climate changes created optimum conditions for effective preservation of terrace fills across this region (Macklin et al., 2012; Soria-Jáuregui et al., 2016).

T1 in the Sneeuberg is an example of a fill terrace that aggraded in a cold, dry climate phase at or around the time of the LGM, with some of the thickest fills (up to 6 m) deposited relative to the later terraces (T2-T4). Both the extent of slope-channel coupling and local catchment lithology were found to be important controls on processes of sediment conveyance to the valley floors. For instance, the vertical sandstone walls in the Ganora Gorge were prone to mechanical weathering along joints and bedding planes by freeze-thaw activity, whilst the strong slope-channel

coupling meant that large quantities of regolith could be delivered to the valley floor by mass-wasting and slopewash processes triggering aggradation. It is possible that this acted as a ‘dam’ behind which sediment from upstream aggraded. In contrast, at Africanders Kloof where slope-channel coupling was relatively low, sedimentation on valley floors occurred through low-energy slopewash processes. Without chronometric dating of this terrace at both locations, it is not possible to evaluate the age structure of these fills or rate of sedimentation, but based on the high energy mode of sedimentation in the gorge, aggradation here likely occurred more quickly than in the tributaries.

It is also unclear as to whether or not incision of T1 occurred in response to an expanded summer-rainfall zone as climate ameliorated in the deglacial period (Chase et al., 2015) or whether a series of large floods within a cool, dry periglacial climate regime initiated cutting. Aggradation and incision may therefore occur without any fundamental change in climate, but this is resolvable in future by better dating control and as the number of palaeoclimatic records across South Africa increases (Stone, 2014).

Negligible rates of tectonic uplift in the Sneeuberg since the Pliocene have not been conducive to terrace formation of the age preserved in many basins across the Mediterranean (Hattingh, 1996; Macklin et al., 2012). Rates of landscape denudation have also been so low, that epeirogenic uplift due to crustal unloading has been negligible (Decker et al., 2011; 2013). Rather, alluvial preservation potential in the valleys reported in this doctoral study has been primarily controlled by thresholds being crossed whereby barriers (geological, sediment slug) have been either overtopped, circumvented or incised and blankets (cemented clay units, calcrete) incised and/or stripped (Fryirs et al., 2007; Bracken et al., 2015).

8.7: Summary

This chapter has synthesised the analytical evidence for the processes and drivers pertaining to terrace development in three headwater valleys of the Upper Sundays River. Different environmental phases have been reconstructed from terrace fills, the extent of connectivity between different parts of the system and the influence of allogenic as well as autogenic drivers of phases of cut, fill and pedogenesis. The

sequences were compared regionally and with records of cut and fill in the SW USA and the Mediterranean.

Chapter 9: Conclusions and further research

9.1 Conclusions

Along tributaries of the upper Sundays River in the Great Karoo, South Africa, extensive exposures of alluvial and colluvial sediments have permitted an investigation into the characteristics, mechanisms and drivers of terrace formation. In this chapter, the major characteristics of each terrace are summarised. This is followed by the major conclusions drawn with respect to the mechanisms and drivers of terrace cut and fill and their wider significance for our understanding of the possible nature and trajectories of valley cut and fill in other drylands.

Multiple terrace fills of varying extent which reflect a range of sedimentary processes within different geomorphic phases were reported. The continuity of four of these terrace fills was a clear indication of catchment scale geomorphic adjustments. The deposits of **terrace 1** were colluvial in origin including: 1) up to 6 m of fine-grained slopewash deposits with lenticular freeze-thaw structures and 2) gelifluctate deposits in the Ganora Gorge. **Terrace 2** was the most continuous terrace, expressed in both tributaries (Africanders and Wilgerbosch Kloof) and the Wilgerbosch River. At Africanders Kloof, an OSL age indicated the terrace was deposited after the Last Glacial Maximum. The deposits of T2 were found to consist of: 1) Laterally impinging alluvial fans, 2) channel bar and floodplain sediments as well as 3) channelized debris-flows. The nature of pedogenic overprinting for both terraces 1 and 2 was controlled primarily by the position of the water table. A spatially extensive rhizogenic calcrete deposited in association with T2 provided an indication of the maximum vertical limits of the palaeo-water table, which was shown to have fluctuated following the first and most prominent phase of calcrete genesis. The soils associated with T2 were found to be polygenetic, reflecting alternating periods of oxidation and reduction, driven by variations in the water-table. The soil magnetic properties were found to reflect the integration of these phases and thus, local topography (via effect on drainage) and subtle variations in source lithology were found to be the most crucial soil forming factors overriding climate. T2 deposits in the upper Wilgerbosch Kloof lacked this calcrete horizon. **Terrace 3** consisted exclusively of channel and floodplain deposits distinctly inset within terrace 2 and above the elevation of the calcrete, but its occurrence restricted to the gorge and

base of Africanders Kloof. **Terrace 4** consisted of Late Holocene gleyed wetland deposits. Compared to T2, these deposits occurred as inset pockets in the valleys.

In addition to terraces that reflected catchment-wide geomorphic adjustments, several discontinuous terraces were reported also. Firstly, in the Africanders Kloof headwaters, four distinct phases of floodout emplacement and intervening periods of local geomorphic inactivity were reconstructed from morphometric and sedimentological analyses of the deposits. The headwater fills were diachronous with those that were the product of catchment-wide geomorphic changes downstream. Secondly, at Wilgerbosch Kloof the headwater fan sequence present lacked the stratigraphic complexity of the fan deposits at Africanders Kloof. In the lower valley, an alluvial terrace intermediate between regional T3 and T4 was found, but highly localised to the lower valley which is carved into mudstone.

Disconnectivity of sediment was shown to be an important mechanism controlling the sensitivity to and propagation of geomorphic changes between different landscape components. Phases of floodout progradation and soil development were found to be an autogenic response to local factors such as fan oversteepening, but primarily, disconnectivity with lower reaches induced by a dolerite barrier downstream which acted as a local base level control. As a result, the Africanders headwaters were found to preserve a local stratigraphic legacy that exceeded the age and complexity of that reported in the Klein Seekoi headwaters (see Section 5.2.4 and Holmes et al., 2003). The effects of intact sandstone rock steps on connectivity were also investigated. Upstream of one such step in the upper Africanders Kloof, regional terraces 2 and 3 were absent. It was demonstrated that the step acted to block headward erosion and thus parts of the catchment remained stable whilst downstream of this barrier, large-scale fluvial adjustments (T2) took place. The reconstructed palaeo-connectivity of these reaches was found to be consistent with the ‘compartmentalised filling’ scenario presented in Chapter 4, where discontinuities disrupt longitudinal linkages in sediment transfer.

The continuity of the regional terraces (1-4) was a clear indication that allogenic forcing had played a more significant role in driving geomorphic changes than localised processes akin to those reported in the headwaters, though processes of autogenesis and complex response were still important, albeit manifesting differently.

The greater sensitivity of landscape response to allogenic drivers was shown to have been amplified by the multitude of incised rock steps and barriers in 2nd–4th order tributaries, the depth of this incision representing the long-term fluvial response to the landward retreat of the Great Escarpment. Reaches that were formerly controlled by localised autogenic processes of cut and fill prior to barrier breach, had become sensitised to catchment-wide geomorphic adjustments. Aggradation of such large volumes of sediment in the tributaries was shown to be consistent with the filling trajectory outlined in the conceptual model.

The periglacial deposits of **T1** were ascribed to cold, dry conditions at or around the time of the LGM. The incision of T1 could have been in response to ameliorating climatic conditions in or just prior to the deglacial period, but rates of knickpoint retreat propagating upstream were amplified by increasing channel gradients and, at time of incision, the lack of connectivity with proximal hillslope as well as upstream channel sediment sources. The rapid aggradation of T2 was shown to be a complex response to this initial knickpoint retreat having propagated into lower order tributaries, re-connecting voluminous upstream sediment sources with the newly formed channel, which then resulted in the valleys becoming choked. The subsequent increase in water-table and formation of calcified root mats was therefore partly a feedback response to the aggraded state of the valleys, but also relatively warm, moist climatic conditions compared to those that occurred during aggradation of T1. A systematic lowering of the water-table in concert with partial incision of T2 and deposition of a 3rd inset terrace was interpreted as a response to climatic aridification. The 4th inset terrace was found to be considerably younger than T1 and T2 (Late Holocene), but the presence of an intermediate terrace in the lithologically softer, wider Wilgerbosch catchment implied that the large apparent age gap between T3 and T4 was to do with restricted alluvial preservation potential. Furthermore, the sensitivity of geomorphic response was shown to have been dampened significantly by the blanketing effect of the calcrete, such that channel incision down to bedrock in the Africanders tributary did not occur again until after 1600AD. The cause of the incision of T4 may relate to land mismanagement associated with the European incursion of the late 18th century, but equally, abrupt late Holocene climate changes such as the ‘Little Ice Age’ was advanced as a possible driver in light of the radiocarbon date from a T4 palaeosol along the

Wilgerbosch River. The cemented nature of terraces 1 and 2 as a product of the complex responses identified accounts for why such thick packages of sediment have been stored for so long in such narrow valleys, as well as the different vulnerability to erosion of different fills.

As part of the long term fluvial response to the retreat of the Great Escarpment, headwater tributaries of the Sundays River preserve a legacy of fluvial activity that contrasts with that reported from valleys draining the northern side of the Escarpment. These contrasts include the fact that the Klein Seekoi valley is not incised to the same extent as the Wilgerbosch River and its tributaries, where there is clear evidence of base level or 'buttress fall' representing multiple cycles of bedrock incision such that dolerite sills and dykes have been, in some cases, completely breached. As a result, channel reaches carved into mudstone are actively downcutting following the process described by Tooth et al. (2004). Consequently, disequilbrium channel forms (floodouts) with no continuous fill terrace architecture occur in the upper Klein Seekoi River, whereas in tributaries of the Wilgerbosch River there are up to four continuous terraces deposited under varied climatological and hydrological conditions. The extent of incision through former barriers to river downcutting, in concert with varied slope-channel coupling and lithological factors have acted to sensitise the Wilgerbosch River and its tributaries to Late Quaternary climate changes. It is these morphological contrasts that are used to explain the differences in fluvial form, process and legacy (preservation potential) between the two valleys (Klein Seekoi and Wilgerbosch).

The reconstruction of the processes and feedbacks pertaining to terrace and soil development in this study are instructive with respect to understanding: 1) how fluvial sediments may be preserved in tectonically stable catchments subject to long-term base level fall; 2) the role of connectivity in enhancing or suppressing sensitivity to and spatial extent of response to allogenic forcing; 3) the relations between periglaciation and subsequent fluvial responses in a South African context.

9.2 Further research

Reconstructing conditions of palaeo-connectivity within different geomorphic phases is critical in order to understand and contextualise landscape evolution. The outcomes of this research highlight a need for more detailed understanding of the

magnitude-frequency conditions under which (dis) connectivity of sediment between different landscape components in drylands occur and how such conditions may change relative to changing system boundary conditions such as: 1) intact barriers; 2) incision (partial or complete), bypassing or overtopping of barriers; 3) abrupt changes in valley confinement. Several strands of future research could be pursued to test and apply the conceptual model of landscape response developed in this study, to other dryland settings.

1. The first proposed research strand is concerned with modelling the processes of connectivity using basin-parameters akin to those observed at the South African field sites. Flume experiments could be designed where discontinuous channel systems with floodouts are simulated upstream of different barriers. For example, identification of the magnitude of allogenic forcing required to override local autogenic controls dictated by the effects of discontinuities on channel slope/confinement may allow the conditions under which propagation of geomorphic change occurs to other parts of the system to be defined. Firstly, a series of episodic flows, mimicking that of a 'flashy' dryland catchment may be input to measure the movement of sediment around or over discontinuities and the linkages and distances of travel between landscape components. The fluvial response may be modelled by incrementally adjusting the magnitude of allogenic input (simulated rainfall) to establish the threshold past which the system becomes fully connected. Secondly, to provide contrast in system boundary conditions, another experiment may be designed where there are headwater reaches impounded by discontinuities, but reaches downstream where discontinuities have been incised. As before, simulated rainfall may be incrementally adjusted in order to determine the major thresholds in connectivity between landscape components. The experiment may be repeated with varying sediment supply and varying discharge to determine the location(s) at which aggradation initiates and model the trajectories of filling.

2. The second proposed research strand is concerned with the acquisition of chronometric data to test for longitudinal age patterns pertaining to theoretical trajectories of valley incision and aggradation. Radiometric dating techniques have been used in novel ways to relate the age of valley fills to varying alluvial storage potential (Keen-Zebert et al., 2013), but otherwise, too often have chronometric data from fluvial records been shoehorned into seductive theories of palaeoclimatic

change, often derived from records that are at great distance from the site of geomorphologic investigation and which may be responding to different palaeoclimatic parameters (Patridge et al., 1997; Temme et al., 2008). Whilst terrace continuity may evidence catchment-wide geomorphic adjustments, complex feedbacks within the system mean that the associated effects take time to propagate up or downstream, depending on the trajectory of filling (Schumm and Hadley, 1957; Brierley and Fryirs, 1999; Grenfell et al., 2014). The application of the conceptual model of valley filling presented in this study to other fluvial environments within source regions which have been proven to yield quartz which is suitable for high precision OSL dating (Rodnight et al., 2006; Tooth et al., 2007; Lyons et al., 2013; 2014) could provide a novel way of modelling longitudinal as well as vertical age patterns within valley fills elsewhere in South Africa, but also in other drylands, to derive trajectories of cutting and filling and evaluate the leads and lags of geomorphic response in different parts of fluvial basins to palaeoclimate change. Acquisition of chronometric data from the valley fills outlined in this study would be extremely beneficial for testing our current model of late Quaternary landscape response. As shown by Colarossi et al. (2015) dating of potassium-feldspar derived from Karoo supergroup rocks may be an alternative approach to determination of the longitudinal and vertical structure of valley fills. K feldspar is concentrated in the laboratory by performing density separation at 2.58 spg. The K-feldspar component (< 2.62 spg) from samples prepared as part of this study have been kept and are thus at an advanced stage of preparation. A pilot study to test the suitability of existing K-feldspar extracts for optical dating could therefore be conducted and, if successful, multiple repeat dates obtained from fills in both the trunk river and tributaries. Such information is crucial for reconstructing the timescales under which gully erosion and soil loss can be reversed. For example, with better chronometric control it may be possible to calculate aggradation rates and establish how long it has taken valleys to refill after phases of erosion under conditions of varied sediment supply availability in the past.

References

Abderrahim H, Candela L, Queralt I, *et al.* 2011. 'X-ray fluorescence analysis for total bromine tracking in the vadose zone: results for Mnsara, Morocco.' *Vadose Zone Journal* **10** (4), pp. 1331-1335.

Aitken MJ and Smith BW. 1988. 'Optical dating: Recuperation after bleaching.' *Quaternary Science Reviews* **7** (3), pp. 387-393.

Allen JRL. 1965. 'Fining-upwards cycles in alluvial successions.' *Geological Journal* **4** (2), pp. 229-246.

Allen JRL. 1982a. *Sedimentary Structures: Their Character and Physical Basis, Volume 1*, Elsevier, Amsterdam, pp. 593.

Anderson NJ and Rippey B. 1988. 'Diagenesis of magnetic minerals in the recent sediments of a eutrophic lake.' *Limnology and Oceanography,* **33** (6), pp. 1476-1492.

Antevs E. 1952. 'Arroyo-Cutting and Filling.' *The Journal of Geology* **60** (4), pp. 375-385

Argobast AF and Johnson WC. 1994. 'Climatic implications of the late Quaternary alluvial record in a small drainage basin in the central Great Plains.' *Quaternary Research* **41** (3), pp. 298-305.

Arnold LJ, Bailey RM and Tucker GE. 2007. 'Statistical treatment of fluvial dose distributions from southern Colorado arroyo deposits.' *Quaternary Geochronology* **2** (1-4), pp. 162-167.

Arnold LJ, Roberts RG, Galbraith RF, *et al.* 2009. 'A revised burial dose estimation procedure for optical dating of young and modern-age sediments.' *Quaternary Geochronology* **4** (4), pp. 306-325.

Bailey RW. 1935. 'Epicycles of erosion in the valleys of the Colorado Plateau province.' *The Journal of Geology* **43** (4), pp. 337-355.

Baker VR. 1987. 'Paleoflood hydrology and extraordinary flood events.' *Journal of Hydrology* **96** (1-4), pp. 79-99.

Baker VR, Kochel RC and Patton PC. 1979. 'Long-term flood frequency analysis using geological data.' *International Association of Hydrological Sciences Publication* **128**, pp. 3-9.

Baker VR, Kochel RC, Patton PC, *et al.* 2009. 'Palaeohydrologic analysis of Holocene flood slackwater sediments,' in, *Modern and Ancient Fluvial Systems,* Blackwell Publishing Ltd, pp. 229-239.

Baker VR, Pickup G and Polach H. 1983. 'Desert palaeofloods in central Australia.' *Nature* **301**, pp. 502-504.

Balling RC and Wells SG. 1990. 'Historical rainfall patterns and arroyo activity within the Zuni River drainage basin, New Mexico.' *Annals of the Association of American Geographers* **80** (4), pp. 603-617.

Balsam W, Ji J and Chen J. 2004. 'Climatic interpretation of the Luochuan and Lingtai loess sections, China, based on changing iron oxide mineralogy and magnetic susceptibility.' *Earth and Planetary Science Letters* **223** (3-4), pp. 335-348.

Barron V and Torrent J. 2002. 'Evidence for a simple pathway to maghemite in Earth and Mars soils.' *Geochemica et Cosmochimica Acta* **66** (15), pp. 2801-2806.

Beinart W. 2003. *The Rise of Conservation in South Africa: Settlers, Livestock and the. Environment 1770–1950.* Oxford University Press, Oxford.

Benito G, Thorndycraft VR, Rico M, *et al.* 2008. 'Palaeoflood and floodplain records from Spain: Evidence for long-term climate variability and environmental changes.' *Geomorphology* **101**, pp. 68-77.

Billi P. 2007. 'Morphology and sediment dynamics of ephemeral stream terminal distributary systems in the Kobo Basin (northern Welo, Ethiopia).' *Geomorphology* **85** (1-2), pp. 98-113.

Blake WH, Wallbrink PJ, Doerr SH, *et al.* 2006. 'Magnetic enhancement in wildfire-affected soil and its potential for sediment-source ascription.' *Earth Surface Processes and Landforms* **31** (2), pp. 249-264.

Blong RJ. 1970. 'The development of discontinuous gullies in a pumice catchment.' *American Journal of Science* **268** (4), pp. 369-383.

Blott SJ and Pye K. 2001. 'GRADISTAT: a grain size distribution and statistics package for the analysis of unconsolidated sediments.' *Earth Surface Processes and Landforms* **26** (11) pp. 1237-1248.

Boardman J. 2014. 'How old are the gullies (dongas) of the Sneeuberg uplands, Eastern Karoo, South Africa?' *Catena* **113**, pp. 79-85.

Boardman J and Foster I. 2008. 'Badland and gully erosion in the Karoo, South Africa.' *Journal of Soil and Water Conservation* **63** (4), pp. 121-125.

Boardman J, Foster I, Rowntree K, *et al*. 2010. 'Environmental stress and landscape recovery in a semi-arid area, the Karoo, South Africa.' *Scottish Geographical Journal* **126** (2), pp. 64-75.

Boardman J, Holmes PJ, Rhodes EJ, *et al.* 2005. 'Colluvial fan gravels, depositional environments and luminescence dating: A Karoo case study.' *South African Geographical Journal* **87** (1), pp. 73-79.

Boardman J, Parsons AJ, Holland R, *et al.* 2003. Development of badlands and gullies in the Sneeuberg, Great Karoo, South Africa. *Catena* **50** (2-4), pp. 165-184.

Boelhouwers JC and Meiklejohn KI. 2002. 'Quaternary periglacial and glacial geomorphology of southern Africa: review and synthesis.' *South African Journal of Science* **98** (1-2), pp. 47-55.

Bond G, Showers W, Cheseby M, *et al.* 1997. 'A pervasive millennial-scale cycle in North Atlantic Holocene and glacial climates.' *Science* **278** (5341), pp. 1257-1266.

Born SM and Ritter DF. 1970. ‘Modern terrace development near Pyramid Lak Nevada, and its geologic implications.’ *Geological Society of America Bulletin* **81** (4), pp. 1233-1242.

Botha GA. 1996. *The geology and palaeopedology of late Quaternary colluvial sediments in northern KwaZulu-Natal.* Memoir 83, Council for Geoscience, South Africa, pp. 165.

Botha GA and Fedoroff N. 1995. ‘Palaeosols in late Quaternary colluvium, northern KwaZulu-Natal, South Africa.’ *Journal of African Earth Sciences* **21** (2), pp. 291-311.

Botha GA, Wintle AG and Vogel JC. 1994. ‘Episodic late Quaternary palaeoguly erosion in northern KwaZulu-Natal, South Africa.’ *Catena* **23** (3-4), pp. 327-340.

Bøtter-Jensen L, Andersen CE, Duller GAT, *et al.* 2003. ‘Developments in radiation, stimulation and observation facilities in luminescence measurements.’ *Radiation Measurements* **37** (4-5), pp. 535-541.

Bousman CB, Partridge PC, Scott L, *et al.* 1988. ‘Palaeoenvironmental implications of late Pleistocene and Holocene valley fills in Blydefontein Basin, Noupoort, C.P. South Africa.’ *Palaeoecology of Africa* **19**, pp. 43-67.

Bracken LJ, Turnbull L, Wainwright J, *et al.* 2015. ‘Sediment connectivity: a framework for understanding sediment transfer at multiple scales.’ *Earth Surface Processes and Landforms* **40** (2), pp. 177-188.

Bridgland D and Westaway R. 2008. ‘Climatically controlled river terrace staircases: A worldwide Quaternary phenomenon.’ *Geomorphology* **98** (3-4), pp. 285-315.

Brierley GJ and Fryirs K. 1997. *River styles in Bega catchment: Implications for management*. Workshop and Field Days, October 1-3 1997. Macquarie University, pp. 24

Brierley GJ and Fryirs K. 1998. ‘A fluvial sediment budget for upper Wolumla Creek, south coast, New South Wales, Australia.’ *Australian Geographer* **29** (1), pp. 107-124.

Brierley GJ and Fryirs K. 1999. ‘Tributary-trunk stream relations in a cut and fill landscape: a case study from Wolumla catchment, New South Wales, Australia.’ *Geomorphology* **28** (1-2), pp. 61-73.

Brierley GJ and Mum CP. 1997. ‘European impacts on downstream sediment transfer and bank erosion in Cobargo catchment, New South Wales, Australia.’ *Catena* **31** (1-2), pp. 119-136.

Bryan K. 1940. ‘Erosion in the valleys of the southwest.’ *New Mexico Quarterly Review* **10**, pp. 227-232.

Bull LJ and Kirkby MJ. 1997. ‘Gully processes and modelling.’ *Progress in Physical Geography* **21** (3), pp. 354-374.

Bull WB.1964. *Geomorphology of segmented alluvial fans in western Fresno County, California*, Report Number 352E, pp. 85-129.

Bull WB. 1972. ‘Recognition of alluvial fan deposits in the stratigraphic record.’ In Hamblin WK and Rigby JK. (Eds). *Recognition of Ancient Sedimentary Environments. Society of Economic Palaeontologists and Mineralogists Special Publication* **16**, pp. 63-83.

Bull WB. 1990. ‘Stream-terrace genesis: implications for soil development.’ *Geomorphology* **3** (3-4), pp. 351-367.

Bull WB. 1991. *Geomorphic Responses to Climate Change.* Oxford University Press, New York, pp. 326.

Bull WB. 1997. ‘Discontinuous ephemeral streams.’ *Geomorphology* **19** (3-4), pp. 227-276.

Burke K and Gunnell Y. 2008. ‘The African Erosion Surface: a continental-Scale synthesis of geomorphology, gectonics, and environmental change over the past 180 million years.’ *GSA Memoirs* **201**, pp. 1-66.

Butzer KW. 1984b. ‘Late Quaternary environments in South Africa.’ In Vogel JC (Ed.). *Late Quaternary Palaeoclimates of the Southern Hemisphere.* Balkema, Rotterdam, pp. 235-264.

Butzer KW, Helgren DM, Fock GJ, *et al.* 1973. ‘Alluvial terraces of the lower Vaal River, South Africa: A reappraisal and reinvestigation.’ *The Journal of Geology* **81** (3), pp. 341-362.

Butzer KW, Stuckenrath R, Bruzewicz AJ, *et al.* 1978. ‘Late Cenozoic palaeoclimates of the Gaap Escarpment, Kalahari margin, South Africa.’ *Quaternary Research* **10** (3), pp. 310-339.

Calvet F and Julia R. 1983. ‘Pisoids in caliche profiles of Tarragona (NE Spain).’ In Peryt TM (Ed.). *Coated Grains.* Berlin, Ed. Springer, pp. 73-79.

Candy I. 2002. ‘Formation of a rhizogenic calcrete during a glacial stage (Oxygen Isotope Stage 12): its palaeoenvironmental stratigraphic significance.’ *Proceedings of the Geologists’ Association* **113** (3), pp. 259-270.

Candy I and Black S. 2009. ‘The timing of Quaternary calcrete development in semi-arid southeast Spain: investigating the role of climate on calcrete genesis.’ *Sedimentary Geology* **218** (1-4), pp. 6-15.

Candy I, Black S, Sellwood BW. 2005. ‘U-series isochron dating of immature and mature calacretes as a basis for constructing Quaternary landform chronologies for the Sorbas basin, southeast Spain.’ *Quaternary Research* **64** (1), pp. 100-111.

Cantuneanu O, Wopfner H, Eriksson PG, *et al.* 2005. ‘The Karoo basins of south-central Africa.’ *Journal of African Earth Sciences* **43** (1-3), pp. 211-253.

Chadwick OA, Nettleton WD and Staidl GJ. 1995. ‘Soil polygenesis as a function of Quaternary climate change, northern Great Basin.’ *Geoderma* **68** (1-2), pp. 1-26.

Chaney RC, Slonim SM, Slonim, SS. 1982. *Determination of Calcium Carbonate Content in Soils.* Construction collection, DOI: 10.1520/STP28907S

Chase BM, Boom A, Carr AS, *et al.* 2015. 'Evolving southwest African response to abrupt deglacial North Atlantic climate change events.' *Quaternary Science Reviews* **121**, pp. 132-136.

Chase BM, Boom A, Carr AS, *et al.* 2013. 'Holocene climate change in southernmost South Africa: rock hyrax middens record shifts in the southern westerlies.' *Quaternary Science Reviews* **82**, pp. 199-205.

Chase BM, Lim S, Chevalier M, *et al.* 2015. 'Influence of tropical easterlies in southern Africa's winter rainfall zone during the Holocene.' *Quaternary Science Reviews* **107**, pp. 138-148.

Chase BM and Meadows ME. 2007. 'Late Quaternary dynamics of southern Africa's winter rainfall zone.' *Earth Science Reviews* **84** (3-4), 103-138.

Chase BM, Scott L, Meadows CE, *et al.* 2012. 'Rock hyrax middens: A palaeoenvironmental archive for southern African drylands.' *Quaternary Science Reviews* **56**, pp. 107-125.

Cheetham MD, Bush, RT, Keene AF, *et al.* 2010. 'Nonsynchronous, episodic incision: Evidence of threshold exceedance and complex response as controls terrace formation.' *Geomorphology* **123** (3-4), pp. 320-329.

Chiverrell RC, Foster GC, Marshall P, *et al.* 2009. 'Coupling relationships: Hillslope-fluvial linkages in the Hodder catchment, NW England.' *Geomorphology* **109** (3-4), pp. 222-235.

Chiverrell RC, Harvey AM and Foster GC. 2007. 'Hillslope gullying in the Solway Firth — Morecambe Bay region, Great Britain: Responses to human impact and/or climatic deterioration?' *Geomorphology* **84** (3-4), pp. 317-343.

Chiverrell RC, Oldfield F, Appleby PG, *et al.* 2008. 'Evidence for changes in Holocene sediment flux in Semer Water and Raydale, North Yorkshire, UK.' *Geomorphology* **100** (1-2), pp. 70-82

Church M and Slaymaker O. 1989. 'Disequilibrium of Holocene sediment yield in glaciated British Columbia.' *Nature* **337** (6206), pp. 452-454.

Clarke ML, Vogel JC, Botha GA, *et al.* 2003. 'Late Quaternary hillslope evolution recorded in eastern South African colluvial badlands.' *Palaeogeography Palaeoclimatology Palaeoecology* **197** (3-4), pp. 199-212.

Cockcroft MJ, Wilkinson MJ and Tyson PD. 1987. 'The application of a present-day climatic model to the late Quaternary in southern Africa.' *Climatic Change* **10** (2), pp. 161-181.

Colarossi D, Duller GAT, Roberts S, *et al.* 2015. 'Comparison of paired quartz OSL and feldspar post-IR IRSL dose distributions in poorly bleached fluvial sediments from South Africa.' *Quaternary Geochronology* **30**, pp. 233-238.

Collinson JD. 1996. 'Chapter 3: Alluvial Sediments.' In: Reading, WG. (Ed.). *Sedimentary Environments: Processes, Facies and Stratigraphy, 3rd edition,* Wiley-Blackwell, Oxford.

Cooke RU and Reeves RW. 1976. *Arroyos and Environmental Change:* Oxford, Oxford University Press, pp. 213.

de Vente J, Poesen J, Arabkhedri M, *et al.* 2007. 'The sediment delivery problem revisited.' *Progress in Physical Geography* **31** (2), pp. 155-178.

Dearing JA (1994). *Environmental Magnetic Susceptibility.* Chi. Publ. Kenilworth, UK.

Dearing JA, Dann RJ, Hay K, *et al.* 1996. 'Frequency-dependent susceptibility measurements of environmental materials.' *Geophysical Journal International* **124** (1), pp. 228-240.

Decker JE, Niedermann S, de Wit M.J. 2011. 'Soil erosion rates in South Africa compared with cosmogenic 3 He-based rates of soil production.' *South African Journal of Geology* **114**, pp. 475–488.

Decker JE, Niedermann S, de Wit M.J. 2013. 'Climatically influenced denudation rates of the southern African plateau: Clues to solving a geomorphic paradox. *Geomorphology* **190**, pp. 48–60.

Dodge RE. 1902. 'Arroyo formation.' *Science* **15**, pp. 746.

Dollar ESJ. (1998). 'Palaeofluvial geomorphology in southern Africa: a review.' *Progress in Physical Geography* **22** (3), pp. 325-349.

Duller GAT. 2003. 'Distinguishing quartz and feldspar in single grain luminescence measurements.' *Radiation Measurements* **37** (2), pp. 161-165.

Duller GAT and Bøtter-Jensen L. 1993. 'Luminescence from potassium feldspars stimulated by infrared and green light.' *Radiation Protection Dosimetry* **47** (1-4), pp. 683-688.

Duller GAT, Bøtter-Jensen L and Poolton NRJ. 1995. 'Stimulation of mineral-specific luminescence from multi-mineral samples.' *Radiation Measurements* **24** (1), pp. 87-93.

Duncan RA, Hooper PR, Rehacek J, *et al.* 1997. 'The timing and duration of the Karoo igneous event, southern Gondwana.' *Journal of Geophysical Research: Solid Earth* **102** (B8), pp. 18127-18138.

Dupont LM and Wyputta U. 2003. 'Reconstructing pathways of aeolian pollen transport to the marine sediments along the coastline of SW Africa.' *Quaternary Science Reviews* **22** (2-4), pp. 157-174.

Ely LL. 1992. *Large floods in the southwestern United States in relation to late Holocene climatic variations.* PhD dissertation, University of Arizona, Tucson.

Ely LL and Baker VR. 1985. 'Reconstructing paleoflood hydrology with slackwater deposits- Verde River, Arizona.' *Physical Geography* **6** (2), pp. 103-126.

Erkens G, Dambeck R, Volleberg KP, *et al.* 2009. 'Fluvial terrace formation in the northern Upper Rhine Graben during the last 20,000 years as a result of allogenic controls and autogenic evolution.' *Geomorphology* **103** (3), pp. 476-495.

Erlanger E, Granger D and Gibbon R. 2012. 'Rock uplift rates in South Africa from isochron burial dating of fluvial and marine terraces.' *Journal of Geology* **40** (11), pp. 1019-1022.

Euler RC, Gumerman GJ, Karlstrom TNV, *et al.* 1979. 'The Colorado Plateaus: cultural dynamics and palaeoenvironment.' *Science* **205** (4411), pp. 1089-1101.

Evans ME and Heller F. 2003. *Environmental Magnetism: Principles and Applications of Enviromagnetics.* Academic Press. ISBN 0-12-243851-5.

Farmer EC, deMenocal PB and Marchitto TM. 2005. Holocene and deglacial ocean temperature variability in the Benguela upwelling region: Implications for low-latitude atmospheric circulation. *Palaeoceanography* **20** (PA2017), DOI: 10.1029/2004PA001049.

Fassbinder JWE and Stanjek H. 1994. Magnetic properties of biogenic soil greigite (Fe3S4). *Geophysical Research Letters* **21** (22), pp. 2349-2352.

Fedotov GN, Shein EV, Putlyaev VI, *et al.* 2007. Physiochemical bases of differences between the sedimentologic and laser-diffraction techniques of soil particle-size analysis. *Eurasian Soil Science* **40** (3), pp. 281-288.

Ferguson RI. 1981. Channel forms and channel changes. In Lewin J. (Ed.). *British Rivers.* Allen and Unwin, London, pp. 90-125.

Fisk HN. 1947. *Fine-grained alluvial deposits and their effects on the Mississippi River activity,* U.S. Corps of Engineers, Mississippi River Commissions, Vicksburg, Mississippi.

Folland CK, Parker D, Colman D, *et al.* 1998. 'Low frequency variability of worldwide ocean surface temperature in the historical record.' In: Navarra A. (Ed.). *Beyond El Nino: Decadal Variability in the Climate System,* Springer-Verlag, pp. 85-114.

Foster IDL, Boardman J and Keay-Bright J. 2007. 'Sediment tracing and environmental history for two small catchments, Karoo Uplands, South Africa,' *Geomorphology* **90** (1-2), pp. 126-143.

Foster IDL, Lees JA, Owens PN, *et al.* 1998. 'Mineral magnetic characterisation of sediment sources from an analysis of lake and floodplain sediments in the catchments of the Old Mil reservoir and Slapton Ley, South Devon, UK,' *Earth Surface Processes and Landforms* **23**, pp. 685-703.

Fryirs K 2013. '(Dis)Connectivity in catchment sediment cascades: a fresh look at the sediment delivery problem.' *Earth Surface Processes and Landforms* **38** (1) pp. 30-46.

Fryirs K and Brierley GJ. 1998. 'The character and age structure of valley fills in upper Wolumla Creek catchment, south coast, New South Wales, Australia.' *Earth Surface Processes and Landforms* **23** (3), pp. 271-287.

Fryirs K and Brierley GJ. 2000. 'A geomorphic approach to the identification of river recovery potential.' *Physical Geography* **21** (3), pp. 244-277.

Fryirs K and Brierley GJ. 2001. 'Variability in sediment delivery and storage along river courses in Bega catchment, NSW, Australia: implications for geomorphic river recovery. *Geomorphology* **38** (3-4), pp. 237-265.

Fryirs K, Brierley GJ, Preston NJ, *et al.* 2007. 'Buffers, barriers and blankets: The (dis)connectivity of catchment-scale sediment cascades.' *Catena* **70** (1), pp.49-67.

Fryirs K, Brierley GJ, Preston NJ, *et al.* 2007. 'Catchment-scale (dis)connectivity in sediment flux in the upper Hunter catchment, New South Wales, Australia. *Geomorphology* **84** (3-4), pp. 297-316.

Galbraith RF and Roberts RG. 2012. 'Statistical aspects of equivalent dose and error calculation and display in OSL dating: An overview and some recommendations,' *Quaternary Geochronology* **11**, pp. 1-27.

Gasse C, Chalié F, Vincens A, *et al.* 2008. 'Climatic patterns in equatorial and southern Africa from 30,000 to 10,000 years ago reconstructed from terrestrial and near-shore proxy data.' *Quaternary Science Reviews* **27**, pp. 2316-2340.

Gellis AC, Pavich MJ, Ellwein AL, *et al.* 2012. 'Erosion, storage and transport of sediment in two subbasins of the Rio Puerco, New Mexico.' *Geological Society of American Bulletin* **124** (5-6), pp. 817-841.

Gilbert GK. 1917. 'Hydraulic mining debris in the Sierra Nevada.' *Geological Survey Professional Paper* **105**, pp. 154.

Gil García MJ, Dorado Valiño M, Valdeolmillos Rodríguez A, *et al.* 2002. Late-glacial and Holocene palaeoclimatic record from Sierra de Cebllorea (northern Iberian range, Spain). *Quaternary International* **93-94**, pp. 13-18.

González-Amuchastegui MJ and Serrano E. 2013. Acumulaciones tobáceas y evolución del paisaje: cronología y fasas morfogenéticas en al Alto Ebro (Burgos). *Cuaternario Geomorfol.* **27**, pp. 9-32.

Graf WL. 1983. 'The arroyo problem – palaeohydrology and palaeohydraulics in the short term. In Gregory KJ (Ed.). *Background to palaeohydrology: a persective.* International geological correlation programme, Wiley, Chichester, pp. 279-302.

Graf WL. 1983. 'Variability of sediment removal in a semiarid watershed.' *Water Resources Research* **19** (3), pp. 643-652.

Grenfell MC, Ellery W and Grenfell SE. 2008. 'Tributary valley impoundment by trunk river floodplain development: a case study from the KwaZulu-Natal Drakesnberg foothills, eastern South Africa.' *Earth Surface Processes and Landforms* **33** (13), pp. 2029-2044.

Grenfell MC, Ellery W and Grenfell SE. 2009. 'Valley morphology and sediment cascades within a wetland system in the KwaZulu-Natal Drakensberg Foothills, Eastern South Africa. *Catena* **78** (1), pp. 20-35.

Grenfell SE, Grenfell MC, Rowntree KM, *et al.* 2014. 'Fluvial connectivity and climate: A comparison of channel pattern and process in two climatically contrasting fluvial sedimentary systems in South Africa,' *Geomorphology* **205**, pp. 142-154.

Grenfell SE, Rowntree KM and Grenfell MC. 2012. 'Morphodynamics of a guly and floodout system in the Sneeuberg Mountains of the semi-arid Karoo, South Africa: Implications for local landscape connectivity. *Catena* **89** (1), pp. 8-21.

Hack JT. 1942. 'The changing physical environment of the Hopi Indians of Arizona. *Peabody Museum of Natural History Papers* **35**, pp. 3-85.

Hadley RF. 1960. *Recent sedimentation and erosional history of Fivemile Creek, Fremont County, Wyoming.* Report Number 352A, pp. 16.

Hadley RF and Schumm SA. 1961. Sediment sources and drainage-basin characteristics in upper Cheyenne River basin. In: *Hydrology of the upper Cheyenne River basin*. U.S. Geological Survey Water-Supply Paper **1531-B**, pp. 137-198

Hanvey PM and Lewis CA. 1990. 'A preliminary report on the age and significance of Quaternary lacustrine deposits at Birnam, north-east Cape Province, South Africa.' *South African Journal of Science* **86**, pp. 271-273.

Hao Q, Oldfield F, Bloemendal J, *et al.* 2008a. 'The magnetic properties of loess and palaeosol samples from the Chinese Loess Plateau spanning the last 22 million years.' *Palaeogeography, Palaeoclimatology, Palaeoecology* **260** (3-4), pp. 389-404.

Hao Q, Oldfield F, Bloemendal J, *et al.* 2008b. 'Particle size separation and evidence for pedogenesis in samples from the Chinese Loess Plateau spanning the past 22 m.y.' *Geology* **36** (9), pp. 727-730.

Harden T, Macklin MG and Baker VR. 2010. 'Holocene flood histories in south-western USA.' *Earth Surface Processes and Landforms* **35** (6), pp. 707-716.

Harnois L. 1988. 'The CIW index: A new chemical index of weathering.' *Sedimentary Geology* **55** (3-4), pp. 319-322.

Harvey AM. 2001. 'Coupling between hillslopes and channels in upland fluvial systems: implications for landscape sensitivity, illustrated from the Howgill Fells, northwest England.' *Catena* **42** (2), pp. 225-250.

Harvey JE, Pederson JL and Rittenour TM. 2011. 'Exploring relations between arroyo cycles and canyon palaeoflood records in Buckskin Wash, Utah: Reconciling scientific paradigms.' *Geological Society of American Bulletin* **123** (11-12), pp. 2266-2276.

Hattingh J. 1996. 'Fluvial response to allocyclic influences during the development of the lower Sundays River, Eastern Cape, South Africa.' *Quaternary International* **33** (0), pp. 3-10.

Hattingh J and Goedhart ML. 1997. 'Neotectonic control on drainage evolution in the Algoa basin, southeastern Cape Province.' *South African Journal of Geology* **100** (1), pp. 43-52.

Hattingh J and Rust IC. 1999. Drainage evolution of the Sundays River, South Africa. In: Miller A and Gupta A. (Eds.). *Varieties in Fluvial Form:* Chichester: John Wiley and Sons, pp. 145-166.

Haynes CV. 1968a. 'Geochronology of late-Quaternary alluvium. In: Morrison RB and Wright HE. (Eds.). *Means of Correlation of Quaternary Successions.* University of Utah Press, Salt Lake City, pp. 591-631.

He F, Shakun JD, Clark PU, *et al.* 2013. 'Northern Hemisphere forcing of Southern Hemisphere climate during the last glaciation.' *Nature* **494** (7435), pp. 81-85.

Hereford R. 1986. 'Modern alluvial history of the Paria River drainage basin, southern Utah.' *Quaternary Research* **25** (3), pp. 293-311.

Hereford R. 2002. 'Valley-fill alluviation during the Little Ice Aage (ca. AD 1400-1880), Paria River basin and southern Colorado Plateau, United States.' *Geological Society of American Special Papers* **114** (12), pp. 1550-1563.

Hereford R, Jacoby GC and McCord VAS. 1996. 'Late Holocene alluvial geomorphology of the Virgin River in the Zion National Park area, southwest Utah.' *Geological Society of America Special Papers* **310**, pp. 1-41.

Hereford R and Webb R. 1992. 'Historic variation of warm-season rainfall, southern Colorado Plateau, southwestern USA.' *Climatic Change* **22** (3), pp. 239-256.

Hogg AG, Hua Q, Blackwell PG, *et al.* 2013. SHCal13 Southern Hemisphere Calibration, 0-50,000 Years cal BP. *Radiocarbon* **51** (4), pp. 1165-1176.

Holmes PJ, Boardman J, Parsons AJ, *et al.* 2003. 'Geomorphological palaeoenvironments of the Sneeuberg Range, Great Karoo, South Africa. *Journal of Quaternary Science* **18** (8), pp. 801-813.

Hooke J. 2003. 'Coarse sediment connectivity in river channel systems: a conceptual framework and methodology.' *Geomorphology* **56** (1-2), pp. 79-94.

Hooke J. 2004. Analysis of coarse sediment connectivity in a semiarid river channel. In: Golosov V, Belyaev V and Walling DE. (Eds). *Sediment Transfer through the Fluvial System, ICCE Moscow, August 2004* **288**, pp. 269-275. Wallingford International Association of the Hydrological Sciences.

Hooke J. 2007. 'Monitoring morphological and vegetation changes and flow events in dryland river channels.' *Environmental Monitoring and Assessment* **127** (1-3), pp. 445-457.

House PK. 1996. *Reports on applied palaeoflood hydrological investigations in western and central Arizona.* PhD dissertation, University of Arizona, Tucson, pp. 355.

Jacobs Z, Wintle AG and Duller GAT. 2006. 'Evaluation of SAR procedures for determination using single aliquots of quartz from two archaeological sites in South Africa.' *Radiation Measurements* **41** (5), pp. 520-533.

Jenny H. 1941. *Factors of Soil Formation.* McGraw-Hill, New York.

Johnson MR. 1976. *Stratigraphy and Sedimentology of the Cape and Karoo sequences in Eastern Cape Province.* Unpublished PhD thesis, Rhodes University, Grahamstown, pp. 366.

Jones LS, Rosenburg M, del Mar Figueroa M, *et al.* 2010. 'Holocene valley-floor deposition and incision in a small drainage basin in western Colorado, USA.' *Quaternary Research* **74** (2), pp. 199-206.

Karlstrom ET and Karlstrom TNV. 1987. 'Late Quaternary alluvial history of the American West: towards a process paradigm.' *Geology* **15** (1), pp. 88-89.

Keay-Bright J and Boardman J. 2009. 'Evidence from field-based studies of rates of soil erosion on degraded land in the central Karoo, South Africa.' *Geomorphology* **103** (3), pp. 455-465.

Keen-Zebert A, Tooth S, Rodnight H, *et al.* 2013. 'Late Quaternary floodplain reworking and the preservation of alluvial sedimentary archives in unconfined and confined river valleys in the eastern interior of South Africa.' *Geomorphology* **185** (0), pp. 54-66.

Kelly SB and Olsen H. 1993. 'Terminal fans – a review with reference to Devonian examples.' *Sedimentary Geology* **85** (1-4), pp. 339-374.

Kelly SD, Newville MG, Cheng L, *et al.* 2003. 'Uranyl incorporation in natural calcite.' *Environmental Science and Technology* **37** (7), pp. 1284-1287.

Kemp RA. 1985. 'The cause of redness in some buried and non-buried soils in eastern England.' *Journal of Soil Science* **36** (3), pp. 329-334.

Kemp RA. 1985. 'The decalcified Lower Loam at Swanscombe, Kent: a buried Quaternary soil.' *Proceedings of the Geologists' Association* **96**, (4), pp. 343-355.

Kemp RA. 1995. 'Distribution and genesis of calcitic pedofeatures within a rapidly aggrading loess-palaeosol sequence in China.' *Geoderma* **65** (3-4), pp. 303-316.

Klappa CF. 1980. 'Brecciation textures and tepee structures in Quaternary calcrete (caliche) profiles from eastern Spain: the plant factor in their formation.' *Geological Journal* **15** (2), pp. 81-89.

Knighton AD. 1998. *Fluvial Forms and Processes: A New Perspective.* Hodder Arnold, London.

Knighton AD. 1989. 'River adjustment to changes in sediment load: the effects of tin mining on the Ringarooma River, Tasmania, 1875-1984.' *Earth Surface Processes and Landforms* **14** (4), pp. 333-359.

Knox JC. 1972. 'Valley alluviation in southwestern Wisconsin.' *Annals of the Association of American Geographers* **62** (3), pp. 401-410.

Knox JC. 1993. 'Large increases in flood magnitude in response to modest changes in climate.' *Nature* **361** (6411), pp. 430-432.

Kochel RC and Baker VR. 1982. 'Palaeoflood hydrology.' *Science* **215** (4531), pp. 353-361.

Kochel RC and Baker VR. 1988. 'Palaeoflood analysis using slackwater deposits. In: Baker VR (Ed.). *Flood Geomorphology.* Wiley-Interscience, pp. 357-376.

Korom SF. 2000. ‘An adsorption isotherm for bromide.’ *Water Resources Research’* **36** (7), pp. 1969-1974.

Lancaster IN. 1979. ‘Quaternary environments of the arid zone of Southern Africa.’ Department of Geography and Environmental Studies *Occasional Paper*, **22**, pp. 77.

Lee-Thorpe JA and Beaumont PB. 1995. ‘Vegetation and seasonality shifts during the late Quaternary deduced from $^{13}C/^{12}C$ ratios of grazers at Equus Cave, South Africa.’ *Quaternary Research* **43**, pp. 426-433.

Le Roux FG. 1989. *The lithostratigraphy of Cenozoic deposits along the southeast Cape coast as related to sea level changes.* Unpublished MSc thesis, University of Stellenbosch, pp. 247.

Leopold LB. 1976. ‘Reversal of the erosion cycle and climatic change.’ *Quaternary Research* **6**, pp. 557-562.

Leopold LB. 1992. Sediment size that determines channel morphology. In: Billi P, Hey RD, Thorne CR, *et al.* (Eds.). *Dynamics of Gravel-bed Rivers* John Wiley and Sons Ltd, Chichester, pp. 297-311.

Leopold LB, Miller JP. 1954. ‘A postglacial chronology for some alluvial valleys in Wyoming.’ *US Geological Survey Water-Supply Paper* **1261**, pp. 90.

Leopold LB, Wolman MG and Miller JP. 1964. *Fluvial Processes in Geomorphology.* W.H. Freeman and Company, San Francisco, CA, pp. 522.

Lewin J and Macklin MG. 2003. ‘Preservatgion potential for late Quaternary river alluvium.’ *Journal of Quaternary Science* **18** (2), pp. 107-120.

Lewis CA. 1999. *Field Guide to the Quaternary in the Eastern and Southern Cape, South Africa.* Rhodes University, Grahamstown, pp. 79.

Lewis CA. 2005. ‘Late Glacial and Holocene palaeoclimatology of the Drakensberg of the Eastern Cape, South Africa.’ *Quaternary International* **129**, pp. 33-48.

Lewis CA. 2008. ‘Late Quaternary climatic changes, and associated human responses, during the last similar to 45000 yr in the Eastern and adjoining Western Cape, South Africa.’ *Earth Science Reviews* **88** (3-4), pp. 167-187.

Lewis CA. 2011. Late Quaternary environmental phases in the Eastern Cape and adjacent Plettenberg Bay-Knysna region and Little Karoo, South Africa. *Proceedings of the Geologists Association* **122** (1), pp. 187-200.

Lewkowicz, AG. 1987a. Headwall retreat of ground-ice slumps, Banks Island, Northwest Territories. *Canadian Journal of Earth Sciences* **24**, pp. 1077-1085.

Lewkowicz AG. 1987b. ‘Nature and importance of thermokast processes, Sand Hills moraine, Banks Island, Canada. *Geografiska Annaler* **69A**, pp. 321-327.

Lindquist AK, Feinberg JM and Waters MR. 2011. ‘Rock magnetic properties of a soil developed on an alluvial deposit at Buttermilk Creek, Texas, USA.’ *Geochemistry, Geophysics, Geosystems* **12** (12), pp. 1-11.

Liu Q, Roberts AP, Torrent J, *et al.* 2007. 'What do the HIRM and S-ratio really measure in environmental magnetism?' *Geochemistry, Geophysics, Geosystems* **8** (9), pp. 1-10.

Liu Q, Sun Y, Qiang X, *et al.* 2015. 'Characterising magnetic mineral assemblages of surface sediments from major Asian dust sources and implications for the Chinese loess magnetism.' *Earth, Planets and Space* **67** (1), pp. 1-17.

Love DW. 1977. *Dynamics of sedimentation and geomorphic history of Chaco Canyon National Monument, New Mexico.* New Mexico Geological Society, Guidebook to 28th Field Conference, pp. 291-300.

Lyons R, Oldfield F and Williams E. 2010. 'Mineral magnetic properties of surface soils and sands across four North African transects and links to climatic gradients. *Geochemistry, Geophysics, Geosystems* **11** (8), pp. 1-22.

Lyons R, Tooth S and Duller GA. 2013. 'Chronology and controls of donga (gully) formation in the upper Blood River catchment, KwaZulu-Natal, South Africa: Evidence for a climatic driver of erosion.' *The Holocene* **23** (12), pp. 1875-1887.

Lyons R, Tooth S and Duller GA. 2014. 'Late Quaternary climatic changes revealed by luminescence dating, mineral magnetism and diffuse reflectance spectroscopy of river terrace palaeosols: a new form of geoproxy data for the southern African interior.' *Quaternary Science Reviews* **95**, pp. 43-59.

Machette MN. 1985. 'Calcic soils of the southwestern United States.' *Geological Society of America Special Papers* **203**, pp.1-22.

Macklin MG, Fuller IC, Lewin J, *et al.* 2002. Correlation of fluvial sequences in the Mediterranean basin over the last 200 ka and their relationship to climate change. *Quaternary Science Reviews* **21**, pp. 1633-1641.

Macklin MG, Lewin J and Woodward, JC. 2012. The fluvial record of climate change. *Philosophical Transactions of the Royal Society* **370**, pp. 2143-2172.

Maher BA. 1986. 'Characterisation of soils by mineral magnetic measurements.' *Physics of the Earth and Planetary Interiors* **42**, (1-2), pp. 76-92.

Maher BA. 1988. 'Magnetic properties of some synthetic sub-micron magnetites.' *Geophysical Journal International* **94** (1), pp. 83-96.

Maher BA. 2011. 'The magnetic properties of Quaternary aeolian dusts and sediments, and their palaeoclimatic significance. *Aeolian Research* **3** (2), pp. 87-144.

Maher BA and Taylor RM. 1989. 'Origin of soil magnetite.' *Nature* **340** (6229), pp. 106-106.

Manjoro M, Rowntree K, Kakembo V, *et al.* 2012. 'Gully fan morphodynamics in a small catchment in the Eastern Cape, South Africa.' *Land Degradation and Development* **23** (6), pp. 569-576.

Marker ME. 1995. 'Late Quaternary environmental implications from sedimentary sequences at 2 high-altitude Lesotho sites.' *South African Journal of Science* **91** (6), pp. 294-298.

Marriott SB and Wright VP. 1993. ‘Palaeosols as indicators of geomorphic stability in two Old Red Sandstone alluvial suites, South Wales.’ *Journal of the Geological Society* **150** (6), pp.1109-1120.

Maud, RR. 1996. The macro-geomorphology of the Eastern Cape. In: Lewis, CA (Ed.): *The Geomorphology of the Eastern Cape, South Africa*. Grahamstown, South Africa, pp. 1-18.

McFadden LD and McAuliffe JR. 1997. ‘Lithologicall influenced geomorphic responses to Holocene climatic changesi n the Southern Colorado Plateau, Arizona: A soil-geomorphic and ecologic perspective.’ *Geomorphology* **19** (3-4), pp. 303-332.

McGowan JH and Garner LE. 1970. ‘Physiographic features and stratification types of coarse-grained pointbars: modern and ancient examples.’ *Sedimentology* **14** (1-2), pp. 77-111.

McKeever SWS, Bøtter-Jensen L, Agersnap Larsen N, *et al.* 1997. ‘Temperature dependence of OSL decay curves: Experimental and theoretical aspects.’ *Radiation Measurements* **27** (2), pp. 161-170.

McManus JF, Francois R, Gherardi JM, *et al.* 2004. ‘Collaspe and rapid resumption of Atlantic meridional circulation linked to deglacial climate changes.’ *Nature* **428** (6985), pp. 834-837.

McManus JF, Oppo DW, Cullen JL. 1999. ‘0.5 million years of millennial scale climate variability in the North Atlantic. *Science* **283**, 971-975.

Meade RH. 1982. ’Sources, sinks and storage of river sediment in the Atlantic drainage of the United States.’ *The Journal of Geology* **90** (3), pp. 235-252.

Merritts DJ, Vincent KR and Wohl EE. 1994. ‘Long river profiles, tectonism, and eustasy: A guide to interpreting fluvial terraces.’ *Journal of Geophysical Research: Solid Earth* **99** (B7), pp. 14031-14050.

Murray AS and Wintle AG. 2000. ‘Luminescence dating of quartz using an improved single-aliquot regenerative-dose protocol.’ *Radiation Measurements* **32** (1), pp. 57-73.

Neal C, Neal M, Hughes S, *et al.* 2007. ‘Bromine and bromide in rainfall, cloud, stream and groundwater in the Plynlimon area of mid-Wales.’ *Hydrology and Earth System Sciences* **11** (1), pp. 301-312.

Nesbitt HW and Young GM. 1982. ‘Early Proterozoic climates and plate motions inferred from major element chemistry of lutites. *Nature* **299** (5885), pp. 715-717.

Neville D. 1996. *European impacts on the Seacow River Valley and its Hunter-Gatherer inhabitants, AD 1770-1990.* Unpublished MA dissertation, University of Cape Town. Part 1: pp. 281. Part 2: pp.63.

Neuumann ER, Svensen H, Galerne CY *et al.* 2011. ‘Multistage evolution of dolerites in the Karoo large igneous province, central South Africa. *Journal of Petrology* **52** (5), pp. 959-984.

Nicholas AP, Ashworth, PJ, Kirkby MJ, *et al.* 1995. 'Sediment slugs: Large-scale fluctuations in fluvial sediment transport rates and storage volumes.' *Progress in Physical Geography* **19** (4), pp. 500-519.

Nichols GJ and Fisher JA. 2007. 'Processes, facies and architecture of fluvial distributary system deposits.' *Sedimentary Geology* **195** (1-2), pp. 75-90.

Nicholson SE, Nash DJ, Chase BM, *et al.* 2013. 'Temperature variability over Africa over the last 2000 years. *The Holocene* **23**, pp. 1085-1094.

O'Connor JE, Ely LL, Wohl EE, *et al.* 1994. 'A 4500-year record of large floods on the Colorado River in the Grand Canyon, Arizona.' *The Journal of Geology* **102** (1), pp. 1-9.

Oldfield F. 1991. 'Environmental magnetism – a personal perspective.' *Quaternary Science Reviews* **10** (1), pp. 73-85.

Oldfield F. 1994. 'Toward the discrimination of fine-grained ferrimagnets by magnetic measurements in lake and near-shore marine sediments.' *Journal of Geophysical ResearchL Solid Earth* **99** (B5), pp. 9045-9050.

Oldfield F and Crowther J. 2007. 'Establishing fire incidence in temperate soils using magnetic measurements.' *Palaeogeography, Palaeoclimatology, Palaeoecology* **249** (3-4), pp. 362-369.

Oldfield F, Hao Q, Bloemendal J, *et al.* 2009. 'Links between bulk sediment particle size and magnetic grain-size: general observations and implications for Chinese loess studies.' *Sedimentology* **56** (7), pp. 2091-2106.

Oldfield F and Yu L. 1994. ' The influence of particle size variations on the magnetic properties of sediments from the north-eastern Irish Sea.' *Sedimentology* **41** (6), pp. 1093-1108.

Otto JC, Schrott L, Jaboyedoff M, *et al.* 2009. 'Quantifying sediment storage in a high alpine valley (Turtmanntal, Switzerland).' *Earth Surface Processes and Landforms* **34** (13), pp. 1726-1742.

Owens PN, Batalla RJ, Collins AJ, *et al.* 2005. 'Fine-grained sediment in river systems: Environmental significance and management issues.' *River Research and Applications* **21** (7), pp. 693-717.

Parkash B, Awasthi AR and Gohain K. 1983. Lithofacies of Markanda terminal fan, Kurukshetra district, Haryana, India. In: Collinson JD and Lewin J (Eds.). *Modern and Ancient Fluvial Systems:* IAS Special Publication **6**, pp. 337-345.

Partridge TC, Demenocal PB, Lorentz SA, *et al.* 1997. 'Orbital forcing of climate over South Africa: A 200,000-year rainfall record from the Pretoria Saltpan.' *Quaternary Science Reviews* **16** (10), pp. 1125-1133.

Partridge TC and Maud RR. 1987. Geomorphic evolution of southern Africa since the Mesozoic. *South African Journal of Geology* **90**, pp. 179-208.

Patton PC, Baker VR and Kochel RC. 1979. Slackwater deposits – a geomorphic technique for the interpretation of fluvial palaeohydrology. In: Rhodes DD and

Williams GP (Eds.). *Adjustments of the Fluvial System.* Dubuque, Iowa, Kendall-hunt, pp. 225-252.

Patton PC and Boison PJ. 1986. 'Processes and rates of formation of Holocene alluvial terraces in Harris Wash, Escalante River basin, south-central Utah.' *Geological Society of America Bulletin* **97** (3), pp. 369-378.

Patton PC and Schumm SA. 1975. 'Gully erosion, northwestern Colorado: a threshold phenomenon.' *Geology* **3** (2), pp. 88-90.

Patton PC and Schumm SA. 1981. 'Ephemeral-stream processes: implications for studies of Quaternary valley fills.' *Quaternary Research* **15** (1), pp. 24-43.

Pelletier JD, Quade J, Goble RJ, *et al.* 2011. 'Widespread hillslope gullying on the southeastern Tibetan Plateau: Human or climate-change induced?' *Geological Society of America Bulletin* **123** (9-10), pp. 1926-1938.

Petit TR, Jouzel D, Raynaud NI, *et al.* 1999. 'Climate and atmospheric history of the past 420,000 years from the Vostok ice core, Antarctica.' *Nature* **399**, pp. 429-436.

Phillips JD. 2014a. 'State transitions in geomorphic responses to environmental change.' *Geomorphology* **204**, pp. 208-216.

Phillips JD. 2014b. 'Thresholds, mode switching, and emergent equilibrium in geomorphic systems.' *Earth Surface Processes and Landforms* **39** (1), pp. 71-79.

Prosser IP and Winchester SJ. 1996. 'History and processes of gully initiation and development in eastern Australia. *Zeitschrift fur Geomorphologie Supplementband* **105**, pp. 91–109.

Prosser IP. 1991. 'A comparison of past and present episodes of gully erosion at Wangrah Creek, southern Tablelands, New South Wales.' *Australian Geographical Studies* **29** (1), pp. 139-154.

Pulley S and Rowntree K. 2016. 'The use of an ordinary colour scanner to fingerprint sediment sources in the South African Karoo.' *Journal of Environmental Management* **165**, pp. 253-262.

Rasbury ET, Meyers WJ, Hanson GN, *et al.* 2000. 'Relationship of uranium to petrography of caliche palaeosols with application to precisely dating the time of sedimentation.' *Journal of Sedimentary Research* **70** (3), pp. 604-618.

Reason CJC, Landman W and Tennant W. 2006. 'Seasonal to decadal prediction of southern African climate and its links with variability of the Atlantic Ocean.' *Bulletin of the American Meteorological Society* **87** (7), pp. 941-955.

Reid SC, Lane SN, Berney JM, *et al.* 2007. 'The timing and magnitude of coarse sediment transport events within an upland, temperate gravel-bed river.' *Geomorphology* **83** (1-2), pp. 152-182.

Renaut RW. 1993. 'Zeolitic diagenesis of late Quaternary fluviolacustrine sediments and associated calcrete formation in the Lake Bogoria Basin, Kenya Rift Valley.' *Sedimentology* **40**, pp. 271-301.

Rienks SM, Botha GA and Hughes JC. 2000. 'Some physical and chemical properties of sediments exposed in a gully (donga) in northern KwaZulu-Natal, South Africa and their relationship to the erodibility of the colluvial layers.' *Catena* **39** (1), pp. 11-31.

Rinaldo A, Dietrich WE, Rigon R, *et al.* 1995. 'Geomorphological signatures of varying climate.' *Nature* **374** (6523), pp. 632-635.

Roberts HM. 2007. 'Assessing the effectiveness of the double-SAR protocol in isolating a luminescence signal dominated by quartz.' *Radiation Measurements* **42** (10), pp. 1627-1636.

Roberts AP and Turner GM. 1993. 'Diagenetic formation of ferrimagnetic iron sulphide minerals in rapidly deposited marine sediments, South Island, New Zealand.' *Earth and Planetary Science Letters* **115**, pp. 257-273.

Roberts HM and Wintle AG. 2001. 'Equivalent dose determinations for polymineralic fine-grains using the SAR protocol: application to a Holocene sequence of the Chinese Loess Plateau.' *Quaternary Science Reviews* **20** (5-9), pp. 859-863.

Rodnight H, Duller GAT, Wintle AG and Tooth S. 2006. 'Assessing the reproducibility and accuracy of optical dating of fluvial deposits.' *Quaternary Geochronology* **1** (2), pp. 109-120.

Rose J, Candy I, Lee JR. 2000. Leet Hill (TM 384926): Pre-glacial and glaciofluvial river deposits – with possible evidence for a major glaciation prior to the deposition of the Lowestoft Till. In: Lewis SG, Whiteman CA and Preece RC. (Eds.). *The Quaternary of Norfolk and Suffolk.* Quaternary Research Association, London, pp. 297-301.

Rowntree K. 2014. 'The evil of sluits: A re-assessment of soil erosion in the Karoo of South Africa as portrayed in century-old sources.' *Journal of Environmental Management* **130**, pp. 98-105.

Rowntree K, Duma M, Kakembo V, *et al.* 2004. 'Debunking the myth of overgrazing and soil erosion.' *Land Degradation and Development* **15** (3), pp. 203-214.

Rowntree K and Foster I. 2012. 'A reconstruction of historical changes in sediment sources, sediment transfer and sediment yield in a small, semi-arid Karoo catchment, South Africa.' *Zeitschrift fur Geomorphologies* **56**, pp. 87-100.

Sadler SP and Kelly SB. 1993. 'Fluvial processes and cyclicity in terminal fan deposits: an example from the Late Devonian of southwest Ireland.' *Sedimentary Geology* **85** (1), pp. 375-386.

Sandercock PJ and Hooke J. 2011. 'Vegetation effects on sediment connectivity and processes in an ephemeral channel in SE Spain.' *Journal of Arid Environments* **75** (3), pp. 239-254.

Sandercock PJ, Hooke J and Mant JM. 2007. 'Vegetation in dryland river channels and its interaction with fluvial processes.' *Progress in Physical Geography* **31** (2), pp. 107-129.

Schultz BR. 1980. *Climate of South Africa, Part 9, General Survey.* Weather Bureau, Department of Transport, Pretoria.

Schumm SA. 1973. 'Geomorphic thresholds and complex response of drainage systems. *Fluvial Geomorphology* **6**, pp. 69-85.

Schumm SA. 1977. *The Fluvial System*. Wiley, New York, pp. 338.

Schumm SA. 1979. 'Geomorphic thresholds: the concept and its applications.' *Transactions of the Institute of British Geographers* **4** (4), pp. 485-515.

Schumm SA and Hadley RF. 1957. 'Arroyos and the semiarid cycle of erosion.' *American Journal of Science* **255** (3), pp. 161-174.

Schumm SA and Parker RS. 1973. 'Implications of complex response of drainage systems for Quaternary alluvial stratigraphy. *Nature* **243**, pp. 99-100.

Schwertmann U and Taylor RM. 1989. Iron oxides. In: Dixon JB and Weed SB. (Eds.). *Minerals in Soil Environments, 2nd edition.* Soil Society of America, Madison, WI, pp. 379-438.

Scott L. 1989. 'Climatic conditions in southern Africa since the last glacial maximum, inferred from pollen analysis.' *Palaeogeography, Palaeoclimatology, Palaeoecology* **70**, pp. 345-353.

Scott L, Holmgren K and Partridge TC. 2008. 'Reconciliation of vegetation and climatic interpretations of pollen profiles and other regional records from the last 60 thousand years in the Savanna Biome of Southern Africa. *Palaeogeography, Palaeoclimatology, Palaeoecology* **257**, pp. 198-206.

Scott L, Marais E and Brook G. 2004. 'Fossil hyrax dung and evidence of Late Pleistocene and Holocene vegetation types in the Namib Desert.' *Journal of Quaternary Science* **19**, pp. 829-832.

Sharp RP and Nobles LH. 1953. 'Mudflow of 1941 at Wrightwood southern California.' *Geological Society of America Bulletin* **64** (5), pp. 547-560.

Shen Z, Bloemendal J, Mauz B, *et al.* 2008. 'Holocene environmental reconstruction of sediment-source linkages at Crummock Water, English Lake District, based on magnetic measurements.' *The Holocene* **18** (1), pp. 129-140.

Shen Z, Mauz B, Lang A, *et al.* 2007. 'Optical dating of Holocene lake sediments: Elimination of the feldspar component in fine silt quartz samples.' *Quaternary Geochronology* **2** (1-4), pp. 150-154.

Shi N, Schneider R, Beug, HJ, *et al.* 2001. 'Southeast trade wind variations during the last 135 kyr: evidence from pollen spectra in eastern South Atlantic sediments.' *Earth and Planetary Science Letters* **187**, pp. 311-321.

Skead CJ. 2007. Historical incidence of the larger land mammals in the Broader Eastern Cape, second edition. In: Boshoff A, Kerley G, Lloyd P. (Eds.). *Centre for African Conservation Ecology*, Nelson Mandela Metropolitan University, Port Elizabeth, South Africa.

Soria-Jáuregui A, González-Amuchastegui MJ, Mauz B, *et al.* 2016. Dynamics of Mediterranean late Quaternary fluvial activity: An example from the River Ebro (north Iberian Peninsula). *Geomorphology* **268**, pp. 110-122.

Stone A. 2014. 'Last Glacial Maximum conditions in southern Africa: Are we any closer to understanding the climate of this period?' *Progress in Physical Geography* **38** (5), pp. 519-542.

Stutt, JBW, Crosta X, van der Borg K, *et al.* 2002. 'Relationship between Antarctic sea ice and southwest African climate during the late Quaternary.' *Journal of Geology* **32** (10), pp. 909-912.

Sugden JM. 1989. *Palaeoecology of the central and marginal uplands of the Karoo, South Africa.* University of Cape Town, Cape Town, pp. 384.

Sundborg Å. 1956. 'The River Klarälven: A study of fluvial processes.' *Geografiska Annaler* **38** (2), pp. 125-237.

Tankard AJ, Jackson M, Eriksson KA, *et al.* 1982. Crustal Evolution of Southern Africa: 3.8 Billion Years of Earth History. Springer-Verlag, Berlin, pp. 523.

Temme A, Baartman JEM, Botha GA, *et al.* 2008. 'Climatic controls on late Pleistocene landscape evolution of the Okhombe valley, KwaZulu-Natal, South Africa. *Geomorphology* **99** (1-4), pp. 280-295.

Thomas DS, Holmes PJ, Bateman MD, *et al.* 2002. 'Geomorphic evidence for late Quaternary environmental change from the eastern Great Karoo margin, South Africa.' *Quaternary International* **89**, pp. 151-164.

Thomas MF. 2001. 'Landscape sensitivity in time and space – an introduction.' *Catena* **42** (2-4), pp. 83-98.

Thompson R and Oldfield F. 1986. *Environmental Magnetism.* Allen and Unwin, London.

Thornthwaite CW, Sharpe CFS and Dosch EF. 1942. *Climate and accelerated erosion in the arid and semi-arid southwest, with special reference to the Polacca Wash drainage basin, Arizona.* Technical Bulletin 808. Washington: U.S. Department of Agriculture.

Tooth S. 1999. Floodouts in central Australia. In: Miller AJ and Gupta A. (Eds.). *Varieties in Fluvial Form*. Wiley, Chichester, pp. 219-247.

Tooth S. 2000. 'Downstream changes in dryland river channels: the Northern Plains of arid central Australia.' *Geomorphology* **34** (1-2), pp. 33-54.

Tooth S, Brandt D, Hancox PJ, *et al.* 2004. 'Geological controls on alluvial river behaviour: a comparative study of three rivers on the South African Highveld.' *Journal of African Earth Sciences* **38** (1), pp. 79-97.

Tooth S, Rodnight H, Duller GAT, *et al.* 2007. 'Chronology and controls of avulsion along a mixed bedrock-alluvial river.' *Geological Society of American Bulletin* **119** (3-4), pp. 452-461.

Trimble SW. 1983. ‘A sediment budget for Coon Creek Basin in the Driftless Area, Wisconsin.’ *American Journal of Science* **283**, pp. 454-474.

Truelsen JL and Wallinga J. 2003. ‘Zeroing of the OSL signal as a function of grain size: investigating bleaching of thermal transfer for a young fluvial sample.’ *Geochronometria* **22**, pp. 1-8.

Tucker ME. 2011. *Sedimentary Rocks in the Field: A Practical Guide. Fourth Edition.* Wiley-Blackwell, Oxford.

Turner BR. 1978. Sedimentary patterns of uranium mineralisation in the Beaufort Group of the southern Karoo (Gondwana) Basin, South Africa. In: Miall AD. (Ed.). *Fluvial Sedimentology, Canadian Association of Petroleum Geologists,* Memoir **5**, pp. 831-848.

Tyson PD. 1986. *Climatic Change and Variability in Southern Africa*. Oxford University Press, Cape Town.

Tyson PD, Odada EO and Partridge TC. 2001. ‘Late Quaternary environmental change in southern Africa.’ *South African Journal of Science* **97** (3), pp. 139-150.

van der Post KD, Oldfield F, Haworth EY, *et al.* 1997. ‘A record of accelerated erosion in the recent sediments of Blelham Tarn in the English Lake District. *Journal of Palaeolimnology* **18**, pp. 103-120.

van Zinderen Bakker EM. 1969a. The Pleistocene vegetation and climate of the Basin. In: JD Clark. (Ed.). *Kalambo Falls prehistoric site*. Cambridge: University Press, pp. 57-84.

van Zinderen Bakker EM. 1976. ‘The evolution of Late Quaternary palaeoclimates of Southern Africa.’ *Palaeoecology of Africa* **9**, pp. 160-202.

Varnes DJ. 1978. Slope movement types and processes. In: Schuster RL and Krizek RJ. (Eds.). *Landslides – Analysis and Control.* National Research Council, Washington DC, Transportation Research Board, Special Report **176**, pp. 11-33.

Vis, GJ, Bohncke SJP, Schneider H, *et al.* 2010. ‘Holocene flooding history of the Lower Tagus Valley (Portugal).’ *Journal of Quaternary Science* **25** (8), pp. 1222-1238.

Vita-Finzi C. 1969. *The Mediterranean Valleys.* Cambridge University Press, London, pp. 91.

Walden J and Ballantyne CK. 2002. ‘Use of environmental magnetic measurements to validate the vertical extent of ice masses at the Last Glacial Maximum.’ *Journal of Quaternary Science* **17** (3), pp. 193-200.

Wang Y, Yu Z, Li G, *et al.* 2009. ‘Discrimination in magnetic properties of different-sized sediments from the Changjiang and Huanghe Estuaries of China and its implication for provenance of sediment on the shelf. *Marine Geology* **260** (1-4), pp. 121-129.

Walden J, Smith JP and Oldfield F. 1999. *Environmental magnetism, a practical guide.* Quaternary Research Association. Technical Guide, pp. 243.

Walling DE. 1983. 'The sediment delivery problem.' *Journal of Hydrology* **65**, pp. 209-237.

Warner RF. 1972. 'River terrace types in the coastal valleys of New South Wales.' *Australian Geographer* **12** (1), pp. 1-22.

Waters MR and Haynes CV. 2001. 'Late Quaternary arroyo formation and climate change in the American Southwest.' *Geology* **29** (5), pp. 399-402.

Webb RH. 1985. *Late Holocene flooding in the Escalante River, south-central Utah.* PhD dissertation, University of Arizona. Tucson, pp. 204.

Webb RH, Blainey JB and Hyndman DW. 2002. Paleoflood Hydrology of the Paria River, Southern Utah and Northern Arizona, USA. In: House PK, Webb VR and Levish DR. (Eds.). *Ancient Floods, Modern Hazards*, American Geophysical Union, WashingtonDC, doi: 10.1029/WS005p0295.

Webb RH, Smith SS and McCord VAS. 1991. 'Historic channel change of Kanab Creek, southern Utah and northern Arizona.' *Grand Canyon Natural History Association Monograph Number* **9**, pp. 91.

Wehmueller WA, Ransom MD and Nettleton WD. 1993. Micromorphology of polygenetic soils in a small watershed, north central Kansas, USA. In: Ringrose-Voase AJ and Humphreys GS. (Eds.). *Developments in Soil Science* **22**, Elsevier, pp. 247-255.

Wentworth CK. 1922. 'A scale of grade and class terms for clastic sediments.' *Journal of Geology* **30**, pp. 377-392.

Westaway R. 2002a. 'Long-term river terrace sequences: evidence for global increases in surface uplift rates in the Late Pliocene and early Middle Pleistocene caused by flow in the lower continental crust induced by surface processes.' *Geologie en Mijnbouw/Netherlands Journal of Geosciences* **81**, pp. 305–328.

Williams M. 1992. 'Evidence for the dissolution of magnetite in recent Scottish peats.' *Quaternary Research* **37** (2), pp. 171-182.

Wintle AG. 1975. 'Thermal quenching of thermoluminescence in quartz.' *Geophysical Journal of the Royal Astronomical Society* **41** (1), pp. 107-113.

Wintle AG, Botha GA, Li SH, *et al.* 1995. 'A chronological framework for colluviation during the last 100 kyr in KwaZulu-Natal.' *South African Journal of Science* **91** (3), pp. 134-139.

Womack WR and Schumm SA. 1977. 'Terraces of Douglas Creek, northwestern Colorado: An example of episodic erosion.' *Geology* **5** (2), pp. 72-76.

Woodward JC, Hamlin RHB, Macklin MG, *et al.* 2008. Glacial activity and catchment dynamics in northwest Greece: Long-term river behaviour and the slackwater sediment record for the last glacial to interglacial transition. *Geomorphology* **101**, pp. 44-67.

Wright VP. 1990. ‘Estimating rates of calcrete formation and sediment accretion in ancient alluvial deposits.’ *Geological Magazine* **127** (3), pp. 273-276.

Wright VP, Platt NH, Marriott SB, *et al.* 1995. ‘A classification of rhizogenic (root-formed) calcretes, with examples from the Upper Jurassic-Lower Cretaecous of Spain and Upper Cretaceous of souithern France.’ *Sedimentary Geology* **100** (1-4), pp. 143-158.

Wright VP, Platt NH and Wimbledon WA. 1988. ‘Biogenic laminar calcretes: evidence of calcified root-mat horizons in paleosols.’ *Sedimentology* **35** (4), pp. 603-620.

Yaalon DH. 1997. ‘Soils in the Mediterranean region: what makes them different?’ *Catena* **28** (3-4), pp. 157-169.

Yamada Y. 1968. ‘Occurrence of bromine in plants and soil.’ *Talanta* **15** (11), pp. 1135-1141.

Young RW and Nanson GC. 1982. ‘Terrace formation in the Illawarra region of New South Wales.’ *Australian Geographer* **15** (4), pp. 212-219.

Yu L and Oldfield F. 1989. ‘A multivariate mixing model for identifying sediment source from magnetic measurements.’ *Quaternary Research* **32** (2), pp. 168-181.

Zhang W, Xing Y, Yu L, *et al.* 2008. ‘Distinguishing sediments from the Yangtze and Yellow rivers, China: a mineral magnetic approach.’ *The Holocene* **18** (7), pp. 1139-1145.

Zheng H, Oldfield F, Yu L, *et al.* 1991. ‘The magnetic properties of particle-sized samples from the Luo Chuan loess section: evidence for pedogenesis.’ *Physics of the Earth and Planetary Interiors* **68** (3-4), pp. 250-258.

Appendix A

Lab-code	Final grain size window (μm)	Initial D_e test	Saturation test	Feldspar test (IR depletion).	Dose recovery test.	Preheat test.	Remarks	Outcome
LV506	90-300	Recuperation evident. Suspected feldspar as exponential-fit not possible	-	-	-	-	Insufficient amount post-etch. Initial D_e test only.	FAIL
LV507	150-300	Failed to recycle low dose – recuperation (High dose 1600s).	Merged into initial De test due to experience of high De's of other samples.	-	-	-	Insufficient amount post-etch. Initial D_e & preheat test.	FAIL
LV508	90-300	40% aliquot acceptance rate: De > 2b = saturation. (High dose 1600s).	Merged into initial De test due to experience of high De's of other samples.	-	-	-	Insufficient amount post-etch. Initial D_e saturation test.	FAIL
LV509	90-300	Successful. De range: 214.1 ± 9.8 to 318.2 ± 8.6	-	2/12 aliquots show feldspar. 4/12 show recuperation .	Success	200^{o}C resulted in best dose recovery (200s).	Normal SAR protocol unsuitable. 'Hotblue wash' SAR variant applied to deal with recuperation.	DATED
LV510	90-300	40% acceptance rate. Regenerative dose points failed to match the 'natural' signal. Suspected saturation.	Saturation indicated by De > 2b.	-	-	-	Insufficient amount post-etch. Appears to be in saturation.	FAIL
LV511	90-200	< 10% aliquot acceptance rate. De > 2b & failure to recycle low dose.	High dose increased to 960s. 67% of aliquots: De > 2b or failed to approach natural. 33% rejected due to recuperation.	-	-	-	Abandoned due to being in 'saturation.'	FAIL
LV512	90-200	De > 2b & failure to recycle low dose.	High dose increased to 960s.	-	-	-	Abandoned due to being in 'saturation.'	FAIL

			75% of aliquots: De > 2b or failed to approach natural.					
LV513	90-200	Regenerative dose points failed to match the 'natural' signal (High dose 1600s). Failure to recycle low dose.	Merged into initial De test due to experience of high De's of other samples.	-	-	-	Abandoned due to insufficient amount post-etch. Initial combined D_e & saturation test only.	FAIL
LV514	90-200	Predominantly insensitive Quartz.	-	-	-	-	Significant amount of sample, but abandoned due to very poor recycling and recuperation.	FAIL
LV515	90-200	Successful.	Close to saturation.	-	Successful recovery of 400s dose.	240^{o}C resulted in best dose recovery (200s).	Normal SAR protocol unsuitable. 'Double-SAR' sequence designed to deal with recuperation.	DATED
LV516	90-300	Regenerative dose points failed to match the 'natural' signal.	-	-	-	-	Insufficient amount post-etch. Initial D_e test only.	FAIL
LV517	90-200	Regenerative dose points failed to match the 'natural' signal. Failure to recycle low dose.	-	-	-	-	Insufficient amount post-etch. Initial D_e test only.	FAIL
LV518	90-200	Weak or no OSL signal.	-	-	-	-	Insufficient amount post-etch. Initial D_e test only.	FAIL

Appendix B

LV509 – The initial SAR test (Murray and Wintle, 2000) measured the equivalent dose on two aliquots (Table B1). Both aliquots recycled the low dose within 10% of unity and feldspar contamination was found to be negligible (IR ratio 0.93–0.95). A preheat test was conducted to assess D_e dependence on temperature (Table B2).

Table B1 – SAR protocol applied to LV509 to determine initial D_e values. Notea a) deliberate exponentially increasing regenerative doses; and **b) applied and equivalent doses (D_e) are given in seconds (Table B1, B2, B4, B7, B8, B10-15). Greys were obtained by applying n x 0.1087 (beta dose rate during time of measurement).**

	Treatment
1	Give dose (30, 60, 120, 240, 480s).
2	Preheat (TL: 220^{o}C for 10s)
3	Optical stimulation 40s (125^{o}C)
4	Give test dose (120^{o}C)
5	Heat (180^{o}C) (as in step 2).
6	Optical stimulation 40s (125^{o}C)
7	Return to 1

Table B2 – preheat test sequence designed for LV509 to determine which preheat temperature yields most consistent dose recovery (n = 15 aliquots). Three aliquots per temperature increment were measured.

	Treatment
1	Bleach natural signal.
2	Applied dose (200s).
3	Preheat (TL: 180, 200, 220, 240,260^{o}C)
4	Optical stimulation 40s (125^{o}C)
5	Give test dose (100s)
6	Heat 1: 180^{o}C (aliquots 180 – 220^{o}C)
7	Heat 2: 220^{o}C (aliquots 220 – 260^{o}C)
8	Optical stimulation 40s (125^{o}C)
9	Return to 3. Use regenerative points 50, 100, 200, 400, 600s.

Preheat temperature of 180^{o}C produces narrowest range of D_e values, but 180^{o}C is not high enough to empty thermally sensitive electron traps (Wintle, 1975). Therefore, 200^{o}C was selected as the most appropriate preheat temperature in subsequent measurements of equivalent dose (Fig. 1).

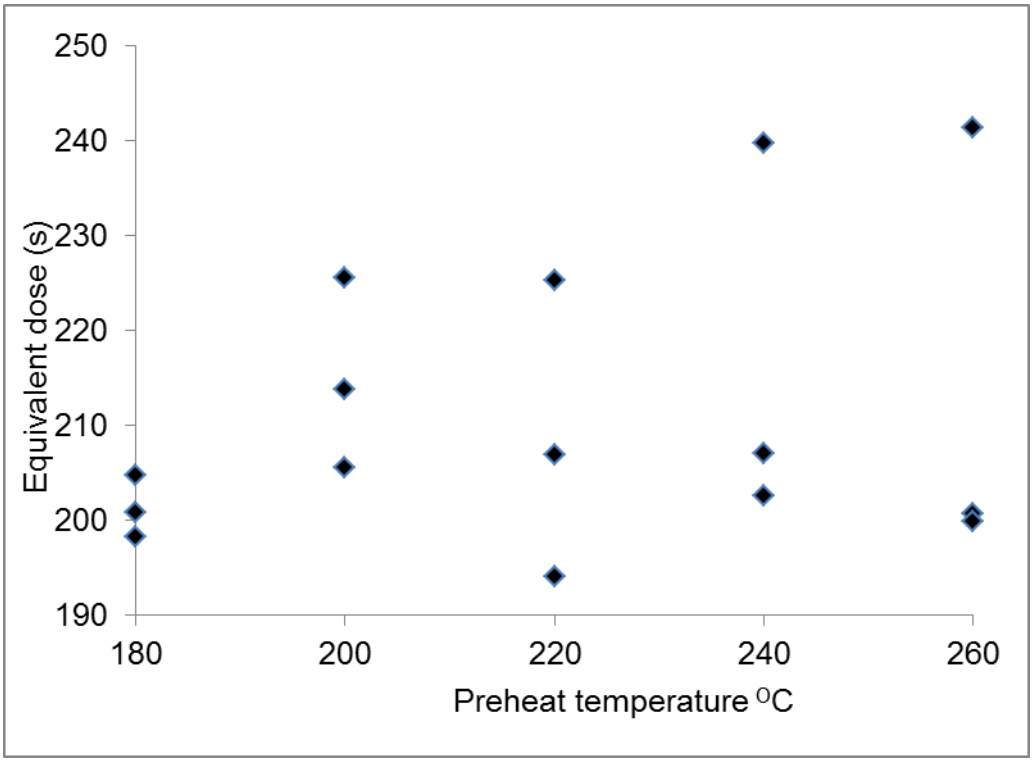

Figure 1 – Results of preheat test for sample LV509 on15 aliquots.

To test the relation between reduced thermal transfer and preheat temperature, the recycling ratios and dose ratio obtained from the same run are plotted in Fig. 2. 200°C produces the best dose recovery reflected in dose ratios of close to unity as well as lowest thermal transfer values reflected in typically low recuperation and effective recycling of both lower (50s) and upper (600s) doses.

A further SAR test was carried out on 12 aliquots to test the effectiveness of 200°C preheat in reducing recuperation. The SAR protocol was largely unsuccessful (2/12 aliquots accepted). Whilst it was possible to fit a saturating exponential curve to the dose response data for most aliquots, thermal transfer is indicated by the nature of the intercept ($y > 0$), confirmed by recuperation values > 10% (see Fig 3 & Table B3 – aliquot 2). Aitken and Smith (1988) proposed a mechanism of 'double charge transfer' whereby charge movement from the 325°C trap to a thermally shallower refuge trap occurred during optical stimulation, followed by re-trapping in the 325°C trap during subsequent heating. Failure to remove this 'recuperated' OSL component could result in equivalent dose overestimation thus causing age overestimation.

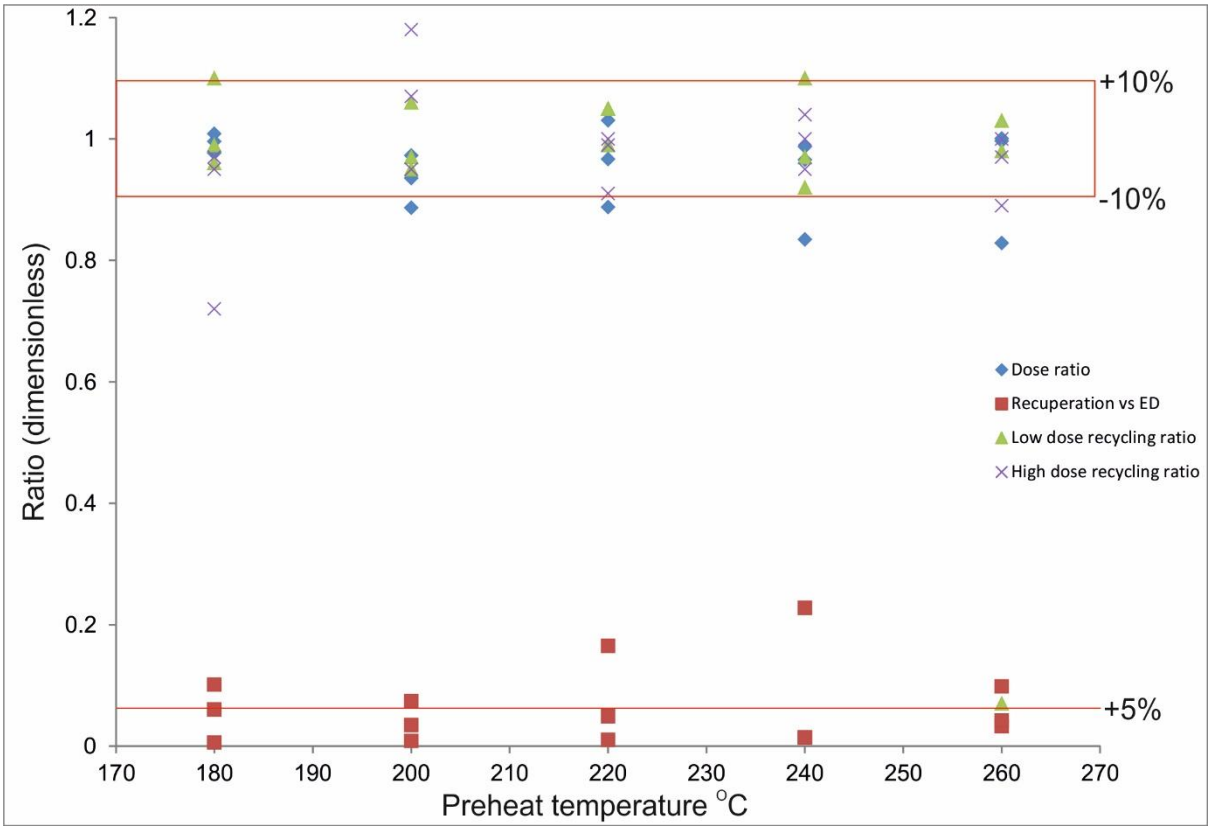

Figure 2 – Results of preheat test for sample LV509. Plotted are dimensionless ratio values for: a) dose; b) recuperation; c and d) recycling ratio of the low and high dose respectively against preheat temperature. Note tolerance levels for a, c & d (± 10%) and b (+ 5%). *Recuperation was calculated by dividing Lx/Tx by Ln/Tn.

IR depletion ratio was only >10% for aliquot 3, but both the shine-down and regenerative growth curves for aliquot 8 may indicate feldspar in spite of the IR being within 10% of unity (Fig. 2 & Table B3).

Table B3 – Results of 2nd SAR test employing 200°C preheat and 100s test dose. Recuperation (Lx/Tx / Ln/Tn) is expressed as %. Accepted aliquots are highlighted bold.

Aliquot	D_e	Recycling (100s)	IR depletion	Recuperation (%)
1	211.6	1.08	1.04	8.4
2	293.2	0.97	1.08	12.2
3	249.1	1.48	0.88	3.9
4	167.3	1.31	0.97	28.3
5	**303.4**	**1.02**	**1.03**	**0**
6	**281.3**	**1.07**	**1.08**	**0.6**
7	72.2	1.05	1.03	38.3
8	3.8	1.8	1.08	180.1

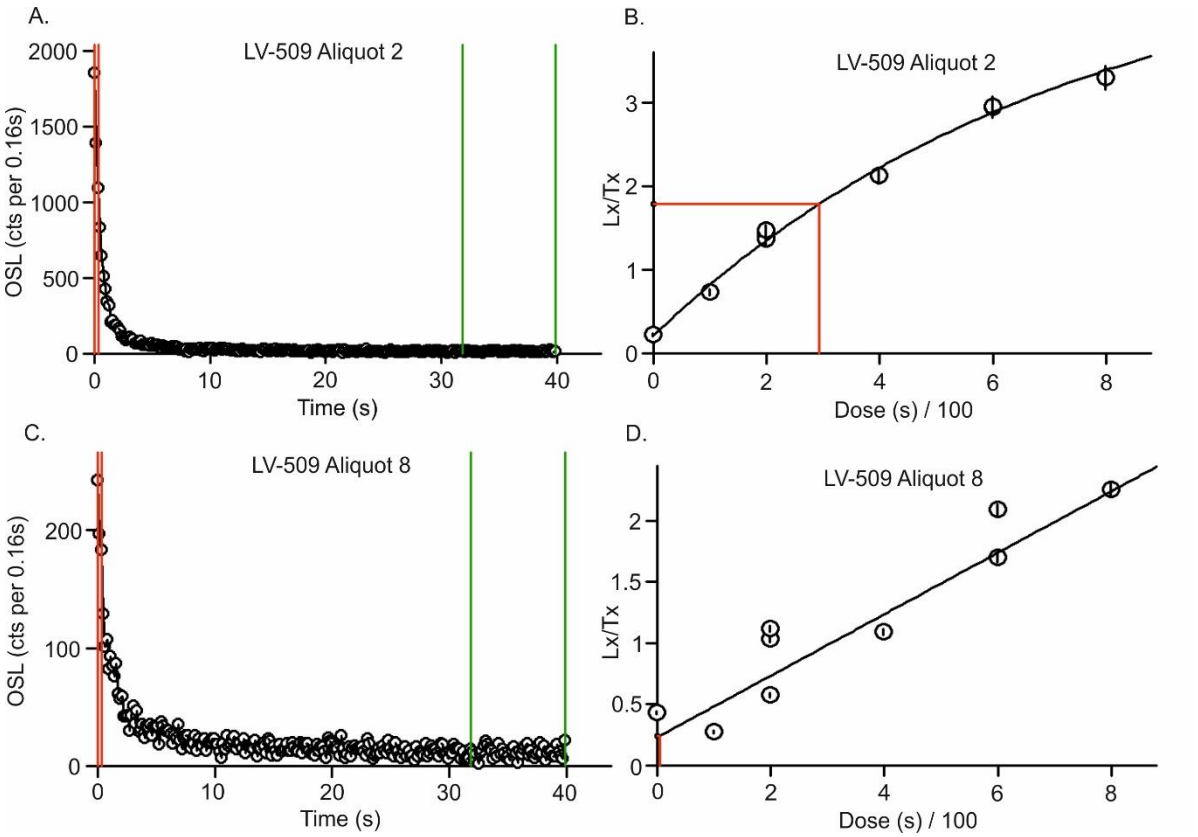

Figure 3 – example of typical results from OSL single aliquot regenerative analysis. A & C show shine-down curves from two aliquots (2 & 8) which exhibit contrasting decay behaviour. B & D show regenerative growth curves from the same aliquots.

This is because of the slow decay curve (Fig. 3) and the fact that exponential growth of Lx/Tx with increasing dose was not possible (Fig. 3). The shine-down curve for aliquot 2 is 'slow' which may indicate OSL dominated by a medium-decay component (Fig. 3). Sampling of the curve was restricted to the first 0.48s at most (3 channels) to avoid sampling the medium or slow OSL components.

On the basis of this evidence, it is questionable as to how useful the IR depletion ratio is as a measure of quartz purity for this sample. Firstly, the ratio was initially used to detect K-feldspar (Duller, 2003); the dolerites are characterised by plagioclase-feldspars (Neuumann et al., 2011), though K-feldspar is present in the sedimentary rock. In these circumstances, it has been recognised that polymineralic samples may not be completely depleted of feldspar OSL following the IR bleach (Duller and Bøtter-Jensen, 1993). Secondly, the large grain-size window used is likely to mask feldspar contamination in the presence of, we assume, light-emitting quartz grains.

To evaluate the purity of the quartz, the thermal quenching (Wintle, 1975; Duller et al., 1995; McKeever et al., 1997; Bøtter-Jensen et al., 2003) of sample LV509 was determined using the following sequence Table B4 (Shen et al., 2007).

Table B4 - modified SAR protocol applied to 12 aliquots (LV509) to determine the thermal quenching of sedimentary quartz with increasing OSL-stimulation temperature (L_x).

	Treatment
1	Bleach sample
2	Give dose (200s).
2	Preheat (TL: 200°C for 10s)
3	Optical stimulation 40s (begin at 50°C; for each cycle, increase temperature in increments of 20°C up to 320°C).
4	Give test dose (100°C)
5	Heat (180°C) (as in step 2).
6	Optical stimulation 40s (125°C)
7	Return to 2 (note step 3 for 2nd cycle will be 70°C etc).

The results of the experiment demonstrate thermal quenching (Fig. 4), comparing well with published curves (see LV150 – Fig. 5).

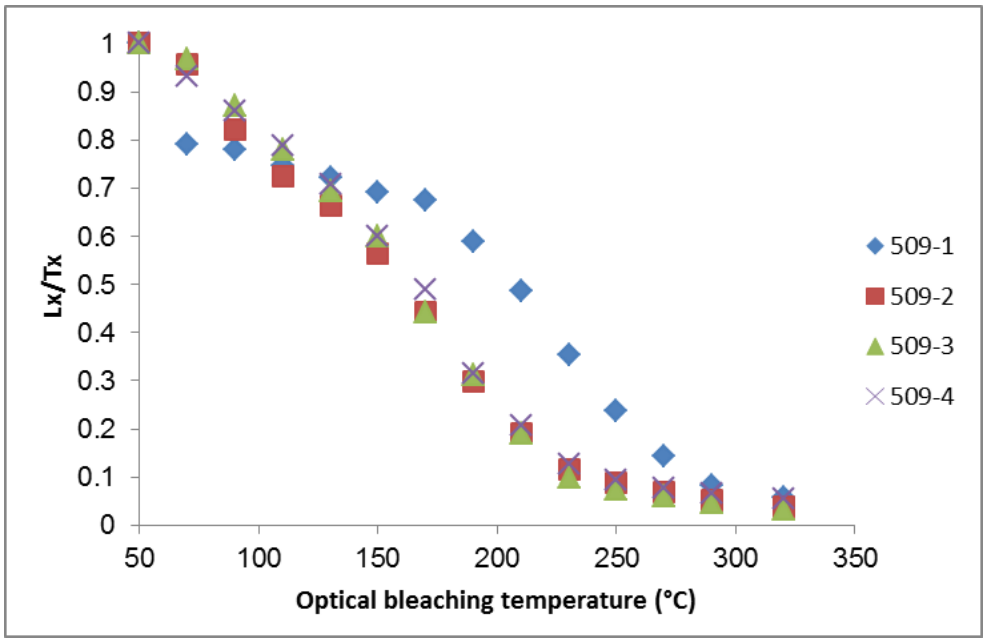

Figure 4 – OSL intensity (L_x/T_x) plotted versus stimulation temperatures for 4/12 representative aliquots. L_x/T_x has been normalised to the 50°C OSL intensity.

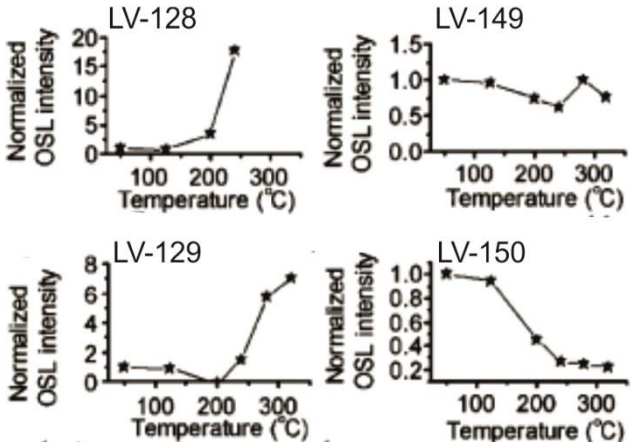

Figure 5 – plot of OSL intensity versus stimulation temperature for four samples by Shen et al. (2007). LV128 & 129 exhibit thermal assistance with increasing stimulation temperature (i.e. normalised L_x/T_x increases. LV149 is intermediate. LV150 displays thermal quenching, with OSL intensity decreasing strongly in stimulation temperature range of 125-280°C.

The OSL intensity versus stimulation temperature curves for LV509 (Fig. 4) were fitted with the thermal quenching formula of McKeever et al. (1997):

(1) $I = I_0 / (1 + C \exp(-W / kT)$

where W is the thermal activation energy, I is the OSL intensity, I_0 is the initial OSL intensity, k is the Boltzmann constant and C is a constant.

Table B5 – Results of non-linear curve fit to thermal quenching data for sample LV509. *Data fitted using Excel.

Aliquot no.	I_0	C	W (eV)
1	1.08	13.28×10^6	0.70
2*	1.70	6×10^6	0.58
3	1.48	0.37×10^6	0.48
4*	1.61	1.7×10^6	0.63
5	1.05	2.97×10^6	0.59
6	1.34	0.0009×10^6	0.36
7	1.60	3.64×10^6	0.62
8	2.97	0.04×10^6	0.37
9	3.24	0.04×10^6	0.37
10	1.51	0.11×10^6	0.42
11	1.33	100×10^6	0.79
12*	1.76	1.6×10^6	0.62

Equation 1 was applied using the OriginPRO9 function fitter (Fig. 6). This was largely successful (aliquots 1, 3, 5-11 – Table. B5), but the other data could not successfully be modelled using Origin. Glitches in the fitting procedure have previously been linked to the initial values specified for each parameter being unsuitable (C, W, I0)

(Shen, 2015 – pers. comm). To this end, for selected aliquots, initial values were varied between 0–10, but the fitting procedure remained unsuccessful.

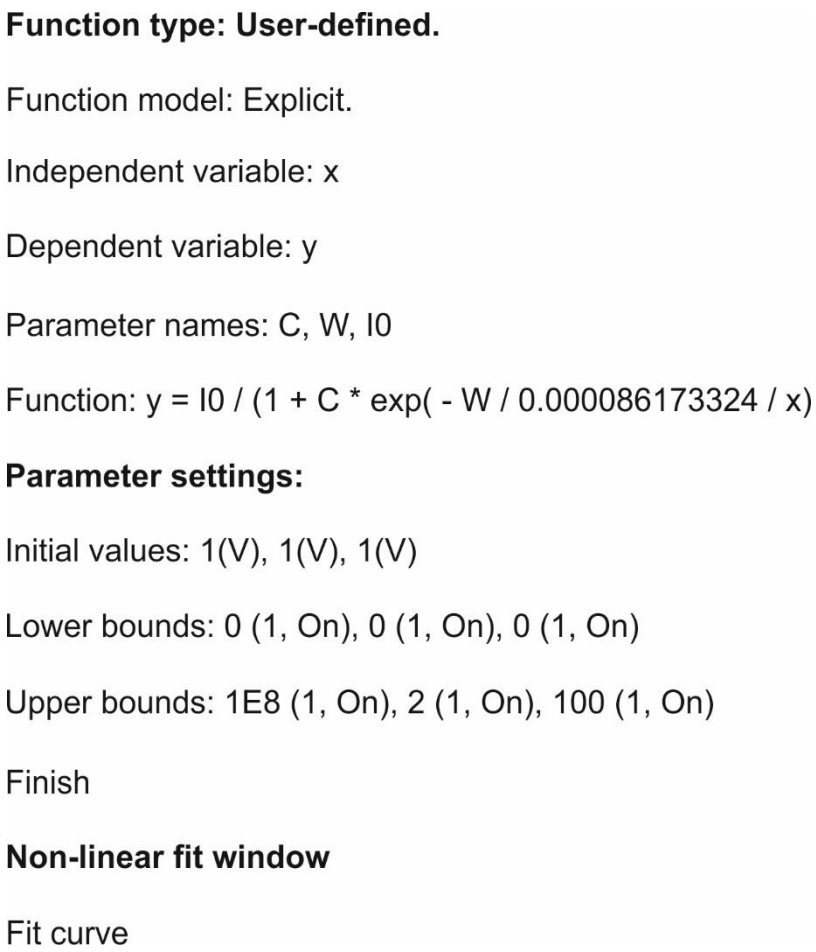

Figure 6 – procedure followed using Origin's "Fitting function builder".

To overcome this difficulty, the thermal activation energy (*W*) was also obtained using Microsoft Excel. The non-linear fit was computed by iteratively adjusting values of *C* & *W* to reduce the squared residuals between L_x/T_x and temperature (Fig. 7 & Table B6). *W* values are variable ranging from 0.36–0.79 (Table B5), but are consistently higher than published values for feldspar (0.19 eV – Shen et al., 2007). On average *W* compares well with values published for sedimentary quartz (Wintle, 1975; 0.51eV – Shen et al., 2007). Aliquots 6, 8 & 9 however exhibit *W* values that are closer to those reported for feldspar. Figure 3 was implicated earlier as showing OSL behaviour characteristic of feldspar. Although these aliquots (6, 8 & 9) show thermal quenching, the technique is not sensitive enough to compensate for the unconventionally large grain size window in which a feldspar component may be

subsumed. Additionally, variations in *W* may be reflective of two sources of sedimentary quartz: one of doleritic and the other of sandstone origin.

The strong OSL signal is clearly reflects the greater number of fine grains (90 μm) giving a higher gross signal than any lithologic-grain size dependence that could attest to inputs from eroding sandstone. Having, as far as possible, demonstrated the purity of quartz, attention is now turned to curing the issue of thermal transfer.

Table B6 – L_x/T_x data (non-normalised), non-linear fit values for *I* (thermal quenching) and residuals for aliquot 2 (Fig. 7 – curve).

L_x/T_x	*I*	*e*
1.70	1.69	8.12E-05
1.62	1.66	1.76E-03
1.39	1.61	4.69E-02
1.23	1.49	6.66E-02
1.13	1.27	2.04E-02
0.96	0.98	3.90E-04
0.75	0.67	5.96E-03
0.51	0.43	5.33E-03
0.33	0.27	3.23E-03
0.20	0.17	8.89E-04
0.15	0.10	2.30E-03
0.12	0.07	2.44E-03
0.09	0.04	2.04E-03
0.07	0.02	1.71E-03

A second preheat/dose recovery test was carried out on 19 aliquots (2 mm) which included a hot-bleach temperature at the end of each measurement cycle (Table A7). 4 aliquots were measured at each temperature. The hot-bleach temperature (T_x) was set at 20^{o}C above the preheat (L_x) temperature (Table A8) to optimise removal of thermal transfer at the end of each cycle.

The test showed that applied dose (200s) was most effectively recovered at 200^{o}C (L_x) with the 220^{o}C hot-bleach (T_x) (Fig. 8). Only 1 of 4 aliquots failed to recover the applied dose (ratio = 0.84). Compared to the previous preheat test, dose recovery is not improved using the hot-bleach step (median = 0.98, σ = 0.11 – Table B8).

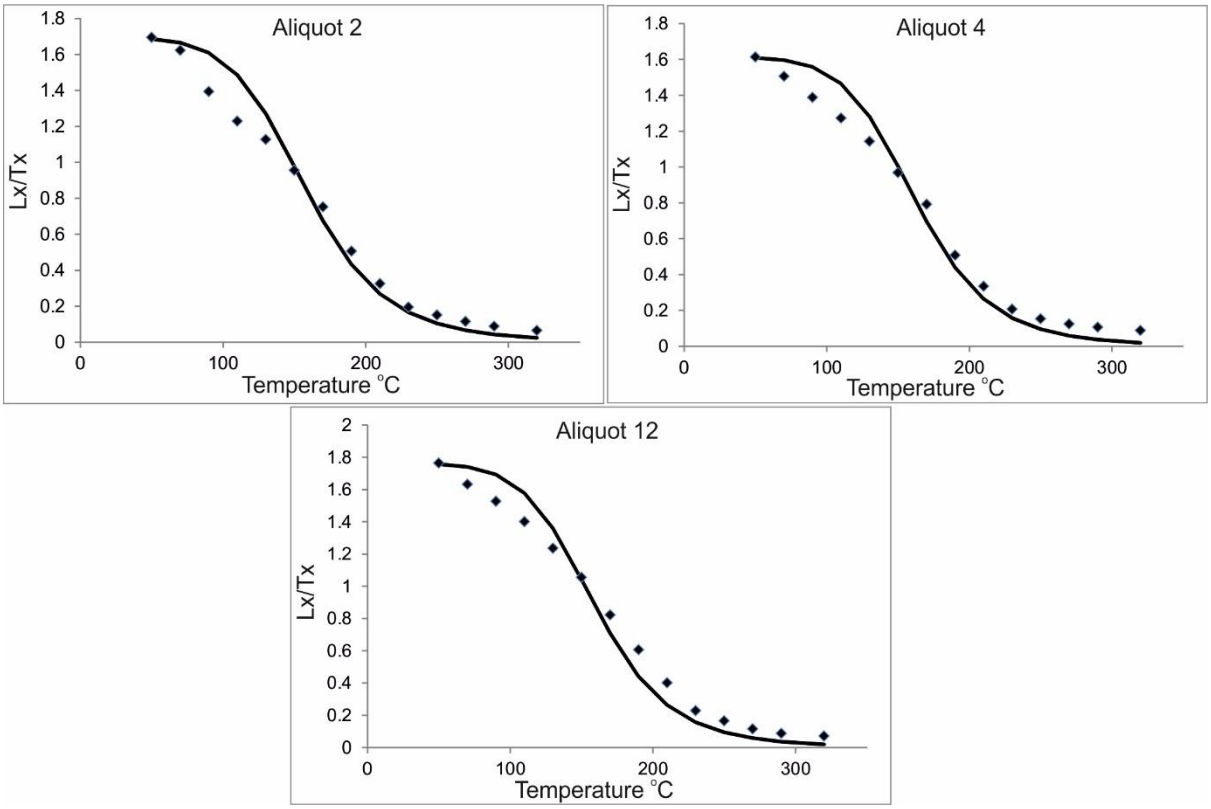

Figure 7 – OSL intensity (L_x/T_x) plotted versus stimulation temperatures for aliquots 2, 4 & 12 with thermal quenching formula fitted using excel.

Table B7 – modified preheat/dose-recovery test applied for sample LV509. Note applied dose values are in seconds.

	Treatment
1	Bleach natural signal.
2	Applied dose (200s).
3	Preheat (TL: 180, 200, 220, 240, 260^{o}C)
4	Optical stimulation 40s (125^{o}C)
5	Give test dose (100^{o}C)
6	Heat 1: 180^{o}C (aliquots 180 – 220^{o}C)
7	Heat 2: 220^{o}C (aliquots 220 – 260^{o}C)
8	Optical stimulation 40s (125^{o}C)
9	**Optical stimulation 40s (200, 220, 240, 260, 280^{o}C)**
10	Return to 3. Use regenerative points 50, 100, 200, 400, 600s.

Table B8 – modified preheat/dose-recovery test applied for sample LV509.

Aliquot no.	**TL temperature (L_x) (^{o}C)**	**Hot bleach temperature (T_x) (^{o}C)**
1-4	180	200
5-8	200	220
9-12	220	240
13-16	240	260
17-20	260	280

Recuperation is very slightly improved (median = 0.02, σ = 0.01) and of the two recycling ratios, the upper dose shows the largest improvement (median = 0.99, σ = 0.06 - see Table B9).

Having demonstrated the usefulness of the 'hot-bleach' step during the T_x part of the sequence, a modified SAR-protocol was written to determine the equivalent dose of the sample (Table B10).

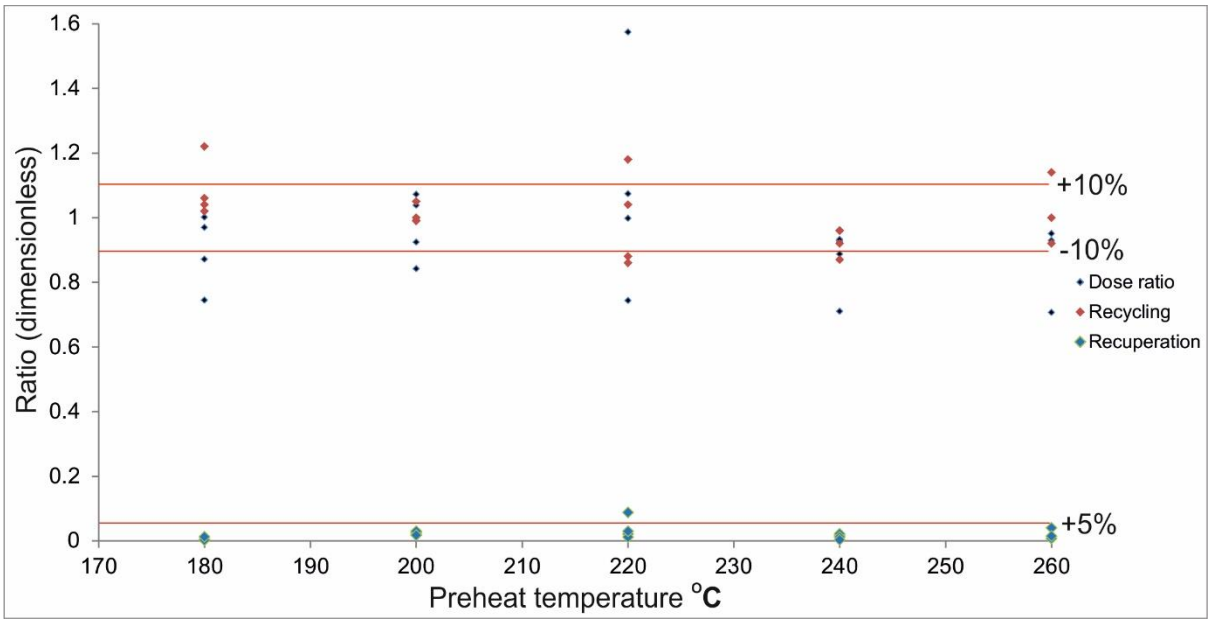

Figure 8 – Results of second preheat test for sample LV509 with extra hot-bleach step as indicated in Table B10. Dose ratio (black diamonds), recycling ratio (red diamonds) and recuperation (blue diamonds) are plotted against preheat temperature °C.

46 accepted D_e values were used in the final burial dose (D_b) of the sample. Ideally, 50 are recommended due to averaging of the luminescence signal associated with the number of grains per aliquot. As a result of this averaging effect, variability in incomplete zeroing of the OSL signal prior to quartz burial will be obscured (Duller, 2008). The Central Age Model (thereafter CAM) was found to be suitable for final age calculation following the protocol of Arnold et al. (2007).

Table B9 – median ([a]) and standard deviation values ([b]) for dose ratio, recuperation and recycling ratios between initial preheat test (i) and subsequent preheat test employing hot bleach-step (ii).

^{o}C	Dose ratio i	Dose ratio ii	Recuperation i	Recuperation ii	Recycling (L) i	Recycling (L) ii	Recycling (H) i	Recycling (H) ii
180	[a]1.00 [b]0.02	[a]0.92 [b]0.12	[a]0.06 [b]0.05	[a]0.00 [b]0.01	[a]0.99 [b]0.07	[a]1.05 [b]0.09	[a]0.95 [b]0.14	[a]0.99 [b]0.03
200	[a]0.94 [b]0.04	[a]0.98 [b]0.11	[a]0.03 [b]0.03	[a]0.02 [b]0.01	[a]0.97 [b]0.06	[a]1 [b]0.03	[a]1.07 [b]0.12	[a]0.99 [b]0.06
220	[a]0.97 [b]0.07	[a]1.04 [b]0.35	[a]0.05 [b]0.08	[a]0.03 [b]0.03	[a]1.05 [b]0.03	[a]0.96 [b]0.15	[a]0.99 [b]0.05	[a]1.01 [b]0.09
240	[a]0.97 [b]0.08	[a]0.91 [b]0.10	[a]0.01 [b]0.12	[a]0.01 [b]0.01	[a]0.97 [b]0.09	[a]0.94 [b]0.04	[a]1 [b]0.05	[a]1.01 [b]0.01
260	[a]1 [b]0.10	[a]0.93 [b]0.14	[a]0.04 [b]0.04	[a]0.01 [b]0.02	[a]0.98 [b]0.54	[a]1 [b]0.11	[a]0.97 [b]0.06	[a] [b]0.08

Table B10 – modified SAR sequence including hot-bleach (step 7) at end of each measurement cycle. *Note repeats of low and high dose to calculate recycling ratios and feldspar test using IR diodes (100 IR). Note: applied dose values given in seconds.

	Treatment
1	Give dose (50s, 100, 200, 400, 600, 0, *100R, *600R, *100IR).
2	Preheat (TL: 200^{o}C for 10s)
3	Optical stimulation 40s (125^{o}C)
4	Give test dose (120s)
5	Heat (180^{o}C) (as in step 2).
6	Optical stimulation 40s (125^{o}C)
7	**Optical stimulation 40s (220^{o}C)**
8	Return to 1

LV515 – Results of initial D_e measurements (Table B1) indicated the quartz was close to saturation (Fig. 9). To test for and evaluate the effect of feldspar on dose recovery, both a double-SAR and normal-SAR dose recovery test were employed (Table B11 and B12).

The 400s applied dose was effectively recovered using both tests (9/12 and 7/12 aliquots accepted respectively (Tables B13 and B14). To save machine time, a normal SAR (Murray and Wintle, 2003) D_e sequence was attempted using a preheat of 240^{o}C and cutheat of 200^{o}C (Table B15). Final age was based from 61 D_e values and modelled using the CAM (Arnold et al., 2007).

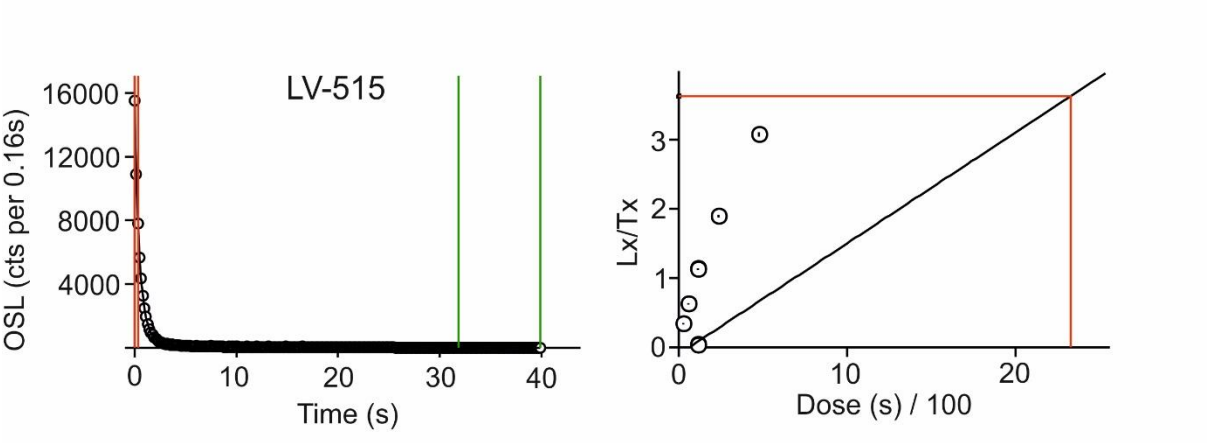

Figure 9 – example of typical shine-down (left) and regenerative dose points (right) from initial D_e test.

Table B11 – dose recovery test sequence employing D-SAR protocol of Roberts and Wintle (2001) on 12 aliquots.

	Treatment
1	Bleach natural signal
2	Applied dose (400s)
3	Preheat (240^{o}C)
4	OSL 50^{o}C IR 100s
5	OSL 125^{o}C IR 40s
6	Give test dose (100s)
7	Preheat 200^{o}C
8	OSL 50^{o}C IR 100s
9	OSL 125^{o}C IR 40s
10	Return to 3. Regenerative dose points 80, 160, 320, 640, 960, 0, 80, 960

Table B12 – dose recovery test sequence employing normal SAR protocol on 12 aliquots.

	Treatment
1	Bleach natural signal
2	Applied dose (400s)
3	Preheat (240^{o}C)
5	OSL 125^{o}C IR 40s
6	Give test dose (100s)
7	Preheat 200^{o}C
9	OSL 125^{o}C IR 40s
10	Return to 3. Regenerative dose points 100s, 200, 400, 600, 800, 0, 100, 100IR

Table B13 – results of D-SAR dose recovery test.

Aliquot no.	D_e	Dose ratio	Recycling (80s)
1	390.4	0.98	1.05
2	417.6	1.04	0.94
3	389	0.97	1
4	384.2	0.96	0.98
5	389.9	0.97	1.03
7	417.8	1.04	1.05
8	358	0.90	1.03
9	362.5	0.91	1.03
11	388.3	0.97	0.98

Table B14 – results of SAR dose recovery test.

Aliquot no.	D_e	Dose ratio	Recycling (100s)	IR depletion (100s)
1	346.1	0.87	0.97	1.03
2	349.2	0.87	0.98	1.07
4	389	0.97	1.03	0.96
5	415.4	1.04	0.96	0.96
6	367	0.92	1.03	1.07
7	388.1	0.97	1.03	0.97
8	384.2	0.96	1.01	0.99
9	388.5	0.97	1.05	1
10	399.5	1	1.01	0.95

Table B15 – SAR protocol for D_e determination.

	Treatment
1	Give dose (100, 200, 400, 600, 900, 0, 100, 600, 100IR).
2	Preheat (TL: 240^{o}C for 10s)
3	Optical stimulation 40s (125^{o}C)
4	Give test dose (120^{o}C)
5	Heat (200^{o}C) (as in step 2).
6	Optical stimulation 40s (125^{o}C)
7	Return to 1